

University of Groningen

In Vivo Models for the Evaluation of Antisense Oligonucleotides in Skin

Bremer, Jeroen; van den Akker, Peter C

Published in:
Methods in Molecular Biology

DOI:
[10.1007/978-1-0716-2010-6_21](https://doi.org/10.1007/978-1-0716-2010-6_21)

IMPORTANT NOTE: You are advised to consult the publisher's version (publisher's PDF) if you wish to cite from it. Please check the document version below.

Document Version
Publisher's PDF, also known as Version of record

Publication date:
2022

[Link to publication in University of Groningen/UMCG research database](#)

Citation for published version (APA):

Bremer, J., & van den Akker, P. C. (2022). In Vivo Models for the Evaluation of Antisense Oligonucleotides in Skin. In *Methods in Molecular Biology* (Vol. 2434, pp. 315-320). (Methods in molecular biology (Clifton, N.J.)). Springer. https://doi.org/10.1007/978-1-0716-2010-6_21

Copyright

Other than for strictly personal use, it is not permitted to download or to forward/distribute the text or part of it without the consent of the author(s) and/or copyright holder(s), unless the work is under an open content license (like Creative Commons).

The publication may also be distributed here under the terms of Article 25fa of the Dutch Copyright Act, indicated by the "Taverne" license. More information can be found on the University of Groningen website: <https://www.rug.nl/library/open-access/self-archiving-pure/taverne-amendment>.

Take-down policy

If you believe that this document breaches copyright please contact us providing details, and we will remove access to the work immediately and investigate your claim.

Downloaded from the University of Groningen/UMCG research database (Pure): <http://www.rug.nl/research/portal>. For technical reasons the number of authors shown on this cover page is limited to 10 maximum.



Virginia Arechavala-Gomez
Alejandro Garanto *Editors*

Antisense RNA Design, Delivery, and Analysis



OPEN ACCESS

 Humana Press

METHODS IN MOLECULAR BIOLOGY

Series Editor

John M. Walker

School of Life and Medical Sciences

University of Hertfordshire

Hatfield, Hertfordshire, UK

For further volumes:

<http://www.springer.com/series/7651>

For over 35 years, biological scientists have come to rely on the research protocols and methodologies in the critically acclaimed *Methods in Molecular Biology* series. The series was the first to introduce the step-by-step protocols approach that has become the standard in all biomedical protocol publishing. Each protocol is provided in readily-reproducible step-by-step fashion, opening with an introductory overview, a list of the materials and reagents needed to complete the experiment, and followed by a detailed procedure that is supported with a helpful notes section offering tips and tricks of the trade as well as troubleshooting advice. These hallmark features were introduced by series editor Dr. John Walker and constitute the key ingredient in each and every volume of the *Methods in Molecular Biology* series. Tested and trusted, comprehensive and reliable, all protocols from the series are indexed in PubMed.

Antisense RNA Design, Delivery, and Analysis

Edited by

Virginia Arechavala-Gomez

*Ikerbasque, Basque Foundation for Science, Bilbao, Spain; Neuromuscular Disorders Research Group,
Biocruces Bizkaia Health Research Institute, Barakaldo, Spain*

Alejandro Garanto

*Department of Pediatrics, Department of Human Genetics, Radboud University Medical Center, Nijmegen,
The Netherlands*

 **Humana Press**

Editors

Virginia Arechavala-Gomez
Ikerbasque, Basque Foundation
for Science
Bilbao, Spain

Neuromuscular Disorders Research Group
Biocruces Bizkaia Health Research Institute
Barakaldo, Spain

Alejandro Garanto
Department of Pediatrics
Department of Human Genetics
Radboud University Medical Center
Nijmegen, The Netherlands

ISSN 1064-3745

ISBN 978-1-0716-2009-0

ISSN 1940-6029 (electronic)

ISBN 978-1-0716-2010-6 (eBook)

<https://doi.org/10.1007/978-1-0716-2010-6>

© The Editor(s) (if applicable) and The Author(s) 2022. This book is an open access publication.

Open Access This book is licensed under the terms of the Creative Commons Attribution 4.0 International License (<http://creativecommons.org/licenses/by/4.0/>), which permits use, sharing, adaptation, distribution and reproduction in any medium or format, as long as you give appropriate credit to the original author(s) and the source, provide a link to the Creative Commons license and indicate if changes were made.

The images or other third party material in this book are included in the book's Creative Commons license, unless indicated otherwise in a credit line to the material. If material is not included in the book's Creative Commons license and your intended use is not permitted by statutory regulation or exceeds the permitted use, you will need to obtain permission directly from the copyright holder.

The use of general descriptive names, registered names, trademarks, service marks, etc. in this publication does not imply, even in the absence of a specific statement, that such names are exempt from the relevant protective laws and regulations and therefore free for general use.

The publisher, the authors and the editors are safe to assume that the advice and information in this book are believed to be true and accurate at the date of publication. Neither the publisher nor the authors or the editors give a warranty, expressed or implied, with respect to the material contained herein or for any errors or omissions that may have been made. The publisher remains neutral with regard to jurisdictional claims in published maps and institutional affiliations.

This Humana imprint is published by the registered company Springer Science+Business Media, LLC part of Springer Nature.

The registered company address is: 1 New York Plaza, New York, NY 10004, U.S.A.

Preface

The field of RNA therapeutics has rapidly changed over the last few years. Particularly, two mRNA vaccines for SARS-CoV-2 and a customized oligonucleotide for an *n*-of-1 trial have revolutionized the expectations in the field. Although the use of RNA-based molecules as treatments has been investigated for several decades, this recent surge of applications has seen more and more researchers embarking on the design and assessment of such therapies. The main objective of this book is to provide basic knowledge and a large collection of methods to facilitate the work of these newcomers to the field who want to exploit antisense technology as a therapeutic intervention.

This book was conceived thanks to the network DARTER (Delivery of Antisense RNA Therapeutics, <https://www.antisenserna.eu>). DARTER is funded by the EU Cooperation of Science and Technology (COST), which aims to enhance interaction and collaborations between researchers in Europe and other countries (<https://www.cost.eu/>). Within DARTER, we aim to exchange knowledge and protocols and explore the full potential of antisense technology in an environment that combines academia, industry, and patient representatives. This book depicts the variety of models, delivery systems, and approaches that can be used to assess RNA technology and has combined the expertise of researchers located in ten different countries.

Among the 28 chapters included in this book, we have commissioned several review chapters that cover aspects from the historical development of nucleic acid therapeutics, the clinical applications of antisense oligonucleotides, and considerations to include in the preclinical evaluation of the oligonucleotide-mediated toxicology, to patent issues that may need to be contemplated. The remaining chapters follow a classical protocol structure, and we have divided them attending to the subject covered: the design of antisense technology and their delivery (Part II), the description of the model systems developed to evaluate their efficacy, both in vitro (Part III) and in vivo (Part IV), methods to evaluate preclinically the toxicity associated with these new potential drugs (Part V), and intellectual property considerations (Part VI).

We thank all contributing authors for their tremendous effort including their secret tips in the notes of their protocols. We also thank COST for facilitating the cooperation between the research groups and for making it possible for this book to be published Open Access. We have learned a lot during the revision of this book, and we hope that readers will, too.

Barakaldo, Spain
Nijmegen, The Netherlands

Virginia Arechavala-Gomez
Alejandro Garanto

Acknowledgments

This book is based upon work from COST Action DARTER (CA 17103), supported by COST (European Cooperation in Science and Technology).

COST (European Cooperation in Science and Technology) is a funding agency for research and innovation networks. Our Actions help connect research initiatives across Europe and enable scientists to grow their ideas by sharing them with their peers. This boosts their research, career, and innovation.

www.cost.eu



COST is supported
by the Horizon 2020
Framework Programme
of the European Union

Contents

<i>Preface</i>	<i>v</i>
<i>Acknowledgments</i>	<i>vii</i>
<i>Contributors</i>	<i>xiii</i>

PART I OVERVIEW

1 Introduction and History of the Chemistry of Nucleic Acids Therapeutics	3
<i>Michael J. Gait and Sudhir Agrawal</i>	
2 Antisense RNA Therapeutics: A Brief Overview	33
<i>Virginia Arechavala-Gomez and Alejandro Garanto</i>	

PART II DESIGN AND FORMULATION OF ANTISENSE TECHNOLOGY

3 Design of Bifunctional Antisense Oligonucleotides for Exon Inclusion	53
<i>Haiyan Zhou</i>	
4 Design and Delivery of SINEUP: A New Modular Tool to Increase Protein Translation	63
<i>Michele Arnoldi, Giulia Zarantonello, Stefano Espinoza, Stefano Gustincich, Francesca Di Leva, and Marta Biagioli</i>	
5 How to Design U1 snRNA Molecules for Splicing Rescue	89
<i>Liliana Matos, Juliana I. Santos, M^a. Francisca Coutinho, and Sandra Alves</i>	
6 Conjugation of Nucleic Acids and Drugs to Gold Nanoparticles	103
<i>Paula Milán-Rois, Ciro Rodriguez-Diaz, Milagros Castellanos, and Alvaro Somoza</i>	
7 Determination of Optimum Ratio of Cationic Polymers and Small Interfering RNA with Agarose Gel Retardation Assay	117
<i>Omer Aydin, Dilek Kanarya, Ummugulsum Yilmaz, and Cansu Ümrhan Tunç</i>	
8 Generation of Protein-Phosphorodiamidate Morpholino Oligomer Conjugates for Efficient Cellular Delivery via Anthrax Protective Antigen	129
<i>Valentina Palacio-Castañeda, Roland Brock, and Wouter P. R. Verdurmen</i>	

PART III IN VITRO MODEL SYSTEMS

9 Development and Use of Cellular Systems to Assess and Correct Splicing Defects	145
<i>Nuria Suárez-Herrera, Tomasz Z. Tomkiewicz, Alejandro Garanto, and Rob W. J. Collin</i>	

10	Modeling Splicing Variants Amenable to Antisense Therapy by Use of CRISPR-Cas9-Based Gene Editing in HepG2 Cells.	167
	<i>Aristides López-Márquez, Ainhoa Martínez-Pizarro, Belén Pérez, Eva Richard, and Lourdes R. Desviat</i>	
11	In Vitro Models for the Evaluation of Antisense Oligonucleotides in Skin.	185
	<i>Jeroen Bremer and Peter C. van den Akker</i>	
12	In Vitro Delivery of PMOs in Myoblasts by Electroporation	191
	<i>Remko Goossens and Annemieke Aartsma-Rus</i>	
13	Rapid Determination of MBNL1 Protein Levels by Quantitative Dot Blot for the Evaluation of Antisense Oligonucleotides in Myotonic Dystrophy Myoblasts	207
	<i>Nerea Moreno, Irene González-Martínez, Rubén Artero, and Estefanía Cerro-Herreros</i>	
14	Evaluation of Exon Skipping and Dystrophin Restoration in In Vitro Models of Duchenne Muscular Dystrophy	217
	<i>Andrea López-Martínez, Patricia Soblechero-Martín, and Virginia Arechavala-Gomeza</i>	
15	Generation of Human iPSC-Derived Myotubes to Investigate RNA-Based Therapies In Vitro	235
	<i>Pablo Herrero-Hernandez, Atze J. Bergsma, and W. W. M. Pim Pijnappel</i>	
16	Eye on a Dish Models to Evaluate Splicing Modulation	245
	<i>Kwan-Leong Hau, Amelia Lane, Rosellina Guarascio, and Michael E. Cheetham</i>	
17	Establishment of In Vitro Brain Models for AON Delivery.	257
	<i>Elena Daoutsali and Ronald A. M. Buijsen</i>	

PART IV IN VIVO MODEL SYSTEMS

18	Considerations for Generating Humanized Mouse Models to Test Efficacy of Antisense Oligonucleotides.	267
	<i>Irene Vázquez-Domínguez and Alejandro Garanto</i>	
19	Generation of Humanized Zebrafish Models for the In Vivo Assessment of Antisense Oligonucleotide-Based Splice Modulation Therapies.	281
	<i>Renske Schellens, Erik de Vrieze, Ralph Slijkerman, Hannie Kremer, and Erwin van Wijk</i>	
20	Use of Small Animal Models for Duchenne and Parameters to Assess Efficiency upon Antisense Treatment	301
	<i>Ngoc Lu-Nguyen, Alberto Malerba, and Linda Popplewell</i>	
21	In Vivo Models for the Evaluation of Antisense Oligonucleotides in Skin	315
	<i>Jeroen Bremer and Peter C. van den Akker</i>	
22	Delivery of Antisense Oligonucleotides to the Mouse Retina	321
	<i>Alejandro Garanto</i>	
23	Delivery of Antisense Oligonucleotides to the Mouse Brain by Intracerebroventricular Injections	333
	<i>Tom Metz, Elsa C. Kuijper, and Willeke M. C. van Roon-Mom</i>	

PART V SAFETY AND TOXICOLOGY

24 Intrathecal Delivery of Therapeutic Oligonucleotides for Potent
Modulation of Gene Expression in the Central Nervous System 345
Zachary Kennedy, James W. Gilbert, and Bruno M. D. C. Godinho

25 Preclinical Safety Assessment of Therapeutic Oligonucleotides..... 355
Patrik Andersson

26 Preclinical Evaluation of the Renal Toxicity of Oligonucleotide
Therapeutics in Mice 371
Lucía Echevarría and Aurelie Goyenvalle

27 Protocol for Isolation and Culture of Mouse Hepatocytes (HCs),
Kupffer Cells (KCs), and Liver Sinusoidal Endothelial Cells
(LSECs) in Analyses of Hepatic Drug Distribution..... 385
Kjetil Elvevold, Ingelin Kyrrestad, and Bård Smedsrød

PART VI INTELLECTUAL PROPERTY

28 Patent Considerations When Embarking on New Antisense Drug
Programs 405
Laurence D. S. Gainey

Index 419

Contributors

- ANNEMIEKE AARTSMA-RUS • *Department of Human Genetics, Leiden University Medical Center, Leiden, The Netherlands*
- SUDHIR AGRAWAL • *University of Massachusetts Medical School, Worcester, MA, USA; Arnay Sciences LLC, Shrewsbury, MA, USA*
- SANDRA ALVES • *Department of Human Genetics, Research and Development Unit, National Health Institute Doutor Ricardo Jorge, Porto, Portugal; Center for the Study of Animal Science, CECA-ICETA, University of Porto, Porto, Portugal*
- PATRIK ANDERSSON • *Respiratory and Immunology Safety, Clinical Pharmacology and Safety Sciences, R&D, AstraZeneca, Gothenburg, Sweden*
- VIRGINIA ARECHAVALA-GOMEZA • *Ikerbasque, Basque Foundation for Science, Bilbao, Spain; Neuromuscular Disorders Research Group, Biocruces Bizkaia Health Research Institute, Barakaldo, Spain*
- MICHELE ARNOLDI • *Neuroepigenetics Laboratory, Department of Cellular, Computational and Integrative Biology (CIBIO), University of Trento, Trento, Italy*
- RUBÉN ARTERO • *Interdisciplinary Research Structure for Biotechnology and Biomedicine (ERI BIOTECMED), Universidad de Valencia, Valencia, Spain; Translational Genomics Group, Incliva Health Research Institute, Valencia, Spain; Joint Unit Incliva-CIPF, Valencia, Spain*
- OMER AYDIN • *NanoThera Lab, Department of Biomedical Engineering, Erciyes University, Kayseri, Turkey; ERNAM - Nanotechnology Research and Application Center, Erciyes University, Kayseri, Turkey; ERKAM - Clinical Engineering and Implementation Center, Erciyes University, Kayseri, Turkey*
- ATZE J. BERGSMA • *Department of Clinical Genetics, Erasmus Medical Center, Rotterdam, The Netherlands; Department of Pediatrics, Erasmus Medical Center, Rotterdam, The Netherlands; Center for Lysosomal and Metabolic Diseases, Erasmus Medical Center, Rotterdam, The Netherlands*
- MARTA BIAGIOLI • *Neuroepigenetics Laboratory, Department of Cellular, Computational and Integrative Biology (CIBIO), University of Trento, Trento, Italy*
- JEROEN BREMER • *Department of Genetics, University of Groningen, University Medical Center Groningen, Groningen, The Netherlands; Department of Dermatology, Center for Blistering Diseases, University of Groningen, University Medical Center Groningen, Groningen, The Netherlands*
- ROLAND BROCK • *Department of Biochemistry, Radboud Institute for Molecular Life Sciences (RIMLS), Radboud University Medical Center, Nijmegen, The Netherlands*
- RONALD A. M. BUIJSEN • *Department of Human Genetics, Leiden University Medical Center, Leiden, The Netherlands*
- MILAGROS CASTELLANOS • *Instituto Madrileño de Estudios Avanzados en Nanociencia (IMDEA Nanociencia), Madrid, Spain*
- ESTEFANÍA CERRO-HERREROS • *Interdisciplinary Research Structure for Biotechnology and Biomedicine (ERI BIOTECMED), Universidad de Valencia, Valencia, Spain; Translational Genomics Group, Incliva Health Research Institute, Valencia, Spain; Joint Unit Incliva-CIPF, Valencia, Spain*
- MICHAEL E. CHEETHAM • *UCL Institute of Ophthalmology, London, UK*

- ROB W. J. COLLIN • *Department of Human Genetics and Donders Institute for Brain, Cognition and Behaviour, Radboud University Medical Center, Nijmegen, The Netherlands*
- M^a. FRANCISCA COUTINHO • *Department of Human Genetics, Research and Development Unit, National Health Institute Doutor Ricardo Jorge, Porto, Portugal; Center for the Study of Animal Science, CECA-ICETA, University of Porto, Porto, Portugal*
- ELENA DAOUTSALI • *Department of Human Genetics, Leiden University Medical Center, Leiden, The Netherlands*
- ERIK DE VRIEZE • *Department of Otorhinolaryngology, Radboud University Medical Center, Nijmegen, The Netherlands; Donders Institute for Brain Cognition and Behaviour, Nijmegen, The Netherlands*
- LOURDES R. DESVIAT • *Centro de Biología Molecular Severo Ochoa CSIC-UAM, CEDEM, CIBERER (ISCIII), IdiPaz (ISCIII), Universidad Autónoma de Madrid, Madrid, Spain*
- FRANCESCA DI LEVA • *Neuroepigenetics Laboratory, Department of Cellular, Computational and Integrative Biology (CIBIO), University of Trento, Trento, Italy; Institute for Biomedicine, Eurac Research, Bolzano, Italy*
- LUCÍA ECHEVARRÍA • *Université Paris-Saclay, UVSQ, Inserm, END-ICAP, Versailles, France; SQY Therapeutics, UVSQ, END-ICAP, Montigny le Bretonneux, France*
- KJETIL ELVEVOLD • *DLiver AS, Tromsø, Norway*
- STEFANO ESPINOZA • *Central RNA Laboratory, Istituto Italiano di Tecnologia, Genova, Italy*
- LAURENCE D. S. GAINES • *HGF Ltd, Manchester, UK*
- MICHAEL J. GAIT • *Medical Research Council Laboratory of Molecular Biology, Cambridge, UK*
- ALEJANDRO GARANTO • *Department of Paediatrics, Amalia Children's Hospital, Nijmegen, The Netherlands; Department of Human Genetics, Radboud University Medical Center, Nijmegen, The Netherlands; Radboud Institute for Molecular Life Sciences (RIMLS), Radboud University Medical Center, Nijmegen, The Netherlands*
- JAMES W. GILBERT • *RNA Therapeutics Institute, University of Massachusetts Medical School, Worcester, MA, USA*
- BRUNO M. D. C. GODINHO • *RNA Therapeutics Institute, University of Massachusetts Medical School, Worcester, MA, USA*
- IRENE GONZALEZ-MARTINEZ • *Interdisciplinary Research Structure for Biotechnology and Biomedicine (ERI BIOTECMED), Universidad de Valencia, Valencia, Spain; Translational Genomics Group, Incliva Health Research Institute, Valencia, Spain; Joint Unit Incliva-CIPE, Valencia, Spain*
- REMKO GOOSSENS • *Department of Human Genetics, Leiden University Medical Center, Leiden, The Netherlands*
- AURELIE GOYENVALLE • *Université Paris-Saclay, UVSQ, Inserm, END-ICAP, Versailles, France*
- ROSELLINA GUARASCIO • *UCL Institute of Ophthalmology, London, UK*
- STEFANO GUSTINCICH • *Central RNA Laboratory, Istituto Italiano di Tecnologia, Genova, Italy; Area of Neuroscience, Scuola Internazionale Superiore di Studi Avanzati (SISSA), Trieste, Italy*
- KWAN-LEONG HAU • *UCL Institute of Ophthalmology, London, UK*
- PABLO HERRERO-HERNANDEZ • *Department of Clinical Genetics, Erasmus Medical Center, Rotterdam, The Netherlands; Department of Pediatrics, Erasmus Medical Center,*

- Rotterdam, The Netherlands; Center for Lysosomal and Metabolic Diseases, Erasmus Medical Center, Rotterdam, The Netherlands*
- DILEK KANARYA • *NanoThera Lab, Department of Biomedical Engineering, Erciyes University, Kayseri, Turkey; ERNAM - Nanotechnology Research and Application Center, Erciyes University, Kayseri, Turkey*
- ZACHARY KENNEDY • *RNA Therapeutics Institute, University of Massachusetts Medical School, Worcester, MA, USA*
- HANNIE KREMER • *Department of Otorhinolaryngology, Radboud University Medical Center, Nijmegen, The Netherlands; Donders Institute for Brain Cognition and Behaviour, Nijmegen, The Netherlands; Department of Human Genetics, Radboud University Medical Center, Nijmegen, The Netherlands*
- ELSA C. KUIJPER • *Department of Human Genetics, LUMC, Leiden, The Netherlands*
- INGELIN KYRRETTAD • *Vascular Biology Research Group, Department of Medical Biology, The Arctic University of Norway (UiT), Tromsø, Norway*
- AMELIA LANE • *UCL Institute of Ophthalmology, London, UK*
- ARÍSTIDES LÓPEZ-MÁRQUEZ • *Centro de Biología Molecular Severo Ochoa CSIC-UAM, CEDEM, CIBERER (ISCIII), IdiPaz (ISCIII), Universidad Autónoma de Madrid, Madrid, Spain*
- ANDREA LÓPEZ-MARTÍNEZ • *Neuromuscular Disorders, Biocruces Bizkaia Health Research Institute, Barakaldo, Spain*
- NGOC LU-NGUYEN • *Department of Biological Sciences, Royal Holloway University of London, Egham, Surrey, UK*
- ALBERTO MALERBA • *Department of Biological Sciences, Royal Holloway University of London, Egham, Surrey, UK*
- AINHUA MARTÍNEZ-PIZARRO • *Centro de Biología Molecular Severo Ochoa CSIC-UAM, CEDEM, CIBERER (ISCIII), IdiPaz (ISCIII), Universidad Autónoma de Madrid, Madrid, Spain*
- LILIANA MATOS • *Department of Human Genetics, Research and Development Unit, National Health Institute Doutor Ricardo Jorge, Porto, Portugal; Center for the Study of Animal Science, CECA-ICETA, University of Porto, Porto, Portugal*
- TOM METZ • *Department of Human Genetics, LUMC, Leiden, The Netherlands*
- PAULA MILÁN-ROIS • *Instituto Madrileño de Estudios Avanzados en Nanociencia (IMDEA Nanociencia), Madrid, Spain*
- NEREA MORENO-CERVERA • *Interdisciplinary Research Structure for Biotechnology and Biomedicine (ERI BIOTECMED), Universidad de Valencia, Valencia, Spain; Translational Genomics Group, Incliva Health Research Institute, Valencia, Spain; Joint Unit Incliva-CIPE, Valencia, Spain*
- VALENTINA PALACIO-CASTAÑEDA • *Department of Biochemistry, Radboud Institute for Molecular Life Sciences (RIMLS), Radboud University Medical Center, Nijmegen, The Netherlands*
- BELÉN PÉREZ • *Centro de Biología Molecular Severo Ochoa CSIC-UAM, CEDEM, CIBERER (ISCIII), IdiPaz (ISCIII), Universidad Autónoma de Madrid, Madrid, Spain*
- W. W. M. PIM PIJNAPPEL • *Department of Clinical Genetics, Erasmus Medical Center, Rotterdam, The Netherlands; Department of Pediatrics, Erasmus Medical Center, Rotterdam, The Netherlands; Center for Lysosomal and Metabolic Diseases, Erasmus Medical Center, Rotterdam, The Netherlands*

- LINDA POPPLEWELL • *Department of Biological Sciences, Royal Holloway University of London, Egham, Surrey, UK*
- EVA RICHARD • *Centro de Biología Molecular Severo Ochoa CSIC-UAM, CEDEM, CIBERER (ISCIII), IdiPaz (ISCIII), Universidad Autónoma de Madrid, Madrid, Spain*
- CIRO RODRIGUEZ-DIAZ • *Instituto Madrileño de Estudios Avanzados en Nanociencia (IMDEA Nanociencia), Madrid, Spain*
- JULIANA I. SANTOS • *Department of Human Genetics, Research and Development Unit, National Health Institute Doutor Ricardo Jorge, Porto, Portugal; Biology Department, Faculty of Sciences, University of Porto, Porto, Portugal*
- RENSKE SCHELLENS • *Department of Otorhinolaryngology, Radboud University Medical Center, Nijmegen, The Netherlands; Donders Institute for Brain Cognition and Behaviour, Nijmegen, The Netherlands*
- RALPH SLIJKERMAN • *Department of Otorhinolaryngology, Radboud University Medical Center, Nijmegen, The Netherlands; Donders Institute for Brain Cognition and Behaviour, Nijmegen, The Netherlands*
- BÅRD SMEDSRØD • *Vascular Biology Research Group, Department of Medical Biology, The Arctic University of Norway (UiT), Tromsø, Norway*
- PATRICIA SOBLECHERO-MARTÍN • *Neuromuscular Disorders, Biocruces Bizkaia Health Research Institute, Barakaldo, Spain; Osakidetza Basque Health Service, Bilbao-Basurto Integrated Health Organisation, Basurto University Hospital, Clinical Laboratory Service, Bilbao, Spain*
- ÁLVARO SOMOZA • *Instituto Madrileño de Estudios Avanzados en Nanociencia (IMDEA Nanociencia), Madrid, Spain*
- NURIA SUÁREZ-HERRERA • *Department of Human Genetics and Donders Institute for Brain, Cognition and Behaviour, Radboud University Medical Center, Nijmegen, The Netherlands*
- TOMASZ Z. TOMKIEWICZ • *Department of Human Genetics and Donders Institute for Brain, Cognition and Behaviour, Radboud University Medical Center, Nijmegen, The Netherlands*
- CANSU ÜMRAN TUNÇ • *NanoThera Lab, Department of Biomedical Engineering, Erciyes University, Kayseri, Turkey*
- PETER C. VAN DEN AKKER • *Department of Genetics, University of Groningen, University Medical Center Groningen, Groningen, The Netherlands; Department of Dermatology, Center for Blistering Diseases, University of Groningen, University Medical Center Groningen, Groningen, The Netherlands; Division of Biological Chemistry and Drug Discovery, School of Life Sciences, University of Dundee, Dundee, Scotland, UK*
- WILLEKE M. C. VAN ROON-MOM • *Department of Human Genetics, LUMC, Leiden, The Netherlands*
- ERWIN VAN WIJK • *Department of Otorhinolaryngology, Radboud University Medical Center, Nijmegen, The Netherlands; Donders Institute for Brain Cognition and Behaviour, Nijmegen, The Netherlands*
- IRENE VÁZQUEZ-DOMÍNGUEZ • *Department of Human Genetics, Donders Institute for Brain, Cognition and Behavior, Radboud University Medical Center, Nijmegen, The Netherlands*
- WOUTER P. R. VERDURMEN • *Department of Biochemistry, Radboud Institute for Molecular Life Sciences (RIMLS), Radboud University Medical Center, Nijmegen, The Netherlands*

- UMMUGULSUM YILMAZ • *NanoThera Lab, Department of Biomedical Engineering, Erciyes University, Kayseri, Turkey; ERNAM - Nanotechnology Research and Application Center, Erciyes University, Kayseri, Turkey*
- GIULIA ZARANTONELLO • *Neuroepigenetics Laboratory, Department of Cellular, Computational and Integrative Biology (CIBIO), University of Trento, Trento, Italy*
- HAIYAN ZHOU • *Genetic and Genomics Medicine Research and Teaching Department, Great Ormond Street Institute of Child Health, University College London, London, UK; NIHR Great Ormond Street Hospital Biomedical Research Centre, London, UK*

Part I

Overview



Chapter 1

Introduction and History of the Chemistry of Nucleic Acids Therapeutics

Michael J. Gait and Sudhir Agrawal

Abstract

This introduction charts the history of the development of the major chemical modifications that have influenced the development of nucleic acids therapeutics focusing in particular on antisense oligonucleotide analogues carrying modifications in the backbone and sugar. Brief mention is made of siRNA development and other applications that have by and large utilized the same modifications. We also point out the pitfalls of the use of nucleic acids as drugs, such as their unwanted interactions with pattern recognition receptors, which can be mitigated by chemical modification or used as immunotherapeutic agents.

Key words Antisense, siRNA, Nucleic acid therapeutics, Oligonucleotides, Toll-like receptors, Pattern recognition receptors, Gapmer, Splice switching

1 Introduction to Synthetic Antisense Oligonucleotides and siRNA

Oligonucleotides are short single-stranded sections of DNA or RNA that contain 2'-deoxyribo-nucleosides or ribo-nucleosides, respectively, which are linked by 3'-5' phosphodiester linkages (Fig. 1a). Antisense oligonucleotides are those that are complementary to a section of naturally occurring RNA, such as an mRNA or a viral RNA, to form Watson-Crick base pairs and to thus inhibit a biological function of that RNA. Zamecnik and Stephenson pioneered this concept in 1978 by utilizing antisense oligodeoxyribonucleotides (ODNs) to bind and inhibit the replication of Rous sarcoma virus (RSV) RNA [1]. This work followed much earlier (1969) studies of De Clercq et al. on interferon induction by synthetic polynucleotides and their phosphorothioate analogues [2] and together these early studies heralded the new field of nucleic acids therapeutics that began to accelerate in the mid to late 1980s.

Many further chemistry developments since then in the use of synthetic oligonucleotide analogues, as outlined below, as well as advances in molecular biology, such as in the newer fields of short

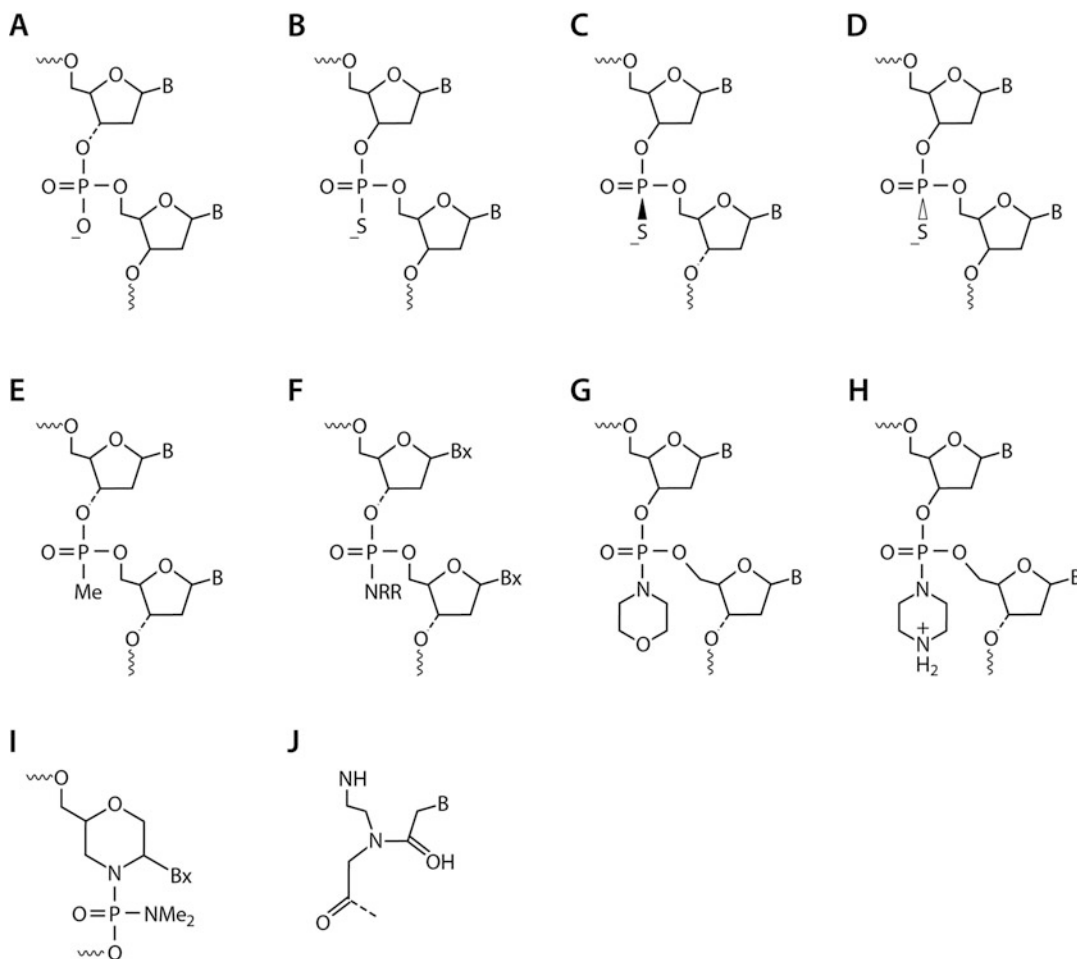


Fig. 1 Chemical structures. (a) DNA oligonucleotides (ODN), (b) phosphorothioate ODN (PS-ODN), (c) *Rp*-PS-ODN, (d) *Sp*-PS-ODN, (e) methylphosphonate ODN (PM-ODN), (f) phosphoramidate ODN (PN-ODN) R = H or alkyl, (g) phosphomorpholidate, (h) phosphopiperazidate, (i) phosphorodiamidate morpholino (PMO), (j) peptide nucleic acids (PNA). B = heterocyclic base

interfering RNA (siRNA) and non-coding RNAs, such as microRNA (miRNA), have led to the widespread and convenient use of synthetic oligonucleotides as antisense and siRNA reagents for gene ablation or targeting of non-coding RNA, as well as their use in animals and in humans leading to the approval of 12 drugs to date. In this chapter we outline the history of oligonucleotide chemistry in antisense and siRNA that has led to preclinical studies that have guided their development with drug-like properties and hence clinical trials (Fig. 2). We go on to discuss the development of the principles of widely used antisense gapmers and siRNAs as well as their immune responses by triggering pattern recognition receptors (PRRs) and how such activities can be controlled or harnessed for

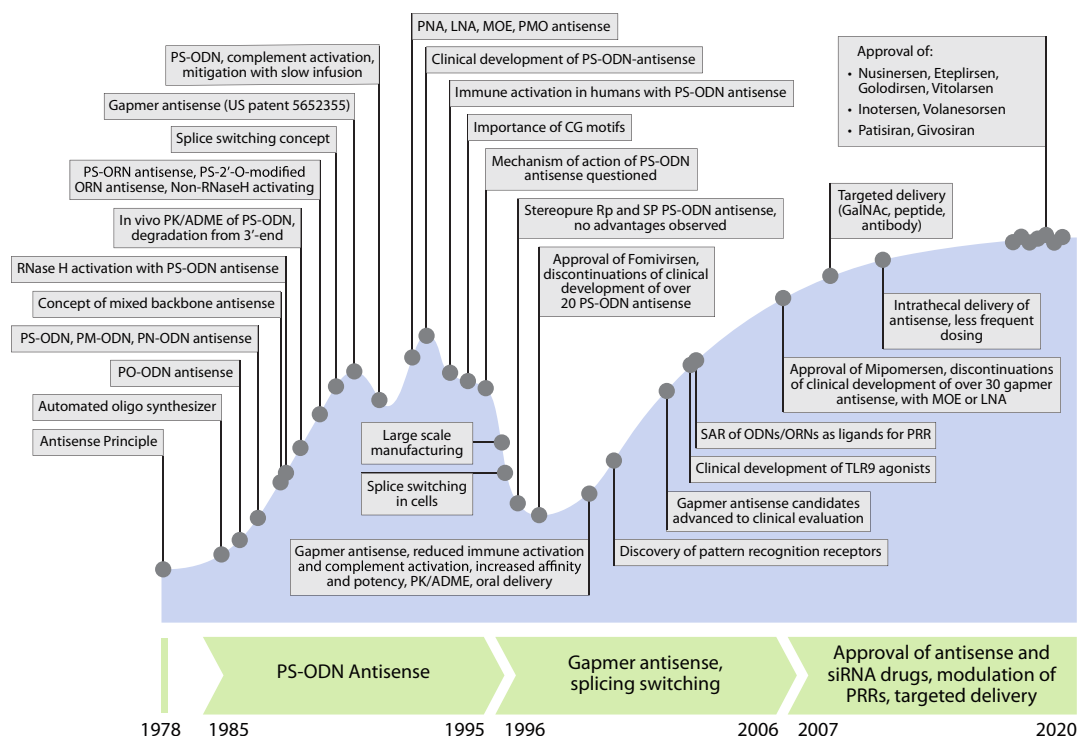


Fig. 2 Evolution of chemical modifications during the development of antisense as therapeutic agents. In the nineties, various modifications of ODNs and ORNs were studied and based on RNase H activation, PS-ODNs became the choice as first-generation antisense agents. Soon it was realized that PS-ODN had off-target activities including complement activation and also sequence specific immune activation. This led to questions on the mechanism of action of PS-ODNs and associated safety signals, and clinical development of most of the PS-ODN ASOs was discontinued. In parallel use of modified ORN for splicing correction in the cells was established. Based on the early work conducted in early nineties, gapmer antisense design provided the key attributes and became the choice as second-generation antisense agents. Studies of chemical modifications in antisense has facilitated development of other therapeutic oligonucleotides. The key modifications which have been identified in the development of antisense, e.g. PS-PDN and PS-ORN, 2'-modified or 2'-O-substituted ribo-nucleosides, bridged ribo-nucleosides, and PMO which are being employed in various nucleic acid therapeutics. In the last few years, a number of drugs based on gapmer ONs (mipomersen, inotersen, volanesorsen), 2'-MOE PS-ORN (nusinersen), PMO (eteplirsen, golodirsen, vitolarsen), and siRNA (patisiran, givosiran) have been approved

use as drugs (Fig. 3). Readers are also referred to a recent book edited by us on recent Advances in Therapeutic Nucleic Acids [3].

2 Oligonucleotide Synthesis

Early work in the 1960s and 1970s on phosphodiester and phosphotriester chemistry for the synthesis of ODNs required armies of nucleic acids chemists for painstaking oligonucleotide synthesis in solution phase that took months to years for each synthesis (for

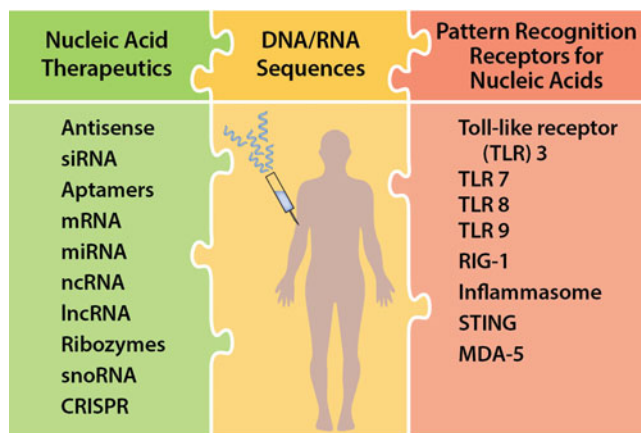


Fig. 3 Pattern recognition receptors (PRRs). The number of PRRs listed in the right-side column which is known to recognize patterns of nucleic acids and induce appropriate immune responses. This recognition is applicable to all use of nucleic acids for therapeutics, and depending on the engagement could affect the mechanism of action and also safety signals. This recognition could be due to PAMPs of the nucleic acid agent being used or due to DAMPs, due to the build-up of administered agent in the tissues and organs, being recognized as endogenous nucleic acids

example [4]). The revolution for molecular biologists came in the late 1970s and early 1980s with the development of solid-phase ODN synthesis first suggested by Letsinger and Mahadevan in 1965 [5] and later developed into working methods in the laboratories of Gait [6–8] and Itakura [9]. These methods were then superseded by the more efficient phosphoramidite chemistry of Caruthers and colleagues [10], which went on to be automated, such as by Applied Biosystems and other companies. The rapid and automated synthesis allowed molecular biologists to obtain synthetic ODNs readily for biological purposes such as for sequencing, cloning, and gene synthesis. The history of oligonucleotide synthesis chemistry has been reviewed [11, 12]. Today standard and modified ODNs can be obtained rapidly and efficiently on a small to large scale through highly automated solid-phase DNA oligonucleotide synthesis for many biological and diagnostic purposes.

Oligoribonucleotide synthesis is also now well established for the synthesis of siRNA or for aptameric RNAs. Currently, several oligonucleotide manufacturing plants are operational to produce oligonucleotides under GMP conditions.

3 Synthetic Oligonucleotide Analogues in Antisense and siRNA

The early work of Zamecnik and colleagues utilized RSV since this was the only viral RNA sequenced at this time. Zamecnik noticed

that both ends of the linear RNA genome bore the same primary sequence in the same polarity and that DNA might be synthesized from the RNA by reverse transcription via circularization of the 5'-end with the 3'-end through base pairing. Zamecnik and Stevenson were able to block this circularization by use of a synthetic ODN via hybridization with the 3'-end of the viral RNA. By use of a cell-free system, translation of the RSV mRNA was impaired, thus leading to inhibition of viral replication. This work was the birth of the antisense concept [1, 13].

Further progress in the antisense field awaited the mid to late 1980s for the availability of genomic DNA (or RNA) sequences for antisense targeting as well as the new automated methods of oligonucleotide synthesis as described above. There was also some scepticism regarding the stability and eukaryotic cell entry ability of unmodified oligonucleotides. Nevertheless Zamecnik and Gallo were able to employ unmodified antisense ODNs to inhibit human immunodeficiency virus 1 (HIV-1) replication [13] and to suppress expression of HIV-1 related markers [14]. Cellular uptake of the ODN was not a limiting factor since experiments were carried out in primary human cells and non-targeted control oligonucleotides showed minimal inhibition of HIV-1 replication, thus demonstrating sequence-specificity. This paper reignited the therapeutic potential of the antisense approach.

The next step was to provide drug-like properties to the unmodified antisense ODNs through chemical modifications. In this context the key consideration was to provide nucleolytic stability to antisense ODNs without affecting their hybridization and affinities with the RNA target. Not much was known at the time about the *in vivo* characteristics of unmodified ODN, or any modified ODNs, which could have guided the study of potential modifications. The first step was to see if modifications of the internucleotide linkages would provide nucleolytic stability to ODNs, while preserving the hybridization affinity to the target RNA. Later on, discovery of PRRs further provided insights into recognition of pathogen associated molecular patterns (PAMPs) of nucleic acids, and how sequence of antisense and nucleic acid-based therapeutic approaches could affect the mechanism of action (Fig. 3).

3.1 Backbone Analogues

3.1.1 Phosphorothioates

The antisense field took inspiration from the very early work of De Clerq, Eckstein, and Merigan [2] where phosphorothioate (PS) modifications were studied in homopolynucleotides as stabilizing agents. By the mid-1980s new chemical synthesis methods for the PS linkage in ODNs became available [15]. Here, a simple sulfur atom replaces a non-bridging oxygen atom (Fig. 1b). However, standard automated synthesis, which in the phosphoramidite method involves treatment with a sulfurizing agent in place of oxidation by iodine, produced a mixture of diastereomeric

oligonucleotide products (*Rp* and *Sp*) (Fig. 1c, d) and thus there was found to be a lower binding affinity to target RNA compared to phosphodiester. However, PS-linked ODNs are much more resistant to nuclease degradation than phosphodiester. Optimization of the synthesis methodology allowed the synthesis of milligram quantities of PS-ODNs for use in cell and in vivo experiments.

Early studies showed dose-dependent inhibition of viral replication and antiviral activity in HIV-1 infected cells by use of antisense PS-ODNs targeted to several regions of HIV-1 mRNA [16, 17]. Surprisingly, homopolymers were also effective and antiviral activity depended on the base composition, suggesting that PS-ODNs also had off-target activity. Longer PS-ODNs were more effective than shorter ones and cellular uptake was efficient in primary human cells without a carrier. In addition, antisense PS-ODNs showed potent and durable inhibition of HIV-1 replication in chronically HIV-1 infected cells [18–20]. Soon after, studies with PS-ODN targeted to influenza virus showed inhibition of virus replication [21]. Based on these early studies and promise, PS-ODNs became the choice for first-generation antisense agents.

Following these studies, work on antisense was pursued in many laboratories around the world for a broad range of applications [22–24]. In addition, several new companies were founded to advance therapeutic applications of antisense, such as Gilead Sciences, Isis Pharmaceuticals (now Ionis Pharmaceuticals), Hybridon (now Idera Pharmaceuticals), and others. Numerous reports appeared on the use of antisense PS-ODNs to target viruses [25, 26], oncogenes [24, 27], and kinases [27, 28], etc. Cellular uptake of PS-ODNs in transformed cells in culture was found to be poor but could be improved substantially by use of cationic lipid carriers. It was also shown that an antisense PS-ODN bound to its target RNA engaged RNase H [19, 20] to excise the RNA strand and this was therefore likely to be the mode of action and not steric block inhibition of translation as observed with other modified ODNs [29, 30]. Nevertheless RNase H cleavage activity was poorer than for a PO-ASO [20].

The first in vivo study in mice of a systemically delivered PS-ODN showed that plasma half-life was very short but that there was a broad tissue disposition with most delivered to liver and kidneys and the lowest amounts in the brain [31]. The PS-ODN was stable in tissues for several days and excreted primarily in urine in degraded form mostly through exonuclease cleavage from the 3'-end. Chemical modifications at the 3'-end increased the stability [32, 33]. The PS-ODN was bound by serum proteins, which increased the plasma half-life and improved tissue disposition [34, 35].

Antisense PS-ODNs showed very potent activity in animal models of viral diseases and cancer [36, 37]. However, in some cases a control PS-ODN also showed some activity, leading to the

possibility of off-target effects [38]. For example, a PS-ODN targeted to human papillomavirus inhibited papillomavirus-induced growth of implanted human foreskin in a mouse xenograft model but unexpectedly was also active in a mouse cytomegalovirus (CMV) model [39]. Studies in immune-compromised mice showed that the effect of the PS-ODN was largely due to immune activation of the host. Sequence-dependent immune stimulation was confirmed during non-clinical safety evaluations of drug candidates. Repeated systemic administration of PS-ODN candidates in mice and rats caused inflammation, splenomegaly, and histological changes in multiple organs [40, 41]. Further in non-human primates, bolus administration of the first antisense PS-ODN (GEM91) led to severe hemodynamic changes due to activation of the alternative complement pathway [42]. Stimulation of the alternative pathway complement activation cascade became the first documented off-target effect, which was due to a plasma concentration effect of the poly-anionic nature of PS-ODNs. It could be mitigated by subcutaneous administration or by slow intravenous infusion. Thereafter, the US Federal Drug Agency (FDA) published guidelines and required the use of non-human primates for non-clinical safety studies of all oligonucleotide drugs [43].

In the 1990s a number of antisense PS-ODN clinical candidates were advanced to human trials [44] through intravenous infusion, intravitreal or subcutaneous delivery [45–47]. Humans showed similar pharmacokinetics and excretion data to those of non-human primates [48, 49]. However, most clinical studies were discontinued due to the lack of activity or a poor therapeutic index [50]. For example, the subcutaneous administration of GEM91 in humans caused flu-like symptoms, swelling of the draining lymph nodes, prolongation of activated partial thromboplastin time (aPTT), and thrombocytopenia [29]. Rather than suppression of HIV-1, HIV-1 RNA levels were increased in blood [51]. However, intravenous delivery had minimal effect on these parameters. There were a few reports of immunostimulatory properties of DNA/ODNs containing CG nucleotides [52, 53]. It only became clear much later that PS-ODNs containing an unmethylated CpG motif activated the immune responses by binding to Toll-like receptor 9 (TLR9), an innate immune receptor present in immune cells that recognizes DNA containing CpG dinucleotide motifs [54]. It became clear that the flu-like symptoms and injection site reactions seen with most of the PS-ODN drug candidates in clinical trials, such as the clinically approved drug fomivirsen, administered intra-vitreally to treat AIDS-related CMV-induced retinitis, contained a CpG motif [55]. Thus, the true mechanism of action of this first-generation drug, now no longer marketed, remains unclear. Altogether, preclinical and clinical studies have provided important insights into the properties of PS-ODNs and its use as drugs [35, 56, 57].

Also of debate for some time has been whether the presence of a mixture of *Rp* and *Sp* diastereoisomers in the synthetic PS-ODNs (Fig. 1c, d) bears any influence on their biological properties. For example, a 20-mer would have 2^{19} isomers. The stereospecificity of enzymes that act on nucleoside phosphates was well known from early work of Eckstein (reviewed in [58]). Since PS-ODN interacting enzymes, such as nucleases, also utilize only a single diastereoisomeric isomer [59], it was plausible that there might be a significant biological effect in cells of utilizing mixed PS diastereoisomers in antisense PS-ODNs. Testing of this only awaited the solid-phase synthesis of stereo-enriched and stereo-pure PS-ODNs. This became possible through pioneering work of Stec and later by use of nucleoside bicyclic oxazaphospholidinium synthons [15, 60]. It is now known that binding strength and recognition by RNase H is generally higher for antisense oligonucleotides containing *Rp* linkages but depends crucially on the placement of these with respect to *Sp* linkages and overall stereospecific PS-ODNs have had limited therapeutic utility [61]. Recently certain stereo-pure antisense oligonucleotides were shown to have improved activity in cell culture and in vivo [62] but the therapeutic significance of such stereospecificity is currently hotly disputed [63]. Even more recently, the clinical development of a stereo-pure PS-ODN, WVEN-531 targeted to DMD has been discontinued due to lack of clinical activity [64]. Furthermore, dosing of this antisense ODN also led to transient increases in complement factors and C-reactive protein [65].

3.1.2 Charge-Neutral Analogues

Two phosphate-containing, charge-neutral oligonucleotide analogues that were particularly used in early antisense studies are the methylphosphonate [66] (Fig. 1e) and the phosphoramidate linkages [67] (Fig. 1f). They both consist of a mixture of diastereoisomers. Methylphosphonate ODNs (MP-ODNs) are stable at physiological pH and are resistant to nucleolytic degradation but are less strongly bound to target RNA compared to PO-ODNs [66, 68]. MP-ODNs targeted to HIV-1 showed dose-dependent inhibition of HIV-1 replication [16], but they are less active than PS-ODNs due to their lack of RNase H activation [19] but instead inhibit protein translation, which is generally a weaker activity in cells. Limited in vivo studies with a MP-ODN showed that while this modification is very resistant to nucleolytic degradation, due to poor protein binding, there was a very poor in vivo disposition and the majority of the administered ODN was eliminated in urine rapidly (Agrawal, unpublished data). In addition, longer MP-ODNs, which bind more strongly to RNA and which are therefore more potent, are poorly soluble under physiological conditions and thus have not been advanced toward clinical trials. By contrast, a 13-mer antisense oligonucleotide containing all phosphoramidate linkages is more soluble. An anticancer agent (GRN163) inhibits the enzyme telomerase [67] and did get into

a clinical trial, however, clinical development was discontinued due to lack of clinical activity. In early work, phosphoramidate-linked antisense oligonucleotides (Fig. 1g, h) targeted to HIV-1 showed similar results in cell-based assays to an MP-ODN and were not pursued [16].

Phosphorodiamidate morpholino oligonucleotides (PMOs) are also charge-neutral but here a morpholino ring replaces the sugar unit (Fig. 1i) [69]. PMOs inhibit translation by a steric block mechanism [70] as they are not recognized by RNase H. They are completely resistant to nucleases but are not taken up well by cells and thus require very high doses for in vivo delivery. They were found to be strong antiviral agents, for example, against Ebola, Marburg, and Chikungunya viruses [71]. Three exon skipping PMO drugs, eteplirsen, golodirsen, and vitolarsen designed to induce alternative splicing and restore the reading frame of mutant dystrophin in patients with Duchenne muscular dystrophy (DMD) [72] have been approved but requires the use of high doses (50 mg/kg or higher). Its therapeutic effectiveness, based on biomarkers, is limited [73], but it is a safe drug at the therapeutic dose. PMO and other chemistries used in exon skipping and other steric block activities have been reviewed [74].

Another initially highly promising, charge-neutral analogue are peptide nucleic acids (PNA), where the sugar-phosphate backbone is replaced by aminoethylglycine units linked by amide bonds (Fig. 1j) [75]. PNA binds strongly to target RNA and, like PMO, they are also completely resistant to degradation by nucleases as well as proteases. Also similar to PMO, duplexes with RNA are not recognized by RNase H and thus PNA acts by a steric block mechanism. Antisense PNAs have been broadly studied as anticancer [76, 77], antiviral [78, 79], and antibacterial agents [80, 81] as well as inhibitors of micro-RNAs [82]. However, once again very high doses are needed in in vivo applications, due to poor cellular uptake and unfavorable pharmacokinetics. Poor in vivo biodistribution is a likely reason for why antisense PNAs have not to date found utility as clinical candidates.

3.2 Sugar Analogues

It has been long established that an RNA-RNA duplex is much stronger than that of DNA-RNA. However, RNA (Fig. 4a) is highly unstable to ribonucleases. Phosphorothioate analogues (PS-ORN) showed an increased affinity to target RNA but they were found to have lower potency as compared to PS-ODNs, probably since RNA-RNA duplexes lack RNase H activation ability [35].

3.2.1 2'-O-Alkyl Sugars

The first sugar analogues to find utility in antisense oligonucleotides are the naturally occurring 2'-O-methylribonucleosides (Fig. 4b) first synthesized by the Ohtsuka laboratory [83]. The phosphoramidites of 2'-O-methylribonucleosides suitable for

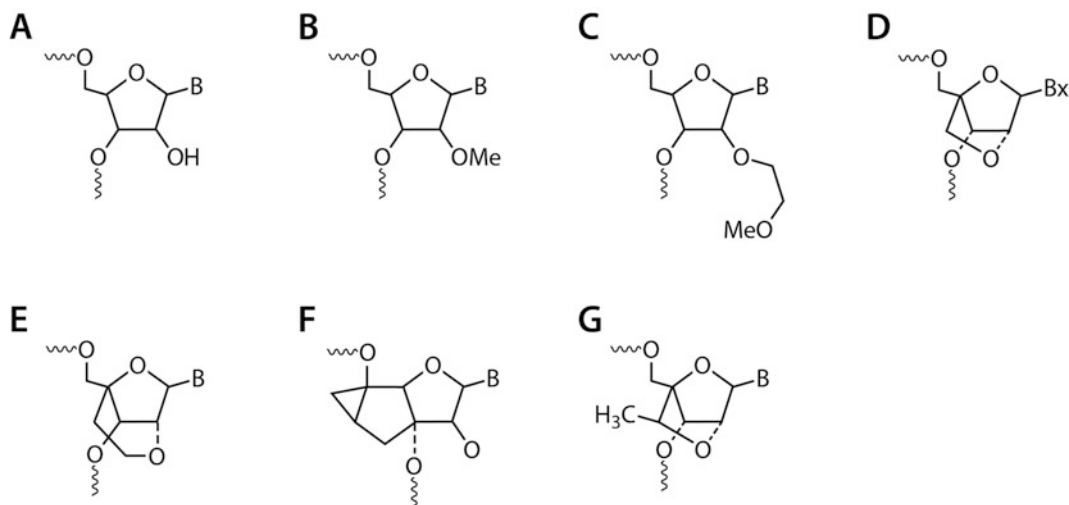


Fig. 4 Chemical structures of the ribo-nucleoside units of therapeutically useful RNA and RNA analogues. (a) ribo-nucleoside (ORN) (b) 2'-*O*-methyl (2'-OMe), (c) 2'-*O*-methoxyethyl (2'-MOE), (d) bridged/locked nucleic acid (LNA), (e) 2'-*O*,4'-*C*-ethylene linked nucleic acid (ENA), (f) tricyclo-DNA (tcDNA), and (g) constrained ethyl (cET). B = heterocyclic bases

solid-phase synthesis became available commercially in the early 1990s [29]. Studies with 2'-*O*-methyloligoribonucleotide phosphorothioates (2'-OMe PS-ORN) showed enhanced stability to nucleases as compared to PS-ORN and showed a higher affinity to target [84]. However, they also showed lower antisense activity compared to PS-ODNs, demonstrating that activation of RNase H was key for this activity [30, 51, 85, 86]. Since then, very many additional 2'-*O*-alkyl analogues have been synthesized and tested in antisense oligonucleotides (ONs), predominantly in gapmer studies (see below) to allow recognition by RNase H. From these studies 2'-*O*-methoxyethylribonucleoside (2'-MOE) (Fig. 4c) has been employed widely in clinical gapmer candidates (Chapters 3 and 4 of Agrawal and Gait [3]).

As described earlier, dose-dependent activation of complement and prolongation of aPTT were found to be unwanted side effects of PS-ODNs. These effects as well as strong binding to serum proteins were thought to be due to the poly-anionic nature of the PS linkage. However, there were found to be significantly less side effects when PS-ORN or 2'-OMe-PS-ASO were used, suggesting that the poly-anionic nature of the PS backbone in PS-ORN and PS 2'-OMe is not as pronounced when placed in the context of an RNA or RNA-like sugar conformation [40, 85–87]. This became crucial to their use in later gapmer antisense studies.

Uniformly 2'-*O*-alkyl modified PS-RNA has also found very high therapeutic use in splice switching (exon skipping or exon inclusion) and other steric blocking applications due to their high binding strength to nuclear pre-mRNA [88, 89]. However, the

exon skipping 2'-OMe PS-ORN antisense drisapersen drug candidate failed to show clinical benefit in patients with DMD and also caused significant adverse side effects and was, therefore, not approved for clinical use [90]. By contrast, the 18-mer 2'-MOE phosphorothioate (2'-MOE PS-ORN, nusinersen), which redirects the splicing of the SMN-2 gene to generate active SMN protein (exon inclusion), administered intrathecally only few times a year was approved by the FDA for the treatment of spinal muscular atrophy (SMA) [91, 92]. The thrombocytopenia and renal toxicity observed with the use of drisapersen could be largely due to the need for repeated subcutaneous dosages of 2'-OMe PS-ORN, which is very stable to nucleolytic degradation and therefore may accumulate in tissues due to its long half-life and potentially interact with PRRs. Nusinersen, a 2'-MOE PS-ORN, is also quite stable to nucleolytic degradation, but its intrathecal administration and need for infrequent and lower doses minimizes the impact of tissue accumulation and avoids the need for passage into the brain and spinal cord from the circulation.

3.2.2 Locked/Bridged Nucleic Acids

A major step forward in the design of antisense ONs was the development in the laboratories of Wengel and also of Imanishi of bicyclic sugar analogues known as locked or bridged nucleic acids (LNA/BNA). Here the conformational flexibility of nucleotides is significantly reduced by linkage of the 2'-oxygen atom to the 4'-carbon atom in the ribose ring (Fig. 4d). This results in a significant increase in the binding affinity of ONs to complementary RNA targets with an increase in the melting temperature of 2–8 °C per residue [93]. Unfortunately, LNA oligomers of 8 units or longer tend to self-aggregate. Therefore they became more useful as mixmers with 2'-deoxynucleotides and here miravirsen, the first microRNA-targeting drug, which acts by sterically blocking microRNA-122, highly expressed in liver, was developed for the treatment of hepatitis C virus infection, a debilitating liver disease [94]. Unfortunately, this drug's clinical development was discontinued because of *safety* issues. LNA has also been used as mixmers with 2'-OMe nucleotides targeting various RNAs in cells (e.g. [93]) and has also found utility in the flanking sequences of gapmers. This had the effect also of modulating the binding strength of the ON and increasing the specificity of the interaction (reviewed in Chapter 3 of Agrawal and Gait [3]).

Another bicyclic analogue that became useful is 2'-O,4'-C-ethylene linked nucleic acid (ENA) [95] (Fig. 4e). In a recent study an antisense ON DS-5141, containing segments of 2'-OMe PS-RNA and ENA, showed good activity in an *mdx* mouse model of DMD and a phase 1/2 clinical trial was carried out in Japan [96]. A further analogue useful in steric block applications is tricyclo-DNA (tcDNA) [97] (Fig. 4f). However, perhaps the

most important bicyclic derivative of LNA that has found considerable therapeutic utility is the methylated analogue known as “constrained Ethyl” (cET), which is being employed in shorter gapmers [98] (Fig. 4g) and being evaluated in preclinical and clinical studies by Ionis Pharmaceuticals Inc. All these types of bridged nucleic acids have shown very strong affinity to target RNA and increased nucleolytic stability, but none of them are substrates for RNase H. Thus, these types of bicyclic sugar analogues are mostly used in steric block/splicing modulation approaches and in the flanking sequences of gapmers.

3.3 Heterocyclic Base Analogues

In early antisense studies it was thought that increased antisense activity might be achievable by improving the affinity of an ODN to target RNA through modification of the heterocyclic bases, for example, by adding an extra hydrogen bond in the base pairing between an ODN and its RNA target or by increasing the base stacking potential in a DNA–RNA duplex. Chemically this was simplest through modifications in the pyrimidine rings, for example, by modifications at positions C-2, C-4, C-5 or at C-6, and many of these base analogues were incorporated into antisense ODNs. However, few of these proved to be of significant value. Incorporation of modified purines generally resulted in a reduced binding affinity of an antisense ODN. Perhaps the most useful study of antisense activity was of incorporation of various heterocyclic bases in ODNs including the increased base stacking analogues C-5 propynyl and 5-methyl cytosine (5-MeC) and the increased hydrogen-bonding analogues phenoxazine, and G-clamp. These studies showed that the increased hydrogen-bonding analogue G-clamp had potent dose-dependent antisense activity [99]. Unfortunately, these antisense ODNs containing G-clamps were found to be highly toxic in *in vivo* studies. Currently, the only significantly used nucleoside base analogue in antisense ODNs is 5-methyl-2'-deoxycytidine (5-MedC) [100]. This methylated base analogue is used mainly to mitigate immune activation in CpG dinucleotide sequences rather than for changing binding strength [101].

4 RNase H Active Gapmer Chemistry for Use as Drugs

Early studies conducted with various modified ODNs, ORNs, and 2'-substituted ORNs as antisense agents provided great insights into what is important for providing drug-like properties to antisense oligonucleotides [3]. Studies with PS-ODNs showed that increased nucleolytic stability and activation of RNase H were key. However, polyanion-related side effects and sequence-dependent immune activation were limiting factors in their broad applicability [50, 57]. Studies with MP-ODNs showed that polyanion-related side effects could be completely mitigated (Agrawal, unpublished

data), and had significant nucleolytic stability. However, with lower affinity and lack of RNase H activation, there was a loss in antisense potency [16]. These observations led to the concept of combining desirable properties of the two modified ODNs to provide drug-like properties to antisense oligonucleotides [29]. The first studies were carried out with antisense containing segments of PS-ODN and PM-ODN or PN-ODN referred to as mixed backbone antisense ONs. These antisense designs showed increased nucleolytic stability and RNase H activation [19, 40]. However, reduced affinity limited their potency. Further insight was obtained from in vivo studies in which a mixed backbone ON containing PS-ODN and PM-ODN showed wide tissue disposition and increased stability and longer half-life in tissues [102].

This led Agrawal and colleagues to design antisense oligonucleotides in which the segments of PS-ODN and 2'-substituted PS-ORN were combined at the appropriate positions [29, 84, 85]. These types of antisense oligonucleotides were referred to as Hybrid ONs, now commonly referred to as gapmers (Fig. 5). In the original design of antisense, a segment of PS-DNA was placed in the middle and segments of 2'-*O*-alkyl PS-ORN or a combination of PO- and PS-linkages were placed at both 3'- and 5'-ends [29, 84, 85, 87, 103]. This design of antisense combined the desirable properties of PS-DNA and 2'-*O*-alkyl PS-ORN, and provided increased affinity to targeted RNA, activation of RNase H, increased nucleolytic stability, and reduced polyanion-related side effects. Furthermore, inflammatory responses were also reduced [35, 40, 56]. In vivo administration in mice showed similar plasma half-life and tissue disposition similar to that observed with PS-ODNs, and with increased in vivo stability and retention in tissues [104]. Also, due to increased in vivo stability, oral and rectal delivery of gapmer antisense was possible [34]. It was postulated that the increased stability and in vivo persistence may allow less frequent dosing to obtain therapeutic benefits.

There was also a concern that increased retention of gapmer antisense in tissues may lead to tissue build up following repeated dosing, which would induce local inflammatory responses and side effects, thereby limiting its therapeutic potential.

Other configurations of gapmer antisense were also evaluated, including the configuration in which a segment of 2'-*O*-alkyl PS-ORN was placed in the center and segments of PS-DNA were placed at both 3'- and 5'-ends. This design of gapmer antisense showed increased potency compared to PS-DNA and reduced polyanion-related side effects. In general, the specificity of RNase H mediated cleavage and its efficiency and excision sites were dependent on the position of the PS-DNA in gapmer antisense ONs [105].

Based on these encouraging results, gapmer antisense became the choice for second-generation antisense agents. In 2001, a

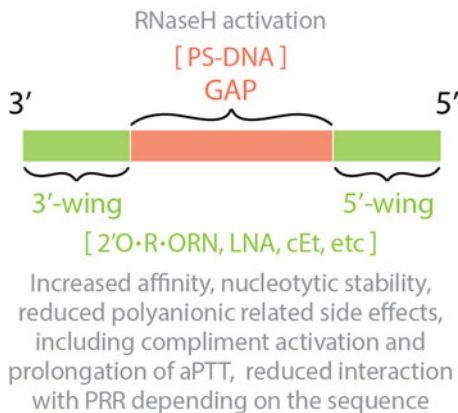


Fig. 5 Design of gapmer antisense oligonucleotides. In a gapmer antisense, segments of PS-DNA and modified RNA are appropriately placed to combine desirable characteristics for antisense agent with both of these modifications. PS-DNA segment provides RNase H activation, and modified RNA segments provide increased nucleolytic stability, affinity to target RNA, decreased polyanionic characteristics and inflammatory responses

licensing agreement between the companies allowed the technology to be widely available [44]. Over the years, studies have been carried out to establish the optimal size of the window of a central PS-DNA segment [105]. Similarly, studies have been carried out to optimize the size of the modified ORN wings at both 3'- and 5'-ends. In the wings of the gapmer antisense, various modified ORNs have been incorporated and evaluated (*see* Chapter 3 of Agrawal and Gait [3]). To date, most promising results have been obtained with gapmer antisense containing segments of 2'-*O*-methyl or 2'-*O*-methoxyethyl at both 3'- and 5'-ends. Over 30 gapmer antisense drug candidates containing 2'-*O*-methoxyethyl or LNA segments have been advanced to clinical evaluations following systemic delivery. To date, three candidates have been approved for clinical use. These include inotersen [106], volanesorsen [107], and mipomersen [108]. Clinical development of several gapmer antisense drug candidates have been discontinued, due to lack of clinical activity and/or safety signals. These include ISIS-FXIRx, ISIS-EIF4ERx, ATL1103, ATL1102, ISIS-GCGRRx, ISIS-PTBRx, ISIS-APOARx, ISIS-SOD1Rx, ISIS-FGFR4Rx, ISIS-405879, OGX-011, OGX-427, LY2181308, ATL1103, ATL1102, etc.

As discussed above, many of the bicyclic sugar analogues including locked/bridged nucleic acids have been studied as antisense agents. These analogues have also been studied as part of the wings in gapmer antisense. These include LNA (Fig. 2d) [109], constrained ethyl 2'-4' bridged nucleic acid (cEt) (Fig. 2g) [110], anhydrohexitol [91], fluorocyclohexenyl (F-CeNA) [111], altritol

nucleic acids [112], and tricyclo-DNA (tcDNA) (Fig. 2f) [97]. These modifications provide very high affinity and have allowed the length of the gapmer antisense to be reduced. A few of these shorter gapmer ASOs are being employed to achieve allele specific knockdown [113]. While the use of shorter antisense may be cost effective, it increases the possibility of off-target effects by binding to non-targeted RNA [114, 115]. Also selected LNA and cET ASOs have been associated with liver toxicity [116, 117].

Several gapmer antisense drug candidates employing LNA in the wings have advanced toward the clinic but development of most of these candidates have been discontinued, primarily due to safety issues and lack of therapeutic index.

Other modifications in the gapmer antisense studies include 2'-deoxy-2'-fluoro-beta-D-arabinonucleic acid (FANA) [118], 3'-fluorohexitolnucleic acid (FHNA) [119], 2'-thiothymine, 5-modified pyrimidine bases, etc. These studies are limited to pre-clinical evaluations.

5 siRNA Chemistry for Use as Drugs

The lessons learned in the development of antisense ONs have allowed the development of siRNA therapeutics to be speeded up. siRNAs have a well-defined structure: a short double stranded RNA of 20–25 base pairs with phosphorylated 5'-ends and hydroxylated 3'-ends and also usually containing two 3'-overhanging nucleotides, although blunt ends are sometimes used. While the key requirement is to provide nucleolytic stability to a siRNA candidate, it requires an understanding of the function of each strand. One strand is called the passenger strand and the other is the active component and is called the antisense or guide strand. It is the guide strand that is incorporated into the enzyme complex called RISC in order to be directed to cleave the target RNA strand, while the passenger strand is displaced.

Studies of various chemical modifications in antisense and their impact on providing drug-like properties have allowed the use of some of these modifications in development siRNA therapeutics. These include PS-linkages, various modified ribose sugars such as 2'-O-methyl, 2'-fluoro 2'-deoxy (2'-F), LNA as well as the sugar ring-opened analogues unlocked nucleic acid (UNA), and glycol nucleic acid (GNA). In siRNA chemical modifications are introduced strategically to provide nucleolytic stability. In addition the passenger strand is usually heavily modified in order to block passenger strand entry into RISC, while to promote RISC loading of the guide strand only light modification is used, such as 2'-F replacement of 2'-OH groups in pyrimidines. At the same time modifications must not be placed centrally in the guide strand so as to block RISC-associated cleavage of the target RNA. The exact

locations of such modifications in guide and passenger strands are generally closely guarded secrets by reagent suppliers. In addition, the 5'-phosphate of a siRNA guide strand is essential for recognition by RISC. Phosphatase-resistant analogues of the 5'-end phosphate have been shown to improve the in vivo efficacy and are used in clinical candidates [120].

In siRNA candidates, chemical modifications provide nucleolytic stability, however, delivery to a desired tissue or cell type requires use of carrier or conjugation with delivery moieties [121]. To date, two main delivery platforms—ionisable lipid nanoparticles (iLNPs) and trivalent *N*-acetylgalactosamine (GalNAc) conjugates—have been employed for delivery to liver hepatocytes. To date, two siRNA drugs have been approved for clinical use patisiran, which uses lipid delivery, and givosiran, which uses a GalNAc conjugation. Third siRNA drug candidate, inclisiran, a GalNAc conjugate has shown positive results in phase 3 trial [122]. Details of these structure activity relationship studies have been discussed in two chapters from a previous book [123, 124].

6 Immune Responses to Nucleic Acids

Over the last five decades there have been several reports on observations that certain nucleic acid sequences showed immune stimulatory properties [52, 125, 126]. In the mid-1990s subcutaneous administration of an antisense PS-ODN targeted to HIV-1 (GEM91) in HIV-1 infected individuals caused flu-like symptoms and systemic immune responses [51]. This observation alone could not be explained until the discovery of PRRs. These receptors are part of the immune system and PAMPs and host-derived damage-associated molecular patterns (DAMPs). These PRRs play an essential role in establishing antiviral and antibacterial responses by recognizing PAMPs. However, PRRs could also induce development of autoimmune and inflammatory diseases by recognizing DAMPs [127, 128].

PAMPs are highly conserved motifs in pathogens, such as bacteria and viruses. There are several PRRs that are known to recognize motifs, sequences, and patterns of nucleic acids and induce receptor-mediated immune responses. These include members of Toll-like receptors (TLRs), of which four TLRs respond to nucleic acids. TLR3, TLR7/8, and TLR9 recognize double-stranded RNA (dsRNA), single-stranded RNA with certain sequence composition and modified bases (ssRNA), and DNA containing unmethylated CpG sequences (CpG DNA), respectively (Chapter 13 of Agrawal and Gait [3]; [129]). These TLRs are localized in endosomes and expressed on various cell types. The type of immune response induced varies dependent on the receptor and the nature of the nucleic acid [130]. In addition to TLRs,

additional receptors are present in the cytoplasm known to recognize nucleic acid-based PAMPs. These include retinoic acid-inducible gene-I (RIG-I), melanoma-associated gene-5 (MDA-5), absent in melanoma 2 (AIM2), cyclic-AMP synthase (cGAS), and stimulator of the interferon gene (STING) (Chapter 13 of Agrawal and Gait [3]).

Following the discovery of TLR9, it became clear that immune activation observed with administration of GEM91 was due to the presence of unmethylated CpG dinucleotides in the antisense sequence [131]. This also provided insights into many of the preclinical studies that the chosen antisense may be exerting antiviral or anticancer activity due to immune activation and not by an antisense mechanism [51, 57]. Interestingly, most of the antisense PS-ODNs in clinical development contained unmethylated CpG motifs, raising questions on the intended mechanism of action [51, 57]. Clinical development of all these antisense drug candidates was discontinued due to lack of activity but also due to safety signals. Similar observations have been made with a few initial siRNA candidates and once again mechanisms of action have been correlated with activation of immune responses [132, 133].

The discovery of PRRs has provided key insights into many of the observations made with use of PS-ODN antisense. For example, TLR9 is a receptor for synthetic ODNs containing unmethylated CpG motifs [131]. Activation of TLR9 leads to induction of Th1 type immune responses in mice, primates, and in humans (Chapter 14 of Agrawal and Gait [3]). Inductions of Th1 type immune responses, which include type interferon (IFN) and interleukin 12 (IL-12), have shown therapeutic potential as antiviral and anticancer agents. This explains the activity of a PS-ODN antisense containing the CpG motif targeted to HPV, also showing activity for CMV and loss of activity in immune compromised mice [39]. This also explains the reason for flu-like symptoms with administration of GEM91, a PS-ODN antisense containing the CpG motif target to HIV-1 [55]. Interestingly, most of the PS-ODN antisense that were advanced to clinical development in the early 1990s contained unmethylated CpG motifs [51]. Thus, their mechanisms of action could be largely due to immune activation or side effects were caused by immune activation.

Detailed structure activity relationships have been carried to elucidate the interaction of PS-ODNs with TLR9. These studies have provided great insights. For example, (a) the presence of unmethylated CpG motif is required, although its position in the sequence is equally important [134], (b) accessibility of the 5'-end is required [111, 135], (c) modifications of the flanking sequence on the 5'-end impacts the immune activity [136], (d) methylation of C in the CpG motif neutralizes immune activation and causes it to act as an antagonist, and (e) certain modified bases could be used in the CpG motif without inducing immune responses. These

insights have been very helpful in designing antisense candidates. These lessons have provided the basis for the creation of optimized agonists and antagonists of TLR9. These classes of compounds have been studied extensively in preclinical models of cancer [106], vaccines [137], viral infection [138], and autoimmune diseases [139], and clinical proof of concept has been established in multiple diseases [3]; Chapters 5 and 14 of Agrawal and Gait [3].

Detailed structure–activity relationship studies have been carried out for TLR3 [134], TLR7 and TLR8 [127, 140], RIG-I [141], and AIM2 [142]. It is important to take these insights into consideration when selecting a sequence and prioritizing chemical modification for use in therapeutic applications.

7 Conjugates and Delivery

The *in vivo* efficacy of ONs is defined by plasma half-life, tissue uptake, nucleolytic stability, and elimination. Systemic administration of several gapmer ASOs has shown a similar profile, i.e., short plasma half-life, wide tissue dispositions, and the presence of intact ASO for longer durations [121]. Even though the delivered gapmer ASO is present in targeted tissues including liver, for sustained clinical activity weekly dosing has been employed. This suggests that the administered ASO is not present in the right cells or cell compartment. Further insights came from intrathecal delivery of the 2'-*O*-methoxyethyl PS-ASO nusinersen (Spinraza) to treat SMA. Patients are being treated with IT delivery, administered only four to five times a year. This suggests that in a local compartment, a delivered ASO exerts pharmacodynamic activity for a longer duration and thereby requires less frequent dosing. In recent studies, both preclinical and clinical, conjugation of gapmer ASO with a GalNac cluster has been shown to improve potency and frequency of treatment for liver targeted RNA/gene targets. Efforts are being made to improve delivery of ASOs to muscles to treat muscular disorders employing antibody conjugates [143, 144].

Peptide conjugation has been researched extensively in recent years in efforts to increase the delivery of oligonucleotides. Numerous cell-penetrating peptides (CPPs) have been developed, which are beyond the scope of this Introduction. Readers are referred to a book describing methods that use cell-penetrating peptides [145]. However, the only peptides that have reached clinical development are Arginine-rich CPPs. These are not suitable for conjugation with negatively charged oligonucleotides because of the tendency of such conjugates to aggregate due to charge–charge interactions between the positively charged peptide part and the negatively charged oligonucleotide part. Instead they have found clinical utility for use as conjugates with charge-neutral PMOs.

Here the company AVI Biopharma (now called Sarepta) developed a series of Arginine-rich CPPs that were taken to toxicological testing in monkeys but were found to have renal toxicity at elevated doses leading to a poor therapeutic index [146]. Recently Sarepta has advocated use of an alternative and shorter Arg-rich peptide, which is (Arg)₆-Gly, as a PMO conjugate as a treatment for the neuromuscular disease DMD. This gave rise to significant improvements in delivery of an attached PMO and increased exon skipping [147]. The peptide-PMO conjugate is currently in Phase 2 clinical trials. Similar Arg-rich peptides, eg ones known as Pip having a short internal hydrophobic domain, have given rise to increased exon skipping for an attached PMO in muscles as well as in heart in an *mdx* mouse model of DMD [148]. Pip peptides and similar derivatives are currently being evaluated as potential therapeutics for other neuromuscular diseases, for example, in myotonic dystrophy [149]. Once again, shorter Arg peptide derivatives as PMO conjugates are likely to be the future clinical candidates in neuromuscular and neurodegenerative diseases.

Delivery of siRNA has been facilitated by the use of lipid complexes or as conjugates with GalNAc, mainly to the liver. Use of lipids provides stability to an siRNA candidate by encapsulating them, along with preferential delivery to the liver. Several lipid encapsulated siRNA candidates have advanced to clinical development. For example, patisiran formulated with lipid nanoparticles (LNP) has received regulatory approval. It is important to note that lipid-nucleic acid mixtures form complexes that create virus-like particle structures and engage PRRs to induce immune responses. In the case of patisiran, subjects were pre-treated with steroids to mitigate inflammatory responses.

The application of the use of GalNAc to hepatocytes has been known for some time and was employed for oligonucleotide delivery more than two decades ago [150]. GalNAc is a ligand for the asialoglycoprotein receptor 9 (ASGPR), which is very abundant on the surface of hepatocytes [151]. Conjugation with GalNAc generally leads to preferential delivery to the liver. However, depending on the nature of modifications of ONs, delivery to other compartments including the kidney has been observed. An siRNA-GalNAc conjugate givosiran has been approved for clinical use, another GalNAc conjugate. Inclisiran has shown positive results in a phase 3 clinical trial (Chapter 11 of Agrawal and Gait [3]).

8 Further Developments in Therapeutics

Over the years many other applications of nucleic acid-based therapeutics have been pursued. These include aptamers, CRISPR/Cas9, and use of modified mRNA for protein overexpression. While the construct and sequence of DNA or RNA employed in

these uses may differ, one common aspect is the need to provide drug like properties to the selected agent. Most of the lessons learned in the development of chemistry in antisense field have facilitated the development of these approaches. In aptamers, modified nucleosides, such as 2'-*O*-methyl, 2'-fluoro or 2'-amino, and modified internucleotide linkages such as PS-linkages or boranophosphate are regularly employed [152, 153]. In the case of mRNA therapy, considerations of use of chemical modifications are different than in other approaches. The 5'-cap and 3'-poly(A) tail are the key contributors to provide long half-life and for efficient translation. New capping agents such as 1,2-dithiodiphosphonate modified caps have been shown to improve RNA translation [154]. Several modified nucleosides including N¹-methyl-pseudouridine and others have been useful in increasing efficiency of translation, and also mitigating immune stimulatory activity [155, 156]. The positional incorporation of modified bases in mRNA affects the secondary structure of the mRNA, which in turn influences its translation. Further stability to mRNA is provided by formulation with LNPs [157].

In studying CRISPR/Cas9-based therapeutic applications, several modifications are being evaluated. These include PS linkages and 2'-fluoro, LNA, c-Et [158], 2'-*O*-methyl [159], 2',4'-BNA (NC) [N-Me] [160], etc. These chemical modifications not only provide stability but also mitigate interactions with PRRs. CRISPR-based technologies have been described in a recent book [161].

9 Summary

Nucleic acid-based therapies are now entering into their fifth decade (*see* Fig. 2 for a timeline of developments). Since the first report of the antisense principle in 1978 using unmodified ODNs, the technology has evolved, and drugs are now being approved. Based on the progress to date and the promise of the results, nucleic acid therapeutics are now being recognized as the third major drug discovery and development approach in addition to small molecules and protein/antibody approaches.

Nucleic acid therapeutic agents are built of A, C, G, T, and U nucleotides and connected through internucleotide bonds. Early work on chemical modifications to provide drug-like properties to antisense and lessons learned have been of tremendous value not only in creating antisense drugs but also in developing therapeutics using synthetic nucleic acids with other mechanisms of action (Fig. 4). Nucleic acid therapeutics could be broadly divided into two classes, the first in which an agent is created to target RNA or DNA and modulate its expression, and in the second an agent is created to bind to proteins or cellular factors. In both of these categories, agents could be recognized by PRRs thereby inducing

immune responses, either unintended or intended affecting the mechanism of action.

The work on the chemistry of antisense has provided us with a few key modifications that have become important tools in nucleic acid therapeutics. The most important of these include PS linkages in ODN and ORN, gapmer design, selected 2'-*O*-substituted nucleosides, and various bridged/locked nucleic acids, etc. The art of creating a nucleic acid agent lies in the understanding of putting together the nucleotide sequence and various modifications for its intended mechanism of action without interacting with PRR (Fig. 3).

Acknowledgments

SA is indebted to Mike Gait for his mentorship during his postdoctoral training in Mike's laboratory and over the last three decades. SA is also grateful to all the colleagues and collaborators whose names appear in the references cited from his laboratory in this chapter.

References

1. Zamecnik PC, Stephenson ML (1978) Inhibition of Rous sarcoma virus replication and cell transformation by a specific oligodeoxynucleotide. *Proc Natl Acad Sci U S A* 75: 280–284
2. De Clercq E, Eckstein F, Merigan TC (1969) Interferon induction increased through chemical modification of a synthetic polynucleotide. *Science* 165:1137–1139
3. Agrawal S, Gait MJ (eds) (2019) *Advances in nucleic acid therapeutics*. Drug discovery series. Royal Society of Chemistry, London
4. Sekiya T, Takeya T, Brown EL, Belagaje R, Contreras R, Fritz H-J, Gait MJ, Lees RG, Ryan MJ, Khorana HG, Norris KE (1979) Total synthesis of a tyrosine suppressor tRNA gene (16). Enzymatic joinings to form the total 208 base-pair long DNA. *J Biol Chem* 254:5787–5801
5. Letsinger RL, Mahadevan V (1965) Oligonucleotide synthesis on a polymer support. *J Am Chem Soc* 87:3526–3527
6. Gait MJ, Sheppard RC (1976) A polyamide support for oligonucleotide synthesis. *J Am Chem Soc* 98:8514–8516
7. Gait MJ, Singh M, Sheppard RC, Edge M, Greene AR, Heathcliffe GR, Atkinson TC, Newton CR, Markham AF (1980) Rapid synthesis of oligodeoxyribonucleotides IV. Improved solid phase synthesis of oligodeoxyribonucleotides through phosphotriester intermediates. *Nucl Acids Res* 8: 1080–1096
8. Sproat BS, Gait MJ (1984) Solid-phase synthesis of oligodeoxyribonucleotides by the phosphotriester method. In: Gait MJ (ed) *Oligonucleotide synthesis: a practical approach*. IRL Press, Oxford, pp 83–114
9. Miyoshi K, Itakura K (1979) Solid phase synthesis of nonadecathymidylic acids by the phosphotriester method. *Tetrahedron Lett* 20:3635–3638
10. Beaucage SL, Caruthers MH (1981) Deoxynucleoside phosphoramidites-A new class of key intermediates for deoxypolynucleotide synthesis. *Tetrahedron Lett* 22:1859–1862
11. Reese CB (2002) The chemical synthesis of oligo- and poly-nucleotides: a personal commentary. *Tetrahedron* 58:8893–8920
12. Reese CB (2005) Oligo- and polynucleotides: 50 years of chemical synthesis. *Org Biomol Chem* 3:3851–3868
13. Barker RH Jr, Metevlev V, Rapaport E, Zamecnik P (1996) Inhibition of *Plasmodium falciparum* malaria using antisense oligodeoxynucleotides. *Proc Natl Acad Sci U S A* 93(1):514–518

14. Zamecnik PC, Goodchild J, Taguchi Y, Sarin PS (1986) Inhibition of replication and expression of human T-cell lymphotropic virus type III in cultured cells by exogenous synthetic oligonucleotides complementary to viral RNA. *Proc Natl Acad Sci U S A* 83(12): 4143–4146
15. Stec WJ, Zon G, Egan W, Stec B (1984) Automated solid-phase synthesis, separation, and stereochemistry of Phosphorothioate analogues of oligodeoxyribonucleotides. *J Am Chem Soc* 106:6077–6079
16. Agrawal S, Goodchild J, Civeira MP, Thornton AH, Sarin PS, Zamecnik PC (1988) Oligodeoxynucleoside phosphoramidates and phosphorothioates as inhibitors of human immunodeficiency virus. *Proc Natl Acad Sci U S A* 85(19):7079–7083
17. Matsukura M, Shinozuka K, Zon G, Mitsuya H, Reitz M, Cohen J, Broder S (1987) Phosphorothioate analogs of oligodeoxyribonucleotides: inhibitors of replication and cytopathic effects of human immunodeficiency virus. *Proc Natl Acad Sci U S A* 84:7706–7710
18. Agrawal S, Ikeuchi T, Sun D, Sarin PS, Konopka A, Maizel J, Zamecnik PC (1989) Inhibition of human immunodeficiency virus in early infected and chronically infected cells by antisense oligodeoxynucleotides and their phosphorothioate analogues. *Proc Natl Acad Sci U S A* 86:7790–7794
19. Agrawal S, Mayrand SH, Zamecnik PC, Pederson T (1990) Site-specific excision from RNA by RNase H and mixed-phosphate-backbone oligodeoxynucleotides. *Proc Natl Acad Sci U S A* 87(4):1401–1405
20. Walder RY, Walder JA (1988) Role of RNase H in hybrid-arrested translation by antisense oligonucleotides. *Proc Natl Acad Sci U S A* 85(14):5011–5015
21. Leiter JM, Agrawal S, Palese P, Zamecnik PC (1990) Inhibition of influenza virus replication by phosphorothioate oligodeoxynucleotides. *Proc Natl Acad Sci U S A* 87(9): 3430–3434
22. Gaudette MF, Hampikian G, Metelev V, Agrawal S, Crain WR (1993) Effect on embryos of injection of phosphorothioate-modified oligonucleotides into pregnant mice. *Antisense Res Dev* 3:391–397
23. Knorre DG, Vlassov VV (1991) Reactive oligonucleotide derivatives as gene-targeted biologically active compounds and affinity probes. *Genetica* 85:53–63
24. Ratajczak MZ, Kant JA, Luger SM, Hijiya N, Zhang J, Zon G, Gewirtz AM (1992) In vivo treatment of human leukemia in a scid mouse model with c-myc antisense oligodeoxynucleotides. *Proc Natl Acad Sci U S A* 89(24): 11823–11827
25. Cowser LM, Fox MC, Zon G, Mirabelli CK (1993) In vitro evaluation of phosphorothioate oligonucleotides targeted to the E2 mRNA of papillomavirus: potential treatment for genital warts. *Antimicrob Agents Chemother* 37(2):171–177
26. Flores-Aguilar M, Freeman WR, Wiley CA, Gangan P, Munguia D, Tatebayashi M, Vuong C, Besen G (1997) Evaluation of retinal toxicity and efficacy of anti-cytomegalovirus and anti-herpes simplex virus antiviral phosphorothioate oligonucleotides ISIS 2922 and ISIS 4015. *J Infect Dis* 175:1308–1316
27. Monia BP, Johnston JF, Geiger T, Muller M, Fabbro D (1996) Antitumor activity of a phosphorothioate antisense oligodeoxynucleotide targeted against C-ras kinase. *Nat Med* 2(6):668–675
28. Dean NM, McKay R (1994) Inhibition of protein kinase C- α expression in mice after systemic administration of phosphorothioate antisense oligodeoxynucleotides. *Proc Natl Acad Sci U S A* 91(24): 11762–11766
29. Agrawal S (1992) Antisense oligonucleotides as antiviral agents. *Trends Biotechnol* 10(5): 152–158
30. Monia BP, Lesnik EA, Gonzalez C, Lima WF, McGee D, Guinosso CJ, Kawasaki AM, Cook PD, Freier SM (1993) Evaluation of 2'-modified oligonucleotides containing 2'-deoxy gaps as antisense inhibitors of gene expression. *J Biol Chem* 268:14514–14522
31. Agrawal S, Tamsamani J, Tang JY (1991) Pharmacokinetics, biodistribution, and stability of oligodeoxynucleotide phosphorothioates in mice. *Proc Natl Acad Sci U S A* 88(17):7595–7599
32. Tamsamani J, Roskey A, Chaix C, Agrawal S (1997) In vivo metabolic profile of a phosphorothioate oligodeoxyribonucleotide. *Antisense Nucl Acid Drug Dev* 7(3):159–165. <https://doi.org/10.1089/oli.1.1997.7.159>
33. Tamsamani J, Tang JY, Padmapriya A, Kubert M, Agrawal S (1993) Pharmacokinetics, biodistribution, and stability of capped oligodeoxynucleotide phosphorothioates in mice. *Antisense Res Dev* 3(3):277–284
34. Agrawal S, Tamsamani J, Galbraith W, Tang J (1995) Pharmacokinetics of antisense oligonucleotides. *Clin Pharmacokinet* 28(1):7–16.

- <https://doi.org/10.2165/00003088-199528010-00002>
35. Agrawal S, Zhang X, Cai Q, Kandimalla ER, Manning A, Jiang Z, Marcel T, Zhang R (1998) Effect of aspirin on protein binding and tissue disposition of oligonucleotide phosphorothioate in rats. *J Drug Target* 5(4):303–312. <https://doi.org/10.3109/10611869808995883>
 36. Dean N, McKay R, Miraglia L, Howard R, Cooper S, Giddings J, Nicklin P, Meister L, Ziel R, Geiger T, Muller M, Fabbro D (1996) Inhibition of growth of human tumor cell lines in nude mice by an antisense of oligonucleotide inhibitor of protein kinase C- α expression. *Cancer Res* 56(15):3499–3507
 37. Moriya K, Matsukura M, Kurokawa K, Koike K (1996) In vivo inhibition of hepatitis B virus gene expression by antisense phosphorothioate oligonucleotides. *Biochem Biophys Res Commun* 218(1):217–223. <https://doi.org/10.1006/bbrc.1996.0038>. S0006-291X(96)90038-8 [pii]
 38. Gura T (1995) Antisense has growing pains. *Science* 270(5236):575–577
 39. Lewis EJ, Agrawal S, Bishop J, Chadwick J, Cristensen ND, Cuthill S, Dunford P, Field AK, Francis J, Gibson V, Greenham AK, Kelly F, Kilkushie R, Kreider JW, Mills JS, Mulqueen M, Roberts NA, Roberts P, Szymkowski DE (2000) Non-specific antiviral activity of antisense molecules targeted to the E1 region of human papillomavirus. *Antivir Res* 48(3):187–196. S0166354200001297 [pii]
 40. Agrawal S, Iyer RP (1997) Perspectives in antisense therapeutics. *Pharmacol Therapeut* 76:151–160
 41. Levin AA (1999) A review of the issues in the pharmacokinetics and toxicology of phosphorothioate antisense oligonucleotides. *Biochim Biophys Acta* 1489(1):69–84. S0167-4781(99)00140-2 [pii]
 42. Galbraith WM, Hobson WC, Giclas PC, Schechter PJ, Agrawal S (1994) Complement activation and hemodynamic changes following intravenous administration of phosphorothioate oligonucleotides in the monkey. *Antisense Res Dev* 4(3):201–206
 43. Black LE, Farrelly JG, Cavagnaro JA, Ahn CH, DeGeorge JJ, Taylor AS, DeFelice AF, Jordan A (1994) Regulatory considerations for oligonucleotide drugs: updated recommendations for pharmacology and toxicology studies. *Antisense Res Dev* 4(4):299–301
 44. Agrawal S (2001) United States Securities and Exchange Commission report. <https://www.sec.gov/Archives/edgar/data/861838/000095013501501616/b39654hye8-k.txt>. Accessed 9 Dec 2020
 45. Bayever E, Iversen PL, Bishop MR, Sharp JG, Tewary HK, Arneson MA, Pirruccello SJ, Ruddon RW, Kessinger A, Zon G et al (1993) Systemic administration of a phosphorothioate oligonucleotide with a sequence complementary to p53 for acute myelogenous leukemia and myelodysplastic syndrome: initial results of a phase I trial. *Antisense Res Dev* 3(4):383–390
 46. de Smet MD, Meenken CJ, van den Horn GJ (1999) Fomivirsen - a phosphorothioate oligonucleotide for the treatment of CMV retinitis. *Ocul Immunol Inflamm* 7(3–4):189–198
 47. Nemunaitis J, Holmlund JT, Kraynak M, Richards D, Bruce J, Ognoskie N, Kwok TJ, Geary R, Dorr A, Von Hoff D, Eckhardt SG (1999) Phase I evaluation of ISIS 3521, an antisense oligodeoxynucleotide to protein kinase C- α , in patients with advanced cancer. *J Clin Oncol* 17(11):3586–3595. <https://doi.org/10.1200/JCO.1999.17.11.3586>
 48. Grindel JM, Musick TJ, Jiang Z, Roskey A, Agrawal S (1998) Pharmacokinetics and metabolism of an oligodeoxynucleotide phosphorothioate (GEM 91) in cynomolgous monkeys following intravenous infusion. *Antisense Nucl Acid Drug Dev* 8:43–52
 49. Sereni D, Tubiana R, Lascoux C, Katlama C, Taulera O, Bourque A, Cohen A, Dvorchik B, Martin RR, Tournier C, Gouyette A, Schechter PJ (1999) Pharmacokinetics and tolerability of intravenous trecovirsen (GEM 91), an antisense phosphorothioate oligonucleotide, in HIV-positive subjects. *J Clin Pharmacol* 39(1):47–54
 50. Agrawal S (1996) Antisense oligonucleotides: towards clinical trials. *Trends Biotechnol* 14(10):376–387. [https://doi.org/10.1016/0167-7799\(96\)10053-6](https://doi.org/10.1016/0167-7799(96)10053-6). 0167-7799(96)10053-6 [pii]
 51. Agrawal S, Kandimalla ER (2004) Role of Toll-like receptors in antisense and siRNA [corrected]. *Nat Biotechnol* 22(12):1533–1537. <https://doi.org/10.1038/nbt1042>. nbt1042 [pii]
 52. Krieg AM, Yi A-K, Matson S, Waldschmidt TJ, Bishop GA, Teasdale R, Koretsky GA, Klinman DM (1995) CpG motifs in bacterial DNA trigger direct B-cell activation. *Nature* 374:546–549
 53. Messina JP, Gilkeson GS, Pisetsky DS (1991) Stimulation of in vitro murine lymphocyte

- proliferation by bacterial DNA. *J Immunol* 147:1759–1764
54. Hemmi H, Takeuchi O, Kawai T, Kaisho T, Sato S, Sanjo H, Matsumoto M, Hoshino K, Wagner H, Takeda K, Akira S (2000) A Toll-like receptor recognizes bacterial DNA. *Nature* 408(6813):740–745. <https://doi.org/10.1038/35047123>
 55. Agrawal S, Martin RR (2003) Was induction of HIV-1 through TLR9? *J Immunol* 171(4): 1621. author reply 1621–1622
 56. Agrawal S (1999) Importance of nucleotide sequence and chemical modifications of antisense oligonucleotides. *Biochim Biophys Acta* 1489:53–68
 57. Agrawal S, Kandimalla ER (2000) Antisense therapeutics: is it as simple as complementary base recognition? *Mol Med Today* 6(2): 72–81. S1357-4310(99)01638-X [pii]
 58. Eckstein F (1985) Nucleoside phosphorothioates. *Annu Rev Biochem* 54:367–402
 59. Kurpiewski MR, Koziolkiewicz M, Wilk A, Stec WJ, Jen-Jacobson L (1996) Chiral phosphorothioates as probes of protein interactions with individual DNA phosphoryl oxygens: essential interactions of EcoRI endonuclease with the phosphate at pGAATTC. *Biochemistry* 35(27):8846–8854. <https://doi.org/10.1021/bi960261e>. bi960261e [pii]
 60. Guo M, Yu D, Iyer RP, Agrawal S (1998) Solid-phase stereoselective synthesis of 2'-O-methyl-oligoribonucleoside phosphorothioates using nucleoside bicyclic oxazaphospholidines. *Bioorg Med Chem Lett* 8:2539–2544
 61. Yu D, Kandimalla ER, Roskey A, Zhao Q, Chen L, Chen J, Agrawal S (2000) Stereo-enriched phosphorothioate oligodeoxynucleotides: synthesis, biophysical and biological properties. *Bioorg Med Chem* 8(1):275–284. S0968-0896(99)00275-8 [pii]
 62. Iwamoto N, Butler DCD, Svrzikapa N, Mohapatra S, Zlatev I, Sah DWY, Meena, Standley SM, Lu G, Apponi LH, Frank-Kamenetsky M, Zhang JJ, Vargeese C, Verdine GL (2017) Control of phosphorothioate stereochemistry substantially increases the efficacy of antisense oligonucleotides. *Nat Biotechnol* 35(9):845–851. <https://doi.org/10.1038/nbt.3948>. nbt.3948 [pii]
 63. Østergaard ME, De Hoyos CL, Wan WB, Shen W, Low A, Berdeja A, Vasquez G, Murray S, Migawa MT, Liang X-H, Swayze EE, Crooke ST, Seth PP (2020) Understanding the effect of controlling phosphorothioate chirality in the DNA gap on the potency and safety of gapmer antisense oligonucleotides. *Nucl Acids Res* 48:1691. <https://doi.org/10.1093/nar/gkaa031>
 64. Wave Life Sciences Press Release (2019) Wave Life Sciences announces discontinuation of Suvodirsens development for Duchenne Muscular Dystrophy. <https://ir.wavelifesciences.com/news-releases/news-release-details/wave-life-sciences-announces-discontinuation-suvodirsens>. Accessed 9 Dec 2020
 65. Wave Life Sciences Press Release (2019) Wave Life Sciences announces Suvodirsens Phase 1 safety and tolerability data and Phase 2/3 Clinical Trial design. <https://ir.wavelifesciences.com/news-releases/news-release-details/wave-life-sciences-announces-suvodirsens-phase-1-safety-and->. Accessed 9 Dec 2020
 66. Miller PS, Agris CH, Murakami A, Reddy PM, Spitz SA, Ts'o POP (1983) Preparation of oligodeoxyribonucleoside methylphosphonates on a polystyrene support. *Nucl Acids Res* 11:6225–6241
 67. Asai A, Oshima Y, Yamamoto Y, Uochi T, Kusaka H, Akinaga S, Yamashita Y, Pongracz K, Pruzan R, Wunder E, Piatyszek M, Li S, Chin AC, Harley CB, Gryaznov S (2003) A novel telomerase template antagonist (GRN163) as a potential anticancer agent. *Cancer Res* 63:3931–3939
 68. Agrawal S, Goodchild J (1987) Oligodeoxynucleoside methylphosphonates: synthesis and enzymic degradation. *Tetrahedron Lett* 28:3539–3542
 69. Summerton J, Weller D (1993) Uncharged Morpholino-based polymers having phosphorus containing chiral intersubunit linkages
 70. Summerton J (1999) Morpholino antisense oligomers: the case for an RNase H-independent structural type. *Biochim Biophys Acta* 1489:141–158
 71. Enterlein S, Warfield KL, Swenson DL, Stein DA, Smith JL, Gamble CS, Kroeker AD, Iversen PL, Bavari S, Mühlberger E (2006) VP35 knockdown inhibits Ebola virus amplification and protects against lethal infection in mice. *Antimicrob Agents Chemother* 50: 984–993
 72. Kinali M, Arechavala-Gomez V, Feng L, Cirak S, Hunt D, Adkin C, Guglieri M, Ashton E, Abbs S, Nihoyanopoulos P, Garraldi EM, Rutherford M, McCulley C, Popplewell LJ, Graham IR, Dickson G, Wood M, Wells DJ, Wilton SD, Holt T, Kole R, Straub V, Bushby K, Sewry C, Morgan JE, Muntoni F (2009) Restoration of dystrophin expression in Duchenne muscular dystrophy: a single blind placebo-controlled dose

- escalation study using morpholino oligomer AVI-4658. *Lancet* 8:918
73. Aartsma-Rus A, Arechavala-Gomez V (2018) Why dystrophin quantification is key in the cteplirs saga. *Nat Rev Neurol* 14: 454–456
74. Järver P, O'Donovan L, Gait MJ (2014) A chemical view of oligonucleotides for exon skipping and related drug applications. *Nucl Acids Ther* 24:37–47
75. Egholm M, Buchardt O, Nielsen PE, Berg RH (1992) Peptide Nucleic Acids (PNA). Oligonucleotide analogues with an achiral backbone. *J Am Chem Soc* 114:1895–1897
76. Rapozzi V, Burm BE, Cogioi S, van der Marel GA, van Boom JH, Quadrifoglio F, Xodo LE (2002) Anti-proliferative effect in chronic myeloid leukaemia cells by antisense peptide nucleic acids. *Nucl Acids Res* 30:3712–3721
77. Villa R, Folini M, Lualdi S, Veronese S, Daidone MG, Zaffaroni N (2000) Inhibition of telomerase activity by a cell-penetrating peptide nucleic acid construct in human melanoma cells. *FEBS Lett* 473:241–248
78. Chaubey B, Tripathi S, Ganguly S, Harris D, Casale RA, Pandey VN (2005) A PNA-Transportan conjugate targeted to the TAR region of the HIV-1 genome exhibits both antiviral and virucidal properties. *Virology* 331:418–428
79. Chaubey B, Tripathi S, Pandey VN (2008) Single acute-dose and repeat-doses toxicity anti-HIV-1 PNATAR-Penetratin conjugates after intraperitoneal administration to mice. *Oligonucleotides* 18:9–20
80. Good L, Awasthi SK, Dryselius R, Larsson O, Nielsen PE (2001) Bactericidal antisense effects of peptide-PNA conjugates. *Nat Biotech* 19:360–364
81. Good L, Nielsen PE (1998) Inhibition of translation and bacterial cell growth by peptide nucleic acid targeted to ribosomal RNA. *Proc Natl Acad Sci U S A* 95:2073–2076
82. Torres AG, Fabani MM, Vigorito E, Williams D, Al-Obaidi N, Wojcechowski F, Hudson RHE, Seitz O, Gait MJ (2012) Chemical structure requirements and cellular targeting of microRNA-122 by peptide nucleic acids anti-miRs. *Nucl Acids Res* 40: 2152–2167
83. Inoue H, Hayase Y, Iwai S, Ohtsuka E (1987) Sequence-dependent hydrolysis of RNA using modified oligonucleotide splints and RNase H. *Nucl Acids Symp Ser* 18:221–224
84. Yu D, Iyer RP, Shaw DR, Lisiewicz J, Li Y, Jiang Z, Roskey A, Agrawal S (1996) Hybrid oligonucleotides: synthesis, biophysical properties, stability studies, and biological activity. *Bioorg Med Chem* 4(10): 1685–1692. 0968089696001605 [pii]
85. Metele V, Lisiewicz J, Agrawal S (1994) Study of antisense oligonucleotide phosphorothioates containing segments of oligodeoxynucleotides and 2'-o-methylribonucleotides. *Bioorg Med Chem Lett* 4:2929–2934
86. Agrawal S, Jiang Z, Zhao Q, Shaw D, Cal Q, Roskey A, Channavajjala L, Saxinger C, Zhang R (1997) Mixed-backbone oligonucleotides as second generation antisense oligonucleotides: in vitro and in vivo studies. *Proc Natl Acad Sci U S A* 94:2620–2625
87. Zhou W, Agrawal S (1998) Mixed-backbone oligonucleotides as second-generation antisense agents with reduced phosphorothioate-related side effects. *Bioorg Med Chem Lett* 8: 3269–3274
88. Sierakowska H, Sambade MJ, Agrawal S, Kole R (1996) Repair of thalassemic human beta-globin mRNA in mammalian cells by antisense oligonucleotides. *Proc Natl Acad Sci U S A* 93(23):12840–12844
89. Wilton SD, Lloyd F, Carville K, Fletcher S, Honeyman K, Agrawal S, Kole R (1999) Specific removal of the nonsense mutation from the mdx dystrophin mRNA using antisense oligonucleotides. *Neuromuscul Disord* 9(5): 330–338. S0960896699000103 [pii]
90. FDA Panel (2015) FDA advisory panel votes BioMarin's drisapersen trials not persuasive. <https://www.fdanews.com/articles/174238-fda-advisory-panel-votes-biomarins-drisapersen-trials-not-persuasive?v=preview>. Accessed 9 Dec 2020
91. Aartsma-Rus A (2017) FDA approval of nusinersen for Spinal Muscular Atrophy makes 2016 the year of splice modulating oligonucleotides. *Nucl Acids Ther* 27:67–69
92. Mercuri E, Darras BT, Chiriboga CA, Day JW, Campbell C, Connolly AM, Iannaccone ST, Kirschner J, Kuntz NL, Saito K, Shieh PB, Tulinius M (2018) Nusinersen versus sham control in later-onset Spinal Muscular Atrophy. *New Engl J Med* 378:625–635
93. Arzumanov A, Walsh AP, Liu X, Rajwanshi VK, Wengel J, Gait MJ (2001) Oligonucleotide analogue interference with the HIV-1 Tat protein-TAR RNA interaction. *Nucleos Nucleot Nucl Acids* 20:471–480
94. Lindow M, Kauppinen S (2012) Discovering the first microRNA targeted drug. *J Cell Biol* 199:407–412
95. Morita K, Hasegawa C, Kaneko M, Tsutsumi S, Sone J, Ishikawa T, Imanishi T, Koizumi M (2001) 2'-O,4'-C-ethylene-

- bridged nucleic acids (ENA) with nuclease-resistance and high affinity for RNA. *Nucl Acids Res Suppl* 1:241–242
96. Lee T, Awano H, Yagi M, Matsumoto M, Watanabe N, Goda R, Koizumi M, Takeshima Y, Matsuo M (2017) 2'-O-methyl RNA/ethylene-bridged nucleic acid chimera antisense oligonucleotides to induce dystrophin exon 45 skipping. *Genes* 8(2):67. <https://doi.org/10.3390/genes8020067>. genes8020067 [pii]
97. Renneberg D, Leumann CJ (2002) Watson-Crick base-pairing properties of tricyclo-DNA. *J Am Chem Soc* 124: 5993–6004
98. Seth PP, Siwkowski A, Allerson CR, Vasquez G, Lee S, Prakash TP, Kinberger G, Migawa MT, Gaus H, Bhat B, Swayze EE (2008) Design, synthesis and evaluation of constrained methoxyethyl (cMOE) and constrained ethyl (cEt) nucleoside analogs. *Nucl Acids Symp Ser* 52:553–554. <https://doi.org/10.1093/nass/nrn280>. nrn280 [pii]
99. Flanagan WM, Wagner RW, Grant D, Lin K-Y, Matteucci M (1999) Cellular penetration and antisense activity by a phenoxazine-substituted heptanucleotide. *Nat Biotech* 17: 48–52
100. Henry S, Stecker K, Brooks D, Monteith D, Conklin B, Bennett CF (2000) Chemically modified oligonucleotides exhibit decreased immune stimulation in mice. *J Pharmacol Exp Ther* 292(2):468–479
101. Yu D, Wang D, Zhu FG, Bhagat L, Dai M, Kandimalla ER, Agrawal S (2009) Modifications incorporated in CpG motifs of oligodeoxynucleotides lead to antagonist activity of toll-like receptors 7 and 9. *J Med Chem* 52(16):5108–5114. <https://doi.org/10.1021/jm900730r>
102. Zhang R, Iyer RP, Yu D, Tan W, Zhang X, Lu Z, Zhao H, Agrawal S (1996) Pharmacokinetics and tissue disposition of a chimeric oligodeoxynucleoside phosphorothioate in rats after intravenous administration. *J Pharmacol Exp Ther* 278(2):971–979
103. Kandimalla ER, Temsamani J, Agrawal S (2007) Synthesis and properties of 2'-O-methylribonucleotide methylphosphonate containing chimeric oligonucleotides. *Nucleos Nucleot* 14:1031–1035
104. Agrawal S, Zhang X, Lu Z, Zhao H, Tamburin JM, Yan J, Cai H, Diasio RB, Habus I, Jiang Z et al (1995) Absorption, tissue distribution and in vivo stability in rats of a hybrid antisense oligonucleotide following oral administration. *Biochem Pharmacol* 50(4): 571–576. 0006295295001602 [pii]
105. Shen LX, Kandimalla ER, Agrawal S (1998) Impact of mixed-backbone oligonucleotides on target binding affinity and target cleaving specificity and selectivity by *Escherichia coli* RNase H. *Bioorg Med Chem* 6:1695–1705
106. Benson MD, Waddington-Cruz M, Berk JL, Polydefkis M, Dyck PJ, Wang AK, Planté-Bordeneuve V, Barroso FA, Merlini G, Obici L, Scheinberg M, Brannagan TH (2018) Inotersen treatment for patients with hereditary transthyretin amyloidosis. *New Engl J Med* 379:22–31
107. Witztum JL, Gaudet D, Freedman SD, Alexander VA, Digenio A, Williams KR, Yang Q, Hughes SG, Geary RS, Arca M, Stroes ESG, Bergeron J (2019) Volanesorsen and triglyceride levels in Familial Chylomicronemia Syndrome. *New Engl J Med* 381:531–542
108. Reeskamp LF, Kastelein JJP, Moriarty PM, Duell PB, Catapano AL, Santos RD, Ballantyne CM (2019) Safety and efficacy of mipomersen in patients with heterozygous familial hypercholesterolemia. *Atherosclerosis* 280: 109–117
109. Frieden M, Orum H (2006) The application of locked nucleic acids in the treatment of cancer. *IDrugs* 9:706–711
110. Hong D, Kurzrock R, Kim Y, Woessner R, Younes A, Nemunaitis J, Fowler N, Zhou T, Schmidt J, Jo M, Lee SJ, Yamashita M, Hughes SG, Fayad L, Piha-Paul S, Nadella MVP, Mohseni M, Lawson D, Reimer C, Blakey DC, Xiao X, Hsu J, Revenko A, Monia BP, MacLeod AR (2015) AZD9150, a next-generation antisense oligonucleotide inhibitor of STAT3 with early evidence of clinical activity in lymphoma and lung cancer. *Sci Transl Med* 7:314ra185
111. Seth PP, Yu J, Jazayeri A, Pallan PS, Allerson CR, Østergaard ME, Liu F, Herdewijn P, Egli M, Swayze EE (2012) Synthesis and antisense properties of Fluoro Cyclohexenyl Nucleic Acid (F-CeNA), a nuclease stable mimic of 2'-fluoro RNA. *J Org Chem* 77: 5074–5085
112. Allart B, Khan K, Rosemeyer H, Schepers G, Hendrix C, Rothenbacher K, Seela F, Van Aerschot A, Herdewijn P (1999) D-Altritol Nucleic Acids (ANA): hybridisation properties, stability, and initial structural analysis. *Chem Eur J* 5:2424–2431
113. Carroll JB, Warby SC, Southwell AL, Doty CN, Greenlee S, Skotte N, Hung G, Bennett CF, Freier SM, Hayden MR (2011) Potent and selective antisense oligonucleotides targeting single nucleotide polymorphisms in the Huntington Disease gene/allele-specific

- silencing of mutant Huntingtin. *Mol Ther* 19:2178–2185
114. Kamola PJ, Kitson JDA, Turner G, Maratou K, Eriksson S, Panjwani A, Warnock LC, Douillard GA, Moores K, Koppe EL, Wixted WE, Wilson PA, Gooderham NJ, Gany TW, Glark KL, Hughes SA, Edbrooke MR, Parry JD (2015) In silico and in vitro evaluation of exonic and intronic off-target effects form a critical element of therapeutic ASO gapmer optimization. *Nucl Acids Res* 43:8638–8650
115. Kasuya T, Hori S, Watanabe A, Nakajima M, Gahara Y, Rokushima M, Yanagimoto T, Kugimiya A (2016) Ribonuclease H1-dependent hepatotoxicity caused by locked nucleic acid-modified gapmer antisense oligonucleotides. *Sci Rep* 6:30377
116. Burel SA, Hart CE, Cauntley P, Hsiao J, Machemer T, Katz M, Watt A, Bul HH, Younis H, Sabripour M, Freier SM, Hung G, Dan A, Prakash TP, Seth PP, Swayze EE, Bennett CF, Crooke ST, Henry SP (2016) Hepatotoxicity of high affinity gapmer antisense oligonucleotides is mediated by RNase H1 dependent promiscuous reduction of very long pre-mRNA transcripts. *Nucl Acids Res* 44:2093–2109
117. Swayze EE, Siwkowski AM, Wancewicz EV, Migawa MT, Wyrzykiewicz TK, Hung G, Monia BP, Bennett CF (2007) Antisense oligonucleotides containing locked nucleic acid improve potency but cause significant hepatotoxicity in animals. *Nucl Acids Res* 35: 687–700
118. Ferrari N, Bergeron D, Tedeschi A-L, Mangos MM, Paquet L, Renzi PM, Damha MJ (2006) Characterization of antisense oligonucleotides comprising 2'-deoxy-2'-fluoro- β -D-arabinonucleic acid (FANA). *Ann N Y Acad Sci* 1082:91–102
119. Egli M, Pallan PS, Allerson CR, Prakash TP, Berdeja A, Yu J, Lee S, Watt A, Gaus H, Bhat B, Swayze EE, Seth PP (2011) Synthesis, improved antisense activity and structural rationale for the divergent RNA affinities of 3'-fluoro hexitol nucleic acid (FHNA and Ara-FHNA) modified oligonucleotides. *J Am Chem Soc* 133:16642–16649
120. Parmar R, Willoughby JLS, Liu J, Foster DJ, Brigham B, Theile CS, Charisse K, Akinc A, Guidry E, Pei Y, Strapps W, Cancilla M, Stanton MG, Rjaev KG, Sepp-Lorenzino L, Manoharan M, Meyers R, Maier MA, Jahdavi V (2016) 5'-(E)-Vinylphosphonate: a stable phosphate mimic can improve the RNAi activity of siRNA-GalNAc conjugates. *Chem-BioChem* 17:985–989
121. Godfrey C, Desviat LR, Smedsrød B, Piétri-Rouxel F, Denti MA, Disterer P, Lorain S, Nogales-Gadea G, Sardon V, Anwar R, El Andaloussi S, Lehto T, Khoo B, Brolin C, van Roon-Mom WM, Goyenvalle A, Aartsma-Rus A, Arechavala-Gomez V (2017) Delivery is key: lessons learnt from developing splice-switching antisense therapies. *EMBO Mol Med* 9:545–557
122. Ray KK, Landmesser U, Leiter LA, Kallend D, Dufour R, Karakas M, Hall T, Troquay RPT, Turner T, Visseren FLJ, Wijngard P, Wright RS (2017) Inclisiran in patients at high cardiovascular risk with elevated LDL cholesterol. *New Engl J Med* 376: 1430–1440
123. Godhino BMDC, Coles AH, Khvorova A (2019) Conjugate-mediated delivery of RNAi-based therapeutics: enhancing pharmacokinetics-pharmacodynamics relationships of medicinal oligonucleotides. In: Agrawal S, Gait MJ (eds) *Advances in nucleic acid therapeutics*. Royal Society of Chemistry, London, pp 206–232
124. Killanthottathil GR, Manoharan M (2019) Liver-targeted RNAi therapeutics: principles and applications. In: Agrawal S, Gait MJ (eds) *Advances in nucleic acid therapeutics*. Royal Society of Chemistry, London, pp 233–265
125. Chirigos MA, Papademetriou V, Bartocci A, Read E, Levy HB (1981) Immune response modifying activity in mice of polyinosinic: polycytidylic acid stabilized with poly-L-lysine, in carboxymethylcellulose [Poly-ICLC]. *Int J Immunopharmacol* 3:329–337
126. Pisetsky DS (1996) Immune activation by bacterial DNA: a new genetic code. *Immunity* 5:303–310
127. Boller T, Felix G (2009) A renaissance of elicitors: perception of microbe-associated molecular patterns and danger signals by pattern-recognition receptors. *Annu Rev Plant Biol* 60:379–406
128. Palm NW, Medzhitov R (2008) Pattern recognition receptors and control of adaptive immunity. *Immunol Rev* 227:221–233
129. Blasius AL, Beutler B (2011) Intracellular toll-like receptors. *Immunity* 32:305–315
130. Kandimalla ER, Agrawal S (2005) Agonists of toll-like receptor 9. In: *Toll and toll-like receptors: an immunologic perspective*. Molecular Biology Intelligence Unit. Springer, Boston, MA, pp 181–212
131. Bauer S, Kirschning CJ, Häcker H, Redecke V, Hausmann S, Akira S, Wagner H, Lipford GB (2001) Human

- TLR9 confers responsiveness to bacterial DNA via species-specific CpG motif recognition. *Proc Natl Acad Sci U S A* 98:9237–9242
132. Cho WG, Albuquerque RJC, Kleinman ME, Taralio V, Greco A, Nozaki M, Green MG, Baffi JZ, Ambati BK, De Falco M, Alexander JS, Brunetti A, De Falco S, Anbelti J (2009) Small interfering RNA-induced TLR3 activation inhibits blood and lymphatic vessel growth. *Proc Natl Acad Sci U S A* 106: 7137–7142
 133. Kleinman ME, Yamada K, Takeda A, Chandrasekaran V, Nozaki M, Baffi JZ, Albuquerque RJC, Yamasaki S, Itaya M, Pan Y, Appukuttan B, Gibbs D, Yang Z, Kariko K, Ambati BK, Eilgus TA, DiPietro LA, Sakurai E, Zhang K, Smith JR, Taylor EW, Ambati J (2008) Sequence- and target-independent angiogenesis suppression by siRNA via TLR3. *Nature* 452:591–597
 134. Lan T, Wang D, Bhagat L, Philbin VJ, Yu D, Tang JX, Putta MR, Sullivan T, La Monica N, Kandimalla ER, Agrawal S (2013) Design of synthetic oligoribonucleotide-based agonists of Toll-like receptor 3 and their immune response profiles in vitro and in vivo. *Org Biomol Chem* 11:1049–1058
 135. Putta MR, Zhu FG, Wang D, Bhagat L, Kandimalla ER, Agrawal S (2010) Peptide conjugation at the 5'-end of oligodeoxynucleotides abrogates Toll-Like Receptor 9-mediated immune stimulatory activity. *Bioconjug Chem* 21:39–45
 136. Agrawal S, Kandimalla ER (2001) Antisense and/or immunostimulatory oligonucleotide therapeutics. *Curr Cancer Drug Targets* 1(3):197–209
 137. Jackson S, Lenting J, Kopp J, Murray L, Ellison W, Rhee M, Shockey G, Akelia L, Ery K, Hayward WL, Janssen RS (2018) Immunogenicity of a two-dose investigational hepatitis B vaccine, HBsAg-1018, using a toll-like receptor 9 agonist adjuvant compared with a licensed hepatitis B vaccine in adults. *Vaccine* 36:668–674
 138. Guyadar D, Bogomolv P, Kobalava Z, Moiseev V, Szlavik J, Astruc B, Varkonyi L, Sullivan T (2011) 1209 IMO-2025 plus Ribavirin gives substantial first-dose viral load reductions, cumulative anti-viral effect, is well tolerated in naive genotype HCV patients: a Phase 1 trial. *J Hepatol* 54(Supp 1):S478
 139. Jiang W, Zhu FG, Bhagat L, Yu D, Tang JX, Kandimalla ER, La Monica N, Agrawal S (2013) A toll-like receptor 7, 8, and 9 antagonist inhibits Th1 and Th17 responses and inflammasome activation in a model of IL-23-induced psoriasis. *J Investig Dermatol* 133:1777–1784
 140. El-Andaloussi S, Johansson HJ, Holm T, Langel U (2007) A novel cell-penetrating peptide, M918, for efficient delivery of proteins and peptide nucleic acids. *Mol Ther* 15: 1820–1826
 141. Poeck H, Besch R, Hartmann G (2008) 5'-triphosphate-siRNA: turning gene silencing and Rig-I activation against melanoma. *Nat Med* 14:1256–1263
 142. Case CL (2011) Regulating caspase-1 during infection: roles of NLRs, AIM2, and ASC. *Yale J Biol Med* 84:333–343
 143. Arnold AE, Malek-Adamian E, Le PU, Meng A, Martinez-Montero S, Petrecca K, Damha MJ, Sholchet MS (2018) Antibody-antisense oligonucleotide conjugate downregulates a key gene in glioblastoma stem cells. *Mol Ther Nucl Acids* 11:518–527
 144. Cuellar TL, Barnes D, Nelson C, Tanguay J, You S-F, Wen X, Scales SJ, Gesch J, Davis D, van Brabant SA, Leake D, Vandlen R, Sieber CW (2015) Systematic evaluation of antibody-mediated siRNA delivery using an industrial platform of THIOMAB-siRNA conjugates. *Nucl Acids Res* 43:1189–1203
 145. Langel U (2015) Cell-penetrating peptides. In: *Methods and protocols. Methods in molecular biology*, 2nd edn. Springer, New York, NY
 146. Jearawiriyapaisarn N, Moulton HM, Buckley B, Roberts J, Sazani P, Fuchareon S, Iversen PL, Kole R (2008) Sustained dystrophin expression induced by peptide-conjugated morpholino oligomers in the muscles of mdx mice. *Mol Ther* 16: 1624–1629
 147. Passini MA, Hanson GJ (2018) Exon skipping oligomer conjugates for muscular dystrophy
 148. Betts C, Saleh AF, Arzumanov AA, Hammond SM, Godfrey C, Coursindel T, Gait MJ, Wood MJA (2012) A new generation of peptide-oligonucleotide conjugates with improved cardiac exon skipping activity for Duchenne muscular dystrophy treatment. *Mol Ther Nucl Acids* 1:e38
 149. Klein AF, Varela M, Arandel L, Holland A, Naouar N, Arzumanov A, Seoane D, Revillod L, Bassez G, Ferry A, Jauvin D, Gourdon G, Puymirat J, Gait MJ, Furling D, Wood MJ (2019) Peptide-conjugated oligonucleotides evoke long-lasting myotonic dystrophy correction in patient-derived cells and mice. *J Clin Investig* 129:4739–4744

150. Juliano RL (2016) The delivery of therapeutic oligonucleotides. *Nucl Acids Res* 14: 6518–6548
151. Bacsa B, Horváti K, Bosze S, Andreae F, Kappe CO (2008) Solid-phase synthesis of difficult peptide sequences at elevated temperatures: a critical comparison of microwave and conventional heating technologies. *J Org Chem* 73:7532–7542
152. Shubham S, Lin L-H, Udofot O, Krupse S, Giangrande PH (2019) Prostate-specific membrane antigen (PMSA) aptamers for prostate cancer imaging and therapy. In: Agrawal S, Gait MJ (eds) *Advances in nucleic acid therapeutics*. Royal Society of Chemistry, London, pp 339–366
153. Zon G (2019) Aptamers and clinical applications. In: Agrawal S, Gait MJ (eds) *Advances in nucleic acids therapeutics*. Royal Society of Chemistry, London, pp 367–399
154. Strenkowska M, Grzela R, Majewski M, Wnek K, Kowalski J, Lukaszewicz M, Zuberek J, Darzynkiewicz E, Kuhn AN, Sahin U, Jemielty J (2016) Cap analogs modified with 1,2-dithiodiphosphate moiety protect mRNA from decapping and enhance its translational potential. *Nucl Acids Res* 44: 9578–9590
155. Andries O, McCafferty S, De Smedt SC, Weiss R, Sanders NN, Kitada T (2015) N (1)-methylpseudouridine-incorporated mRNA outperforms pseudouridine-incorporated mRNA by providing enhanced protein expression and reduced immunogenicity in mammalian cell lines and mice. *J Control Release* 217:337–344
156. Svitkin YV, Cheng YM, Chakraborty T, Presnyak V, John M, Sonenberg N (2017) N1-methyl-pseudouridine in mRNA enhances translation through eIF2- α -dependent and independent mechanisms by increasing ribosome density. *Nucl Acids Res* 45:6023–6036
157. Oberli MA, Rechmuth AM, Dorkin JR, Mitchell MJ, Fenton OS, Jaklenec A, Anderson DG, Langer R, Blankschtein D (2017) Lipid nanoparticle assisted mRNA delivery for potent cancer immunotherapy. *Nano Lett* 17:1326–1335
158. Yin H, Song C-Q, Suresh S, Wu Q, Walsh S, Rhym LH, Mintzer E, Bolukbasi MF, Zhu LJ, Kauffman K, Mou H, Ovberholzer A, Ding J, Kwan S-Y, Bogorad RL, Zatzepin TS, Koteliansky V, Wolfe SA, Xue W, Langer R, Anderson DG (2017) Structure-guided chemical modification of guide RNA enables potent non-viral in vivo genome editing. *Nat Biotech* 35:1179–1187
159. Hendel A, Bak RO, Clark JT, Kennedy AB, Ryan DE, Roy S, Steinfeld I, Lunstad BD, Kaiser RJ, Wilkens AB, Bacchette R, Tsalenko A, Dellinger D, Bruhn L, Porteus MH (2015) Chemically modified guide RNAs enhance CRISPR-Cas genome editing in human primary cells. *Nat Biotech* 33: 985–989
160. Cromwell CR, Sung K, Park J, Krysler AR, Jovel J, Kim SK, Hubbard BP (2018) Incorporation of bridged nucleic acids into CRISPR RNAs improves Cas9 endonuclease specificity. *Nat Commun* 9:1448
161. Geny S, Hosseini ES, Concordet J-P, Giovannangeli C (2019) CRISPR-based technologies for genome engineering: properties, current improvements and applications in medicine. In: Agrawal S, Gait MJ (eds) *Advances in nucleic acid therapeutics*. Royal Society of Chemistry, London, pp 400–433

Open Access This chapter is licensed under the terms of the Creative Commons Attribution 4.0 International License (<http://creativecommons.org/licenses/by/4.0/>), which permits use, sharing, adaptation, distribution and reproduction in any medium or format, as long as you give appropriate credit to the original author(s) and the source, provide a link to the Creative Commons license and indicate if changes were made.

The images or other third party material in this chapter are included in the chapter's Creative Commons license, unless indicated otherwise in a credit line to the material. If material is not included in the chapter's Creative Commons license and your intended use is not permitted by statutory regulation or exceeds the permitted use, you will need to obtain permission directly from the copyright holder.





Chapter 2

Antisense RNA Therapeutics: A Brief Overview

Virginia Arechavala-Gomez  and Alejandro Garanto 

Abstract

Nucleic acid therapeutics is a growing field aiming to treat human conditions that has gained special attention due to the successful development of mRNA vaccines against SARS-CoV-2. Another type of nucleic acid therapeutics is antisense oligonucleotides, versatile tools that can be used in multiple ways to target pre-mRNA and mRNA. While some years ago these molecules were just considered a useful research tool and a curiosity in the clinical market, this has rapidly changed. These molecules are promising strategies for personalized treatments for rare genetic diseases and they are in development for very common disorders too. In this chapter, we provide a brief description of the different mechanisms of action of these RNA therapeutic molecules, with clear examples at preclinical and clinical stages.

Key words RNA therapy, Antisense oligonucleotides, Clinical trials, Splicing, Personalized medicine

1 Introduction

Nucleic acid therapeutics is still a growing field. With the irruption of the mRNA vaccines against SARS-CoV-2 special attention has been given to this type of therapies but other types of nucleic acid therapeutics, coined antisense oligonucleotides (AONs), have been studied for many years. Although only a dozen therapeutic oligonucleotides have been formally approved for clinical use, there are many new such drugs in the pipeline for a plethora of (mainly rare) diseases. These AON molecules interact with different nucleic acids (mRNA, non-coding RNA, and DNA) thanks to sequence specific Watson–Crick base pairing. Their mechanism of action, that may be designed to bind specific targets, makes these drugs easy to design, less likely to cause side effects and, therefore, potential candidates to lead the next wave of precision medicine. In this chapter, we describe the most frequently used AON-based therapeutic strategies, their mechanisms of action (Fig. 1), and the results of several clinical trials, with special emphasis in eye and muscle diseases.

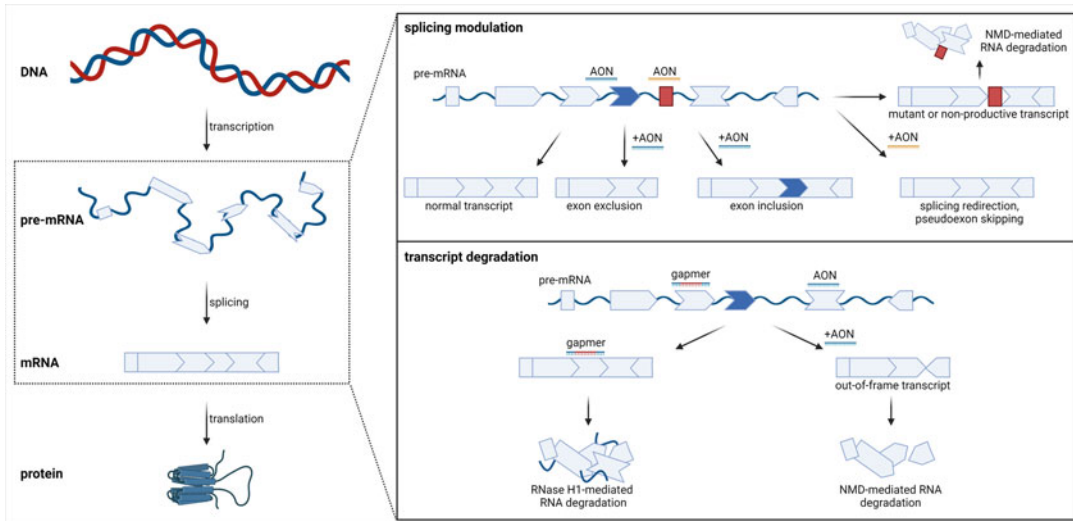


Fig. 1 Schematic representation of the multiple mechanisms of action of antisense oligonucleotide (AON) molecules. AONs can act at pre- and mRNA levels of the synthesis of a functional protein (left panel). They can be used to modulate splicing (upper right panel) or to degrade (pre-)mRNA (lower right panel). Splice-modulating AONs bind to pre-mRNA and promote the insertion or skipping of regular exons. In addition, they can redirect splicing when mutations in a gene lead to splicing defects (such as pseudoexon insertions). This splicing modulation causes the degradation of the transcript and a consequent reduction of protein levels. Alternatively, transcript degradation can also be achieved by using AONs binding to the pre-mRNA to disrupt the open reading frame and degrade transcripts via nonsense-mediated decay (NMD). Gapmers, in contrast, can bind to both pre-mRNA and mRNA and activate RNase-H1 RNA degradation. (Created with [BioRender.com](https://www.biorender.com))

2 Mechanisms of Action

2.1 Splicing Modulation

The majority of existing therapeutic AONs are designed to alter the splicing pattern of specific pre-mRNAs [1]. This can be used to treat disorders caused by splicing alterations, which with the current widespread availability of better and cheaper sequencing options are being identified more easily and can be specifically targeted [2].

2.1.1 Exon Exclusion (Shortened Proteins)

In many genes, deleting an exon would result in the production of a non-functional protein, as their structure and function would be compromised. However, there are some cases in which internally “trimmed” proteins could be partially functional due to the existence of less-vital structures within a large protein. Mutations in the *DMD* gene disrupt the open reading frame (ORF) and the expression of the dystrophin protein, leading to Duchene muscular dystrophy (DMD). In contrast, in the much milder Becker muscular dystrophy mutations in the same gene that maintain the ORF produce an internally deleted but functional protein. This real-life example was rapidly seized as an opportunity to achieve the same

effect using therapeutic AONs, and several of the recently approved AON molecules target different *DMD* exons [3–9]. Because there are many different *DMD* mutations, the skipping specific exons would be therapeutic for different subsets of patients.

This concept has also been employed in the development of new AONs to skip in-frame exons carrying single-nucleotide changes generating premature stop codons in large genes. Mutations in *USH2A* cause either Usher syndrome (deafness combined with blindness) or isolated blindness in the form of retinitis pigmentosa. Exon 13 of *USH2A* is prone to carry truncating variants and by deleting it, a protein with residual function is potentially produced [10, 11]. This is also the case of a stop codon introduced by a variant in exon 36 of *CEP290*, which is naturally skipped at low levels in the retina and involved in retinal dystrophy. AONs designed to skip exon 36 restored the reading frame and produced a functional protein able to rescue the cellular phenotype in patient-derived cells [12]. Following the same strategy, AON molecules to skip different exons of *COL7A1* have been developed for dystrophic epidermolysis bullosa, a skin disease inherited in both dominant and recessive fashion [13–16].

2.1.2 Exon Inclusion

A seemingly opposite mechanism of action is at the core of nusinersen, an AON approved for the treatment of spinal muscular atrophy (SMA). In this case, mutations in the *SMN1* gene cause low or lack of SMN protein production. However, SMN protein can be produced by two nearly identical genes, *SMN1* and *SMN2*. The latter, however, contributes at very low levels due to the high rate of exon-7 skipping that disrupts the ORF. Nusinersen is used to alter the splicing of *SMN2* and include exon 7, and therefore produce sufficient amounts of SMN protein to ameliorate the patient's disease [17, 18].

2.1.3 Splicing Redirection

Variants close to the splice sites result often in either exon skipping or exon elongation. In the second scenario, mutations decrease the recognition of the original splice site and a cryptic splice site present in the intron is recognized; in the most extreme case, the entire intron is retained. Exonic variants may cause a synonymous or a predicted non-deleterious missense change at protein level, and in addition they can have a dramatic effect at RNA level by creating a novel splice site. In any case, these splicing defects are also amenable for AON intervention. For instance, a mutation in exon 3 of *USH1C* linked to deafness generates a novel splice donor site (SDS) upstream the regular SDS of the exon. This new SDS is preferentially used by the cells, leading to a disrupted reading frame. By using AONs to block the newly generated SDS, the normal transcript can be produced [19]. A similar approach has been used to target the exon elongation caused by near-exon

intronic variants in *ABCA4* linked to Stargardt macular degeneration. This study showed that by blocking the newly created SDS the normal splicing can be restored. However, this approach turned out to be not that successful when targeting exon elongations caused by variants in the splice acceptor site (SAS) [20].

Another elegant way to modulate splicing using AONs is by targeting the non-productive transcripts. These transcripts often are generated by (a) alternative splicing causing insertion or skipping of exons; (b) using alternative cryptic splice sites; and (c) retaining the introns. In any case, these splicing events lead to a disrupted ORF being the transcript degraded via nonsense-mediated decay (NMD). A very recent study has shown that 1246 potentially disease-associated genes present at least one of these non-productive transcripts. By targeting these splicing events to insert or skip an exon, exclude a retained intron, or redirect splicing when a cryptic splice site is used, the overall protein levels can be increased and this might be a promising therapeutic tool for haploinsufficiency cases [21].

2.1.4 Deep-Intronic Variants

For many years intronic variants have been ignored. This is mainly because they lay in the non-informative regions of our genome, the introns. However, the implementation of novel and more robust sequencing tools has contributed to solve the missing heritability in several diseases by discovering deep-intronic mutations with a detrimental effect on pre-mRNA splicing. The study of these variants is complex but with the help of novel bioinformatic (e.g. SpliceAI [22]) and molecular tools (mini/midi/maxi-genes [23]), it is possible to predict the effect at pre-mRNA level. These variants often result in the insertion of a pseudoexon, a piece of the intron that it is recognized as an exon and leads to a disruption of the ORF and consequently the generation of a premature stop codon. Pseudoexon exclusion can be achieved by using AONs. In the *ABCA4* gene, AONs have shown splicing correction for most of the 35 intronic variants identified as cause of Stargardt disease [24–30].

2.2 Transcript Degradation

Antisense technology can be extremely useful to degrade transcripts and cause gene silencing (knockdown). From the therapeutic perspective, this might be a potential tool to treat autosomal dominant diseases caused by dominant-negative mutations. In this case, by degrading specifically the mutant allele, the correct protein can perform its function properly.

2.2.1 RNase H1-Activating Antisense Oligonucleotides (Gapmers)

These antisense molecules are characterized for being able to actively reduce the levels of the mRNAs in the nucleus and cytoplasm [31], therefore they are very useful to downregulate gene expression. These RNase H1-activating AONs or gapmers are chimeric molecules linked using a phosphorothioate (PS) backbone that usually present a conformation 5-10-5, where the two arms

consist of five modified RNA nucleotides (2'-*O*-methoxyethyl (2'MOE), 2'-*O*-methyl (2'OMe) or locked nucleic acid (LNA)) flanking ten DNA nucleotides [32]. The first-ever AON approved by the FDA was fomivirsen, a first-generation RNase H1-activating AON [33–36] (*see* Subheading 3). However, this is the only RNase H1-activating AON that does not have the chimeric RNA/DNA structure. So far, four molecules using this mechanism of action have received FDA and/or EMA approval to treat different disease conditions [32].

Gapmers can be used to downregulate genes in allele-independent and allele-specific manner. Below, we review some examples of each case.

Allele-independent mRNA degradation is often used to target genes or pathways that are overexpressed in certain disease conditions or can worsen the disease progression. Thus, reducing the levels of particular genes can be very beneficial. This is the case for two of the approved AON drugs: mipomersen and volanesorsen. These molecules target the mRNA of the apolipoprotein B-100 in familial hypercholesterolemia or apolipoprotein C3 in familial chylomicronaemia syndrome, hypertriglyceridemia and familial partial lipodystrophy, respectively, to lower the levels of specific lipids increased in these diseases [37–41].

In contrast, allele-specific mRNA degradation aims to target only the mutant allele. This way, specific mutations that cause a dominant-negative effect can be targeted. This is the case of inotersen, a gapmer designed to target the mRNA encoding the transthyretin (TTR) protein in autosomal dominant hereditary transthyretin amyloidosis [42, 43]. A single-nucleotide change in the gene produces misfolding of the TTR protein. As TTR protein needs to tetramerize in order to conduct its function, the addition of mutant monomers into the tetramer affects the overall function. Systemic amyloid depositions are formed, leading to progressive polyneuropathy of the sensory and motor systems with multiorgan dysfunction in late-disease stages. The therapeutic gapmer targets the mutant allele to reduce the amount of tetramers containing the mutant protein, and therefore prevent the aforementioned depositions [42, 43]. Another recent example is the use of gapmers to specifically degrade the mutant allele introduced by a mutation in the *COCH* gene, which causes autosomal dominant hearing impairment [44]. In this study, two strategies were used to degrade the mutant transcript: directly targeting the mutation or other single-nucleotide polymorphisms (SNPs) in *cis* with the mutation that are part of the mutant haplotype.

2.2.2 Disrupting Reading Frame

Splice-switching AONs can also be used to induce transcript degradation. Skipping regular exons can also be used to knockdown the function of an undesired gene, by creating mRNA isoforms that

encode non-functional proteins or trigger degradation of the mRNA by NMD [45]. For instance, exon skipping of hepatic APOB100 was able to sustainably reduce LDL cholesterol levels in mice [46], downregulation of *MAPT* gene has been proposed as a possible treatment for tauopathies [47], and skipping exon 2 of *ALK5* may modulate the TGF- β signaling cascade, reducing the components related to the overproduction of extracellular matrix in hypertrophic scar [48].

3 Therapeutic Potential

While years ago oligonucleotides were considered a useful research tool and just a curiosity in the clinical market, this has rapidly changed into approved therapeutic strategies for several diseases and promising personalized treatments for many other (rare inherited) diseases. In this section, we will focus on the development of AON-based therapeutic strategies for two particular tissues: muscle and retina.

3.1 Examples of Clinical Trials for Muscle Diseases

The use of AONs to treat neuromuscular disorders has been at the forefront of the clinical development of AON-based therapies and more than half of the AONs currently in the market target either Duchenne muscular dystrophy (DMD) or spinal muscular atrophy (SMA). As previously described, AONs targeting the *DMD* gene aim to skip specific exons to restore the reading frame. This gene has 79 exons and patients present a large variety of mutations, mostly deletions and duplications, that require the design of specific AONs to treat a small subset to patients. The first such drug, eteplirsen, targeted exon 51 of *DMD*. Skipping this exon could potentially be therapeutic for 13% of DMD patients [3, 6]. Since then, golodirsen, viltolarsen, and casimersen have been approved, all applicable to decreasing percentages of patients [9, 49, 50].

All DMD exon-skipping drugs currently in the market are phosphorodiamidate morpholino oligomers (PMO). In contrast, the development of the first AON drug in clinical trials for this disorder, drisapersen (a 2'OMe/PS oligonucleotide) [51] as well as that of many others targeting *DMD* with the same chemistry were halted due to side effects [52]. Despite the apparent success of PMO chemistries to reach the market, these drugs are yet not very efficient, and their clinical outcomes are still poor. This is the main reason why they are yet to be approved in Europe, while in the USA and Japan have been given “accelerated approval” based on dystrophin protein expression as a surrogate endpoint, which is very low and there is debate about its clinical relevance [53]. Currently, several efforts are driven toward increasing the delivery efficacy of these drugs to the target tissue [32, 54]. Several next generation AONs targeting the same exon as eteplirsen (exon 51)

have been or are being developed. This is the case of the stereopure suvodirsén, which was halted after poor results in a phase I clinical trial (NCT03907072) or the peptide-conjugated PMO currently in Phase I/II clinical trials (MOMENTUM, NCT04004065).

While AONs for DMD do not offer yet the clinical benefits that were hoped to achieve at initial stages, the journey to their development has provided very valuable lessons to stakeholders interested in developing these drugs, particularly in the context of orphan drugs [55]. A drug that benefited from some of the previous knowledge was nusinersén, a 2'MOE/PS AON targeting another neuromuscular disorder (SMA). Nusinersén was approved only months after eteplirsén and has been quickly approved worldwide due to the robust clinical data derived from the clinical trials [18, 56]. As described before, this AON is based on an exon inclusion approach to restore the expression of SMN protein in motoneurons. In this case, the target tissue is treated directly by intrathecal infusion, circumventing any delivery hurdles that may have hampered the efficacy of AONs targeting muscle or other organs when delivered systemically. Indeed, nusinersén's delivery approach, chosen chemistry and formulation has been replicated in several *n*-of-1 clinical trials of other AONs targeting motoneurons, such as milasén and jacifusén (NCT04768972) [57] (*see* Subheading 4).

3.2 Examples of Clinical Trials for Eye Diseases

The eye is one of the most promising organs for therapeutic development. Among other characteristics, it is contained, easily accessible, and immune-privileged [58]. In fact, the first-ever FDA-approved AON (fomiversén) was a first-class oligonucleotide to treat human cytomegalovirus retinitis, an eye condition in immunocompromised patients [33–36]. Furthermore, a growing group of genes and mutations causing retinal diseases have been targeted at preclinical level using AONs. This includes pseudoexon exclusion for *CEP290* [59–63], *OPAI* [64], *CHM* [65] *USH2A* [66], and *ABCA4* [24–29]; splicing modulation for *USH2A* [10] and *CEP290* [12]; or transcript degradation for *NR2E3* [67] and *RHO* [68]. Three of these molecules are currently in different clinical trial phases detailed below.

The most advanced molecule in a clinical setting is sepfarsén (QR-110). This is a 17-mer 2'OMe/PS oligonucleotide aiming to correct the inclusion of a pseudoexon caused by a deep-intronic mutation in *CEP290*-associated autosomal recessive Leber congenital amaurosis [69]. In the phase 1/2 clinical trial (NCT03140969), all patients were injected with an initial loading dose of either 320 or 160 µg followed by a maintenance dose every 3 months (160 or 80 µg) [70, 71]. Interim results showed that sepfarsén was well tolerated and safe with no serious adverse events [70, 71]. Although the final results of the trial have not yet been published, the improvement that most patients showed led to the design and approval of a phase 2/3 clinical trial (Illuminate,

NCT03913143). This is a multi-center, double-masked, randomized, controlled, multiple-dose study to evaluate efficacy, safety, tolerability, and systemic exposure in patients older than 8 years carrying the specific mutation in at least one of the two alleles. Two different doses and a sham-procedure group will be assessed, for a total period of 2 years. In addition, two other clinical trials for the same molecule are ongoing. One is the extension of the phase 1/2 clinical trial to continue treating the patients of the first trial by administering sepfarsen every 3 months in both the already intervened and the contralateral eye (NCT03913130). The second is a multi-center, open-label, dose-escalation, and double-masked randomized controlled trial to evaluate safety and tolerability in children below age of 8 years old (Brighten, NCT04855045).

A multi-center phase 1/2 clinical trial to assess safety and tolerability of QR-421a (Stellar, NCT03780257) is currently ongoing. This 21-mer 2'MOE/PS oligonucleotide aims to skip the frequently mutated exon 13 of *USH2A* [10] causing autosomal recessive Usher syndrome or isolated retinitis pigmentosa. Preliminary results, presented in a press release seem to indicate that QR-421a is well tolerated with no serious adverse events. Furthermore, after treatment with this molecule, improvements in several measures of vision were detected. With these encouraging results, two preliminary phase 2/3 clinical trials have been designed in order to study different patient populations based on the best corrected visual acuity. Both trials will be double-masked, randomized, controlled, 24-month, and multiple-dose study (Sirius and Celeste).

The third molecule in a clinical setting is QR-1123, a gapmer designed to degrade the mutant allele (known as P23H) in the *RHO* gene [68], which has a dominant-negative effect leading to autosomal dominant retinitis pigmentosa. Thus, the hypothesis is that by degrading the allele carrying the mutation, the other allele will be able to produce a functional protein. This molecule is in an early stage of a multi-center open-label, double-masked, randomized, phase 1/2 trial (NCT04123626).

Other molecules for eye-related genetic diseases in late stages of preclinical development are QR-504a for *TCF4*-associated Fuchs endothelial corneal dystrophy and QR-411 for pseudoexon exclusion in *USH2A*-associated Usher syndrome or isolated retinitis pigmentosa.

As well as to target specific mutations, AONs have also been explored for multifactorial eye conditions. This is the case of primary open angle glaucoma, in which *TGF- β 2* was targeted with a 14-mer 3 + 3 LNA-modified gapmer in a phase I clinical trial. Results showed that the molecule was tolerated, safe and potentially clinically efficacious [72]. Besides this, other type of antisense molecules (small interference RNA, siRNA) have been clinically tested for glaucoma [73], dry eye syndrome [74], diabetic macular edema [75], and age-related macular degeneration [73, 76, 77].

4 Future of AON Trials and Personalized Medicine: $n = 1$ Trials?

In 2019, an AON molecule (milasen) to treat a single patient pushed the bounds of personalized medicine and raised many regulatory and ethical questions never explored before for genetic treatments [57, 78].

Milasen was customized exclusively for Mila, a child suffering from a form of Batten disease (neuronal ceroid lipofuscinosis 7) caused by the insertion of an SVA (SINE–VNTR–Alu) retrotransposon, with a detrimental effect on splicing, in the intron 6 of the *MFSD8* gene [57]. Using a 22-mer 2'MOE/PS AON it was possible to redirect splicing avoiding the insertion of the SVA in the final mRNA transcript. Besides the exclusivity of this treatment, another extraordinary achievement was that it took only 13 months to go from the clinical diagnosis to the first dosing: Mila had a clinical diagnosis in mid-November of 2016, the genetic defect was identified in May 2017, approval to proceed was received in January 2018 and first patient dosing occur in the same month.

The AON delivery regime via intrathecal bolus injection was highly similar to the one of nusinersen, the AON used for SMA [17, 18, 56]. The treatment did not show any safety concerns and the frequency and duration of the seizures was reduced. Unfortunately, despite the treatment had some effect, Mila passed away early 2021. Nevertheless, this study is the hallmark of personalized medicine, and although not all diseases are amenable for this type of therapies, it has highlighted this as a possible approach and managed to re-evaluate the speed and type of safety studies and regulatory requirements. In a similar development, a drug was designed and provided to patient suffering from amyotrophic lateral sclerosis (ALS) with mutations *FUS* gene, following the same delivery route as nusinersen and milasen. Unfortunately, this patient, Jaci Hermsstad, also died recently. However, the drug originally developed for this single patient, ION363 or jacifusen, is currently being tested in a phase III trial for patients with the same disease (NCT04768972). Thus, AON technology can be considered as a platform for individualized treatments which may, sometimes, be extended to other patients.

5 Hurdles

A drawback when compared to small molecule drugs is the relatively large size of AON molecules which limits their delivery into the cells where they exert their action. Therefore, their distribution is limited, their naked uptake is poor, and it is highly determined by the chemistry of their backbones [54]. Often, these AON molecules are not even able to reach their target organ. To circumvent

this, most of these AONs rely on their conjugation or formulation with different delivery systems to be able to reach and access their intracellular targets [32]. In addition, when delivered systemically, these molecules can barely reach the central nervous system due to the blood retina and brain barriers. However, as described before, local delivery of naked modified AONs to these specific organs have shown to be efficient and safe in several clinical trials [17, 18, 56, 70, 71, 79].

Another drawback is the high exposure of certain organs upon systemic delivery of AONs. For instance, after intravenous injection of AONs a significant proportion is taken by the liver and kidney. This limits the biodistribution to other tissues and derivate on toxic effects in these organs. However, many of the liver and kidney injuries were found when using high and not clinically relevant doses of AONs [32]. In that sense, novel delivery methods or conjugates are required to be able to target the organs of interest and bypass the high clearance by the liver and kidneys.

Finding proper models to assess the sequence-dependent efficacy and safety of AONs is still a pending issue. Their safety assessment is often performed in rodents, non-human primates, and human plasma. However, these studies only provide sequence- and chemical modification-specific effects. The generation of humanized models have provided very good results, however, generating a humanized animal model for every mutation to be targeted is not feasible nor ethical. It is also possible to generate almost any human cell from patient-derived cells reprogrammed to a pluripotent stage. While these models can provide good readouts at RNA, protein, or even functional levels the entire context will still be missing. Currently, significant efforts are being made in the generation of organ-on-chips. This technology allows the combination of multiple tissues or even organs to study the interaction between them and test therapeutic interventions [80, 81]. In addition, this technology enables other type of measurements that in the near future might be very valuable to perform drug screenings and evaluate the efficacy and safety of many molecules, including AONs [80–83].

Finally, clear guidelines and novel clinical trial designs are needed to explore the full therapeutic potential of AONs when investigated as treatments for rare diseases. The case of milasen has proven that this is possible and new of such trials are being planned.

6 Conclusions

The therapeutic potential of AONs has been, for many years, subject of speculation and theoretical discussion and, while these molecules were widely applied in a research laboratory setting, their

clinical application was anecdotal and limited to rare diseases. However, this landscape has recently changed completely thanks to several factors. On one hand, many of such drugs have been approved, being splice-switching AON and siRNA drugs at the forefront of this wave. Secondly, several breakthroughs in the delivery formulation of these drugs have increased the uptake of AONs targeting the liver and this has open wide open the field to consider these as reliable treatment options for several disorders where the liver is the target tissue. Thirdly, much more attention has been given to antisense technology due to the *n*-of-1 case of milasen. Lastly, RNA-therapies have gained extraordinary popularity due to vaccines against SAR-CoV-2 based on mRNA technology, highlighting the development of drugs based on nucleic acids. All of this will contribute to make these drugs a main resource in the therapeutic toolbox of the twenty-first century.

Acknowledgments

V.A-G holds a Miguel Servet Fellowship from the ISCIII (grants CP12/03057 and CPII17/00004), part-funded by ERDF/FEDER. V.A-G also acknowledges funding from Ikerbasque (Basque Foundation for Science). A.G. group is financially supported by the Foundation Fighting Blindness (PPA-0517-0717-RAD), the Curing Retinal Blindness Foundation as well as the Landelijke Stichting voor Blinden en Slechtienden and Stichting Oogfonds via Uitzicht 2019-17, together with Stichting Blindenhulp, Rotterdamse Stichting Blindenbelangen and Dowilwo. The funding organizations had no role in the design or conduct of this research and provided unrestricted grants. Both authors are members of the European COST Action DARTER (CA17103).

References

1. Arechavala-Gomez V, Khoo B, Aartsma-Rus A (2014) Splicing modulation therapy in the treatment of genetic diseases. *Appl Clin Genet* 7:245–252. <https://doi.org/10.2147/TACG.S71506>
2. Lewandowska MA (2013) The missing puzzle piece: splicing mutations. *Int J Clin Exp Pathol* 6(12):2675–2682
3. Arechavala-Gomez V, Graham IR, Popplewell LJ, Adams AM, Aartsma-Rus A, Kinali M, Morgan JE, van Deutekom JC, Wilton SD, Dickson G, Muntoni F (2007) Comparative analysis of antisense oligonucleotide sequences for targeted skipping of exon 51 during dystrophin pre-mRNA splicing in human muscle. *Hum Gene Ther* 18(9):798–810. <https://doi.org/10.1089/hum.2006.061>
4. Popplewell LJ, Adkin C, Arechavala-Gomez V, Aartsma-Rus A, de Winter CL, Wilton SD, Morgan JE, Muntoni F, Graham IR, Dickson G (2010) Comparative analysis of antisense oligonucleotide sequences targeting exon 53 of the human DMD gene: implications for future clinical trials. *Neuromuscul Disord* 20(2):102–110. <https://doi.org/10.1016/j.nmd.2009.10.013>
5. Kinali M, Arechavala-Gomez V, Feng L, Cirak S, Hunt D, Adkin C, Guglieri M, Ashton E, Abbs S, Nihoyannopoulos P, Garalda ME, Rutherford M, McCulley C,

- Popplewell L, Graham IR, Dickson G, Wood MJ, Wells DJ, Wilton SD, Kole R, Straub V, Bushby K, Sewry C, Morgan JE, Muntoni F (2009) Local restoration of dystrophin expression with the morpholino oligomer AVI-4658 in Duchenne muscular dystrophy: a single-blind, placebo-controlled, dose-escalation, proof-of-concept study. *Lancet Neurol* 8(10): 918–928. [https://doi.org/10.1016/S1474-4422\(09\)70211-X](https://doi.org/10.1016/S1474-4422(09)70211-X)
6. Cirak S, Arechavala-Gomez V, Guglieri M, Feng L, Torelli S, Anthony K, Abbs S, Garralda ME, Bourke J, Wells DJ, Dickson G, Wood MJ, Wilton SD, Straub V, Kole R, Shrewsbury SB, Sewry C, Morgan JE, Bushby K, Muntoni F (2011) Exon skipping and dystrophin restoration in patients with Duchenne muscular dystrophy after systemic phosphorodiamidate morpholino oligomer treatment: an open-label, phase 2, dose-escalation study. *Lancet* 378(9791):595–605. [https://doi.org/10.1016/S0140-6736\(11\)60756-3](https://doi.org/10.1016/S0140-6736(11)60756-3)
7. Anwar S, Yokota T (2020) Golodirsen for Duchenne muscular dystrophy. *Drugs Today* 56(8):491–504. <https://doi.org/10.1358/dot.2020.56.8.3159186>
8. Clemens PR, Rao VK, Connolly AM, Harper AD, Mah JK, Smith EC, McDonald CM, Zaidman CM, Morgenroth LP, Osaki H, Satou Y, Yamashita T, Hoffman EP, Investigators CD (2020) Safety, tolerability, and efficacy of viltolarsen in boys with Duchenne muscular dystrophy amenable to exon 53 skipping: a phase 2 randomized clinical trial. *JAMA Neurol* 77: 1. <https://doi.org/10.1001/jamaneurol.2020.1264>
9. Shirley M (2021) Casimersen: first approval. *Drugs* 81:875. <https://doi.org/10.1007/s40265-021-01512-2>
10. Dulla K, Slijkerman R, van Diepen HC, Albert S, Dona M, Beumer W, Turunen JJ, Chan HL, Schulkens IA, Vorthoren L, Besten CD, Buil L, Schmidt I, Miao J, Venselaar H, Zang J, Neuhauss SCF, Peters T, Broekman S, Pennings R, Kremer H, Platenburg G, Adamson P, de Vrieze E, van Wijk E (2021) Antisense oligonucleotide-based treatment of retinitis pigmentosa caused by USH2A exon 13 mutations. *Mol Ther* 29:2441. <https://doi.org/10.1016/j.ymthe.2021.04.024>
11. Pendse N, Lamas V, Maeder M, Pawlyk B, Gloskowski S, Pierce EA, Chen Z-Y, Liu Q (2020) Exon 13-skipped USH2A protein retains functional integrity in mice, suggesting an exon-skipping therapeutic approach to treat USH2A-associated disease. *bioRxiv*. <https://doi.org/10.1101/2020.02.04.934240>
12. Barny I, Perrault I, Michel C, Goudin N, Defoort-Dhellemmes S, Ghazi I, Kaplan J, Rozet JM, Gerard X (2019) AON-mediated exon skipping to bypass protein truncation in retinal dystrophies due to the recurrent CEP290 c.4723A>T mutation. Fact or fiction? *Genes (Basel)* 10(5):368. <https://doi.org/10.3390/genes10050368>
13. Goto M, Sawamura D, Nishie W, Sakai K, McMillan JR, Akiyama M, Shimizu H (2006) Targeted skipping of a single exon harboring a premature termination codon mutation: implications and potential for gene correction therapy for selective dystrophic epidermolysis bullosa patients. *J Invest Dermatol* 126(12): 2614–2620. <https://doi.org/10.1038/sj.jid.5700435>
14. Bremer J, Bornert O, Nystrom A, Gostynski A, Jonkman MF, Aartsma-Rus A, van den Akker PC, Pasmooij AM (2016) Antisense oligonucleotide-mediated exon skipping as a systemic therapeutic approach for recessive dystrophic epidermolysis bullosa. *Mol Ther Nucl Acids* 5(10):e379. <https://doi.org/10.1038/mtna.2016.87>
15. Ham KA, Aung-Htut MT, Fletcher S, Wilton SD (2020) Nonsequential splicing events alter antisense-mediated exon skipping outcome in COL7A1. *Int J Mol Sci* 21(20):7705. <https://doi.org/10.3390/ijms21207705>
16. Bornert O, Hogervorst M, Nauroy P, Bischof J, Swildens J, Athanasiou I, Tufa SF, Keene DR, Kiritsi D, Hainzl S, Muraier EM, Marinkovich MP, Platenburg G, Hausser I, Wally V, Ritsema T, Koller U, Haisma EM, Nystrom A (2021) QR-313, an antisense oligonucleotide, shows therapeutic efficacy for treatment of dominant and recessive dystrophic epidermolysis bullosa: a preclinical study. *J Invest Dermatol* 141(4):883–893.e886. <https://doi.org/10.1016/j.jid.2020.08.018>
17. Finkel RS, Chiriboga CA, Vajsar J, Day JW, Montes J, De Vivo DC, Yamashita M, Rigo F, Hung G, Schneider E, Norris DA, Xia S, Bennett CF, Bishop KM (2016) Treatment of infantile-onset spinal muscular atrophy with nusinersen: a phase 2, open-label, dose-escalation study. *Lancet* 388(10063):3017–3026. [https://doi.org/10.1016/S0140-6736\(16\)31408-8](https://doi.org/10.1016/S0140-6736(16)31408-8)
18. Finkel RS, Mercuri E, Darras BT, Connolly AM, Kuntz NL, Kirschner J, Chiriboga CA, Saito K, Servais L, Tizzano E, Topaloglu H, Tulinius M, Montes J, Glanzman AM, Bishop K, Zhong ZJ, Gheuens S, Bennett CF, Schneider E, Farwell W, De Vivo DC, Group ES (2017) Nusinersen versus sham control in infantile-onset spinal muscular atrophy. *N Engl*

- J Med 377(18):1723–1732. <https://doi.org/10.1056/NEJMoa1702752>
19. Lentz JJ, Jodelka FM, Hinrich AJ, McCaffrey KE, Farris HE, Spalitta MJ, Bazan NG, Duelli DM, Rigo F, Hastings ML (2013) Rescue of hearing and vestibular function by antisense oligonucleotides in a mouse model of human deafness. *Nat Med* 19(3):345–350. <https://doi.org/10.1038/nm.3106>
 20. Tomkiewicz TZ, Suárez-Herrera N, Cremers FPM, Collin RWJ, Garanto A (2021) Antisense oligonucleotide-based rescue of aberrant splicing defects caused by 15 pathogenic variants in ABCA4. *Int J Mol Sci* 22(9):4621
 21. Lim KH, Han Z, Jeon HY, Kach J, Jing E, Weyn-Vanhentenryck S, Downs M, Corrionero A, Oh R, Scharner J, Venkatesh A, Ji S, Liao G, Ticho B, Nash H, Aznarez I (2020) Antisense oligonucleotide modulation of non-productive alternative splicing upregulates gene expression. *Nat Commun* 11(1):3501. <https://doi.org/10.1038/s41467-020-17093-9>
 22. Jaganathan K, Kyriazopoulou Panagiotopoulou S, McRae JF, Darbandi SF, Knowles D, Li YI, Kosmicki JA, Arbelaez J, Cui W, Schwartz GB, Chow ED, Kanterakis E, Gao H, Kia A, Batzoglu S, Sanders SJ, Farh KK (2019) Predicting splicing from primary sequence with deep learning. *Cell* 176(3):535–548.e524. <https://doi.org/10.1016/j.cell.2018.12.015>
 23. Sangermano R, Khan M, Cornelis SS, Richelle V, Albert S, Garanto A, Elmelik D, Qamar R, Lugtenberg D, van den Born LI, Collin RWJ, Cremers FPM (2018) ABCA4 midigenes reveal the full splice spectrum of all reported noncanonical splice site variants in Stargardt disease. *Genome Res* 28(1):100–110. <https://doi.org/10.1101/gr.226621.117>
 24. Albert S, Garanto A, Sangermano R, Khan M, Bax NM, Hoyng CB, Zernant J, Lee W, Allikmets R, Collin RWJ, Cremers FPM (2018) Identification and rescue of splice defects caused by two neighboring deep-intronic ABCA4 mutations underlying Stargardt disease. *Am J Hum Genet* 102(4):517–527. <https://doi.org/10.1016/j.ajhg.2018.02.008>
 25. Bauwens M, Garanto A, Sangermano R, Naessens S, Weisschuh N, De Zaeytjij J, Khan M, Sadler F, Balikova I, Van Cauwenbergh C, Rosseel T, Bauwens J, De Leeneer K, De Jaegere S, Van Laethem T, De Vries M, Carss K, Arno G, Fakin A, Webster AR, de Ravel de l'Argentiere TJL, Sznajer Y, Vuylsteke M, Kohl S, Wissinger B, Cherry T, Collin RWJ, Cremers FPM, Leroy BP, De Baere E (2019) ABCA4-associated disease as a model for missing heritability in autosomal recessive disorders: novel noncoding splice, cis-regulatory, structural, and recurrent hypomorphic variants. *Genet Med* 21(8):1761–1771. <https://doi.org/10.1038/s41436-018-0420-y>
 26. Garanto A, Duijkers L, Tomkiewicz TZ, Collin RWJ (2019) Antisense oligonucleotide screening to optimize the rescue of the splicing defect caused by the recurrent deep-intronic ABCA4 variant c.4539+2001G>A in Stargardt disease. *Genes* 10(6):425. <https://doi.org/10.3390/genes10060452>
 27. Sangermano R, Garanto A, Khan M, Runhart EH, Bauwens M, Bax NM, van den Born LI, Khan MI, Cornelis SS, Verheij J, Pott JR, Thiadens A, Klaver CCW, Puech B, Meunier I, Naessens S, Arno G, Fakin A, Carss KJ, Raymond FL, Webster AR, Dhaenens CM, Stohr H, Grassmann F, Weber BHF, Hoyng CB, De Baere E, Albert S, Collin RWJ, Cremers FPM (2019) Deep-intronic ABCA4 variants explain missing heritability in Stargardt disease and allow correction of splice defects by antisense oligonucleotides. *Genet Med* 21(8):1751–1760. <https://doi.org/10.1038/s41436-018-0414-9>
 28. Khan M, Arno G, Fakin A, Parfitt DA, Dhooge PPA, Albert S, Bax NM, Duijkers L, Niblock M, Hau KL, Bloch E, Schiff ER, Piccolo D, Hogden MC, Hoyng CB, Webster AR, Cremers FPM, Cheetham ME, Garanto A, Collin RWJ (2020) Detailed phenotyping and therapeutic strategies for intronic ABCA4 variants in Stargardt disease. *Mol Ther Nucl Acids* 21:412–427. <https://doi.org/10.1016/j.omtn.2020.06.007>
 29. Tomkiewicz TZ, Suarez-Herrera N, Cremers FPM, Collin RWJ, Garanto A (2021) Antisense oligonucleotide-based rescue of aberrant splicing defects caused by 15 pathogenic variants in ABCA4. *Int J Mol Sci* 22(9):4621. <https://doi.org/10.3390/ijms22094621>
 30. Cremers FPM, Lee W, Collin RWJ, Allikmets R (2020) Clinical spectrum, genetic complexity and therapeutic approaches for retinal disease caused by ABCA4 mutations. *Prog Retin Eye Res* 79:100861. <https://doi.org/10.1016/j.preteyeres.2020.100861>
 31. Liang XH, Sun H, Nichols JG, Crooke ST (2017) RNase H1-dependent antisense oligonucleotides are robustly active in directing RNA cleavage in both the cytoplasm and the nucleus. *Mol Ther* 25(9):2075–2092. <https://doi.org/10.1016/j.ymthe.2017.06.002>

32. Hammond SM, Aartsma-Rus A, Alves S, Borges SE, Buijsen RAM, Collin RWJ, Covello G, Denti MA, Desvial LR, Echevarria L, Foged C, Gaina G, Garanto A, Goyenvallé AT, Guzowska M, Holodnuka I, Jones DR, Krause S, Lehto T, Montolio M, Van Roon-Mom W, Arechavala-Gomez V (2021) Delivery of oligonucleotide-based therapeutics: challenges and opportunities. *EMBO Mol Med* 13(4):e13243. <https://doi.org/10.15252/emmm.202013243>
33. Crooke ST (1998) Vitravene--another piece in the mosaic. *Antis Nucl Acid Drug Dev* 8(4): vii–viii. <https://doi.org/10.1089/oli.1.1998.8.vii>
34. Mulamba GB, Hu A, Azad RF, Anderson KP, Coen DM (1998) Human cytomegalovirus mutant with sequence-dependent resistance to the phosphorothioate oligonucleotide fomivirsen (ISIS 2922). *Antimicrob Agents Chemother* 42(4):971–973. <https://doi.org/10.1128/AAC.42.4.971>
35. Roehr B (1998) Fomivirsen approved for CMV retinitis. *J Int Assoc Phys AIDS Care* 4(10): 14–16
36. Jabs DA, Griffiths PD (2002) Fomivirsen for the treatment of cytomegalovirus retinitis. *Am J Ophthalmol* 133(4):552–556
37. Graham MJ, Lee RG, Bell TA III, Fu W, Mullick AE, Alexander VJ, Singleton W, Viney N, Geary R, Su J, Baker BF, Burkey J, Crooke ST, Crooke RM (2013) Antisense oligonucleotide inhibition of apolipoprotein C-III reduces plasma triglycerides in rodents, nonhuman primates, and humans. *Circ Res* 112(11): 1479–1490. <https://doi.org/10.1161/CIRCRESAHA.111.300367>
38. Geary RS, Baker BF, Crooke ST (2015) Clinical and preclinical pharmacokinetics and pharmacodynamics of mipomersen (kynamro ((R))): a second-generation antisense oligonucleotide inhibitor of apolipoprotein B. *Clin Pharmacokinet* 54(2):133–146. <https://doi.org/10.1007/s40262-014-0224-4>
39. Digenio A, Dunbar RL, Alexander VJ, Hompesch M, Morrow L, Lee RG, Graham MJ, Hughes SG, Yu R, Singleton W, Baker BF, Bhanot S, Crooke RM (2016) Antisense-mediated lowering of plasma apolipoprotein C-III by volanesorsen improves dyslipidemia and insulin sensitivity in type 2 diabetes. *Diabetes Care* 39(8):1408–1415. <https://doi.org/10.2337/dc16-0126>
40. Pechlaner R, Tsimikas S, Yin X, Willeit P, Baig F, Santer P, Oberhollenzer F, Egger G, Witztum JL, Alexander VJ, Willeit J, Kiechl S, Mayr M (2017) Very-low-density lipoprotein-associated apolipoproteins predict cardiovascular events and are lowered by inhibition of APOC-III. *J Am Coll Cardiol* 69(7): 789–800. <https://doi.org/10.1016/j.jacc.2016.11.065>
41. Aslesh T, Yokota T (2020) Development of antisense oligonucleotide gapmers for the treatment of dyslipidemia and lipodystrophy. *Methods Mol Biol* 2176:69–85. https://doi.org/10.1007/978-1-0716-0771-8_5
42. Benson MD, Waddington-Cruz M, Berk JL, Polydefkis M, Dyck PJ, Wang AK, Plante-Bordeneuve V, Barroso FA, Merlini G, Obici L, Scheinberg M, Brannagan TH III, Litchy WJ, Whelan C, Drachman BM, Adams D, Heitner SB, Conceicao I, Schmidt HH, Vita G, Campistol JM, Gamez J, Gorevic PD, Gane E, Shah AM, Solomon SD, Monia BP, Hughes SG, Kwok TJ, McEvoy BW, Jung SW, Baker BF, Ackermann EJ, Gertz MA, Coelho T (2018) Inotersen treatment for patients with hereditary transthyretin amyloidosis. *N Engl J Med* 379(1):22–31. <https://doi.org/10.1056/NEJMoal716793>
43. Dyck PJB, Coelho T, Waddington Cruz M, Brannagan TH III, Khella S, Karam C, Berk JL, Polydefkis MJ, Kincaid JC, Wiesman JF, Litchy WJ, Mauermann ML, Ackermann EJ, Baker BF, Jung SW, Guthrie S, Pollock M, Dyck PJ (2020) Neuropathy symptom and change: inotersen treatment of hereditary transthyretin amyloidosis. *Muscle Nerve* 62(4):509–515. <https://doi.org/10.1002/mus.27023>
44. de Vrieze E, Canas Martin J, Peijnenborg J, Martens A, Oostrik J, van den Heuvel S, Neveling K, Pennings R, Kremer H, van Wijk E (2021) AON-based degradation of c.151C>T mutant COCH transcripts associated with dominantly inherited hearing impairment DFNA9. *Mol Ther Nucl Acids* 24:274–283. <https://doi.org/10.1016/j.omtn.2021.02.033>
45. Maquat LE (2004) Nonsense-mediated mRNA decay: splicing, translation and mRNP dynamics. *Nat Rev Mol Cell Biol* 5(2):89–99. <https://doi.org/10.1038/nrm1310>
46. Disterer P, Al-Shawi R, Ellmerich S, Waddington SN, Owen JS, Simons JP, Khoo B (2013) Exon skipping of hepatic APOB pre-mRNA with splice-switching oligonucleotides reduces LDL cholesterol in vivo. *Mol Ther* 21(3): 602–609. <https://doi.org/10.1038/mt.2012.264>
47. Sud R, Geller ET, Schellenberg GD (2014) Antisense-mediated exon skipping decreases tau protein expression: a potential therapy for tauopathies. *Mol Ther Nucl Acids* 3:e180. <https://doi.org/10.1038/mtna.2014.30>

48. Raktoc RS, Rietveld MH, Out-Luiting JJ, Kruihof-de Julio M, van Zuijlen PP, van Doorn R, Ghalbzouri AE (2020) Exon skipping of TGFbetaRI affects signalling and ECM expression in hypertrophic scar-derived fibroblasts. *Scars Burn Heal* 6: 2059513120908857. <https://doi.org/10.1177/2059513120908857>
49. Aartsma-Rus A, Corey DR (2020) The 10th oligonucleotide therapy approved: golodirsen for Duchenne muscular dystrophy. *Nucl Acids Ther* 30(2):67–70. <https://doi.org/10.1089/nat.2020.0845>
50. Dhillon S (2020) Viltolarsen: first approval. *Drugs* 80(10):1027–1031. <https://doi.org/10.1007/s40265-020-01339-3>
51. van Deutekom JC, Janson AA, Ginjaar IB, Frankhuizen WS, Aartsma-Rus A, Bremmer-Bout M, den Dunnen JT, Koop K, van der Kooi AJ, Goemans NM, de Kimpe SJ, Ekhardt PF, Venneker EH, Platenburg GJ, Verschuuren JJ, van Ommen GJ (2007) Local dystrophin restoration with antisense oligonucleotide PRO051. *N Engl J Med* 357(26): 2677–2686. <https://doi.org/10.1056/NEJMoa073108>
52. Hilhorst N, Spanoudi-Kitrimi I, Goemans N, Morren MA (2019) Injection site reactions after long-term subcutaneous delivery of drisapersen: a retrospective study. *Eur J Pediatr* 178(2):253–258. <https://doi.org/10.1007/s00431-018-3272-1>
53. Aartsma-Rus A, Arechavala-Gomez V (2018) Why dystrophin quantification is key in the eteplirsen saga. *Nat Rev Neurol* 14(8): 454–456. <https://doi.org/10.1038/s41582-018-0033-8>
54. Godfrey C, Desviat LR, Smedsrod B, Pietri-Rouxel F, Denti MA, Disterer P, Lorain S, Nogales-Gadea G, Sardone V, Anwar R, El Andaloussi S, Lehto T, Khoo B, Brolin C, van Roon-Mom WM, Goyenvall A, Aartsma-Rus A, Arechavala-Gomez V (2017) Delivery is key: lessons learnt from developing splice-switching antisense therapies. *EMBO Mol Med* 9(5):545–557. <https://doi.org/10.15252/emmm.201607199>
55. Straub V, Balabanov P, Bushby K, Ensini M, Goemans N, De Luca A, Pereda A, Hemmings R, Campion G, Kaye E, Arechavala-Gomez V, Goyenvall A, Niks E, Veldhuizen O, Furlong P, Stoyanova-Beninska V, Wood AJ, Johnson A, Mercuri E, Muntoni F, Sepodes B, Haas M, Vroom E, Aartsma-Rus A (2016) Stakeholder cooperation to overcome challenges in orphan medicine development: the example of Duchenne muscular dystrophy. *Lancet Neurol* 15(8): 882–890. [https://doi.org/10.1016/S1474-4422\(16\)30035-7](https://doi.org/10.1016/S1474-4422(16)30035-7)
56. Mercuri E, Darras BT, Chiriboga CA, Day JW, Campbell C, Connolly AM, Iannaccone ST, Kirschner J, Kuntz NL, Saito K, Shieh PB, Tulinius M, Mazzone ES, Montes J, Bishop KM, Yang Q, Foster R, Gheuens S, Bennett CF, Farwell W, Schneider E, De Vivo DC, Finkel RS, Group CS (2018) Nusinersen versus sham control in later-onset spinal muscular atrophy. *N Engl J Med* 378(7):625–635. <https://doi.org/10.1056/NEJMoa1710504>
57. Kim J, Hu C, Moufawad El Achkar C, Black LE, Douville J, Larson A, Pendergast MK, Goldkind SF, Lee EA, Kuniholm A, Soucy A, Vaze J, Belur NR, Fredriksen K, Stojkovska I, Tsytyskova A, Armant M, DiDonato RL, Choi J, Cornelissen L, Pereira LM, Augustine EF, Genetti CA, Dies K, Barton B, Williams L, Goodlett BD, Riley BL, Pasternak A, Berry ER, Pflock KA, Chu S, Reed C, Tyndall K, Agrawal PB, Beggs AH, Grant PE, Urion DK, Snyder RO, Waisbren SE, Poduri A, Park PJ, Patterson A, Biffi A, Mazzulli JR, Bodamer O, Berde CB, Yu TW (2019) Patient-customized oligonucleotide therapy for a rare genetic disease. *N Engl J Med* 381(17):1644–1652. <https://doi.org/10.1056/NEJMoa1813279>
58. Vazquez-Dominguez I, Garanto A, Collin RWJ (2019) Molecular therapies for inherited retinal diseases-current standing, opportunities and challenges. *Genes* 10(9):654. <https://doi.org/10.3390/genes10090654>
59. Collin RW, den Hollander AI, van der Velde-Visser SD, Bennicelli J, Bennett J, Cremers FP (2012) Antisense oligonucleotide (AON)-based therapy for leber congenital amaurosis caused by a frequent mutation in CEP290. *Mol Ther Nucl Acids* 1:e14. <https://doi.org/10.1038/mtna.2012.3>
60. Gerard X, Perrault I, Hancin S, Silva E, Bigot K, Defoort-Delhemmes S, Rio M, Munnich A, Scherman D, Kaplan J, Kichler A, Rozet JM (2012) AON-mediated exon skipping restores ciliation in fibroblasts harboring the common leber congenital amaurosis CEP290 mutation. *Mol Ther Nucl Acids* 1: e29. <https://doi.org/10.1038/mtna.2012.21>
61. Garanto A, Chung DC, Duijkers L, Corral-Serrano JC, Messchaert M, Xiao R, Bennett J, Vandenberghe LH, Collin RW (2016) In vitro and in vivo rescue of aberrant splicing in CEP290-associated LCA by antisense oligonucleotide delivery. *Hum Mol Genet* 25(12): 2552–2563. <https://doi.org/10.1093/hmg/ddw118>
62. Duijkers L, van den Born LI, Neidhardt J, Bax NM, Pierrache LHM, Klevering BJ, Collin

- RWJ, Garanto A (2018) Antisense oligonucleotide-based splicing correction in individuals with leber congenital amaurosis due to compound heterozygosity for the c.2991+1655A>G mutation in CEP290. *Int J Mol Sci* 19(3):753. <https://doi.org/10.3390/ijms19030753>
63. Dulla K, Aguila M, Lane A, Jovanovic K, Parfitt DA, Schulkens I, Chan HL, Schmidt I, Beumer W, Vorthoren L, Collin RWJ, Garanto A, Duijkers L, Brugulat-Panes A, Semo M, Vugler AA, Biasutto P, Adamson P, Cheetham ME (2018) Splice-modulating oligonucleotide QR-110 restores CEP290 mRNA and function in human c.2991+1655A>G LCA10 models. *Mol Ther Nucl Acids* 12:730–740. <https://doi.org/10.1016/j.omtn.2018.07.010>
 64. Bonifert T, Gonzalez Menendez I, Battke F, Theurer Y, Synofzik M, Schols L, Wissinger B (2016) Antisense oligonucleotide mediated splice correction of a deep intronic mutation in OPA1. *Mol Ther Nucl Acids* 5(11):e390. <https://doi.org/10.1038/mtna.2016.93>
 65. Garanto A, van der Velde-Visser SD, Cremers FPM, Collin RWJ (2018) Antisense oligonucleotide-based splice correction of a deep-intronic mutation in CHM underlying choroideremia. *Adv Exp Med Biol* 1074: 83–89. https://doi.org/10.1007/978-3-319-75402-4_11
 66. Slijkerman RW, Vache C, Dona M, Garcia-Garcia G, Claustres M, Hettterschijs L, Peters TA, Hartel BP, Pennings RJ, Millan JM, Aller E, Garanto A, Collin RW, Kremer H, Roux AF, Van Wijk E (2016) Antisense oligonucleotide-based splice correction for USH2A-associated retinal degeneration caused by a frequent deep-intronic mutation. *Mol Ther Nucl Acids* 5(10):e381. <https://doi.org/10.1038/mtna.2016.89>
 67. Naessens S, Ruysschaert L, Lefever S, Coppieeters F, De Baere E (2019) Antisense oligonucleotide-based downregulation of the G56R pathogenic variant causing NR2E3-associated autosomal dominant retinitis pigmentosa. *Genes* 10(5):363. <https://doi.org/10.3390/genes10050363>
 68. Murray SF, Jazayeri A, Matthes MT, Yasumura D, Yang H, Peralta R, Watt A, Freier S, Hung G, Adamson PS, Guo S, Monia BP, LaVail MM, McCaleb ML (2015) Allele-specific inhibition of rhodopsin with an antisense oligonucleotide slows photoreceptor cell degeneration. *Invest Ophthalmol Vis Sci* 56(11):6362–6375. <https://doi.org/10.1167/iovs.15-16400>
 69. den Hollander AI, Koenekoop RK, Yzer S, Lopez I, Arends ML, Voeselek KE, Zonneveld MN, Strom TM, Meitinger T, Brunner HG, Hoyng CB, van den Born LJ, Rohrschneider K, Cremers FPM (2006) Mutations in the CEP290 (NPHP6) gene are a frequent cause of Leber congenital amaurosis. *Am J Hum Genet* 79(3):556–561. <https://doi.org/10.1086/507318>
 70. Cideciyan AV, Jacobson SG, Drack AV, Ho AC, Charng J, Garafalo AV, Roman AJ, Sumaroka A, Han IC, Hochstedler MD, Pfeiffer WL, Sohn EH, Taiel M, Schwartz MR, Biasutto P, Wit W, Cheetham ME, Adamson P, Rodman DM, Platenburg G, Tome MD, Balikova I, Nerinckx F, Zaeytijd J, Van Cauwenbergh C, Leroy BP, Russell SR (2019) Effect of an intravitreal antisense oligonucleotide on vision in Leber congenital amaurosis due to a photoreceptor cilium defect. *Nat Med* 25(2):225–228. <https://doi.org/10.1038/s41591-018-0295-0>
 71. Cideciyan AV, Jacobson SG, Ho AC, Garafalo AV, Roman AJ, Sumaroka A, Krishnan AK, Swider M, Schwartz MR, Girach A (2021) Durable vision improvement after a single treatment with antisense oligonucleotide sepo-farsen: a case report. *Nat Med* 27:785. <https://doi.org/10.1038/s41591-021-01297-7>
 72. Pfeiffer N, Voykov B, Renieri G, Bell K, Richter P, Weigel M, Thieme H, Wilhelm B, Lorenz K, Feindor M, Wosikowski K, Janicot M, Packert D, Rommich R, Mala C, Fettes P, Leo E (2017) First-in-human phase I study of ISTH0036, an antisense oligonucleotide selectively targeting transforming growth factor beta 2 (TGF-beta2), in subjects with open-angle glaucoma undergoing glaucoma filtration surgery. *PLoS One* 12(11): e0188899. <https://doi.org/10.1371/journal.pone.0188899>
 73. Moreno-Montanes J, Sadaba B, Ruz V, Gomez-Guiu A, Zarranz J, Gonzalez MV, Paneda C, Jimenez AI (2014) Phase I clinical trial of SYL040012, a small interfering RNA targeting beta-adrenergic receptor 2, for lowering intraocular pressure. *Mol Ther* 22(1): 226–232. <https://doi.org/10.1038/mt.2013.217>
 74. Benitez-Del-Castillo JM, Moreno-Montanes J, Jimenez-Alfaro I, Munoz-Negrete FJ, Turman K, Palumaa K, Sadaba B, Gonzalez MV, Ruz V, Vargas B, Paneda C, Martinez T, Bleau AM, Jimenez AI (2016) Safety and efficacy clinical trials for SYL1001, a novel short interfering RNA for the treatment of dry eye disease. *Invest Ophthalmol Vis Sci* 57(14):

- 6447–6454. <https://doi.org/10.1167/iov.16-20303>
75. Nguyen QD, Schachar RA, Nduaka CI, Sperling M, Basile AS, Klamerus KJ, Chi-Burris K, Yan E, Paggiarino DA, Rosenblatt I, Aitchison R, Erlich SS, Group DCS (2012) Dose-ranging evaluation of intravitreal siRNA PF-04523655 for diabetic macular edema (the DEGAS study). *Invest Ophthalmol Vis Sci* 53(12):7666–7674. <https://doi.org/10.1167/iov.12-9961>
 76. Kaiser PK, Symons RC, Shah SM, Quinlan EJ, Tabandeh H, Do DV, Reisen G, Lockridge JA, Short B, Guercioli R, Nguyen QD, Sirna-027 Study I (2010) RNAi-based treatment for neovascular age-related macular degeneration by Sirna-027. *Am J Ophthalmol* 150(1):33–39.e32. <https://doi.org/10.1016/j.ajo.2010.02.006>
 77. Nguyen QD, Schachar RA, Nduaka CI, Sperling M, Klamerus KJ, Chi-Burris K, Yan E, Paggiarino DA, Rosenblatt I, Aitchison R, Erlich SS, Group MCS (2012) Evaluation of the siRNA PF-04523655 versus ranibizumab for the treatment of neovascular age-related macular degeneration (MONET Study). *Ophthalmology* 119(9):1867–1873. <https://doi.org/10.1016/j.optha.2012.03.043>
 78. Mullard A (2020) N-of-1 drugs push biopharma frontiers. *Nat Rev Drug Discov* 19(3):151–153. <https://doi.org/10.1038/d41573-020-00027-x>
 79. Tabrizi SJ, Leavitt BR, Landwehrmeyer GB, Wild EJ, Saft C, Barker RA, Blair NF, Craufurd D, Priller J, Rickards H, Rosser A, Kordasiewicz HB, Czech C, Swayze EE, Norris DA, Baumann T, Gerlach I, Schobel SA, Paz E, Smith AV, Bennett CF, Lane RM, Phase 1-2a I-HSST (2019) Targeting huntingtin expression in patients with Huntington's disease. *N Engl J Med* 380(24):2307–2316. <https://doi.org/10.1056/NEJMoa1900907>
 80. Bhise NS, Ribas J, Manoharan V, Zhang YS, Polini A, Massa S, Dokmeci MR, Khademhosseini A (2014) Organ-on-a-chip platforms for studying drug delivery systems. *J Control Release* 190:82–93. <https://doi.org/10.1016/j.jconrel.2014.05.004>
 81. Kimura H, Sakai Y, Fujii T (2018) Organ/body-on-a-chip based on microfluidic technology for drug discovery. *Drug Metab Pharmacokinet* 33(1):43–48. <https://doi.org/10.1016/j.dmpk.2017.11.003>
 82. Mittal R, Woo FW, Castro CS, Cohen MA, Karanxha J, Mittal J, Chhibber T, Jhaveri VM (2019) Organ-on-chip models: implications in drug discovery and clinical applications. *J Cell Physiol* 234(6):8352–8380. <https://doi.org/10.1002/jcp.27729>
 83. Jodat YA, Kang MG, Kiaee K, Kim GJ, Martinez AFH, Rosenkranz A, Bae H, Shin SR (2018) Human-derived organ-on-a-chip for personalized drug development. *Curr Pharm Des* 24(45):5471–5486. <https://doi.org/10.2174/1381612825666190308150055>

Open Access This chapter is licensed under the terms of the Creative Commons Attribution 4.0 International License (<http://creativecommons.org/licenses/by/4.0/>), which permits use, sharing, adaptation, distribution and reproduction in any medium or format, as long as you give appropriate credit to the original author(s) and the source, provide a link to the Creative Commons license and indicate if changes were made.

The images or other third party material in this chapter are included in the chapter's Creative Commons license, unless indicated otherwise in a credit line to the material. If material is not included in the chapter's Creative Commons license and your intended use is not permitted by statutory regulation or exceeds the permitted use, you will need to obtain permission directly from the copyright holder.



Part II

Design and Formulation of Antisense Technology



Design of Bifunctional Antisense Oligonucleotides for Exon Inclusion

Haiyan Zhou 

Abstract

Bifunctional antisense oligonucleotide (AON) is a specially designed AON to regulate pre-messenger RNA (pre-mRNA) splicing of a target gene. It is composed of two domains. The antisense domain contains sequences complementary to the target gene. The tail domain includes RNA sequences that recruit RNA binding proteins which may act positively or negatively in pre-mRNA splicing. This approach can be designed as targeted oligonucleotide enhancers of splicing, named TOES, for exon inclusion; or as targeted oligonucleotide silencers of splicing, named TOSS, for exon skipping. Here, we provide detailed methods for the design of TOES for exon inclusion, using *SMN2* exon 7 splicing as an example. A number of annealing sites and the tail sequences previously published are listed. We also present methodology of assessing the effects of TOES on exon inclusion in fibroblasts cultured from a SMA patient. The effects of TOES on *SMN2* exon 7 splicing were validated at RNA level by PCR and quantitative real-time PCR, and at protein level by western blotting.

Key words Antisense oligonucleotide, Bifunctional antisense, Pre-mRNA splicing, TOES, Splice switching, Exon inclusion, Exon skipping

1 Introduction

Harnessing antisense oligonucleotides (AONs) to redirect the altered pre-messenger RNA (pre-mRNA) splicing and modulate target gene expression is an efficient therapeutic strategy for genetic disorders associated with alternative splicing. A number of AON approaches have been investigated on redirecting pre-mRNA splicing. The original strategy is to use AONs complementary to a cryptic splice site to prevent its use and favored selection of the authentic site [1]. This approach has been used regularly to alter the proportion of splice isoforms produced from mutated genes or alternative splicing units. In addition to blocking the splice sites, alternative splicing events are often controlled by regulatory proteins bound to exonic and intronic elements located beyond the alternative splice sites. A valid approach is to use AONs to directly

target exonic or intronic elements by blocking the binding of regulatory proteins to these elements that are involved in pre-mRNA splicing. This strategy has been successfully used to augment the exon 7 inclusion in *SMN2* gene by using a short AON to target an intronic splicing silencer (ISS) within the gene [2–5]. Nusinersen, an 18-mer AON annealing to the ISS-N1 element in *SMN2* intron 7 is the first antisense drug approved by the US Food and Drug Administration (FDA) for treatment of any types of spinal muscular atrophy (SMA) [6–8]. This strategy has also been proved to be very effective in Duchene muscular dystrophy (DMD) by promoting the skipping of an exon in the *DMD* gene to restore the interrupted reading frame hence partial rescue of the functional dystrophin protein [9, 10]. Three AON drugs, eteplirsen for exon 51 skipping and golodirsen and viltolarsen for exon 53 skipping in the *DMD* gene, have been approved by the FDA for treatment of DMD [11–13].

The other splice switching approach is the use of bifunctional oligonucleotides to increase the number of positively or negatively acting signals in an exon or intron and to regulate the alternative splicing. The oligonucleotides were designed with one domain (the antisense domain) annealing to the target exon or intron, and another domain (the tail domain) containing a sequence that either recruits RNA binding proteins involved in pre-mRNA splicing [14] or is made of a synthetic protein domain covalently linked to the antisense domain [15]. This approach may be designed as targeted oligonucleotide enhancers of splicing (TOES) for exon inclusion [14, 16], or as targeted oligonucleotide silencers of splicing (TOSS) for exon skipping [17].

The effectiveness of TOES as a potential therapy for SMA by augmenting exon 7 splicing in *SMN2* gene has been approved both in vitro in cellular model [14, 16] and in vivo in mouse model [18–20]. A bifunctional oligonucleotide targeted to *SMN2* exon 7 was expressed in transgenic mice within a modified U7 snRNA gene. Expression of the TOES-U7 RNA in a mouse model of SMA produced a substantial improvement in function and lifespan [20]. Two other bifunctional oligonucleotides targeting the intronic splicing silencers in *SMN2* intron 6 and intron 7, which have the dual effects of blocking the silencer and recruiting activator proteins, also showed the potential therapeutic effects in the transgenic mouse models of SMA [18, 19].

We describe here the details in design of bifunctional oligonucleotide for exon inclusion by correcting *SMN2* exon 7 splicing as an example (Fig. 1). TOES oligonucleotides are designed to contain two domains, an antisense domain complementary to sequences of *SMN2* gene and a tail domain comprising sequences known as binding moieties for splicing activator proteins. The following design principles for TOES oligonucleotides are followed: (1) the antisense sequence may anneal to the potential

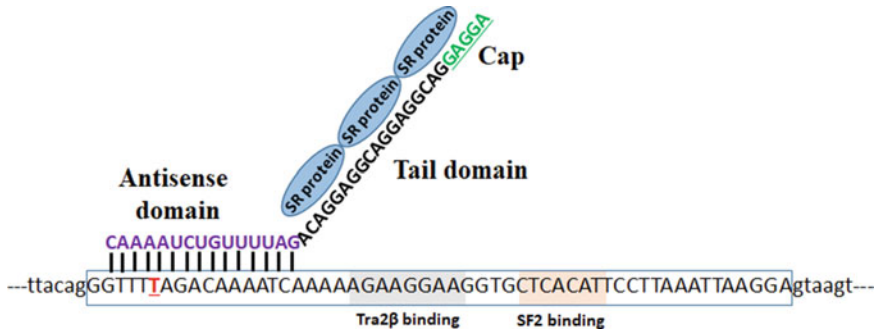


Fig. 1 Design of TOES to promote *SMN2* exon 7 inclusion. The sequence of *SMN2* exon 7 is in upper case and the flanking introns in lower case. Nucleotide 6 in *SMN2* exon 7 is T (in red). Two shaded sequences are the binding sites of Tra2 β and SF2/ASF, respectively. TOES is designed with two functional parts, the antisense domain to anneal to nucleotides 2–16 in *SMN2* exon 7, the tail domain containing 3 repeats of “GGAGGAC” motifs to recruit the SR protein SRSF1. Cap contains five nucleotides at the 5'-end of the tail (in green, which is chemically modified)

splicing silencer binding sites in either intron 6, exon 7 or intron 7, and should avoid any splicing enhancer binding sites; (2) a number of splicing enhancer motifs (e.g. SF2/ASF, SRSF1, and hTra2 β 1) may be included in the tail domain to improve the effectiveness of the oligonucleotides; (3) chemical modification can be applied to the antisense sequence, but not to the tail domain, which may inactive protein binding to the tail domain. The effects on exon inclusion are evaluated at RNA and protein levels in fibroblasts cultured from a patient with type II SMA carrying three copies of *SMN2* gene.

2 Materials

2.1 AON Design

1. Online software to identify splicing motifs, e.g., Human Splicing Finder (<http://www.umd.be/HSF/HSF.shtml>).
2. Online software to predict the secondary structures of the target gene and AONs (<http://rna.urmc.rochester.edu/RNAstructure.html>).
3. Online software to calculate oligonucleotide properties on annealing temperature, GC content, and self-complementary (<http://biotools.nubic.northwestern.edu/OligoCalc.html>).

2.2 Synthesis and Preparation of Bifunctional Oligonucleotides

1. Oligonucleotides are synthesized commercially by Eurogentec Ltd. (www.eurogentec.com).
2. RNase and DNase-free distilled water (*see Note 1*).
3. RNase and DNasefree 1.5 mL Eppendorf tubes.

2.3 Culture of Skin Fibroblasts from SMA Patient

1. Growth medium: Dulbecco's modified eagle medium (DMEM), 10% Fetal Bovine Serum (FBS), 1% Glutamax.
2. Trypsin-EDTA.
3. Phosphate-buffered saline (PBS).
4. Incubator set at 37 °C and 5% CO₂.

2.4 Fibroblast Transfection

1. Transfection reagent (e.g. Lipofectamine 2000).
2. Reduced serum medium for transfection (e.g. Opti-MEM).
3. 6 well plate or 35 mm diameter culture dish.
4. Sterile 1.5 mL Eppendorf tubes.

2.5 RNA Extraction

1. RNA isolation kit.
2. β-mercaptoethanol.
3. 70% ethanol (molecular grade).
4. RNase-free water.
5. 1.5 mL RNase-free Eppendorf tubes.
6. NanoDrop spectrophotometer.

2.6 cDNA Synthesis

1. cDNA synthesis kit.
2. Thermocycler.
3. 0.2 mL PCR tubes.

2.7 Polymerase Chain Reaction (PCR)

1. cDNA template from Subheading 2.6.
2. Taq Polymerase.
3. Primers (10 μM forward primer and 10 μM reverse primer). Primers sequences are shown in Table 1.
4. PCR buffer: 10× PCR buffer, 10 mM dNTPs, 50 mM MgCl₂, Taq DNA polymerase (5 U/μL), and nuclease-free water.
5. 0.2 mL PCR tubes.
6. Thermocycler.
7. Tris–Borate–EDTA 1× (TBE) buffer.
8. Agarose.
9. DNA gel stain.
10. Loading buffer.
11. DNA ladder.
12. Gel imaging system.

2.8 Quantitative Real-Time PCR

1. cDNA template from Subheading 2.6.
2. qPCR primers (10 pmol/μL each). Sequences are shown in Table 1.

Table 1**Sequences of primers used for exon 7 inclusion quantification by PCR and quantitative real-time PCR**

Assay	Products	Sequences (5'–3')	Annealing T _m (°C)
PCR	Full-length SMN2 (505 bp)	F: CTC CCA TAT GTC CAG ATT CTC TT	55
	Δ7 SMN2 (451 bp)	R: CTA CAA CAC CCT TCT CAC AG	
qRT-PCR	Full-length SMN2 (133 bp)	F: ATA CTG GCT ATT ATA TGG GTT TT	60
	Δ7 SMN2 (125 bp)	R: TCC AGA TCT GTC TGA TCG TTT C F: TGG ACC ACC AAT AAT TCC CC R: ATG CCA GCA TTT CCA TAT AAT AGC C	

3. Universal SYBR Green Master Mix.
4. 96-well real-time PCR plate.
5. Sealing film.
6. Real-Time PCR Thermal Cycler.

2.9 Western Blotting

1. Protein extraction buffer: 0.25% SDS, 75 mM Tris–HCl (pH 6.8), or RIPA buffer.
2. Protease inhibitor cocktail tablets.
3. Pierce BCA Protein Assay Kit.
4. PBST washing buffer (PBS, pH 7.4, 0.1% Tween 20).
5. Mini gel tank and blot transfer set.
6. NuPAGE 10% Bis-Tris precast gels, LDS sample buffer (4×), SDS running buffer (20×), antioxidant, sample reducing buffer, transfer buffer (20×), methanol.
7. Protein molecular weight ladder.
8. PVDF membrane.
9. Odyssey blocking buffer for PVDF membrane blocking.
10. Antibodies: mouse anti-SMN monoclonal antibody (BD Transduction Laboratories), mouse anti-β-tubulin monoclonal antibody (Sigma), IRDye 800CW-conjugated goat anti-mouse secondary antibody (Li-Cor).
11. Odyssey imaging instrument to quantify western blot signals.

3 Methods**3.1 Design of Bifunctional Oligonucleotides**

1. Predict the potential binding motifs of the negative splicing regulator heterogeneous nuclear ribonucleoprotein A1 (hnRNP A1) in the target intron or exon sequences, using *Human Splicing Finder* online software.

2. Other splicing repressors, such as intronic splicing silencers and exonic splicing silencers, may also be identified in the literature. A number of annealing sites in intron 6, exon 7, and intron 7 have been reported to augment *SMN2* exon 7 splicing by bifunctional AONs (Table 2) (*see Note 2*).
3. AONs, of 15–20 mer in length, are designed to anneal to the potential binding sites of hnRNP A1 or other splicing silencers.
4. The GC content of each AON sequence should be 40–65%, with an ideal content of approximately 60%.
5. Avoid four consecutive “G,” strong secondary structure or self-complementary sequences, and self-dimers.
6. Chemical modifications, e.g., 2'-*O*-methyl and locked nucleic acid (LNA), may be applied to the antisense sequence to improve stability and increase binding affinity.
7. Select the tail domain. Examples are listed in Table 2.
8. No chemical modifications are recommended in the tail domain except the cap sequence (Fig. 1) [16] (*see Note 3*).

3.2 Transfection of SMA Fibroblasts

1. Seed the cells in a 6-well plate at a concentration of 2×10^5 cells per well, which gives 80% confluence on the next day.
2. Cells are cultured in 2 mL of growth medium for 24 h.
3. 24 h later, change the growth medium to 1 mL Opti-MEM and leave the cells in the incubator during the preparation of transfection mixes.
4. Prepare the transfection reagent mixes in sterile 1.5 mL tubes. For each sample, prepare two mixes: the first mix (Mix A) contains 100 μ L Opti-MEM and 1 μ L AON at desired concentration (e.g. 1 μ L AON at 100 μ M to get a 100 nM final concentration). While for the mock control add only 100 μ L Opti-MEM. The second mix (Mix B) contains 100 μ L Opti-MEM and 5 μ L Lipofectamine 2000.
5. Mix the AON-containing tube (Mix A) with the lipofectamine-containing tube (Mix B) at a ratio of 1:1 (100 μ L + 100 μ L).
6. Incubate the transfection mix for 20 min at room temperature (RT).
7. Add 800 μ L Opti-MEM in the transfection mix to top it up to a final volume of 1 mL.
8. Remove Opti-MEM from the 6 well plate and replace with 1 mL transfection mix in each well.
9. Incubate the plate for at least 6 h at 37 °C with 5% CO₂ (*see Note 4*).

Table 2
The reported bi-functional AONs designed for SMN2 exon 7 inclusion

Intron/ exon	Antisense binding domain	Sequence of the antisense domain (5'–3')	Sequence of the tail domain (5'–3')	Recruiting protein	Reference
Exon 7	hnRNP A1 (ESS)	GAUUUUGUCUAAAAC	ACAGGAGGCAGGAGGAGGA	SRSF1	[5, 7]
Intron 7	hnRNP A1 binding site (ISS-N1)	GAUUCACUUUUCAUAAUUGCUGG	CACACGACACACGACACACGA	SF2/ASF	[10]
Intron 7	hnRNP A1 binding site (ISS-N1)	GAUUCACUUUUCAUAAUUGCUGG	GAAGGAGGGAAGGAGGGAAGGAGG	hTra2β1	[10]
Intron 6	Element 1 (E1)	CUAUUAUAGAUAGUUA UUCAACAAA	CACACGACACACGACACACGA	SF2/ASF	[9]
Intron 6	Element 1 (E1)	CUAUUAUAGAUAGUUA UUCAACAAA	GAAGGAGGGAAGGAGGGAAGGAGG	hTra2β1	[9]
Intron 7	hnRNP A1 binding site (ISS-N1)	AGUAAGAUUCACUUU	UGUGUGUGUGUGUGUGUG	TDP-43	[8]

3.3 Splicing Assay of Bifunctional AONs on SMN2 Exon 7 Inclusion at RNA Level

1. Extract RNA from SMA fibroblasts using RNeasy Mini Kit according to manufacturer's instruction.
2. Reverse transcription: the cDNA is synthesized from 500 ng RNA using cDNA Synthesis kit according to manufacturer's instruction.
3. PCR of *SMN2* transcripts: Use 1 μ L cDNA in a 25 μ L PCR reaction with 500 pmol of each primer (Table 1), 200 μ M of dNTPs, 1.5 mM $MgCl_2$, 2.5 units of Taq polymerase and 1 \times PCR buffer. The PCR amplification program is as follows: 1 cycle with 3 min at 94 $^{\circ}$ C (initial denaturation), 25–30 subsequent cycles of 30 s at 94 $^{\circ}$ C (denaturation), 30 s at 55 $^{\circ}$ C (annealing), and 30 s at 72 $^{\circ}$ C (extension), followed by a final 10-min extension at 72 $^{\circ}$ C. Check an aliquot of the PCR product (5–10 μ L) in 1.5% agarose gel electrophoresis and SYBR safe DNA stain using an UV transilluminator. The top band is the full-length *SMN2* product (505 bp). The lower band is the product without exon 7 ($\Delta 7$ *SMN2*, 451 bp).
4. Quantitative real-time PCR of full-length and $\Delta 7$ *SMN2* transcripts: product specific primers (Table 1), cDNA and 1 \times PCR Master mix are mixed in a 20 μ L PCR reaction. The program includes activation at 95 $^{\circ}$ C for 3 min, 40 cycles of 95 $^{\circ}$ C for 10 s, and 60 $^{\circ}$ C for 1 min. The cycle at which the amount of fluorescence is above the threshold (C_t) is detected. For quantification, it is possible to use the standard curve method produced from serial dilutions of cDNA from untreated SMA fibroblasts, or the $\Delta\Delta C_t$ method. Normalize the ratios of full-length *SMN2* and $\Delta 7$ *SMN2* to a housekeeping gene (e.g. *HPRT1* or *GAPDH*) (see Note 5).

3.4 Bifunctional AONs on Restoring SMN Protein Measured by Western Blotting

1. Remove culture medium from the well. Add 100 μ L ice-cold lysis buffer to the cells. Keep on ice for 5–10 min. Collect lysates using cell scrapers to fresh 1.5 mL Eppendorf tube and homogenize thoroughly with pipette.
2. Centrifuge at 12,000 $\times g$ and 4 $^{\circ}$ C for 10 min. Transfer the supernatant to a fresh tube.
3. Measure protein concentration by a NanoDrop spectrophotometer using the Pierce BCA Protein Assay Kit according to the manufacturer's instructions.
4. Load 5 mg total protein into NuPAGE precast gels and then electrophorese.
5. Transfer electrophoretically separated proteins from the gel to a PVDF membrane.
6. Block the PVDF membrane for 1 h in blocking buffer.
7. Incubate the membrane with the primary antibodies at 4 $^{\circ}$ C overnight on a shaker.

8. Wash the PVDF membrane for 3×10 min in PBST buffer.
9. Incubate the PVDF membrane with fluorescence secondary antibody for 1 h at room temperature.
10. Wash for 3×10 min in PBST and detect bands using the Odyssey Imaging software (Image Studio).

4 Notes

1. DEPC-treated RNase-free water should be avoided to dissolve oligonucleotides. Dissolved AONs should be aliquoted and stored at -20°C and avoid repeated freeze-thaw.
2. For TOES design, the most efficient binding sites of the antisense domain will be the validated exonic or intronic splicing silencers. For exonic silencers, the binding site is favorable to the upstream of the exon.
3. If the antisense domain anneals to an exon, it should avoid inducing any potential exon skipping of the binding exon.
4. Chemical modification of all the RNA nucleotides through the entire tail domain may reduce the binding affinity to protein. However, chemical modification may be only added to the last five nucleotides at the 5'-end of the tail domain (cap, as shown in Fig. 1) to improve the stability while still keep its binding affinity.
5. The duration of transfection can be prolonged to overnight or 24 h. For cells less tolerant to lipofectamine transfection, shorter incubation period, e.g. 6 h, is recommended.
6. It is recommended at least two housekeeping genes are used in the quantitative real-time PCR assay.

Acknowledgments

This work was supported by the Wellcome Trust, University College London, UK Medical Research Council (MRC), SMA-Europe, SMA Trust, Muscular Dystrophy UK and NIHR Great Ormond Street Hospital and Institute of Child Health Biomedical Research Centre.

References

1. Dominski Z, Kole R (1993) Antisense oligonucleotides. *Proc Natl Acad Sci U S A* 90: 8673–8677
2. Mitropant C, Porensky P, Zhou H, Price L, Muntoni F, Fletcher S et al (2013) Improved antisense oligonucleotide design to suppress aberrant SMN2 gene transcript processing: towards a treatment for spinal muscular atrophy. *PLoS One* 8:2–11

3. Hua Y, Sahashi K, Rigo F, Hung G, Horev G, Bennett F et al (2011) Peripheral SMN restoration is essential for long-term rescue of a severe spinal muscular atrophy mouse model. *Nature* 478:123–126
4. Zhou H, Janghra N, Mitropant C, Dickinson R, Anthony K, Price L et al (2013) A novel morpholino oligomer targeting ISS-N1 improves rescue of severe spinal muscular atrophy transgenic mice. *Hum Gene Ther* 24:331–342
5. Singh NK, Singh NN, Androphy EJ, Eliot J, Singh RN (2006) Splicing of a critical exon of human Survival Motor Neuron is regulated by a unique silencer element located in the last intron. *Mol Cell Biol* 26:1333–1346
6. Mercuri E, Darras BT, Chiriboga CA, Day JW, Campbell C, Connolly AM et al (2018) Nusinersen versus sham control in later-onset spinal muscular atrophy. *N Engl J Med* 378:625–635
7. Finkel RS, Mercuri E, Darras BT, Connolly NL, Kuntz J, Kirschner CA et al (2017) Nusinersen versus sham control in infantile-onset spinal muscular atrophy. *N Engl J Med* 377:1723–1732
8. Hoy SM (2017) Nusinersen: first global approval. *Drugs* 77:473–479
9. Cirak S, Arechavala-Gomez V, Guglieri M, Feng L, Torelli S, Anthony K et al (2011) Exon skipping and dystrophin restoration in patients with Duchenne muscular dystrophy after systemic phosphorodiamidate morpholino oligomer treatment: an open-label, phase 2, dose-escalation study. *Lancet* 378:595–605
10. Kinali M, Arechavala-Gomez V, Feng L, Cirak S, Hunt D, Adkin C et al (2009) Local restoration of dystrophin expression with the morpholino oligomer AVI-4658 in Duchenne muscular dystrophy: a single-blind, placebo-controlled, dose-escalation, proof-of-concept study. *Lancet Neurol* 8:918–928
11. Aartsma-Rus A, Corey DR (2020) The 10th oligonucleotide therapy approved: golodirsen for Duchenne muscular dystrophy. *Nucl Acids Ther* 30:67. <https://doi.org/10.1089/nat.2020.0845>
12. Frank DE, Schnell FJ, Akana C, El-Husayni SH, Desjardins CA, Morgan J et al (2020) Increased dystrophin production with golodirsen in patients with Duchenne muscular dystrophy. *Neurology* 94:e2270. <https://doi.org/10.1212/WNL.0000000000009233>
13. Heo YA (2020) Golodirsen: first approval. *Drugs* 80:329–333
14. Skordis LA, Dunkley MG, Yue B, Eperon IC, Muntoni F (2003) Bifunctional antisense oligonucleotides provide a trans-acting splicing enhancer that stimulates SMN2 gene expression in patient fibroblasts. *Proc Natl Acad Sci U S A* 100:4114–4119
15. Cartegni L, Krainer AR (2003) Correction of disease-associated exon skipping by synthetic exon-specific activators. *Nat Struct Biol* 10:120–125
16. Owen N, Zhou H, Malygin AA, Sangha J, Smith LD, Muntoni F et al (2011) Design principles for bifunctional targeted oligonucleotide enhancers of splicing. *Nucl Acids Res* 39:7194–7208
17. Brosseau JP, Lucier JF, Lamarche AA, Shkreta L, Gendron D, Lapointe E et al (2014) Redirecting splicing with bifunctional oligonucleotides. *Nucl Acids Res* 42:e40
18. Baughan TD, Dickson A, Osman EY, Lorson CL (2009) Delivery of bifunctional RNAs that target an intronic repressor and increase SMN levels in an animal model of spinal muscular atrophy. *Hum Mol Genet* 18:1600–1611
19. Osman EY, Yen PF, Lorson CL (2012) Bifunctional RNAs targeting the intronic splicing silencer N1 increase SMN levels and reduce disease severity in an animal model of spinal muscular atrophy. *Mol Ther* 20:119–126
20. Meyer K, Marquis J, Trüb J, Nlend R, Verp S, Ruepp MD et al (2009) Rescue of a severe mouse model for spinal muscular atrophy by U7 snRNA-mediated splicing modulation. *Hum Mol Genet* 18:546–555

Open Access This chapter is licensed under the terms of the Creative Commons Attribution 4.0 International License (<http://creativecommons.org/licenses/by/4.0/>), which permits use, sharing, adaptation, distribution and reproduction in any medium or format, as long as you give appropriate credit to the original author(s) and the source, provide a link to the Creative Commons license and indicate if changes were made.

The images or other third party material in this chapter are included in the chapter's Creative Commons license, unless indicated otherwise in a credit line to the material. If material is not included in the chapter's Creative Commons license and your intended use is not permitted by statutory regulation or exceeds the permitted use, you will need to obtain permission directly from the copyright holder.





Design and Delivery of SINEUP: A New Modular Tool to Increase Protein Translation

Michele Arnoldi, Giulia Zarantonello, Stefano Espinoza, Stefano Gustincich, Francesca Di Leva, and Marta Biagioli

Abstract

SINEUP is a new class of long non-coding RNAs (lncRNAs) which contain an inverted Short Interspersed Nuclear Element (SINE) B2 element (invSINEB2) necessary to specifically upregulate target gene translation. Originally identified in the mouse *AS-Uchl1* (antisense Ubiquitin carboxyl-terminal esterase L1) locus, natural SINEUP molecules are oriented head to head to their sense protein coding, target gene (*Uchl1*, in this example). Peculiarly, SINEUP is able to augment, in a specific and controlled way, the expression of the target protein, with no alteration of target mRNA levels. SINEUP is characterized by a modular structure with the Binding Domain (BD) providing specificity to the target transcript and an effector domain (ED)—containing the invSINEB2 element—able to promote the loading to the heavy polysomes of the target mRNA. Since the understanding of its modular structure in the endogenous *AS-Uchl1* ncRNA, synthetic SINEUP molecules have been developed by creating a specific BD for the gene of interest and placing it upstream the invSINEB2 ED. Synthetic SINEUP is thus a novel molecular tool that potentially may be used for any industrial or biomedical application to enhance protein production, also as possible therapeutic strategy in haploinsufficiency-driven disorders.

Here, we describe a detailed protocol to (1) design a specific BD directed to a gene of interest and (2) assemble and clone it with the ED to obtain a functional SINEUP molecule. Then, we provide guidelines to efficiently deliver SINEUP into mammalian cells and evaluate its ability to effectively upregulate target protein translation.

Key words SINEUP, Long non-coding RNA, Antisense, Translational increase, Physiological increase, Therapeutic tool, Haploinsufficiency, Protein manufacturing

1 Introduction

The quantitative improvement of protein production in mammalian systems is a compelling need for the industrial manufacturing of commercially available enzymes, antibodies and supplements, but also for gene therapy-based treatments of medical conditions. Several technologies are available to address such a need, however, they usually consist of introducing exogenously constructs containing the protein of interest or directly the target

peptide [1]. These approaches still struggle to overcome hazardous but invariable hurdles, especially when used as therapeutic tools, such as ectopic expression and protein quantity modulation, sometimes associated with toxicity [2]. As an alternative, newly identified RNA-based techniques such as small activating RNAs (RNAs) are able to target and upregulate endogenous gene transcription [3]. In 2012, Carrieri et al. discovered a new class of lncRNAs, belonging to the category of natural antisense transcripts (NATs), that have the property to increase the protein translation of the target mRNA [4]. These transcripts were named SINEUP based on their ability to upregulate target protein translation by means of an invSINEB2 repeat, leaving unaltered the transcriptional levels of the target mRNA. They were first discovered in mice, where *AS-Uchl1* was found to have a post-transcriptional upregulating activity on its sense protein coding counterpart, *Uchl1* mRNA [4]. Later studies confirmed and validated the expression of SINEUP in human cells [5, 6]. SINEUP molecular mechanism relies on its modular structure, composed of two fundamental domains: a Binding Domain (BD)—a region at the 5' of the lncRNA overlapping head to head to the 5' of the target mRNA—and an Effector Domain (ED)—constituted by an invSINEB2 repetitive element. The BD is crucial for target gene pairing and it confers molecular specificity, while the ED is the functional part of SINEUP required for loading the target transcript on polyosomes and driving the translational increase [4].

The initial discovery was then supported by the crucial finding that the BD could be engineered in order to target a specific mRNA of interest, as first demonstrated with Green Fluorescent Protein (*GFP*) [4]. Additionally, miniSINEUP containing only the BD and a shorter version of the original ED were also proven to be effective [7]. This characteristic would enable to overcome the difficulties of long molecules delivery, especially for therapeutic purposes in which naked RNA molecules administration can be proposed. Recently, TranSINE Therapeutics Limited (Cambridge, UK) has been founded to translate the SINEUP technology into the clinics as therapeutics for haploinsufficiency.

All together, these findings qualified SINEUP as a flexible tool able to upregulate the protein production of virtually any mRNA target of interest, affecting solely the translational levels. As such, SINEUP molecules demonstrated to be a suitable tool for protein manufacturing, able to boost, for instance, the production of recombinant proteins and monoclonal antibodies in mammalian cells [8–10]. SINEUP molecules are also being studied from a therapeutic point of view, since their functional characteristics could confer advantages with respect to other gene therapy approaches. SINEUP molecules generally upregulate the endogenous protein of about two- to fivefold (almost within a physiologic range) and they are only effective in those districts where the target

mRNA is physiologically expressed, therefore avoiding unspecific effects [10]. Finally, by targeting mRNA molecules, SINEUP does not introduce stable or unwanted changes in the host genome. Thus far, several synthetic SINEUP molecules were successfully designed and delivered as potential therapeutic molecules. For instance, synthetic SINEUP were designed and successfully used to increase the levels of disease-associated proteins in vitro, such as Parkinson's disease-associated DJ-1 in three human neuronal cell lines [7] and Glial-cell derived neurotrophic factor (GDNF) in mouse cell line [11]. Moreover, SINEUP have been used to rescue frataxin levels in a cellular model of Friedreich's Ataxia [12]. Concerning in vivo model systems, SINEUP could effectively rescue some phenotypes associated with microphthalmia with linear skin defects (MLS) syndrome in a medaka fish model of *cox7B* haploinsufficiency [13]. More recently, SINEUP targeting GDNF mRNA was tested in a neurochemical Parkinson's disease (PD) mouse model [11]. Interestingly, SINEUP-GDNF increased endogenous GDNF level for at least 6 months which lead to an enhancement of dopamine release in the striatum and an amelioration of motor behavior and neurodegeneration, without affecting body weight or food intake, common side effects of the ectopic expression of GDNF [11].

Here, we describe in detail the fundamental steps in order to design, clone, and deliver SINEUP molecular tools in the cellular system of interest.

2 Materials

2.1 Design and Cloning of SINEUP

1. Zenbu browser (<https://fantom.gsc.riken.jp/zenbu/>).
2. Ensembl genome browser (<https://www.ensembl.org/index.html>).
3. UCSC genome browser (<https://genome.ucsc.edu/>).
4. NCBI (<https://www.ncbi.nlm.nih.gov/genome/>).
5. RNA Fold web server (<http://rna.tbi.univie.ac.at/cgi-bin/RNAWebSuite/RNAfold.cgi>).
6. Salt free primers. Use primers to clone the Effector Domain from Carrieri et al. [4]:
 - (a) For mAS *Uchl1*Δ5': 5- CAGTGCTAGAGGAGGTCA GAAGAG-3
 - (b) Rev mAS *Uchl1* fl: 5-CATAGGAGTGTTCATT-3
 Or primers from Zucchelli et al. [7]:
 - (a) FWD EcoRI *invSINEB2*: 5-TATAGAATTCCAGTGCTA GAGGAGG-3

(b) 3REV HindIII *invSINEB2*: 5- GAGAAAGCTTAAGA
GACTGGAGC-3

7. Ultrapure water.
8. Mammalian expression plasmid vector of your choice.
9. Restriction enzymes.
10. T4 DNA ligase.
11. *E. coli* competent cells.
12. Luria-Bertani (LB-10 g/L Tryptone, 10 g/L NaCl, 5 g/L Yeast Extract) broth.
13. Antibiotics of your choice.
14. Maxiprep kit.
15. Molecular grade agarose.
16. DNA gel staining.
17. DNA loading dye.
18. DNA ladder.
19. Electrophoresis apparatus.

2.2 SINEUP Delivery into Cellular Model

1. Target cells of interest. In this protocol we used human iPS-derived neuronal progenitor cells (hiNPCs) [14].
2. Poly-L-ornithine hydrobromide (20 µg/mL).
3. Laminin (3 µg/mL).
4. Dulbecco's Modified Eagle's Medium (DMEM).
5. Ham's F-12 Nutrient (HAM F12).
6. B27.
7. Penicillin-Streptomycin solution.
8. L-Glutamine.
9. EGF (20 ng/mL).
10. bFGF (20 ng/mL).
11. Heparin (5 µg/mL).
12. hiNPCs culturing medium: 70% v/v DMEM completed with 30% v/v HAM F12, 2% v/v B27, 1% v/v Penicillin-Streptomycin solution, and 1% v/v L-Glutamine and supplemented with EGF (20 ng/mL), bFGF (20 ng/mL) and Heparin (5 µg/mL). Semi-confluent monolayers of hiNPCs were maintained in 5% CO₂, 37 °C humidified incubator.
13. Enzyme for adherent cellular culture detachment (e.g. TripLE in this example).
14. Transfection solution (e.g. Nucleofector Solutions—Lonza).
15. Nucleofector™ Device (Lonza).

2.3 RNA and Protein Analysis

1. RadioImmunoPrecipitation Assay—RIPA—buffer.
2. Protease and Phosphatase inhibitors (PI and PhI, respectively).
3. Bicinchoninic acid (BCA) or Bradford protein assay kit.
4. Bovine serum albumin (BSA) standard curve.
5. Western blot apparatus.
6. Specific antibody for the target protein and a housekeeping protein.
7. Enhanced ChemiLuminescence (ECL) or equivalent assay.
8. Eurofins PCR primer design tool or equivalent (<https://eurofinsgenomics.eu/en/ecom/tools/pcr-primer-design/>).
9. ThermoFisher primer analyzer tool or equivalent (<https://www.thermofisher.com/it/en/home/brands/thermo-scientific/molecular-biology/molecular-biology-learning-center/molecular-biology-resource-library/thermo-scientific-web-tools/multiple-primer-analyzer.html>).
10. DNase.
11. DEPC-treated (nuclease-free) water.
12. Retro-transcriptase containing both oligo(dT) and Random Hexamer primers.
13. SYBR Green or Taqman reagents.

3 Methods

Prepare all the solutions using analytical grade reagents with ultra-pure water at room temperature, unless otherwise indicated. Solutions used with cells are filtered or sterilized at the beginning. Cells are handled under biological hoods while all the other reactions are performed on the bench. Follow safety instructions indicated by safety team in your institution.

3.1 Binding Domain Design and Cloning

1. Retrieve the sequence of your transcript of interest from Zenbu browser (<https://fantom.gsc.riken.jp/zenbu/>) [15].
2. In Zenbu, select the organism in which you will perform the experiments (e.g. human or mouse) and search for the target gene of interest (*see* **Note 1** and Fig. 1a).
3. Check how many TSS have been characterized for your gene and in which tissue/cell line they are expressed (Fig. 1b) by selecting the “CAGE libraries” (or other libraries in which you are interested).
4. Expand the window in the 5'UTR region containing the TSS in order to better appreciate how many TSS have been identified. You will see a bar plot in which each bar represents a TSS

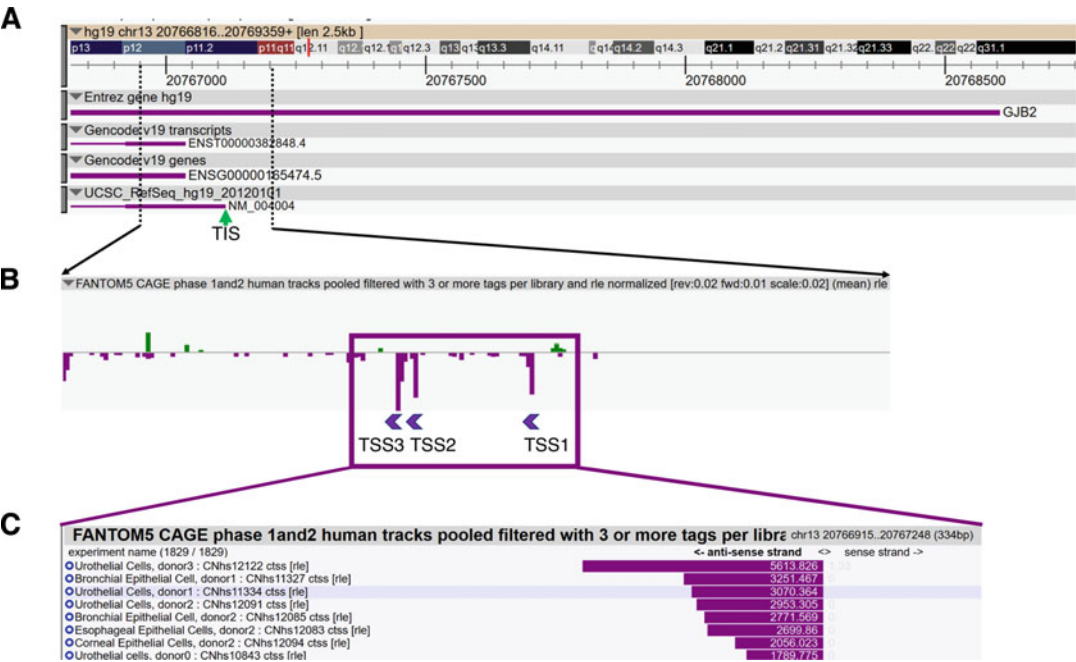


Fig. 1 Zenbu genome browser interrogation of transcript of interest showing TSS usage in selected model system. **(a)** Zenbu genome browser screenshot showing the genomic location of the gene of interest (in this example *GJB2*) in the human genome assembly 19 (hg19), green arrow identifies the Translation Initiation Site (TIS). RefSeq accession number for the transcript of interest (NM_004004, in this case) is also visible. In the enlargement in **(b)** alternative TSS usage identified by FANTOM5 CAGE library (reported as purple bar plots) is shown. Both TSSs in the same orientation (reverse strand, purple bar plots) and in the opposite orientation (forward strand, green bar plots) of the gene are depicted. The purple box highlights the chosen region in which interrogates the browser about the expression of your target transcript. Main TSSs, TSS1, TSS2, and TSS3, are indicated by purple arrows. **(c)** Displays the tracks (experiments) in which the transcript is more expressed

(Fig. 1b); in the window below, the tracks expressing your transcript will be displayed (Fig. 1c). Among them, you can select the tissue/cells/organ of your interest.

5. In the identified TSS and the 5'UTR region, design an efficient SINEUP molecule in which the BD overlaps the Translational Initiation Site (TIS) and expands in the upstream region characterized for your transcript.
6. Further test the expression of your transcript(s) using genome browsers such as Ensembl genome browser (<https://www.ensembl.org/index.html>), UCSC genome browser (<https://genome.ucsc.edu/>), or NCBI (<https://www.ncbi.nlm.nih.gov/genome/>).
7. Design forward primer (FW) on the 5'UTR and reverse primer (RV) on coding DNA sequence (CDS) downstream Translational Initiation Site (TIS).

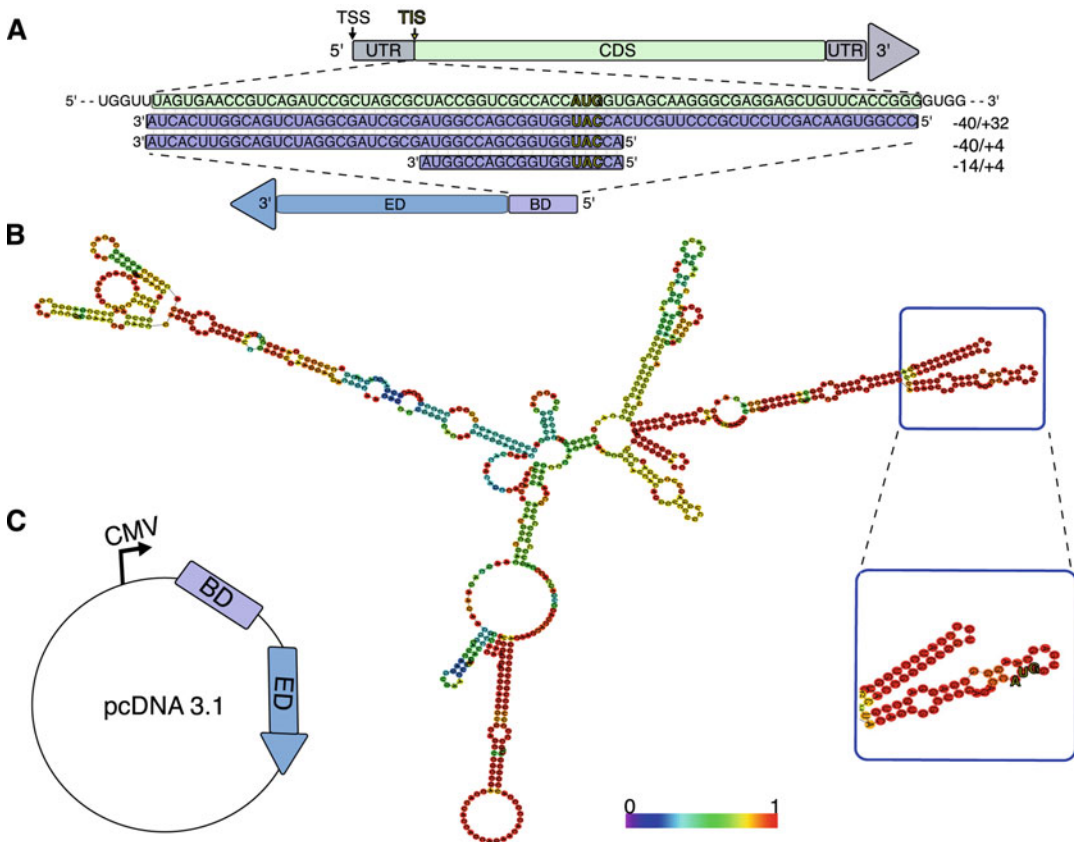


Fig. 2 SINEUP modular structure: Binding domain (BD) design and cloning. (a) Representation of the modular structure of SINEUP and the design strategy to obtain BD oriented head to head to its target gene. BDs, in light purple, targeting the gene of interest (as an example, the CDS of EGFP is depicted in light green), untranslated region (UTR) in gray, Transcriptional Start Site (TSS) in black, and Transcriptional Initiation Site (TIS) in yellow, are shown. Different suggested lengths for BD are reported. SINEUP effector domain (ED) in light blue, with the antisense region, overlapping TIS is depicted in black-shadowed yellow. Adenine (A) of the TIS is set as 0, BDs lengths vary between -40 from the A and $+32$ nucleotides, -40 and $+4$ nucleotides, and -14 and $+4$ nucleotides, respectively. (b) Example of RNA folding prediction results using RNA Fold web server (<http://rna.tbi.univie.ac.at/cgi-bin/RNAWebSuite/NAfold.cgi>) with default parameters, here reported for EGFP transcript. The blue box displays an enlargement of the TIS (in yellow AUG) surrounding region, in which packed structures without big hairpin-loop are reported. Minimum free energy (MFE) prediction is used to create the output, with base-pair probability in form of a dot plot it depicted. Scale bar reports both base-pair and unpair probability for every base colored dot, with 1 highest probability that the base pair as well as 1 highest probability that the base unpair with the neighbors (c). (Schematic representation of pcDNA 3.1 vector structure obtained from Carrieri C. et al. 2012 [4], BD is depicted in light purple followed by ED in light blue are under CMV promoter)

8. Dissolve salt free quality primers in ultrapure water to obtain equal molarity for each primer to a final concentration of $10 \mu\text{M}$.

9. Confirm the expression of your target transcript(s) by PCR in your selected model system.
10. Run the PCR product onto agarose gel to confirm amplicon size, purify PCR product, and sequence with both FW and RV primers to validate transcript identity and specificity (*see Note 2*).
11. The BD will be designed spanning the TIS of the transcript of interest. You can start selecting the “canonical” target sequence corresponding to 40 bases upstream and 4 bases downstream the TIS (−40/+4) in which 0 correspond to the A of the TIS ATG (*see Note 3*).
12. Additional sequences of different length can be designed both on the TIS and in region(s) targeting downstream, in-frame methionines (*see Note 4* and Fig. 2a). A full list of published BDs is reported in Table 1.
13. On the target region of interest where the BD will be designed, evaluate the GC content and the mRNA secondary structure using RNA Fold web server (<http://rna.tbi.univie.ac.at/cgi-bin/RNAWebSuite/RNAfold.cgi>—Fig. 2b, *see Note 5*) [19, 20].
14. Further analysis can be performed to understand if other lncRNA(s) are generated endogenously from the same genetic locus. Albeit not mandatory, this information can give you an idea of the specific gene’s structure as well as highlight possible competition in SINEUP binding to the target TIS.
15. Once selected BDs of interest, perform off-targets prediction by interrogating Basic local Alignment (BLAST, <https://blast.ncbi.nlm.nih.gov/Blast.cgi>) or BLAT (<https://genome.ucsc.edu/cgi-bin/hgBlat>). This information can help to avoid SINEUP off-target issues and to prioritize experiments with the more specific molecules (*see Note 6*).
16. When you select the region of the transcript in which you want to design the BD, you must reverse complement the sense mRNA sequence to obtain a SINEUP able to interact with the target gene (Fig. 2a).
17. For each BD of interest, synthesize the FW primer in a sense orientation (5′–3′ orientation) with the restriction enzyme needed for insertion into the chosen vector at its 5′ end. On the other hand, synthesize the RV primer in an inverted orientation (3′–5′) with the compatible restriction site at the 5′ end, in order to allow primer annealing.
18. Equimolar concentration of both primers must be denatured for 5′ at 100 °C and cooled slowly (1 °C every minute) to obtain double stranded DNA (dsDNA) BD.

Table 1

List of natural and synthetic SINEUP tested to upregulate protein production. Binding Domain (BD—A and B columns, the overlapping sequence with the sense spliced mRNA is reported) and Effector Domain (ED—C column) administered with different delivery methods (F columns) in diverse model systems (H and I columns) are listed. Position relatively to the targeted Methionine (A column) of the gene of interest (E column) are reported (AUG with A set as 0, M1 refers to first Methionine corresponding to TIS, whereas M76 refers to Methionine in position 76 in the amino acid chain)

BD length	BD specificity	Class of ED	Target gene	Delivery method	Model organism	Increase level of target protein	Reference
−40/−49 M1 −9/+34 M1	<i>Uchl1</i>	invSINEB2/ Alu	<i>Uchl1</i>	Lipofectamine 2000	MN9D	Yes	[4]
−40/+32 M1	<i>Uchl1</i>	invSINEB2/ Alu	<i>Uchl1</i>	Lipofectamine 2000	HEK293T/17	Yes	[4]
−54/−6 M1 +65/+98 M1	<i>Uxt</i>	invSINEB2/ Alu	<i>Uxt</i>	Lipofectamine 2000	MN9D	Yes	[4]
−40/+32 M1	<i>GFP</i>	invSINEB2/ Alu	<i>GFP</i>	Lipofectamine 2000	HEK293T/17	Yes	[4]
−40/+32 M1	FLAG	invSINEB2	FLAG-TRAF6, FLAG-DJ-1, FLAG-Hba, FLAG-TTRAP	Lipofectamine 2000	HEK293T/17	Yes	[7]
−40/+32 M1	<i>DJ1</i>	invSINEB2	<i>DJ1</i>	Lipofectamine 2000	SH-SY5Y, BE(2)-M17 and SK-N-SH	Yes	[7]
−40/+4 M1	<i>DJ1</i>	invSINEB2	<i>DJ1</i>	Lipofectamine 2000	SH-SY5Y	Yes	[7]

(continued)

Table 1
(continued)

BD length	BD specificity	Class of ED	Target gene	Delivery method	Model organism	Increase level of target protein	Reference
−40/+32 M1	EGFP	invSINEB2 or invSINEB2/Alu	EGFP	Lipofectamine 2000	HEK 293T/17, HepG2, HcLa	Yes	[7]
−40/+32 M1	EGFP	invSINEB2/Alu	EGFP	Lipofectamine 3000	HcLa, HEK293A, HEK293T and CHO-K1	Yes	[16]
−40/+32 M1	EGFP	invSINEB2/Alu	EGFP-BBCK	Lipofectamine 3000	HEK293T	Yes	[16]
−40/+32 M1	EGFP	invSINEB2/Alu	EGFP-βB2-crystallin	Lipofectamine 3000	HEK293T	Yes	[16]
−40/+32 M1	Sox9	invSINEB2/Alu	Sox9	Lipofectamine 3000	C5.18 and rat primary chondrocyte	Yes	[16]
−40/+32 M1	met-luciferase	invSINEB2/Alu	met-luciferase	Lipofectamine 3000	HEK293T	Yes	[16]
−40/0 M1	EGFP	invSINEB2/Alu	EGFP	Lipofectamine 3000	HEK293T	No	[16]
−100/0 M1	EGFP	invSINEB2/Alu	EGFP	Lipofectamine 3000	HEK293T	No	[16]
0/+32 M1	EGFP	invSINEB2/Alu	EGFP	Lipofectamine 3000	HEK293T	No	[16]
0/+100 M1	EGFP	invSINEB2/Alu	EGFP	Lipofectamine 3000	HEK293T	No	[16]
0/+200 M1	EGFP	invSINEB2/Alu	EGFP	Lipofectamine 3000	HEK293T	Yes	[16]

−40/+360 M1	EGFP	invSINEB2/ Alu	EGFP	Lipofectamine 3000	HEK293T	Yes	[16]
−40/+560 M1	EGFP	invSINEB2/ Alu	EGFP	Lipofectamine 3000	HEK293T	No	[16]
−40/+760 M1	EGFP	invSINEB2/ Alu	EGFP	Lipofectamine 3000	HEK293T	No	[16]
−40/+100 M1	EGFP	invSINEB2/ Alu	EGFP	Lipofectamine 3000	HEK293T	Yes	[16]
−40/+200 M1	EGFP	invSINEB2/ Alu	EGFP	Lipofectamine 3000	HEK293T	Yes	[16]
−100/+32 M1	EGFP	invSINEB2/ Alu	EGFP	Lipofectamine 3000	HEK293T	Yes	[16]
−100/ +100 M1	EGFP	invSINEB2/ Alu	EGFP	Lipofectamine 3000	HEK293T	Yes	[16]
−40/+32 M1	<i>anti-HIV</i> antibody 10E8	invSINEB2 or invSINEB2/ Alu	<i>anti-HIV</i> antibody 10E8	Lipofectamine 3000	HEK293T	Yes	[16]
−40/+100 M1	<i>anti-HIV</i> antibody 10E8	invSINEB2 or invSINEB2/ Alu	<i>anti-HIV</i> antibody 10E8	Lipofectamine 3000	HEK293T	Yes	[16]
−100/+32 M1	<i>anti-HIV</i> antibody 10E8	invSINEB2 or invSINEB2/ Alu	<i>anti-HIV</i> antibody 10E8	Lipofectamine 3000	HEK293T	Yes	[16]
−200/+48 M1	<i>anti-HIV</i> antibody 10E8	invSINEB2 or invSINEB2/ Alu	<i>anti-HIV</i> antibody 10E8	Lipofectamine 3000	HEK293T	Yes	[16]
−40/+32 M1	EGFP	invSINEB2/ Alu	EGFP	FreeStyle MAX reagent	CHO-S	Yes	[8]

(continued)

Table 1
(continued)

BD length	BD specificity	Class of ED	Target gene	Delivery method	Model organism	Increase level of target protein	Reference
-40/+4 M1	<i>NLuc</i>	invSINEB2/ Alu	<i>NLuc</i>	Lipofectamine 2000; FreeStyle MAX reagent	HEK293T; CHO-S	Yes	[8]
-40/+33 M1	<i>mIgG</i> secretory leader	invSINEB2/ Alu	<i>scFv; Periostin</i>	FreeStyle MAX reagent	CHO-S	Yes	[8]
-13/+82 M1	<i>mEln</i> secretory leader	invSINEB2/ Alu	<i>NLuc</i>	FreeStyle MAX reagent	CHO-S	Yes	[8]
-40/+32 M1	<i>EGFP</i>	invSINEB2/ Alu	<i>EGFP</i>	Lipofectamine 2000	HEK293T/17	Yes	[13]
-40/+32 M1	<i>EGFP</i>	invSINEB2/ Alu	<i>EGFP</i>	RNA injection	Zebrafish embryo	Yes	[13]
-40/+32 M1	<i>cox7B</i>	invSINEB2/ Alu	<i>cox7B</i>	RNA injection	Zebrafish embryo	Yes	[13]
-67/+31 M1	<i>PPP1R12A</i>	FRAM	<i>PPP1R12A</i>	Lipofectamine 2000	HEK293T, HeLa	Yes	[5]
-35/+4 M1	<i>PPP1R12A</i>	FRAM	<i>PPP1R12A</i>	Lipofectamine 2000	HEK293T	Yes	[5]
-35/+4 M1	<i>PPP1R12A</i>	invSINEB2	<i>PPP1R12A</i>	Lipofectamine 2000	HEK293T	Yes	[5]
-93/+95 M1	<i>ITFG2</i>	MIRb	<i>ITFG2</i>	Lipofectamine 2000	HEK293T	Yes	[5]

−28/+32 M1	<i>GFP</i>	invSINEB2/ Alu	<i>GFP</i>	Lipofectamine 2000	HEK293T/17	Yes	[17]
−28/+27 M1	<i>GFP</i>	invSINEB2/ Alu	<i>GFP</i>	Lipofectamine 2000	HEK293T/17	No	[17]
−28/+22 M1	<i>GFP</i>	invSINEB2/ Alu	<i>GFP</i>	Lipofectamine 2000	HEK293T/17	No	[17]
−28/+18 M1	<i>GFP</i>	invSINEB2/ Alu	<i>GFP</i>	Lipofectamine 2000	HEK293T/17	No	[17]
−28/+12 M1	<i>GFP</i>	invSINEB2/ Alu	<i>GFP</i>	Lipofectamine 2000	HEK293T/17	No	[17]
−28/+8 M1	<i>GFP</i>	invSINEB2/ Alu	<i>GFP</i>	Lipofectamine 2000	HEK293T/17	No	[17]
−28/+4 M1	<i>GFP</i>	invSINEB2/ Alu	<i>GFP</i>	Lipofectamine 2000	HEK293T/17	Yes	[17]
−28/0 M1	<i>GFP</i>	invSINEB2/ Alu	<i>GFP</i>	Lipofectamine 2000	HEK293T/17	No	[17]
−28/−4 M1	<i>GFP</i>	invSINEB2/ Alu	<i>GFP</i>	Lipofectamine 2000	HEK293T/17	No	[17]
−28/ −8 M1	<i>GFP</i>	invSINEB2/ Alu	<i>GFP</i>	Lipofectamine 2000	HEK293T/17	No	[17]
−28/−12 M1	<i>GFP</i>	invSINEB2/ Alu	<i>GFP</i>	Lipofectamine 2000	HEK293T/17	No	[17]
−20/+32 M1	<i>GFP</i>	invSINEB2/ Alu	<i>GFP</i>	Lipofectamine 2000	HEK293T/17	No	[17]
−10/+32 M1	<i>GFP</i>	invSINEB2/ Alu	<i>GFP</i>	Lipofectamine 2000	HEK293T/17	No	[17]
0/+32 M1	<i>GFP</i>	invSINEB2/ Alu	<i>GFP</i>	Lipofectamine 2000	HEK293T/17	No	[17]
10/+32 M1	<i>GFP</i>	invSINEB2/ Alu	<i>GFP</i>	Lipofectamine 2000	HEK293T/17	No	[17]

(continued)

Table 1
(continued)

BD length	BD specificity	Class of ED	Target gene	Delivery method	Model organism	Increase level of target protein	Reference
-18/+4 M1	GFP	invSINEB2/ Alu	GFP	Lipofectamine 2000	HEK293T/17	No	[17]
-40/+4 M1	FXN	invSINEB2/ Alu	FXN	Lipofectamine 2000	HEK 293T/17	Yes	[12]
-40/0 M1	FXN	invSINEB2/ Alu or invSINEB2	FXN	Lipofectamine 2000	HEK 293T/17	Yes	[12]
-14/0 M1	FXN	invSINEB2/ Alu or invSINEB2	FXN	Lipofectamine 2000	HEK 293T/17	Yes	[12]
-14/+4 M1	FXN	invSINEB2/ Alu or invSINEB2	FXN	Lipofectamine 2000	HEK 293T/17	Yes	[12]
-40/+4 M76	FXN	invSINEB2/ Alu	FXN	Lipofectamine 2000	HEK 293T/17	Yes	[12]
-40/ 0 M76	FXN	invSINEB2/ Alu or invSINEB2	FXN	Lipofectamine 2000	HEK 293T/17	Yes	[12]
-10/ -60/+0 M76	FXN	invSINEB2	FXN	Lipofectamine 2000	HEK 293T/17	No	[12]
-40/+4 M1	FXN	invSINEB2	FXN	lentiviral particles	GM04078 fibroblasts	Yes	[12]
-40/0 M1	FXN	invSINEB2	FXN	lentiviral particles	GM04078 fibroblasts	Yes	[12]

–14/0 M1	<i>FXN</i>	invSINEB2	<i>FXN</i>	lentiviral particles	GM04078 fibroblasts; SH-SY5Y	Yes	[12]
–14/+4 M1	<i>FXN</i>	invSINEB2	<i>FXN</i>	lentiviral particles	GM04078 fibroblasts; SH-SY5Y	Yes	[12]
–40/+4 M76	<i>FXN</i>	invSINEB2	<i>FXN</i>	lentiviral particles	GM04078 fibroblasts	Yes	[12]
–40/+4 M1	<i>FXN</i>	invSINEB2	<i>FXN</i>	electroporation	GM16214 lymphoblasts	Yes	[12]
–40/0 M1	<i>FXN</i>	invSINEB2	<i>FXN</i>	electroporation	GM16214 lymphoblasts	Yes	[12]
–40/+4 M1	<i>GDNF</i>	invSINEB2/ Alu	<i>GDNF</i>	Lipofectamine 2000; AAV9 injection	Neuro2a; C8-D1A	Yes	[11]
–14/+4 M1	<i>GDNF</i>	invSINEB2/ Alu	<i>GDNF</i>	Lipofectamine 2000; AAV9 injection	Neuro2a; C8-D1A	Yes	[11]
–14/+4 M1	<i>GDNF</i>	invSINEB2/ Alu	<i>GDNF</i>	AAV9 vectors injection	Dorsal striatum of adult C57BL/6J mice	Yes	[11]
–31/+4 M1	<i>SOX9</i>	invSINEB2/ Alu	<i>SOX9</i>	Lipofectamine 2000	HepG2 and Hepa 1–6	Yes	[18]
–28/+4 M1	<i>EGFP</i>	invSINEB2/ Alu	<i>EGFP</i>	Lipofectamine 2000	HEK293T/17	Yes	[18]

19. By taking advantage of the restriction sites present in the BD and in the selected plasmid of interest, clone every BD upstream of the *AS-Uchl1* ED. A shorter version of ED called miniSINEUP, which still comprehends the invSINEB2 element present in *AS-Uchl1*, should preferentially be used to obtain shorter SINEUP (*see Note 7*) in expression plasmid (e.g. pcDNA 3.1 vector from Clontech, Fig. 2c) using T4 DNA ligase (Fig. 2b). If necessary, inducible or tissue specific promoters can be used.

3.2 Effector Domain Design and Cloning

You can design the ED and insert in a different plasmid as needed. The ED comprehends an invSINEB2, free right Alu monomer (FRAM) or MIRb (Mammalian-wide Interspersed Repeat type b) transposable element sequence from natural SINEUP (*see Note 8*). Virtually any of those elements can present SINEUP activity, however, the element present in *AS-Uchl1* was previously inserted in miniSINEUP vectors and it was the most widely characterized. For this reason, in this section, we will refer to invSINEB2 cloning as ED.

1. To amplify ED from *AS-Uchl1* you can use primers “For mAS *Uchl1*Δ5′” and “Rev mAS *Uchl1* fl” from Carrieri et al. [4]. Moreover, to obtain a 170 bp long ED, primers “FWD EcoRI *invSINEB2*” and “REV HindIII *invSINEB2*” from Zucchelli et al. [7] which produce a shorter SINEUP called miniSINEUP, can be selected. Albeit miniSINEUP retains only the invSINEB2 and not the Alu element, this construct was successfully used to increase GFP translation [7].
2. Add restriction enzymes sites at the 5′ end to the primers of interest to clone the ED into the desired vector.
3. After performing PCR, purify the amplicon and confirm the correct sequence.
4. Clone the purified ED in the vector of interest downstream the BD.
5. Transform the ligation product into *E. coli* competent cells.
6. Cultured the bacteria in LB broth at 37 °C supplemented with the antibiotic required for selection (e.g. kanamycin sulfate).
7. The empty vector and/or a vector containing only the ED (in the case you clone only the BD targeting the gene of interest in the vector already containing the ED) must be produced as control for ligation.
8. Verify positive clones by restriction analysis or colony PCR and sequencing.
9. Produce and purify the plasmids containing SINEUP for the gene of interest and the empty vector.

10. Analyze plasmids integrity on agarose gel and confirm again the presence of the insert and its correct orientation by restriction map and sequencing.

3.3 SINEUP Delivery into Cellular Model

Different methods such as transfection, electroporation, or viral vectors transduction, can be chosen to deliver your plasmid into the cells of choice. The selected method should meet a criterion of high plasmid internalization efficiency (>60–70% positive cells). In fact, SINEUP molecules upregulate protein translation in a physiologic range (approximately two- to fivefold) so if few cells receive the plasmid this effect can be hidden or under-estimated. Here, we describe the method which best fits our expectations in hiNPCs [14]. For additional information on SINEUP delivery in animal and cellular models *see* **Note 9**.

In this protocol we focused on our target cells of choice, hiNPCs, for which electroporation represents an optimal method of transfection for transient expression. For this purpose, we used Nucleofector™ Device (Lonza) and selected the recommended protocol for our specific cell line, as well as the advised program (A033) of the device. Dealing specifically with SINEUP, we recommend the following:

1. Start by using 1 µg of SINEUP for every one million cells (*see* **Note 10**).
2. Prepare the electroporation mix using the recommended electroporation solution and each SINEUP you want to deliver as well as a solution containing the empty vector as negative control.
3. Resuspend the cellular pellet with the electroporation mix and electroporate with the device and program of choice (e.g. Nucleofector™ Device, Lonza program A033 for hiNPCs).
4. Collect the electroporated cells and seed them in a mix of 1:2 = old:new pre-warmed medium. We recommend seeding the cells to reach roughly 40% confluency.
5. Replace the medium after 6 h of incubation (be careful that cells are attached on the well) with new, pre-warmed medium.
6. If any fluorescent protein (e.g. GFP) reporter gene is present, check the fluorescence levels to evaluate delivery efficiency (Fig. 3a).
7. We recommend harvesting the electroporated cells after 24–48 h, when cells have fully recovered and are transiently expressing the delivered constructs (containing SINEUP or empty control).

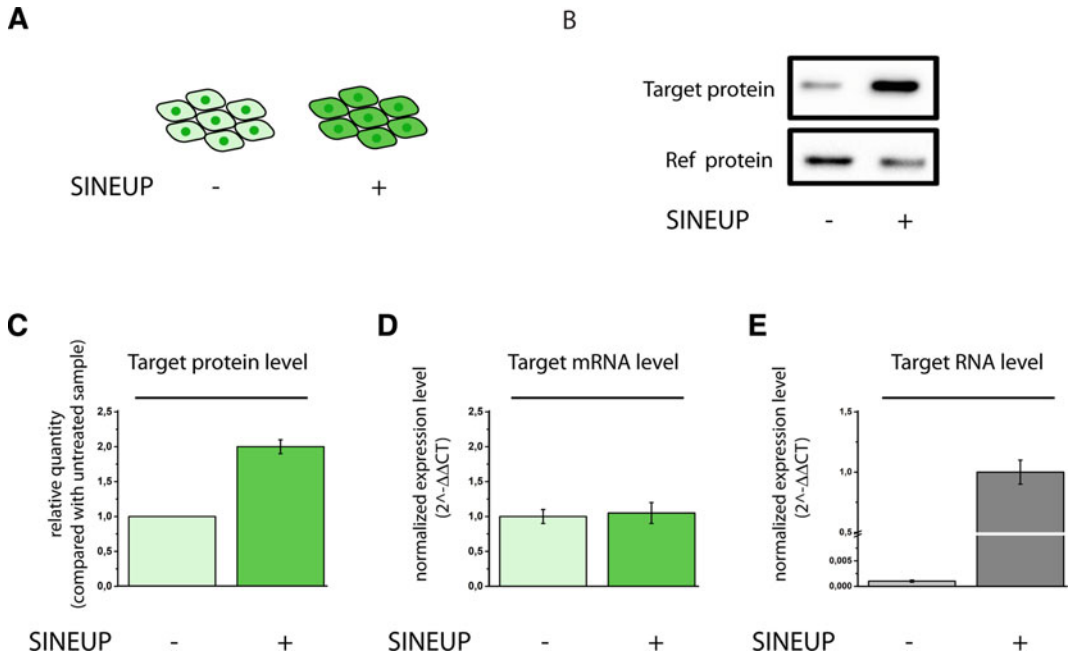


Fig. 3 Expected results when SINEUP positively increases target mRNA translation without altering its transcriptional level in human induced neural progenitor cells (hiNPCs). **(a)** Representative image of hiNPCs expressing EGFP after electroporation with control vector (SINEUP -) or with SINEUP targeting *EGFP* (SINEUP +). **(b)** Western Blot image reports target protein expression relative to a chosen reference protein in the presence (+) or absence (-) of SINEUP against the target mRNA, *EGFP*, in this example. **(c)** Bar graph representing fold change quantification of target protein from WB experiments in **(b)**. **(d)** Bar graphs representing normalized expression level of target mRNA upon SINEUP administration (- control SINEUP, + SINEUP against target *EGFP* mRNA). SINEUP presence is depicted in **(e)**. Transcripts expression was obtained from qPCR quantification and normalized with a chosen reference gene

3.4 SINEUP Efficacy Assessment:
Transcription and Translation Evaluation

Successful SINEUP function needs to be assessed by transcriptional and translational analysis, such as qPCR and WB, respectively. In particular, an increase in protein production between two- and fivefold changes is expected (Fig. 3b, c) without dysregulation of the target mRNA expression (Fig. 3d) when SINEUP is present (Fig. 3e).

1. Apply protocols you routinely use in your lab to extract proteins from the electroporated cells. We used commercial RIPA buffer supplemented with Protease and Phosphatase inhibitors (PI and PhI, respectively).
2. Carefully quantify your proteins using BCA or Bradford protein assay kit. Always include the BSA standard curve for protein quantification. It is fundamental reliable quantification in order to appreciate standard two- to fivefold changes in the protein level due to SINEUP delivery.

3. Perform Western blot experiments using a protocol you are familiar with; the optimization of WB depends on the target protein of interest.
4. Load the same amount of protein (e.g. 20 µg) for all the samples.
5. It is crucial to use specific antibodies to recognize the protein isoform of interest targeted by SINEUP. In particular, the resolved band of the target gene (Fig. 3b) should be clearly distinguishable after WB analysis to perform a correct quantification of the protein of interest (Fig. 3c).
6. Be careful with your choice of ECL or equivalent assay. If the reagent is not sensitive enough you will not see the band of interest; on the other side, many sensitive reagents will not allow you to appreciate subtle changes in protein level due to saturated bands.
7. Albeit in standard experiments three/five biological replicates are considered enough to achieve robust results and to assess reproducibility, in this case you may need more replicates (*see Note 11*).
8. Design Quantitative Polymerase Chain Reaction (qPCR) primers for the target of interest, a housekeeping gene and SINEUP ED by using Eurofins PCR Primer Design online tool (<https://eurofinsgenomics.eu/en/ecom/tools/pcr-primer-design/>), but equivalent systems could also be employed (*see Note 12*).
9. All primers should be tested for hairpin and primer dimer formation. Here we used multiple primer analyzer (ThermoFisher; <https://www.thermofisher.com/it/en/home/brands/thermo-scientific/molecular-biology/molecular-biology-learning-center/molecular-biology-resource-library/thermo-scientific-web-tools/multiple-primer-analyzer.html>) and Oligo Calc (Northwestern; <http://biotools.nubic.northwestern.edu/OligoCalc.html>), but similar tools might also be evaluated.
10. Apply protocols you routinely use in your lab to obtain high quality RNA from the electroporated cells.
11. Preferentially, perform DNase treatment on your RNA samples before proceeding with retro-transcription in order to avoid issues due to DNA contamination.
12. Always resuspend RNA in DEPC-treated (nuclease-free) water.
13. To retro-transcribe RNA to produce cDNA we used a mix containing both oligo(dT) and Random Hexamer primers.

14. For qPCR, the Master Mix reagents should be preferred to DNA polymerase in order to minimize errors. You can use SYBR Green or Taqman systems equally.
15. Perform qPCR assay with the cDNA using primers or Taqman probes targeting a reference housekeeping gene (such as *ACTB*), the target transcript(s) and SINEUP to assess correct expression.
16. Calculate the relative mRNA expression level of the target gene by normalizing treated samples with SINEUP against the empty vector and by using $2^{-\Delta\Delta C_t}$ method [21].
17. Normalize the empty vector against the SINEUP sample for SINEUP expression (*see Note 13*).
18. Stable mRNA expression from your target transcript should be observed (Fig. 3d) when SINEUP is expressed (Fig. 3e).

4 Notes

1. The first step is to identify the specific transcript isoform(s) of your transcript of interest that is expressed in the selected model system. This step is necessary since your target might express alternative isoforms that differ from cell to cell and in different tissues. Moreover, the expressed isoform in your cell model/tissue would not necessarily be the most characterized. Zenbu browser is an on-demand freely available interface that allows visualizing data, such as RNA-seq, CAGE (cap analysis of gene expression), short-RNA-seq, and ChIP-seq (chromatin immunoprecipitation) in the chosen model system. The broad spectrum of systems that are annotated could give information especially on annotated promoters and transcriptional starting sites (TSS) usage. However, not all the systems have been characterized and reported in Zenbu [15]. Additional information about how to use Zenbu genome browser, as well as methods to detect and analyze SINEUP in cell culture can be found in Takahashi et al. [22].
2. When you design SINEUP BD, it is important to seek for possible Single Nucleotide Variants (SNV) that might hamper the annealing capability of SINEUP or the expression of your target.
3. Most of the efficient SINEUP BDs characterized until now have been designed in this region in order to specifically recognize the target gene. Specific recognition of transcript originating from the gene of interest allows increase in translation of the full-length target. We recommend designing BD of different lengths. Optimization of the Binding Domain sequence and length is an important step in designing the experiment

[17]. Among others, we suggest $-40/+32$, $-40/+4$, and $14/+4$ BD regions as the most promising target to be chosen for the experiments (as reported in Fig. 2a).

4. Additional SINEUP targeting in-frame, internal methionine can be design if the TIS surrounding region is poorly accessible. Although many more experimental evidences support the importance of targeting the TIS, the internal, in-frame methionine of the *Frataxin* gene was successfully tested and provided efficient upregulation of Frataxin protein [12]. In fact, SINEUP mechanism is not completely characterized and we cannot exclude that target mRNA can be loaded on polyosomes by internal bait which does not interfere with translational initiation. Moreover, alternative translation might occur to downstream AUG codon in the presence of internal ribosomal entry site (IRES) [23]. In summary, we prompt researchers to explore also the possibility of targeting internal in-frame methionines.
5. As mentioned in the methods, packed secondary structures can impair the sense-antisense pairing of SINEUP molecules, decreasing its efficacy. In addition, GC rich region and stem-and-loop structures might inhibit translation by blocking ribosome binding [23]. RNA fold web server predicts in vitro secondary structure of single stranded nucleic acid by energy minimization and/or minimum entropy. This analysis will provide hints on the accessibility of the transcript area in order to optimize SINEUP binding. Although RNA fold tool can be a useful tool, it only mimics the complex physiological condition of RNA fold present in vivo. Recently, a novel approach called icShape (in vivo click selective 2-hydroxyl acylation and profiling experiment) was established to capture the RNA structure in vivo in order to overcome the RNA Fold tool issues [24]. Although not essential for SINEUP design, we recommend analysing icShape data to better understand the binding capacity of SINEUP to the target area of interest.
6. While performing off-target analysis, keep in mind that the possible off-target transcripts need also to be expressed in the model system of your choice to be targeted by SINEUP. On the other hand, the TIS or the internal in-frame methionine you choose to design SINEUP must be present in the transcript(s) expressed in the tissue of interest for translation to occur.
7. To clone SINEUP you can use a mammalian expression plasmid vector of your choice. Since the aim is to obtain an abundant and efficient production of SINEUP, the expression should be driven by a suitable promoter, Cytomegalovirus (CMV) or SV40, frequently employed in mammalian cells plasmids. An inducible/tissue specific promoter may be used, if needed.

8. Long sequences of in vitro synthesized RNA molecules can generate issues especially during delivery in cells. For this reason, starting from the original complete sequence containing the invSINEB2, Alu sequence, and 3' tail of the natural *AS-Uchl1*, a short functional version was created, called miniSINEUP, encompassing only the invSINEB2 [7, 17]. We suggest performing the SINEUP experiment using miniSINEUP construct, composed by the specific BD and 170 nucleotides length ED of invSINEB2 element. Notably, the human transcriptome does not present invSINEB2 sequences, but functional SINEUP were discovered in human containing embedded FRAM and MIRb transposable element. These two functional domains worked as Eds [5]. Although ED can be designed either with invSINEB2, FRAM, and MIRb domains, we recommend to generate initially ED by using invSINEB2 motif that has been extensively and successfully used to increase protein translation in different cell lines, in vivo in Medaka fish and in a mouse model for Parkinson Disease [4–6, 10–13]. Notably, by nuclear magnetic resonance (NMR) analysis, it was observed that the secondary structure of the invSINEB2 motif is crucial for its function. For this reason, when designing the ED containing invSINEB2, it is important to include the region between 43 and 58 stem-loop structure since this region is likely to be vital for SINEUP function [25].
9. In vitro and in vivo delivery can be optimized and changed if needed. To date, successful SINEUP deliveries were previously reported in vitro using Lipofectamine and lentiviral particles in human derived fibroblasts [12], in vivo by RNA injection in zebrafish embryo [13] and AAV9 vectors injection in the dorsal striatum of adult mice [11]. For both in vitro and in vivo, the delivery method can vary according to the model of choice, the stage and the time window of interest (e.g. transient expression, conditional expression or stable expression). The methods described here for BD design, cloning and SINEUP efficacy assessment steps in cellular models also apply for animal systems. However, concerning the delivery step in vivo, SINEUP molecules can be delivered and expressed in animal models similarly to other RNA-based therapeutics, e.g. by viral vectors. Moreover, it is possible to administer in vitro transcribed SINEUP targeting the transcript of interest instead of the plasmid carrying it. If this method is used, you should chemically modify the in vitro transcribed SINEUP to better stabilize the molecule, by replacing CTP with 5-methylcytidine-50-triphosphate (m5C); and replacing UTP with pseudouridine-50-triphosphate (Ψ) or N1-methylpseudouridine-50-triphosphate (N1m Ψ) [18]. In our experience, it is best to test whether the experimental cell system chosen for the

experiment is positively responding to SINEUP administration. For this reason, we suggest testing the previously characterized SINEUP against *GFP* [4, 7], before moving to SINEUP targeting the gene of interest. To analyze the SINEUP efficacy on GFP translation, WB analysis as well as imaging analysis with semi-automatic detection methods can be performed [22]. Of importance, to underlie that protein translation is increased due to SINEUP mechanism, qPCR should be conducted and report stable expression of the target transcript.

10. SINEUP molecule can act in a dose dependent manner to control protein translation without affecting transcript level [7]. To assess the optimal efficiency, different concentrations of SINEUP should be tested.
11. SINEUP delivery experiments as well as WB and qPCR analysis should be performed at least in triplicate to observe statistically significant changes. However, depending on the model system used, additional experiments may be needed to reach significance. The crucial step is the WB quantification: if the band of your target(s) and the reference proteins are not well resolved, changes ascribed to SINEUP positive upregulation can be difficult to examine. In our experience it is better to set specific conditions for WB detection in the chosen model system before performing SINEUP experiment.
12. Primers or Taqman probes for target gene(s) of interest and stable housekeeping gene(s) must be designed in order to assess the stability of the target gene(s) upon SINEUP administration. In addition, primers or probes targeting SINEUP ED must be designed in order to check the correct expression of SINEUP into the chosen model system after plasmid delivery (if the chosen ED contain the invSINEB2 and Alu elements the desired primer can be found in Zucchelli et al. [7]). Primers for qPCR should be designed in regions spanning exon-exon junctions to minimize DNA residual contamination, maximize PCR efficiency and specificity.
13. The different methods for analysing SINEUP and the target mRNA expression is needed since for SINEUP, the quantification in qPCR of the empty vector should be close to the detection limit of the instrument since little signal can be recorded by using the SINEUP specific primer or probes. On the contrary, SINEUP expression is expected to be high upon delivery of the plasmid containing SINEUP sequence, hence that amount is set as default condition one, whereas the empty vector quantification should be close to zero (Fig. 3e).

References

1. Wahlestedt C (2013) Targeting long non-coding RNA to therapeutically upregulate gene expression. *Nat Rev Drug Discov* 12(6):433–446. <https://doi.org/10.1038/nrd4018>
2. Wang D, Gao G (2014) State-of-the-art human gene therapy: part I. Gene delivery technologies. *Discov Med* 18(97):67–77
3. Li LC (2017) Small RNA-guided transcriptional gene activation (RNAa) in mammalian cells. *Adv Exp Med Biol* 983:1–20. https://doi.org/10.1007/978-981-10-4310-9_1
4. Carrieri C, Cimatti L, Biagioli M, Beugnet A, Zucchelli S, Fedele S, Pesce E, Ferrer I, Collavin L, Santoro C, Forrest AR, Carninci P, Biffo S, Stupka E, Gustincich S (2012) Long non-coding antisense RNA controls Uchl1 translation through an embedded SINEB2 repeat. *Nature* 491(7424):454–457. <https://doi.org/10.1038/nature11508>
5. Schein A, Zucchelli S, Kauppinen S, Gustincich S, Carninci P (2016) Identification of antisense long noncoding RNAs that function as SINEUPs in human cells. *Sci Rep* 6:33605. <https://doi.org/10.1038/srep33605>
6. Zucchelli S, Cotella D, Takahashi H, Carrieri C, Cimatti L, Fasolo F, Jones MH, Sblattero D, Sanges R, Santoro C, Persichetti F, Carninci P, Gustincich S (2015) SINEUPs: a new class of natural and synthetic antisense long non-coding RNAs that activate translation. *RNA Biol* 12(8):771–779. <https://doi.org/10.1080/15476286.2015.1060395>
7. Zucchelli S, Fasolo F, Russo R, Cimatti L, Patrucco L, Takahashi H, Jones MH, Santoro C, Sblattero D, Cotella D, Persichetti F, Carninci P, Gustincich S (2015) SINEUPs are modular antisense long non-coding RNAs that increase synthesis of target proteins in cells. *Front Cell Neurosci* 9:174. <https://doi.org/10.3389/fncel.2015.00174>
8. Patrucco L, Chiesa A, Soluri MF, Fasolo F, Takahashi H, Carninci P, Zucchelli S, Santoro C, Gustincich S, Sblattero D, Cotella D (2015) Engineering mammalian cell factories with SINEUP noncoding RNAs to improve translation of secreted proteins. *Gene* 569(2):287–293. <https://doi.org/10.1016/j.gene.2015.05.070>
9. Sasso E, Latino D, Froechlich G, Succio M, Passariello M, De Lorenzo C, Nicosia A, Zambrano N (2018) A long non-coding SINEUP RNA boosts semi-stable production of fully human monoclonal antibodies in HEK293E cells. *MAbs* 10(5):730–737. <https://doi.org/10.1080/19420862.2018.1463945>
10. Zucchelli S, Patrucco L, Persichetti F, Gustincich S, Cotella D (2016) Engineering translation in mammalian cell factories to increase protein yield: the unexpected use of long non-coding SINEUP RNAs. *Comput Struct Biotechnol J* 14:404–410. <https://doi.org/10.1016/j.csbj.2016.10.004>
11. Espinoza S, Scarpato M, Damiani D, Manago F, Mereu M, Contestabile A, Peruzzo O, Carninci P, Santoro C, Papaleo F, Mingozzi F, Ronzitti G, Zucchelli S, Gustincich S (2020) SINEUP non-coding RNA targeting GDNF rescues motor deficits and neurodegeneration in a mouse model of Parkinson's disease. *Mol Ther* 28(2):642–652. <https://doi.org/10.1016/j.ymthe.2019.08.005>
12. Bon C, Luffarelli R, Russo R, Fortuni S, Pierattini B, Santulli C, Fimiani C, Persichetti F, Cotella D, Mallamaci A, Santoro C, Carninci P, Espinoza S, Testi R, Zucchelli S, Condo I, Gustincich S (2019) SINEUP non-coding RNAs rescue defective frataxin expression and activity in a cellular model of Friedreich's Ataxia. *Nucl Acids Res* 47(20):10728–10743. <https://doi.org/10.1093/nar/gkz798>
13. Indrieri A, Grimaldi C, Zucchelli S, Tammaro R, Gustincich S, Franco B (2016) Synthetic long non-coding RNAs [SINEUPs] rescue defective gene expression in vivo. *Sci Rep* 6:27315. <https://doi.org/10.1038/srep27315>
14. Sheridan SD, Theriault KM, Reis SA, Zhou F, Madison JM, Daheron L, Loring JF, Haggarty SJ (2011) Epigenetic characterization of the FMR1 gene and aberrant neurodevelopment in human induced pluripotent stem cell models of fragile X syndrome. *PLoS One* 6(10):e26203. <https://doi.org/10.1371/journal.pone.0026203>
15. Severin J, Lizio M, Harshbarger J, Kawaji H, Daub CO, Hayashizaki Y, Consortium F, Bertin N, Forrest AR (2014) Interactive visualization and analysis of large-scale sequencing datasets using ZENBU. *Nat Biotechnol* 32(3):217–219. <https://doi.org/10.1038/nbt.2840>
16. Yao Y, Jin S, Long H, Yu Y, Zhang Z, Cheng G, Xu C, Ding Y, Guan Q, Li N, Fu S, Chen XJ, Yan YB, Zhang H, Tong P, Tan Y, Yu Y, Fu S, Li J, He GJ, Wu Q (2015) RNAe: an effective method for targeted protein translation enhancement by artificial non-coding

- RNA with SINEB2 repeat. *Nucl Acids Res* 43(9):e58. <https://doi.org/10.1093/nar/gkv125>
17. Takahashi H, Kozhuharova A, Sharma H, Hirose M, Ohyama T, Fasolo F, Yamazaki T, Cotella D, Santoro C, Zucchelli S, Gustincich S, Carninci P (2018) Identification of functional features of synthetic SINEUPs, antisense lncRNAs that specifically enhance protein translation. *PLoS One* 13(2): e0183229. <https://doi.org/10.1371/journal.pone.0183229>
 18. Toki N, Takahashi H, Zucchelli S, Gustincich S, Carninci P (2020) Synthetic in vitro transcribed lncRNAs (SINEUPs) with chemical modifications enhance target mRNA translation. *FEBS Lett* 594(24):4357–4369. <https://doi.org/10.1002/1873-3468.13928>
 19. Gruber AR, Lorenz R, Bernhart SH, Neubock R, Hofacker IL (2008) The Vienna RNA websuite. *Nucl Acids Res* 36(Web Server Issue):W70–W74. <https://doi.org/10.1093/nar/gkn188>
 20. Lorenz R, Bernhart SH, Honer Zu Siederdisen C, Tafer H, Flamm C, Stadler PF, Hofacker IL (2011) ViennaRNA Package 2.0. *Algor Mol Biol* 6:26. <https://doi.org/10.1186/1748-7188-6-26>
 21. Segundo-Val IS, Sanz-Lozano CS (2016) Introduction to the gene expression analysis. *Methods Mol Biol* 1434:29–43. https://doi.org/10.1007/978-1-4939-3652-6_3
 22. Takahashi H, Sharma H, Carninci P (2019) Cell based assays of SINEUP non-coding RNAs that can specifically enhance mRNA translation. *J Vis Exp* (144). <https://doi.org/10.3791/58627>
 23. Kozak M (2002) Pushing the limits of the scanning mechanism for initiation of translation. *Gene* 299(1–2):1–34. [https://doi.org/10.1016/s0378-1119\(02\)01056-9](https://doi.org/10.1016/s0378-1119(02)01056-9)
 24. Flynn RA, Zhang QC, Spitale RC, Lee B, Mumbach MR, Chang HY (2016) Transcriptome-wide interrogation of RNA secondary structure in living cells with icSHAPE. *Nat Protoc* 11(2):273–290. <https://doi.org/10.1038/nprot.2016.011>
 25. Ohyama T, Takahashi H, Sharma H, Yamazaki T, Gustincich S, Ishii Y, Carninci P (2020) An NMR-based approach reveals the core structure of the functional domain of SINEUP lncRNAs. *Nucl Acids Res* 48(16):9346–9360. <https://doi.org/10.1093/nar/gkaa598>

Open Access This chapter is licensed under the terms of the Creative Commons Attribution 4.0 International License (<http://creativecommons.org/licenses/by/4.0/>), which permits use, sharing, adaptation, distribution and reproduction in any medium or format, as long as you give appropriate credit to the original author(s) and the source, provide a link to the Creative Commons license and indicate if changes were made.

The images or other third party material in this chapter are included in the chapter's Creative Commons license, unless indicated otherwise in a credit line to the material. If material is not included in the chapter's Creative Commons license and your intended use is not permitted by statutory regulation or exceeds the permitted use, you will need to obtain permission directly from the copyright holder.





Chapter 5

How to Design U1 snRNA Molecules for Splicing Rescue

Liliana Matos, Juliana I. Santos, M^a. Francisca Coutinho,
and Sandra Alves

Abstract

Mutations affecting constitutive splice donor sites (5'ss) are among the most frequent genetic defects that disrupt the normal splicing process. Pre-mRNA splicing requires the correct identification of a number of *cis*-acting elements in an ordered fashion. By disrupting the complementarity of the 5'ss with the endogenous small nuclear RNA U1 (U1 snRNA), the key component of the spliceosomal U1 ribonucleoprotein, 5'ss mutations may result in exon skipping, intron retention or activation of cryptic splice sites. Engineered modification of the U1 snRNA seemed to be a logical method to overcome the effect of those mutations. In fact, over the last years, a number of in vitro studies on the use of those modified U1 snRNAs to correct a variety of splicing defects have demonstrated the feasibility of this approach. Furthermore, recent reports on its applicability in vivo are adding up to the principle that engineered modification of U1 snRNAs represents a valuable approach and prompting further studies to demonstrate the clinical translatability of this strategy.

Here, we outline the design and generation of U1 snRNAs with different degrees of complementarity to mutated 5'ss. Using the *HGSNAT* gene as an example, we describe the methods for a proper evaluation of their efficacy in vitro, taking advantage of our experience to share a number of tips on how to design U1 snRNA molecules for splicing rescue.

Key words U1 snRNA-based therapy, Splicing modulation, 5'ss mutations, Aberrant exon skipping, Modified U1 snRNA, Mucopolysaccharidosis IIIC

1 Introduction

The U1 small nuclear ribonucleoprotein (U1 snRNP) is a key molecule involved in an early event of the splicing process. Like other snRNPs involved in the overall splicing regulation process, it contains a small RNA complexed with several proteins, namely seven Smith antigen (Sm) proteins and three U1-specific proteins (U1A, U1C, and U170K) [1]. U1 snRNA, the RNA component of the U1 snRNP is a 164 nucleotides-long molecule whose 5' end interacts by complementarity with the 5' splice donor site (5'ss). That interaction between the single stranded 5' tail of the U1 snRNA molecule and the moderately conserved stretch of nucleotides that constitutes the 5'ss (CAG/GURAGU, where R is a

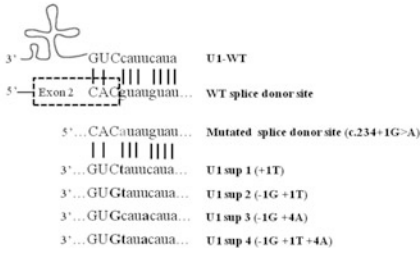
purine) marks the exon-intron boundary and initiates spliceosome assembly [2]. About 40%, 22%, and 5% of normal 5'ss contain two, three, or four mismatches towards the U1 snRNA, respectively [3, 4]. This variable degree of degeneration is among the major factors that significantly contribute to hinder a clear prediction of the effect of mutations flanking the canonical GU site. Furthermore, there is a number of additional elements, which may influence the splice site selection and need to be taken into account such as splicing silencer and enhancer motifs, the presence of alternative splice sites, secondary structures, and regulatory proteins [5]. Therefore, a straightforward prediction of the effect of mutations flanking the canonical GU site without a direct assessment of the mature mRNA produced can be quite challenging. Interestingly, however, it is also the variable degree of degeneration of 5'ss and the surprising heterogeneity existing among human spliceosomal snRNA, which allows for splicing correction using modified exogenous U1 snRNAs.

Overall, the rationale on the use of modified U1 snRNAs to correct splicing defects is as simple as it can be: as 5'ss mutations alter the 5'ss recognition by the endogenous U1 snRNA, exogenous U1 snRNAs may be engineered through complementary base pairing in order to correctly recognize the mutated allele and initiate spliceosome assembly, thus suppressing the mutation effect.

So far, the effects of modified U1 snRNAs have been tested in vitro in a number of cellular platforms from patient-derived cells to model cell lines overexpressing the splicing defects under study, and their potential to either fully or partially correct those mutations was demonstrated for a number of different diseases [5, 6]. Importantly, the application of this sort of modified U1 snRNAs in animal models has also been addressed in recent studies, with a few promising results reported to date [7–10] (*see Note 1*).

Globally, mutations affecting constitutive 5'ss represent roughly 8% of all known genetic disease-causing variants. Their pathogenicity derives from the reduced complementarity of the U1 snRNA to the 5'ss. 5'ss mutations mostly result in exon skipping but their effect over splicing may vary. Currently, there are a number of in silico tools that may help predict disease-causing effects, but cDNA analysis remains mandatory for a proper assessment of their consequence over splicing. For example, mutations affecting RNA splicing represent more than 20% of the mutant alleles in Mucopolysaccharidosis type IIIC (MPS IIIC; *HGSNAT* gene), a rare lysosomal storage disorder that causes severe neurodegeneration. Many of these mutations are located in the conserved splice donor or acceptor sites, while few are found in the nearby nucleotides. For three mutations that affect the donor site, we have previously developed different modified U1 snRNAs with compensatory changes that may allow for proper recognition of the mutated 5'ss, in an attempt to rescue the normal splicing process.

A



B

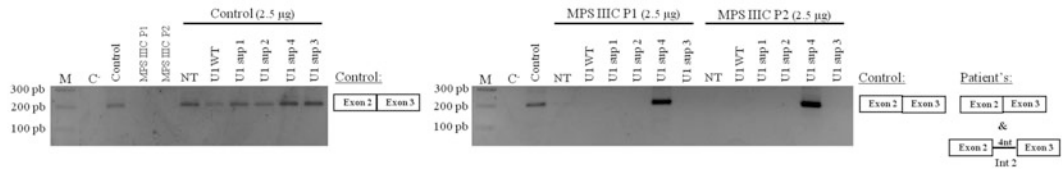


Fig. 1 Modified U1 snRNA therapeutic approach to correct the pathogenic effect of a 5' splice site mutation on the *HGSNAT* gene. **(a)** Schematic illustration of base pairing between the wild-type U1 (U1-WT) and the 5'ss of wild-type and mutant exon 2 of the *HGSNAT* gene. The mutation position in the 5'ss is marked in grey and it is in italics. The different U1 snRNAs used for the mutated 5'ss of *HGSNAT* (designated as U1-sup, for suppressor) are also shown. The U1 sequence modifications are illustrated in bold. **(b)** RT-PCR analysis of the endogenous splicing pattern of control and MPS IIIC patients derived fibroblasts after transfection with different U1 isoforms. The constitutive splicing of exon 2 of the *HGSNAT* gene was not altered in control fibroblasts after overexpression of U1-WT or any of the modified U1 constructs. In the MPS IIIC patients 1 (MPS IIIC P1) and 2 (MPS IIIC P2), bearing the homozygous mutation c.234+1G>A, only the fully adapted U1 (U1-sup4) resulted in partial correction of exon 2 skipping

For the c.234+1G>A mutation, a totally complementary U1 snRNA allowed for partial correction of exon 2 aberrant splicing in patients' fibroblasts (Fig. 1) [11]. Here, we take advantage of our experience on the development of modified U1 snRNAs to compensate for those *HGSNAT* mutations, to present a practical overview on how to design U1 snRNA molecules for splicing rescue.

In summary, we present an overview of the experimental design for in vitro testing the potential of modified U1 snRNA vectors to correct aberrant splicing caused by 5'ss mutations. Briefly, we show: (a) how to design in silico U1's with different degrees of complementarity to each mutated 5'ss by introducing a number of sequence changes, and (b) how the different U1 vectors harboring those alterations are obtained by site-directed mutagenesis of the original wild-type (WT) human U1 snRNA-harboring pG3U1 vector [12], a derivative of pHU1 [13]. We also describe how these molecules are transfected into patients' fibroblasts and how their effectiveness on splicing redirection can be assessed by post-transfection cDNA analysis and sequencing. Finally, we elaborate on the relevance of further addressing the treatment's effect at protein level.

2 Materials

2.1 Generating Modified U1 snRNA Vectors Adapted to the 5' ss of Interest

1. The *Homo sapiens* U1 snRNA gene sequence is required to design primers for site-directed mutagenesis PCR and can be found in the Ensembl database (ENSG00000104852).
2. The sequence of the 5' ss of interest for splicing rescue can be found in Ensembl or other reference sequence databases (in this particular chapter we used the *Homo sapiens* HGSNAT gene sequence, ENSG00000165102).
3. pG3U1 vector [12] a derivative of pHU1 [13] (*see Note 2*).
4. Sense and antisense mutagenic primers.
5. PCR mutagenesis kit.
6. PCR thermocycler.
7. Chemically *Escherichia coli* competent cells (Homemade or commercial; usually are included in the PCR mutagenesis kits).
8. Water bath.
9. Thermomixer.
10. Ice.
11. Super optimal broth with catabolite repression (SOC) medium (commercially available).
12. Luria-Bertani (LB) agar medium (commercially available; sterilize by autoclaving) plates with selection antibiotic (100 µg/mL, ampicillin; *see Note 3*).
13. Sterile bacterial cell spreaders.
14. Plasmid DNA miniprep purification kit.
15. LB liquid medium (commercially available; sterilize by autoclaving).
16. Ampicillin.
17. 15 mL conical centrifuge tubes.
18. Sterile tips.
19. Orbital shaking incubator.
20. pG3U1 forward primer (U1-seq Fw—5' CACGAAG GAGTTCCCGTG 3').
21. Sterile flasks (1 L).
22. Endotoxin-free maxiprep plasmid DNA purification kit.
23. 40% Glycerol (sterilize by autoclaving).
24. 2 mL polypropylene conical tubes.

2.2 In Vitro Therapeutic Evaluation of Modified U1 snRNA Vectors in Human Fibroblasts

2.2.1 Transfection of Modified U1 snRNA Vectors in Human Fibroblasts

1. Human Dermal Fibroblasts from patients harboring the mutation under analysis (e.g. fibroblasts from patients' with MPS IIIC, carrying the c.234+1G>A mutation in homozygosity) and WT Human Dermal Fibroblasts to use as control.
2. Dulbecco's Modified Eagle's Medium (DMEM) + Glutamax supplemented with 10% Fetal Bovine Serum (FBS), 5% penicillin/streptomycin (PenStrep) antibiotics, and 5% amphotericin B (Fungizone®).
3. Phosphate buffered saline 1x (PBS).
4. Trypsin-EDTA.
5. CO₂ incubator.
6. 15 mL conical centrifuge tubes.
7. Refrigerated centrifuge.
8. Neubauer chamber (hemocytometer).
9. Inverted Microscope.
10. Hand cell counter.
11. T-75 cm² cell culture flasks.
12. 6-well cell culture plates.
13. Opti-MEM™ Reduced Serum Medium.
14. Transfection reagent.
15. 1.5 and 2 mL polypropylene conical tubes.
16. Modified U1 snRNA constructs (*see* Subheading 2.1).

2.2.2 Analysis of Splicing Rescue by RT-PCR

1. RNA isolation kit.
2. Refrigerated centrifuge.
3. 1.5 mL polypropylene conical tubes.
4. Spectrophotometer for nucleic acids measurement.
5. cDNA synthesis kit.
6. Taq DNA polymerase.
7. Oligo(dT)₁₈ primer mix (if required).
8. Gene-specific primers (e.g. *HGSNAT* primers—Exon 2 Fw: 5' ACATGCAGAGCTGAAGATGGA 3'; Exon 3 Rv: 5' GATAGATCCGTGCTGGGTG 3').
9. Ice.
10. RNase free water.
11. PCR thermocycler.
12. Agarose gel with ethidium bromide for electrophoresis.

- 13. DNA Ladder (molecular weight size marker).
- 14. UV transilluminator.
- 15. Sterile scalpel blades.
- 16. PCR products purification kits.

3 Methods

3.1 Generating the Modified U1 snRNA Vectors

To design the primers for producing the desired modified human U1 snRNA vectors, it is first necessary to know the sequences of the 5'ss under study, both WT and mutant. Then, it is necessary to analyze the complementarity of those sequences with that of U1 snRNA. Next, several modified U1 snRNA vectors can be designed and constructed to have different complementarities to the target sequences (Fig. 2). To generate those constructs, the plasmid pG3U1 [12] (kindly provided by Prof. Dr. Belén Pérez) a derivative of pHU1 [13], containing the coding sequence of the human U1 can be used as template for site-directed mutagenesis PCR reactions (*see Note 2*). Depending on the number of mutations to insert in the U1 snRNA vector sequence, different mutagenic primer pairs need to be designed.

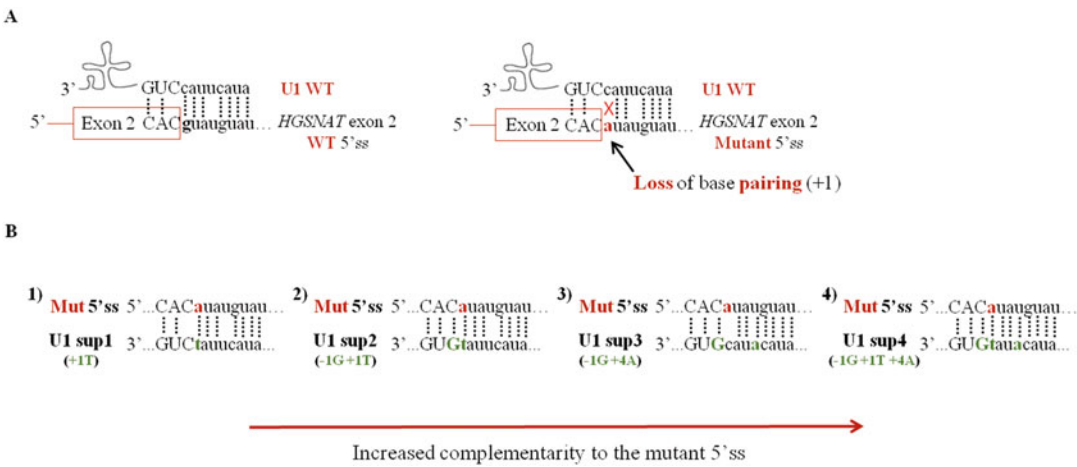


Fig. 2 Design and construction of modified U1 snRNA vectors. (a) Schematic representation of base pair interactions between the U1 snRNA and the wild-type and mutant 5'ss of *HGSNAT* exon 2, respectively. (b) Illustration of the strategy followed to increase the complementarity of U1 snRNA with the mutated 5'ss of *HGSNAT* gene. U1 complementarity was increased stepwise, and to try to compensate for the *HGSNAT* mutation at +1 position, four different U1-adaptations were designed [U1 sup1 (+1T); U1 sup2 (-1G +1T); U1 sup3 (-1G +4A); U1 sup4 (-1G +1T +4A)]. Upper case letters show exonic nucleotides, whereas the lower case letters denote intronic nucleotides. Base pairing is indicated by vertical lines and its loss by an X. The mutant nucleotide is highlighted in red and the changed nucleotides in the U1 sequence are illustrated in green

3.1.1 Engineering

Modified U1 snRNA Vectors

Adapted to the 5' ss of Interest

1. According to the different modifications to be introduced in the U1 snRNA vector sequence, design sense and antisense primers with the desired mutation(s) to be introduced by site-directed mutagenesis (*see* **Note 4**).
2. Using the mutagenic primers, perform the site-directed mutagenesis of the WT U1 snRNA vector using the mutagenesis kit (*see* **Note 5**). Briefly, mix the U1 snRNA plasmid DNA (~40 ng) with primers, buffer, dNTPs (according to the kit), apyrogenic water, a High Fidelity Taq polymerase and subject the mixture to recommended PCR conditions from the mutagenesis kit. The number of PCR cycles varies according to the type of the desired mutation(s) (*see* **Note 6**); and the number (n) of min of the PCR extension step depends on the plasmid length, n is calculated as 1 min/kb; *see* **Note 7**. After the PCR reaction is completed, add 1 μ L (10 U) of *DpnI* restriction enzyme to the amplified products and incubate for 1 h at 37 °C to digest the parental dsDNA.
3. Use 1–4 μ L of the *DpnI* treated DNA reaction to transform *E. coli* competent cells. Briefly, thaw on ice a 50 μ L aliquot of competent cells and add 1–4 μ L of the digested reaction. Swirl the tube gently to mix and incubate on ice for 30 min. In a water bath or dry thermomixer, heat pulse the tube at 42 °C for 45 s and then place the reaction tube on ice for 2 min. Add room temperature SOC medium (5 \times the volume of competent cells) and incubate for 1 h with shaking at 600 rpm in a dry thermomixer (*see* **Note 8**). After incubation spread the appropriate volume (*see* **Note 9**) of transformation reaction on pre-warmed (37 °C) LB-agar plates containing ampicillin (100 μ g/mL) and incubate at 37 °C for 16–18 h (*see* **Note 10**).
4. To obtain plasmid DNA minipreps, prepare minicultures of selected bacterial colonies to allow their growth. Add 3 mL (*see* **Note 11**) of LB medium containing ampicillin (100 μ g/mL) to a 15 mL tube and using a sterilized pipette tip pick a colony and add it into the medium by pipetting up and down (or, simply, place the pipet tip into the medium). Repeat the procedure for 3–5 colonies. Incubate the tubes in an orbital shaking incubator at 220 rpm and 37 °C for 16–18 h. To purify the plasmid DNA prepare DNA minipreps using a plasmid miniprep purification kit (*see* **Note 12**). Select the mutant(s) U1 snRNA plasmid(s) by Sanger sequencing analysis (U1-seq Fw primer) using ~100 ng of purified miniprep.
5. Once the desired modified U1 snRNA construct(s) are selected, propagate them in maxicultures to obtain a high quantity of the modified construct(s) that can be used for transfection. First, prepare a miniculture of each case according to **step 4** (*see* **Note 13**). Then add 100–150 mL of LB medium

containing ampicillin (100 µg/mL) to a sterilized flask(s) (*see Note 11*) and inoculate all the bacterial growth from the miniculture(s). Incubate the flask(s) in an orbital shaking incubator at 37 °C and 220 rpm for 16–18 h. Using an endotoxin-free maxiprep plasmid DNA purification kit, maxiprep the plasmid(s) containing the modified U1 snRNA construct(s) and perform its sequencing analysis for validation.

3.2 In Vitro Therapeutic Evaluation of Modified U1 snRNA Vectors in Human Fibroblasts

3.2.1 Modified U1 snRNA Vectors Transfection in Human Fibroblasts

Even though we must always find a balance between the best possible experimental design and the resources available, adequate controls may never be forgotten. Still, there is a minimum standard for cell culture experiments that must always be met if we want to draw strong conclusions out of them. Therefore, adequate controls to the variables under test should always be included (*see Note 14*).

1. Grow both WT control and patient fibroblasts in T-75 flasks with DMEM + Glutamax medium supplemented with 10% FBS, 5% antibiotics, and 5% amphotericin B, in an incubator at 37 °C with 95% humidity and 5% CO₂ following standard cell culture procedures.
2. On the day before transfection, detach the cells by trypsinization. Briefly, discard the growth medium and wash cells with 3 mL of PBS buffer. Then, discard the PBS and add 2 mL of trypsin-EDTA. Subsequently, incubate cells with the solution for 5 min at 37 °C. After this period, check in an inverted microscope that cells are detached and add 4 mL of fresh medium to inactivate trypsin-EDTA action.
3. Harvest the cells to a 15 mL tube and centrifuge at $500 \times g$ for 5 min to eliminate any traces of trypsin.
4. Discard the supernatant and resuspend cells in 4 mL of fresh medium.
5. Count cells in suspension with an hemocytometer (Neubauer chamber). Pipette a small volume of cell suspension (approximately 15 µL) to both hemocytometer chambers and count the cells present in all four external quadrants of each chamber by observing it in an inverted microscope. Considering the dimensions of the chamber (1 mm × 1 mm × 0.1 mm), each quadrant has a total volume of 0.1 mm³, which equals 10⁻⁴ mL. Therefore, the total number of cells in the original suspension can be calculated with the following equation:

$$N = \frac{\sum n}{8} \times 10^4$$

where N is the total number of cells per milliliter, n is the number of cells counted in each quadrant of the Neubauer chamber and the 10⁴ factor allows for the correction of the total number of cells in 1 mL of cell suspension.

6. For modified U1 snRNA vectors transfection, seed a total of $\sim 2.5\text{--}3 \times 10^5$ fibroblast cells into 6-well plates and grow cells in DMEM + Glutamax medium supplemented with 10% FBS, 5% antibiotics and 5% amphotericin B, in an incubator at 37 °C with 95% humidity and 5% CO₂.
7. On the next day (cells at 80–90% confluence), transfect the cells with quantities between 1 and 3.5 µg of the modified U1 snRNA constructs using a transfection reagent according to the manufacturer's protocol (*see* **Notes 15** and **16**).
8. 24–48 h after transfection, harvest cells by trypsinization. Discard the growth medium of each plate well and wash cells with 1 mL of PBS buffer. Discard the PBS, add 500 µL of trypsin-EDTA to each well and incubate for 5 min at 37 °C. Then, check by microscopy that cells are rounding up and add 1 mL of DMEM + Glutamax medium to inactivate trypsin-EDTA. Harvest cells to 2 mL tubes and centrifuge at $500 \times g$ for 5 min at 4 °C; discard the supernatant; wash cells with 1 mL of PBS buffer and centrifuge again. Proceed to RNA extraction or store the pellet(s) at –80 °C for future use.

3.2.2 Analysis of Splicing Rescue by RT-PCR

1. Extract total RNA from the transfected human fibroblasts using a RNA extraction kit according to the manufacturer's protocol. Then, perform RNA quantification using a spectrophotometer.
2. For reverse transcription, use a cDNA synthesis kit following the manufacturer's protocol, and start with 1–2 µg of total RNA. The cDNA synthesis reaction can be stored at –20 °C or used immediately for PCR amplification.
3. Perform a PCR in standard conditions using a Taq polymerase supplemented with its buffer, dNTPs, gene-specific primers for a final concentration of 0.4 µM each (e.g. *HGSNAT* primers), 2 µL of cDNA, and RNase free water to a final volume of 50 µL.
4. To evaluate the splicing rescue, analyze the amplification products through agarose gel electrophoresis in an agarose gel stained with 5 µL of ethidium bromide (*see* **Note 17**). Choose a DNA ladder according to the size of the amplified band. After separation, visualize the gel using an UV transilluminator. As an example, Fig. 1 shows the results of the partial correction of *HGSNAT* exon 2 splicing after expression of a modified U1 snRNA (totally complementary to the 5'ss of exon 2) in patients' fibroblasts.
5. Assess the identity of the obtained band(s) by sequencing analysis (*see* **Note 18**). For this purpose, purify the PCR products directly with a PCR clean-up kit if there is only one amplified band or when multiple bands are present excise each band from the gel and purify them using a gel band

purification kit. Whatever the case, follow the indications present in the manufacturer's protocol.

6. Subject the purified bands to standard automated sequencing using gene-specific primers for the amplification (e.g. *HGSNAT* primers). Compare the obtained sequence (s) with the reference sequence of the gene of interest (retrieved from the Ensembl database) using the Clustal Omega bioinformatic tool (<https://www.ebi.ac.uk/Tools/msa/clustalo/>), in order to analyze the effect of the modified U1 snRNA's in rescuing the normal splicing pattern.

3.2.3 Assessment of the Effect of U1 snRNA-Induced Splicing Rescue at Protein Level

While not included in this chapter, for it is case-specific, the effect of modified U1 snRNAs-treatment at protein level is mandatory whenever we want to proceed to *in vivo* studies in order to address the true therapeutic potential of a given U1 snRNA molecule.

Ideally, as soon as we get an RT-PCR pattern that confirms splicing correction to some extent, and that rescue is confirmed by band excision and Sanger sequencing, the overall effect of that rescue at protein level should also be checked. There is a variety of methods we can choose in order to address this issue, from the direct quantification of enzymatic activity (whenever the gene product under analysis has a catalytic activity) to that of the protein itself (through Western blot).

Usually, the method of choice depends on two major factors: the protein itself and the assays available *in house* to assess it. Virtually every method from Western blot to immunofluorescence may be informative and provide extra support to the conclusions drawn from the RT-PCR. Therefore, as a take-home message, we would recommend that, whenever designing U1 snRNA molecules for splicing rescue, the effect should be checked not only at cDNA level, but also at protein level.

4 Notes

1. This chapter is exclusively focused on mutation-adapted U1 snRNAs. Nevertheless, it is important to refer that there is a novel, second generation, of engineered U1 snRNAs, which may be used for therapeutic purposes: the so-called Exon-Specific U1 snRNAs (ExSpeU1). These ExSpeU1s are complementary to non-conserved sequences downstream of mutant 5'ss. In theory, ExSpeU1 is expected to decrease the potential of off-target effects of U1 snRNA-based therapies, while allowing for a single ExSpeU1 to rescue multiple splicing defects that affect a single exon [4–6].
2. The pG3U1 vector [12] {Susani, 2004, TCIRG1-dependent recessive osteopetrosis: mutation analysis, functional

identification of the splicing defects, and in vitro rescue by U1 snRNA} was used, but the human U1 snRNA sequence can be cloned in other standard expression vector(s).

3. Store LB-agar plates with antibiotics at 4 °C in the dark.
4. Mutagenic primers can be designed using the web-based Quik-Change Primer Design Program, available online at www.agilent.com/store/primerDesignProgram.jsp (we recommend to read the “help” section of the program). However, it is important to take into account a number of considerations:
 - (a) both mutagenic primers must contain the desired mutation(s) and anneal to the same sequence on opposite strands of the plasmid;
 - (b) each primer should have between 25 and 45 bases in length with a melting temperature (T_m) of ≥ 78 °C;
 - (c) the desired mutation(s) should be located in the middle of the primer (~12–15 nucleotides of the correct sequence on both sides);
 - (d) the primers should have a minimum GC content of 40% and should terminate in one or more C or G bases;
 - (e) the primers do not need to be 5' phosphorylated and purification may either be performed by liquid chromatography (HPLC) or by polyacrylamide gel electrophoresis (PAGE).
5. To modify the pG3U1 we recommend to use the Quik-Change™ II mutagenesis kit (Agilent). However, other site-directed mutagenesis commercial kits can be used. The kit should be chosen according to the plasmid length and the type of mutations to introduce.
6. According to the type of mutation(s) to be inserted in the U1 snRNA WT sequence, the number of PCR cycles varies. For point mutations (1 nucleotide change) use 12 cycles; for single amino acid changes (3 nucleotides) use 16 cycles and for multiple amino acid deletions or insertions (≥ 4 nucleotides) use 18 cycles.
7. The number (n) of min of PCR extension step recommended is usually 1 min/kb. However, using the QuikChange™ II mutagenesis kit (Agilent) we usually increment the time for 2 min/kb. For the pG3U1 plasmid length, 8 min should work, but from our experience adding one more min to this step (in this case 9 min for extension) gives the best results.
8. If a thermomixer is not available, follow the site-directed mutagenesis kit manufacturer's recommendations concerning shaking of transformation reactions.

9. The entire volume of transformation reaction can be plated on a single LB-agar plate. However, depending on the transformation efficiency this may originate a huge number of colonies which are then difficult to select. Therefore, we recommend to use more than one plate and spread different volumes to increase the probability to obtain individualized colonies (e.g. 200 and 100 μ L). When plaquing lower volumes a small quantity (1:1) of SOC medium can be added to the transformation reaction to dilute and help to spread the transformation product.
10. If colonies cannot be selected immediately, store plate(s) at 4 °C.
11. The total volume of the tube should allow a volume of air that is 5 \times the volume of LB medium (e.g. 3 mL of LB medium in a 15 mL tube; 5 mL of LB medium in a 25 mL tube, etc.).
12. Before starting the miniprep(s) procedure, a sample of bacterial culture can be preserved in a “glycerolate” for future use. For a final volume of 1 mL, add a part of bacterial culture and a part of sterilized glycerol to a 2 mL tube for a final concentration of ~10–15% of glycerol. Vortex immediately and store at –80 °C.
13. To avoid the need to pick another bacterial colony from an LB-agar plate, the glycerolate(s) (*see* **Note 12**) can be used to prepare a new miniculture. Briefly, defrost the glycerolate on ice, scrape it lightly with a pipette tip or aspirate few microliters and pipet them up and down into a tube containing the desired volume of LB medium and ampicillin (100 μ g/mL). Incubate the tube(s) in an orbital shaking incubator as recommended in **step 4** of Subheading 3.1.1.
14. In the transfection experiments here referred (*see* **step 7** of Subheading 3.2.1) we included two negative controls: one where only the transfection reagent was added to the cells and other where the minigene expressing the WT U1 sequence was transfected on cells.
15. For liposome-based transfection of fibroblasts, Lipofectamine[®] 2000 (Invitrogen) or other commercial lipofection reagent can also be tested. To further increase transfection efficacy, the modified U1's can also be inserted into the cells by the electroporation technique. For both methods we recommend to optimize the amount of transfection reagent according to the quantity of modified U1 and number of cells to transfect.
16. To assess transfection efficiency, transfect fibroblasts with a control plasmid encoding GFP or RFP and monitor fluorescence by microscopy. Also, the cell uptake of the modified U1's can be confirmed by PCR with specific primers (U1 Fw—5' A TCGAAATTAATACGACTCA 3' and U1 Rv—5' CTGGGA AAACCACCTTCGT 3'). Otherwise, clone the WT human U1

snRNA cassette from pG3U1 vector in a plasmid encoding GFP and monitor fluorescence and U1 expression simultaneously.

17. Adjust the agarose gel percentage according to the molecular weight of the target amplified products.
18. In RT-PCR analysis after U1 snRNA's transfection, the size of the amplified band(s) seen on the agarose gel can give an idea of whether the aberrantly spliced exon under study is included in the cDNA or not. However, it is necessary to sequence the amplified band(s) from control and patient fibroblasts treated with the different modified U1 snRNAs, to confirm the correct splicing pattern.

Acknowledgments

The authors would like to acknowledge Prof. Dr. Belén Pérez (Molecular Biology Department, Faculty of Sciences, University Autonoma of Madrid, Spain) for kindly provide the pG3U1 vector. In addition, the authors would like to acknowledge BioMedCentral, Part of Springer Nature for allowing the reproduction in this chapter of an adapted version of a figure originally published in Matos, L. et al. Therapeutic strategies based on modified U1 snRNAs and chaperones for Sanfilippo C splicing mutations. *Orphanet J Rare Dis* 9, 180 (2014). <https://doi.org/10.1186/s13023-014-0180-y>. Copyright © 2014, Springer Nature. This work was partially supported by *Fundação para a Ciência e Tecnologia* (FCT) IP (project: FCT/PTDC/BBBBMD/6301/2014) and by *The National MPS Society* (project: 2019DGH1642).

References

1. van der Feltz C, Anthony K, Brilot A, Pomeranz Krummel DA (2012) Architecture of the spliceosome. *Biochemistry* 51(16): 3321–3333. <https://doi.org/10.1021/bi201215r>
2. Buratti E, Baralle D (2010) Novel roles of U1 snRNP in alternative splicing regulation. *RNA Biol* 7(4):412–419
3. Carmel I, Tal S, Vig I, Ast G (2004) Comparative analysis detects dependencies among the 5' splice-site positions. *RNA* 10(5):828–840. <https://doi.org/10.1261/rna.5196404>
4. Pinotti M, Bernardi F, Dal Mas A, Pagani F (2011) RNA-based therapeutic approaches for coagulation factor deficiencies. *J Thromb Haemost* 9(11):2143–2152. <https://doi.org/10.1111/j.1538-7836.2011.04481.x>
5. Coutinho MF, Matos L, Santos JI, Alves S (2019) RNA therapeutics: how far have we gone? *Adv Exp Med Biol* 1157:133–177. https://doi.org/10.1007/978-3-030-19966-1_7
6. Hwu WL, Lee YM, Lee NC (2017) Gene therapy with modified U1 small nuclear RNA. *Expert Rev Endocrinol Metab* 12(3): 171–175. <https://doi.org/10.1080/17446651.2017.1316191>
7. Balestra D, Faella A, Margaritis P, Cavallari N, Pagani F, Bernardi F, Arruda VR, Pinotti M (2014) An engineered U1 small nuclear RNA rescues splicing defective coagulation F7 gene expression in mice. *J Thromb Haemost* 12(2): 177–185. <https://doi.org/10.1111/jth.12471>

8. Lee NC, Lee YM, Chen PW, Byrne BJ, Hwu WL (2016) Mutation-adapted U1 snRNA corrects a splicing error of the dopa decarboxylase gene. *Hum Mol Genet* 25(23):5142–5147. <https://doi.org/10.1093/hmg/ddw323>
9. Lee B, Kim YR, Kim SJ, Goh SH, Kim JH, Oh SK, Baek JI, Kim UK, Lee KY (2019) Modified U1 snRNA and antisense oligonucleotides rescue splice mutations in SLC26A4 that cause hereditary hearing loss. *Hum Mutat* 40(8): 1172–1180. <https://doi.org/10.1002/humu.23774>
10. Breuel S, Vorm M, Bräuer AU, Owczarek-Lipska M, Neidhardt J (2019) Combining engineered U1 snRNA and antisense oligonucleotides to improve the treatment of a BBS1 splice site mutation. *Mol Ther Nucl Acids* 18: 123–130. <https://doi.org/10.1016/j.omtn.2019.08.014>
11. Matos L, Canals I, Dridi L, Choi Y, Prata MJ, Jordan P, Desviat LR, Pérez B, Pshezhetsky AV, Grinberg D, Alves S, Vilageliu L (2014) Therapeutic strategies based on modified U1 snRNAs and chaperones for Sanfilippo C splicing mutations. *Orphanet J Rare Dis* 9:180. <https://doi.org/10.1186/s13023-014-0180-y>
12. Susani L, Pangrazio A, Sobacchi C, Taranta A, Mortier G, Savarirayan R, Villa A, Orchard P, Vezzoni P, Albertini A, Frattini A, Pagani F (2004) TCIRG1-dependent recessive osteopetrosis: mutation analysis, functional identification of the splicing defects, and in vitro rescue by U1 snRNA. *Hum Mutat* 24(3):225–235. <https://doi.org/10.1002/humu.20076>
13. Lund E, Dahlberg JE (1984) True genes for human U1 small nuclear RNA. Copy number, polymorphism, and methylation. *J Biol Chem* 259(3):2013–2021

Open Access This chapter is licensed under the terms of the Creative Commons Attribution 4.0 International License (<http://creativecommons.org/licenses/by/4.0/>), which permits use, sharing, adaptation, distribution and reproduction in any medium or format, as long as you give appropriate credit to the original author(s) and the source, provide a link to the Creative Commons license and indicate if changes were made.

The images or other third party material in this chapter are included in the chapter's Creative Commons license, unless indicated otherwise in a credit line to the material. If material is not included in the chapter's Creative Commons license and your intended use is not permitted by statutory regulation or exceeds the permitted use, you will need to obtain permission directly from the copyright holder.





Conjugation of Nucleic Acids and Drugs to Gold Nanoparticles

Paula Milán-Rois, Ciro Rodriguez-Diaz, Milagros Castellanos,
and Álvaro Somoza 

Abstract

Gold nanoparticles (AuNPs) can be used as carriers for biomolecules or drugs in cell culture and animal models. Particularly, AuNPs ease their internalization into the cell and prevent their degradation. In addition, engineered AuNPs can be employed as sensors of a variety of biomarkers, where the electronic and optical properties of the AuNPs are exploited for a convenient, easy, and fast read out. However, in all these applications, a key step requires the conjugation of the different molecules to the nanoparticles. The most common approach exploits the great affinity of sulfur for gold. Herein, we summarize the methods used by our group for the conjugation of different molecules with AuNPs. The procedure is easy and takes around 2 days, where the reagents are slowly added, following an incubation at room temperature to ensure the complete conjugation. Finally, the unbound material is removed by centrifugation.

Key words Gold nanoparticles, Spherical nucleic acid, Functionalization, Oligonucleotides, Nano-medicine, Metal nanoparticles, Conjugation, Drug delivery, Sensors

1 Introduction

Oligonucleotides and drugs face some challenges for their optimal delivery in cells and animal models. Particularly, oligonucleotides (e.g., antisense, gapmers, and siRNAs) usually present low stability and suffer from reduced cell internalization and selectivity [1, 2] and, for these reasons, transfection reagents such as lipofectamine are usually employed to improve delivery. On the other hand, drugs can be too hydrophobic and require solubilizing molecules (e.g., dimethylsulfoxide [DMSO], ethanol). However, these kinds of chemicals present critical restrictions such as cytotoxicity or limited loading. To overcome these drawbacks, delivery systems based on nanoparticles can be employed [3]. There are different types of nanoparticles such as liposomes, micelles, dendrimers, inorganic

particles, carbon-based nanostructures, viral nanocarriers, polymeric, peptide or metallic nanoparticles, etc. [4–12]. Each vehicle presents different characteristics that can be exploited to address specific challenges related to the delivery of bioactive molecules.

Among the different systems, gold nanoparticles (AuNPs) present excellent properties for the delivery of oligonucleotides because of their low toxicity, cost, and particularly their ease of preparation and functionalization [13]. AuNPs can be synthesized in the laboratory through simple methods, such as the one described by Turkevich [14] and detailed in Subheading 3.1.

The properties of AuNPs can be tuned through their modification with oligonucleotides. When the nanoparticles are densely loaded with oligonucleotides, the resulting nanostructures are known as spherical nucleic acids (SNA) [15]. This kind of nanostructure presents interesting features, such as high internalization in a wide variety of cells and low toxicity. Therefore, these derivatives can be employed for multiple applications, such as drug delivery systems, gene therapy and regulation, or molecular diagnosis [16, 17].

Regarding the vehiculization of therapeutics, AuNPs can be used for the delivery of hydrophobic drugs such as paclitaxel, doxorubicin, or AZD8055 without affecting their effectiveness [18, 19]. On the other hand, AuNPs functionalized with oligonucleotides (e.g., siRNAs, gapmers) could be used as a substitute for transfection reagents in different applications involving gene regulation, or even immunomodulatory processes, for the treatment of diseases such as cancer, sepsis, skin disorders, diabetes, etc. [16, 20–22].

In the case of diagnostics, it is worth mentioning that fast and accurate point-of-care diagnostic systems are critical in personalized medicine. In particular, nucleic acid detection is of great importance for the diagnosis and treatment of many diseases caused by genetic mutations, infectious agents, or other physiologically abnormal circumstances. Conventional methods such as RT-PCR offer high accuracy and sensitivity; however, these methods are not suitable for routine diagnosis because they are time-consuming and need highly trained personnel and expensive equipment. One development that seems to simplify the nucleic acid detection and we study in the lab is the use of SNA based on a single-stranded oligonucleotide with a unique stem-loop structure (Molecular Beacon, MB) [23, 24].

This chapter describes how to conjugate drugs or oligonucleotides to AuNPs, which can be further used as delivery systems of therapeutics and sensors.

To attach any compound to AuNPs, the high affinity of thiol groups to gold could be exploited. Thus, the molecules (e.g., oligonucleotides, drugs) should be functionalized with linkers

containing sulfur-based moieties, such as thiols or dithiolanes [25], which are commented in this chapter.

AuNPs conjugation requires a few simple steps of addition, incubation, and washes. The method might change slightly depending on the linker employed for the conjugation, which can be designed to control the release or stability of the cargo. In general, the use of dithiolane provides more robust structures and can be achieved in few hours, whereas the use of thiols implies more than 1 day. For the reader's convenience, we have included the preparation of the dithiolane linkers used in our group. The approach can be used for the conjugation of drugs, polymers (e.g., polyethylene glycol [PEG]), or the preparation of oligonucleotides in a DNA synthesizer using a tailored solid support, usually based on controlled pore glass (CPG).

2 Materials

2.1 AuNP Synthesis

2.1.1 Materials

- 250 mL round-bottom glass flask.
- Septum for a 250 mL round-bottom flask.
- 3.5 cm long magnet.
- 0.3 μm fritted filter for vacuum filtration.
- 250 mL Erlenmeyer flask with an output for vacuum.
- Plastic material such as conical centrifuge tubes and microcentrifuge tubes.
- 1 mL quartz cuvette.

2.1.2 Reagents

- Gold solution: 945.2 μM Hydrogen tetrachloroaurate (III) hydrate ($\text{AuCl}_4\text{H}_3\text{O}$) in 100 mL autoclaved Milli-Q grade water.
- Ultrapure reagent-grade water.
- Sodium citrate solution: 40 mM sodium citrate tribasic dihydrate (118 mg) in 10 mL autoclaved Milli-Q grade water.

2.1.3 Equipment

- Hot plate (7 cm radius) with magnetic stirring.
- Reflux column.
- Vacuum pump.
- UV-Vis spectrophotometer.

2.2 Dithiolane-Based Linkers Synthesis

2.2.1 Materials

- 50 mL round-bottom flask.
- 2-cm long magnet.
- 1 septum.
- Thin-layer chromatography (TLC) (sheets of silica gel 60F254).
- Filter paper.
- 2000 KDa tubing membrane.

2.2.2 Reagents

- Lipoic acid.
- *N*-hydroxysuccinimide (NHS).
- Tetrahydrofuran (THF).
- *N,N'*-dicyclohexylcarbodiimide (DCC).
- Ethyl acetate (AcOEt).
- Methoxypolyethylene glycol amine (PEG-NH₂).
- Drug with a primary amine (e.g., Gemcitabine).
- Dimethylformamide (DMF).
- Dichloromethane (CH₂Cl₂).
- Methanol (MeOH).
- Threoninol.
- 4,4'-Dimethoxytrityl chloride (DMTrCl).
- Dry pyridine (Py).
- Hexane.
- Succinic anhydride.
- Dry CH₂Cl₂.
- 4-(Dimethylamino)pyridine (DMAP).
- *N,N*-Diisopropylethylamine (DIPEA).
- Distilled water.
- Magnesium sulfate anhydrous (MgSO₄).
- 1-Hydroxybenzotriazole (HBO^t).
- Acetonitrile (MeCN).
- CPG: Aminopropyl-CPG, 1000 Å.
- Caping reagent A (CAP A): THF/pyridine/acetic anhydride (8:1:1).
- Caping reagent B (CAP B): 10% Methylimidazole in THF.

2.2.3 Equipment

- Flash column chromatography using silica gel (60 Å, 230 × 400 mesh).
- Rotavapor.

2.3 Functionalization of AuNPs

2.3.1 Materials

- Plastic material: one microcentrifuge tube per condition.
- A 96-well plate for absorbance measurements in a plate reader.

2.3.2 Reagents

- Oligonucleotides with sulfide-based modifications at micromolar concentration.
- Annealing buffer 3×: 30 mM Tris-HCl, 3 mM EDTA, 150 mM NaCl.
- Tris (2-carboxyethyl) phosphine hydrochloride solution (TCEP).
- Gold nanoparticles (AuNP) with a diameter of 13 ± 2 nm (*see* Subheading 3.1).
- Sodium chloride solution: 5 M NaCl.
- Oligonucleotide quantification kit (e.g., Quant-iT™ OliGreen™ ssDNA Assay Kit, Qubit™ ssDNA Assay Kit), including the Quant-iT OliGreen® ss DNA Reagent, TE 20× buffer, and oligonucleotide standard.
- Autoclaved Milli-Q grade water.
- PEG modified with a dithiolane group (*see* Subheading 3.2.2).
- Chemotherapeutic drugs with dithiolane-based linker (e.g., gemcitabine) (*see* Subheading 3.2.3).

2.3.3 Equipment

- Benchtop centrifuge.
- Vortex mixer.
- Orbital shaker.
- Plate reader suitable for absorbance and fluorescence determinations using 96-well plates.
- Evaporating centrifuge.

3 Methods

3.1 AuNP Synthesis

For the preparation of AuNP (13 ± 2 nm) the Turkevich method is used [14] as follows:

1. Turn on the heating plate to 140 °C.
2. Add 100 µL of HAuCl₄ solution (94.52 µmol) in a 250 mL round bottom flask containing 100 mL of sterile water.
3. Add the magnet to the round bottom flask.
4. Place the round bottom flask in the heating plate while stirring at 700 rpm approximately, with a reflux system, and heat it to reflux.

5. Prepare the sodium citrate tribasic dihydrate solution in a 50 mL conical centrifuge tube.
6. When the mixture boils, add the citrate solution quickly while stirring at 700 rpm.
7. Wait for 15 min and then remove the round bottom flask from the heating plate. During this period, the color of the solution turns from yellow to red (*see Note 1*).
8. Leave the mixture stirring at 300 rpm at room temperature and protect from the light for 16 h.
9. Filter the solution using a 0.3 μm fritted filter with the help of vacuum.
10. Determine nanoparticles' size: for proper characterization of gold nanoparticles, the size should be measured by TEM and the concentration determined by UV-Vis spectrophotometry using the Beer-Lambert law. It requires measuring the UV-Vis absorbance at 520 nm and using the corresponding extinction coefficient (ϵ) for its size [26]. For instance, to determine the concentration of 13 ± 1 nm AuNPs, which have an extinction coefficient (ϵ) of $2.7 \times 10^8 \text{ M}^{-1} \text{ cm}^{-1}$, you should use the following equation (Eq. 1):

$$\text{concentration} = \frac{A}{\epsilon \times l} \quad (1)$$

where A is the absorbance at 520 nm, l is the optical path in cm, and ϵ extinction coefficient in $\text{M}^{-1} \text{ cm}^{-1}$.

3.2 Dithiolane-Based Linkers Synthesis

The preparation of the dithiolane-based derivatives of drugs (**3**) and PEG (**2**) is summarized in Fig. 1 and described in the following instructions. In the case of oligonucleotides, the required solid support (CPG) containing a dithiolane moiety for the preparation of oligonucleotides is also described (7).

3.2.1 Compound **1** [2,5-Dioxopyrrolidin-1-yl(R)-5-(1,2-Dithiolan-3-yl)Pentanoate]

1. Dissolve lipoic acid (1 equiv.) and *N*-hydroxysuccinimide (1.2 equiv.) in tetrahydrofuran (0.5 M).
2. Stir the solution at 0 °C for 10 min.
3. Dissolve *N,N'*-dicyclohexylcarbodiimide (1.2 equiv.) in tetrahydrofuran (3.5 M) and add it slowly to the lipoic acid and *N*-hydroxysuccinimide solution obtained in **step 1**.
4. Stir the reaction at room temperature for 5 h.
5. Filter the mixture using a filter paper and wash the solid with cold ethyl acetate. Evaporate the solvent under vacuum to obtain compound **1** as a yellow oil.

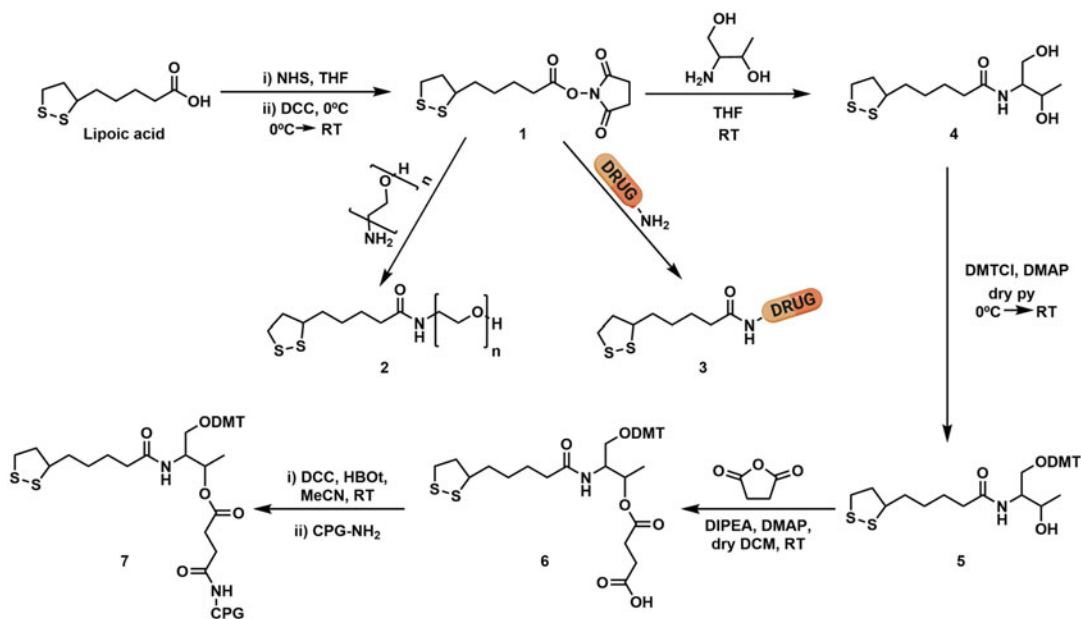


Fig. 1 Schematic representation of the synthesis of dithiolane-modified products: PEG, drug, and CPG

3.2.2 PEG (**2**)

1. Dissolve compound **1** (2 equiv.) and PEG-NH₂ (1 equiv.) in tetrahydrofuran.
2. Stir the reaction at room temperature for 18 h.
3. Purify the crude by dialysis with a 2000 KDa tubing membrane.
4. Stir the solution for 18 h to obtain compound **2**.

3.2.3 Drug-Modified Linker (**3**)

1. Dissolve compound **1** (2 equiv.) and a drug containing a primary amine (e.g., Gemcitabine) (1 equiv.) in dimethylformamide (0.1 M).
2. Stir the reaction at room temperature for 24 h.
3. Eliminate the solvent in vacuum.
4. Purify the crude by flash chromatography (CH₂Cl₂:MeOH/25:1) to obtain compound **3**.

3.2.4 Compound **4**: N-(1,3-Dihydroxybutan-2-yl)-5-(1,2-Dithiolan-3-yl) Pentanamide

1. Dissolve compound **1** (1 equiv.) and threoninol (1.1 equiv.) in THF (0.15 M).
2. Stir the solution at room temperature for 18 h.
3. Eliminate the solvent in vacuum.
4. Purify the crude by flash chromatography (CH₂Cl₂:MeOH/25:1) to obtain compound **4** as a yellow oil.

3.2.5 Compound 5: N-(1-(bis(4-Methoxyphenyl)(Phenyl)methoxy)-3-Hydroxybutan-2-yl)-5-(1,2-Dithiolan-3-yl)Pentanamide

1. Dissolve compound **4** (1 equiv.) in dry pyridine (0.3 M).
2. Dissolve DMTrCl (1.2 equiv.) in dry pyridine (1 M) and add to the compound **4** solution in dry pyridine at 0 °C.
3. Stir the reaction at 0 °C for 30 min, then at room temperature for 18 h.
4. Eliminate the solvent in vacuum.
5. Purify the crude by flash chromatography (Hexane:AcOEt/1:1) to obtain compound **5** as a beige foam.

3.2.6 Compound 6: 4-((3-(5-(1,2-Dithiolan-3-yl)Pentanamido)-4-(bis(4-Methoxyphenyl)(Phenyl)methoxy)Butan-2-yl)oxy)-4-Oxobutanoic Acid

1. Dissolve compound **5** (1 equiv.), DMAP (0.1 equiv.) and DIPEA (1.4 equiv.) in dry CH₂Cl₂ (0.13 M).
2. Dissolve succinic anhydride (1.3 equiv.) in dry CH₂Cl₂ (0.3 M) and add the solution slowly to the mixture prepared in the previous step at 0 °C.
3. Stir the reaction at room temperature for 18 h.
4. Wash the solution with water 3 times.
5. Dry the organic layer with MgSO₄.
6. Eliminate the solvent in vacuum to obtain compound **6**.

3.2.7 Compound 7: 4-((3-(5-(1,2-Dithiolan-3-yl)Pentanamido)-4-(bis(4-Methoxyphenyl)(Phenyl)methoxy)Butan-2-yl)oxy)-4-Oxobutanamide CPG

1. Dissolve compound **6** (1 equiv.) in MeCN (0.05 M).
2. Dissolve DCC (1 equiv.) and HBO^t (1 equiv.) in MeCN (0.2 M) and add to compound **6** solution at room temperature for 3 h.
3. Filter the solution with filter paper and add to the CPG (5 equiv. in mg).
4. Stir the mixture for 3 h at room temperature.
5. Remove the solvent and wash the CPG with MeOH three times and with CH₂Cl₂ three times.
6. Dry the CPG.
7. Add a mixture of capping reagents [CAP A:CAP B (1:1)] (1 mL per 175 mg of CPG).
8. Stir the solution for 1 h at RT.
9. Remove the solvent and wash the CPG with MeOH three times and with MeCN three times.

3.3 AuNP Functionalization with Thiol-Modified Oligonucleotides

Oligonucleotides can be easily attached to AuNPs using a thiol-based linker, which is commercially available, and most oligonucleotide providers offer this modification. However, the thiol group should be deprotected, as detailed below, before incubating the oligonucleotides with AuNPs (Fig. 2).

1. Incubate the oligonucleotide with TCEP (*see Note 2*) using a 100× excess relative to the oligonucleotide's thiol (*see Note 3*)

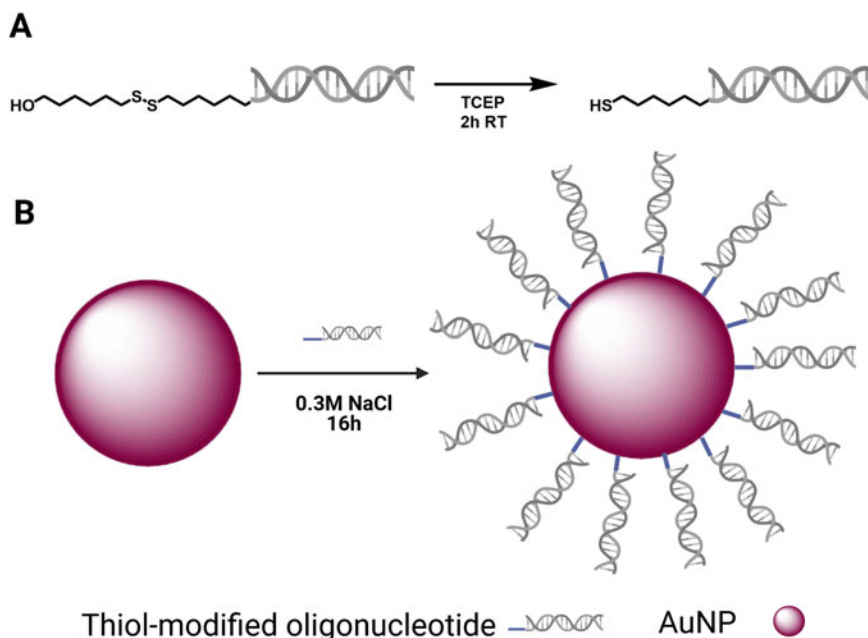


Fig. 2 Schematic representation of: (a) Deprotection of oligonucleotides bearing a thiol moiety. (b) Functionalization of AuNPs with thiol-modified oligonucleotides

for 2 h at room temperature and moderate agitation on a mini-shaker (e.g., for deprotect 500 μL of an oligonucleotide solution at 20 μM (i.e., 20 pmol/ μL) use 2 μL of TCEP at 0.5 M) (*see Note 4*).

2. Add the deprotected oligonucleotide slowly to the AuNP solution prepared at 12 nM.
3. Incubate the mixture for 45 min at room temperature and moderate agitation.
4. Add 60 μL NaCl solution to a final concentration of 0.3 M through the addition of small volumes (e.g., 5–10 μL) (*see Note 5*). Vortex the solution quickly after each addition of NaCl solution and incubate the sample for at least 10 min on a mini-shaker between each addition.
5. Incubate the sample for 16 h at room temperature on a mini-shaker with moderate agitation.
6. Remove any unbound material by centrifugation at 13.2 rpm and 4 $^{\circ}\text{C}$ for 30 min. After the centrifugation, remove the supernatant and save it for later use. The pellet should be resuspended by vortexing in sterile water using the same volume of water removed to keep the concentration constant. Repeat the cleaning **step 3** times (*see Note 6*).
7. Evaporate the collected supernatants and use the Quant-iT™ OliGreen™ ssDNA Assay Kit protocol to determine the

unbound oligonucleotide from the solution (*see* Subheading 3.4) (*see* **Note 7**).

3.4 Oligonucleotide Quantification

For the quantification of oligonucleotides in the supernatant, use an oligonucleotide quantification kit. In this case, the Quant-iT OliGreen kit is used. The general procedure is as follows.

3.4.1 Standard Curve Preparation

1. Prepare a standard curve for each oligonucleotide using at least 5 dilutions of the specific oligonucleotide in TE buffer (1×), e.g., 0, 1000, 750, 500, 250 ng/mL.
2. Prepare a solution of Quant-iT OliGreen® ss DNA Reagent (2 µg/mL) in TE (1×).
3. Mix each oligonucleotide dilution from **step 1** with 1 mL OliGreen solution prepared in **step 2**. Incubate the solution for 5 min at room temperature protected from light.
4. Take 200 µL of each solution prepared in **step 3** and measure it in a plate reader (excitation 480 nm, emission 520 nm).
5. Plot the data in a concentration (ng/mL, *X*-axis) vs. absorbance (a.u., *Y*-axis) graph. Fit the data to a simple linear regression model and use this equation to calculate future concentrations.

3.4.2 Oligonucleotide Quantification in AuNPs

1. Evaporate to dryness the supernatant collected during the cleaning of modified AuNPs (*see* **step 7** in Subheading 3.3).
2. Resuspend the pellet in 1 mL TE (1×).
3. Prepare a solution of OliGreen reagent (2 µg/mL) in TE (1×).
4. Mix the resuspended supernatant with 1 mL OliGreen solution (*see* **step 2** in Subheading 3.4.1). Incubate the solution for 5 min at room temperature protected from light.
5. Take 200 µL of each solution prepared in **step 4** and measure it in a plate reader (excitation 480 nm, emission 520 nm).
6. Interpolate the data obtained in the standard curve equation (*see* **step 5** in Subheading 3.4.1) to determine the amount of unbounded oligonucleotide.

3.5 AuNP Functionalization with Dithiolane-Modified Oligonucleotides or Drugs

Oligonucleotides could be attached to AuNPs in a faster way using a dithiolane-based linker, which does not require a deprotection step, as in the case of thiols (Fig. 3).

3.5.1 AuNP Functionalization with Dithiolane-Modified Oligonucleotides

1. Add the oligonucleotide to 1 mL 12 nM of 13 ± 2 nm gold nanoparticles (AuNP) (*see* **Note 3**).
2. Incubate the solution for 15 min at room temperature on a mini-shaker at a moderate speed.
3. Add 60 µL NaCl solution to a final concentration of 0.3 M through the addition of small volumes (e.g., 5–10 µL) (*see*

Note 5). Vortex the solution quickly after each addition of NaCl solution and incubate the sample for at least 10 min on a mini-shaker between each addition.

4. Incubate the sample for 4 h at room temperature on a mini-shaker at a moderate speed.
5. Continue with the washing steps, as described previously (*see step 6* in Subheading 3.3) and the quantification of the unbound material (*see* Subheading 3.4) (*see Notes 6 and 7*).

3.5.2 AuNP

Functionalization with Dithiolane-Modified Drugs

In this case, the drugs have to be modified with a dithiolane-based linker (Fig. 4), and the AuNPs should be stabilized with oligonucleotides or PEG containing a sulfide-based linker. In this case, for 1 mL of 13 ± 2 nm AuNP (12 nM) add at least 2000 pmol of stabilizing agent (e.g., PEG, oligonucleotide) and then the required amount of the modified drug for a total of 10,000 pmol (stabilizing agent + drug) in the solution.

1. Add the stabilizing agent and incubate it for 15 min at room temperature on a mini-shaker at a moderate speed.
2. Add the modified drug very slowly and incubate it for 16 h at room temperature on a mini-shaker at a moderate speed (*see Note 5*).
3. Wash the nanoparticles as described in **step 6** in Subheading 3.3 (*see Note 6*).
4. Evaporate the collected supernatant to the initial volume (1 mL) to quantify the drug and determine the nanoparticles' loading.
5. Measure the supernatant in a spectrophotometer (according to the specific absorbance of the drug) and calculate the unbound drug using the Beer-Lambert formula (*see Note 8*).

4 Notes

1. AuNP solution should be kept in darkness.
2. Keep TCEP under an inert atmosphere to prevent its oxidation. Once opened, store the compound in 20 μ L aliquots at -20 $^{\circ}$ C.
3. Duplexes should be annealed from their corresponding oligonucleotides before conjugation. In short, combine equal concentration and volume of each strand and add the same volume of annealing buffer ($3\times$). Then, incubate the sample at 95 $^{\circ}$ C for 10 min and leave to cool slowly to room temperature.

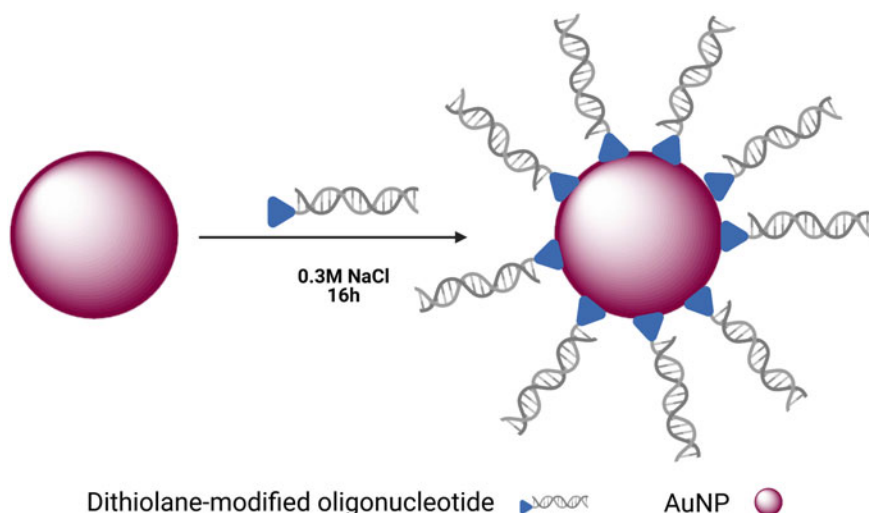


Fig. 3 Schematic representation of AuNPs functionalization with dithiolane-modified oligonucleotides

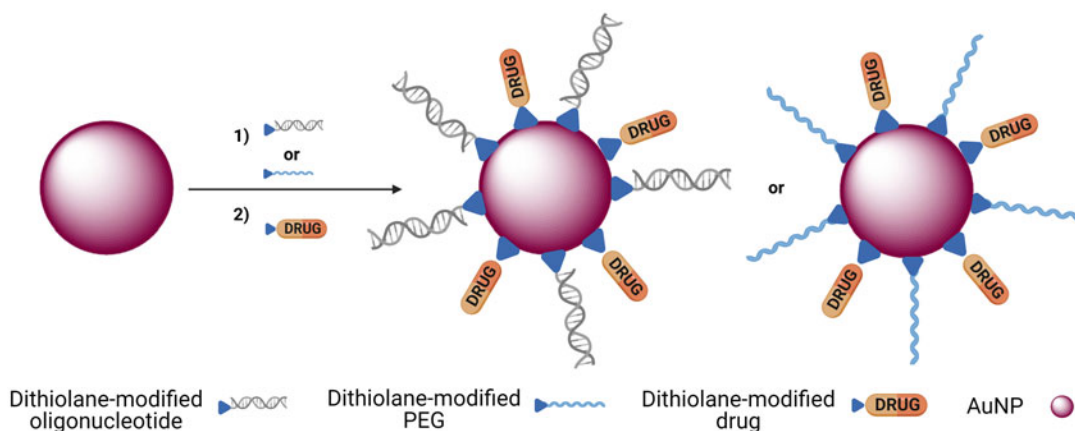


Fig. 4 Schematic representation of AuNPs functionalization with a dithiolane-modified drug using oligonucleotides or PEG as stabilizers

4. To get a complete functionalization of the nanoparticles, we recommend adding 10,000 pmol of the oligonucleotide to 1 mL AuNP (12 nM, 13 nm).
5. If you see that the AuNPs are being attached to the plastic tubes, move the solution to other plastic tubes immediately.
6. When AuNPs are changing their color to blue, it is due to aggregation. If vortexing the solution does not re-solubilize them, discard the preparation.
7. Oligonucleotide quantification could also be done by releasing the attached oligonucleotide [27]. To do so, treat the sample with 1 mM GSH for 8 h 37 °C. Then centrifuge the sample for

30 min at 13.2 rpm. Collect the supernatant and measure it as described in Subheading 3.3 and 3.4.

8. Drug quantification could also be done by comparing the drug supernatant absorbance or fluorescence with a proper standard linear calibration curve of the drug [19] or using analytical chromatography (HPLC).

References

1. Milán Rois P, Latorre A, Rodriguez Diaz C et al (2018) Reprogramming cells for synergistic combination therapy with nanotherapeutics against uveal melanoma. *Biomimetics* 3:28. <https://doi.org/10.3390/biomimetics3040028>
2. Hammond SM, Aartsma-Rus A, Alves S et al (2021) Delivery of oligonucleotide-based therapeutics: challenges and opportunities. *EMBO Mol Med* 13:e13243. <https://doi.org/10.15252/emmm.202013243>
3. Godfrey C, Desviat LR, Smedsrød B et al (2017) Delivery is key: lessons learnt from developing splice-switching antisense therapies. *EMBO Mol Med* 9:545–557. <https://doi.org/10.15252/emmm.201607199>
4. Bregoli L, Movia D, Gavigan-Imedio JD et al (2016) Nanomedicine applied to translational oncology: a future perspective on cancer treatment. *Nanomed Nanotechnol Biol Med* 12: 81–103. <https://doi.org/10.1016/j.nano.2015.08.006>
5. Gou Y, Miao D, Zhou M et al (2018) Bio-inspired protein-based nanoformulations for cancer theranostics. *Front Pharmacol* 9: 421–462. <https://doi.org/10.3389/fphar.2018.00421>
6. Mahajan S, Patharkar A, Kuche K et al (2018) Functionalized carbon nanotubes as emerging delivery system for the treatment of cancer. *Int J Pharm* 548:540–558. <https://doi.org/10.1016/j.ijpharm.2018.07.027>
7. Singh P, Pandit S, Mokkapati VRSS et al (2018) Gold nanoparticles in diagnostics and therapeutics for human cancer. *Int J Mol Sci* 19:1979. <https://doi.org/10.3390/ijms19071979>
8. Mishra DK, Shandilya R, Mishra PK (2018) Lipid based nanocarriers: a translational perspective. *Nanomed Nanotechnol Biol Med* 14:2023–2050. <https://doi.org/10.1016/j.nano.2018.05.021>
9. Núñez C, Estévez SV, del Pilar CM (2018) Inorganic nanoparticles in diagnosis and treatment of breast cancer. *J Biol Inorg Chem* 23: 331–345. <https://doi.org/10.1007/s00775-018-1542-z>
10. Manzano M, Vallet-Regí M (2018) Mesoporous silica nanoparticles in nanomedicine applications. *J Mater Sci Mater Med* 29:65. <https://doi.org/10.1007/s10856-018-6069-x>
11. Pattni BS, Chupin VV, Torchilin VP (2015) New developments in liposomal drug delivery. *Chem Rev* 115:10938–10966. <https://doi.org/10.1021/acs.chemrev.5b00046>
12. Steinmetz NF (2013) Viral nanoparticles in drug delivery and imaging. *Mol Pharm* 10: 1–2. <https://doi.org/10.1021/mp300658j>
13. Daraee H, Eatemadi A, Abbasi E et al (2016) Application of gold nanoparticles in biomedical and drug delivery. *Artif Cells Nanomed Biotechnol* 44:410–422. <https://doi.org/10.3109/21691401.2014.955107>
14. Turkevich J, Stevenson PC, Hillier J (1951) A study of the nucleation and growth processes in the synthesis of colloidal gold. *Discuss Faraday Soc* 11:55. <https://doi.org/10.1039/d89511100055>
15. Cutler JL, Auyeung E, Mirkin CA (2012) Spherical nucleic acids. *J Am Chem Soc* 134: 1376–1391. <https://doi.org/10.1021/ja209351u>
16. Mokhtarzadeh A, Vahidnezhad H, Youssefian L et al (2019) Applications of spherical nucleic acid nanoparticles as delivery systems. *Trends Mol Med* 25(12):1066–1079. <https://doi.org/10.1016/j.molmed.2019.08.012>
17. Mioc A, Mioc M, Ghiulai R et al (2019) Gold nanoparticles as targeted delivery systems and theranostic agents in cancer therapy. *Curr Med Chem* 26(35):6493–6513. <https://doi.org/10.2174/0929867326666190506123721>
18. Heo DN, Yang DH, Moon H-J et al (2012) Gold nanoparticles surface-functionalized with paclitaxel drug and biotin receptor as theranostic agents for cancer therapy. *Biomaterials* 33: 856–866. <https://doi.org/10.1016/j.biomaterials.2011.09.064>
19. Latorre A, Posch C, Garcimartín Y et al (2014) DNA and aptamer stabilized gold nanoparticles for targeted delivery of anticancer

- therapeutics. *Nanoscale* 6:7436–7442. <https://doi.org/10.1039/C4NR00019F>
20. Kapadia CH, Melamed JR, Day ES (2018) Spherical nucleic acid nanoparticles: therapeutic potential. *BioDrugs* 32:297–309. <https://doi.org/10.1007/s40259-018-0290-5>
 21. Randeria PS, Seeger MA, Wang X-Q et al (2015) siRNA-based spherical nucleic acids reverse impaired wound healing in diabetic mice by ganglioside GM3 synthase knock-down. *Proc Natl Acad Sci* 112:5573–5578. <https://doi.org/10.1073/pnas.1505951112>
 22. Wang X, Hao L, Bu HF et al (2016) Spherical nucleic acid targeting microRNA-99b enhances intestinal MFG-E8 gene expression and restores enterocyte migration in lipopolysaccharide-induced septic mice. *Sci Rep* 6:1–13. <https://doi.org/10.1038/srep31687>
 23. Latorre A, Posch C, Garcimartín Y et al (2014) Single-point mutation detection in RNA extracts using gold nanoparticles modified with hydrophobic molecular beacon-like structures. *Chem Commun* 50(23):3018–3020. <https://doi.org/10.1039/c3cc47862a>
 24. Coutinho C, Somoza Á (2019) MicroRNA sensors based on gold nanoparticles. *Anal Bioanal Chem* 411(9):1807–1824
 25. Posch C, Latorre A, Crosby MB et al (2015) Detection of GNAQ mutations and reduction of cell viability in uveal melanoma cells with functionalized gold nanoparticles. *Biomed Microdev* 17:15–37. <https://doi.org/10.1007/s10544-014-9908-7>
 26. Liu X, Atwater M, Wang J, Huo Q (2007) Extinction coefficient of gold nanoparticles with different sizes and different capping ligands. *Colloids Surf B Biointerfaces* 58:3–7. <https://doi.org/10.1016/J.COLSURFB.2006.08.005>
 27. Melamed JR, Riley RS, Valcourt DM et al (2017) Quantification of siRNA duplexes bound to gold nanoparticle surfaces. *Methods Mol Biol* 1570:1–15

Open Access This chapter is licensed under the terms of the Creative Commons Attribution 4.0 International License (<http://creativecommons.org/licenses/by/4.0/>), which permits use, sharing, adaptation, distribution and reproduction in any medium or format, as long as you give appropriate credit to the original author(s) and the source, provide a link to the Creative Commons license and indicate if changes were made.

The images or other third party material in this chapter are included in the chapter's Creative Commons license, unless indicated otherwise in a credit line to the material. If material is not included in the chapter's Creative Commons license and your intended use is not permitted by statutory regulation or exceeds the permitted use, you will need to obtain permission directly from the copyright holder.





Chapter 7

Determination of Optimum Ratio of Cationic Polymers and Small Interfering RNA with Agarose Gel Retardation Assay

Omer Aydin, Dilek Kanarya, Ummugulsum Yilmaz, and Cansu Ümran Tunç

Abstract

Nanomaterials have aroused attention in the recent years for their high potential for gene delivery applications. Most of the nanoformulations used in gene delivery are positively charged to carry negatively charged oligonucleotides. However, excessive positively charged carriers are cytotoxic. Therefore, the complexed oligonucleotide/nanoparticles should be well-examined before the application. In that manner, agarose gel electrophoresis, which is a basic method utilized for separation, identification, and purification of nucleic acid molecules because of its poriferous nature, is one of the strategies to determine the most efficient complexation rate. When the electric field is applied, RNA fragments can migrate through anode due to the negatively charged phosphate backbone. Because RNA has a uniform mass/charge ratio, RNA molecules run in agarose gel proportional according to their size and molecular weight. In this chapter, the determination of complexation efficiency between cationic polymer carriers and small interfering RNA (siRNA) cargos by using agarose gel electrophoresis is described. siRNA/cationic polymer carrier complexes are placed in an electric field and the charged molecules move through the counter-charged electrodes due to the phenomenon of electrostatic attraction. Nucleic acid cargos are loaded to cationic carriers via the electrostatic interaction between positively charged amine groups (N) of the carrier and negatively charged phosphate groups (P) of RNA. The N/P ratio determines the loading efficiency of the cationic polymer carrier. In here, the determination of N/P ratio, where the most efficient complexation occurs, by exposure to the electric field with a gel retardation assay is explained.

Key words Small interfering ribonucleic acid (siRNA), Agarose gel retardation assay, siRNA/cationic polymer carrier complex, Nanoparticles, N/P ratio, Gene delivery

1 Introduction

Regulation of a specific gene has been used for the treatment of a wide range of diseases such as cardiovascular diseases [1], neurodegenerative diseases [2], and cancer [3]. RNA Interference (RNAi) has become a powerful tool for gene silencing studies due to its advantageous properties such as high specificity, effectiveness, a minimum amount of side effect, and easy preparation [4]. RNAi mechanism was first determined by Andrew Z. Fire, Craig

C. Mello, and their colleagues [5]. As a result of their studies, they received the Nobel Prize in Physiology or Medicine in 2006. Interfering RNAs have the ability to silence target genes in cells [6]. At this silencing process, 18–31 nucleotides length small RNA molecules are introduced into cells and induce a sequence-specific gene silencing at the post-transcriptional level by blocking mRNAs containing a matched sequence.

siRNA is the most commonly used interfering RNA and has shown high potential as a therapeutic RNA for gene-based treatments [7]. It regulates the expression of various genes by binding to mRNAs in the cell cytoplasm and causing degradation of their mRNA target. The siRNA is double stranded in nature and is about 22 nucleotides in length. Its precursor is initially recognized by Dicer RNase and then incorporated with the RNA-induced silencing complex (RISC). The siRNA-RISC complex can bind the targeting region of the mRNA and lead to a sequence-specific cleavage with endonuclease Argonaute-2 (AGO2), thereby reducing the expression of the targeted protein [8].

Although siRNA has had particular interest in research, there are some limitations. The major limitations of siRNAs-based therapeutics are their rapid degradation by serum nucleases, poor cellular uptake due to the negatively charged backbone, rapid renal clearance following systemic delivery, off-target effects, and induction of immune responses [9]. In addition, even after siRNA is released from the endosome without being exposed to the lysosome and released into the cell cytoplasm, gene silencing of the siRNA may not be immediately observed [10]. Thereby, before the silencing therapeutic effect of siRNA begins, there is always an induction period due to the intracellular half-life of the target protein. The silencing effect of the given siRNA decreases over time owing to the natural degradation of the siRNA molecules in the cell. Moreover, the therapeutic effect persists for a limited time in rapidly dividing cells such as cancer cells, due to the continuous dilution of siRNA in the replication.

Bare siRNA molecules have poor cellular internalization and they need a carrier to enter cells, where their mechanism of action occurs. The major challenge in the delivery of nucleic acids is the availability of a suitable carrier for transferring siRNA to target cells. To do that, there are two main approaches such as viral and non-viral vectors [11]. The suitable vectors should provide a high degree of transfection for a long period without causing systemic toxicity and immunogenicity [12]. Despite the high transfection activity of viral vectors, possible damage to host genes, immune system stimulation, and infection potential limit its application for gene therapy [13].

To overcome these limitations different types of delivery systems have been designed such as lipid [14, 15], polymer [16], peptide [17, 18], dendrimer [19–21], and micelle [22] based

vehicles. An ideal siRNA delivery system should be non-toxic, safe, and effective. Thus, many studies have focused on the development of non-viral vectors with minimal toxicity. Furthermore, the carrier systems should assure entrance of siRNA cargos to the cell cytoplasm without being interrupted by biological barriers such as serum, cell membrane, and endosome/lysosome [23]. In detail, the cell entry of siRNA/cationic polymer carriers is mostly facilitated by the mechanism known as “endocytosis” [10]. In particular, siRNA/cationic polymer carriers should be able to have endosomal escape. Otherwise, siRNA could be degraded in the acidic and enzymatic milieu of endosome/lysosome [24].

Cationic polymers and lipids have frequently been employed in research due to their advantages in gene delivery such as biodegradability, low cytotoxicity, structure variety, and easy scale-up production [25]. Therapeutic nucleic acid cargoes are loaded into the carrier systems mostly through the positive–negative charge interactions between positive charges of carrier and negative charges of phosphate groups in RNA. However, cationic polymer carriers with excess of positive charge may cause toxicity. Cationic carriers cause considerable disruption of cellular membrane integrity because of the negatively charged constitution of cell membrane [26]. Moreover, cationic nanocarriers induce cell necrosis due to the positive charge [27]. They also cause mitochondrial and lysosomal damage and formation of a high number of autophagosomes [28]. In order to overcome this problem, smart carriers have been developed not to cause cell membrane hydrolysis and necrosis so that they can deliver the therapeutic agents to the target site [29]. Although the benefits of nanocarriers in drug delivery have attracted much attention and great efforts have been made to investigate better cationic carriers, toxicity has always been the main problem of cationic carrier applications [30]. Because of this toxicity issue, the number of positive charges of polymer carriers should be kept low. In that case, the required therapeutic concentration of siRNA could not be achieved. Thus, N/P ratio has a great importance for gene delivery. Consequently, it is essential to keep the N/P ratio low, which indicates the complexation efficiency of the anionic therapeutic agents and the cationic carriers, in order to prevent cytotoxicity from excess amount of cationic polymer carriers. As a result, the main aim for optimum N/P ratio is to carry the most efficient number of siRNA with minimum number of cationic polymer carriers.

To identify the optimum ratio of N and P, the gel retardation assay commonly used for nucleic acid separation could be chosen for determination of N/P ratio [31]. This technique is frequently utilized for the determination of DNA or RNA fragments based on their molecular weight [32]. The phosphate backbone of the DNA or RNA is negatively charged, and therefore RNA fragments

migrate to the positively charged anode when placed in the electric field for separation, identification, and purification [33].

Agarose which, is a pure linear polymer obtained from seaweed, is frequently used for gel electrophoresis [34]. The polymer is boiled to dissolve in a buffer solution and polymerized in gel form by hydrogen bonding when left to cool at room temperature. There is no other component such as catalysts required than agarose. Therefore, preparing agarose gel is simple and fast. The advantages of agarose gel electrophoresis are being non-toxic gel medium, rapid, and easy to cast of gels and providing well separation of high molecular weight nucleic acids [35]. In addition, the samples can be recovered from the gel by melting or digesting the gel with any agarose enzyme or by treating a chaotropic salt [36].

The movement of molecules in an agarose gel depends on their size, charge, the type of electrophoresis buffer, and the pore size of the gel. In this method, siRNA is forced to migrate through an extremely cross-linked agarose base in response to an electric field. In the solution, the phosphate groups of the siRNA are negatively charged so the siRNA molecule migrates to the positive pole (Fig. 1).

This technique is also being used for determination of the complexation efficiency of siRNA/cationic polymer carriers. By adding a positively charged polymer to the siRNA, the overall charge of the complex is neutralized. Because of decreasing the negative charge density of siRNA complex, the movement of siRNA/cationic polymer carriers in the gel is getting difficult. If the complexation does not happen completely, for example, there are free forms of siRNA with siRNA/cationic polymer carriers, the free siRNAs travel far away than the complexation forms [37].

All in all, the movement of a siRNA/cationic polymer carrier complexation through a gel depends on (a) size of the complexation structure, (b) agarose concentration, (c) type of agarose, (d) applied voltage, (e) presence of staining dye, and (f) electrophoresis buffer type [38]. After running the samples in a suitable dye-containing gel, the complexed and free siRNA can be visualized under UV light.

2 Materials

1. siRNA.
2. Agarose.
3. Tris-HCl.
4. Acetic acid or boric acid.
5. EDTA.
6. DNA Ladder.

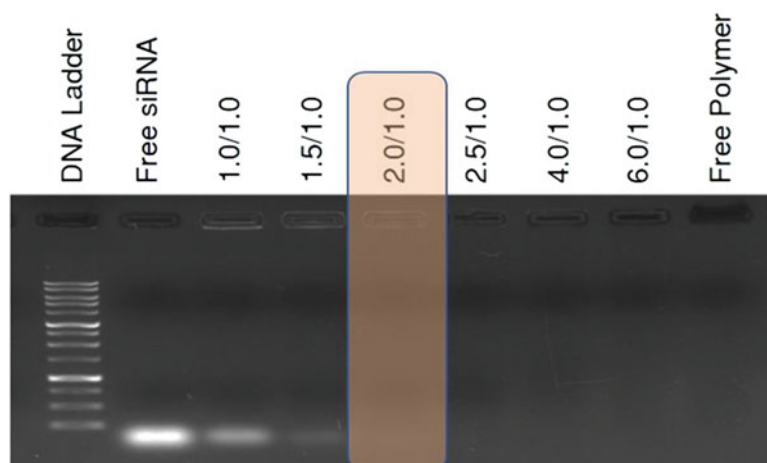


Fig. 1 Agarose gel retardation assay to evaluate siRNA binding efficiency of 15 kDa cationic polymer complexation with siRNA at different N/P (amine/phosphate) ratios. The gel retardation assay is set as the number of carriers is increasing, siRNA is kept constant. The orange-colored rectangle marking in the figure shows the optimal N/P ratio (2/1) which is siRNA completely complexed with the carriers

7. Loading Dye.
8. RedSafe nucleic acid staining solution.
9. Ethidium bromide.
10. dH₂O.
11. Microwave oven.
12. Gel casting device.
13. Glass beaker.
14. Graduated cylinder.

Prepare solutions with distilled water and nuclease-free water. Store all reagents (except siRNA and loading dye) at room temperature.

2.1 Agarose Gel

1. Preparation of tris acetate-ethylenediaminetetraacetic (TAE) buffer reagents: Prepare 50× TAE buffer (pH 8.0) with 40 mM ethylenediaminetetraacetic (EDTA) disodium salt (M_W : 336.21 g/mol), 2 mM tris base (M_W : 121.14 g/mol), 1 M Acetic Acid (M_W : 60.05 g/mol) (*see Note 1*).
2. Preparation of stock solution 5.0 l 50× TAE buffer (pH 8.0): Weight 1.21 g of Tris base, 67.24 g of EDTA, and draw 285.95 mL of acetic acid and dissolve all of them in 5.0 L distilled water, carefully. Perform this step on the magnetic stirrer and adjust pH 8.0 with hydrochloric acid (HCl) (*see Note 2*). Store the solution at room temperature.

3. Preparation of $1\times$ TAE buffer: Draw 20.0 mL of $50\times$ TAE buffer solution and complete it to final 1000.0 mL in a glass beaker (*see Note 3*).
4. Preparation of 1% agarose gel: Weight 1.0 g agarose powder, add 100.0 mL of electrophoresis buffer. Agarose powder is dissolved in the electrophoresis buffer to the desired concentration (*see Note 4*).

2.2 Polymer and siRNA

1. Preparation of polymer solution: Add 1.0 mg of polymer in 1.0 mL of nuclease-free water. Store at 4°C .
2. Stock siRNA solution: Dissolve siRNA in nuclease-free water at a concentration of $50\text{ }\mu\text{mol}$. Afterwards, allocate 800.0 μL of stock siRNA solution into microcentrifuge tubes (*see Note 5*) and store at -20°C .

3 Methods

3.1 Calculation of Nitrogen to Phosphate (N/P) Ratio for Complexation for siRNA/Cationic Polymer Carriers

Following the steps below, the number of siRNA, cationic polymers, and N/P ratios will be calculated. It is good to create a table containing the amounts of siRNA, polymer, loading dye, and distilled water, which will be helpful for setting the experiment (*see Table 1*). After the calculation, the complexation siRNA/cationic polymer carriers at the different N/P ratios are loaded into gel wells, run in the electrophoresis, and visualized under UV light.

To sum up, the procedure can be simply separated into four steps: (1) preparation of materials to be loaded into wells and carried out of complexation, (2) preparation of agarose gel and loading of samples into wells, (3) running the samples at appropriate voltage and time, and (4) obtained data and identification of the optimum N/P ratio (Fig. 2).

3.1.1 Calculation of the Amine Groups of Polymer

1. Calculate the molecular weight and the number of amine groups of the cationic polymer (or look at the datasheet of your polymer if you purchase from a vendor) (*see Note 6*), i.e.;
 - (a) The molecular weight of a cationic polymer: 180,000.0 g/mol.
 - (b) Amine groups per the cationic polymer: 235 amines.
2. Determine the initial dose of the cationic polymer to be used and calculate the mole of the cationic polymer, i.e.;
 - (a) The cationic polymer dose: 1.0 mg.
 - (b) The number of the cationic polymer moles: 5.5×10^{-9} mol.

Table 1
The siRNA/cationic polymer carrier complexation for different N/P ratios

Well number	Treatment (N/P)	Stock siRNA solution (μL)	Stock polymer solution (μL)	Loading dye (μL)	Nuclease free H ₂ O (μL)
1	DNA ladder	–	–	–	–
2	Free siRNA	1.0	–	4.0	15.0
3	1.0/1.0	1.0	1.6	4.0	13.4
4	1.5/1.0	1.0	2.4	4.0	12.6
5	2.0/1.0	1.0	3.2	4.0	11.8
6	2.5/1.0	1.0	4.0	4.0	11.0
7	4.0/1.0	1.0	6.4	4.0	8.6
8	6.0/1.0	1.0	9.6	4.0	5.4
9	Free polymer	–	10.6	4.0	5.4

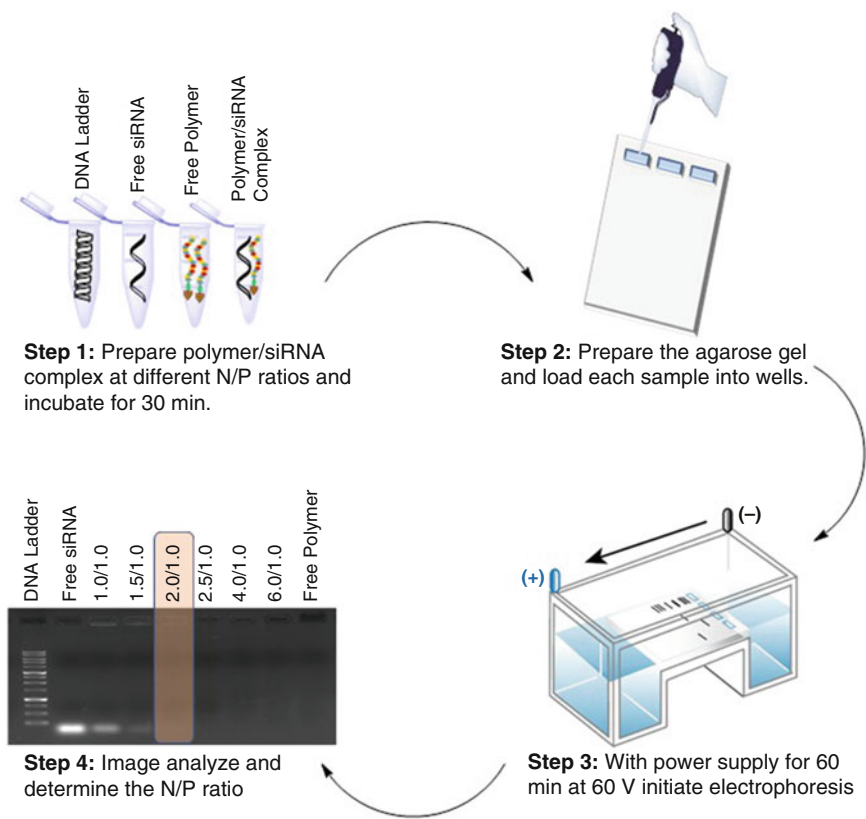


Fig. 2 Brief summary of the creation stages of gel retardation assay

3. Multiply the number of amine groups in the cationic polymer by the number of cationic polymer moles. This number will be the number of total amine moles.

(a) The mole of amine groups: 1.3×10^{-6} mol.

3.1.2 Calculation of Phosphate Groups of siRNAs

1. Calculate the average molecular weight of siRNAs (*see Note 7*), i.e.;

(a) The average molecular weight of a siRNA molecule: 340.0 g/mol.

(b) siRNA consists of double stranded 21 bp so it has a total of 42 bp unit/siRNA molecule.

(c) The molecular weight of 21 bp siRNA (siRNA molecule * number of bp * 2) 14,280.0 g/mol ($340.0 \times 21 \times 2$). This is the value used in the subsequent calculations.

2. Determine the initial dose of the siRNA to be used and calculate the mole of the siRNA.

(a) The siRNA dose: 0.7 µg.

(b) The number of siRNA moles: 4.9×10^{-11} mol.

3. Multiply the number of Phosphate (PO_4^{3-}) groups in the siRNA to get the total number of phosphate groups.

(a) The mole of PO_4^{3-} groups (siRNA moles * nr PO_4^{3-} groups): 2.06×10^{-9} mol (4.9×10^{-11} mol * 42).

3.1.3 Calculation of N/P Ratios

One milligram of cationic polymer (1.3×10^{-6} mol obtained from Subheadings 3.1.1–3.1.3) dissolved in 1.0 mL of distilled water as a stock solution. For the calculation of 1:1 N/P ratio, calculate the amount of amine groups in the polymer which equals to the same mole of PO_4^{3-} groups (2.1×10^{-9} mol obtained from the Subheadings 3.1.2 and 3.1.3). Based on this calculation, 1.60 µL of the polymer solution is taken. For 1.5:1, 2:1, 2.5:1, 4:1, 6:1 N/P ratios, this volume is multiplied with 1.5, 2.0, 2.5, 4.0, and 6.0, respectively (*see Table 1*).

3.2 Preparation of 1% Agarose Gel Electrophoresis

1. To prepare $1\times$ TAE buffer, get 50.0 mL of $50\times$ TAE buffer stock solution and complete to 1000.0 mL volume with distilled water in a beaker.
2. Add 1.0 g of agarose powder into 100.0 mL of $1\times$ TAE buffer and mix it to make 1% agarose gel. After that, boil the agarose mixture in a microwave oven to melt it (*see Note 8*).
3. Cool the solution to approximately 50–60 °C.
4. Add the RedSafe nucleic acid staining solution (5.0 µL) (*see Note 9*).

5. Poured into a casting tray containing a sample comb and allowed to solidify at room temperature (*see* **Note 10**).
6. Remove the sample comb from the cooling casting tray (*see* **Note 11**).

3.3 Loading siRNA/ Cationic Polymer Carrier Complex into 1% Agarose Gel

1. Prepare mixture of nuclease-free water, polymer, and siRNA in separated microcentrifuge tubes as given in Table 1.
2. Allow 30 min for the complexation of siRNA/cationic polymer carrier.
3. Add 4.0 μL of DNA gel loading dye to each centrifuge tube. The loading dye ($6\times$) is added to the gel for the visualization of siRNA during sample loading and running.
4. Load a total 20.0 μL volume from each sample into agarose gel wells.
5. Set power supply at 60 V for 60 min (*see* **Note 12**).
6. The electrophoretic mobility of the siRNAs of each sample is visualized under UV light (*see* Fig. 1).

4 Notes

1. Agarose gel electrophoresis of siRNA is performed using either TAE buffer or tris-borate-EDTA (TBE) buffer [39].
2. Wear a mask and gloves when preparing buffer agents. TAE buffer solution can be stored at room temperature for a month. In our laboratory, we prepare fresh solution every month.
3. The most reliable strategy for TAE usage, prepare a fresh $1\times$ TAE buffer for each time just before the experiment.
4. The percentage of agarose gels used is generally in the range of 0.2–3%. This percentage could be changed based on the size of siRNA and total molecular weight of the carrier [40].
5. Allocate all the samples (i.e. siRNA) to avoid damaging the main source.
6. Calculation/determination of the molecular weight, chemical formulation, surface charge, and size of the polymer are carried out according to ^1H -NMR, zeta potential, and size analysis.
7. The average molecular weight of siRNA base is 340 g/mol. Average molecular weight of a double-stranded DNA (dsDNA) base pair and a single-stranded DNA (ssDNA) base pair are 600 and 330 g/mol, respectively [41].
8. Initially, the agarose solution is boiled for 45–60 s in the microwave at 180 $^{\circ}\text{C}$. If the agarose powder does not dissolve well, repeat the step for another 20–25 s until it totally dissolves.

9. Instead of using RedSafe nucleic acid staining dye, ethidium bromide, bromophenol blue or xylene cyanole could be preferred [35].
10. The casting tray containing sample comb must be on a flat surface. Otherwise, the thickness of the gel may not be uniform. While pouring the solution, one should be careful about the formation of bubbles, which may affect the migration efficiency.
11. To solidify the gel, wait 1–1.5 h before removing the comb from the tray to ensure that the loading wells are intact and well-opened.
12. The optimum running time is 45–90 min to identify the N/P ratio of siRNA/cationic polymer carrier complexation. In the case of gel electrophoresis is performed at a higher voltage, the running time is decreased. However, if the running time is increased that leads to heating up which leading to siRNA banding artifacts [39].

Acknowledgments

This work was supported by Scientific and Technological Research Council of Turkey (TUBITAK)-2515 COST Program Grant number: 118Z952 and Research Fund of Erciyes University (Project number: MAP-2020-9692).

References

1. Zhang X, Li DY, Reilly MP (2019) Long intergenic noncoding RNAs in cardiovascular diseases: challenges and strategies for physiological studies and translation. *Atherosclerosis* 281:180–188. <https://doi.org/10.1016/j.atherosclerosis.2018.09.040>
2. Conejos-Sanchez I, Gallon E, Nino-Pariente A, Smith JA, De la Fuente AG, Di Canio L, Pluchino S, Franklin RJM, Vicent MJ (2019) Polyornithine-based polyplexes to boost effective gene silencing in CNS disorders. *Nanoscale* 12(11):6285–6299. <https://doi.org/10.1039/c9nr06187h>
3. Liu T, Wang L, Xin H, Jin L, Zhang D (2020) Delivery systems for RNA interference-based therapy and their applications against cancer. *Sci Adv Mater* 12(1):75–86. <https://doi.org/10.1166/sam.2020.3694>
4. Subhan MA, Torchilin VP (2019) Efficient nanocarriers of siRNA therapeutics for cancer treatment. *Transl Res* 214:62–91. <https://doi.org/10.1016/j.trsl.2019.07.006>
5. Fire A, Xu S, Montgomery MK, Kostas SA, Driver SE, Mello CC (1998) Potent and specific genetic interference by double-stranded RNA in *Caenorhabditis elegans*. *Nature* 391(6669):806–811. <https://doi.org/10.1038/35888>
6. Dong Y, Siegwart DJ, Anderson DG (2019) Strategies, design, and chemistry in siRNA delivery systems. *Adv Drug Deliv Rev* 144: 133–147. <https://doi.org/10.1016/j.addr.2019.05.004>
7. Kapadia CH, Luo B, Dang MN, Irvin-Choy ND, Valcourt DM, Day ES (2020) Polymer nanocarriers for MicroRNA delivery. *J Appl Polym Sci* 137(25):48651. <https://doi.org/10.1002/app.48651>
8. Lin Y-X, Wang Y, Blake S, Yu M, Mei L, Wang H, Shi J (2020) RNA nanotechnology-mediated cancer immunotherapy. *Theranostics* 10(1):281–299. <https://doi.org/10.7150/thno.35568>

9. Karimi F, Azizi Jalilian F, Hossienkhani H, Ezati R, Amini R (2019) siRNA delivery technology for cancer therapy: promise and challenges. *Acta Med Iran* 57:83–93. <https://doi.org/10.18502/acta.v57i2.1760>
10. Tsouris V, Joo MK, Kim SH, Kwon IC, Won Y-Y (2014) Nano carriers that enable co-delivery of chemotherapy and RNAi agents for treatment of drug-resistant cancers. *Biotechnol Adv* 32(5):1037–1050. <https://doi.org/10.1016/j.biotechadv.2014.05.006>
11. Shirley JL, de Jong YP, Terhorst C, Herzog RW (2020) Immune responses to viral gene therapy vectors. *Mol Ther* 28(3):709–722. <https://doi.org/10.1016/j.ymthe.2020.01.001>
12. Sabouri-Rad S, Oskuee RK, Mahmoodi A, Gholami L, Malaekheh-Nikouei B (2017) The effect of cell penetrating peptides on transfection activity and cytotoxicity of polyallylamine. *Bioimpacts* 7(3):139–145. <https://doi.org/10.15171/bi.2017.17>
13. Rezaee M, Oskuee RK, Nassirli H, Malaekheh-Nikouei B (2016) Progress in the development of lipopolyplexes as efficient non-viral gene delivery systems. *J Control Release* 236:1–14. <https://doi.org/10.1016/j.jconrel.2016.06.023>
14. Parashar D, Rajendran V, Shukla R, Sistla R (2020) Lipid-based nanocarriers for delivery of small interfering RNA for therapeutic use. *Eur J Pharm Sci* 142:105159. <https://doi.org/10.1016/j.ejps.2019.105159>
15. Jorge A, Pais A, Vitorino C (2020) Targeted siRNA delivery using lipid nanoparticles. *Methods Mol Biol* 2059:259–283
16. Liao X (2019) Development of a cationic polymer-based siRNA delivery system for the regeneration of tendon injury. University of East Anglia, Norwich
17. Qiu Y, Tam B, Chung WY, Mason J, Lam JK (2019) Relationship between the secondary structure of the peptide base siRNA carrier and effective gene silencing effect on lung epithelial cells. *J Aerosol Med Pulmonary Drug Delivery* 2:A16–A17
18. Cummings JC, Zhang H, Jakymiw A (2019) Peptide carriers to the rescue: overcoming the barriers to siRNA delivery for cancer treatment. *Transl Res* 214:92–104. <https://doi.org/10.1016/j.trsl.2019.07.010>
19. Pan J, Mendes LP, Yao M, Filipczak N, Garai S, Thakur GA, Sarisozen C, Torchilin VP (2019) Polyamidoamine dendrimers-based nanomedicine for combination therapy with siRNA and chemotherapeutics to overcome multidrug resistance. *Eur J Pharm Biopharm* 136:18–28. <https://doi.org/10.1016/j.ejpb.2019.01.006>
20. Laurini E, Marson D, Aulic S, Fermeleglia M, Priel S (2019) Evolution from covalent to self-assembled PAMAM-based dendrimers as nanovectors for siRNA delivery in cancer by coupled in silico-experimental studies. Part II: self-assembled siRNA Nanocarriers. *Pharmaceutics* 11(7):324. <https://doi.org/10.3390/pharmaceutics11070324>
21. Jain A, Mahira S, Majoral J-P, Bryszewska M, Khan W, Ionov M (2019) Dendrimer mediated targeting of siRNA against polo-like kinase for the treatment of triple negative breast cancer. *J Biomed Mater Res A* 107(9):1933–1944. <https://doi.org/10.1002/jbm.a.36701>
22. Lu Y, Zhong L, Jiang Z, Pan H, Zhang Y, Zhu G, Bai L, Tong R, Shi J, Duan X (2019) Cationic micelle-based siRNA delivery for efficient colon cancer gene therapy. *Nanoscale Res Lett* 14(1):193. <https://doi.org/10.1186/s11671-019-2985-z>
23. Kandil R, Xie Y, Heermann R, Isert L, Jung K, Mehta A, Merkel OM (2019) Coming in and finding out: blending receptor-targeted delivery and efficient endosomal escape in a novel bio-responsive siRNA delivery system for gene knockdown in pulmonary T cells. *Adv Ther* 2(7):1900047. <https://doi.org/10.1002/adtp.201900047>
24. Prantner AM, Scholler N (2014) Biological barriers and current strategies for modifying nanoparticle bioavailability. *J Nanosci Nanotechnol* 14(1):115–125. <https://doi.org/10.1166/jnn.2014.8899>
25. Patil S, Gao Y-G, Lin X, Li Y, Dang K, Tian Y, Zhang W-J, Jiang S-F, Qadir A, Qian A-R (2019) The development of functional non-viral vectors for gene delivery. *Int J Mol Sci* 20(21):5491. <https://doi.org/10.3390/ijms20215491>
26. Chen J, Hessler JA, Putschakayala K, Panama BK, Khan DP, Hong S, Mullen DG, Dimaggio SC, Som A, Tew GN, Lopatin AN, Baker JR, Holl MMB, Orr BG (2009) Cationic nanoparticles induce nanoscale disruption in living cell plasma membranes. *J Phys Chem B* 113(32):11179–11185. <https://doi.org/10.1021/jp9033936>
27. Wei X, Shao B, He Z, Ye T, Luo M, Sang Y, Liang X, Wang W, Luo S, Yang S, Zhang S, Gong C, Gou M, Deng H, Zhao Y, Yang H, Deng S, Zhao C, Yang L, Qian Z, Li J, Sun X, Han J, Jiang C, Wu M, Zhang Z (2015) Cationic nanocarriers induce cell necrosis through impairment of Na⁺/K⁺-ATPase and cause subsequent inflammatory response. *Cell Res*

- 25(2):237–253. <https://doi.org/10.1038/cr.2015.9>
28. Fröhlich E (2012) The role of surface charge in cellular uptake and cytotoxicity of medical nanoparticles. *Int J Nanomedicine* 7: 5577–5591. <https://doi.org/10.2147/IJN.S36111>
29. Durmaz YY, Lin Y-L, ElSayed MEH (2013) Development of degradable, pH-sensitive star vectors for enhancing the cytoplasmic delivery of nucleic acids. *Adv Funct Mater* 23(31): 3885–3895. <https://doi.org/10.1002/adfm.201203762>
30. Lv H, Zhang S, Wang B, Cui S, Yan J (2006) Toxicity of cationic lipids and cationic polymers in gene delivery. *J Control Release* 114(1): 100–109. <https://doi.org/10.1016/j.jconrel.2006.04.014>
31. Scott V, Clark AR, Docherty K (1994) The gel retardation assay. In: *Protocols for gene analysis*. Springer, Berlin, pp 339–347
32. Hellman LM, Fried MG (2007) Electrophoretic mobility shift assay (EMSA) for detecting protein–nucleic acid interactions. *Nat Protoc* 2(8):1849
33. Helling RB, Goodman HM, Boyer HW (1974) Analysis of endonuclease R-EcoRI fragments of DNA from lambdoid bacteriophages and other viruses by agarose-gel electrophoresis. *J Virol* 14(5):1235–1244
34. Magdeldin S (2012) *Gel electrophoresis: principles and basics*. BoD–Books on Demand, Norderstedt
35. Chawla H (2002) *Introduction to plant biotechnology*. Routledge, Milton Park. <https://doi.org/10.1201/9781315275369>
36. Tietz D (2012) *Nucleic acid electrophoresis*. Springer, Berlin
37. Loening UE (1968) Molecular weights of ribosomal RNA in relation to evolution. *J Mol Biol* 38(3):355–365. [https://doi.org/10.1016/0022-2836\(68\)90391-4](https://doi.org/10.1016/0022-2836(68)90391-4)
38. Rio DC, Ares M Jr, Hannon GJ, Nilsen TW (2010) Nondenaturing agarose gel electrophoresis of RNA. *Cold Spring Harb Protoc* 2010(6):pdb.prot5445. <https://doi.org/10.1101/pdb.prot5445>
39. Sanderson BA, Araki N, Lilley JL, Guerrero G, Lewis LK (2014) Modification of gel architecture and TBE/TAE buffer composition to minimize heating during agarose gel electrophoresis. *Anal Biochem* 454:44–52. <https://doi.org/10.1016/j.ab.2014.03.003>
40. Murphy D, Carter DA, Evans MJ (1993) *Transgenesis techniques: principles and protocols*. Springer, Berlin
41. He F (2011) DNA molecular weight calculation. *Bio-Protocol* 1(6):e46. <https://doi.org/10.21769/BioProtoc.46>

Open Access This chapter is licensed under the terms of the Creative Commons Attribution 4.0 International License (<http://creativecommons.org/licenses/by/4.0/>), which permits use, sharing, adaptation, distribution and reproduction in any medium or format, as long as you give appropriate credit to the original author(s) and the source, provide a link to the Creative Commons license and indicate if changes were made.

The images or other third party material in this chapter are included in the chapter's Creative Commons license, unless indicated otherwise in a credit line to the material. If material is not included in the chapter's Creative Commons license and your intended use is not permitted by statutory regulation or exceeds the permitted use, you will need to obtain permission directly from the copyright holder.





Chapter 8

Generation of Protein-Phosphorodiamidate Morpholino Oligomer Conjugates for Efficient Cellular Delivery via Anthrax Protective Antigen

Valentina Palacio-Castañeda, Roland Brock, and Wouter P. R. Verdurmen

Abstract

Phosphorodiamidate morpholino oligomers (PMOs) offer great promise as therapeutic agents for translation blocking or splice modulation due to their high stability and affinity for target sequences. However, in spite of their neutral charge as compared to natural oligonucleotides or phosphorothioate analogs, they still show little permeability for cellular membranes, highlighting the need for effective cytosolic delivery strategies. In addition, the implementation of strategies for efficient cellular targeting is highly desirable to minimize side effects and maximize the drug dose at its site of action. Anthrax toxin is a three-protein toxin of which the pore-forming protein anthrax protective antigen (PA) can be redirected to a receptor of choice and lethal factor (LF), one of the two substrate proteins, can be coupled to various cargoes for efficient cytosolic cargo delivery. In this protocol, we describe the steps to produce the proteins and protein conjugates required for cytosolic delivery of PMOs through the cation-selective pore generated by anthrax protective antigen. The method relies on the introduction of a unique cysteine at the C-terminal end of a truncated LF (aa 1–254), high-yield expression of the (truncated) toxin proteins in *E. coli*, functionalization of a PMO with a maleimide group and coupling of the maleimide-functionalized PMO to the unique cysteine on LF by maleimide-thiol conjugation chemistry. Through co-administration of PA with LF-PMO conjugates, an efficient cytosolic delivery of PMOs can be obtained.

Key words Antisense, Anthrax toxin, Protective antigen, Phosphorodiamidate morpholino oligomers, DNA analog, Drug delivery, Cellular internalization, Bioconjugate chemistry

1 Introduction

Phosphorodiamidate morpholino oligomers (PMOs) are uncharged DNA analogs with therapeutic potential due to their ability to specifically bind to target sites on RNA. By steric inhibition of translation initiation complexes, PMOs can block translation. Alternatively, by targeting sites associated with splicing of pre-mRNAs, PMOs can mediate splice modulation and thereby correct the consequences of splicing mutations at the pre-mRNA level, for instance those in inherited retinal dystrophies [1]. PMOs

have several qualities that are excellent for therapeutic development, including nuclease-resistance, long-term activity, low toxicity, and high specificity [2, 3]. However, a major challenge remains, which is achieving an efficient cellular delivery, particularly in vivo. PMOs are neutral molecules that because of their size are impermeable to cellular membranes. Delivery approaches that have been developed up to now include scraping of cells, particle-based approaches, and cell-penetrating peptide (CPP)-based delivery [3–5]. Cell scraping cannot be translated to in vivo applications and particle-based approaches suffer from delivery challenges in vivo such as poor tissue penetration and liver enrichment [6]. CPP-mediated delivery has demonstrated potential, but still does not target specific cell-surface receptors, indicating the need for a novel approach.

Recently, several groups have demonstrated that anthrax toxin, a sophisticated protein-based molecular machine that has evolved to efficiently deliver toxic catalytic proteins into the cytosol, can be employed for the functional delivery of various types of cargoes, including antisense oligonucleotides (AON) [7, 8]. The full anthrax toxin consists of three proteins: a pore-forming protein, called protective antigen (PA), that generates cation-selective pores and two enzyme components [9], called lethal factor (LF) and edema factor (EF). LF and EF in turn consist of two domains: the first domain binds the protein pore and the second domain is the enzymatically active domain and is thus responsible for the actual toxicity. For the delivery of PMOs via this mechanism, only PA and the PA pore-binding domain of LF are needed as protein components. For LF, this means that the enzymatic (toxicity-causing) domain of LF is replaced with a PMO.

In this chapter, we describe the preparation of the components needed to mediate cytosolic delivery of PMOs by the anthrax toxin translocation mechanism (Fig. 1a). The individual protein components, PA and LF (1–254) are produced in high quantity in soluble form in the cytosol of *E. coli*. LF (1–254) is by itself cysteine-free, so through the introduction of a unique C-terminal cysteine, a site-specific conjugation via maleimide-thiol conjugation chemistry can be achieved. Maleimide-thiol conjugation chemistry is useful for coupling biologically active molecules because it is fast, highly selective and it can be done in physiological buffers at 37 °C or at 4 °C [10].

To enable the conjugation of the PMO to the protein, PMOs containing a primary amine at the 3' end are functionalized with a maleimide moiety through a bifunctional linker containing an NHS-ester and a maleimide group separated by a cyclohexane spacer. After coupling maleimide-functionalized PMOs with LF, uncoupled PMO is removed via dialysis, producing LF-PMO conjugates that can be delivered to the cytosol via anthrax protective antigen (Fig. 1b).

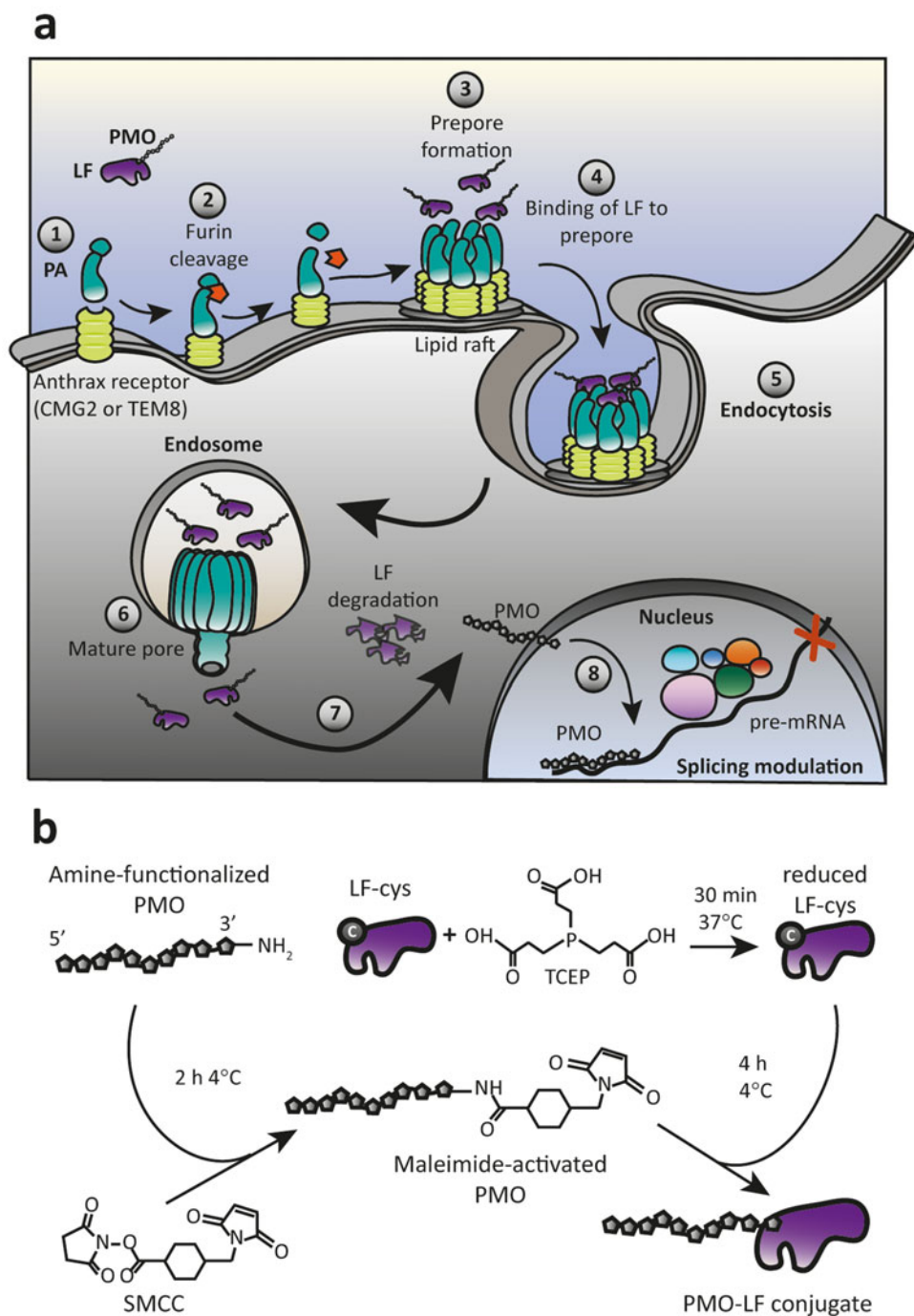


Fig. 1 Cytosolic delivery of PMO using the anthrax toxin mechanism. **(a)** Schematic representation of the cytosolic delivery of the LF-PMO conjugate via anthrax protective antigen. Numbers indicate the distinct steps in the delivery process. **(b)** Schematic representation of the coupling of a PMO to LF-cys. *LF* lethal factor, *PA* protective antigen, *PMO* phosphorodiamidate morpholino oligomer, *SMCC* succinimidyl 4-(*N*-maleimido-methyl)cyclohexane-1-carboxylate, *TCEP* tris(2-carboxyethyl)phosphine

2 Materials

All buffers should be prepared with double-distilled water to ensure highly pure buffers. It is not necessary to work under sterile conditions. However, to perform experiments in the absence of antibiotics, make sure that the final conjugates are filter-sterilized before use.

2.1 Protein Expression

1. BL21(DE3) competent cells (*see Note 1*).
2. *E. coli* expression vector coding for anthrax protective antigen (*see Note 2*).
3. *E. coli* expression vector coding for LF (1–254) with a C-terminal cysteine (LF-cys) (*see Note 3*).
4. LB agar plates: add demi water to 10 g peptone, 5 g yeast, 8 g NaCl, and 15 g agar until a volume of 1 L is reached. Mix well, autoclave and store at room temperature. To make plates, heat the LB agar in the microwave until fully liquid, allow to cool until it is lukewarm before adding the antibiotic of choice. Pour liquid into a Petri dish until you reach a thickness of approximately 0.5 cm. Wait until the agar solidifies and store upside down at 4 °C.
5. 2× YT medium: For 1 L, add demi water to 16 g peptone, 10 g yeast, and 5 g NaCl until a volume of 1 L is reached. Mix well, autoclave, and store at room temperature.
6. Terrific Broth (TB): 12 g/L tryptone, 24 g/L yeast extract, and 4 mL/L glycerol, 17 mM KH₂PO₄ and 72 mM K₂HPO₄. Store at room temperature (*see Note 4*).
7. Autoclaved 20% (w/v) glucose solution in demi water.
8. Isopropyl β-D-1-thiogalactopyranoside (IPTG): 1 M stock solution in double-distilled water. Aliquot and store at –20 °C.
9. High-speed centrifuge.
10. Incubator shaker.

2.2 Protein Purification

1. 4-(2-Hydroxyethyl)-1-piperazineethanesulfonic acid (HEPES)-buffered saline (HBS)-wash: 50 mM HEPES, pH 8.0, 150 mM NaCl, 1 mM MgCl₂, 20 mM imidazole. Adjust the pH with NaOH to reach pH 8.0. Store at 4 °C. The buffer can be stored at 4 °C for up to 12 months.
2. HBS-resuspension buffer: HBS wash containing 250 µg/mL lysozyme and 1× complete EDTA-free protease inhibitor cocktail. Prepare fresh on the day of the experiment.
3. HBS-low salt: 50 mM HEPES, pH 8.0, 20 mM NaCl, 20 mM imidazole. Adjust the pH with NaOH to reach pH 8.0. Store at 4 °C. The buffer can be stored at 4 °C for up to 12 months.

4. HBS-high salt: 50 mM HEPES, pH 8.0 1 M NaCl, 20 mM imidazole. Adjust the pH with NaOH to reach pH 8.0. Store at 4 °C. The buffer can be stored at 4 °C for up to 12 months.
5. PBS-elution buffer: PBS, pH 7.4, 300 mM imidazole. Adjust the pH with HCl to reach pH 7.4. Store at 4 °C. The buffer can be stored at 4 °C for up to 12 months.
6. Ni-NTA superflow resin (e.g. Qiagen) equilibrated with HBS wash.
7. His-tagged tobacco etch virus (TEV) protease (commercially available).
8. PBS-EDTA-DTT: PBS containing 0.5 mM ethylenediamine-tetraacetic acid (EDTA) and 1 mM dithiothreitol (DTT). Prepare fresh for each experiment.
9. Sonicator.
10. Low-protein binding syringe filter for small volumes (<1 mL) with 0.22 µm pore size.
11. Äkta Pure or alternative chromatography system with UV detector.
12. Superdex 200 10/300 GL column or equivalent column.
13. 4 mL centrifugal filter with a 30 kDa cut-off.

2.3 Protein-PMO Conjugation

1. Tris-buffered saline (TBS): 20 mM Tris-HCl, pH 7.4, 150 mM NaCl. Adjust the pH with NaOH to reach pH 7.4 Store at 4 °C. The buffer can be stored at 4 °C for up to 12 months.
2. 7 kDa MWCO ZEBA spin columns (Thermo Fisher Scientific).
3. Degassed HBS: 50 mM HEPES, pH 7.2, 150 mM NaCl (*see Note 5*). Store at 4 °C. The buffer can be stored at 4 °C for up to 12 months. Degas again for 5–10 min before every use.
4. Phosphate-buffered saline (PBS): 10 mM phosphate, pH 7.2, 137 mM NaCl, 2.7 mM KCl. Store at room temperature. Adjust the pH with HCl to set the pH to 7.2 upon dilution from a 10× PBS stock solution prepared with 14.4 g/L Na₂HPO₄, 2.4 g/L KH₂PO₄, 80 g/L NaCl, and 2 g/L KCl, which gives a pH of ~6.8. The buffer can be stored at least for 1 year at room temperature.
5. 1 M lysine solution: For 10 mL, add double-distilled water to 1.46 g lysine until the volume reaches 10 mL. Store at –20 °C. The solution can be kept at –20 °C for at least 1 year.
6. 0.5 M tris(2-carboxyethyl)phosphine (TCEP) solution in double-distilled water, pH 7.0 (*see Note 6*) Store aliquots at –20 °C.
7. PMO with a 3' primary amine modification (Gene tools).

8. Succinimidyl 4-(*N*-maleimidomethyl)cyclohexane-1-carboxylate (SMCC) linker (Thermo Fisher Scientific).
9. Dialysis membrane (e.g. 20 kDa MWCO).

3 Methods

3.1 Expression of PA and LF-cys

1. Mix 20 μ L of BL21(DE3) competent *E. coli* bacteria with 0.5 μ L of pure plasmid encoding either PA or LF-cys in a centrifuge tube and place on ice for 15–30 min.
2. Heat shock for 45 s in a water bath at 42 °C, place back on ice for 2 min and subsequently add 200 μ L of LB medium. Place horizontally in an incubator shaker at 37 °C for 45 min and plate 10 μ L out on an LB agar plate containing the appropriate type and concentration of antibiotic. After an overnight growth, confirm a proper density of colonies and place the plate upside down at 4 °C until starting the next step. It is recommended to start the following step on the same day.
3. Prepare a starter culture by picking a single colony and inoculating 50 mL of 2 \times YT medium containing 1% (w/v) glucose and antibiotic. Let the bacteria grow overnight at 37 °C with shaking at 150 rpm, orbit diameter 50 mm.
4. Use the starter culture to inoculate 1 L of TB supplemented with 0.8% (w/v) glucose and antibiotic to a starting OD₆₀₀ of 0.1.
5. Allow the bacteria to grow at 37 °C with shaking at 150 rpm, orbit diameter 50 mm, until an OD₆₀₀ of 0.7–0.8 is reached. At this point the expression can be induced by adding 100 μ M IPTG. Decrease the temperature to 25 °C (*see Note 7*).
6. After 4 h of expression, centrifuge the cells for 10 min at 5000 $\times g$ in 500 mL containers. Discard the supernatant and resuspend the pellets in 20 mL of medium. Transfer the resuspended cells to 50 mL conical tubes and centrifuge again for 10 min at 5000 $\times g$. Discard the medium and snap-freeze the pellets in liquid nitrogen. Store at –80 °C until purification is commenced.

3.2 Purification of PA and LF-cys

PA and LF are susceptible to denaturation or aggregation when exposed to higher temperatures, so it is recommended to perform all of the subsequent steps at 4 °C.

1. Resuspend bacteria pellets from 1 L expression culture in 20 mL HBS-resuspension buffer.
2. Lyse the bacteria on ice by sonication (60 W with 15 pulses of 10 and 30 s pause between pulses in order to avoid excessive heat or formation of foam (*see Note 8*)).

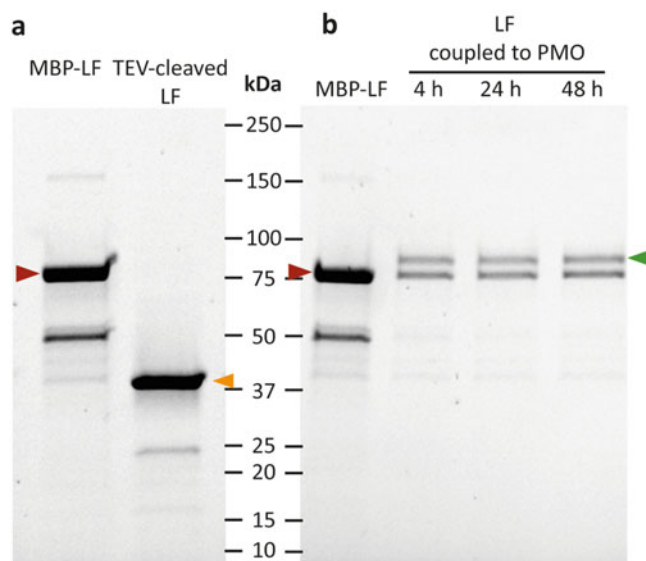


Fig. 2 TEV cleavage of MBP-LF and time dependency of coupling efficiency of LF to PMO. **(a)** SDS-PAGE gel showing LF fused to MBP before TEV cleavage (red arrow) and LF after cleavage and purification via reverse IMAC (orange arrow). **(b)** SDS-PAGE gel illustrating the effect of incubation time on the conjugation efficiency of coupling LF to the PMO. Red arrow indicates 86 kDa band corresponding to MBP-LF before coupling. Green arrow shows a band with increased molecular weight at approximately 92 kDa corresponding to the coupled fraction (MW of PMO: 6.8 kDa). No marked differences are seen between the incubation time and the coupling efficiency, indicating that 4 h incubation is sufficient to achieve 50% coupling. Proteins on gels were visualized by stain-free imaging technology (Bio-Rad). *IMAC* immobilized metal ion affinity chromatography, *LF* lethal factor, *MBP* maltose-binding protein, *PMO* phosphorodiamidate morpholino oligomer, *TEV* tobacco etch virus

3. Centrifuge the bacterial lysates at $28,000 \times g$ for 40 min and filter the supernatant using 0.22 μm pore size filters.
4. Incubate the supernatants containing the His-tagged proteins with 1 mL of HBS wash-equilibrated Ni-NTA superflow resin for 1 h on a roller shaker.
5. Transfer the resin-containing solution to a column containing a bottom filter and wash with 20 column volumes (CV) of HBS-low salt, followed by 20 CV of HBS-high salt and 20 CV of HBS wash.
6. Pre-elute the proteins with 1 CV of PBS-elution buffer, followed by eluting with 4×1 CV. Each elution step should be for 10 min on a roller shaker (*see Note 9*).
7. Dialyze the eluted proteins overnight against 2 L $1 \times$ PBS. In the morning, exchange for fresh PBS and dialyze for two more hours.

8. The purified proteins His₆-MBP-LF-cys and His₆-MBP-PA can be cleaved with TEV protease to generate LF-cys and PA, respectively (Fig. 2a). To cleave off the His₆-MBP add a His-tagged TEV protease at a 1:20 (w/w) ratio in PBS-EDTA-DTT.
9. In order to separate the His₆-MBP and the His-tagged TEV from LF-cys or PA, a reverse immobilized metal ion affinity chromatography (IMAC) purification step must be done in which the *unbound* fraction is kept. Because the Ni-NTA resin is incompatible with high concentrations of EDTA and DTT, solutions must first be dialyzed against a 100-fold excess of HBS wash for at least 2 h to sufficiently remove the EDTA and DTT.
10. Incubate the dialyzed samples with 1 mL equilibrated Ni-NTA superflow resin for 1 h on a roller shaker.
11. Collect the unbound fraction, which should contain only LF-cys or PA. An SDS-PAGE gel can be run at this stage in order to confirm correct cleavage (Fig. 2a). To prepare LF-cys for reduction, perform a dialysis against HBS (*see* Note 10). Dialyze PA against PBS, after which it will be ready for further purification via size-exclusion chromatography (SEC) (Subheading 3.3).
12. LF needs to be reduced in order to generate the free thiol groups required for maleimide-thiol conjugation chemistry. To reduce LF-cys add a 100-fold molar excess of TCEP, incubate for 30 min at 37 °C, and remove excess TCEP using a 7 kDa MCWO ZEBRA spin column. To calculate the amount of TCEP needed, determine the protein concentration using the absorption at 280 nm and the extinction coefficient ϵ_{280} of the protein (i.e. 91,680 M⁻¹ cm⁻¹ for MBP-containing LF and 23,840 M⁻¹ cm⁻¹ for cleaved LF).

3.3 Purification of PA by Size-Exclusion Chromatography (SEC)

After purification of PA via IMAC, we typically see some co-purification of degraded fragments, which can be removed via SEC (*see* Note 11). We generally purify our PA or PA fusion constructs via SEC using an Äkta pure chromatography system equipped with an S200 column (*see* Note 12), which yields pure and active proteins [11, 12].

1. Concentrate the sample to a volume of less than 500 μ L, which is the maximal volume that can be loaded on an S200 column. Make sure that the protein solution is sufficiently concentrated so that in the maximally 500 μ L several milligrams of proteins can be loaded (ideally 2–5 mg). For lower amounts, the separation of individual peaks can become problematic. Filtration of the protein using a low protein-binding syringe filter (0.22 μ m pore size) before loading is recommended since protein

aggregates may clog the column. Alternatively, centrifugation of the sample at high speed ($\sim 20,000 \times g$) for 5 min and loading the supernatant can be done.

2. Connect the column to the chromatography system drop to drop (i.e. without introducing air) and equilibrate the column with PBS. Connect one or multiple injection loops (i.e. depending on the system) that can hold twice the volume of the sample to the chromatography system. For example, for a 500 μL sample, use a 1 mL injection loop. Wash the loop extensively with PBS before loading the sample.
3. When the sample has been loaded, start the run. A typical speed is 0.5 mL/min. Start fraction collection after the dead volume (~ 7 – 8 mL on an S200 column connected to an Äkta Pure system). A suitable fraction size is 0.5 mL. PA should elute at around 12 mL, which should give a major peak detectable by the UV detector.
4. Run an SDS-PAGE gel with collected fractions of any major peaks to determine the molecular weight and purity of the collected proteins. Full-length PA will have a size of approximately 83 kDa.
5. Combine all fractions that contain pure PA, concentrate with a 4 mL centrifugal filter (cut-off: 30 kDa) until a concentration of 2–5 mg/mL is obtained and freeze in aliquots. Aliquots should be snap-frozen in liquid nitrogen and kept at -80°C . Thawed aliquots of PA can be refrozen in liquid nitrogen at least three times without a noticeable decrease in activity.

3.4 Functionalizing PMO with a Maleimide Moiety

1. Dissolve PMO containing a primary amine in double-distilled water to a concentration of 1 mM. The PMO can be stored either at room temperature or aliquoted and stored at -80°C for long-term storage (*see Note 13*).
2. Calculate the amount needed of the SMCC linker for the PMO coupling, taking into account that a 20-fold molar excess of the linker is needed for the reaction. Weigh the desired amount of the SMCC linker and dissolve in anhydrous DMF (e.g. 1.5 mg SMCC in 100 μL of DMF to make a stock solution of 45 mM). Freeze aliquots at -20°C and only thaw briefly for use. The NHS moiety of the linker is very reactive and may hydrolyze already through the presence of trace amounts of water.
3. Mix the PMO with a 20-fold molar excess of the SMCC linker with minimal dilution (e.g. 900 μM PMO and 18 mM SMCC linker) and incubate for 2 h at 4°C (*see Note 14*).
4. Quench unreacted linker by adding lysine to a final concentration of 100 mM using a 1 M lysine solution.

5. Separate the reacted PMO from the unreacted linker using a buffer-exchange procedure (e.g. 7 kDa ZEBRA spin column, depending on the molecular weight of the PMO).

3.5 Coupling of Anthrax Lethal Factor to Maleimide- Functionalized PMO

1. Assuming full recovery of the PMO after the ZEBRA spin column and equal volume, add a tenfold molar excess of the maleimide-functionalized PMO to the reduced LF-cys proteins (e.g. 800 μ M PMO to 80 μ M LF) and incubate for 4 h at 4 °C (Fig. 2b) (see **Note 15**).
2. Dialyze overnight to remove the unreacted PMO. Exchange dialysis buffer the next morning and dialyze for two more hours. Upon complete removal of the excess uncoupled PMO, the concentration of the PMO-conjugate can be calculated using the absorption coefficient of the PMO at 265 nm, while correcting for the absorption of the protein at 265 nm (see **Note 16**). The conjugates can be snap-frozen in liquid nitrogen and stored at -80 °C.

4 Notes

1. There are many *E. coli* strains suitable for high-level protein expression of the proteins described in this chapter, but we have good experience with the strain BL21(DE3). For the proteins in question, BL21(DE3) achieves high-level *and* soluble protein expression upon IPTG-mediated induction of T7 polymerase from a *lacUV5* promoter.
2. We typically express full-length PA fused to an N-terminal His₆-maltose-binding protein (MBP) sequence in a pQIq backbone [11]. MBP serves in this context as a solubility enhancer, leading to tens of mg of soluble protein produced in the cytosol of *E. coli* per liter expression culture in shake flasks. We include a TEV protease site between MBP and protective antigen that can be used to cleave off His₆-MBP and generate native PA.
3. Similar to the expression of PA, we express truncated LF (aa 1–254) fused to an N-terminal His₆-MBP sequence. For maleimide-thiol conjugations, we introduce a single cysteine at the most C-terminal position (LF-cys). Similar to PA, this construct gives us very high levels of soluble expression in the cytosol of *E. coli*.
4. 1 L Terrific broth is prepared by autoclaving 12 g tryptone, 24 g yeast extract, and 4 mL glycerol in 800 mL distilled water, followed by the addition of 100 mL of a separately autoclaved (or filter sterilized) solution of 0.17 M KH₂PO₄ and 0.72 M

K₂HPO₄. Adjust volume to 1 L. Mixing the separately autoclaved solutions can be done at the day of the experiment.

5. Degassing should be done at least for several minutes, which generally gives us good results. We flush with nitrogen gas at a speed which generates some, but not excessive, bubbling. Extending the degassing time to 1 h can be considered for optimal results.
6. Dissolving TCEP hydrochloride at 0.5 M in double-distilled water will result in an acidic solution with a pH between 2 and 3. Adjust the pH of the 0.5 M TCEP solution with concentrated NaOH or KOH to pH 7.0.
7. For expression of PA and LF constructs, we decrease the temperature to 25 °C in order to express maximal amounts of soluble proteins. The growth is much slower at 25 °C than at 37 °C, so it is normal that during 4 h of expression, bacteria will not grow much denser (final OD₆₀₀ between 2 and 3). Increasing the shaking speed improves aeration and can give better yields.
8. Even though the protocol describes lysing of cells by sonication, we typically obtain equally good results when we use French press bacterial cell lysis. With both methods, it is important to avoid excessive heat that may quickly denature or aggregate the proteins.
9. During the preelution, very little His-tagged protein will be eluted since the purpose is to equilibrate the resin with the elution buffer. Nevertheless, we prefer not to discard the preelution fractions since they still may contain *some* protein. Upon measuring the concentration, we make the decision to discard it and/or take it along for dialysis (our typical threshold is an A280 of 0.4).
10. Since the reduction in this protocol is done with TCEP, we prefer to use HBS over PBS because TCEP is more stable in HBS.
11. Next to SEC, PA can also be further purified via ion-exchange chromatography or both sequentially if a very high purity is needed.
12. For purification by SEC, we prefer to use a Superdex 200 10/300 GL column (GE Healthcare), which is suitable for separating proteins ranging in molecular weight from 10 to 600 kDa. We get a good separation when separating PA from its degraded fragments with this column. We have not compared with other comparable columns, which may perform equally well. Similarly, while we work with an Äkta pure system, alternative systems for SEC are likely to work equally well and the protocol described would only require small modifications.

13. PMOs can be dissolved in double-distilled water by pipetting up and down. The solution can be frozen at -80°C or kept at room temperature. We have not seen any differences in coupling efficiency following freezing and rethawing.
14. The reaction can be performed at room temperature for 30 min or at 4°C for 2 h. We get slightly better results when performing the latter protocol.
15. We observed an already high efficiency of coupling after 4 h (Fig. 2b), which did not noticeably increase during longer incubation times. It is possible that longer reaction times may still be better for some protein-PMO conjugations, in which case reaction times up to 48 h can be attempted. Higher excesses of PMO lead to greater efficiency but can be cost limiting. Furthermore, removal of much greater excesses of PMO using dialysis will take significantly longer. Additionally, more concentrated solutions of proteins (up to 5 mg/mL) and PMO are desired, taking into account the solubility of each.
16. PMOs absorb much more strongly than proteins at 265 and 280 nm, implying that absorption measurements at either wavelength will be dominated by the absorption of the PMO. For an accurate estimation of the protein-PMO conjugate, it is therefore important to completely remove the uncoupled PMO, which can be achieved either by extensive dialysis or by ion-exchange chromatography. By measuring the absorption of the conjugate at 265 nm and correcting for the absorption of the protein at 265 nm (for this, measure the pure protein and estimate the $\epsilon_{265\text{ nm}}$ as follows: $[(A_{265\text{ nm}}/A_{280\text{ nm}}) * \epsilon_{280}]$), one can use the extinction coefficient of the PMO at 265 nm (provided by the manufacturer) to calculate the concentration of the protein-PMO conjugate. For a proper correction, take into account the labeling efficiency of the protein through analysis of conjugates by SDS-PAGE.

Acknowledgments

This work was supported by funding from Landelijke Stichting voor Blinden en Slechtzienden, grant number: UitZicht 2017-14.

References

1. Gerard X, Garanto A, Rozet JM et al (2016) Antisense oligonucleotide therapy for inherited retinal dystrophies. *Adv Exp Med Biol* 854: 517–524
2. Summerton J, Weller D (1997) Morpholino antisense oligomers: design, preparation, and properties. *Antisense Nucleic Acid Drug Dev* 7(3):187–195
3. Shabanpoor F, McClorey G, Saleh AF et al (2015) Bi-specific splice-switching PMO oligonucleotides conjugated via a single peptide active in a mouse model of Duchenne muscular dystrophy. *Nucleic Acids Res* 43(1):29–39

4. Partridge M, Vincent A, Matthews P et al (1996) A simple method for delivering morpholino antisense oligos into the cytoplasm of cells. *Antisense Nucleic Acid Drug Dev* 6(3): 169–175
5. Summerton JE (2005) A novel reagent for safe, effective delivery of substances into cells. *Ann N Y Acad Sci* 1058:62–75
6. Juliano RL (2016) The delivery of therapeutic oligonucleotides. *Nucleic Acids Res* 44(14): 6518–6548
7. Dyer PDR, Shepherd TR, Gollings AS et al (2015) Disarmed anthrax toxin delivers antisense oligonucleotides and siRNA with high efficiency and low toxicity. *J Control Release* 220(Pt A):316–328
8. Wright DG, Zhang Y, Murphy JR (2008) Effective delivery of antisense peptide nucleic acid oligomers into cells by anthrax protective antigen. *Biochem Biophys Res Commun* 376(1):200–205
9. Young JAT, Collier RJ (2007) Anthrax toxin: receptor binding, internalization, pore formation, and translocation. *Annu Rev Biochem* 76: 243–265
10. Hansen RE, Winther JR (2009) An introduction to methods for analyzing thiols and disulfides: reactions, reagents, and practical considerations. *Anal Biochem* 394(2): 147–158
11. Verdurmen WP, Luginbühl M, Honegger A et al (2015) Efficient cell-specific uptake of binding proteins into the cytoplasm through engineered modular transport systems. *J Control Release* 200:13–22
12. Verdurmen WPR, Mazlami M, Plückthun A (2017) A quantitative comparison of cytosolic delivery via different protein uptake systems. *Sci Rep* 7(1):13194

Open Access This chapter is licensed under the terms of the Creative Commons Attribution 4.0 International License (<http://creativecommons.org/licenses/by/4.0/>), which permits use, sharing, adaptation, distribution and reproduction in any medium or format, as long as you give appropriate credit to the original author(s) and the source, provide a link to the Creative Commons license and indicate if changes were made.

The images or other third party material in this chapter are included in the chapter's Creative Commons license, unless indicated otherwise in a credit line to the material. If material is not included in the chapter's Creative Commons license and your intended use is not permitted by statutory regulation or exceeds the permitted use, you will need to obtain permission directly from the copyright holder.



Part III

In Vitro Model Systems



Chapter 9

Development and Use of Cellular Systems to Assess and Correct Splicing Defects

Nuria Suárez-Herrera, Tomasz Z. Tomkiewicz, Alejandro Garanto, and Rob W. J. Collin

Abstract

A significant proportion of mutations underlying genetic disorders affect pre-mRNA splicing, generally causing partial or total skipping of exons, and/or inclusion of pseudoexons. These changes often lead to the formation of aberrant transcripts that can induce nonsense-mediated decay, and a subsequent lack of functional protein. For some genetic disorders, including inherited retinal diseases (IRDs), reproducing splicing dynamics in vitro is a challenge due to the specific environment provided by, e.g. the retinal tissue, cells of which cannot be easily obtained and/or cultured. Here, we describe how to engineer splicing vectors, validate the reliability and reproducibility of alternative cellular systems, assess pre-mRNA splicing defects involved in IRD, and finally correct those by using antisense oligonucleotide-based strategies.

Key words *ABCA4*, Antisense oligonucleotide, Exon skipping, Genetic therapy, Inherited retinal diseases, Maxigene, Midigene, Pre-mRNA, Pseudoexon, Splicing modulation, Splicing vectors

1 Introduction

Technologies such as next generation sequencing (NGS) expanded the discovery of genetic variants from coding regions to the entire genome. As a consequence of high-throughput data analysis, it is crucial to be able to correctly identify and distinguish disease-causing variants from single nucleotide polymorphisms (SNPs). This is especially relevant for intronic variants, as many of them have an unknown functional significance. In the field of inherited retinal diseases (IRDs), a common autosomal recessive condition known as Stargardt disease (STDG1) [1] lacks the bi-allelic molecular diagnosis in 30% of cases, i.e. the second variant cannot be identified in the coding regions of adenosine triphosphate (ATP) binding cassette type A4 (*ABCA4*) gene [2, 3].

Nuria Suárez-Herrera and Tomasz Z. Tomkiewicz contributed equally to this work.

Virginia Arechavala-Gomez and Alejandro Garanto (eds.), *Antisense RNA Design, Delivery, and Analysis*, Methods in Molecular Biology, vol. 2434, https://doi.org/10.1007/978-1-0716-2010-6_9, © The Editor(s) (if applicable) and The Author(s) 2022

According to the Human Gene Mutation Database, mis-splicing mutations have been estimated to represent 8.6% of the total mutations underlying inherited diseases (23,868/275,716) [4]. In vitro functional assays can provide insight into the underlying mechanisms behind aberrant splicing and identify the mutations that interfere with this process. Currently, the ideal model to assess and correct mis-splicing mutations in STGD1 are iPSC-derived retina-like cells (such as photoreceptor precursor cells (PPCs) or retinal organoids) from a patient harboring the genetic variants of interest, as these represent the right cell type(s) with the proper genetic context. In parallel, great efforts have been made to develop a more cost-effective and less time-consuming strategy to reach the same goal, by trying to mimic the pathological situation in a reliable and controlled manner. Engineering and use of multi-exon splice vectors have been proven to be extremely effective [2, 5–7] in gaining insight into IRDs and, more specifically, STGD1. In general, splice vectors or midigenes refer to a specific type of vector containing a large genomic region that allows to study the splicing processes between the included exons. An even longer genomic content allows for inclusion of long-range cis-acting elements to more accurately reflect the dynamics of splicing [8]. These “artificial” genomic vectors were shown to be very valuable when it comes to *ABCA4*, as the entire 128-kb gene has been successfully spanned in a set of midigenes representing an alternative to the impossibility of cloning such a large genomic region in a single vector [6].

The suitability of midigenes for some cell lines reduced the complexity of the study of pathologic deep-intronic variants (among other types of mutations) and their effect on splicing. In addition, validated midigenes harboring splicing variants represent a system for reliable and relatively quick identification of potential therapeutic molecules such as antisense oligonucleotides (AONs). AON-based therapies represent a very effective approach to target mis-splicing mutations. AONs are chemically modified RNA molecules that have the ability of modulating splicing by binding to pre-mRNA and interfering with the spliceosome [9]. They are used in the field of IRDs [10], as well as in other genetic diseases as the purpose of AONs is not limited to splice-switch function only [11]. Generating a reliable artificial splicing system is of major importance when it comes to the development of a potential therapeutic molecule. For the early investigation of possible causative variant affecting pre-mRNA splicing in retinal genes and subsequent assessment of AON potency, midigene technology is a suitable approach that has been shown to produce reliable results [6, 12].

Following transfection of the vector into HEK293T cells, AONs are co-transfected, and the splicing correction can be assessed at RNA level. Subsequently, the AONs that are identified

as most potent can be tested in more advanced and precise cell models such as iPSC-derived retina-like cells.

Despite the proven efficiency of the HEK293T cells, they are not derived from ocular tissue, which allows to speculate whether the splicing dynamics enforced by HEK293T represents that of the retina. As an alternative, with the aim to better represent the retina-like splicing dynamics in in vitro splice assays, we also describe the use of retinoblastoma WERI-Rb-1 cells. These cells are also suitable for midigene transfection and in some cases demonstrate splicing dynamics that are more similar to that of the retina when compared to HEK293T cells.

In this chapter, we describe how to design multi-exon splice vectors followed by appropriate validation and correction of mis-splicing mutations by performing in vitro studies in cellular systems.

2 Materials

2.1 Design of Midigene and Maxigene Splice Vector

1. Donor and destination vector (*see Note 1*).
2. BP-Clonase cloning kit: BP-Clonase, buffer, proteinase K, etc. (i.e. Gateway[®] enzymes).
3. LR-Clonase cloning kit: LR-Clonase, buffer, proteinase K, etc. (i.e. Gateway[®] enzymes).
4. Genomic DNA, in this example, the bacterial artificial chromosome (BAC) clone, CH17-325O16 (insert g.94,434, 639–94,670,492), containing the entire *ABCA4* gene.
5. Generated midigenes (*see Subheading 3.1.1*).
6. Primers flanking the region of interest with attB sites. In this chapter we use *ABCA4* as an example. Forward primer sequence (attB sites underlined): 5'-GGGGACAAGTTTGT-ACAAAAAAGCAGGCTTC aacactgtgtggcaattggag-3' and reverse primer sequence: 5'-GGGGACCACTTTGTACAA GAAAGCTGGGTG agctactgtgtggaggggtg-3'. Primers are located in intron 6 and intron 11 of *ABCA4*, and serve as an example [6].
7. In silico cloning software (VectorNTI, SnapGene or Benchling).
8. High-fidelity *Taq* polymerase PCR kit: High-fidelity *Taq* polymerase, dNTPs, buffer, MgCl₂ and Q-solution or DMSO if applicable.
9. Unique restriction enzymes for sites present in your constructs, in our example are shown as A and B (*see Subheading 3.2.1*).
10. Commercially available DNA purification and cleanup kit.
11. Shrimp Alkaline Phosphatase.

12. T4 ligation kit.
13. Competent cells (preferably commercial ones).
14. LB medium: Autoclave 10 g NaCl, 10 g tryptone, and 5 g yeast extract in 1 L of deionized water.
15. LB plates: Autoclave 10 g NaCl, 10 g tryptone, 5 g yeast extract, and 30 g agar in 1 L of deionized water.
16. Selection antibiotics (usually ampicillin and kanamycin) at 50 mg/mL (this is the stock 1000× concentrated).
17. Commercially available Mini/Midiprep kit for plasmid DNA purification.
18. Electrophoresis equipment and agarose gels.

2.2 Site-Directed Mutagenesis

1. Generated midigene and maxigene vectors (*see* Subheadings 3.1.1 and 3.2.2).
2. Primers to introduce the desired mutation, in this chapter we use the c.859-506G > C mutation in the *ABCA4* midigene as an example (the variant is in bold and underlined):
Forward primer 5'- CTGTGATTTGTTGTTGTTGTTGTTGTTGTTT **G** AGACGGAGTAT -TGCTCAG-3' and reverse primer 5'- GACACTAAACAACAACAACAACAACAA CAA-AA**C**CTCTGCCTCATAACGAGTC-3' [3].
3. Primers to amplify the region within selected restriction sites of the midi-/maxigene.
4. High-fidelity *Taq* polymerase PCR kit: High-fidelity *Taq* polymerase, dNTPs, buffer, MgCl₂ and Q-solution or DMSO if applicable.
5. Standard *Taq* polymerase kit.
6. pGEM®-T Easy Vector System kit.
7. IPTG and X-Gal.
8. EcoRI restriction enzyme.
9. DpnI restriction enzyme.
10. Competent cells (preferably commercial ones).
11. LB medium: Autoclave 10 g NaCl, 10 g tryptone, and 5 g yeast extract in 1 L of deionized water.
12. LB plates: Autoclave 10 g NaCl, 10 g tryptone, 5 g yeast extract, and 30 g agar in 1 L of deionized water.
13. Selection antibiotics (usually Ampicillin and Kanamycin) at 50 mg/mL.
14. Commercially available Mini/Midiprep kit for plasmid DNA purification.
15. Electrophoresis equipment and agarose gels.

16. Corresponding restriction enzymes C and D (*see* Subheading 3.2.3).
17. Shrimp Alkaline Phosphatase.
18. Commercially available DNA purification and cleanup kit.
19. T4 ligation kit.

2.3 Culture Conditions and Cell Lines

1. HEK293T cells (ATCC[®] CRL-3216[™]). Culture medium: DMEM 10% FCS medium (DMEM medium supplemented with 10% Fetal Calf Serum (FCS), 100 U/mL of penicillin, 100 µg/mL streptomycin, and 1% (v/v) 100 mM sodium pyruvate).
2. WERI-Rb-1 cells (ATCC[®] HTB-169[™]). Culture medium: DMEM 15% FCS medium (DMEM medium supplemented with 15% FCS, 100 U/mL of penicillin, 100 µg/mL streptomycin and 10 mL of 1 M HEPES).
3. T75 flasks to culture cell lines.
4. 0.25% trypsin solution for cell dissociation.
5. 1× PBS.

2.4 Midigene and AON Transfection

1. HEK293T or WERI-Rb-1 cells and corresponding culture medium.
2. Midigene vector, as an example we used *ABCA4* BA7 midigene [6].
3. AON stock: resuspend the lyophilized AONs at final concentration of 0.1–1 mM in 1× PBS previously autoclaved twice.
4. 6-well plates and 24-well plates.
5. OptiMEM and transfection reagents (i.e., FuGene[®] or Lipofectamine[®]).
6. 0.25% trypsin solution for cell dissociation.
7. 1× PBS.

2.5 RT-PCR

1. Commercially available RNA isolation kit.
2. Commercially available cDNA synthesis kit.
3. Primers located in the flanking exons of your region of interest. In the example described in this chapter:
 - (a) Region of interest.
 - *ABCA4* exon 7 forward: 5'- TCTGAGATCTTGGG GAGGAA-3'.
 - *ABCA4* exon 8 reverse: 5'- TGGAGTCAATCCCCA GAAAG-3'.
 - (b) Actin loading control (*see* **Note 2**).

- *ACTB* exon 3 forward: 5'-ACTGGGACGACATGGA GAAG-3'.
- *ACTB* exon 4 reverse: 5'-TCTCAGCTGTGGTGGT GAAG-3'.
- (c) *RHO* transfection control.
 - *RHO* exon 5 forward: 5'- ATCTGCTGCGGCAA GAAC-3'.
 - *RHO* exon 5 reverse: 5'-AGGTGTAGGGGATGGGA GAC-3'.
- 4. PCR kit: Polymerase, dNTPs, buffer, MgCl₂, water, and Q-solution or DMSO if applicable.
- 5. Electrophoresis equipment and agarose gels.

3 Methods

Retina-specific genes are not readily expressed outside the ocular tissue. The inability to express or poorly express the genes of interest in non-ocular tissues makes it difficult to study variants affecting pre-mRNA splicing. Generation of PPCs from patient-derived reprogramed fibroblasts is an alternative to this, but is time-consuming and expensive.

3.1 Design of Midigene Splice Vectors

3.1.1 Gateway Cloning

In here, we describe the generation and use of pCI-NEO-*RHO* Gateway-adapted in-house vector (*see* Fig. 1).

1. Identify the gene and sequence of interest in genomic databases such as Ensembl Genome Browser or UCSC [13, 14] and then identify the region of interest. In this case, the region of interest is a deep-intronic variant causing guanine to cytosine substitution at position c.859-506 of the *ABCA4* gene. The base substitution strenghtes a cryptic deep-intronic splice acceptor side and causes generation of a 56-nts long pseudoexon between exon 7 and 8.
2. Design primers suitable for Gateway[®] BP cloning (*see* Note 3).
3. Use the BAC clone, CH17-325O16 (insert g.94,434, 639–94,670,492), containing the entire *ABCA4* gene. Isolate the BAC DNA using commercially available midiprep kit and use it as a PCR template to generatet the midigenes. Prepare the PCR reaction with 0.5 μM of each forward and reverse primer, 0.2 mM dNTPs, Phusion High-Fidelity DNA polymerase, 1× Phusion GC buffer, 3% DMSO, and 2.5 ng of BAC DNA in a total of 50 μL. Run the PCR program where the initial denaturation is at 98 °C for 30 s; 15–20 cycles of denaturation at 98 °C for 10 s each, annealing at 58 °C and

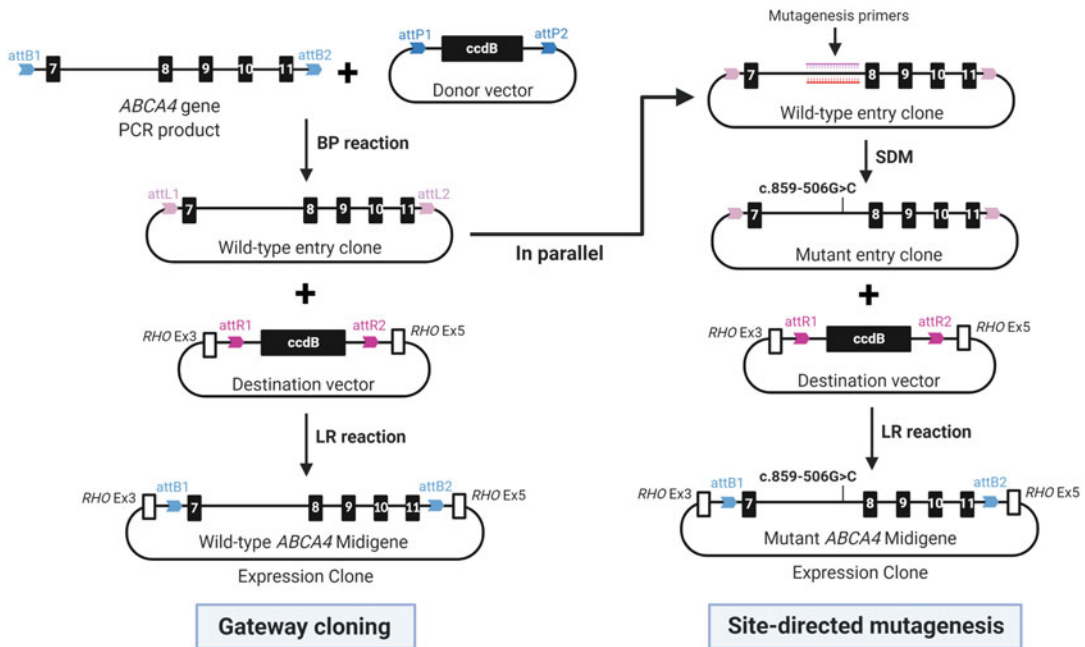


Fig. 1 Schematic representation of wild-type and mutant *ABCA4* midigene engineering. The simplified protocol for Gateway[®] system cloning and site-directed mutagenesis are shown on the left and right section, respectively. *SDM*: site-directed mutagenesis

extension at 72 °C for at least 1 min per kb of insert, with a final extension at 72 °C for 15 min [6].

4. Resolve the PCR product by gel electrophoresis by loading 10% of the reaction. The presence of a single band at a corresponding size indicates a successful PCR amplification step. The band needs to be purified using any available commercial DNA purification and cleanup kit.
5. Set-up the BP reaction as instructed by the manufacturer of the BP-clonase cloning kit. The procedure used in-house includes 1 μ L of donor vector (150 ng), 2 μ L of buffer, 150 ng of purified and sequenced PCR product (max. 5 μ L), milli-Q water up to 8 and 2 μ L of BP-Clonase enzyme. The BP reaction has to be incubated at 25 °C for a minimum of 2 h.
6. Terminate the reaction by adding 2 μ L of Proteinase K and incubating for 10 min at 37 °C.
7. Transform up to 5 μ L of the reaction using competent cells (*see Note 4*) and incubate for 30 min on ice.
8. Perform the heat shock between 45 and 60 s at 42 °C and immediately place the cells back on ice for a minimum of 2 min.
9. Add 250 μ L of SOC medium into the tube and incubate for 1 h at 37 °C.

10. Plate the content of the tube on a plate containing the corresponding antibiotic (the in-house vector has a kanamycin-resistance cassette) and incubate O/N at 37 °C.
11. Pick between 5 and 10 colonies and grow them in a 3 mL of LB medium supplemented with the corresponding antibiotic (1: 1000 ratio of antibiotic to medium) O/N.
12. Perform the plasmid isolation using commercially available miniprep kit for plasmid DNA purification.
13. Verify the presence of insert by conducting restriction analysis. Use donor vector as a control (*see Note 5*).
14. Sequence the entire wild-type clone to make sure that the *Taq* did not introduced new mutations during the amplification step (*see Note 6*).
15. Perform side-directed mutagenesis (*see Subheading 3.1.2*).

3.1.2 Side-Directed Mutagenesis

In this section, we describe the side-directed mutagenesis protocol for midigene constructs:

1. Design the mutagenesis primers to have approximately 20-nts flanking both regions of the c.859-506 position (*see Fig. 1*).
2. Prepare mutagenesis mastermix with 1 U of high-fidelity *Taq* polymerase, 0.5 µM of forward and reverse primer, 0.2 mM dNTPs, 1× high-fidelity reaction buffer, 2× Q-solution, and 10–35 ng of the wild-type midigene vector in a total of 50 µL. Run the PCR program where the initial denaturation is at 94 °C for 5 min; 15 cycles of denaturation at 94 °C for 30 s each, annealing between 50 and 58 °C for 30 s and extension time at least 1 min per each kb of the complete plasmid with a final extension at 72 °C for 20 min.
3. Add 1 µL DpnI directly to 20 µL of the PCR reaction to digest the original template (the wild-type sequence). Incubate the reaction at 37 °C for 3 h. The reaction is terminated at 80 °C for 20 min.
4. Perform the transformation using up to 5 µL of the reaction (*see steps 7–13* in Subheading 3.1.1).
5. Sequence the entire mutant clone to confirm the presense of the desired mutation and also to identify all of the undesired substitutions present in the mutant clone (*see Note 6*).

3.2 Design of Maxigene Splice Vectors

There are some variants that may need larger genomic environment in order to correctly assess them. This could be the case for mutations whose effect is only detected when other splice regulatory motifs are present, generally located in introns. As a consequence, larger genomic context should be included and based on our experience, it is difficult to obtain a splicing vector of this size because of several reasons. The first one is the probability of

inducing single nucleotide changes during the amplification of the genomic region of interest. Long-range PCR and high-fidelity DNA *Taq* polymerases may prevent this from happening, although these chances increase when amplifying >10 kb fragments. Recombination efficiency between the fragment and the donor vector is also affected, as well as the efficiency of site-directed mutagenesis on the entry clone. Both cases are highly associated with the size of the vector. To overcome these limitations, we propose to use the already engineered midgenes completely covering the whole gene in order to generate a maxigene, which combines the genomic context of more than one midgene. In this section, we show an example of the mentioned cloning strategy.

3.2.1 *In Silico Design of Maxigene Strategy*

1. Select the two midgenes that include the introns and exons of interest.
2. Find a common region within both vectors (generally, it is the overlapping sequence between the first midgene and the following).
3. Look for restriction sites in the common region (A) as well as in the backbone of the vector (B) (*see* Fig. 2). Restriction sites A and B should be unique in both midgenes (*see* **Note 7**).
4. Simulate the engineering of the final construct by selecting the fragments flanked by restriction sites A and B in both midgenes. From the first vector (based on sequence), select the fragment B → A (backbone to common region), whereas in the second vector the fragment goes A → B (common region to backbone).

3.2.2 *Cloning of Maxigene Vectors*

1. Check if the enzymes are compatible in terms of incubation time/temperature, reaction buffer and stability in order to avoid partial digestions (*see* **Note 8**).
2. Set the digestion reaction for midgene 1 and 2 with restriction enzymes A and B (*see* Fig. 2). Digest at least 0,5–1 µg of DNA and check the digestion product by gel electrophoresis (*see* **Note 9**).
3. Cut the band corresponding to the fragment of interest and purify the DNA by using the kit of your convenience (*see* **Note 10**).
4. Measure DNA concentration and perform the ligation reaction as described by the manufacturer of the T4 ligase kit (make sure to include a negative control the vector only).
5. Transform 5 µL of the ligation product using DH10β competent cells (*see* **Note 4**) and incubate for 20–30 min on ice.
6. Perform the heat shock for 30 s at 42 °C and cool down the cells for 2 min on ice.

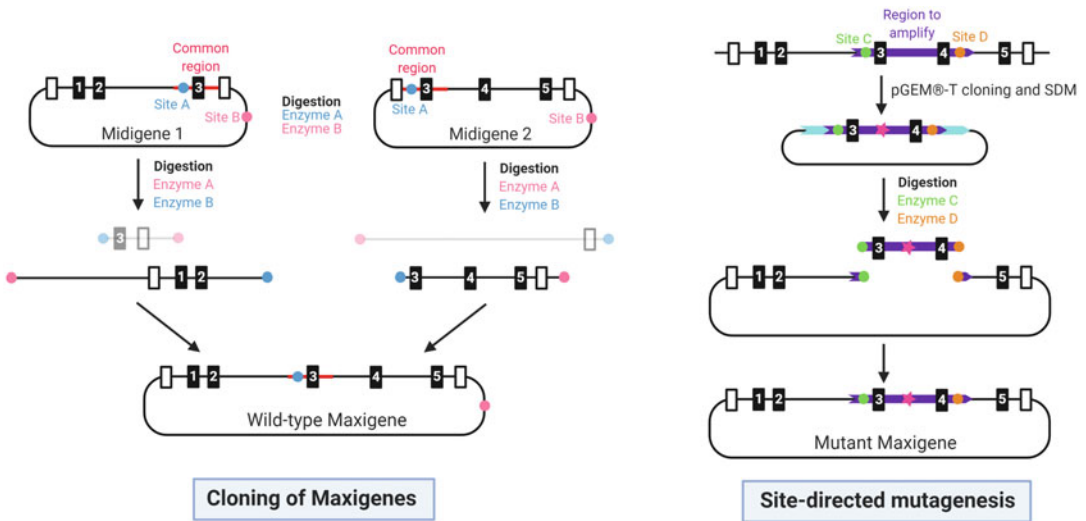


Fig. 2 Schematic representation of wild-type and mutant maxigene engineering. Cloning steps and site-directed mutagenesis are shown on the left and right section, respectively. This example of maxigene strategy is based on the alternative procedures explained in Subheading 3.2. *SDM*: site-directed mutagenesis

7. Add 250 μ L of 10 β /Stable Outgrowth Medium into the tubes and incubate for 1 h at 37 °C in the shaking incubator (250 rpm).
8. Plate everything on LB-agar plates containing the corresponding antibiotic (as we are referring to expression clones, these have ampicillin resistance).
9. Incubate O/N at 37 °C.
10. Take the plates from the incubator in the morning and in the same afternoon, pick colonies and let them grow at 37 °C in 3 mL of LB medium supplemented with the corresponding antibiotic, i.e., ampicillin.
11. Perform plasmid isolation and verify if the ligation worked by restriction analysis or colony PCR. As a negative control, use midigene 1 in parallel.
12. Sequence the positive clones in order to verify that they do not contain any additional mutations.

3.2.3 Site-Directed Mutagenesis

To obtain the mutant maxigene, you can either use midigene 1 or 2 containing the mutation of interest and follow the same protocol indicated in the previous section or perform the site-directed mutagenesis on the wild-type maxigene. In order to perform the second option, we propose the following strategy as an example for a maxigene (*see* Fig. 2):

1. Look for unique restriction sites flanking the region of interest (containing the position where single-nucleotide change has to be performed, in this case would be C and D).
2. Amplify this region by using high-fidelity PCR kit.
3. Incubate with normal *Taq* Polymerase for 20 min at 72 °C to add the A overhangs to the final PCR product.
4. Clone the fragment into a pGEM[®]-T vector following the instructions of the kit's manufacturer. Incubate O/N at 4 °C.
5. The next day, transform 5 µL of the previous reaction using DH5α competent cells.
6. Perform the heat shock for 60 s at 42 °C and cool down the cells for 2 min on ice.
7. Add 250 µL of stable outgrowth medium into the tubes and incubate for 1 h at 37 °C in the shaking incubator (250 rpm).
8. Just before plating, add IPTG and X-Gal in the tube and immediately, plate everything on LB-agar plates containing the corresponding antibiotic (pGEM[®]-T vectors have ampicillin resistance).
9. Incubate O/N at 37 °C.
10. Pick white colonies and let them grow at 37 °C in 3 mL of LB medium supplemented with antibiotic.
11. Perform plasmid isolation using available commercial miniprep kit for plasmid DNA purification, followed by restriction analysis using EcoRI to check if the region is cloned. Keep in mind that your insert may contain an EcoRI restriction site.
12. Sequence the positive clones to check if they contain any additional mutations.
13. Perform site-directed mutagenesis as previously indicated for midigene vectors.
14. Verify the mutation by Sanger sequencing.
15. Digest both the pGEM[®]-T vector and the maxigene with restriction enzymes C and D.
16. Set the ligation reaction as indicated in the maxigene cloning with either the purified digestion products directly (incubating one of the fragments with phosphatase) or the purified fragments from the agarose gel.
17. Pick colonies and perform restriction analysis or colony PCR to check the correct ligation between the fragment containing the mutation and the rest of the maxigene.
18. Analyze the new inserted region by Sanger sequencing.

3.3 In Vitro Evaluation of Splice Vectors in Cell Lines

The constructed midi/maxigenes need to be validated and assessed in vitro. In the functional studies of IRDs, the cell line of choice is usually HEK293T. These cells are easy to transfect and do not express retina-specific genes. Therefore, the expression of retina-specific gene delivered with the vector is not interfered by the endogenous expression of such gene. This advantage is counterbalanced by fact that the HEK293T cells have different properties compared to retina cells. As a consequence, the splicing dynamics are often but not always the same. As an alternative to better represent the retina-like splicing dynamics, we also describe the use of WERI-Rb-1 cells, which are retinoblastoma cells. These cells are still suitable for midigene transfection and sometimes mimic retina-specific splicing patterns better in comparison with HEK293T cells (*see* Fig. 3).

3.3.1 Transfection in HEK293T

1. Seed 0.5×10^6 cells/well in DMEM 10% FCS medium in 6-well plate if you can transfect the midigene 4 h post-seeding (*see* **Note 11**).
2. Once the cells are attached, transfect 1.2 μg of plasmid in a 6-well plate. In this example we used FuGENE (ratio is 3:1 FuGENE:plasmid). To make transfection mix, to 200 μL of OptiMEM medium, add 3.6 μL of FuGENE. To the transfection mix add 1.2 μg of plasmid and incubate at RT for 15–20 min.
3. Dispense the transfection mix on top of the corresponding well (*see* **Note 12**).
4. Incubate the plate at 37 °C for 24 (*see* Subheading 3.4.1) or 48 h (*see* **Note 13**).
5. After the incubation, gently rinse the cells with pre-warmed $1 \times$ PBS and then detach the cells using 500 μL trypsin. Collect the detached cells into a 1.5 mL Eppendorf using P1000 pipette.
6. Centrifuge the Eppendorf tubes for 5 min at $1000 \times g$ to pellet the cells, remove the supernatant and wash the cells again in $1 \times$ PBS for 5 min at $1000 \times g$.
7. Discard the supernatant and:
 - (a) freeze the cell pellets at -80 °C (storage) after 48 h incubation and proceed with further analysis at another moment or,
 - (b) proceed with the RNA isolation (validation of the midigene expression and splicing) after 48 h incubation.

3.3.2 Transfection in WERI-Rb-1

1. Dispense 1 to 2×10^6 cells to 1.5 mL Eppendorf tube in a total volume of 500 μL of DMEM 15% FCS.
2. Transfect 1.2 μg of plasmid. In this example, we used FuGENE (ratio is 3:1 FuGENE:plasmid). To make transfection mix

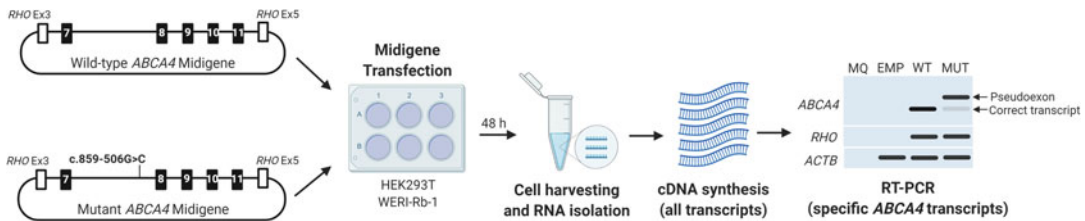


Fig. 3 Experimental strategy to assess splicing defects in HEK293T or WERI-Rb-1 cell lines. The cells are first transfected with a wild-type (WT) or mutant (MUT) *ABCA4* midigene and, following a 48-h incubation, splicing is validated by RT-PCR as outlined in Subheading 3.4.3. The gel picture shows an approximate read-out of the expected *ABCA4* transcripts. MQ, negative control of the PCR reaction; EMP, empty transfection mix (endogenous expression of the selected genes within the cell line used).

200 μ L of OptiMEM medium with 3.6 μ L of FuGENE. And to this tube, add 1.2 μ g of plasmid and incubate at RT for 15–20 min.

3. Dispense the transfection mix to 1.5 mL Eppendorf tube with WERI-Rb-1 cells and incubate for 2 h at 37 °C.
4. After the incubation, transfer the cells to the corresponding well on the 6-well plate and add medium to a total volume of 2 mL.
5. Incubate the plate at 37 °C for either 24 (see Subheading 3.4.1) or 48 h (see **Note 13**).
6. After incubation, collect the cells in 1.5 mL Eppendorf tube and spin it for 5 min at 1000 $\times g$.
7. Remove the medium and wash the cells again in 1 \times PBS for 5 min at 1000 $\times g$.
8. Discard the PBS and:
 - (a) freeze the cell pellets at –80 °C (storage) after 48 h incubation and proceed with further analysis at another moment or,
 - (b) proceed immediately with the RNA isolation (validation of the midigene expression and splicing) after 48 h incubation.

3.3.3 Validation of Splicing Events by Reverse Transcriptase PCR (RT-PCR)

Before starting to use midigenes as an artificial system, it is necessary to check the effect of the variant at pre-mRNA level, and therefore, the RT-PCR is used as a validation method for splicing events.

1. Design forward and reverse primers to flank the region of interest. If the cell line used presents endogenous expression of your target gene, design one of the primers in the artificial exon of the midigene (*RHO*) (see **Note 14**).

2. Isolate the RNA from the pellets obtained in Subheading 3.3.1 or 3.3.2 and measure the concentration using NanoDrop.
3. Use 1 μg of RNA to synthesize cDNA by following the instruction of the kit's manufacturer.
4. Prepare RT-PCR master mix with 1 U *Taq* polymerase, 1 \times PCR buffer with MgCl_2 , 0.2 mM dNTPs, and 50–60 ng of cDNA in a total volume of 25 μL . In parallel, prepare the corresponding PCR mixes for actin (loading control) and *RHO* (midigene transfection control) using the mastermix recipe outlined above with appropriate actin and *RHO* primers. Run the PCR program where the initial denaturation is at 94 °C for 5 min; 35 cycles of denaturation at 94 °C for 30 s each, annealing at 58 °C for 30 s and extension time at 72 °C for 3 min, with a final elongation step at 72 °C for 5 min.
5. Resolve PCR products by gel electrophoresis. Load 10 μL from *ABCA4* PCR products and 5 μL from actin and *RHO* PCR products as well.
6. Excise the bands coming from each midigene transfection and extract the DNA using a PCR cleanup kit of choice.
7. Measure DNA concentration and if it is not sufficient for Sanger sequencing (minimum of 200 ng per sample), clone the bands in pGEM[®]-T vector following the manufacturer's instructions.
8. Verify all bands corresponding to different splicing events comparing the mutant to the wild-type condition.
9. Correctly identify and remove midigene artifacts (*see* **Note 15**) or heteroduplexes (*see* **Note 16**).

3.4 Correcting Splicing Defects in Artificial Systems

In this part of the chapter, we describe the experimental design to correctly compare a set of AON sequences by using midigenes as a model system and how to determine the efficacy of aberrant splicing correction. The utilization of photoreceptor precursor cells and/or retinal organoids is a recommended step in the final stages of AON potency validation in in vitro studies.

3.4.1 Midigene Vector and AON Co-transfection

Seeding 0.5×10^6 cells/well in 6-well plate provides enough cells to seed 6 wells on the 24-well plate. It is recommended to perform early calculations into how many wells will be required for the splice correction assay as this will influence the number of wells on the 6-well plate required for midigene transfection. If 6 or less wells on the 24-well plate are needed, one 6-well plate seeded with 0.5×10^6 HEK293T cells and transfected with midigene is enough.

When setting up splice assay with AONs, do not forget about the minimum required controls. These include non-transfected control or empty transfection mix (EMP), cells transfected with

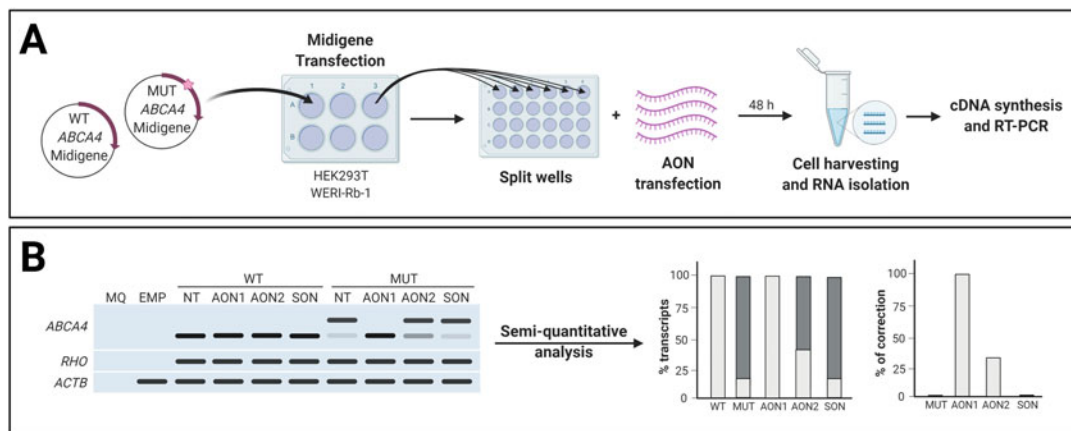


Fig. 4 Analysis of AON-mediated splicing correction in midigene-based splice assays. **(a)** Experimental strategy to correct splicing defects by co-transfection of wild-type (WT) or mutant (MUT) *ABCA4* midigenes with AONs in cell lines as described in Subheading 3.4.1. **(b)** Representation of splicing read-out on agarose gel and further semi-quantitative analysis. The gel picture represents an approximation of expected *ABCA4* transcripts, further semi-quantitative analysis and graphs are based on this estimation. MQ: negative control of the PCR reaction, EMP: empty transfection mix (endogenous expression of the selected genes within the cell line used), NT: non-treated (transfected with midigene but no AONs), SON: scrambled or sense oligonucleotide

wild-type (WT) midigene or mutant (MUT) midigene but not transfected with AONs (NT), and cells transfected with wild-type or mutant midigene and co-transfected with the corresponding scrambled or sense oligonucleotide (SON). The controls cells have to be seeded together with test cells and exposed to the exact same treatment conditions, which include medium change and transfer from 6-well plate to 24-well plate.

1. Refer to Subheadings 3.4.1 and 3.4.2 for cell seeding and midigene transfection procedures, then incubate for the next 24 h.
2. Use 500 μ L of trypsin to detach the HEK293T. Neutralize the effect of trypsin with 500 μ L of HEK293T specific medium and collect the cells in a 15 mL Falcon tube. Wash the well with extra 1 mL of medium to collect all the remaining cells. Add 1 mL of HEK293T medium to make 3 mL cell suspension and seed 500 μ L of the suspension per well in the 24-well plate using P1000 pipette (see Note 17).
3. Place the 24-well plate in the 37 $^{\circ}$ C incubator and allow for at least 4 h incubation or until cells become attached to the wells.
4. In this example, the final concentration of the AON was at 0.5 μ M (see Note 18). To co-transfect two wells on a 24-well plate (wild-type and mutant midigene) with the same AON at 0.5 μ M, mix 50 μ L of OptiMEM medium with 1 μ L of FuGENE[®]. To this mixture add 5 μ L of resuspended AON at

100 μM stock concentration. Incubate the transfection reaction for 15–20 min at RT. After incubation add enough medium to make 1 mL.

5. On a 24-well plate, remove all the medium from the transfected wells and gently dispense 500 μL of the transfection mix to the wells transfected with wild-type and mutant midigenes. (*see Note 19*).
6. Place the well plate back in the incubator and allow for 48 h incubation (*see Fig. 4a*).
7. After incubation, collect the cells in an 1.5 mL Eppendorf tube and centrifuge for 5 min at $1000 \times g$. Remove the medium and wash the cells again in $1 \times \text{PBS}$ for 5 min at $1000 \times g$.
8. Discard the PBS and
 - (a) freeze the cell pellets at -80°C (storage) and proceed with further analysis at another moment or,
 - (b) proceed immediately with the RNA isolation and the cDNA synthesis following manufacturer's instructions.
9. After the cDNA synthesis perform RT-PCR as previously described (*see Subheading 3.3.3*).
10. Resolve PCR products by gel electrophoresis.
11. Similar strategy is used for WERI-Rb-1 transfection with AONs. First, refer to Subheading 3.3.3 for midigene transfection to WERI-Rb-1 cells, and follow the protocol outlined above.

3.4.2 Quantification of Splicing Redirection with Image J

Measuring efficiency of an AON-based strategy represents the last step in order to discard or select a potential therapeutic molecule for further clinical studies. There are several methods available to calculate this efficiency and, in this chapter, we focus on a semi-quantification strategy for RT-PCR readouts (*see Fig. 4b*).

1. Open the gel image (TIFF format) in Image J or Fiji (same software).
2. Use the rectangle tool to make selections of the bands you want to quantify (*see Note 20*).
3. Select the first lane and press Ctrl + 1.
4. Move the newly generated rectangle to the right and put it on top of the next lane, then press Ctrl + 2.
5. Repeat **step 4** as many times as samples you have in your gel image.
6. After selecting all bands, press Ctrl + 3 and a new window with all intensity peaks will appear.

7. Using the straight-line tool, draw a line at the bottom of every peak and close it in order to remove the background signal from the band intensity signal.
8. Use the wand tracing tool and click on the closed peak to measure its area. Automatically, a new window will appear showing area value while measuring all the peaks (*see Note 21*).
9. Copy all area values into an Excel sheet (replace dots by commas if necessary).
10. Calculate the total area of every condition. Use this value as a reference to calculate the % of correct transcript or aberrant transcript (*see Note 22*) as indicated below:

$$\% \text{ of Transcript} = \frac{\text{Area Transcript}}{\text{Total Area}} \times 100$$

11. Introduce the values in Graphpad Prism and calculate the average of the other replicates as well (*see Note 23*).
12. Create a graph of the % of correct/aberrant transcript for every condition.
13. Calculate the percentage of aberrant transcript decrease by setting the aberrant transcript of non-treated mutant midigene value as your reference, this will represent the % of correction.
14. Take the average of the decrease in all samples per groups and compare the data using a One-Way ANOVA for statistical analysis.

3.4.3 How to Know If an AON Is Effective?

Once you assess the aberrant transcript rescue of the different AONs that are being tested, it is possible to classify them in several groups depending on their splicing redirection efficiency (*see Note 24*). In previous studies [15], we classified AONs in the following five groups in order to analyze their properties in a straightforward way (*see Fig. 4b*): highly effective (>75% correction), effective (between 75% and 50% correction), moderately effective (between 50% and 25% correction), poorly effective (between 25% and 0% correction), and noneffective (when correction is not detected).

However, there are some limitations as this protocol is based on a semi-quantitative strategy, such as the interference of heteroduplexes and midigene artifacts. Even though we presented different ways of overcoming these limitations, there is the possibility of using other quantitative strategies [16]. As an example, Fragment Analyzer, TapeStation or digital droplet PCR can be implemented in order to get more accurate splicing readouts (*see Note 25*).

4 Notes

1. The donor vector used in this example was pDONR201 vector supplied from Invitrogen. The destination vector used was pCI-NEO-*RHO* vector, which was adapted to contain genomic region encompassing exons 3 through 5 of *RHO*.
2. In the example, we used in-house primers designed for mouse because of the high sequence conservation between mouse *Actb* and human *ACTB* gene.
3. Design the primers to capture as much of the *ABCA4* genomic content for the Gateway[®]-adapted vector cloning. The primers have to be able to insert *attB* sites for Gateway BP cloning.
4. Transformation efficiency for >15 kb constructs is significantly increased when using DH10 β cells instead of DH5 α .
5. Selection of enzyme(s) used to verify the insert depend on the backbone and the insert. We recommend to use an enzyme that cuts in at least two distinct places across the vector. If such enzyme cannot be found, we recommend to use one enzyme that cuts the insert and one enzyme that cuts the backbone of the vector.
6. If new undesired mutations are present within the insert, assess their potential effect on the splicing, in silico, by using tools designed to study pre-mRNA splicing (<http://www.umd.be/HSF/HSF.shtml>).
7. If that is not the case, uniqueness of restriction site A is not strictly needed for both vectors, but it is not recommended having more than two in one of the midigenes. On the contrary, restriction site B should always be unique in both cases. In our case, restriction site A was located twice in the midigene 1. For that reason, we amplified a part of midigene 1 including restriction site B until the beginning of the common region where the second restriction site A was (reverse primer included half of the restriction site A and phosphate group at 5'), then we used this product to proceed with the strategy.
8. If this is not the case, sequential digestion is also possible.
9. In our case, the amplified fragment from midigene 1 had to be digested with restriction enzyme B only as restriction site A was located twice in this plasmid, whereas midigene 2 needed sequential digestion with both enzymes A and B.
10. Based on our experience, even if agarose gels prepared with TAE buffer are recommended to obtain a better resolution of large fragments, the loss of DNA after purification with TAE-specific kits is very high. As an alternative, you can always do a cleanup directly from the digestion product, but

incubation with phosphatase is needed at least in one of the digested midigenes and screening of colonies afterwards might be more extensive. In our case, phosphatase incubation was performed in digestion product from midigene 2 to avoid re-ligation with itself.

11. Seed at lower density ($0.2\text{--}0.25 \times 10^6$ cells/well) if you have to wait 24 h until transfection.
12. Dispense the transfection mix drop by drop across the well. After dispensing all the midi-/maxigenes to all the wells, gently swirl the plate to ensure homogenous distribution of the midigene.
13. Twenty-four hours incubation is recommended for AON co-transfection in transcript rescue experiments, 48 h incubation is recommended for assessing the expression of the wild-type midi-/maxigene or assessing the effect of mutation on the transcript.
14. Using *RHO* primers for the RT-PCR might reveal other splicing events induced by the artificial exons. However, you can reduce this artifact by performing nested PCR afterwards, substituting the *RHO* primer by one binding to the next available exon of your transcript.
15. Reduce the amount of transfected midigene if artifacts are masking other splicing events or change the combination of primers, narrowing the region of interest could reduce the amplification of these artifacts.
16. To remove heteroduplexes from the read out, we suggest set a 3–5 cycles PCR in the same conditions by adding 1 μL from the product obtained in **step 5**. However, this may affect the reliability of the method as one extra PCR step is added, for that reason it is important to validate the observed final read-out [17].
17. If you are working with more than one 6-well plate, pool all the cells transfected with the same midigene together. Calculate how much medium needs to be added. If you are working with less than 6 wells on the 24-well plate collect the cells in the total of 3 mL as described, seed the required number of wells and discard of the remaining cell suspension if not needed.
18. The AONs can be tested at varying molarities to assess the concentration at which AONs are most efficient. The concentration can vary between 0.1 and 1 μM .
19. As an alternative, it is also possible to remove from each well the exact volume of the transfection mix to be added, making sure the final concentration of AON does not change.

20. The rectangle size and position (in Y -axis) will be equal for all lanes and cannot be changed in further steps, so make sure to select a region that can cover all bands from the same lane.
21. Try to follow a consistent order through all the analysis, start measuring the band corresponding to the correct transcript and moving to the one of either pseudoexon inclusion (larger) or exon skipping (smaller) band for every different lane/condition.
22. In the aberrant transcript band, total/partial pseudoexon inclusion or total/partial exon skipping can be counted as aberrant. If heteroduplexes were also included in the band quantification, half of the value of that band should be counted as correct transcript, whereas the other half should be included in the aberrant transcript.
23. It is recommended to repeat the same experiment at least three times (replicates) in order to perform further statistical analysis and make proper comparisons between all conditions
24. This is especially useful when screening a set of AONs with the aim of covering entire regions at pre-mRNA levels [15].
25. In a same study, you can include more than one splicing analysis and compare between them to obtain a more robust result.

Acknowledgments

This work was supported by European Union's Horizon 2020—Marie Skłodowska-Curie Actions grant no. 813490 (to R.W.J.C.) and Retina UK Foundation grant no. GR596 (to R.W.J.C.), Algemene Nederlandse Vereniging ter Voorkoming van Blindheid, Stichting Blinden-Penning, Landelijke Stichting voor Blinden en Slechtienden, Stichting Oogfonds Nederland, Stichting Macula Degeneratie Fonds, and Stichting Retina Nederland Fonds (who contributed through UitZicht 2015-31 and 2018-21), together with the Rotterdamse Stichting Blindenbelangen, Stichting Blindenhulp, Stichting tot Verbetering van het Lot der Blinden, Stichting voor Ooglijders, and Stichting Dowilvo (to A.G. and R.W.J.C.). This work was also supported by the Foundation Fighting Blindness USA, grant no. PPA-0517-0717-RAD (to A.G. and R.W.J.C.). The funding organizations had no role in the design or conduct of this research. They provided unrestricted grants.

References

1. Tanna P et al (2017) Stargardt disease: clinical features, molecular genetics, animal models and therapeutic options. *Br J Ophthalmol* 101(1):25–30
2. Fadaie Z et al (2019) Identification of splice defects due to noncanonical splice site or deep-intronic variants in ABCA4. *Hum Mutat* 40(12):2365–2376
3. Sangermano R et al (2019) Deep-intronic ABCA4 variants explain missing heritability in Stargardt disease and allow correction of splice defects by antisense oligonucleotides. *Genet Med* 21(8):1751–1760
4. Stenson PD et al (2017) The human gene mutation database: towards a comprehensive repository of inherited mutation data for medical research, genetic diagnosis and next-generation sequencing studies. *Hum Genet* 136(6):665–677
5. Bauwens M et al (2019) ABCA4-associated disease as a model for missing heritability in autosomal recessive disorders: novel noncoding splice, cis-regulatory, structural, and recurrent hypomorphic variants. *Genet Med* 21(8):1761–1771
6. Sangermano R et al (2018) ABCA4 midgenes reveal the full splice spectrum of all reported noncanonical splice site variants in Stargardt disease. *Genome Res* 28(1):100–110
7. Garanto A et al (2016) In vitro and in vivo rescue of aberrant splicing in CEP290-associated LCA by antisense oligonucleotide delivery. *Hum Mol Genet* 25(12):2552–2563
8. Khan M et al (2019) Identification and analysis of genes associated with inherited retinal diseases. In: Weber BHF, Langmann T (eds) *Retinal degeneration: methods and protocols*. Springer, New York, pp 3–27
9. Hammond SM, Wood MJ (2011) Genetic therapies for RNA mis-splicing diseases. *Trends Genet* 27(5):196–205
10. Collin RW, Garanto A (2017) Applications of antisense oligonucleotides for the treatment of inherited retinal diseases. *Curr Opin Ophthalmol* 28(3):260–266
11. Sharma VK, Sharma RK, Singh SK (2014) Antisense oligonucleotides: modifications and clinical trials. *MedChemComm* 5(10):1454–1471
12. Tomkiewicz TZ et al (2021) Antisense oligonucleotide-based rescue of aberrant splicing defects caused by 15 pathogenic variants in ABCA4. *Int J Mol Sci* 22(9):4621
13. Cunningham F et al (2018) Ensembl 2019. *Nucleic Acids Res* 47(D1):D745–D751
14. Kent WJ et al (2002) The human genome browser at UCSC. *Genome Res* 12(6):996–1006
15. Garanto A et al (2019) Antisense oligonucleotide screening to optimize the rescue of the splicing defect caused by the recurrent deep-intronic ABCA4 variant c.4539+2001G>A in Stargardt disease. *Genes* 10(6):452
16. Hiller M et al (2018) A multicenter comparison of quantification methods for antisense oligonucleotide-induced DMD exon 51 skipping in Duchenne muscular dystrophy cell cultures. *PLoS One* 13(10):e0204485
17. Thompson JR, Marcelino LA, Polz MF (2002) Heteroduplexes in mixed-template amplifications: formation, consequence and elimination by ‘reconditioning PCR’. *Nucleic Acids Res* 30(9):2083–2088

Open Access This chapter is licensed under the terms of the Creative Commons Attribution 4.0 International License (<http://creativecommons.org/licenses/by/4.0/>), which permits use, sharing, adaptation, distribution and reproduction in any medium or format, as long as you give appropriate credit to the original author(s) and the source, provide a link to the Creative Commons license and indicate if changes were made.

The images or other third party material in this chapter are included in the chapter’s Creative Commons license, unless indicated otherwise in a credit line to the material. If material is not included in the chapter’s Creative Commons license and your intended use is not permitted by statutory regulation or exceeds the permitted use, you will need to obtain permission directly from the copyright holder.





Modeling Splicing Variants Amenable to Antisense Therapy by Use of CRISPR-Cas9-Based Gene Editing in HepG2 Cells

Aristides López-Márquez, Ainhoa Martínez-Pizarro, Belén Pérez, Eva Richard, and Lourdes R. Desviat 

Abstract

The field of splice modulating RNA therapy has gained new momentum with FDA approved antisense-based drugs for several rare diseases. In vitro splicing assays with minigenes or patient-derived cells are commonly employed for initial preclinical testing of antisense oligonucleotides aiming to modulate splicing. However, minigenes do not include the full genomic context of the exons under study and patients' samples are not always available, especially if the gene is expressed solely in certain tissues (e.g. liver or brain). This is the case for specific inherited metabolic diseases such as phenylketonuria (PKU) caused by mutations in the liver-expressed *PAH* gene.

Herein we describe the generation of mutation-specific hepatic cellular models of PKU using CRISPR/Cas9 system, which is a versatile and easy-to-use gene editing tool. We describe in detail the selection of the appropriate cell line, guidelines for design of RNA guides and donor templates, transfection procedures and growth and selection of single-cell colonies with the desired variant, which should result in the accurate recapitulation of the splicing defect.

Key words Splicing, Gene editing, CRISPR/Cas9, HepG2, Inherited metabolic diseases, Phenylketonuria, Cellular models

1 Introduction

Splicing defects account for up to one-third of human disease-causing variants, according to the current estimates [1–3]. Constitutive splicing relies on the recognition of consensus splicing sequences (5' splice site, 3' splice site, branch point, and polypyrimidine tract) by spliceosomal components, as well as of other less conserved regulatory elements, referred to as exonic or intronic splicing enhancers or silencers (ESE, ISE, ESS, or ISS), that modulate spliceosome recruitment [4]. These cis-regulatory elements are recognized by trans-acting factors including the serine/arginine-rich domain-containing (SR) protein and heterogeneous nuclear

ribonucleoprotein (hnRNP) families that may act co-ordinately to accurately regulate exon inclusion.

Pathogenic splicing variants disrupt conserved splice sites or regulatory elements or cause aberrant splicing by creating/activating alternative splice sites or by promoting the aberrant inclusion of intronic pseudoexons [4]. Splicing can be modulated therapeutically using antisense approaches, and to date, the clinically approved splice-switching antisense oligonucleotides (SSO) for spinal muscular atrophy, Duchenne muscular atrophy and for an individual patient with a rare, fatal neurodegenerative disease [5–7], represent landmarks in the field, opening new avenues for treatment of patients with defects amenable to splice-mediated correction.

The first requirement for the accurate design and testing of antisense splice correction therapy is the availability of relevant experimental models in which to dissect the underlying molecular mechanisms of pathogenic variants and to test candidate molecules. In this sense, the development of clustered-regulatory interspaced short palindromic repeats (CRISPR)-CRISPR associated nuclease (Cas) genome editing has paved the way to the rapid and easy generation of new and improved cell/animal models of disease. This has facilitated the understanding of the specific pathogenic effect and has allowed efficient testing of targeted therapies, including allele-specific repair for splicing mutations, in tissue types with native expression levels [8–13]. Based on a naturally employed bacterial defense mechanism [14, 15], CRISPR/Cas9 technology was developed as a programmable system of genetic editing that commonly uses the Cas9 nuclease from *Streptococcus pyogenes* and a RNA duplex comprised of a sequence-specific CRISPR RNA (crRNA) and a generic trans-activating CRISPR RNA (tracrRNA) that directs the nuclease to a cut site point, three base pairs upstream of the protospacer adjacent motif or PAM. The PAM is a three-nucleotide motif essential for the nuclease to recognize its DNA target which in the case of Cas9 is NGG. The crRNA and the tracrRNA can be delivered individually or linked in a single RNA molecule. These elements can be delivered to cells as plasmids or as a ribonucleoprotein (RNP) complex [16].

Once Cas9 nuclease cuts the DNA introducing a double stranded break (DSB), the cell can repair this through two different mechanisms: non-homologous end-joining (NHEJ) which usually results in small insertions or deletions, useful for the generation of gene knockouts, or homology driven repair (HDR), used to introduce specific changes via a DNA template with homology arms to our target locus and containing the sequence or point mutation desired [16].

In our laboratory we have used CRISPR/Cas9 technology to introduce splicing mutations causing inherited metabolic diseases (IMD) in cellular and animal models. IMD are monogenic diseases

characterized by dysregulation of the metabolic networks that underlie development and homeostasis [17]. They belong to the category of rare diseases due to their low individual prevalence and are generally enzyme deficiencies of autosomal recessive inheritance, characterized by the toxic accumulation of precursors and of their derivatives or by lack of downstream metabolites. Several of the most frequent and well characterized IMD, e.g. organic acidemias and amino acid disorders, are of major hepatic expression and, as in other genetic diseases, 13–25% of all disease-causing variants interfere with mRNA splicing (HGMD statistics, Professional Release 2019.3). These data warrant further investigation of the therapeutical potential of SSOs in these diseases and the generation of liver specific cellular models for these studies.

The generation of a cell model using CRISPR/Cas9 system can be done in a huge variety of cell lines. In this chapter we describe the protocol for efficient introduction of a specific splicing variant in the *PAH* gene, coding for phenylalanine hydroxylase, and responsible for the well characterized disease phenylketonuria (PKU, MIM#261600), inherited in autosomal recessive fashion. Human *PAH* is exclusively expressed in liver, so in this protocol we use hepatoma cell line HepG2 seeking to attain edition in both alleles (homozygous phenotype). We explain how to select for the appropriate cell line in each particular case, describe the design of RNA guides and donor templates, transfection procedures, growth of single-cell colonies, selection and testing to confirm genomic edition, and accurate recapitulation of the splicing defect (Fig. 1). Appropriate controls to be included in each step are explained, as well as the necessary precautions to be taken especially for intronic splicing variants. We use as example the CRISPR/Cas9-mediated introduction of the recently characterized *PAH* intronic variant, c.1199 + 20G > C, that causes exon skipping due to disruption of a splicing regulatory element [18]. This variant creates a PshAI restriction site, which is used to screen for gene edition in the transfected cells.

2 Materials

2.1 Cell Culture

1. Laminar flow-hood.
2. Humid CO₂ incubator.
3. Centrifuge.
4. Phase-contrast microscope.
5. Hemocytometer–double chamber with Neubauer rulings.
6. Manual Counter.
7. Consumables: Tissue culture plates, filtered tips, falcon tubes, Eppendorf tubes.

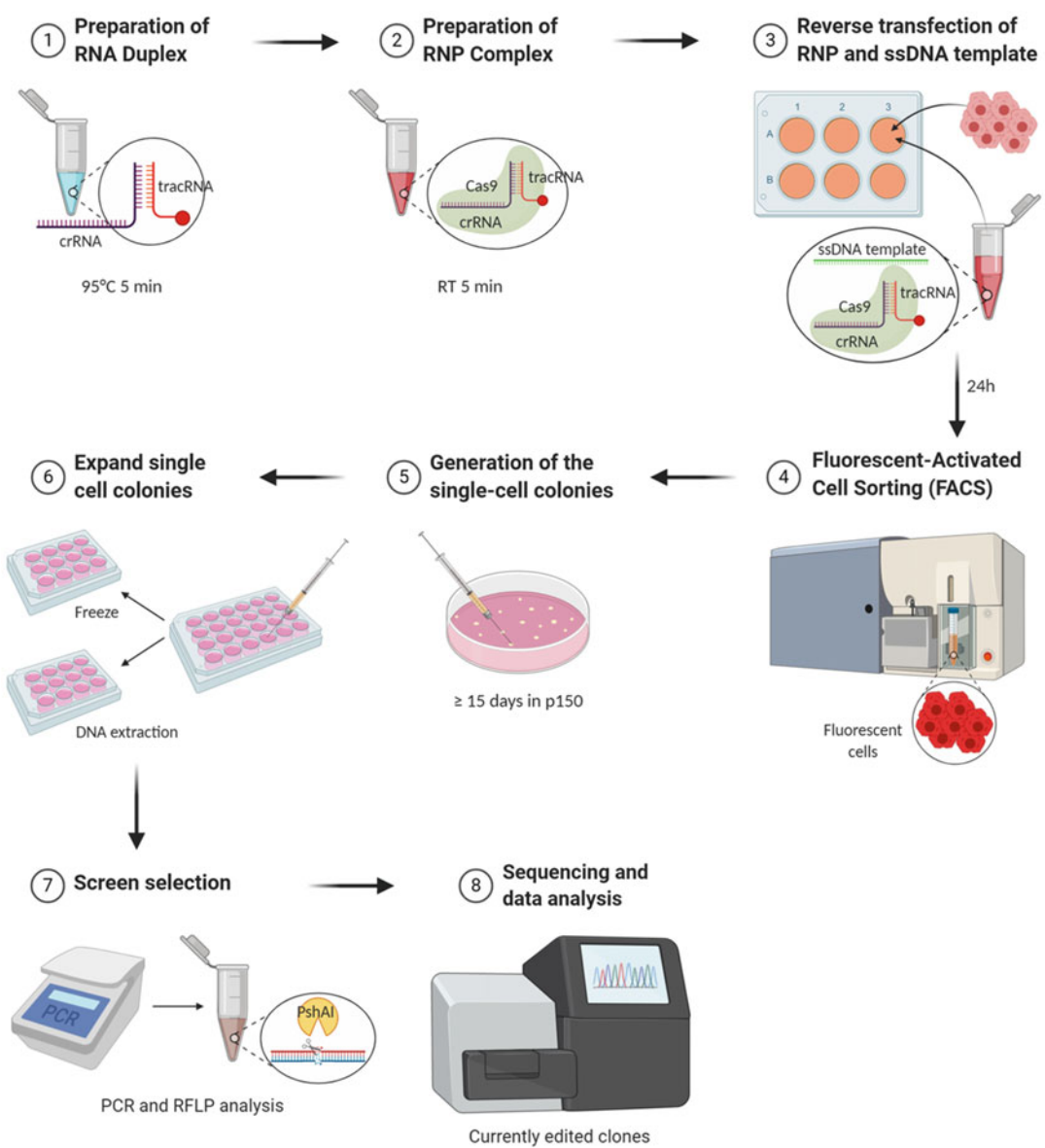


Fig. 1 Outline of the gene editing experimental protocol. (This image was created using BioRender)

8. Phosphate Buffered Saline (PBS).
9. Minimum Essential Medium (MEM) supplemented with 10% Fetal Bovine Serum (FBS), 1% L-Glutamine, and antibiotics.
10. Solution of trypsin–EDTA: 0.25% trypsin, 1 mM EDTA.
11. Trypan Blue Solution: 0.4% trypan blue in PBS.
12. Micropipettes.
13. Stripper micropipettes and 150 μ m tips (Origio Inc).

2.2 Ribonucleoprotein (RNP) Transfection

1. Cas9 Nuclease (*see Note 1*).
2. Fluorescently labeled tracrRNA (tracrRNA-ATTO550) (*see Note 1*).
3. Single-stranded (ss) DNA Template (*see Note 1*).
4. crRNA (*see Note 1*).
5. RNA Duplex Buffer supplied by the manufacturer (*see Note 1*).
6. Nuclease-Free Water.
7. OptiMEM media.
8. Lipofectamine Transfection Reagent (*see Note 2*).

2.3 Fluorescence Activated Cell Sorting

1. Sorting buffer: PBS, 5 mM EDTA, 25 mM Hepes pH 7.0 supplemented with 2% FBS.
2. 5-mL polystyrene tubes with cell strainer.
3. Cell Sorter.

2.4 Genomic DNA Isolation

1. QIAamp DNA Mini Kit for DNA purification (Qiagen).
2. Centrifuge.
3. NanoDrop One spectrophotometer (Thermo Fisher Scientific).

2.5 Polymerase Chain Reaction (PCR)

1. Thermal cycler.
2. PCR tubes.
3. Nuclease-Free Water.
4. dNTPs.
5. FastStart Taq DNA Polymerase (Roche) and PCR buffer 10× (25 mM MgCl₂).
6. Target-specific primers.
7. Agarose gel with ethidium bromide (0.4 µg/mL) and UV transilluminator.
8. DNA Molecular Weight Marker.
9. Kit to purify PCR products, e.g., Cycle Pure Kit for PCR product purification (Omega).

2.6 Restriction Fragment Length Polymorphism Assay (RFLP)

1. PshAI restriction enzyme and enzyme reaction buffer.
2. Agarose gel with ethidium bromide (0.4 µg/mL) and UV transilluminator.
3. DNA Molecular Weight Marker.

2.7 RNA Isolation and Reverse Transcription

1. Trizol isolation reagent (Ambion).
2. 2-Propanol and chloroform.
3. Ethanol 75%.

4. RNase-Free Water and RNase free-consumables.
5. NanoDrop One spectrophotometer (Thermo Fisher Scientific).
6. Thermal cycler.
7. NZY First-Strand cDNA Synthesis Kit.

2.8 Web Resources

1. Sequences and genomes: <https://www.ensembl.org/>.
2. Sequences alignments: <https://blast.ncbi.nlm.nih.gov/Blast.cgi>.
3. Design and analysis of crRNAs: <https://bioinfogp.cnb.csic.es/tools/breakingcas/>.
4. Design, analysis and/or ordering of crRNAs, tracrRNA, ssDNA Templates: https://eu.idtdna.com/site/order/designtool/index/CRISPR_SEQUENCE.
5. PCR primer design: <http://bioinfo.ut.ee/primer3-0.4.0/>.
6. Primer and PCR product analysis: <https://www.ncbi.nlm.nih.gov/tools/primer-blast/>.

3 Methods

3.1 HepG2 Cell Culture

1. Culture the selected HepG2 cell line following standard procedures in P-100 culture dishes with MEM supplemented with 10% FBS, antibiotics, and glutamine at 37 °C in an incubator with 95% humidity and 5% CO₂ (*see* **Notes 3–6**).
2. Just before transfection (*see* Subheading 3.5 below) detach cells by trypsinization. First, aspirate the media and wash the cells with PBS. Once the PBS has been aspirated from the plate, add 0.25% trypsin-EDTA into the plate and incubate at 37 °C for 5 min. Check by microscopy that the cells are rounding up. Once the cells are detached from the plate add 10% FBS in MEM to stop the trypsin reaction. Pipette the cells up and down to dissociate detached cell clumps into single cells. Transfer the cells to a falcon tube and spin them in a centrifuge at $218 \times g$ for 5 min. Discard the supernatant and resuspend the cell pellet in fresh medium.
3. Count the resuspended cells using a hemocytometer. Prepare a dilution 1:8 of the cells in Trypan Blue solution to distinguish dead cells (stained blue). Add the cell suspension to both chamber sides of the hemocytometer and count the cells with the help of a manual counter.

3.2 Design of Guide RNAs and Donor Template

1. Design the specific crRNA guides with the help of bioinformatics software and their potential off-targets (*see* **Notes 7–12**) (Fig. 2).

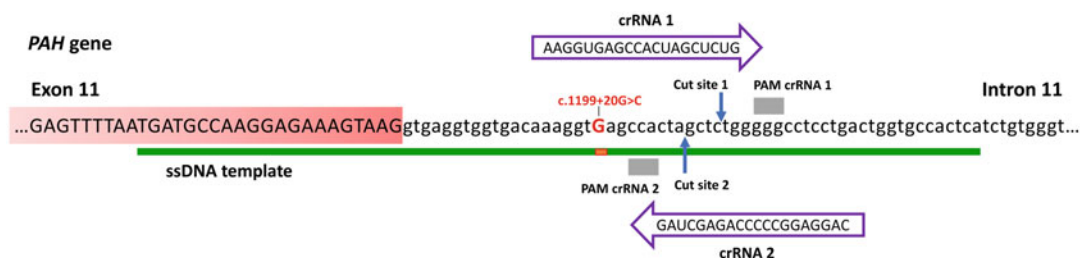


Fig. 2 Schematic representation of the *PAH* gene region surrounding the c.1199 + 20G > C mutation, showing the sequence of the ssDNA template which will include the desired change (green line with red box) and the crRNA guides used (purple arrows), indicating the corresponding PAM sequences (gray rectangles) and the Cas9 nuclease cut sites 3 nucleotides upstream of PAM (blue arrows)

2. Design the ssDNA donor template (*see* **Notes 13–15**) (Fig. 2).
3. Order the crRNA guides, tracrRNA, ssDNA donor template, Cas9 nuclease, transfection reagent, and all the necessary reagents for the CRISPR/Cas9 system (*see* **Note 1**).

3.3 Preparation of RNA Duplex

1. Resuspend the crRNA and tracrRNA-ATTO550 in 20 and 50 μL of Nuclease-Free Duplex Buffer, respectively, resulting in 100 μM stock concentrations (*see* **Notes 16–19**).
2. Prepare the RNA Duplex at a final concentration of 1 μM by mixing the tracrRNA and the crRNA in equimolar concentrations in Nuclease-Free Duplex Buffer (add 1 μL of each crRNA and tracrRNA-ATTO550 to 98 μL of buffer) (*see* **Note 20**).
3. Heat at 95 $^{\circ}\text{C}$ for 5 min.
4. Cool to room temperature (25 $^{\circ}\text{C}$).

3.4 Preparation of the Ribonucleoprotein Complex (RNP)

1. Dilute Cas9 nuclease to a working concentration of 1 μM in OptiMEM (*see* **Note 21**).
2. Prepare the RNP by mixing in independent tubes for each crRNA the following: 24 μL of RNA duplex (1 μM), 24 μL of Cas9 (1 μM), 9.6 μL of Cas9 PLUS reagent from CRISPR MAX kit (*see* **Note 21**), and 342.4 μL of OptiMEM, adding to a total 400 μL .
3. Incubate at room temperature for 5 min.

3.5 Reverse Transfection of RNP and DNA Donor Template

1. Prepare the ssDNA Donor Template at a working concentration of 1 μM in Nuclease-Free Water.
2. Prepare the transfection mixing the following for each well of a 6-well plate: 7.2 μL of 1 μM ssDNA donor template, 400 μL of RNP complex, 19.2 μL of CRISPRMAX Transfection reagent and 373.6 μL of OptiMEM, adding to a total 800 μL (*see* **Notes 22 and 23**).
3. Incubate at room temperature for 20 min.

4. During the incubation of the transfection mix proceed to detach HepG2 cells by trypsinization as explained above (Subheading 3.1) (*see Note 24*).
5. Prepare a dilution of 4×10^5 cells/mL with complete MEM without antibiotics.
6. Once the incubation of the transfection mix is complete, add 800 μ L to each well of the 6-well plate.
7. Add 1600 μ L of the cell suspension to each well containing the transfection mix, for a final volume of 2400 μ L. The number of cells should be 6.4×10^5 cells/well; final concentration of RNP is 10 nM and final concentration of the ssDNA donor template is 3 nM (*see Note 22*).
8. Incubate the cells in an incubator at 37 °C and 5% CO₂ for 24 h. If you are not using tracrRNA-ATTO550 and performing FACS analysis, incubate for 48 h and skip (Subheading 3.6).

3.6 Fluorescent-Activated Cell Sorting (FACS)

1. Trypsinize the cells as explained above 24 h after transfection.
2. Dilute 1.5×10^6 cells in 300 μ L of sorting buffer.
3. For each sample to be collected, a 15 mL Falcon tube with 2 mL of FBS supplemented with 2 μ L of antibiotics mix must be prepared.
4. Collect fluorescent cells for each crRNA.
5. Centrifuge at $218 \times g$ for 5 min.
6. Seed 1×10^5 cells per well of 6-well plate. One complete 6-well plate for each crRNA is enough.
7. Incubate the cells in an incubator at 37 °C and 5% CO₂. Change the medium every 2 days. Expand the cell culture and freeze several cryotubes of the total pool of transfected cells (*see Note 25*).

3.7 Generation of the Single-Cell Colonies

1. Trypsinize the cells as explained above.
2. Count the cells with the help of a hemocytometer.
3. Seed 150–200 cells in a 150-mm plate.
4. Incubate the cells in an incubator at 37 °C and 5% CO₂ for, at least 15 days (*see Note 5*).
5. Once the colonies can be seen with the naked eye, select and pick the colonies with a stripper micropipette and 150 μ m tips. This should be done by observing colonies under a microscope inside a laminar flow-hood under sterile conditions (*see Notes 26 and 27*).
6. Put each colony in a 1.5 mL Eppendorf tube with 50 μ L of trypsin and incubate at 37 °C for 5 min.

7. Individualize the cells by pipetting up and down several times. Seed the cells derived from the colonies into 24-well plates. It is not necessary to centrifuge previously.
8. Expand the culture and change the medium every 48 h. Once the cells are confluent, trypsinize the cells and split them into two wells of a 12-well plate. One of the wells will be used to isolate DNA for analysis, while the other will be used to freeze and/or expand the colony (*see* **Notes 28** and **29**).

3.8 Genomic DNA Extraction and RFLP Analysis

1. Trypsinize the cells as indicated above, centrifuge the cells at $300 \times g$ for 5 min and discard the supernatant.
2. Resuspend the pellet with 200 μ L of PBS.
3. Isolate the DNA using QIAamp DNA Mini kit (Qiagen) following the manufacturer's protocol (*see* **Note 30**).
4. Quantify the DNA concentration in the isolate using Nano-drop One spectrophotometer.
5. Design primers using Primer3 software (<http://bioinfo.ut.ee/primer3-0.4.0/>) for amplification of the region surrounding the desired edited change (500–600 bp) (*see* **Note 31**).
6. Prepare pools of DNA mixing equal amounts (circa 50 ng) of DNA from individual colonies (4 or 5) in a PCR tube to obtain a final amount of 200 ng (*see* **Note 32**).
7. Perform PCR according to standard procedures. Use 200 ng of genomic DNA in a 50 μ L PCR reaction with 1 μ M of each primer, 200 μ M of each dNTP, 2 unit of Taq polymerase and PCR buffer 1 \times . The PCR amplification program is as follows: 1 cycle with 5 min at 95 $^{\circ}$ C, 36 subsequent cycles of 25 s at 95 $^{\circ}$ C, 25 s at 50–60 $^{\circ}$ C (depending on the primers), and 40 s at 72 $^{\circ}$ C, with a final 7-min extension at 72 $^{\circ}$ C.
8. Run 5 μ L of each sample in a 2% agarose gel with ethidium bromide (or other safer dye, such as GelRed or SYBR Safe) to confirm amplification.
9. Digest 5 μ L of each amplified sample in a final volume of 20 μ L with the restriction enzyme using the appropriate buffer and following the manufacturer's indications (*see* **Notes 33** and **34**).
10. Run the restriction reaction volume in a 2% agarose gel with ethidium bromide to visualize the resulting DNA bands.
11. Repeat the PCR and the restriction assay for each individual clone included in the pools for which a positive RFLP analysis is observed (in our example, digestion with PbsAI) (Fig. 3).

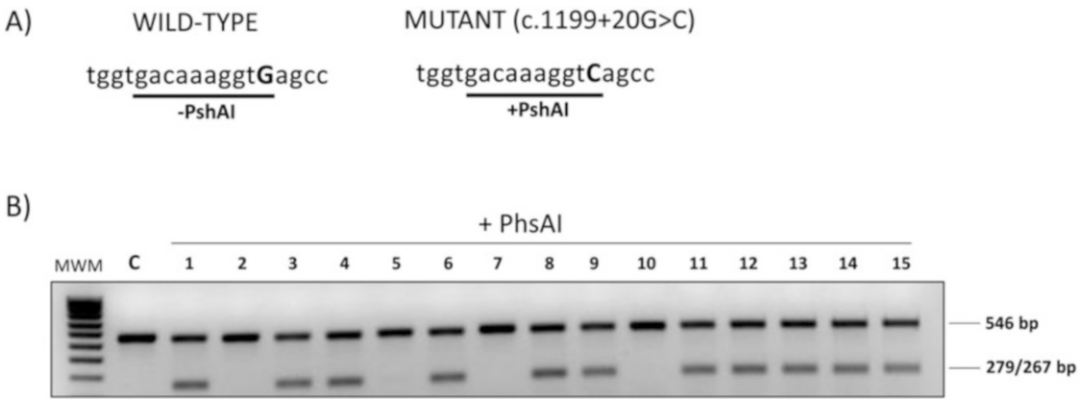


Fig. 3 RFLP analysis to monitor for gene edition. The wild-type and mutant sequences are shown in panel **a** and panel **b** is a representative gel showing RFLP analysis of single-cell colonies. Top bands correspond to the amplified PCR products and lower-sized bands correspond to the products obtained by digestion with PshAI enzyme due to the introduction of a restriction site with the point mutation c.1199 + 20G > C. C undigested control. Colonies 1, 3, 4, 6, 8, 9, 11–15 are positive and heterozygous (one allele edited)

3.9 Sequencing Analysis of Candidate Clones and Off-Targets Analysis

1. Using DNA from positive clones, perform a PCR to amplify the edited region and those regions where potential off-targets were identified by the software (*see Note 6*), using specific primers designed using Primer3 software (*see Note 35*).
2. Purify the PCR products using a PCR purification kit (*see Note 36*).
3. Prepare the mix for the sequencing reaction according to the instructions of the genomics facility and/or the sequencer. Carry out the sequencing with the forward and the reverse primers in separate reactions.
4. Analyze the sequences with the help of a chromatogram viewer (*see Notes 35 and 37*).

3.10 RNA Isolation

1. Once a correctly edited clone has been identified, expand the culture to obtain enough cells for RNA isolation.
2. Wash with PBS and trypsinize the cells. Centrifuge the cells at $16,000 \times g$ for 5 min and discard the supernatant. Cells can be frozen at -70°C in this step.
3. Add 1 mL of Trizol per sample. Incubate the homogenate for 5 min at room temperature to achieve complete dissociation of nucleoprotein complexes.
4. Add 200 μL of chloroform. Mix by vortexing for 15 s and incubate for 2 min at room temperature.
5. Centrifuge at $12,000 \times g$ for 15 min at 4°C to separate the phases.
6. Transfer the aqueous phase (upper and transparent) to a new Eppendorf tube.

7. Add 500 μL of 2-propanol. Mix by vortexing for 15 s.
8. Incubate the samples at room temperature for 10 min followed by an incubation of, at least, 20 min at -20°C .
9. Centrifuge the samples at $12,000 \times g$ for 30 min at 4°C . Discard the supernatant.
10. Add 1 mL of 75% ethanol and wash the precipitate by vortexing (it can be stored in 75% ethanol for a week at 4°C or a year at -20°C).
11. Centrifuge at $12,000 \times g$ for 5 min at 4°C and discard the supernatant.
12. Centrifuge at $7500 \times g$ for 1 min at 4°C . Let the pellet dry at room temperature until they become transparent.
13. Dissolve the dry RNA in 30 μL of “Nuclease-Free Water” by pipetting and incubate it at least 10 min on ice (if it does not dissolve well it can be incubated 10–15 min at $55\text{--}60^\circ\text{C}$).
14. Measure the concentration of the isolated RNA using NanoDrop One and keep the samples at -70°C until use.

3.11 RT-PCR and Sequencing Analysis to Confirm the Splicing Defect

1. For reverse transcription with the NZYRT System, use 1 μg of RNA, following the manufacturer’s protocol. Random hexamers, oligo(dT) or vector-specific primer can be used. Mix RNA with NZYRT Master mix and NZYRT Enzyme mix in a final volume of 20 μL in PCR tubes, incubate 10 min at 25°C , followed by 30 min at 50°C , 5 min at 85°C and cool to 4°C .
2. Add 1 μL of NZY RNase H and incubate at 37°C for 20 min.
3. Perform a standard PCR reaction using 1 μL cDNA and a final volume of 25 μL .
4. Run 5 μL of each sample in a 2% agarose gel.
5. Purify, quantify, and sequence the PCR product as explained above (*see* **Note 38**).

4 Notes

1. All the specific reagents for gene editing (crRNA, tracrRNA-ATTO550, ssDNA template, Cas9 Nuclease) explained in this protocol were obtained from IDT (Integrated DNA Technology). However, it is important to note that there are several other companies that sell these same products performing equally well. It is the researcher’s decision to decide which company he wants to work with.
2. The method of delivery and/or the transfection reagent will depend on our cell line or on our preferences. Lipofection with Lipofectamine™ CRISPRMAX™ Cas9 and its Transfection

Reagent (Thermofisher) has been the method and the reagent chosen is this protocol.

3. Before starting the gene editing experiment, it is important to check that the chosen cell line expresses the gene of interest (mRNA and protein) and corresponds to a tissue relevant for your studies, i.e., splicing defect was observed in this type of cells, as splicing outcomes may depend on tissue-specific splice factors. It is also essential to take into account the organism from which the cell line is derived. For example, intronic sequences are not well conserved among species, and this is crucial when, for example, the aim is to study intronic splicing mutations.
4. It is necessary to verify the karyotype of the chosen cell line, to confirm it is normal, at least in relation to the pair of chromosomes where the gene that is going to be edited is located. Most established cell lines show aneuploidies and structural chromosomal alterations that will hinder the desired gene edition if the corresponding chromosome is affected. In our case, we tested a battery of human hepatoma cell lines, Hep3B, HepG2, Huh7 among others and selected an HepG2 cell line with two chromosomes 12 where the PAH gene is located. Karyotype analysis is a routine service offered by many human genetic diagnosis laboratories.
5. The chosen cell line should have the ability to form “single-cell colonies.” This is necessary to isolate individual cells after transfection that will be subsequently expanded for genetic characterization to confirm and select correctly gene edited clones. There are different procedures for the generation of “single-cell colonies”: (a) cell sorting: 1 cell/96-well-plate well using a cell sorter, (b) serial dilutions, and (c) seeding the cells at a high dilution (approximately 100 cells in one 150 mm plate).

The election of one method or another will depend on the cell line, so it is advisable to test this before generating the colonies with the edited cells. In our hands, for example, HepG2 cells exhibited high mortality after sorting and plating in 96-well plates, so we selected option c. For some cell lines the use of conditioned medium (filtered culture medium collected from control cells) can aid the growth in the form of a colony derived from a single cell. The time of growth and appearance of single-cell colonies will depend on the type of cells you are working with. With HepG2 cells, colonies emerged and reached the correct size after circa 20 days.

6. It is advisable to have the region sequenced before starting the editing experiment to identify single-nucleotide polymorphisms in the specific cell line used which may affect the design

of RNA guides and DNA templates, as well as result in erroneous interpretation of the sequencing analysis of the edited clones (concluding there has been an extra change introduced during DNA repair after Cas9 reaction when it was already present in the sequence prior to editing).

7. There are multiple softwares for designing RNA guides for CRISPR assays. In our case we have used Breaking Cas software (<http://bioinfogp.cnb.csic.es/tools/breakingcas>) [19], which we find user-friendly, and the one offered by the company IDT, obtaining nearly identical results. In this sense, it is advisable to use and compare the results from at least two different softwares, to be sure that the selected guides are the most suitable.
8. It is advisable to test at least two RNA guides in a parallel and independent way. Generally, according to IDT, in 2/3 of the cases, sense sequence guides will work better than antisense guides. As we cannot predict which ones will do best for a given locus, we recommend testing both orientations.
9. As an optional step, you can pretest your RNA guides with an in vitro digestion after PCR amplification of the target region to confirm their efficiency (following IDT protocol).
10. SnapGene Viewer (<https://www.snapgene.com/>) has been the software used for visualization of sequences used in this project, location of crRNA, DNA templates, restriction sites, etc. and for sequence analysis of the individual edited clones. However, other programs and software can be used.
11. Cas9 nuclease cut site should be as close as possible to the sequence (nucleotide) which is to be edited. This requirement limits the region where we will design the RNA guides, especially if we want to introduce a point mutation as is the case here. It should be noted that this does not generally apply for the generation of a *knock-out* model, or in general, if we are not focused on introducing a mutation in a specific DNA position; in those cases the cut site can be in any position, so the design and choice of the RNA guide is much easier.
12. If possible, it is recommended to choose an RNA guide targeting the region that includes the nucleotide we intend to edit. Once the edition of that locus has occurred, the affinity of our RNA guide is reduced (because of a mismatch due to the mutation introduced), thus hindering possible reediting.
13. A ssDNA oligonucleotide containing the desired point mutation to be introduced is used as a template by the cell to repair the double strand break induced by Cas9 through HDR. The mutation of interest included in the ssDNA template should be in the middle of the sequence flanked by the homology arms. The length of the homology arms should be 35–40 nucleotides if it is a single-nucleotide change. Using longer homology arms

does not increase the homologous recombination success rate. However, for longer edits (e.g. insertion/deletion of several nucleotides), the length of the homology arms must also be increased.

14. For small insertions or single-nucleotide changes, ssDNA template is recommended. In other experimental situations (introduction of >100 nucleotide sequences) it may be advisable to use double stranded DNA templates.
15. In most gene editing protocols, introducing translationally silent sequence changes in the DNA template eliminating the PAM sequence is recommended, to avoid reediting of our target which may introduce unwanted changes. However, when dealing with intronic or exonic splice mutations, any extra change may alter the final splicing outcome so this should be avoided.
16. Standard desalting or HPLC are the purification methods recommended when ordering the ssDNA template. Also, especially in rich nucleases environments, phosphorothioate bonds (PS Bonds) at the extremes of the oligonucleotide are advisable, ideally putting at least two for each end of the template.
17. This protocol is written to use separate crRNA and tracrRNA. There is also the possibility of working with single guide RNA, where both are linked together, so this step will be different, refer to manufacturer's recommendations.
18. The resuspension volumes depend on the amount of purchased crRNA and tracrRNA. A table of equivalences for different quantities is available in the IDT protocols. It is important to keep in mind that the resuspended RNA oligonucleotides can be stored at -20°C . The volumes and quantities referred to in this protocol are calculated for a 6-well plate, which has been the format used by the authors. Refer to the protocols available on the IDT website for other formats (e.g. 96-well plate).
19. The use of tracrRNA fused to the ATTO550 fluorophore is not strictly necessary but, in our hands, it was very useful for measuring transfection efficiency and to select transfected cells by fluorescence activated cell sorting (FACS) before clone generation. However, in cell types where transfection efficiency is known to be high/very high this step may be waived. In addition, there are certain cell types that are more prone to damage during the sorting process, so it would not be advisable to use this procedure to avoid increasing cell mortality. The protocol described can also be used for tracrRNA without ATTO550. In addition, it is important not to confuse transfection efficiency rate with editing efficiency, since a cell may have been transfected, but not edited. It is important to keep in mind that the success rate of the gene editing will not

only depend on the quality of the guide, but also on the transfection method, the locus we are editing, the cell type, etc.

20. The RNA Duplex can be prepared at a final concentration $>1\text{ }\mu\text{M}$ and stored at $-20\text{ }^{\circ}\text{C}$ during, at least, 6 months. Before use, it should be diluted in Nuclease-Free Duplex Buffer to a working concentration of $1\text{ }\mu\text{M}$.
21. IDT provides Cas9 nuclease at a stock concentration of $62\text{ }\mu\text{M}$. It can be diluted in different buffers, such as PBS or Cas9 Working Buffer (20 mM HEPES, 150 mM KCl, pH 7.5). This will depend on our cell type. In our case we have used OptiMEM to dilute the Cas9 enzyme. It will be important to take these details into account when purchasing Cas9 nuclease from other companies.
22. The final concentration of the ssDNA template is variable depending on the cell type, delivery method, etc. In this case (transfection of HepG2 cells with Lipofectamine (CRISPR-Max)), a final concentration of 3 nM ssDNA template was used, following the manufacturer's recommendations. Transfecting higher amounts of ssDNA template does not ensure a higher rate of editing success. In addition, large amounts of DNA oligonucleotide can become toxic for the cells and increase cell mortality.
23. In initial experiments, it is advisable to perform the reverse transfection of each crRNA guide in triplicate (three 6-well plate wells/crRNA).
24. As with any transfection assay, it is advisable to split and pass the cells at least once after defrosting before starting the test.
25. Before generating colonies derived from a single cell, it is important to freeze the remaining total pool of cells transfected with each crRNA. In the event of any problem we could defrost those cells to generate the colonies again without the need to repeat the transfection.
26. Once the colonies have grown to a size allowing us to handle them efficiently, they must be expanded for analysis. You can select as many colonies as you can manage. You must consider that expansion, cultivation, and analysis of individual colonies require considerable effort and dedication. Normally we grow around 50–70 colonies for each crRNA used.
27. The system used to select colonies and pick them can be very variable. For example, cloning cylinders can be used or other methods of choice of the researcher.
28. We expanded the single-cell colonies in 24-well plates, but this can be modified according to the researcher's preferences and/or cell line characteristics using plates with different formats. In our case, once the cells are confluent, we divide each

well of the 24-well plate into two wells of a 12-well plate. It is important to keep accurate record of each duplicate, since one of them will be used to extract DNA for analysis, and the other will be used to freeze the colony and, in case it is the one selected, expand it for further characterization and use.

29. The analysis of the colonies derived from a single cell is necessary to identify edited ones. In our case, the point mutation that we are introducing generates a new restriction site for the PshAI enzyme. This is very useful to rapidly and easily screen by RFLP analysis for the presence of the introduced mutation, although the edited region must be verified by sequence analysis. In some applications, translationally silent changes are introduced in the donor template near the mutation to create/destroy a restriction site, thus allowing RFLP screening. However, this is not recommended for splicing mutations as any nearby change may alter the splicing outcome. Alternative approaches to evaluate edition efficiency include next-generation sequencing approaches or digital droplet PCR.
30. Other commercial kits or in-house methods can be used for DNA extraction.
31. Other alternative software and resources can be used with the same objective. Primers are designed to amplify the region with the desired change, which should ideally be in the middle of the amplicon, so after digesting with the corresponding enzyme and running the products in an agarose gel we can easily distinguish digested and undigested DNA bands, which will facilitate the identification of the positive clone. Care should be taken during primer design to ensure that there are no other restriction sites for the corresponding enzyme (in our case PshAI) within the amplicon.
32. Due to the high number of colonies, it is very laborious to analyze all of them individually. Therefore, it is advisable to make pools with DNA extracted from 4 or 5 colonies, mixing them to obtain 200 ng of total DNA. Once edition is observed in the RFLP analysis, colonies will then be analyzed individually.
33. It is not necessary to purify the PCR products before restriction enzyme digestion. Purification of PCR products does not improve digestion efficiency, as the PCR product is diluted enough so that the different components of the PCR reaction do not interfere with the enzymatic activity.
34. The conditions, temperatures, and times of the restriction reaction may depend on the enzyme and/or the trademark.
35. Usually, amplification and subsequent sequencing of the three possible off-targets with the highest scores identified by the software used is enough. Based on our experience we can

conclude that off-targets, although it is important to sequence and validate them, are not the biggest problem. However, we frequently found extra changes in the area near the edited nucleotide (on-target). In this sense, these errors have been the main problem and the cause of having had to discard many clones before finding the final positive one.

36. There are many commercially available kits for purification of PCR products. We routinely use Cycle Pure Kit (Omega).
37. Sequencing is necessary for the validation of the positive clone. And to discard off-target effects in the correctly edited clone. We should confirm that no extra changes have been made in the edited region. IMPORTANT: Do not confuse these random changes that CRISPR introduces when repairing the DSB in the DNA (on-target effects) with potential off-targets, which are locus to which our crRNAs can bind and induce a DSB in the DNA.
38. It is important, once the positive clone is selected and genetically analyzed, to carry out the phenotypic characterization as cellular model of the disease phenotype, to confirm that it accurately recapitulates the splicing defect, resulting (in our case) in the absence of protein and activity. To that aim, RT-PCR and cDNA sequencing, followed by Western blot analysis of PAH protein and PAH activity assay were performed. The specific analyses to be performed will depend on each case according to the aim of the study, but, in the case of splicing mutations they should include at least RT-PCR and subsequent cDNA sequencing analysis.

References

1. Montes M, Sanford BL, Comiskey DF, Chandler DS (2019) RNA splicing and disease: animal models to therapies. *Trends Genet* 35(1): 68–87. <https://doi.org/10.1016/j.tig.2018.10.002>
2. Lim KH, Ferraris L, Filloux ME, Raphael BJ, Fairbrother WG (2011) Using positional distribution to identify splicing elements and predict pre-mRNA processing defects in human genes. *Proc Natl Acad Sci U S A* 108(27): 11093–11098. <https://doi.org/10.1073/pnas.1101135108>
3. Sterne-Weiler T, Howard J, Mort M, Cooper DN, Sanford JR (2011) Loss of exon identity is a common mechanism of human inherited disease. *Genome Res* 21(10):1563–1571. <https://doi.org/10.1101/gr.118638.110>
4. Scotti MM, Swanson MS (2016) RNA mis-splicing in disease. *Nat Rev Genet* 17(1): 19–32. <https://doi.org/10.1038/nrg.2015.3>
5. Aartsma-Rus A (2016) New momentum for the field of oligonucleotide therapeutics. *Mol Ther* 24(2):193–194. <https://doi.org/10.1038/mt.2016.14>
6. Kim J, Hu C, Moufawad El Achkar C, Black LE, Douville J, Larson A, Pendergast MK, Goldkind SF, Lee EA, Kuniholm A, Soucy A, Vaze J, Belur NR, Fredriksen K, Stojkovska I, Tsytsykova A, Armant M, DiDonato RL, Choi J, Cornelissen L, Pereira LM, Augustine EF, Genetti CA, Dies K, Barton B, Williams L, Goodlett BD, Riley BL, Pasternak A, Berry ER, Pflock KA, Chu S, Reed C, Tyndall K, Agrawal PB, Beggs AH, Grant PE, Urion DK, Snyder RO, Waisbren SE, Poduri A, Park PJ, Patterson A, Biffi A, Mazzulli JR, Bodamer O, Berde CB, Yu TW (2019) Patient-customized oligonucleotide therapy for a rare genetic disease. *N Engl J Med* 381(17):1644–1652. <https://doi.org/10.1056/NEJMoa1813279>

7. Aartsma-Rus A, Corey DR (2020) The 10th oligonucleotide therapy approved: golodirsen for Duchenne muscular dystrophy. *Nucleic Acid Ther* 30(2):67–70. <https://doi.org/10.1089/nat.2020.0845>
8. Kemaladewi DU, Maino E, Hyatt E, Hou H, Ding M, Place KM, Zhu X, Bassi P, Baghestani Z, Deshwar AG, Merico D, Xiong HY, Frey BJ, Wilson MD, Ivakine EA, Cohn RD (2017) Correction of a splicing defect in a mouse model of congenital muscular dystrophy type 1A using a homology-directed-repair-independent mechanism. *Nat Med* 23(8):984–989. <https://doi.org/10.1038/nm.4367>
9. Schneller JL, Lee CM, Bao G, Venditti CP (2017) Genome editing for inborn errors of metabolism: advancing towards the clinic. *BMC Med* 15(1):43. <https://doi.org/10.1186/s12916-017-0798-4>
10. Bollen Y, Post J, Koo BK, Snippert HJG (2018) How to create state-of-the-art genetic model systems: strategies for optimal CRISPR-mediated genome editing. *Nucleic Acids Res* 46(13):6435–6454. <https://doi.org/10.1093/nar/gky571>
11. Maule G, Casini A, Montagna C, Ramalho AS, De Boeck K, Debyser Z, Carlon MS, Petris G, Cereseto A (2019) Allele specific repair of splicing mutations in cystic fibrosis through AsCas12a genome editing. *Nat Commun* 10(1):3556. <https://doi.org/10.1038/s41467-019-11454-9>
12. Xu S, Luk K, Yao Q, Shen AH, Zeng J, Wu Y, Luo HY, Brendel C, Pinello L, Chui DHK, Wolfe SA, Bauer DE (2019) Editing aberrant splice sites efficiently restores beta-globin expression in beta-thalassemia. *Blood* 133(21):2255–2262. <https://doi.org/10.1182/blood-2019-01-895094>
13. Doudna JA (2020) The promise and challenge of therapeutic genome editing. *Nature* 578(7794):229–236. <https://doi.org/10.1038/s41586-020-1978-5>
14. Mojica FJ, Diez-Villasenor C, Garcia-Martinez J, Soria E (2005) Intervening sequences of regularly spaced prokaryotic repeats derive from foreign genetic elements. *J Mol Evol* 60(2):174–182. <https://doi.org/10.1007/s00239-004-0046-3>
15. Jinek M, Chylinski K, Fonfara I, Hauer M, Doudna JA, Charpentier E (2012) A programmable dual-RNA-guided DNA endonuclease in adaptive bacterial immunity. *Science* 337(6096):816–821. <https://doi.org/10.1126/science.1225829>
16. Knott GJ, Doudna JA (2018) CRISPR-Cas guides the future of genetic engineering. *Science* 361(6405):866–869. <https://doi.org/10.1126/science.aat5011>
17. Morava E, Rahman S, Peters V, Baumgartner MR, Patterson M, Zschocke J (2015) Quo vadis: the re-definition of “inborn metabolic diseases”. *J Inher Metab Dis* 38(6):1003–1006. <https://doi.org/10.1007/s10545-015-9893-x>
18. Martinez-Pizarro A, Dembic M, Perez B, Andresen BS, Desviat LR (2018) Intronic PAH gene mutations cause a splicing defect by a novel mechanism involving U1snRNP binding downstream of the 5' splice site. *PLoS Genet* 14(4):e1007360. <https://doi.org/10.1371/journal.pgen.1007360>
19. Oliveros JC, Franch M, Tabas-Madrid D, San-Leon D, Montoliu L, Cubas P, Pazos F (2016) Breaking-Cas-interactive design of guide RNAs for CRISPR-Cas experiments for ENSEMBL genomes. *Nucleic Acids Res* 44(W1):W267–W271. <https://doi.org/10.1093/nar/gkw407>

Open Access This chapter is licensed under the terms of the Creative Commons Attribution 4.0 International License (<http://creativecommons.org/licenses/by/4.0/>), which permits use, sharing, adaptation, distribution and reproduction in any medium or format, as long as you give appropriate credit to the original author(s) and the source, provide a link to the Creative Commons license and indicate if changes were made.

The images or other third party material in this chapter are included in the chapter's Creative Commons license, unless indicated otherwise in a credit line to the material. If material is not included in the chapter's Creative Commons license and your intended use is not permitted by statutory regulation or exceeds the permitted use, you will need to obtain permission directly from the copyright holder.





In Vitro Models for the Evaluation of Antisense Oligonucleotides in Skin

Jeroen Bremer and Peter C. van den Akker

Abstract

The genodermatosis dystrophic epidermolysis bullosa (DEB) is caused by mutations in the *COL7A1* gene which encodes type VII collagen (C7). In the cutaneous basement membrane zone, C7 secures attachment of the epidermal basal keratinocyte to the papillary dermis by means of anchoring fibril formation. The complete absence of these anchoring fibrils leads to severe blistering of skin and mucosa upon the slightest friction and early mortality. To date, although preclinical advances toward therapy are promising, treatment for the disease is merely symptomatic. Therefore, research into novel therapeutics is warranted.

Antisense oligonucleotide (ASO)-mediated exon skipping is such a therapy. Clinical examination of naturally occurring exon skipping suggested that this mechanism could most likely benefit the most severely affected patients. The severe form of DEB is caused by biallelic null mutations. Exon skipping aims to bind an ASO to the mutated exon of the pre-mRNA in the cell nucleus. Thereby, the ASO inhibits the recognition of the mutated exon by the splicing machinery, and as a result, the mutated exon is spliced out from the mRNA with its surrounding introns, i.e., it is skipped. Here, we describe in vitro methods to evaluate ASO-mediated exon skipping in a preclinical setting.

Key words Epidermolysis bullosa, Therapy, Exon skipping, Antisense RNA, Fibroblasts, Keratinocytes, Splice modulating

1 Introduction

In this chapter, we describe the evaluation of ASO-mediated exon skipping as a therapeutic approach for DEB in a preclinical in vitro setting. DEB is caused by mutations in the *COL7A1* gene which encodes type VII collagen (C7) [1]. DEB is a rare disease affecting 1–9 in every one million births, worldwide. The disease is characterized by severe blistering of skin and mucosae. DEB can be inherited both dominantly and recessively, and the severity of the disease strongly depends on the quantity and functionality of the C7 protein present at the cutaneous basement membrane zone. The most severe recessive form of DEB (RDEB-gen sev) is caused by biallelic null mutations and the complete absence of C7 in the skin. Previously, we have shown that for RDEB-gen sev caused by

biallelic null mutations, exon skipping is anticipated to be clinically beneficial [2].

Exon skipping relies on specifically designed ASOs that bind to the pre-mRNA in the cell nucleus. When bound, these ASOs inhibit the recognition of the mutated exon by the splicing machinery through steric hindrance [3]. As a result, the mutated exon is spliced out (skipped) of the mRNA together with its surrounding introns. If the skipped exon is in frame, the reading frame of the transcript is maintained and produces a slightly shorter but functional protein [4].

Exon skipping affects the pre-mRNA; therefore, it is essential for the ASO to pass the cell membrane and the nuclear envelope. The commonly used 2'-O-methyl phosphorothioate (2OMePS) and 2'-methoxyethyl phosphorothioate (2MOE) ASOs are negatively charged and therefore not able to easily pass the cell membrane in cell cultures. Therefore, active transfer across the cell membrane is essential. Cationic lipid transfection is such a way of active transfer and widely used to achieve efficient uptake by in vitro cultured cells. Widely studied cells of the skin are dermal fibroblasts and epidermal keratinocytes. Here, we describe the in vitro evaluation of distribution and activity of ASOs in cultured fibroblasts and keratinocytes, as C7 is expressed by both the cell types. However, cationic lipid transfection of fibroblasts and keratinocytes can be used to evaluate the activity of antisense RNA for many diseases, as they express many proteins.

2 Materials

2.1 Cell Culture

1. Trypsin/EDTA (2.5% trypsin/0.2% EDTA).
2. Dispase II (2.4 U/mL).
3. Penicillin/Streptomycin (100 U/mL and 100 µg/mL, respectively).
4. Saline solution: 0.9% NaCl in dH₂O sterilized through 0.22-µm filter.
5. Antisense oligonucleotides: 50 µM stock solution in dH₂O (final concentration depends on experimental setup).
6. Fibroblast medium: DMEM 4.5 g/L glucose, L-glutamate, 10% fetal bovine serum (FBS), 1× penicillin/streptomycin.
7. Phosphate-buffered saline (PBS).
8. Fibroblast transfection agent: Polyethylenimine (PEI) 1 mg/mL.
9. Keratinocyte medium: CellnTec Prime (CnT-PR).
10. HEPES-buffered saline solution (HBSS).

11. Keratinocyte transfection medium: Opti-MEM.
12. Keratinocyte transfection agent: Lipofectamine-2000.

3 Methods

3.1 Isolation and Culture of Epidermal Keratinocytes and Dermal Fibroblasts

Full-thickness skin biopsies (4–6 mm) or larger skin tissue (1–2 cm) are used to isolate cells.

1. On day 1, incubate the tissue at room temperature overnight in $2\times$ penicillin/streptomycin solution protected from light.
2. On day 2, using tweezers and a scalpel, scrape off excess fatty tissue from the dermal side of the tissue.
3. Place the tissue in a 100-mm petri dish, floating with the dermal side down in 10 mL Dispase II and incubated overnight at 4 °C.
4. On day 3, separate the epidermis from the dermis as a sheet using tweezers. After separation, place the dermis into a glass petri dish and set aside. Transfer the epidermal sheets into a clean 100-mm petri dish containing 10 mL trypsin/EDTA and incubate for 10 min at 37 °C.
5. During the 10 min incubation time, cut the dermis into small pieces of around 1–2 mm in size, using two scalpels in a “scissor” fashion on the glass surface of the petri dishes. Transfer the tissue fragments onto the bottom of the well of a six-well plate and add complete fibroblast medium dropwise onto the tissue and refresh every other day. Within 2 weeks, fibroblasts should be growing out from the tissue. When proliferation of these fibroblasts starts to stagnate due to confluency, remove the tissue remnants, and harvest and passage the cells.
6. After 10 min trypsinization of the epidermal sheets, pipette the trypsin/EDTA solution up and down repeatedly to dissociate the sheets into individual cells.
7. Transfer the cell suspension into a 15-mL tube containing 500 μ L FBS to inactivate trypsinization.
8. Spin the cells down by centrifugation for 10 min at $200 \times g$.
9. Discard the supernatant and resuspend the pellet in Cnt-PR medium.
10. Seed the cells into the culture vessel. Usually, keratinocytes isolated from one 6 mm biopsy are seeded in two 35-mm petri dishes. Refresh the medium three times a week and harvest and passage the cells once they reach 75–90% confluence.

3.2 Transfection of Primary Fibroblasts and Keratinocytes

In this protocol, we describe the transfection of cells with an ASO in a well of a 12-well plate at a concentration of 250 nM, as an example. This is the final concentration of ASOs in the wells after the transfection. All concentrations can be adjusted according to the needs of the individual experiments.

3.2.1 Fibroblasts

Fibroblasts are cultured and transfected in normal fibroblast medium (*see* Subheading 2.1, step 6)

1. Seed the fibroblasts in 12-well plates at a density at which the cells reach 70–80% confluence within 24–48 h (*see* **Note 1**), depending on proliferation rate.
2. When the cells reach 70–80% confluence, wash the cells three times with PBS and carefully remove the PBS with a pipet or vacuum aspiration system.
3. Add 900 μ L fresh medium and place the plate back in the incubator (*see* **Note 2**).
4. To prepare the lipid-ASO complexes, for each transfected well, pipette 91.5 μ L sterile saline solution in a sterile Eppendorf cup.
5. Add 5 μ L of ASO, and 3.5 μ L PEI and immediately vortex for 10 s (*see* **Note 3**).
6. Incubate the saline-ASO-PEI solution at room temperature for 10 min.
7. After incubation, add the transfection mix dropwise to the well.
8. Shake the plate in a north to south and east to west motion and place in the incubator (*see* **Note 4**).
9. After 5–6 h, gently remove the transfection medium, wash twice with PBS, and add 1 mL fresh medium and place back into the incubator (*see* **Note 5**).
10. After 48–72 h, analyze the cells for exon skipping at RNA or protein level.
11. As a positive control, a fluorescently labeled nonspecific AON is used. In case exon skipping exerts its effect in the nuclei, localization in nuclei corresponds to transfection efficiency (Fig. 1).

3.2.2 Keratinocytes

Keratinocytes are cultured in CnT-PR serum-free low-calcium keratinocyte medium and transfected in Opti-MEM medium.

1. Seed keratinocytes in 12-well plates at a density at which the cells reach 70–80% confluence within 24–48 h.
2. When the cells reach 70–80% confluence, wash the cells three times with HBSS and add 900 μ L Opti-MEM to the well and place back in the incubator.

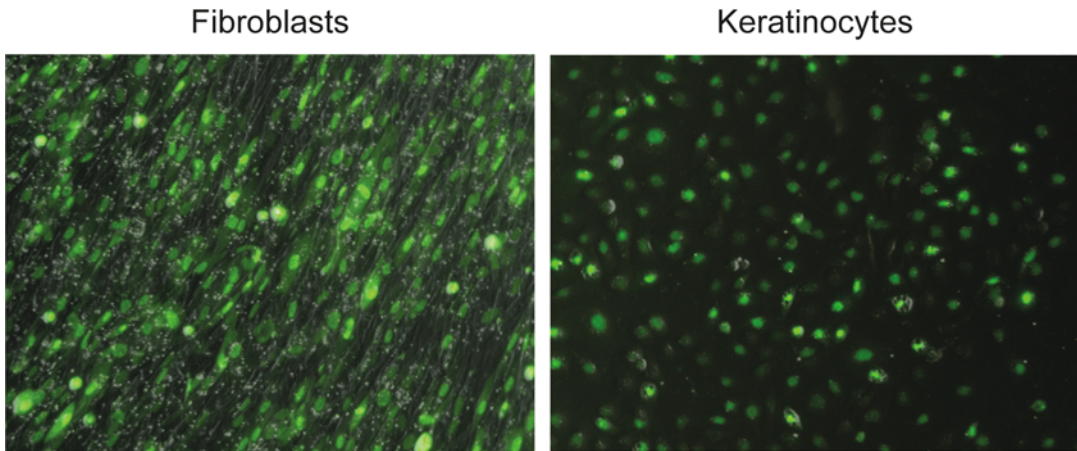


Fig. 1 Microscopy image of cells transfected with fluorescently labeled AON. **Left:** Fibroblasts transfected with a fluorescently labeled (green) AON using polyethylenimine. **Right:** Keratinocytes transfected with the same fluorescently labeled AON. A transfection efficiency of more than 95% is observed in both fibroblasts and keratinocytes, as shown by the green signal in the nuclei

3. In an 1.5-mL tube, add 45 μ L Opti-MEM, then add 5 μ L ASO and gently mix by pipetting in and out.
4. In a second 1.5-mL tube, add 48 μ L Opti-MEM and 2 μ L Lipofectamine-2000 and gently mix by pipetting in and out and incubate at room temperature for 5 min.
5. Add the Lipofectamine-2000 solution to the ASO solution and gently mix by pipetting up and down.
6. Incubate at room temperature for 30 min.
7. Add the lipid-ASO complexes dropwise to the wells and place back in the incubator.
8. After 6 h of incubation, remove the medium and gently wash the cells twice with HBSS. Add fresh keratinocyte medium and place the plate in the incubator.
9. After 24–72 h cells can be analyzed for exon skipping and protein expression.

4 Notes

1. For both fibroblasts and keratinocytes: usually between 0.5 and 1.5×10^5 of primary cultured cells is sufficient depending on passage and viability.
2. Do not pipet the PBS, HBSS, or medium directly onto the cells. Instead, gently pipet the liquid against the side wall of the well to prevent unnecessary stress to the cells.

3. It is essential to pipet in the order saline, ASO, PEI. Do not vortex longer than 10 s.
4. During incubation, prevent the solution from agitating. When pipetting the solution from the Eppendorf tube onto the wells, do not pipet repeatedly up and down, as this might disrupt the lipid-ASO complexes. Additionally, when placing the plate back into the incubator, prevent swirling motions, as this will concentrate the AON-transfection reagent complexes in the middle of the wells.
5. Transfection using cationic lipids induces, to some extent, cell death and will have an effect on the cell membrane as the lipids bind and pass them. Therefore, when washing cells and refreshing media, gently and smoothly pipet via the side of the well.

References

1. Has C, Bauer JW, Bodemer C, Bolling MC, Bruckner-Tuderman L, Diem A, Fine JD, Heagerty A, Hovnanian A, Marinkovich MP, Martinez AE, McGrath JA, Moss C, Murrell DF, Palisson F, Schwieger-Briel A, Sprecher E, Tamai K, Uitto J, Woodley DT, Zambruno G, Mellerio JE (2020) Consensus reclassification of inherited epidermolysis bullosa and other disorders with skin fragility. *Br J Dermatol* 183(4): 614–627. <https://doi.org/10.1111/bjd.18921>
2. Bremer J, van der Heijden EH, Eichhorn DS, Meijer R, Lemmink HH, Scheffer H, Sinke RJ, Jonkman MF, Pasmooij AMG, Van den Akker PC (2019) Natural exon skipping sets the stage for exon skipping as therapy for dystrophic epidermolysis bullosa. *Mol Ther Nucleic Acids* 18: 465–475
3. Aartsma-Rus A, van Vliet L, Hirschi M, Janson AA, Heemskerk H, de Winter CL, de Kimpe S, van Deutekom JC, t Hoen PA, van Ommen GJ (2009) Guidelines for antisense oligonucleotide design and insight into splice-modulating mechanisms. *Mol Ther* 17(3):548–553. <https://doi.org/10.1038/mt.2008.205>
4. Bornert O, Köhl T, Bremer J, van den Akker PC, Pasmooij AM, Nyström A (2016) Analysis of the functional consequences of targeted exon deletion in COL7A1 reveals prospects for dystrophic epidermolysis bullosa therapy. *Mol Ther* 24(7): 1302–1311. <https://doi.org/10.1038/mt.2016.92>

Open Access This chapter is licensed under the terms of the Creative Commons Attribution 4.0 International License (<http://creativecommons.org/licenses/by/4.0/>), which permits use, sharing, adaptation, distribution and reproduction in any medium or format, as long as you give appropriate credit to the original author(s) and the source, provide a link to the Creative Commons license and indicate if changes were made.

The images or other third party material in this chapter are included in the chapter's Creative Commons license, unless indicated otherwise in a credit line to the material. If material is not included in the chapter's Creative Commons license and your intended use is not permitted by statutory regulation or exceeds the permitted use, you will need to obtain permission directly from the copyright holder.





Chapter 12

In Vitro Delivery of PMOs in Myoblasts by Electroporation

Remko Goossens and Annemieke Aartsma-Rus

Abstract

Antisense oligonucleotides (AONs) are small synthetic molecules of therapeutic interest for a variety of human disease. Their ability to bind mRNA and affect its splicing gives AONs potential use for exon skipping therapies aimed at restoring the dystrophin transcript reading frame for Duchenne muscular dystrophy (DMD) patients. The neutrally charged phosphorodiamidate morpholino oligomers (PMOs) are a stable and relatively nontoxic AON modification. To assess exon skipping efficiency in vitro, it is important to deliver them to target cells. Here, we describe a method for the delivery of PMOs to myoblasts by electroporation. The described protocol for the Amaxa 4D X unit nucleofector system allows efficient processing of 16 samples in one nucleocuvette strip, aiding in high-throughput PMO efficacy screens.

Key words AON, PMO, Electroporation, Nucleofection, Myocytes, Duchenne muscular dystrophy, DMD

1 Introduction

Antisense oligonucleotides (AONs) are versatile, powerful tools for the potential treatment of a variety of diseases. AONs are short synthetic oligonucleotides consisting of modified DNA or RNA nucleic acid analogs. AONs can be exploited in multiple ways, including the modulation of splicing. Here, AONs bind to the unspliced mRNA and mask splice sites or exonic splice enhancer or silencer sites, resulting in an exon being ex- or included in the mature mRNA. Examples of such AONs are eteplirsen, golodirsen, viltolarsen, and casimersen to treat Duchenne muscular dystrophy (DMD) patients with eligible mutations, and nusinersen to treat spinal muscular atrophy (SMA). For DMD, antisense-mediated exon skipping is used to restore the reading frame of the dystrophin (*DMD*) transcript, allowing the production of an internally deleted partially functional dystrophin protein [1]. This approach is mutation specific. Currently, for Duchenne, four AONs have been approved by the Food and Drug Administration (FDA, USA),

which induce skipping of exon 51 (eteplirsen), exon 53 (golodirsen and viltolarsen) or exon 45 (casimersen).

Various different AON chemistries have been developed, such as 2'-*O*-methyl phosphorothioate (2'-*O*-MePS), 2'-*O*-methoxyethyl phosphorothioate (2'-MOE-PS), and phosphorodiamidate morpholino oligomer (PMO) [2]. These different chemistries have unique chemical properties and were developed to enhance stability, solubility, and cellular uptake of AONs [2]. AONs are sometimes covalently conjugated to other molecules, in an attempt to improve their uptake by target tissues after systemic delivery [3]. For treatment of SMA, intrathecal injection of the AON into the cerebrospinal fluid (CSF) leads to efficient uptake by neurons and other cells in the nervous system with a long half-life [4]. However, in DMD all of the >700 different skeletal muscles are affected, and as such systemic delivery of AONs is required, which currently involves weekly intravenous infusions [5].

DMD consists of 79 exons, and there is a wide variety of unique patient mutations [6, 7], with a mutation hotspot spanning exon 45 through 53 [6, 8]. Approximately 55% of total *DMD* mutations causative for Duchenne would be eligible for some form of exon skipping therapy [7]. While skipping certain exons is applicable to larger groups of patients, it is crucial to skip also additional exons, which individually apply to small groups of patients, to increase the general applicability of this approach to as many patients as possible. To optimally design AONs for most of the *DMD* exons, it is important to have the ability for high-throughput screening of AON exon skipping efficacy. To perform reliable initial testing of AONs in vitro, it is essential to establish a reproducible, efficient means of delivery to a target cell. This can be achieved using electroporation of immortalized muscle cells [9]. Using immortalized cells has the advantage of theoretically unlimited proliferation, so large amounts of cells with homogenous characteristics can be generated. Primary cell sources are finite, and each new donor will have to be validated for reproducibility, which hampers screening potential when a large number of different AONs are to be tested simultaneously. Furthermore, it is our experience that the capacity of primary cultures to differentiate into myotubes declines with advanced passages.

Unlike 2'-*O*-MePS AONs and dsDNA (e.g., plasmids), PMO AONs are neutrally charged, impeding the delivery by cationic lipid transfection systems. An alternative method for delivery of PMOs to mammalian cells is electroporation [9]. Electroporation relies on the formation of pores in the cell membrane by the application of an electric pulse through the transfection medium, mediating delivery of the particle of interest. The pore-forming pulse either serves to simultaneously deliver a charged molecule or is followed by a dedicated secondary delivery pulse. While electroporation efficiency is aided by active mobilization of charged molecules of

interest into the cells by the electric current applied, the pore formation itself is already able to allow passive entry of inert molecules such as PMOs, albeit potentially at a lower efficiency. In fact, efficiency of in vitro PMO electroporation is relatively high when compared to other methods such as gymnosis and calcium-enriched medium (CEM) [10].

Classic electroporation is performed with cells in suspension, requiring dissociation of adherent cells from the culture vessel prior to the procedure. For studying *DMD* exon skipping, a cell line which expresses full-length *DMD* (Dp427m) is required. Alternatively, if available, a patient-derived cell line with a specific mutation can be used where skipping of a specific exon restores dystrophin production. However, as *DMD* expression in proliferating myoblasts is very low, myoblasts need to differentiate after electroporation with the Amaxa 4D X unit to form mature myotubes, expressing higher levels of *DMD*. Novel electroporation techniques also allow for electroporation of adherent cell layers, which can be advantageous when working with cells that grow slowly or have limited proliferation capacity upon differentiation, such as mature myotubes or neuronal cells. These methods, just like other electroporation techniques, require thorough characterization and optimization of conditions for maximum efficiency and are not included in this chapter.

In this chapter, we provide a protocol for the delivery of PMOs to immortalised myoblasts by electroporation with the Lonza Amaxa 4D-nucleofector X unit, and their subsequent differentiation to *DMD* expressing myotubes. The procedure for further sample processing and analysis of the skipped transcript by end-point reverse transcription polymerase chain reaction (RT-PCR) and quantitative PCR (RT-qPCR) are also outlined.

2 Materials

2.1 Cell Culture

1. Immortalized myoblasts: 0.5×10^6 up to 1×10^6 cells per reaction (for transfer to a 6-well plate) (*see Note 1*).
2. Culture medium (proliferation): For myoblasts either: F10 Nutrient mix (nutmix) medium supplemented with 20% fetal bovine serum (FBS), 1% PenStrep, 10 ng/mL rhFGF and 1 mM dexamethasone, **or** Skeletal Muscle Cell Growth Medium (SMCGM) supplemented with 15% FBS and 50 µg/mL gentamicin (*see Note 2*).
3. Culture medium (resuspension): F10 Nutmix + 20% FBS + 1% PenStrep.
4. Culture medium (differentiation): DMEM (4.5 g/L glucose) + 2% FBS **or** 2% knockout serum replacement (KOSR) + 50 µg/mL Gentamicin **or** 1% PenStrep (*see Note 2*).

5. Trypsin-EDTA (0.05%).
6. Dulbecco's phosphate-buffered saline (dPBS (-MgCl₂, -CaCl₂)).
7. Culture vessels (e.g., T182 flask and 6-well plates).

2.2 Electroporation

1. Lonza 4D nucleofector core unit.
2. Lonza 4D nucleofector X-unit for cells in suspension (*see Note 3*).
3. Sutable 4D-nucleofector X kit (e.g., primary cell optimization kit) containing 16-well nucleofector strips and nucleofection buffer.
4. PMOs at 1 mM concentration in saline, 0.2- μ m filter sterilized (*see Notes 4 and 5*).

2.3 RNA Isolation

1. TRI-reagent (e.g., TRIsure).
2. Chloroform.
3. 2-Propanol.
4. 70% Ethanol (EtOH).
5. RNase-free water (DEPC treated).

2.4 cDNA Synthesis

1. Random hexamer primers (N6) (20 ng/ μ L).
2. dNTP mix (10 mM each).
3. 5 \times reverse transcriptase (RT) reaction buffer.
4. Reverse transcriptase enzyme.
5. RNase inhibitor.
6. RNase-free water (DEPC treated).

2.5 RT-PCR Analysis of Skipping Efficiency

1. cDNA generated from >1 μ g total RNA by random hexamer primers (Subheading 3.3, step 5).
2. Forward and reverse primer set (preferably intron spanning) (10 μ M stock).
3. dNTP mix (10 mM each).
4. 10 \times Reaction buffer.
5. Taq polymerase.
6. Molecular biology grade agarose.
7. TRIS-Borate-EDTA (TBE) buffer (1 \times).
8. Ethidium bromide (EtBr).
9. 100 bp DNA marker.

2.6 RT-qPCR of Skipping Efficiency

1. cDNA generated from >1 μ g total RNA by random hexamer primers (Subheading 3.3, step 5).

2. Forward and reverse primer set for the gene of interest (one of the primers should span the exon boundary of the skipped product (e.g., the primer should consist of the last 10 nucleotides of exon 1, and the first 10 nucleotides of exon 3 of the gene of interest when skipping exon 2)) (10 μ M stock).
3. Forward and reverse primer set for a suitable reference gene (e.g., *GUSB* or *GAPDH*) (10 μ M stock).
4. 2 \times SYBR-green PCR mastermix.

3 Methods

RNA isolated from the nucleofected myotube cultures is used to generate cDNA, which can subsequently be used for RT-PCR or RT-qPCR analysis of exon skipping efficiency. To purify a sufficient amount of total RNA from myotube cultures, we usually transfer cells to six-well plates after nucleofection. Smaller culture vessel might be suitable, or more optimal, for other purposes. We use up to 1×10^6 myoblast cells per 20 μ L nucleofection reaction, requiring 1.6×10^7 cells in total for a full 16-well cuvette strip. A T182 culture vessel of high confluence contains about 2×10^7 myoblast cells. A graphical overview of the procedure is outlined in Fig. 1. All steps described in Subheading 3.1, **steps 1–17** should be performed under aseptic conditions. Subheading 3.1, **steps 18** through Subheading 3.2, **step 11** should be performed using suitable personal protection according to local regulations.

3.1 Nucleofection and Maintenance of Cells

This example assumes an experiment involving 1 full 16-well nucleocuvette strip, using 1×10^6 cells per reaction. Scale volumes up or down according to experimental design. Prior to starting the procedure, make sure that the nucleofector buffer has been supplemented as indicated. Prior to handling the cells, make sure that the desired programs to be used have been entered into the 4D-nucleofector core unit to avoid delays in the procedure when handling resuspended cells (*see* **Note 6**).

1. Preferentially subculture myoblasts 1 day prior to nucleofection to ensure proper viability and growth phase of cells. Cells from confluent cultures might exhibit a decreased efficiency or survival.
2. Label wells and add media to the culture vessels used to transfer cells post-nucleofection, e.g., 3 mL proliferation media per well of a 6-well plate. Place plates in a 37 °C CO₂ incubator to warm and equilibrate the media.
3. On the day of the nucleofection experiment, wash the cells with dPBS and trypsinize the cells. Use 2 mL trypsin 0.05% for a

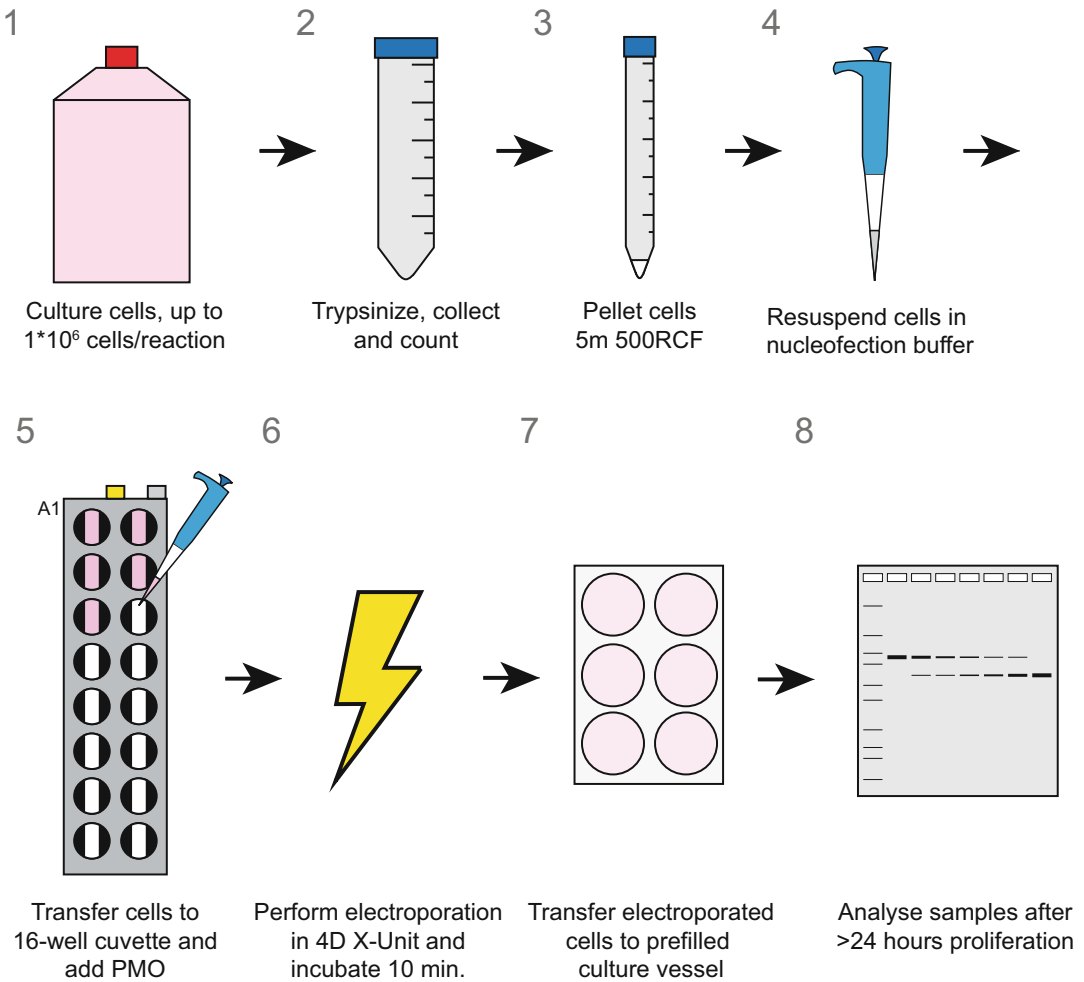


Fig. 1 Schematic workflow of nucleofecting PMO in myoblast cells

T182 and carefully tilt flask to cover all cells. Place cells with trypsin in a 37 °C incubator.

4. When cells are properly detached from the surface (cell line dependent, but generally after 2 min), add resuspension media to a total volume of 10 mL to inhibit trypsin activity.
5. Resuspend cells and transfer to a 50-mL tube (*see Note 7*). If multiple flasks are needed to obtain the required number of cells need for the experiment performed, pool cells at this step.
6. Count the number of cells in the 50-mL tube (at least twice) using available cell counting methods. Transfer a total of 1.7×10^7 cells ($16 \times 1 \times 10^6$ reactions + 1 surplus) to a fresh conical tube, and pellet cells by centrifugation for 5 min at 200 relative centrifugal force (RCF).

7. Aspirate medium completely and gently resuspend cell pellet in 20 μL nucleofection buffer per reaction (i.e., here we use 340 μL for 16 reactions + 1 surplus) (*see Note 8*).
8. Aliquot 20 μL cell suspension in each of the chambers in the 16-well nucleofector strip using a P20 micropipette. Avoid creating air bubbles (*see Note 9*). When placing the cuvette strip with the yellow notch away from the user, the top left well is well A1 (*see Note 10*).
9. Add 1 μL of PMO diluted to the desired concentration. For example, 1 μL PMO from a 1 mM stock will result in a final concentration in the cuvette of 50 μM . Gently mix by stirring with the pipet tip, do **not** vigorously pipet up and down (*see Notes 11 and 12*).
10. Replace the lid on the cuvette strip (*see Note 13*) and place it in the 4D-Nucleofector X unit tray (yellow notch away from user, toward the machine).
11. Start nucleofection by selecting start on the 4D-nucleofector core unit touch screen.
12. After the machine has finished electroporating, check the status on the display. Green crosses mean the samples have been electroporated without issues. When other symbols are shown, an error might have occurred. Refer to the 4D-nucleofector user manual.
13. Leave the nucleocuvette strip on the bench for 10 min for the cells to recover (*see Note 14*).
14. Gently add 180 μL prewarmed media to each of the wells of the cuvette strip.
15. Carefully resuspend (maximum 2–3 times up and down) the cells in the cuvette, and transfer to the culture vessel prepared in Subheading 3.1, **step 2** (*see Note 15*).
16. Allow cells to proliferate for 24 up to 72 h and monitor viability of electroporated cells (*see Note 16*). Let cells proliferate until reaching 100% confluency.
17. Upon reaching confluency, replace myoblast proliferation media with differentiation media to induce myotube formation.
18. After 72 h, wash cells with dPBS and lyse in 500 μL TRI-reagent (for a 6 well plate).
19. Collect samples using a cell scraper and transfer to 1.5-mL microcentrifuge tubes on ice.
20. Store samples ($-80\text{ }^{\circ}\text{C}$) or immediately isolate total RNA from cells according to available protocols (e.g., 3.2).

3.2 RNA Isolation

1. Thaw the lysate obtained at Subheading 3.2, step 17 and add 1/5th volume (100 μ L) of chloroform (*see* Notes 17 and 18).
2. Mix thoroughly by shaking for 30 s.
3. Incubate on ice for 5 min.
4. Centrifuge samples for 15 min at 16,000 RCF at 4 °C.
5. Carefully transfer the upper aqueous phase to a new microcentrifuge tube, without disturbing the organic- and interphase.
6. Add an equal volume of 2-propanol to transferred aqueous phase.
7. Mix well and incubate for >30 min on ice, then centrifuge for 15 min at 16,000 RCF at 4 °C.
8. Discard supernatant and wash pellet with 1 mL 70% EtOH.
9. Centrifuge for 5 min at 16,000 RCF at 4 °C.
10. Discard supernatant and air-dry pellet.
11. Dissolve the pellet in RNase-free water (e.g., 25 μ L).
12. Determine RNA concentration using a Nanodrop ND-1000.
13. Store RNA at -80 °C (*see* Note 19).

3.3 cDNA Synthesis

1. To generate first-strand cDNA using random hexamer using at least 1 μ g of total RNA in a 20 μ L reaction. In a 12.5 μ L reaction mix the following components (*see* Note 20):
 - (a) X μ L RNA for a total of 1 μ g.
 - (b) 1 μ L dNTP mix (10 mM each).
 - (c) 1 μ L Random hexamer primers (N6) (20 ng/ μ L).
 - (d) X μ L RNase-free water up to 12.5 μ L.
2. Incubate reaction for 5 min at 65 °C. Chill on ice for 2 min.
3. To each tube add:
 - (a) 4 μ L 5 \times RT-reaction buffer.
 - (b) 1 μ L Reverse transcriptase enzyme.
 - (c) 0.5 μ L RNase inhibitor.
4. Incubate at 42 °C for 1 h.
5. Incubate at 85 °C for 5 min.
6. Dilute the 20 μ L cDNA reaction to a final volume of 100 μ L with ultrapure MQ.
7. Store cDNA at -20 °C.

3.4 RT-PCR Analysis

1. Set up RT-PCR (25 μ L reactions) according to the follow set-up per reaction (*see* Note 21):
 - (a) 2.5 μ L 10 \times Reaction buffer.
 - (b) 1 μ L Forward primer (10 μ M).

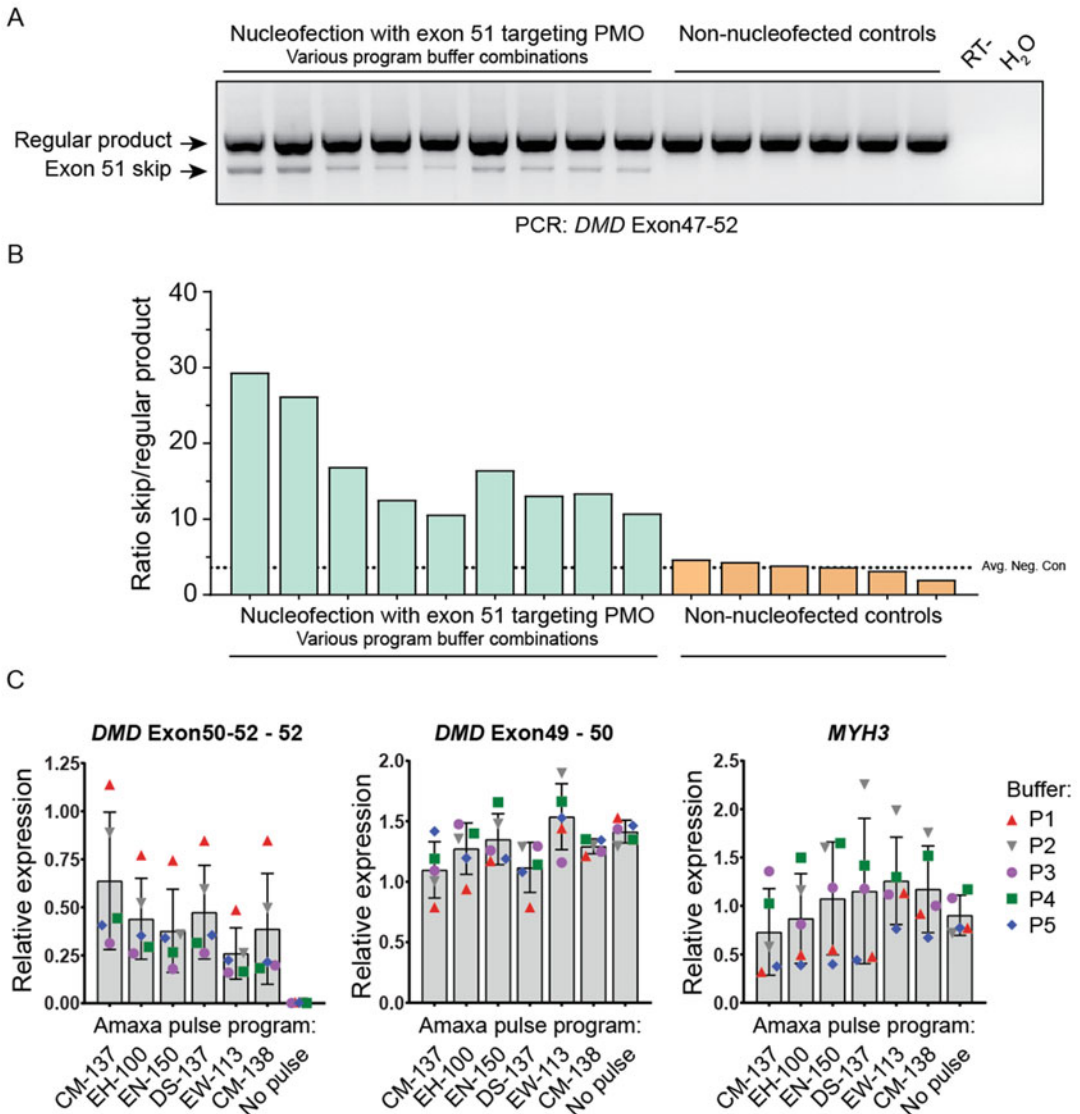


Fig. 2 Example of the result of RT-PCR analysis after successful nucleofection of a *DMD* exon 51 targeting PMO in KM155 myotubes using various programs of the 4D-nucleofector. (a) Agarose gel electrophoresis of endpoint RT-PCR products using primers specific for *DMD* exon 47 through 52. Skipping of exon 51 will lead to the production of a smaller PCR product as indicated. Different lanes consist of different experimental combination of nucleofection buffers and programs. (b) Approximate quantification of agarose gel shown in A by FIJI analysis. Ratios of Exon 51 skipped product intensities over the regular (exon 51 containing) product are plotted. The average of the negative controls (no PMO/no pulse samples (orange bars)) is shown as a dotted line. (c) RT-qPCR analysis of *DMD* exon 51 skipping in KM155 myotubes with 6 nucleofection programs and 5 nucleofection buffers. Exon skipping was determined with a primer set only amplifying the *DMD* transcript without exon 51 (Exon 50-52F + Exon 52R). A primer set specific for *DMD* exon 49 through 50 shows all *DMD* transcript, and *MYH3* is used as a marker for myogenic differentiation. Cells resuspended in nucleofection buffer not subjected to an electric pulse were used as a negative control. In our hands, exon skipping efficiency was highest using a combination of program CM-137 and buffer P1

- (c) 1 μL Reverse primer (10 μM).
 - (d) 1 μL dNTP mix (10 mM each).
 - (e) 0.2 μL Taq polymerase (5 U/ μL).
 - (f) 10 μL cDNA from Subheading 3.3, step 5.
 - (g) 9.3 μL ultrapure water (up to 25 μL).
2. Gently mix and place samples in a thermal cycler using the following program:
 - (a) 1: 5 min, 95 °C—initial melt.
 - (b) 2: 30 s, 95 °C—melt.
 - (c) 3: 30 s, 60 °C—annealing (change for specific primers).
 - (d) 4: 40 s, 72 °C—extension (~30 s per kb).
 - (e) 5: Go to **step 2**, 34 additional times (35 cycles total).
 - (f) 6: 5 min, 72 °C—final extension.
 3. Analyze PCR samples by standard ethidium bromide (EtBr) agarose gel electrophoresis, using a 2% agarose gel (for products <1000 bp) in TBE buffer at 125 V (Fig. 2) (*see Note 22*). Alternatively, accurate analysis of signal intensity can be measured by use of, e.g., an Agilent 2100 Bioanalyzer (*see Note 23*).

3.5 RT-qPCR Analysis

1. For RT-qPCR analysis, measure the gene of interest and at least one reference gene. Always measure a technical triplicate of each cDNA-primer combination. Set up RT-qPCR according to the following set-up per reaction (we use 8 μL reactions in a 384-well plate):
 - (a) 4 μL 2 \times SYB green master mix.
 - (b) 1 μL Forward primer (10 μM).
 - (c) 1 μL Reverse primer (10 μM).
 - (d) 2 μL cDNA from Subheading 3.3, step 5.
2. Seal the plate and mix by inversion and briefly spinning down the plate in a centrifuge.
3. Place samples in a real-time PCR enabled thermal cycler and run the following program:
 - (a) 1: 5 min, 95 °C—initial melt.
 - (b) 2: 10 s, 95 °C—melt.
 - (c) 3: 30 s, 60 °C—Annealing and extension (change temperature for specific primers).
 - (d) 4: Read plate, go to **step 2**, 39 additional times (40 cycles total).
 - (e) 5: Melt curve analysis.

4. A suitable primer pair for the skipped product will yield little to no signal in the un-nucleofected control samples and will have increased abundance when the exon was successfully skipped.

4 Notes

1. The procedure described herein has been optimized and validated using immortal muscle cell line KM155, which has been described previously [11, 12]. Use of this protocol for primary muscle cells or other immortalized cell lines might require additional optimization.
2. Different media are described in the literature for proliferation and/or differentiation of myoblasts. These different media can have considerable effects on gene expression and morphology. For example, differentiation of myoblasts with 2% FCS leads to slower formation of multinucleated myotubes compared to 2% KOSR. However, myotubes formed with 2% KOSR are harder to handle due to faster release from the vessel surface, presumably due to spontaneous contraction of the myotubes. We recommend that different media are tested to compare optimal experimental conditions.
3. For electroporation of adherent cells, a few of the options available are the Lonza 4D nucleofector Y-unit or the Nepa-gene NEPA21 electroporator.
4. Delivery of PMOs by nucleofection can be prohibitively expensive for many laboratories, as prices for consumables are steep compared to common laboratory transfection reagents, some of which can be cheaply prepared in-house. On the other hand, if the material to be transfected is expensive or rare, nucleofection allows for relatively high concentrations to be applied directly to the cells due to the low reaction volume (as low as 20 μ L), saving costs on oligonucleotides.
5. While small molecules such as siRNAs and AONs are easily delivered into myoblasts by electroporation (e.g., siRNA, PMOs) or transfection (e.g., siRNA, 2OMePS AONs), delivery of (large) plasmids is notoriously inefficient.
6. For our immortalized myoblast cell line (KM155), we have tested various different nucleofector pulse programs in combination with the nucleofection buffers present in the primary cell line optimization kit (i.e., P1, P2, P3, P4, and P5). We noticed that the trend of *DMD* exon skipping efficiency was similar for each buffer and depended largely on the nucleofection program used for the 4D X unit (Fig. 2c, bars). Buffers did however largely contribute to overall efficiency of a set of nucleofections (Fig. 2c, individual data points per bar).

7. When trypsinizing cells from the culture vessel, dissociate cells by controlled but forceful pipetting with a 10-mL pipet and a pipetboy to generate a single-cell suspension. Cell clumps will severely hamper nucleofection.
8. Cells should not be kept in nucleofection buffer for a prolonged amount of time, as this can reduce efficiency and viability. After diluting the cell pellet in nucleofection buffer, working swiftly and accurately is key.
9. At any step of the procedure, but especially upon loading of the nucleocuvette, avoid air bubbles in the reagents containing cells. Cavitation shearing and electric arcing can occur when air bubbles are present. Loading the cuvette with a P20 and reverse pipetting (i.e., not pressing the piston to the second stop) are useful for avoiding air bubbles in the cuvette strip.
10. We have tested the re-use of single cuvette strips for the delivery of the same PMO without any noticeable effect on delivery efficiency or cell viability. If the proprietary nucleofector solutions have not finished upon finishing the cuvette strips of a kit, this method can prolong the use of a single ordered kit. To clean a cuvette strip: after transferring cells from a nucleofection experiment from the 16-well strip to a culture vessel, immediately submerge the strip (without lid) in a 100 mL glass bottle filled with sterile milli-Q (MQ). Shake vigorously for 30 s. Decant MQ and add 70% EtOH for disinfection and shake vigorously. Do not leave the cuvette strip in ethanol for extended periods of time to prevent damage to the electrode. Decant EtOH and rinse twice with sterile MQ, air-dry strip and store for future use. We have not tested degradation of efficiency after more than two re-uses. Different nucleofection programs with higher voltages might affect electrode degradation and result in poor efficiency upon re-use. Re-usability should always be tested in the experimental setup used to avoid problems in reproducibility.
11. As an alternative to loading the PMO directly in the cell suspension, it is possible to mix PMO, cells and nucleofection buffer prior to dispensing in the 16-wells nucleocuvette. For example, in bulk when multiple pulse programs are tested, or in sterile strips/plates for testing large amounts of different PMOs. For the latter, it is possible to transfer cells to the nucleocuvette by use of a multichannel pipette.
12. It is possible to add the PMO to the nucleocuvette wells prior to adding the cells, in which addition of the cells and handling of the strip will sufficiently mix the substrate with the cell suspension. However, as PMO solutions tend to be slightly viscous, it can be hard to reliably dispense a small volume (e.g., 1 or 2 μ L) in a dry well, compared to dispensing in solution.

13. The cell suspension (20 μ L) in the nucleocuvette strip should cover the entire bottom of the well in the nucleocuvette. After loading the cell suspension and prior to placing the cuvette in the X-unit, tap it several times on the working surface with appropriate force.
14. Excessive cell death may warrant changes in recovery steps. For example, after electroporation, add 180 μ L warm culture media to each well of the cuvette strip, and incubate the strip 10 min at 37 °C. Afterwards, transfer cells carefully as described above.
15. Cells are fragile immediately after electroporation. Avoid shear stress by over-resuspension with small diameter tip orifices. Use a P200 or P1000 micropipette, resuspend two or three times in the cuvette, and immediately transfer to the pre-warmed culture plate. Avoid creation of air bubbles by aggressive pipetting.
16. Certain cell types might show increased viability after nucleofection when treated with ROCK inhibitors to block apoptosis 4 h prior and 24 h post nucleofection.
17. RNA is extremely sensitive to degradation by environmental RNases, such as present on human skin. When handling/preparing RNA samples, always wear suitable gloves, and clean work surfaces with RNase removal agents (e.g., RNaseZAP).
18. To compare samples properly, it is important to process sample sets in the same way. This includes but is not limited to simultaneous isolation of RNA, simultaneous generation of cDNA, identical input of RNA for cDNA reactions, etc.
19. For assessing the efficiency of *DMD* exon skipping with RT-PCR, we generally do not incorporate a DNase I treatment step in the RNA isolation protocol.
20. Generation of cDNA can be performed in PCR strips with caps, allowing for easy incubations in a thermal cycler and transfer of sample to another PCR strip with a multichannel pipette.
21. For analysis of exon skipping efficiency by RT-PCR, we strongly recommend the use of single-reaction RT-PCR instead of nested PCR amplifications. Nested PCR amplifications have a high tendency to induce preferential amplification bias and are less quantitatively reliable [13]. Different polymerases and protocols might be better suited for specific transcripts and should be tested.
22. When using software such as ImageJ/FIJI to analyze agarose gel band intensities, it is of the utmost importance that the user keeps the limitations of the software in mind. Saturated signal on the source image will lead to misleading results if analyzed

incorrectly. Therefore, while useful for estimating relative intensity, many applications will require more sensitive methods to reliably quantify exon skipping efficiency. Furthermore, detection of DNA in agarose gels is facilitated by the amount of EtBr intercalating with the DNA, resulting in signal when exposed to UV light. As shorter PCR products bind less EtBr, their intensity is inherently underestimated when measured in analysis software.

23. Prior to analyzing PCR products on an Agilent 2100 bioanalyzer, it is advised to always run some of the sample on an EtBr agarose gel to confirm successful PCR amplification.

References

1. Aartsma-Rus A, van Ommen GJ (2007) Antisense-mediated exon skipping: a versatile tool with therapeutic and research applications. *RNA* 13(10):1609–1624. <https://doi.org/10.1261/rna.653607>
2. Douglas AG, Wood MJ (2013) Splicing therapy for neuromuscular disease. *Mol Cell Neurosci* 56:169–185. <https://doi.org/10.1016/j.mcn.2013.04.005>
3. Jirka SM, Heemskerk H, Tanganyika-de Winter CL, Muilwijk D, Pang KH, de Visser PC, Janson A, Karnaoukh TG, Vermue R, t Hoen PA, van Deutekom JC, Aguilera B, Aartsma-Rus A (2014) Peptide conjugation of 2'-O-methyl phosphorothioate antisense oligonucleotides enhances cardiac uptake and exon skipping in mdx mice. *Nucleic Acid Ther* 24(1):25–36. <https://doi.org/10.1089/nat.2013.0448>
4. Neil EE, Bisaccia EK (2019) Nusinersen: a novel antisense oligonucleotide for the treatment of spinal muscular atrophy. *J Pediatric Pharmacol Ther* 24(3):194–203. <https://doi.org/10.5863/1551-6776-24.3.194>
5. Aartsma-Rus A, Krieg AM (2017) FDA approves Eteplirsen for Duchenne muscular dystrophy: the next chapter in the Eteplirsen saga. *Nucleic Acid Ther* 27(1):1–3. <https://doi.org/10.1089/nat.2016.0657>
6. Aartsma-Rus A, Van Deutekom JC, Fokkema IF, Van Ommen GJ, Den Dunnen JT (2006) Entries in the Leiden Duchenne muscular dystrophy mutation database: an overview of mutation types and paradoxical cases that confirm the reading-frame rule. *Muscle Nerve* 34(2):135–144. <https://doi.org/10.1002/mus.20586>
7. Bladen CL, Salgado D, Monges S, Foncuberta ME, Kekou K, Kosma K, Dawkins H, Lamont L, Roy AJ, Chamova T, Guergueltcheva V, Chan S, Korngut L, Campbell C, Dai Y, Wang J, Barišić N, Brabec P, Lahdetic J, Walter MC, Schreiber-Katz O, Karcagi V, Garami M, Viswanathan V, Bayat F, Buccella F, Kimura E, Koeks Z, van den Bergen JC, Rodrigues M, Roxburgh R, Lusakowska A, Kostera-Pruszyk A, Zimowski J, Santos R, Neagu E, Artemieva S, Rasic VM, Vojinovic D, Posada M, Bloetzer C, Jeannet PY, Joncourt F, Díaz-Manera J, Gallardo E, Karaduman AA, Topaloglu H, El Sherif R, Stringer A, Shatillo AV, Martin AS, Peay HL, Bellgard MI, Kirschner J, Flanigan KM, Straub V, Bushby K, Verschuuren J, Aartsma-Rus A, Bérout C, Lochmüller H (2015) The TREAT-NMD DMD global database: analysis of more than 7,000 Duchenne muscular dystrophy mutations. *Hum Mutat* 36(4):395–402. <https://doi.org/10.1002/humu.22758>
8. Tuffery-Giraud S, Bérout C, Leturcq F, Yaou RB, Hamroun D, Michel-Calemard L, Moizard MP, Bernard R, Cossée M, Boisseau P, Blayau M, Creveaux I, Guiochon-Mantel A, de Martinville B, Philippe C, Monnier N, Bieth E, Khau Van Kien P, Desmet FO, Humbertclaude V, Kaplan JC, Chelly J, Claustres M (2009) Genotype-phenotype analysis in 2,405 patients with a dystrophinopathy using the UMD-DMD database: a model of nationwide knowledgebase. *Hum Mutat* 30(6):934–945. <https://doi.org/10.1002/humu.20976>
9. Aung-Htut MT, McIntosh CS, West KA, Fletcher S, Wilton SD (2019) In vitro validation of phosphorodiamidate morpholino oligomers. *Molecules* 24(16):2922. <https://doi.org/10.3390/molecules24162922>
10. Hori S-I, Yamamoto T, Waki R, Wada S, Wada F, Noda M, Obika S (2015) Ca²⁺ enrichment in culture medium potentiates

- effect of oligonucleotides. *Nucleic Acids Res* 43(19):e128. <https://doi.org/10.1093/nar/gkv626>
11. Mamchaoui K, Trollet C, Bigot A, Negroni E, Chaouch S, Wolff A, Kandalla PK, Marie S, Di Santo J, St Guily JL, Muntoni F, Kim J, Philippi S, Spuler S, Levy N, Blumen SC, Voit T, Wright WE, Aamiri A, Butler-Browne G, Mouly V (2011) Immortalized pathological human myoblasts: towards a universal tool for the study of neuromuscular disorders. *Skelet Muscle* 1:34. <https://doi.org/10.1186/2044-5040-1-34>
 12. Echigoya Y, Lim KRQ, Trieu N, Bao B, Miskew Nichols B, Vila MC, Novak JS, Hara Y, Lee J, Touznik A, Mamchaoui K, Aoki Y, Takeda S, Nagaraju K, Mouly V, Maruyama R, Duddy W, Yokota T (2017) Quantitative antisense screening and optimization for exon 51 skipping in Duchenne muscular dystrophy. *Mol Ther* 25(11):2561–2572. <https://doi.org/10.1016/j.ymthe.2017.07.014>
 13. Spitali P, Heemskerk H, Vossen RHAM, Ferlini A, den Dunnen JT, t Hoen PAC, Aartsma-Rus A (2010) Accurate quantification of dystrophin mRNA and exon skipping levels in duchenne muscular dystrophy. *Lab Invest* 90(9):1396–1402. <https://doi.org/10.1038/labinvest.2010.98>

Open Access This chapter is licensed under the terms of the Creative Commons Attribution 4.0 International License (<http://creativecommons.org/licenses/by/4.0/>), which permits use, sharing, adaptation, distribution and reproduction in any medium or format, as long as you give appropriate credit to the original author(s) and the source, provide a link to the Creative Commons license and indicate if changes were made.

The images or other third party material in this chapter are included in the chapter's Creative Commons license, unless indicated otherwise in a credit line to the material. If material is not included in the chapter's Creative Commons license and your intended use is not permitted by statutory regulation or exceeds the permitted use, you will need to obtain permission directly from the copyright holder.





Rapid Determination of MBNL1 Protein Levels by Quantitative Dot Blot for the Evaluation of Antisense Oligonucleotides in Myotonic Dystrophy Myoblasts

Nerea Moreno, Irene González-Martínez, Rubén Artero, and Estefanía Cerro-Herreros

Abstract

Western blot assays are not adequate for high-throughput screening of protein expression because it is an expensive and time-consuming technique. Here we demonstrate that quantitative dot blots in plate format are a better option to determine the absolute contents of a given protein in less than 48 h. The method was optimized for the detection of the Muscleblind-like 1 protein in patient-derived myoblasts treated with a collection of more than 100 experimental oligonucleotides.

Key words Myotonic dystrophy, Oligonucleotides, Quantitative dot blot, Muscleblind-like protein 1, DM1 myoblasts

1 Introduction

Myotonic dystrophy type 1 (DM1) is a degenerative genetic disease that is classified as rare because it affects less than 1 in 2000 people (1/3000 to 1/8000; [1]). DM1 originates from an expansion of the CTG trinucleotide repeat in the 3'-untranslated region (UTR) of the DMPK gene that, upon transcription, forms CUG hairpins that behave as toxic RNAs. CUG expansion RNA aberrantly binds and sequesters essential developmental proteins of the Muscleblind-like (MBNL) family, which are key regulators of alternative splicing. The depletion in MBNL protein function causes alterations in RNA metabolism that originate defined symptoms of the disease [2]. Studies in animal models have shown that the increase of MBNL in a genetic background of DM improves the

Nerea Moreno and Irene González-Martínez contributed equally to this work.

pathological phenotypes and that the overexpression of MBNL1 in control mice is well tolerated [3].

Patients suffer from myotonia and muscle atrophy and weakness, which, in advanced stages of the disease, lead to respiratory distress and early death. Currently, there is no effective treatment for DM1, and management of symptoms is the only option to preserve the quality of life of people living with DM1. In its most common form, the onset of symptoms occurs during adolescence, and affected people have a significantly shortened lifespan of 48–55 years. Because of its prevalence and the severity of the clinical manifestations, finding a cure for DM1 is a social and medical need [4, 5].

The development of effective high-throughput tools in drug discovery research has increased the demand for complementary high capacity immunoblot methods in which to assess the consequences of drug candidates at protein level. One example is the need to quickly evaluate the levels of MBNL1 protein in patient-derived myoblasts [6] treated with hundreds of oligonucleotide variants to block repressive miRNAs miR-23b and miR-218, as a means to boost endogenous levels and compensate sequestration by CUG expansions in mutant DMPK [7]. To this end, we have generated a diversity (>100) of highly modified antisense oligonucleotides (AONs) to block miR-23b and miR-218. Examples of these modifications are the substitution of natural ribose rings by locked nucleic acid (LNAs), C2' hydroxyl substitutions with a methoxy (2'OMe) or methoxyethyl (2'-MOE), or the use of phosphorothioates to link two nucleotides, instead of natural phosphodiester bonds, to improve stability in vivo as they make these ASOs resistant to intracellular and extracellular nucleases. AON can also be made electrostatically neutral by using phosphorodiamidate morpholino oligomers (PMO) and can be conjugated to a cholesterol moiety to improve the diffusion through cell membranes and cell uptake [8, 9].

For this purpose, we propose the use of quantitative dot blot (QDB) analysis as an alternative to Western blot. For the development of the QDB assay, we have modified two previously published protocols [10, 11]. Dot blot was developed to simplify the process of Western blot analysis (Fig. 1) when the antibody is very specific for the detection of the protein of interest, and there is no need to determine its molecular weight, for example, when screening the effects of several molecules on the expression of a single protein. Specifically, QDB transforms traditional immunoblots into quantitative assays and allows expression analysis of a certain protein in your samples in 96-well format, being more efficient and faster than a Western blot.

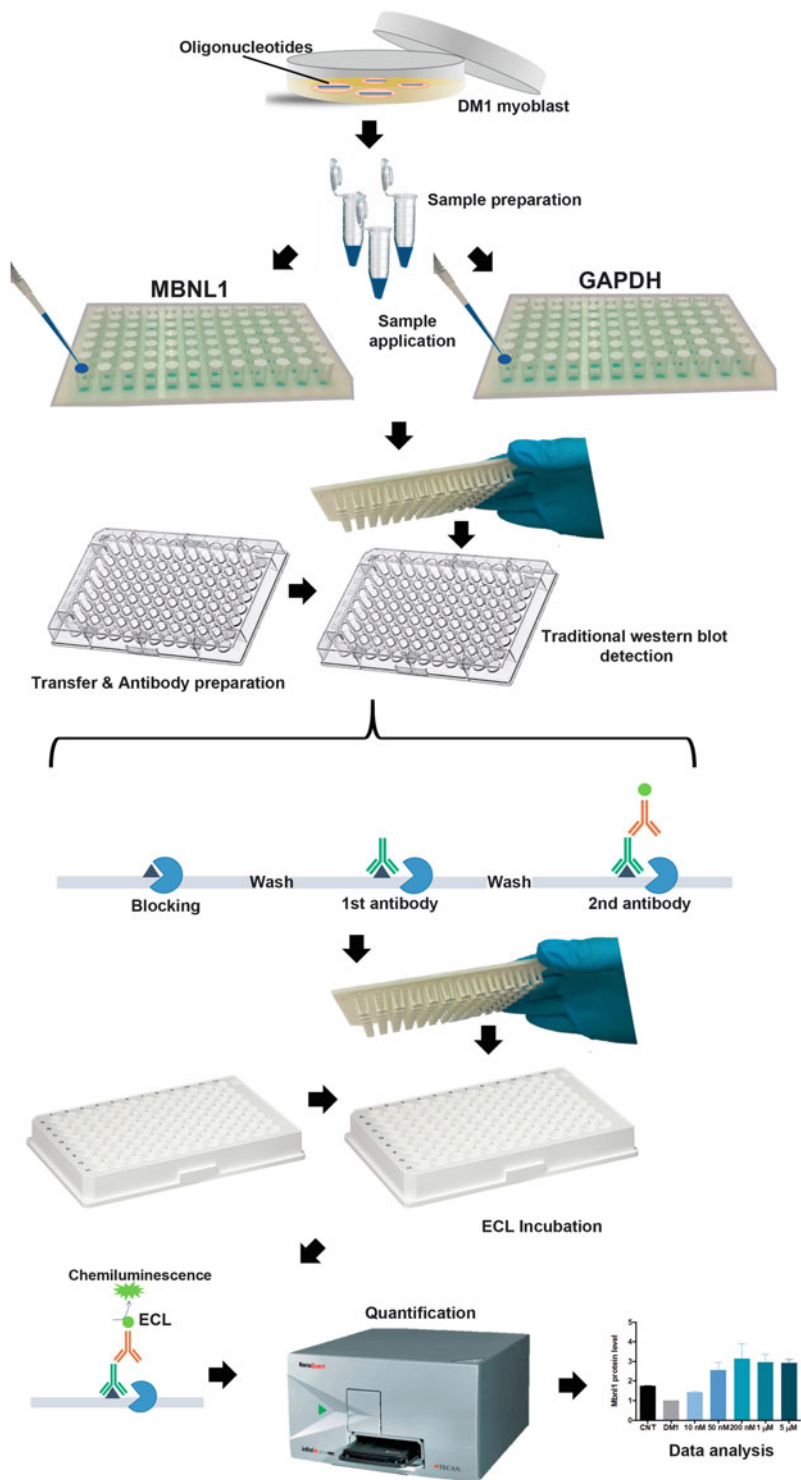


Fig. 1 Illustration of the entire QDB process for evaluation of antisense oligonucleotides in DM1 myoblast

2 Materials

2.1 Cell Culture and Transfection

1. Standard tissue culture facilities.
2. Six-well plates.
3. PBS 1×.
4. Opti-MEM Reduced Serum medium.
5. Transfection Reagent (*see Note 1*).
6. Complete medium (for 500 mL): 445 mL DMEM Dulbecco's Modified Eagle Medium 4500 mg/glucose, 50 mL FBS, and 5 mL penicillin-streptomycin.
7. Differentiation medium (for 100 mL): 1 mL penicillin-streptomycin, 2 mL Horse Serum, 1 mL apotransferrin, 100 μ L insulin, 20 μ L doxycyclin and 95.88 mL DMEM 4500 mg/glucose.

2.2 QDB Assay

1. Protein quantification kit (*see Note 2*).
2. QDB plates (Quanticision Diagnostics, Inc.).
3. Primary and secondary antibodies:
 - (a) Anti-MBNL1 (Abcam, ab77017).
 - (b) Anti-GAPDH (Santa Cruz Biotechnology, G-9: sc-365062).
 - (c) Anti-mouse POD.
4. Pierce™ ECL Western blotting substrate.
5. White 96-well plate, flat bottom.
6. TECAN infinite M200 Pro.
7. Orbital shaker.
8. Transfer buffer: 14.4 g glycine, 3 g Tris base, 700 mL ddH₂O, 200 mL methanol and fill to 1 L with ddH₂O. Store at 4 °C.
9. 10× TBS: 24.2 g Tris base, 80 g NaCl, bring to 0.8 L with ddH₂O, adjust the pH to 7.6 with HCl and fill to 1 L with ddH₂O. Store at 4 °C.
10. 1× TBST: 100 mL 10× TBS, 5 mL Tween 20 and fill to 1 L with ddH₂O. Store at 4 °C.
11. Blocking buffer: 5 g milk powder and bring to 100 mL with TBST 1×. Store at 4 °C.
12. 4× Loading buffer: 0.8 mL 3 M Tris-HCl pH 6.8, 4 mL glycerol, 0.8 g SDS, 0.04 g bromophenol blue, 4 mL β -mercaptoethanol and fill to 10 mL with ddH₂O. Store at −20 °C.
13. RIPA solution: 10 mL RIPA and 1 tablet of protease inhibitor cocktail. Storage in 4 °C.

3 Methods

3.1 Cell Transfection

1. Seed cells in 6-well plates at a density of 200,000 cells per well in complete medium and are incubated for 24 h at 37 °C 5% CO₂.
2. Prepare the mixes for transfection. Volumes in this example are calculated for 3 wells of a 6-well plate and in 5 different concentrations in the range between 10 and 5000 nM, diluted in Opti-MEM in a sterile tube in a final volume of 600 µL. For example, to transfect AO at 200 µM mix 594 µL of Opti-MEM and add 6 µL of AO at 100 µM. To test other concentrations, adapt the volumes accordingly. Pipet gently to mix.
3. Add 3 µL of X-tremeGENE HP DNA transfection reagent to the diluted mix. Incubate for 30 min at RT while preparing the following step.
4. Remove medium from wells and wash twice with PBS 1×.
5. Add 200 µL of transfection mix to each well in a dropwise manner. Swirl the wells to ensure the distribution over the entire plate.
6. Leave the cells in the incubator for 4 h.
7. Add 2.3 mL of differentiation medium per well.

3.2 Sample Collection and Quantification

1. After 72 h of incubation of the DM1 myoblasts with the test oligonucleotides, wash each well with PBS before protein collection.
2. Collect cells in RIPA solution (120 µL/well).
3. Lyse cells with an ultrasonic homogenizer such as the UP100H. Sonication is at an ultrasonic cycle mode of 30 s and an amplitude of 60%. The sample must be kept in ice during the entire procedure.
4. Centrifuge the lysate at 16,000 × *g* for approximately 15 min after ultrasonic homogenization/extraction.
5. After centrifuging, collect the supernatant and determine the protein concentration by a protein assay such as Pierce protein assay BCA.

3.3 Sample Preparation

1. Calculate enough protein extract for ten replicate wells at 1 µg/well to account for pipetting errors, as they will be later loaded in quadruplicates in two different plates: one for detection of MBNL1 and the other for GAPDH, as an endogenous control (*see Note 3*).
2. Add the protein extract at the indicated concentration, add 10.4 µL of loading buffer 4× and complete to a final volume of 50 µL of ddH₂O (*see Note 4*).

3. Boil the freshly prepared sample for 5 min in a water bath and after denaturation of the protein leave it on ice.

3.4 Sample Application and Transference

1. Place the plates upside down to load the samples. Pipette 5 μ L of the previously prepared protein sample on each membrane circle (Fig. 2).
2. Dry loaded QDB plates for 30 min at room temperature in a well-ventilated space.
3. After drying, dip the QDB plate in transfer buffer for 1 min. During this minute, shake it with an orbital movement until the blue color in the wells is eliminated.
4. Rinse QDB plates gently with TBST in constant shaking for 1 min three times.
5. Block QDB plates with blocking buffer for 1 h with constant shaking.

3.5 Primary Antibody Incubation

1. Dilute primary antibodies in blocking buffer at the appropriate concentrations (anti-MBNL1: 1/1000 and anti-GAPDH: 1/500) and aliquot into the wells of two 96-well plates, one for each antibody, at 100 μ L/well (*see Note 5*).
2. Insert each QDB plate into the 96-well plates and incubate overnight at 4 °C in constant shaking.
3. Rinse the plates briefly with TBST and then wash with TBST in constant shaking for 5 min, three times.

3.6 Secondary Antibody Incubation

1. Dilute the appropriate secondary antibody (anti-mouse POD) in blocking buffer at the final concentration of 1/2000 and aliquot it in the 96-well plates at 100 μ L/well. QDB plates are inserted into the 96-well plates and incubated in constant shaking for 2 h.
2. Rinse QDB plates gently three times with TBST and then wash with TBST in constant shaking for 5 min, three times.

3.7 Quantification

1. Before the last washes, prepare the ECL substrate by following the manufacturer's instructions.
2. Aliquot 50 μ L of ECL substrate into each well of a 96-well plate, and insert the QDB plate inside the 96-well plates for 1 min.
3. After a minute, remove the QDB plate from the 96-well plate and shake it briefly to remove the remaining reagent and introduce it into a clean white 96-well plate.
4. For data acquisition, use a TECAN infinite M200 Pro using an initial acquisition time of 1 s/well in the luminescence and select "plate with cover."

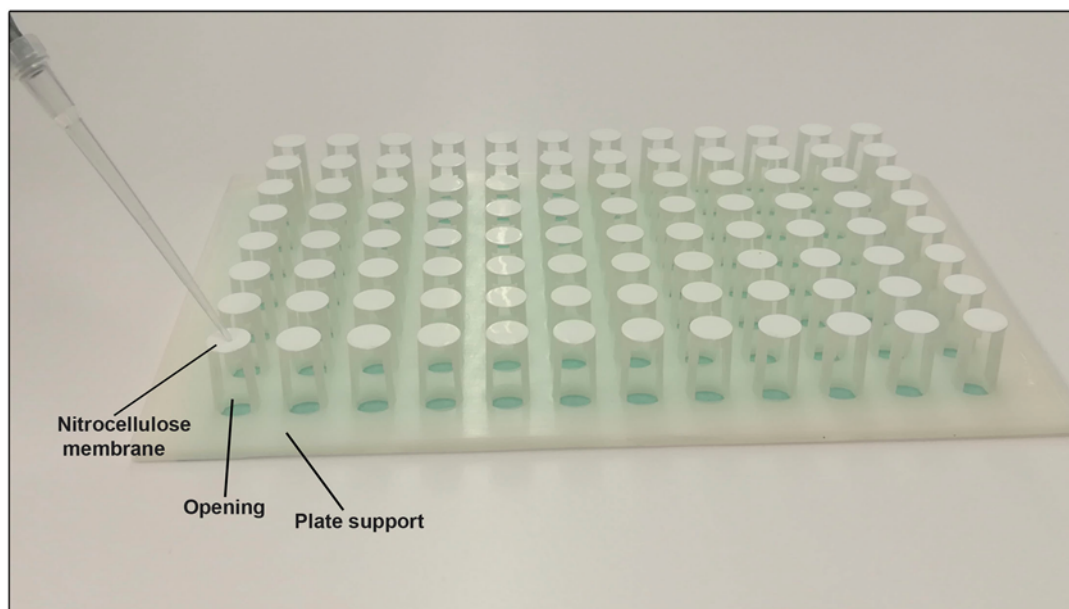


Fig. 2 A photograph of a QDB plate upside down. The figure shows the different components of the plate and how to load the sample

3.8 Data Analysis

1. First, look at the negative control values, which have to be below the rest of the samples. Pay also attention to the integrity of the plate since any alteration of the membrane in one of the wells may lead to artifactually low chemiluminescence values.
2. Next, subtract the average value of the negative controls from all the samples, thus removing the contribution of the background to the quantification.
3. Obtain the average of the quadruplicates for both the MBNL1 and the GAPDH plates. Divide the average of the replicates of the MBNL1 samples by those of GAPDH.
4. GAPDH normalized values can be further normalized to values in mock-transfected DM1 cells to obtain fold changes.
5. As a positive control, confirm in each plate that the difference between the average values of MBNL1 in control and untreated DM1 cells is around 1.6 times.

4 Notes

1. Could be done with any transfection reagent, but we have tested only X-tremeGENE HP DNA Transfection Reagent.
2. Could be done with any protein quantification kit, but we have tested only Pierce™ BCA Protein Assay kit.

3. Always include positive and negative controls in each of the plates. Our positive controls were healthy cell samples while the negative contained RIPA buffer only. Negative control wells provide the background luminescence reading, which must be significantly lower than our experimental data.
4. It is very important to prepare the protein and load the samples in the gas hood since β -mercaptoethanol is toxic by inhalation.
5. To ensure a valid result, the specificity of the antibody used needs to be verified through Western blot analysis.

Acknowledgments

The project leading to these results has received funding from “la Caixa” Banking Foundation under the project code HR17-00268 (TATAMI project to R.A.). I.G.-M. was funded by the Precipita Project titled “Desarrollo de una terapia innovadora contra la distrofia miotónica”; E.C.-H. was supported by the post-doctoral fellowship APOSTD/2019/142; and N.M.-C was supported by the pre-doctoral fellowship PRE2019-090622. Part of the equipment employed in this work has been funded by Generalitat Valenciana and cofinanced with ERDF funds (OP ERDF of Comunitat Valenciana 2014-2020).

References

1. Ashizawa T, Gagnon C, Groh WJ, Gutmann L, Johnson NE, Meola G, Moxley R III, Pandya S, Rogers MT, Simpson E, Angeard N, Bassez G, Berggren KN, Bhakta D, Bozzali M, Broderick A, Byrne JLB, Campbell C, Cup E, Day JW, De Mattia E, Duboc D, Duong T, Eichinger K, Ekstrom AB, van Engelen B, Esparis B, Eymard B, Ferschl M, Gadalla SM, Gallais B, Goodglick T, Heatwole C, Hilbert J, Holland V, Kierkegaard M, Koopman WJ, Lane K, Maas D, Mankodi A, Mathews KD, Monckton DG, Moser D, Nazarian S, Nguyen L, Nopoulos P, Petty R, Phetteplace J, Puymirat J, Raman S, Richer L, Roma E, Sampson J, Sansone V, Schoser B, Sterling L, Statland J, Subramony SH, Tian C, Trujillo C, Tomaselli G, Turner C, Venance S, Verma A, White M, Winblad S (2018) Consensus-based care recommendations for adults with myotonic dystrophy type 1. *Neurol Clin Pract* 8(6):507–520. <https://doi.org/10.1212/CPJ.0000000000000531>
2. Jiang H, Mankodi A, Swanson MS, Moxley RT, Thornton CA (2004) Myotonic dystrophy type 1 is associated with nuclear foci of mutant RNA, sequestration of muscleblind proteins and deregulated alternative splicing in neurons. *Hum Mol Genet* 13(24):3079–3088. <https://doi.org/10.1093/hmg/ddh327>
3. Chamberlain CM, Ranum LP (2012) Mouse model of muscleblind-like 1 overexpression: skeletal muscle effects and therapeutic promise. *Hum Mol Genet* 21(21):4645–4654. <https://doi.org/10.1093/hmg/dds306>
4. Landfeldt E, Nikolenko N, Jimenez-Moreno C, Cumming S, Monckton DG, Gorman G, Turner C, Lochmuller H (2019) Disease burden of myotonic dystrophy type 1. *J Neurol* 266(4):998–1006. <https://doi.org/10.1007/s00415-019-09228-w>
5. Mathieu J, Allard P, Potvin L, Prevost C, Begin P (1999) A 10-year study of mortality in a cohort of patients with myotonic dystrophy. *Neurology* 52(8):1658–1662
6. Arandel L, Polay Espinoza M, Matloka M, Bazinet A, De Dea DD, Naouar N, Rau F, Jollet A, Edom-Vovard F, Mamchaoui K, Tarnopolsky M, Puymirat J, Battail C, Boland A, Deleuze JF, Mouly V, Klein AF, Furling D (2017) Immortalized human

- myotonic dystrophy muscle cell lines to assess therapeutic compounds. *Dis Model Mech* 10(4):487–497. <https://doi.org/10.1242/dmm.027367>
7. Cerro-Herreros E, Sabater-Arcis M, Fernandez-Costa JM, Moreno N, Perez-Alonso M, Llamusi B, Artero R (2018) miR-23b and miR-218 silencing increase Muscleblind-like expression and alleviate myotonic dystrophy phenotypes in mammalian models. *Nat Commun* 9(1):2482. <https://doi.org/10.1038/s41467-018-04892-4>
 8. Croke ST, Witzum JL, Bennett CF, Baker BF (2019) RNA-targeted therapeutics. *Cell Metab* 29(2):501. <https://doi.org/10.1016/j.cmet.2019.01.001>
 9. Smith CIE, Zain R (2019) Therapeutic oligonucleotides: state of the art. *Annu Rev Pharmacol Toxicol* 59:605–630. <https://doi.org/10.1146/annurev-pharmtox-010818-021050>
 10. Tian G, Tang F, Yang C, Zhang W, Bergquist J, Wang B, Mi J, Zhang J (2017) Quantitative dot blot analysis (QDB), a versatile high throughput immunoblot method. *Oncotarget* 8(35):58553–58562. <https://doi.org/10.18632/oncotarget.17236>
 11. Qi X, Zhang Y, Zhang Y, Ni T, Zhang W, Yang C, Mi J, Zhang J, Tian G (2018) High throughput, absolute determination of the content of a selected protein at tissue levels using quantitative dot blot analysis (QDB). *J Vis Exp* (138):56885. <https://doi.org/10.3791/56885>

Open Access This chapter is licensed under the terms of the Creative Commons Attribution 4.0 International License (<http://creativecommons.org/licenses/by/4.0/>), which permits use, sharing, adaptation, distribution and reproduction in any medium or format, as long as you give appropriate credit to the original author(s) and the source, provide a link to the Creative Commons license and indicate if changes were made.

The images or other third party material in this chapter are included in the chapter's Creative Commons license, unless indicated otherwise in a credit line to the material. If material is not included in the chapter's Creative Commons license and your intended use is not permitted by statutory regulation or exceeds the permitted use, you will need to obtain permission directly from the copyright holder.





Chapter 14

Evaluation of Exon Skipping and Dystrophin Restoration in In Vitro Models of Duchenne Muscular Dystrophy

Andrea López-Martínez, Patricia Soblechero-Martín,
and Virginia Arechavala-Gomeza 

Abstract

Several exon skipping antisense oligonucleotides (eteplirsen, golodirsen, viltolarsen, and casimersen) have been approved for the treatment of Duchenne muscular dystrophy, but many more are in development targeting an array of different *DMD* exons. Preclinical screening of the new oligonucleotide sequences is routinely performed using patient-derived cell cultures, and evaluation of their efficacy may be performed at RNA and/or protein level. While several methods to assess exon skipping and dystrophin expression in cell culture have been developed, the choice of methodology often depends on the availability of specific research equipment.

In this chapter, we describe and indicate the relevant bibliography of all the methods that may be used in this evaluation and describe in detail the protocols routinely followed at our institution, one to evaluate the efficacy of skipping at RNA level (nested PCR) and the other the restoration of protein expression (myoblot), which provide good results using equipment largely available to most research laboratories.

Key words Dystrophin, Antisense oligonucleotide, Duchenne muscular dystrophy, Eteplirsen, Myoblot, Exon skipping

1 Introduction

Duchenne muscular dystrophy (DMD) is an X-linked inherited neuromuscular disorder caused by mutations in the dystrophin gene (*DMD*) and characterized by rapid progression of muscle weakness and loss of ambulation in early adolescence. Most *DMD* mutations are deletions that disrupt the open reading frame (ORF), preventing the synthesis of dystrophin protein. On the other hand, Becker's muscular dystrophy (BMD) is a milder neuromuscular disorder caused by in-frame mutations in the same gene. In this case, mutations do not disrupt the ORF and a shorter but semi-functional form of dystrophin is produced resulting in a milder form of disease [1, 2].

The reading-frame rule, exemplified in Becker patients, is the basis of the concept of exon skipping by antisense oligonucleotides (AONs) as a possible therapy for DMD. In this case, AONs are designed to attach to specific RNA sequences and disrupt the binding of the spliceosome, which in turn causes the skipping of a particular exon and the restoration of the expression of a truncated, but semi-functional, dystrophin [3]. This therapeutic approach could benefit around 83% of DMD patients, but due to the vast array of different *DMD* deletions and mutations causing DMD, to treat each subset of DMD patients, different exons would need to be targeted by specific AONs [4, 5]. Eteplirsen, golodirsen, viltolarsen, and casimersen are AONs that facilitate the skipping of *DMD* exons 51, 53, 53, and 45 respectively, and have been approved by the FDA (2016, 2019, 2020, and 2021) [6–10]. These drugs would only be applicable to 13% (eteplirsen) and 8% of DMD patients (golodirsen, viltolarsen, and casimersen). New AONs, skipping other exons, are being designed for the remaining deletions that may benefit from this approach [11–14].

The preclinical development of new exon-skipping AONs relies on the use of cell cultures from patients harboring specific deletions. It is common practice to design a panel of candidate AONs and evaluate their efficacy in culture before advancing to preclinical testing, and many methods are followed to evaluate them, at both RNA and protein levels, as represented in Fig. 1.

1.1 Evaluating Exon Skipping at RNA Level

When evaluating exon skipping at RNA level, several methods, both quantitative and semi-quantitative, are routinely used. A recent publication compared five different quantification techniques: quantitative real-time PCR (qPCR) [18], digital droplet PCR (ddPCR) [23], single PCR assessed with an Agilent bioanalyzer, and nested PCR with agarose gel image analysis [15–17]. They concluded that ddPCR was the most precise and less dispersed quantitative method for exon-skipping detection, while the other techniques may overestimate exon skipping and present high data variation.

The ddPCR protocol is based on the mix of the DNA sample with an oil–water media to divide the template in several thousand droplets. Each droplet contains none or one single template strand that would provide individual amplification reactions and absolute quantification. It is a highly reproducible and efficient technique as it does not depend on the PCR efficiency and may be adapted to quantify exon skipping using specific probes. Nevertheless, the technique requires highly specific equipment not available in most laboratories [23].

Quantitative real-time PCR for *DMD* transcripts uses custom probes to specifically detect skipped transcripts that are lately amplified for transcript quantification. Data are normalized with endogenous transcript controls but the requirement of a pre-amplification

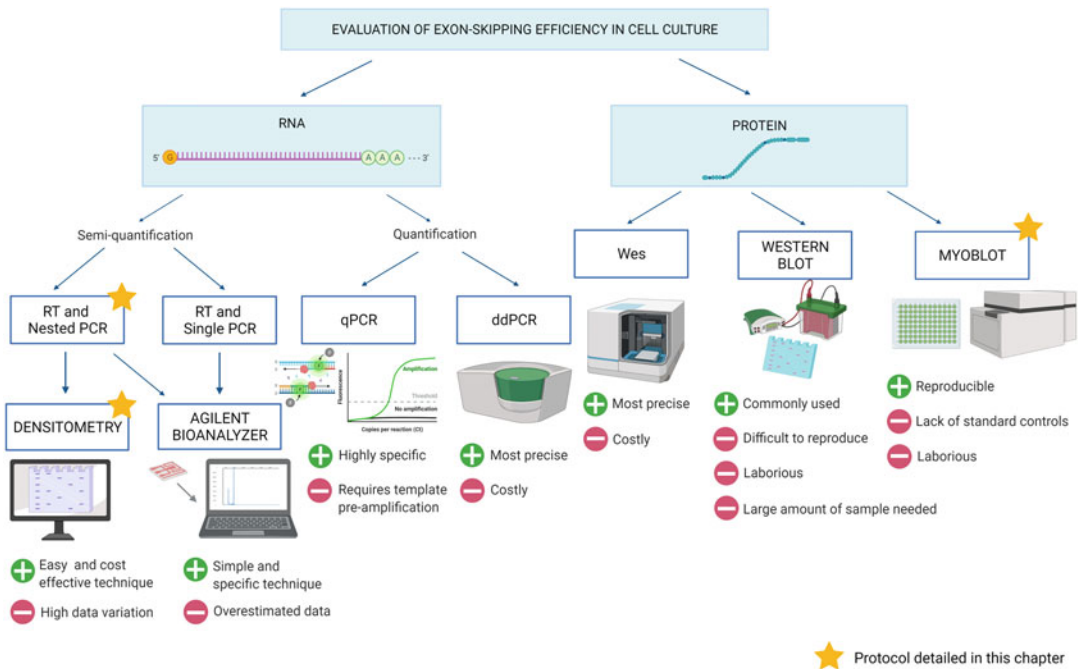


Fig. 1 Methods that may be used to evaluate exon skipping in cell culture. Currently, the most accurate methods are digital droplet PCR (ddPCR) and capillary western immunoassay (Wes), but the equipment required to perform these experiments is not present in the majority of research laboratories. Advantages (green) and disadvantages (red) of each method are presented in this figure. Main bibliographical references for these methods are: RT-PCR followed by gel densitometry analysis [15, 16], single-round PCR followed by bioanalyzer [16, 17], qPCR [18], ddPCR [13], capillary western immunoassay (Wes) [19], Western blotting [20], myoblots [21]. Several attempts to compare these methods have been published by a consortium to evaluate dystrophin protein quantification methods [20] and another to compare methods to quantify exon skipping [17]. A recent meeting to find consensus among stakeholders on all dystrophin protein quantification methods described was also recently published [22]. Created with [Biorender.com](https://biorender.com)

step and specific probes for each of the deletions tested may decrease linearity and increase costs [18].

Most methods are semi-quantitative at best and provide an indication of efficacy that should be evaluated further by assessing the downstream consequences of exon skipping (dystrophin restoration). Our approach combines the study of exon skipping at RNA level by a rather simple nested PCR plus gel densitometry analysis method, with a quantitative evaluation of dystrophin protein by myoblots.

1.2 Evaluating Dystrophin Restoration in Cell Culture

Dystrophin protein quantification can be challenging due to its large size (3685 amino acids) and expression pattern, and it has been an extremely hot topic when evaluating the results of dystrophin restoration clinical trials [24]. A recent meeting of stakeholders interested in dystrophin quantification methodology highlighted the problems derived from the variability of dystrophin

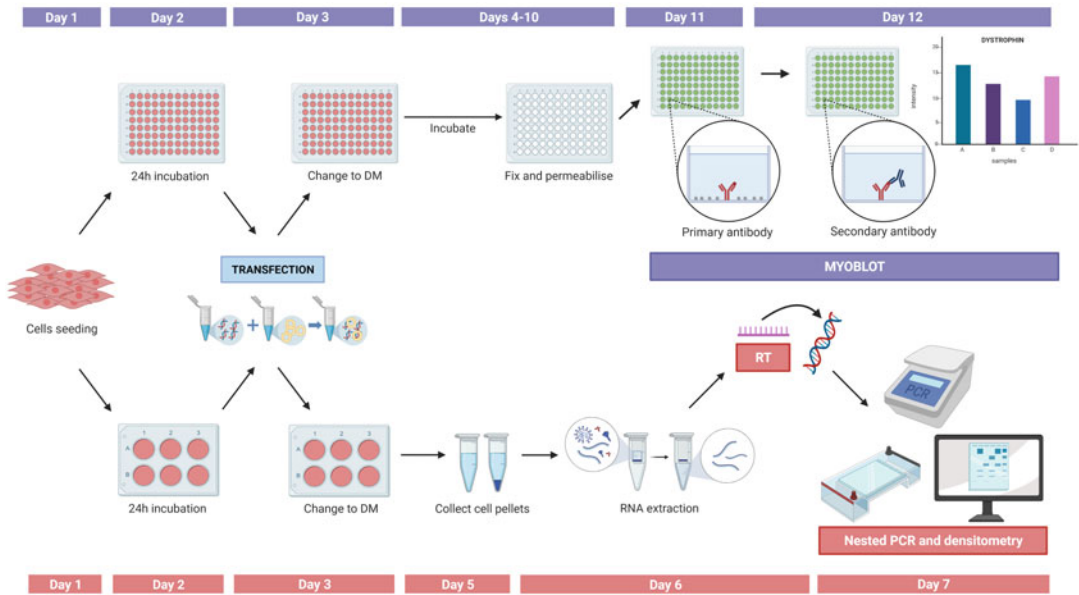


Fig. 2 Workflow of an exon skipping evaluation experiment. *RNA evaluation*: a 6-well plate is seeded and transfected with two different AON concentrations. Cells are collected after 48 h for RNA extraction, reverse transcription (RT), and nested PCR analysis by densitometry. *Dystrophin protein quantification*: a 96-well plate is seeded, transfected, and allowed to differentiate for a week. Plates are fixed before being analyzed by myoblot. Created with [Biorender.com](https://biorender.com)

levels between different muscles and individuals as well as the lack of standardized controls [22]. When analyzing preclinical in vitro experiments, other points need to be considered: patient-derived cell cultures are difficult to expand and differentiate, and dystrophin expression is only detectable when cells are differentiated into myotubes. Western blotting analysis from cultured cells requires very large amounts of protein lysate that does not produce good quantitative results while using a lot of sample.

A novel advance in protein quantification is the capillary Western immunoassay (Wes), based on the use of capillary as separation modules for protein isolation followed by dystrophin detection by an immunoassay that allows accurate quantification. The Wes system is said to detect low protein concentrations, in a range of 0.125–1.25 μg [19, 22]. However, this equipment is not yet commonly found in most laboratories.

We detail in this chapter the quantitative method developed at our department: myoblots, a method based on the in-cell western blotting optimized for the quantification of muscle proteins in cell culture [21]. Myoblots are performed in 96-well plates seeded with patient-derived cells, which are allowed to differentiate. Signal is normalized by cell number, and the differentiation status of the cultures is assessed as a quality control of the experiment.

A summary of our strategy to evaluate exon skipping drugs in cell culture is shown in Fig. 2. In the example used in this chapter, we evaluated two concentrations of an AON skipping exon 51 on immortalized cell cultures [25] from a patient harboring a mutation that causes the deletion of exon 52 from the CNMD Biobank (London, UK).

2 Materials

2.1 Cell Culture and Transfection

1. Standard tissue culture facilities.
2. Low background fluorescence and low evaporation 96-well plates with clear, flat bottom.
3. The AON used in the example was synthesized by Eurogentec, Belgium with the following sequence: 5'-[T*C*A*-A*G*G*-A*A*G*-A*T*G*-G*C*A*-T*T*T*-C*T]-3'; where * is a 2' MOE phosphorothioate linkage. AON stock at 100 μ M in distilled H₂O is stored at -80 °C.
4. SMMC: Skeletal Muscle Cell Growth Medium Complete. SMMC is supplemented with 5% Supplement Mix, 10% fetal bovine serum, 1% GlutaMax (dipeptide L-alanine-L-glutamine), 2% PenStrep, and 0.06% Gentamicine.
5. DMEM: Dulbecco's Modified Eagle Medium.
6. Opti-MEM Reduced Serum Media.
7. Differentiation medium: DMEM supplemented with 2% horse serum.
8. 0.05% Trypsin-EDTA.
9. Lipofectamine™ 2000 Transfection Reagent.

2.2 RT and Nested PCR Analysis

1. Access to thermocycler, electrophoresis equipment, and gel documentation system.
2. Nanodrop or other equipment to measure RNA concentration.
3. RNeasy Mini Kit.
4. SuperScript™ IV First-Strand Synthesis System (*see Note 1*).
5. PCR Master Mix including: 33.5 μ l RNase free-water, 5 μ l 10 \times PCR Buffer, 3 μ l 50 mM MgCl₂, 1 μ l 10 mM dNTPs, 0.5 μ l Taq DNA Polymerase recombinant (5 U/ μ L), plus two sets of specific primers (10 μ M) described in Table 1 (*see Note 2*).
6. Agarose.
7. 1 \times TAE buffer.
8. SYBR safe DNA gel stain.
9. 5 \times PCR Loading Buffer.

Table 1
Primer sequences

Primers			Sequence	Length
RT	55R	Exon 55 reverse	AACTGCCAATGTCCTACAGGAT	22 bases
First PCR	48F	Exon 48 forward	AAAAGACCTTGGGCAGCTTG	20 bases
	54R	Exon 54 reverse	TGACTTGGCCCTGAAACTTC	20 bases
Second PCR	49F	Exon 49 forward	CCAGCCACTCAGCCAGTG	18 bases
	53R	Exon 53 reverse	CCTTCAGAACCGGAGGCAA	19 bases

Specific primer 55R was used in the RT reaction. Two different sets of primers targeting regions between exons 48F-54R (first PCR) and 49F-53R (second PCR) were used for the nested-PCR method

- 10. HyperLadder 100 bp.
- 11. Gel extraction kit to isolate PCR fragments for sequencing.

2.3 Myoblots

- 1. Access to an Odyssey CLx Scan (LI-COR Biosciences).
- 2. Orbital shaker.
- 3. Ice-cold methanol.
- 4. 1× PBS.
- 5. Permeabilization Buffer (PB): 1× PBS, Triton 0.1%.
- 6. Intercept® Blocking Buffer (LI-COR Biosciences).
- 7. Washing Buffer (WB): 1× PBS, Tween 0.1%.
- 8. Primary antibodies:
 - (a) MF20 antibody (Developmental Studies Hybridoma Bank (DSHB)).
 - (b) Mandys1, kindly provided by Prof. G Morris, The MDA Monoclonal Antibody Resource.
 - (c) Mandys106, kindly provided by Prof. G Morris, The MDA Monoclonal Antibody Resource.
 - (d) Dys1 (Leica Biosystems).
- 9. Secondary antibodies:
 - (a) Goat Anti-Mouse IgG H&L (Biotin, Abcam).
 - (b) IRDye 800CW Streptavidin (LI-COR Biosciences).
 - (c) IRDye 800CW Goat anti-Mouse IgG (LI-COR Biosciences).
 - (d) CellTag™ 700 Stain from (LI-COR Biosciences).

3 Methods

3.1 Cell Culture and Transfection

1. Cells are seeded in 6-well plates: 350,000 cells per well or 96-well plates: 7500 cells per well in SMMC:DMEM (1:1) (*see Note 3*).
2. The following day, when 80% confluence is reached, growth medium is replaced by differentiation medium (DM).
3. On day 3, AON transfection is performed as follows [18]. Some examples of the distribution of the experimental conditions in the 96-well plate are described in Fig. 3 (*see Note 4*).
4. Remove DM from wells.
5. Wash with PBS.
6. Add 50 μ l of Opti-MEM per well in the 96-well plate and 1 ml per well in the 6-well plate.
7. Incubate at 37 °C and 5% CO₂ while preparing the following steps.
8. Dilute the AON to 100 μ M in distilled H₂O.
9. Prepare mixes for transfection. Volumes in this example are calculated for a single well of a 6-well plate and two different antisense conditions, 100 nM and 300 nM, adjust the volumes for the number of replicates. In 96-well plates, adjust volumes for a final volume of 50 μ l per well.
10. The transfection is performed with Lipofectamine 2000[®] Reagent using 2 μ l per 1 ml of final transfection volume. In this particular example, volumes are calculated as: prepare one tube with 250 μ l of Opti-MEM and 1 μ l of AON at 100 μ M (for AON 100 nM condition), another with 250 μ l of Opti-MEM and 3 μ l of AON at 100 μ M (for AON 300 nM condition), a third tube with 250 μ l of Opti-MEM alone (no AON control), and a fourth tube with 750 μ l Opti-MEM and 6 μ l of lipofectamine.
11. Add 250 μ l of the lipofectamine mix to each AON tube and incubate all three tubes (100 nM, 300 nM, and lipofectamine only) for 30 min at RT to allow for complex formation.
12. Add 500 μ l of Opti-MEM to each tube for a final transfection volume of 1 ml per well of the 6-well plate.
13. Add 1 ml of transfection mix to each well of the 6-well plate and 50 μ l of mix to each well of the 96-well plate. Incubate for 5 h at 37 °C and 5% CO₂.
14. Five hours after AON transfection, medium is changed to differentiation medium, and plates are placed again in the incubator.

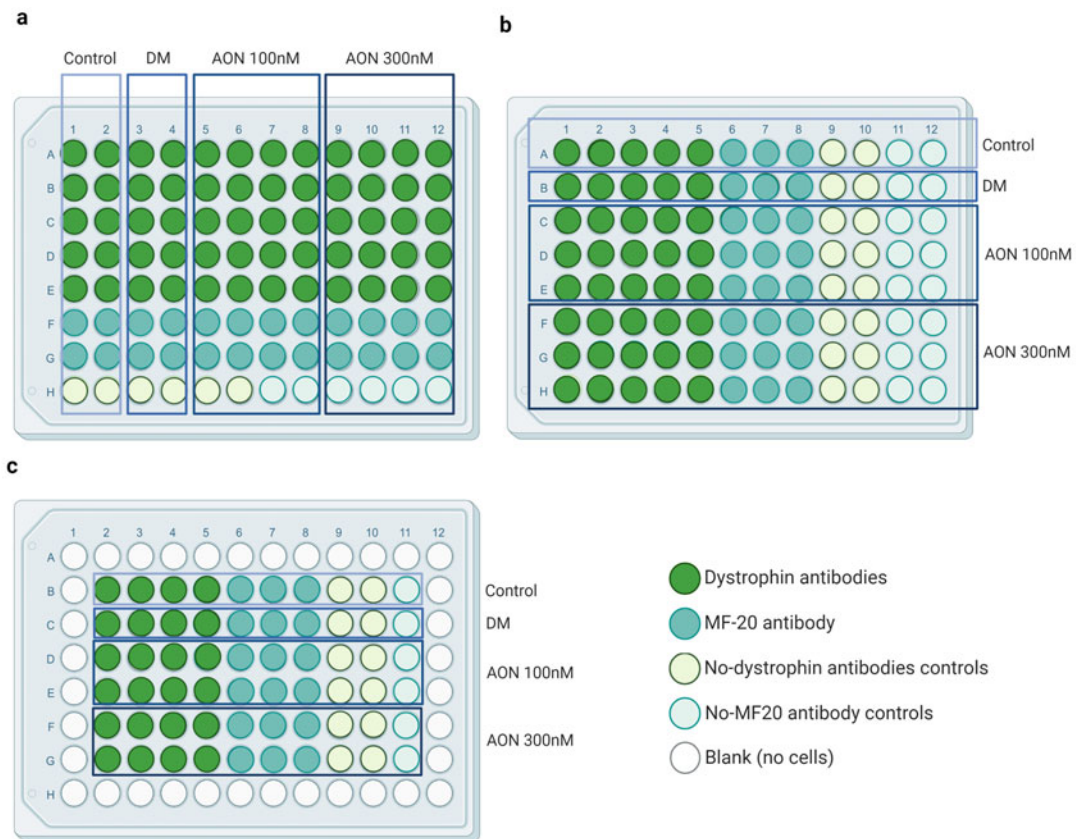


Fig. 3 Examples of plate distribution for exon skipping evaluation at protein level. **(a)** The four experimental conditions are distributed as follows in the 96-well plate: 2 columns for control (Lipofectamine only), 2 columns for DM (differentiation medium only), 4 columns for 100 nM AON, and 4 columns for 300 nM AON, both transfected with Lipofectamine. **(b)** The four experimental conditions are distributed as follows in the 96-well plate: 1 row for control (Lipofectamine only), 1 row for DM (differentiation medium only), 3 rows for 100 nM AON, and 3 rows for 300 nM AON, both transfected with Lipofectamine. **(c)** Reduction of the edge effect by filling edge wells with 100 μ l of preferred buffer, but not cells. Then, the four experimental conditions are distributed as follows in the 96-well plate: 1 row for control (Lipofectamine only), 1 row for DM (differentiation medium only), 2 rows for 100 nM AON, and 2 rows for 300 nM AON, both transfected with Lipofectamine. Each experimental condition will be probed with different antibodies in the 800-nm channel (green): the majority of wells will be probed with a dystrophin antibody mix, some with an MF20 antibody (experimental quality control to assess differentiation), and the remaining wells will have no primary antibody to eliminate background. In the 700-nm channel (red), every well will be probed with a cell number stain (CellTag™ 700 Stain) to allow for cell number normalization. Created with [Biorender.com](https://biorender.com)

15. After 48 h, cell pellets are collected from 6-well plates for RNA extraction using RNeasy Mini Kit to be used in the nested PCR (*see* Subheading 3.2).
16. Incubate the 96-well plates for 7 days and fix with ice-cold methanol. Myoblots can be performed immediately, or plates

may be stored in PBS at 4 °C until analysis (*see* Subheading 3.3).

3.2 Nested PCR and Gel Image Analysis Method

3.2.1 Reverse Transcription

1. After RNA extraction, RNA concentrations are measured with Nanodrop and 1 µg of template RNA is used for reverse transcription (RT).
2. RT is performed following the SuperScript™ IV First-Strand Synthesis System manufacturer's instructions with a specific primer (*see* **Note 5**), as described in Table 1.

3.2.2 Nested PCR

1. For the first PCR, prepare the PCR mastermix and add 2 µl of each primer of the first set of primers at 10 µM. In the example they target exon 48 and 54 (*see* Fig. 4a for primer location strategy).
2. Add 3 µl of cDNA (direct RT product) to the PCR mastermix.
3. Run the first PCR as follows: 94 °C for 5 min, 30 cycles of 94 °C for 40 s, 60 °C for 40 s, and 72 °C for 1 min and 20 s, and finally, 72 °C for 7 min.
4. Three microliters of the first PCR product are used as template in the second PCR, which has the same PCR mastermix plus 2 µl of each of the second pair of primers at 10 µM (49F and 53R in the example) (*see* **Note 6**).
5. The second PCR (or nested) should be run as follows: 94 °C for 5 min, 35 cycles of 94 °C for 40 s, 60 °C for 40 s, and 72 °C for 1 min and 20 s, and finally, 72 °C for 7 min.
6. Run a 2% agarose gel with the whole PCR product (50 µl) for 1 h at 100 mV.
7. Place gel on the transilluminator of the gel documentation system and acquire the image. A representative image is shown in Fig. 4b. This figure shows the skipped and non-skipped product highlighting the bands selected for quantification.
8. Cut the relevant PCR bands for DNA extraction and verification by Sanger sequencing.

3.2.3 Band Semi-Quantification

For the image analysis, if the available gel documentation system has quantification software you may use this, if not you may quantify the intensity of the bands with image J (<https://imagej.nih.gov/ij/download.html>):

1. Select the lanes that include the relevant bands using the region of interest (ROI) selection tool.
2. Use the gel analysis tool to create Analyze>Gels>Plot lanes.
3. Draw lines to separate the peaks corresponding to the required bands and use the wand tool to select them.

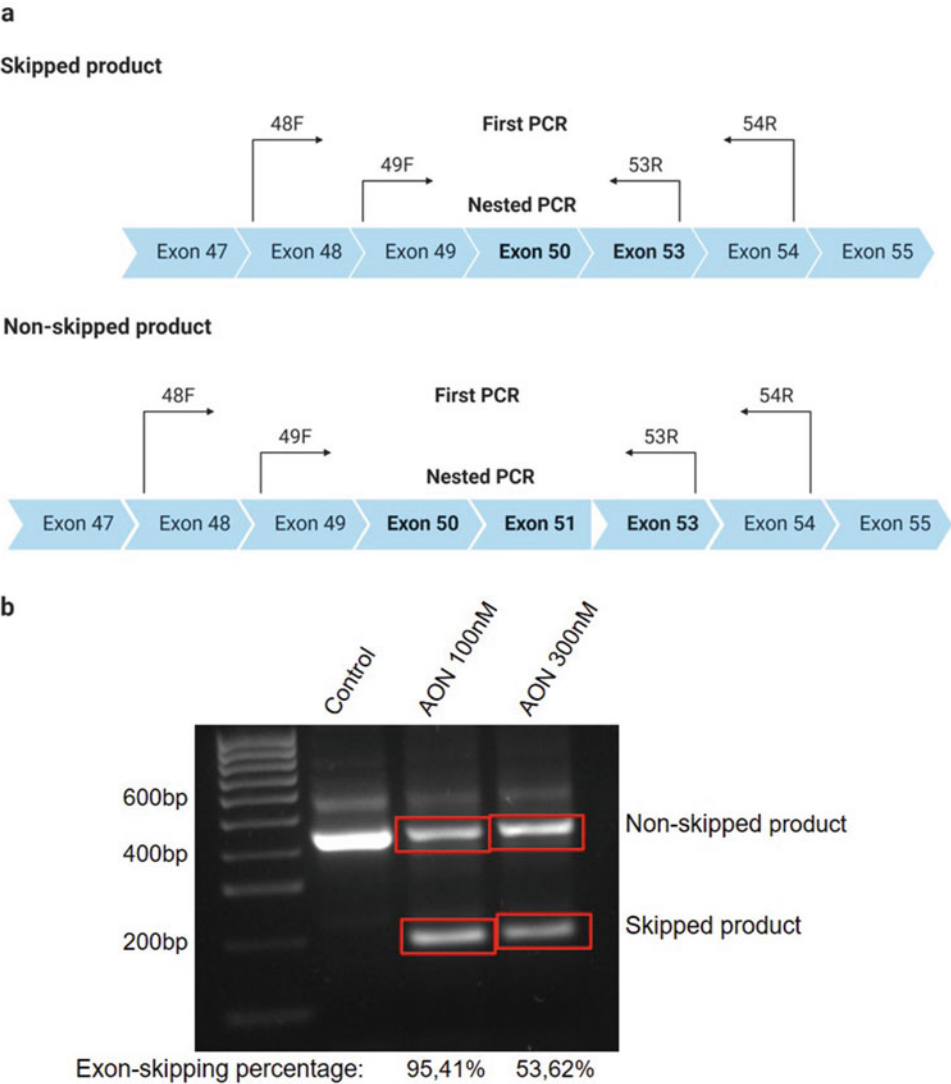


Fig. 4 Nested PCR results. **(a)** Skipped and non-skipped product schematic representations. Primers 48F and 54R were used in the first PCR and primers 49F and 53R in the second. Skipped product size is reduced due to the lack of exon 51 and 52 while the non-skipped product is just lacking exon 52. Created with [Biorender.com](https://www.biorender.com). **(b)** Agarose gel image from AON transfection. Fifty microliter of PCR product were examined in a 2% agarose gel stained with SYBRSafe. Image was captured in a Gel Doc™ EZ Imager (BIORAD). Red boxes indicate the quantified bands. The described relative percentage of exon skipping for 100 nM AON was 95.41% and for 300 nM AON was 53.62%

4. Analyze by clicking Analyze>Gels>LabelPeak to obtain each peak's area.
5. Normalize peak areas by amplicon sizes and calculate exon skipping percentages according to the formula [17]:

$$\text{Exon skipping\%} = \frac{(\text{normalized peak area skipped fragment})}{(\text{normalized peak area skipped fragment}) + (\text{normalized area non - skipped fragment})} \times 100$$

3.3 Myoblot Method

In our example, we are interested in dystrophin restoration, and the plate will be probed with the different antibodies as described in Fig. 3a.

3.3.1 Myoblot Procedure

1. If plates were stored at 4 °C, remove PBS. If not, remove methanol and wash with PBS.
2. Add 100 µl of Permeabilization Buffer (PB) per well.
3. Place the plates in an orbital shaker at RT for 5 min.
4. Remove PB and repeat four times the previous process.
5. Remove PB and add 50 µl of Intercept[®] (PBS) blocking buffer per well.
6. Incubate for 2 h in the orbital shaker at RT.
7. Remove blocking buffer.
8. Add 50 µl of the corresponding primary antibodies diluted in the blocking buffer. In the example (Fig. 3a), plate distribution was the following:
 - (a) Sixty wells for dystrophin detection. Add a dystrophin-Ab mix: Mandys1, Mandys106, and Dys1 at 1/100 dilution.
 - (b) Twenty-four wells for the differentiation marker. Add MF20 antibody at 1/50 dilution.
 - (c) Twelve wells as negative controls without any primary antibody. Add 50 µl of blocking buffer.
9. Incubate overnight at 4 °C in the orbital shaker.
10. Remove antibodies and add 100 µl per well of Washing Buffer (WB).
11. Wash for 5 min in the orbital shaker at RT.
12. Remove WB and repeat the wash four times.
13. For dystrophin detection, an amplification of the signal is needed. Biotin antibody (1/2000 dilution in blocking buffer) is used for signal amplification in those wells where dystrophin mix is added and also to 6 wells of the negative controls: after 1 h incubation at RT with this antibody, WB washes are repeated four times more as indicated in steps 10–12.
14. Add 50 µl of the corresponding secondary antibody diluted in the blocking buffer.
 - (a) Add CellTag[™] 700 Stain to all secondary antibody mixes at 1/1000 dilution.

- (b) For dystrophin mix amplified with biotin: add IRDye 800CW Streptavidin at 1/2000 dilution. Also added to 6 wells of the negative controls where biotin was added before (background control for the streptavidin secondary).
 - (c) For MF20: add IRDye 800CW Goat anti-Mouse IgG at 1/500 dilution. Also added to 6 wells of the negative controls (background control for the goat antibody).
15. Incubate for 1 h at RT in the orbital shaker.
 16. Remove the secondary antibodies and add 100 µl of WB per well.
 17. Wash for 5 min at the orbital shaker at RT.
 18. Remove the WB and repeat the wash process four times.
 19. Add 100 µl of PBS per well and prepare the Odyssey CLx Scan (*see* **Note 7**).

3.3.2 Myoblot Analysis

1. In the Image Studio™ Software from your computer, select “In Cell Western analysis” and start the acquisition.
2. Once acquired, align channels using the Image Studio™ Software.
3. Select all the wells in the “ICW wells” tab, and in the lower menu, go to “Grid Sheet” Tab and click in Copy (*see* **Note 8**).
4. Paste intensity measurements in an Excel sheet. Figure 5a shows an example of the raw data directly copied, without any modification, to an Excel sheet.
5. Revise the plate image and the raw intensity measurements to discard any outliers such as scraping the cells with the pipette tip or antibody specks, as in the case of the highlighted value represented in Fig. 5b, in which the antibody specks increase the 800-nm signal of the well. These wells are not included in the calculations, and they are highlighted for auditing purposes.
6. As shown in Fig. 5a, select in the 800-nm channel the rows without primary antibody to calculate the average background intensity.
7. Subtract from each sample’s intensity measurement acquired at the 800-nm channel the corresponding average background intensity value.
8. Normalize the previous values, dividing them by the corresponding intensity value measured in the 700-nm channel (CellTag™ 700 Stain), as shown in Fig. 5a (*see* **Note 9**).
9. Calculate average and SEM for each condition tested (i.e., non-treated, 100 nM AON and 300 nM AON).

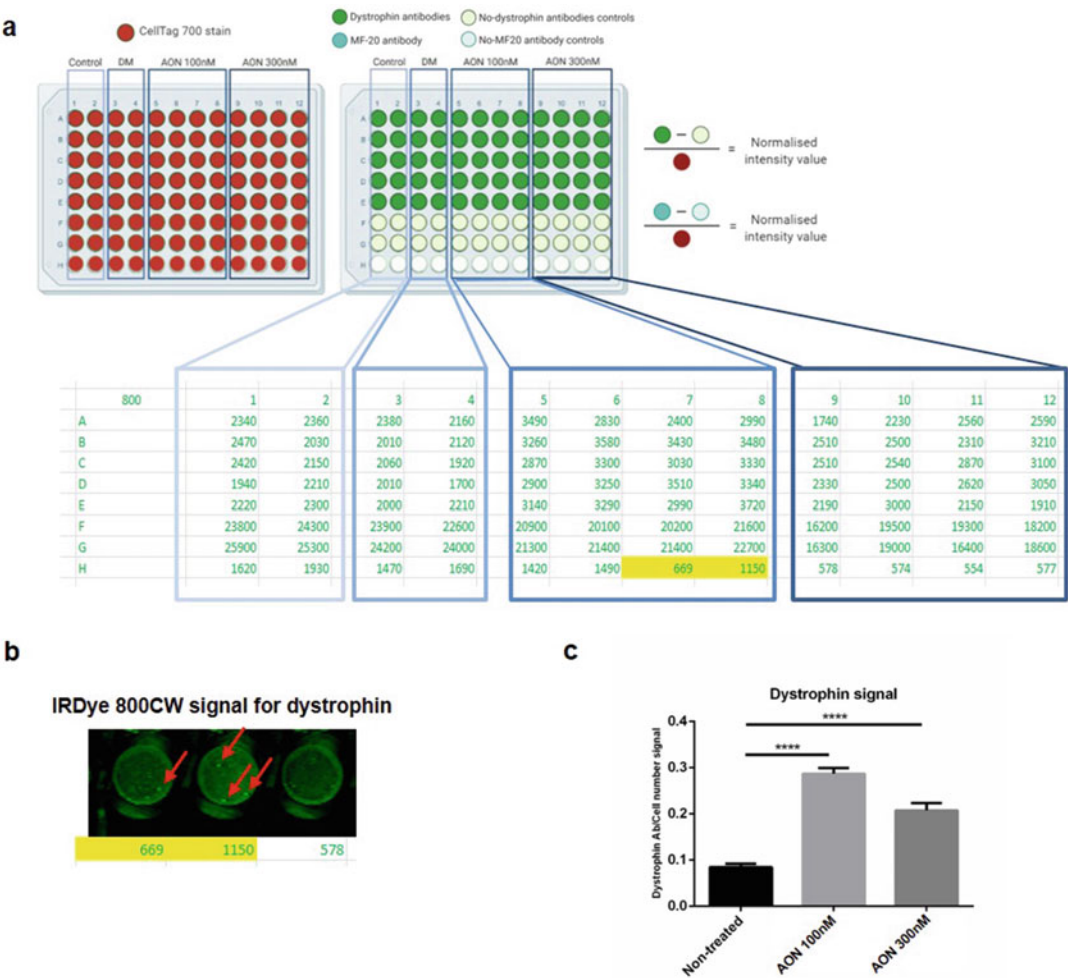


Fig. 5 In cell Western analysis. **(a)** Readings performed by the Odyssey Scan at 700 nm (Red, CellTag™ 700 Stain) and 800 nm (Green, Dystrophin, MF20 and background) provide a single intensity value for each well at each channel. To normalize each value, the corresponding background average value (no primary antibody) is subtracted from each value and later divided by its corresponding one for the CellTag™ 700 Stain signal (700 nm value). Created with [Biorender.com](#). **(b)** Example of omitted wells by antibody specks (marked with arrows) and its corresponding eliminated value. **(c)** Bar graph of data: average ± SEM of the two AON concentrations against control (lipofectamine only) and analysis by two-way ANOVA with multiple comparisons (**** $p < 0.0001$)

10. Evaluate MF20 values (as a measurement of culture differentiation) to critically assess the experiment: poor differentiation of the cultures may render unacceptable results (*see* **Note 10**).
11. Plot mean ± SEM in a bar graph as represented in Fig. 5c.

3.4 Concluding Remarks

The two methods described are complementary in their assessment of the exon skipping capacity of an AON: semi-quantification of the skipped product at RNA level plus dystrophin quantification at

protein level. As seen in the example we used, they show concordant results supports AON suitability for dystrophin restoration in preclinical studies.

4 Notes

1. Different RNA extraction and RT-PCR kits or techniques may be used according to the usual protocols of the laboratory.
2. The AON used in this example skips exon 51, and the cell culture is missing exon 52. We are using primers in the vicinity; these will need to be adapted to the specific regions studied. Many different primer combinations may be used, but they should always produce a larger product in the first round and a smaller one in the second one. In our example, the first PCR primers (Table 1) target exons 48 (forward) and 54 (reverse), and the product of this reaction will be the template of the second PCR, using primers 49 (forward) and 53 (reverse). The final PCR product that will be visualized by gel electrophoresis will include exons 49, 50, 51, and 53 if not skipped, and the skipped product contains exons 49, 50, and 53 (Fig. 4a).
3. Cell number in 96-well plates for myoblot analysis should be adjusted as required depending on the proliferation rate and differentiation facility of the cell culture used. To improve cell attachment, it is advisable to incubate the plates for an hour at RT.
4. An edge effect might be observed when analyzing some plates. In that case, the plate layout in Fig. 3c is recommended in order to avoid non-reliable well signals. Blank wells should be filled with 100 µl of the preferred buffer to prevent evaporation.
5. Random or hexamer primers may be used for the RT reaction, but in our hands specific primers work best for *DMD* amplification.
6. In case some regions are difficult to amplify, one of the primers (forward or reverse) can be used again in the second PCR (e.g., first PCR primers 48F+54R and second PCR primers 48F + 53R).
7. Plates can be read with or without liquid (e.g., PBS or WB) indistinctly, although it is important to evaluate the Odyssey CLx Scan focus at least once with the desired condition in the plates selected for ICW.
8. This process needs to be done individually for each channel (700 nm and 800 nm measurements), as each time one set of values (700 nm or 800 nm) is added to the clipboard. Pay special attention to which channel is active at the time of copying the data.

9. CellTag™ 700 Stain accumulates in both nucleus and cytoplasm of permeabilized cells and provides a linear fluorescent signal across a wide range of cell types and cell numbers (<https://www.licor.com/bio/reagents/celltag-700-stain-for-in-cell-western-assays>). It is highly recommended to test linearity of fluorescent signal for each cell line of interest by staining different cell number wells with CellTag™ 700 Stain. Also, it is advisable to revise raw and normalized data values to assess normalization and variability for each experimental condition.
10. Assessing the cultures by visual examination is a good first quality control. MF20 values are expected to be similar and consistent for the experiment shown, and values may vary depending on the cell type, as patient's cells usually differentiate worse than controls.

Acknowledgments

This work was supported by funding from Health Institute Carlos III (ISCIII, Spain) and the European Regional Development Fund (ERDF/FEDER), “A way of making Europe” (grants CP12/03057 and PI15/00333), Basque Government (grants 2016111029), and Duchenne Parent Project Spain (grant 05/2016). V.A.-G. holds a Miguel Servet Fellowship from the ISCIII (CP117/00004), part-funded by ERDF/FEDER. P. S-M holds a Rio Hortega Fellowship from ISCIII (CM19/00104), part funded by ERDF/FEDER. P. S-M holds a Rio Hortega Fellowship from ISCIII (CM19/00104) V.A.-G. also acknowledges funding from Ikerbasque (Basque Foundation for Science). The authors declare that they have no conflict of interest.

References

1. Birnkrant DJ, Bushby K, Bann CM, Apkon SD, Blackwell A, Brumbaugh D, Case LE, Clemens PR, Hadjiyannakis S, Pandya S, Street N, Tomezsko J, Wagner KR, Ward LM, Weber DR, DMD Care Consideration Working Group (2018) Diagnosis and management of Duchenne muscular dystrophy, part 1: diagnosis, and neuromuscular, rehabilitation, endocrine, and gastrointestinal and nutritional management. *Lancet Neurol* 17:251. [https://doi.org/10.1016/S1474-4422\(18\)30024-3](https://doi.org/10.1016/S1474-4422(18)30024-3)
2. Anthony K, Cirak S, Torelli S, Tasca G, Feng L, Arechavala-Gomez V, Armaroli A, Guglieri M, Straathof CS, Verschuuren JJ, Aartsma-Rus A, Helderma-van den Enden P, Bushby K, Straub V, Sewry C, Ferlini A, Ricci E, Morgan JE, Muntoni F (2011) Dystrophin quantification and clinical correlations in Becker muscular dystrophy: implications for clinical trials. *Brain* 134(pt 12): 3547–3559. <https://doi.org/10.1093/brain/awr291>
3. Arechavala-Gomez V, Khoo B, Aartsma-Rus A (2014) Splicing modulation therapy in the treatment of genetic diseases. *Appl Clin Genet* 7:245–252. <https://doi.org/10.2147/TACG.S71506>
4. Echevarria L, Aupy P, Goyenvalle A (2018) Exon-skipping advances for Duchenne muscular dystrophy. *Hum Mol Genet*. <https://doi.org/10.1093/hmg/ddy171>
5. Aartsma-Rus A, Fokkema I, Verschuuren J, Ginjaar I, van Deutekom J, van Ommen GJ, den Dunnen JT (2009) Theoretic applicability

- of antisense-mediated exon skipping for Duchenne muscular dystrophy mutations. *Hum Mutat* 30(3):293–299. <https://doi.org/10.1002/humu.20918>
6. US Food and Drug Administration (FDA) (2016) FDA grants accelerated approval to first drug for Duchenne muscular dystrophy. <http://www.fda.gov/NewsEvents/Newsroom/PressAnnouncements/ucm521263.htm>. Accessed 24 Jan 2017
 7. Frank DE, Schnell FJ, Akana C, El-Husayni SH, Desjardins CA, Morgan J, Charleston JS, Sardone V, Domingos J, Dickson G, Straub V, Guglieri M, Mercuri E, Servais L, Muntoni F (2020) SKIP-NMD Study Group. Increased dystrophin production with golodirsen in patients with Duchenne muscular dystrophy. *Neurology* 94(21):e2270–e2282. <https://doi.org/10.1212/WNL.0000000000009233>. Epub 2020 Mar 5. PMID: 32139505; PMCID: PMC7357297
 8. Cirak S, Arechavala-Gomez V, Guglieri M, Feng L, Torelli S, Anthony K, Abbs S, Garralda ME, Bourke J, Wells DJ, Dickson G, Wood MJ, Wilton SD, Straub V, Kole R, Shrewsbury SB, Sewry C, Morgan JE, Bushby K, Muntoni F (2011) Exon skipping and dystrophin restoration in patients with Duchenne muscular dystrophy after systemic phosphorodiamidate morpholino oligomer treatment: an open-label, phase 2, dose-escalation study. *Lancet* 378(9791):595–605. [https://doi.org/10.1016/S0140-6736\(11\)60756-3](https://doi.org/10.1016/S0140-6736(11)60756-3)
 9. Dhillon S (2020) Viltolarsen: first approval. *Drugs* 80(10):1027–1031. <https://doi.org/10.1007/s40265-020-01339-3>
 10. US Food and Drug Administration (FDA) (2021) FDA approves targeted treatment for rare Duchenne muscular dystrophy mutation. <https://www.fda.gov/news-events/press-announcements/fda-grants-accelerated-approval-first-targeted-treatment-rare-duchenne-muscular-dystrophy-mutation>
 11. Popplewell LJ, Graham IR, Malerba A, Dickson G (2011) Bioinformatic and functional optimization of antisense phosphorodiamidate morpholino oligomers (PMOs) for therapeutic modulation of RNA splicing in muscle. *Methods Mol Biol* 709:153–178. https://doi.org/10.1007/978-1-61737-982-6_10
 12. Popplewell LJ, Adkin C, Arechavala-Gomez V, Aartsma-Rus A, de Winter CL, Wilton SD, Morgan JE, Muntoni F, Graham IR, Dickson G (2010) Comparative analysis of antisense oligonucleotide sequences targeting exon 53 of the human DMD gene: implications for future clinical trials. *Neuromuscul Disord* 20(2):102–110. <https://doi.org/10.1016/j.nmd.2009.10.013>
 13. Nguyen Q, Yokota T (2017) Immortalized muscle cell model to test the exon skipping efficacy for Duchenne muscular dystrophy. *J Pers Med* 7(4):13. <https://doi.org/10.3390/jpm7040013>
 14. Aartsma-Rus A, De Winter CL, Janson AA, Kaman WE, Van Ommen GJ, Den Dunnen JT, Van Deutekom JC (2005) Functional analysis of 114 exon-internal AONs for targeted DMD exon skipping: indication for steric hindrance of SR protein binding sites. *Oligonucleotides* 15(4):284–297. <https://doi.org/10.1089/oli.2005.15.284>
 15. Arechavala-Gomez V, Graham IR, Popplewell LJ, Adams AM, Aartsma-Rus A, Kinali M, Morgan JE, van Deutekom JC, Wilton SD, Dickson G, Muntoni F (2007) Comparative analysis of antisense oligonucleotide sequences for targeted skipping of exon 51 during dystrophin pre-mRNA splicing in human muscle. *Hum Gene Ther* 18(9):798–810. <https://doi.org/10.1089/hum.2006.061>
 16. Aartsma-Rus A, Janson AA, Kaman WE, Bremmer-Bout M, van Ommen GJ, den Dunnen JT, van Deutekom JC (2004) Antisense-induced multiexon skipping for Duchenne muscular dystrophy makes more sense. *Am J Hum Genet* 74(1):83–92. <https://doi.org/10.1086/381039>
 17. Hiller M, Falzarano MS, Garcia-Jimenez I, Sardone V, Verheul RC, Popplewell L, Anthony K, Ruiz-Del-Yerro E, Osman H, Goeman JJ, Mamchaoui K, Dickson G, Ferlini A, Muntoni F, Aartsma-Rus A, Arechavala-Gomez V, Datson NA, Spitali P (2018) A multicenter comparison of quantification methods for antisense oligonucleotide-induced DMD exon 51 skipping in Duchenne muscular dystrophy cell cultures. *PLoS One* 13(10):e0204485. <https://doi.org/10.1371/journal.pone.0204485>
 18. Anthony K, Feng L, Arechavala-Gomez V, Guglieri M, Straub V, Bushby K, Cirak S, Morgan J, Muntoni F (2012) Exon skipping quantification by quantitative reverse-transcription polymerase chain reaction in Duchenne muscular dystrophy patients treated with the antisense oligomer eteplirsén. *Hum Gene Ther Methods* 23(5):336–345. <https://doi.org/10.1089/hgtb.2012.117>
 19. Beekman C, Janson AA, Baghat A, van Deutekom JC, Datson NA (2018) Use of capillary Western immunoassay (Wes) for quantification of dystrophin levels in skeletal muscle of healthy controls and individuals with Becker and Duchenne muscular dystrophy. *PLoS One*

- 13(4):e0195850. <https://doi.org/10.1371/journal.pone.0195850>
20. Anthony K, Arechavala-Gomez V, Taylor LE, Vulin A, Kaminoh Y, Torelli S, Feng L, Janghra N, Bonne G, Beuvin M, Barresi R, Henderson M, Laval S, Loubakos A, Campion G, Straub V, Voit T, Sewry CA, Morgan JE, Flanigan KM, Muntoni F (2014) Dystrophin quantification: biological and translational research implications. *Neurology* 83(22):2062–2069. <https://doi.org/10.1212/WNL.0000000000001025>
 21. Ruiz-Del-Yerro E, Garcia-Jimenez I, Mamchaoui K, Arechavala-Gomez V (2018) Myoblots: dystrophin quantification by in-cell western assay for a streamlined development of Duchenne muscular dystrophy (DMD) treatments. *Neuropathol Appl Neurobiol* 44(5):463–473. <https://doi.org/10.1111/nan.12448>
 22. Aartsma-Rus A, Morgan J, Lonkar P, Neubert H, Owens J, Binks M, Montolio M, Phadke R, Datson N, Van Deutekom J, Morris GE, Rao VA, Hoffman EP, Muntoni F, Arechavala-Gomez V, workshop p (2019) Report of a TREAT-NMD/world Duchenne organisation meeting on dystrophin quantification methodology. *J Neuromuscular Dis* 6 (1): 147–159. doi:<https://doi.org/10.3233/JND-180357>
 23. Verheul RC, van Deutekom JC, Datson NA (2016) Digital droplet PCR for the absolute quantification of exon skipping induced by antisense oligonucleotides in (pre-)clinical development for Duchenne muscular dystrophy. *PLoS One* 11(9):e0162467. <https://doi.org/10.1371/journal.pone.0162467>
 24. Aartsma-Rus A, Arechavala-Gomez V (2018) Why dystrophin quantification is key in the eteplirsén saga. *Nat Rev Neurol* 14(8):454–456. <https://doi.org/10.1038/s41582-018-0033-8>
 25. Mamchaoui K, Trollet C, Bigot A, Negroni E, Chaouch S, Wolff A, Kandalla PK, Marie S, Di Santo J, St Guily JL, Muntoni F, Kim J, Philippi S, Spuler S, Levy N, Blumen SC, Voit T, Wright WE, Aamiri A, Butler-Brown G, Mouly V (2011) Immortalized pathological human myoblasts: towards a universal tool for the study of neuromuscular disorders. *Skelet Muscle* 1:34. <https://doi.org/10.1186/2044-5040-1-34>

Open Access This chapter is licensed under the terms of the Creative Commons Attribution 4.0 International License (<http://creativecommons.org/licenses/by/4.0/>), which permits use, sharing, adaptation, distribution and reproduction in any medium or format, as long as you give appropriate credit to the original author(s) and the source, provide a link to the Creative Commons license and indicate if changes were made.

The images or other third party material in this chapter are included in the chapter's Creative Commons license, unless indicated otherwise in a credit line to the material. If material is not included in the chapter's Creative Commons license and your intended use is not permitted by statutory regulation or exceeds the permitted use, you will need to obtain permission directly from the copyright holder.





Chapter 15

Generation of Human iPSC-Derived Myotubes to Investigate RNA-Based Therapies In Vitro

Pablo Herrero-Hernandez, Atze J. Bergsma, and W. W. M. Pim Pijnappel

Abstract

Alternative pre-mRNA splicing can be cell-type specific and results in the generation of different protein isoforms from a single gene. Deregulation of canonical pre-mRNA splicing by disease-associated variants can result in genetic disorders. Antisense oligonucleotides (AONs) offer an attractive solution to modulate endogenous gene expression through alteration of pre-mRNA splicing events. Relevant in vitro models are crucial for appropriate evaluation of splicing modifying drugs. In this chapter, we describe how to investigate the splicing modulating activity of AONs in an in vitro skeletal muscle model, applied to Pompe disease. We also provide a detailed description of methods to visualize and analyze gene expression in differentiated skeletal muscle cells for the analysis of muscle differentiation and splicing outcome. The methodology described here is relevant to develop treatment options using AONs for other genetic muscle diseases as well, including Duchenne muscular dystrophy, myotonic dystrophy, and facioscapulohumeral muscular dystrophy.

Key words Splicing, Human iPSC, Skeletal muscle, Antisense oligonucleotides, In vitro models

1 Introduction

Pre-mRNA splicing is a highly conserved process in eukaryotes that plays a role in pre-mRNA processing. Alternative splicing can diversify gene function to produce isoforms with specific functions in distinct cell types [1, 2]. Genetic variations can lead to defects in pre-mRNA splicing that cause human disease [3]. Modulation of pre-mRNA splicing can be directed to correct aberrant splicing, to skip protein coding variants, to restore the reading frame, or to prevent expression of toxic gene products. This is possible by targeting antisense oligonucleotides (AONs) toward canonical splice sites or to *cis*-acting regulatory elements such as cryptic splice sites or splicing silencers/enhancers [4]. Alternative splicing in skeletal muscle is abundant and essential for muscle development and function [5]. Deregulation of pre-mRNA splicing in skeletal muscle is known to be the underlying cause of multiple human

myopathies [5]. Suitable in vitro and in vivo models are crucial to investigate novel splicing modulating drugs in target cells and tissues.

In vitro human skeletal muscle models can be obtained directly from muscle biopsies, or these can be generated by (*trans*-)differentiation of primary fibroblasts, pluripotent stem cells, or non-muscle cells with myogenic capacity like pericytes and mesoangioblasts [6–8]. Several protocols have been described to generate muscle progenitor cells (MPCs) derived from human patient-derived induced pluripotent stem cells (hiPSCs) using directed differentiation methods for disease modeling [9–11].

Here we describe how purified, expandable hiPSC-derived MPCs, generated using a transgene-free procedure [11] can be differentiated into multinucleated myotubes to test the modulating activity of AONs. These methods can be used to analyze splicing correction in vitro to develop RNA-based therapies for muscle disorders. We have used this strategy to test AONs for Pompe disease [12] and describe the methodology here in detail.

2 Materials

All cell culture work needs to be performed under sterile conditions in safety cabinets. All cell lines should be tested for mycoplasma following the manufacturer instructions (Lonza; LT07-318). Cell lines are cultured at 5% CO₂ and 37 °C in humidified incubators.

2.1 Skeletal Muscle Progenitor Cell Culture

1. Human MPC lines (*see Note 1*).
2. DMEM 4.5 g/L Glucose.
3. Fetal Bovine Serum.
4. Penicillin/Streptomycin/Glutamine 100× (p/s/g).
5. Fibroblast Growth Factor 2 (FGF2) (*see Note 2*).
6. Sterile cell culture grade Bovine Serum Albumin (7.5% BSA).
7. TrypLE™ Express Enzyme (1×), phenol red.
8. Phosphate Buffered Saline (DPBS).
9. Extracellular Matrix gel from Engelbreth (ECM; 1×).
10. DMEM:F12.
11. Insulin/Transferrin/Selenium 100×.
12. DMSO.
13. Freezing containers.

2.2 Cell Culture Media

1. Proliferation medium: DMEM 4.5 g/L Glucose, supplemented with 10% FBS, 1× Pen/Strep, and 100 ng/ml FGF2 (added directly to plate/well).

2. Differentiation medium: DMEM:F12, supplemented with 1× ITS-X and 1× Pen/Strep.

2.3 Antisense Oligonucleotide Design and Delivery

1. Phosphorodiamidate morpholino oligomer (PMO) AONs (Gene Tools, LLC.)
2. Endoportor (Gene Tools, LLC.)
3. MilliQ filtered sterile water.

2.4 Immunofluorescence

1. 4% Paraformaldehyde (diluted from a 32% solution in PBS).
2. 0.1% Tween (diluted in PBS from a 100% solution).
3. 0.3% Triton-X100 (diluted in PBS from a 100% solution).
4. Bovine Serum Albumin (BSA).
5. Primary antibodies: Mouse-α-MYH1E (1:50, MF20 supernatant, DSHB), Rabbit-α-MYOGENIN (1:100, sc-576, Santa Cruz), Rabbit-α-MYOD (1:100, sc-304, Santa Cruz), Mouse-α-PAX7 (1:100, concentrate, DSHB).
6. Secondary antibodies: Horse-α-mouse biotin (1:250, Vector Laboratories), Alexa Fluor-594-a-goat, Alexa Fluor-488-α-mouse, Alexa Fluor-594-α-rabbit, Alexa Fluor-488-α-rabbit (1:500, Invitrogen).
7. Tertiary: Streptavidin 594 (1:500, Invitrogen, S-32356).
8. Hoechst 33342 (1:15,000, Invitrogen, H3570).
9. Nikon wide field microscope (10× and 20× objectives).

2.5 RNA Isolation, cDNA Synthesis, and Quantitative RT-PCR (RT-qPCR)

1. RNA isolation kit.
2. cDNA Synthesis kit.
3. iTaq Universal SYBR Green Supermix.
4. Hard-Shell 96-Well PCR Plates.
5. Thermocycler.
6. Real-time thermocycler.
7. Spectrophotometer.
8. Agarose.
9. Ethidium Bromide.
10. Primers (*see* Table 1).

Table 1
Primers used for RT-qPCR

Primer target	Sequence (5' to 3')
<i>MYOD</i> fw	CACTCCGGTCCCAAATGTAG
<i>MYOD</i> rv	TTCCCTGTAGCACCACACAC
<i>MYOG</i> fw	CACTCCCTCACCTCCATCGT
<i>MYOG</i> rv	CATCTGGGAAGGCCACAGA
<i>LAMP1</i> fw	GTGTTAGTGGCACCCAGGTC
<i>LAMP1</i> rv	GGAAGGCCTGTCTTGTTTCAC
<i>LAMP2</i> fw	CCTGGATTGCGAATTTTACC
<i>LAMP2</i> rv	ATGGAATTCTGATGGCCAAA

3 Methods

3.1 Expansion, Cryopreservation, and Differentiation of MPCs

3.1.1 Expansion

1. MPCs grow optimally when the confluency is between 30 and 90%. It is important to maintain this cell density throughout the expansion (*see Note 3*).
2. Plate cells onto ECM coated plates (*see Note 4*). Coat plates using a solution of ECM (1:200) diluted in Proliferation medium without FGF2. Coating solution is left on the plates for 30 min at RT.
3. For cell detachment, first wash plates in pre-warmed PBS at 37 °C and then treat the cells with a 1:1 pre-warmed solution of TrypLE™ Express Enzyme and PBS (3 ml for 10 cm plates) for 3–5 min at 37 °C.
4. Collect cells using 5 volumes of Proliferation medium and centrifuge for 4 min at $200 \times g$.
5. Resuspend cells using Proliferation medium, transfer to pre-coated plates (remove coating solution, do not wash), and add 100 ng/ml of FGF2 directly into the plate (*see Note 5*).
6. Immediately transfer plates to a humidified incubator and perform cross movements to ensure appropriate cell spreading and mixing of FGF2.

3.1.2 Freeze-Thaw

1. Thaw vials of MPCs in a pre-warmed water bath, transfer cell suspension slowly into 5 volumes of Proliferation medium (no FGF2), and centrifuge for 4 min at $200 \times g$.
2. Plate cells in pre-coated plates using Proliferation medium plus 100 ng/ml of FGF2 freshly added to the cells.

- Freeze cells using Proliferation medium (plus 100 ng/ml FGF2) and 10% DMSO in 1 ml cryovials and store in freezing containers at -80°C for 24 h (at least) prior to long-term storage in liquid nitrogen tanks.

3.1.3 Differentiation into Multinucleated Myotubes

- Grow cells to reach $>90\%$ confluency (avoid 100% confluency) and then switch to Differentiation medium for 4 days without refreshing (*see* **Note 6**). Wide field images of differentiated myotubes are shown in Fig. 1.

3.2 Delivery and Efficacy of Antisense Oligonucleotides in Patient-Derived Myotubes

3.2.1 Transfection

- Resuspend the PMO AONs in RNase-free MilliQ at a concentration of 1 mM.
- Add 4.5 μl of Endoport reagent per ml of medium directly to the cells and mix by gentle shaking (*see* **Note 7**).
- Add the desired amount of PMO AONs to the cells and mix by gentle shaking.
- Transfect AONs 1 day prior differentiation (day -1). Cells should be 60–80% confluent.
- Switch to differentiation medium (day 0).
- Leave cells to differentiate for 4 days and either collect protein or RNA or fix cells for immunofluorescence.

3.2.2 Immunofluorescence

- For immunofluorescence analysis of patient-derived myotubes, prepare cells using 48-well plates.
- Wash cells once in PBS.
- Fix cells using 4% PFA in PBS for 10 min at RT, remove and add PBS. Cells can be stored at 4°C before proceeding.
- Wash twice in PBS for 2 min each.
- Incubate for 10 min with 0.3% Triton-X100 in PBS for permeabilization.
- Incubate for 30 min with 3% BSA, 0.1% Tween in PBS for blocking.
- Repeat washing **step 4**.
- Incubate with primary antibodies for 1 h at RT in 0.1% BSA, 0.1% Tween in PBS (*see* **Note 8**).
- Repeat washing **step 4**.
- Incubate with secondary antibodies for 45 min at RT in 0.1% BSA, 0.1% Tween in PBS.
- Repeat washing **step 4**.
- If biotinylated antibodies were used, incubate with tertiary for 30 min at RT in 0.1% BSA, 0.1% Tween in PBS.
- Repeat washing **step 4**.

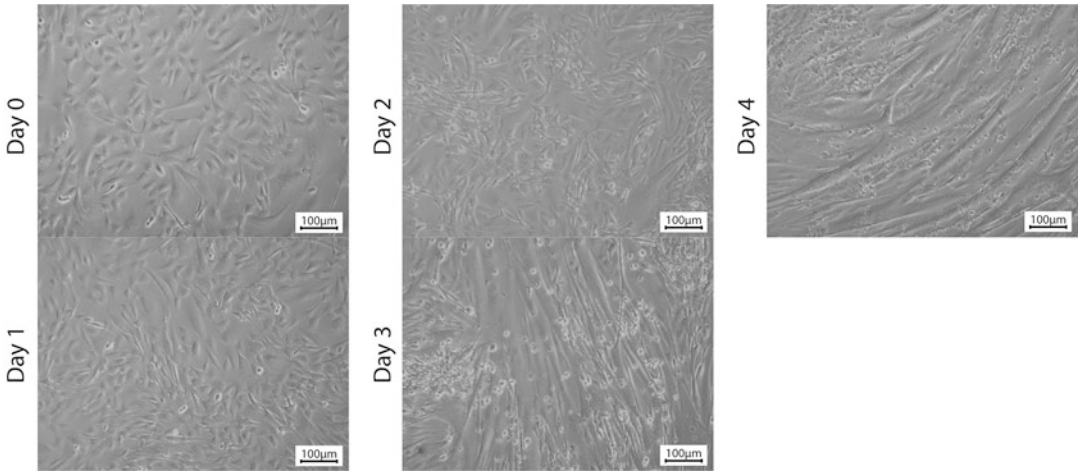


Fig. 1 Wide field images of differentiating MPCs. Representative images of the differentiation of MPCs over 4 days. Scale bar 100 μ m

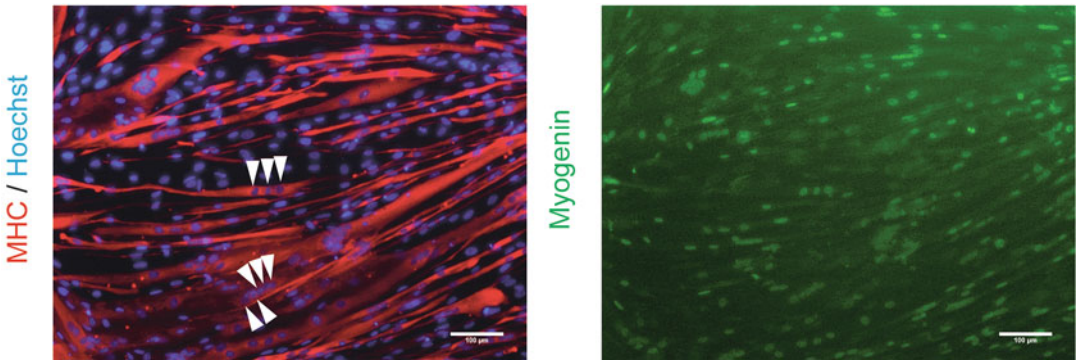


Fig. 2 Immunofluorescence images of 4 days differentiated MPCs. MPCs were stained with MYH1E (red), MYOGENIN (green), and the nuclei with Hoechst (blue). Arrowheads indicate nuclei present in multinucleated myotubes. Scale bar 100 μ m

14. Counterstain with Hoechst nuclear staining (1:15,000) in PBS for 10 min.
15. Remove and add PBS.
16. Take images of five random fields with 10 \times or 20 \times lens in MYH1E-stained myotubes (*see* Fig. 2) to calculate the fusion index. The fusion index is determined as the percentage of nuclei present in multinucleated MYH1E-positive cells (>2 nuclei in one cell) with respect to the total number of nuclei.

3.2.3 RT-qPCR

1. Harvest RNA after 4 days of differentiation using 350 μ l of the lysis buffer (or the amount indicated in the first step of the RNA isolation kit) per well of a 12 well-plate.

2. Purify RNA following the instructions of the preferred RNA isolation kit.
3. Retrotranscribe 300–500 ng of total RNA into cDNA using a cDNA Synthesis Kit.
4. Dilute cDNA samples 10× and prepare the qPCR using iTaq Universal SYBR Green Supermix.
5. Amplify the cDNA of interest using a Real Time System.
6. To analyze alternative splice variants in patient-derived myotubes, we normalize gene expression using each of the following four genes: *MYOD*, *MYOG* (*Myogenin*), *LAMP1*, and *LAMP2* (see **Note 9**). Gene expression is calculated using the ΔCt method for each housekeeping gene. Thereafter, the average value of the four normalized expression values is calculated.

4 Notes

1. Here we only used transgene-free derived muscle progenitor cells from hiPSCs as described in [11]. However, we anticipate that other sources of myogenic cells would also be applicable.
2. The FGF2 stock powder is dissolved in 0.1% BSA (sterile cell culture-grade BSA diluted in PBS and filtered using a 0.22- μm filter) and aliquoted using tips and tubes that were coated with 0.2% BSA in PBS. The dissolved FGF2 can be stored at $-80\text{ }^{\circ}\text{C}$. Each aliquot is used for maximally 1 week after thawing (kept at $4\text{ }^{\circ}\text{C}$) and 100 ng/ml is added directly to the cell culture medium every 2 days. When adding FGF2 every 2 days, this can be done without refreshing cell culture media. However, cell culture media must be refreshed every 3 days.
3. MPCs spontaneously differentiate at a confluency of $>90\%$ and loose proliferative capacity in culture.
4. Here we only used ECM for our studies. However, we anticipate that other coating materials can be used as well.
5. We typically plate a 1/4 or 1/6 dilution of cells to get a 60–90% confluency in 2 days and 3 days, respectively, using the same plate surface area.
6. There are different methods to differentiate MPCs into multinucleated myotubes [9–12]. For these studies we used DMEM:F12, $1\times$ ITS-X, $1\times$ p/s/g for 4 days without refreshing. Longer differentiation periods might result in cell detachment due to spontaneous contraction.
7. Endoport reagent is specifically designed for transfection of PMO AONs and was used by us in the following studies [4, 11]. Endoport reagent does not form a complex with AONs, but it enhances endocytosis in cells. The amount of

Endoporters used are independent of the concentration of PMO AONs. Other backbones might require different delivery reagents.

8. The following proteins are commonly used to assess myogenic potential of differentiating MPCs across species: Myosin heavy chain (MYH1E, cytoplasmic), Myogenin (MYOG, nuclear), and MYOD (nuclear). PAX7 (nuclear) can be used to identify the muscle stem cell fraction.
9. To normalize gene expression, we observed that the following genes involved in myogenesis: *MYOD* and *MYOG*; and the following involved in lysosome biogenesis: *LAMP1* and *LAMP2*; do not change expression levels among patient and healthy donor derived myotubes. We used these genes in this study [12].

Acknowledgments

We thank Erik van der Wal for the critical reading and the revisions of this manuscript. This work was funded by Tex net, the Prinses Beatrix Spierfonds/Stichting Spieren voor Spieren (grant W. OR13-21), the Sophia Children's Hospital Foundation (SSWO) (grant S-687 and S17-32), and Metakids (grant 2016-063).

References

1. Shapiro MB, Senapathy P (1987) RNA splice junctions of different classes of eukaryotes: sequence statistics and functional implications in gene expression. *Nucleic Acids Res* 15(17): 7155–7174. <https://doi.org/10.1093/nar/15.17.7155>
2. Lei Q, Li C, Zuo Z, Huang C, Cheng H, Zhou R (2016) Evolutionary insights into RNA trans-splicing in vertebrates. *Genome Biol Evol* 8(3):562–577. <https://doi.org/10.1093/gbe/evw025>
3. Bergsma AJ, van der Wal E, Broeders M, van der Ploeg AT, Pijnappel WWM (2018) Alternative splicing in genetic diseases: improved diagnosis and novel treatment options. *Int Rev Cell Mol Biol* 335:85–141. <https://doi.org/10.1016/bs.ircmb.2017.07.008>
4. van der Wal E, Bergsma AJ, Pijnenburg JM, van der Ploeg AT, Pijnappel W (2017) Antisense oligonucleotides promote exon inclusion and correct the common c.-32-13T>G GAA splicing variant in Pompe disease. *Mol Ther Nucleic Acids* 7:90–100. <https://doi.org/10.1016/j.omtn.2017.03.001>
5. Pistoni M, Ghigna C, Gabellini D (2010) Alternative splicing and muscular dystrophy. *RNA Biol* 7(4):441–452. <https://doi.org/10.4161/rna.7.4.12258>
6. Baghdadi MB, Tajbakhsh S (2018) Regulation and phylogeny of skeletal muscle regeneration. *Dev Biol* 433(2):200–209. <https://doi.org/10.1016/j.ydbio.2017.07.026>
7. Ito N, Kii I, Shimizu N, Tanaka H, Takeda S (2017) Direct reprogramming of fibroblasts into skeletal muscle progenitor cells by transcription factors enriched in undifferentiated subpopulation of satellite cells. *Sci Rep* 7(1): 8097. <https://doi.org/10.1038/s41598-017-08232-2>
8. Selvaraj S, Kyba M, Perlingeiro RCR (2019) Pluripotent stem cell-based therapeutics for muscular dystrophies. *Trends Mol Med* 25(9): 803–816. <https://doi.org/10.1016/j.molmed.2019.07.004>
9. Choi IY, Lim H, Estrellas K, Mula J, Cohen TV, Zhang Y, Donnelly CJ, Richard JP, Kim YJ, Kim H, Kazuki Y, Oshimura M, Li HL, Hotta A, Rothstein J, Maragakis N, Wagner KR, Lee G (2016) Concordant but varied

- phenotypes among Duchenne muscular dystrophy patient-specific myoblasts derived using a human iPSC-based model. *Cell Rep* 15(10):2301–2312. <https://doi.org/10.1016/j.celrep.2016.05.016>
10. Hicks MR, Hiserodt J, Paras K, Fujiwara W, Eskin A, Jan M, Xi H, Young CS, Evseenko D, Nelson SF, Spencer MJ, Handel BV, Pyle AD (2018) ERBB3 and NGFR mark a distinct skeletal muscle progenitor cell in human development and hPSCs. *Nat Cell Biol* 20(1):46–57. <https://doi.org/10.1038/s41556-017-0010-2>
 11. van der Wal E, Herrero-Hernandez P, Wan R, Broeders M, In 't Groen SLM, van Gestel TJM, van Ijcken WFJ, Cheung TH, van der Ploeg AT, Schaaf GJ, Pijnappel W (2018) Large-scale expansion of human iPSC-derived skeletal muscle cells for disease modeling and cell-based therapeutic strategies. *Stem cell Rep* 10(6):1975–1990. <https://doi.org/10.1016/j.stemcr.2018.04.002>
 12. van der Wal E, Bergsma AJ, van Gestel TJM, In 't Groen SLM, Zachres H, Arauzo-Bravo MJ, Scholer HR, van der Ploeg AT, Pijnappel W (2017) GAA deficiency in Pompe disease is alleviated by exon inclusion in iPSC-derived skeletal muscle cells. *Mol Ther Nucleic Acids* 7:101–115. <https://doi.org/10.1016/j.omtn.2017.03.002>

Open Access This chapter is licensed under the terms of the Creative Commons Attribution 4.0 International License (<http://creativecommons.org/licenses/by/4.0/>), which permits use, sharing, adaptation, distribution and reproduction in any medium or format, as long as you give appropriate credit to the original author(s) and the source, provide a link to the Creative Commons license and indicate if changes were made.

The images or other third party material in this chapter are included in the chapter's Creative Commons license, unless indicated otherwise in a credit line to the material. If material is not included in the chapter's Creative Commons license and your intended use is not permitted by statutory regulation or exceeds the permitted use, you will need to obtain permission directly from the copyright holder.





Eye on a Dish Models to Evaluate Splicing Modulation

Kwan-Leong Hau, Amelia Lane, Rosellina Guarascio,
and Michael E. Cheetham

Abstract

Inherited retinal dystrophies, such as Leber congenital amaurosis, Stargardt disease, and retinitis pigmentosa, are characterized by photoreceptor dysfunction and death and currently have few treatment options. Recent technological advances in induced pluripotent stem cell (iPSC) technology and differentiation methods mean that human photoreceptors can now be studied in vitro. For example, retinal organoids provide a platform to study the development of the human retina and mechanisms of diseases in the dish, as well as being a potential source for cell transplantation. Here, we describe differentiation protocols for 3D cultures that produce retinal organoids containing photoreceptors with rudimentary outer segments. These protocols can be used as a model to understand retinal disease mechanisms and test potential therapies, including antisense oligonucleotides (AONs) to alter gene expression or RNA processing. This “retina in a dish” model is well suited for use with AONs, as the organoids recapitulate patient mutations in the correct genomic and cellular context, to test potential efficacy and examine off-target effects on the translational path to the clinic.

Keywords Retinal organoids, Induced pluripotent stem cells, Differentiation, 3D culture, Retinal degeneration, Photoreceptor, Retina in a dish

1 Introduction

The dysfunction and death of photoreceptor cells are associated with inherited retinal diseases (IRDs), which are a major cause of blindness. The lack of effective treatment to prevent loss of photoreceptors means these diseases are currently irreversible. Recent progress in the differentiation of stem cells to retinal cells has enabled the generation of functional retinal organoids in vitro or a “retina in a dish” [1–4]. By recapitulating the retina from patient-derived induced pluripotent stem cells (iPSC), retinal organoids offer a platform for developing therapeutic treatments and modeling patient disease [5, 6].

A dynamic and complex microenvironment is involved in eye development, including direct and indirect cell–cell interaction and specific signaling regulation in different stages of development

[7]. Because of this complex microenvironment, retinal organoids have the potential to develop a more mature retina than photoreceptors differentiated in 2D conditions only. Several studies have shown that with defined culture conditions, embryonic stem cells (ESC), and iPSC can be differentiated into retinal organoids in a 3D environment, producing a laminated retina that mimics the in vivo human retina [2, 3, 8]. In addition to recapitulating the structure of native eye development, rudimentary disorganized outer segments can be observed in photoreceptors from retinal organoids.

In this chapter, we describe three different methods to differentiate iPSC to retinal organoids in 3D. Retinal organoids generated from these protocols are well laminated with photoreceptors in their outer layer and develop rudimentary outer segments. Importantly, they also recapitulate photoreceptor mRNA processing and the exquisite pattern of alternative splicing they present [9–11]. This makes retinal organoids ideal for studying aberrant splicing events associated with patient variants in several forms of IRDs [9, 12]. Furthermore, they can then be applied to the development of antisense oligonucleotides (AONs) as potential treatments [9, 13].

2 Materials

2.1 General Materials

1. U-bottom ultra-low 96-well plate.
2. 25-well plate low attachment.
3. 6-well plate.
4. Ultra-low adhesion 6-well plate.
5. Crescent knife.
6. Retinoic acid (RA).

2.2 iPSC Culture

1. Essential 8 Flex medium.
2. Geltrex.
3. Cell dissociation buffer (ThermoFisher).

2.3 EB Suspension Protocol

1. EB2 base medium: GMEM, 20% Knock-Out Serum, 1% Sodium pyruvate, 1% NEAA, and 110 μ M 2-Mercaptoethanol (*see Note 1*).
2. NR media (NRM): DMEM/F12, 1% N₂ Supplement, 10% FBS, and 1% NEAA (*see Note 1*).
3. V-bottom 96-well plate.
4. IWR-1c (Wnt inhibitor).
5. Rock inhibitor (Y-27632).

6. Matrigel (growth factor reduced).
7. Hedgehog smoothened agonist (SAG).
8. TrypLE.

2.4 EB Adherent Protocol

1. Neural induction medium (NIM): DMEM/F-12 (1:1), 1% N₂ supplement, 1% NEAA, and Heparin 2 µg/ml (*see Note 1*).
2. Retinal Differentiation Medium (RDM): DMEM/F12 (3:1), 2% B27 (without Vitamin A), 1% NEAA, and 1% Pen/Strep (*see Note 1*).
3. Neural Retina Maturation Medium 1 (RMM1): DMEM/F12 (3:1), 2% B27 (without vitamin A), 1% NEAA, 1% Pen/Strep, 10% FBS, 100 µM Taurine, and 1% Glutamax (*see Note 1*).
4. Neural Retina Maturation Medium 2 (RMM2): DMEM/F12 (3:1), 1% N₂, 1% NEAA, 1% Pen/Strep, 10% FBS, 100 µM Taurine, and 1% Glutamax (*see Note 1*).
5. Blebbistatin.

2.5 Non-EB Adherent Protocol

1. Essential 6 medium (ThermoFisher).
2. Neural induction Medium (NIM): Advanced DMEM/F12, 1% N₂ supplement, 1% NEAA, 1% Glutamax, and 1% Pen/Strep (*see Note 1*).
3. Retinal Differentiation Media (RDM): DMEM/F12 (3:1), 1% Pen/Strep, 1% NEAA, and 2% B27 (*see Note 1*).
4. Neural Retina Maturation Medium 1 (RMM1): DMEM/F12 (3:1), 1% Pen/Strep, 2% B27, 10% FBS, 100 µM Taurine, 1% NEAA, and 1% Glutamax (*see Note 1*).
5. Neural Retina Maturation Medium 2 (RMM2): DMEM/F12 (3:1), 1% Pen/Strep, 2% B27 (without vitamin A), 1% N₂, 10% FBS, 100 µM Taurine, 1% NEAA, and 1% Glutamax (*see Note 1*).

2.6 RNA Extraction

1. RNA mini kit.
2. PBS.
3. Micropestle.

3 Methods

iPSC are maintained with Essential 8 Flex (E8F) in Geltrex coated 6-well plates (*see Note 2*). Once they reach 70% confluence, iPSC are treated with 500 µl cell dissociation buffer for 2 min at 37 °C in the incubator. After the incubation, remove the cell dissociation buffer and add 1 ml of E8F into a well. Use 1 ml tip scraping the well to collect iPSC in small clumps. Cell clumps are collected and

transferred into a new Geltrex-coated plate with 1 ml tip. Medium is changed every other day, and iPSC can be double-fed with 4 ml E8F to cover the weekend (*see* **Note 3**).

3.1 EB Suspension Protocol

This protocol is adapted from the method initially described by Sasai and colleagues [3].

1. Maintain iPSC in a 6-well plate as described earlier. Use 1 ml TrypLE to disperse cells into single cells. Collect the cell pellet after centrifugation at $300 \times g$ for 5 min and resuspend in 2 ml E8F with 10 μ M Rock inhibitor (ROCKi).
2. Place 10,000 cells per well with 100 μ l E8F with ROCKi in a V-bottom low attachment 96-well plate.
3. The next day, add 100 μ l E8F with ROCKi (Day 1).
4. Change half medium, 100 μ l, with EB2 with 10 μ M ROCKi, 3 μ M IWRe-1, and 2% Matrigel twice a week until Day 12.
5. Change half medium, 100 μ l, with EB2 with 3 μ M IWRe-1, 2% Matrigel, 10% FBS, and 100 nM SAG twice a week until Day 18.
6. Transfer cells into U-bottom ultra-low attachment 96-well plates, and the medium is switched to NRM supplemented with 0.5 μ M RA from Day 20 until Day 100. Change medium three times a week (Fig. 1) (*see* **Note 4**).
7. From Day 100, select and maintain laminated organoids in 25-well plates in NRM with no RA till collection day (Fig. 1) (*see* **Note 5**).

3.2 EB Adherent Protocol

This protocol is adapted from the method initially described by Canto-Soler and colleagues [2].

1. Collect the iPSC clusters, as described earlier, from three confluent wells (or one T25 flask) with E8F + 10 μ M Blebbistatin (*see* **Note 6**) and transfer the cell clumps into three wells (2 ml per well) of ultra-low adhesion 6-well plate to form the embryoid bodies (EB).
2. After 24 h (Day 1), use a 10-ml pipette to collect the EB into 15-ml falcon and centrifuge at $110 \times g$ for 2 min. Remove the supernatant and collect the EB with 6 ml medium of 75% E8F + 10 μ M Blebbistatin and 25% neural induction medium (NIM). Transfer the EB back to the wells, 2 ml in each well (*see* **Note 7**).
3. With the same technique described in **step 2**, change the medium to 50% E8F + 10 μ M Blebbistatin and 50% NIM on Day 2 and 100% NIM on Day 3 and Day 5 (*see* **Note 8**).
4. On Day 7, transfer EB from three wells to six wells of Geltrex-coated 6-well plate in NIM, 4 ml in each well. Gently mix the

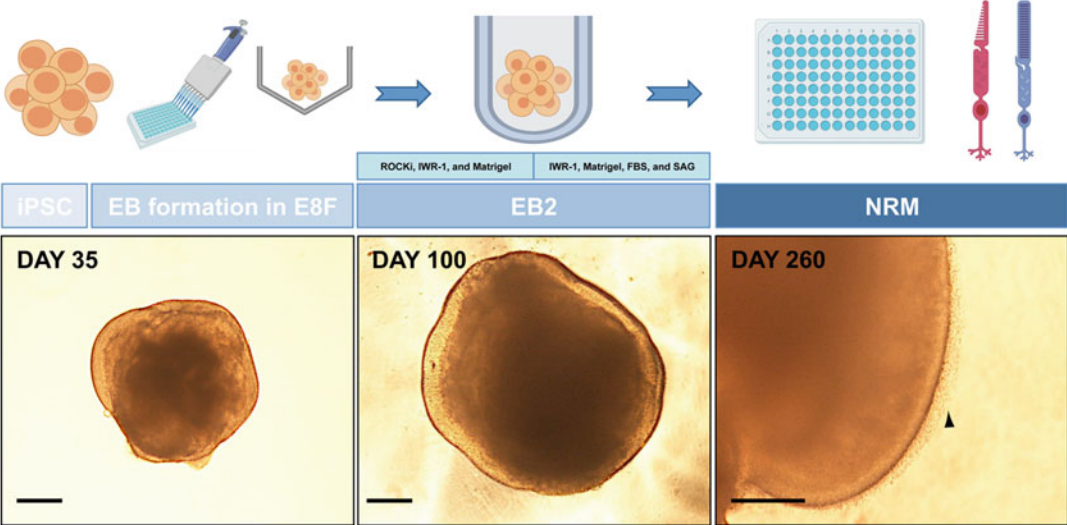


Fig. 1 EB suspension protocol. Top row: Schematic diagram of EB suspension protocol steps and media. Lower row: Representative organoids at different stages of differentiation are shown. Visible lamination can be observed at approximately Day 35 and good organoids can maintain the lamination and mature during differentiation to form an outer nuclear layer of photoreceptors with inner segment and outer segment (which can be seen by the “brush border,” arrowhead). Scale bar is 250 μm . The cartoon images are made with BioRender

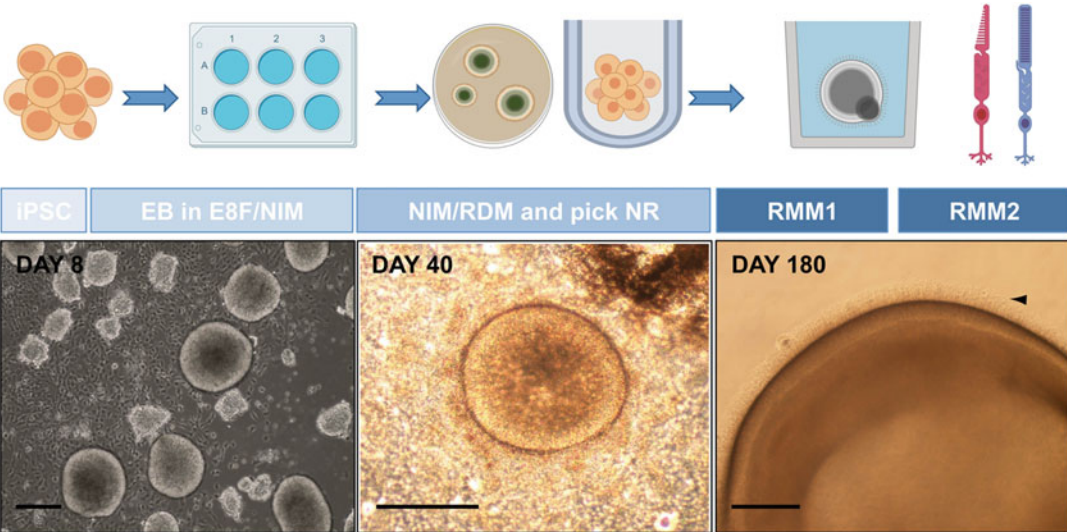


Fig. 2 EB adherent protocol. Top row: Schematic diagram of EB adherent protocol steps and media. Lower row: Representative images at different stages of differentiation are shown. EB formation in suspension is followed by attachment to Geltrex-coated wells and formation of NR. Picked NR successfully mature through the differentiation form an outer nuclear layer of photoreceptors with inner segment and outer segment (which can be seen by the “brush border,” arrowhead). Scale bar is 250 μm . The cartoon images are made with BioRender

medium in the wells to let the EB equally distributed in the wells (Fig. 2) (*see* **Note 2**).

5. Change 4 ml NIM medium twice a week until Day 15.
6. Feed the cells daily with retinal differentiation medium (RDM) from Day 16 until neural retina (NR) domains [9] are formed (Fig. 2).
7. Pick individual NR mechanically with a crescent knife using an inverted brightfield microscope (EvoSXL Core) in the safety cabinet in between Day 28 and Day 35 and culture in suspension in U-bottom ultra-low 96-well plates with RDM, one NR per well. Change medium three times a week (*see* **Notes 4 and 11**).
8. Switch medium to RMM1 from Day 42. Of note, 1 μ M RA is introduced from Day 63.
9. Switch medium to RMM2 with 0.5 μ M RA from Day 90 and RMM2 only from Day 100.
10. On Day 100, laminated retinal organoids can be observed with a microscope and are selected and transferred to 25-well plates with 1 ml medium (*see* **Note 5**).
11. Maintain retinal organoids in RMM2 until collection day.

3.3 Non-EB Adherent Protocol

This protocol is adapted from the method initially described by Ali and colleagues [8].

1. iPSC are maintained in 6-well plates as described earlier. E8F is switched to Essential 6 medium for 2 days when the cells reach 90–100% confluence (*see* **Note 9**).
2. Introduce 4 ml NIM from Day 3 and change the medium three times a week until the NR are formed (Fig. 3) (*see* **Note 10**).
3. Pick NR, as described in EB Adherent Protocol (*see* Subheading 3.2, **step 7**), and maintain in U-bottom ultra-low attachment 96-well plates with RDM up to 1 week (*see* **Notes 4 and 11**).
4. Switch medium from RDM to RMM1 for 4 weeks.
5. After 4 weeks with RMM1 only, introduce 1 μ M RA in RMM1 for 2 weeks.
6. Switch medium to RMM2 with 0.5 μ M RA until Day 100.
7. Visually confirmed laminated organoids are transferred to 25-well plates and maintained in RMM2 without B27 until collection day (Fig. 3) (*see* **Note 12**).

3.4 AON Treatment of Organoids

1. Mature organoids are generated from protocols described in the above sections.
2. Dilute AONs into working concentration (e.g., 0.1–10 μ M) with culture medium, depending on the methods (*see* **Note 13**).

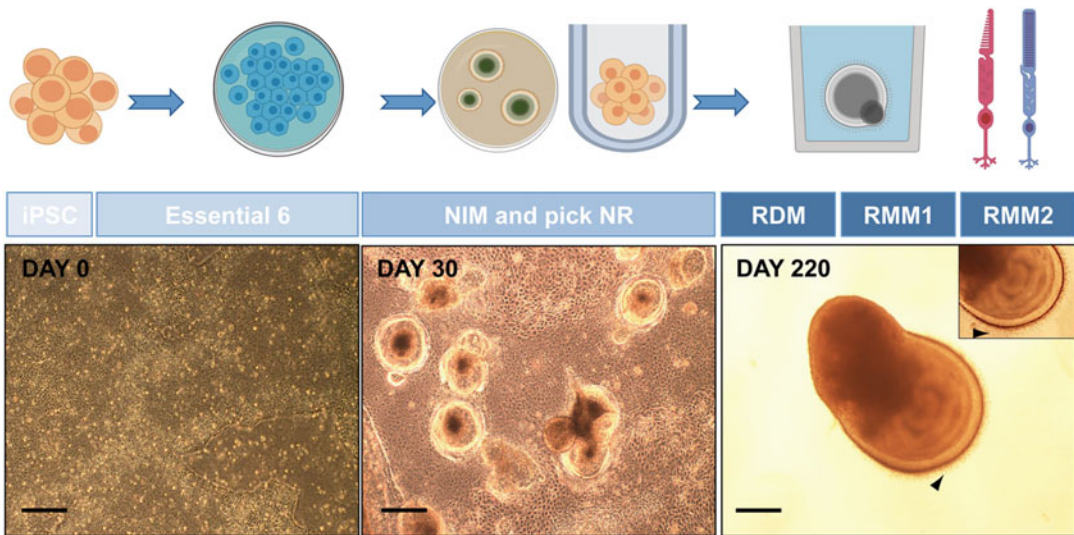


Fig. 3 Non-EB adherent protocol. Top row: Schematic diagram of non-EB adherent protocol steps and media. Lower row: Representative images at different stages of differentiation are shown. NR are formed in NIM medium, and picked NR cultured in suspension going through differentiation mature to form organoids with an outer nuclear layer of photoreceptors with inner segment and outer segment projecting outwards (which can be seen by the “brush border,” arrowhead). Scale bar is 250 μm . The cartoon images are made with BioRender

3. Remove the medium and treat organoids with media containing AONs (*see Note 14*).
4. Treat organoids with AONs two times a week with a full change of the medium containing the AON (*see Note 15*).
5. On the collection day, transfer the organoids into 1.5-ml microcentrifuge tubes with 1 ml PBS individually.
6. Remove PBS and keep the microcentrifuge tube on dry ice for 10 min.
7. RNA can be extracted immediately or the samples can be stored at -80°C (*see Note 16*).

3.5 RNA Extraction from Organoids

1. Samples are prepared as described in the previous step.
2. Homogenize organoids individually with micropestle in the microcentrifuge tube.
3. Add lysis buffer from RNA mini kit, in this case from Qiagen, and homogenize organoids again (*see Note 17*).
4. Follow the instruction of RNA extraction kit to finish RNA extraction and cDNA can then be synthesized.

3.6 Read-out

These methods can be used to produce laminated retinal organoids for the study of RNA processing and morphological changes associated with genomic variants and their potential correction with

AONs. The assays used for downstream analyses are dependent on the specific questions being asked. Routine analyses would usually involve RT-PCR and qPCR, but the organoids are also amenable to RNAseq, single-cell sorting, next-generation sequencing, or long-range sequencing. This can provide a unique insight into human photoreceptor splicing and its manipulation for discovery science or therapeutic benefit.

4 Notes

1. General. Once supplemented, the complete medium is stable for up to 2 weeks when stored in the fridge at 4 °C. Freshly made medium can be aliquoted and stored in the freezer at −20 °C for longer storage.
2. Geltrex from stock solution is diluted 50 times in DMEM/F12 medium and 1 ml diluted Geltrex is used to coat a well in a 6-well plate. Plate is coated at 37 °C in the incubator for an hour. EB will attach in the wells from this step.
3. General. Different iPSC clones might have different efficiency of differentiation using these methods. It is recommended to start with at least two of the protocols to test which method is more efficient for that specific clone. The retinal identity and correct lamination of organoids produced by any of the three described methods can be predicted by careful visual inspection under a microscope, but it must be verified by expression of mature retinal markers (e.g., recoverin, cone arrestin, rhodopsin, LM opsin) by immunofluorescence staining and/or gene expression assays.
4. Medium is changed three times a week for 96-well plates and two times a week for 25-well plates.
5. Cut the end of a 1-ml pipette tip off to transfer organoids from 96-well plates to 25-well plates. One retinal organoid per well of 25-well plates. More than one organoid in a well might cause them to merge together.
6. Three wells from a 6-well plate or one T25 flask are optimized conditions we use, but this vary depending on the size of the clumps and confluence of the iPSC. So this step may need to be optimized in each lab.
7. Be gentle while collecting and transferring EB from and into wells. Avoid breaking the EB into single cells.
8. Gamm and colleagues reported that a single dose of BMP4 at day 6 of differentiation, followed by one-half media changes every 3 days until day 16, improved NR production [14].

9. iPSCs need to reach almost 100% confluence, this is crucial for non-EB adherent protocol. Lower density might cause cell death and failure of the protocol. Essential 6 medium is changed daily.
10. For weekend feeding, 6 ml of NIM is used on Friday instead of 4 ml. NR are usually formed between week 4 and week 6.
11. At the NR picking step, it is recommended to pick as many as possible (or needed) to increase the number of mature organoids. Between 50% and 90% of the NR picked will not make it to mature laminated retinal organoids (dependent on cell line). Some fail to form organized neuroepithelium in suspension and some collapse in a later stage forming a ball of neuro-retinal rosettes that will not develop the full outer and inner retinal layers. It is necessary to account for this when designing experiments.
12. We find media without B27 from this stage may improve the organization of the inner retinal cell layers in organoids.
13. 0.1–10 μ M is the concentration range that we have tested for AONs (with phosphorothioate backbone and either 2'-*O*-methyl or 2'-*O*-methoxyethyl modifications). The working concentration might vary with different AONs, as this is empirical.
14. Gymnotic treatment with phosphorothioate backbone AONs is effective for retinal organoids. Addition of 6 μ M EndoPorter will assist morpholino uptake. To treat the organoids, 200 μ l of total volume is used in 96-well plates and 1 ml in 25-well plates.
15. Treatment time is empirical and will depend on the specific target or assay being used. We have used treatment times between 72 h and 4 weeks.
16. Nonsense mediated decay can be inhibited with emetine prior to sample collection, if it is suspected this is affecting the detection of aberrant transcripts.
17. A 30-gauge needle can be used to help homogenize organoids. 200–500 ng of RNA can be extracted per organoid.

Acknowledgments

This work is supported by Wellcome Trust, Fight for Sight, Foundation Fighting Blindness, Retina UK, Moorfields Eye Charity and NC3Rs. We would like to thank the other members of the Cheetham, Hardcastle, and van der Spuy groups past and present for their support, encouragement and help in iPSC and organoid

maintenance. We would also like to thank Anai Gonzalez-Cordero for advice on the non-EB adherent protocol.

References

- Gonzalez-Cordero A, West EL, Pearson RA, Duran Y, Carvalho LS, Chu CJ, Naeem A, Blackford SJI, Georgiadis A, Lakowski J, Hubank M, Smith AJ, Bainbridge JWB, Sowden JC, Ali RR (2013) Photoreceptor precursors derived from three-dimensional embryonic stem cell cultures integrate and mature within adult degenerate retina. *Nat Biotechnol* 31(8):741–747. <https://doi.org/10.1038/nbt.2643>
- Zhong X, Gutierrez C, Xue T, Hampton C, Vergara MN, Cao LH, Peters A, Park TS, Zambidis ET, Meyer JS, Gamm DM, Yau KW, Canto-Soler MV (2014) Generation of three-dimensional retinal tissue with functional photoreceptors from human iPSCs. *Nat Commun* 5:4047. <https://doi.org/10.1038/ncomms5047>
- Nakano T, Ando S, Takata N, Kawada M, Muguruma K, Sekiguchi K, Saito K, Yonemura S, Eiraku M, Sasai Y (2012) Self-formation of optic cups and storable stratified neural retina from human ESCs. *Cell Stem Cell* 10(6):771–785. <https://doi.org/10.1016/j.stem.2012.05.009>
- Meyer JS, Shearer RL, Capowski EE, Wright LS, Wallace KA, McMillan EL, Zhang SC, Gamm DM (2009) Modeling early retinal development with human embryonic and induced pluripotent stem cells. *Proc Natl Acad Sci U S A* 106(39):16698–16703. <https://doi.org/10.1073/pnas.0905245106>
- Gamm DM, Phillips MJ, Singh R (2013) Modeling retinal degenerative diseases with human iPS-derived cells: current status and future implications. *Expert Rev Ophthalmol* 8(3):213–216. <https://doi.org/10.1586/eop.13.14>
- Sasai Y (2013) Next-generation regenerative medicine: organogenesis from stem cells in 3D culture. *Cell Stem Cell* 12(5):520–530. <https://doi.org/10.1016/j.stem.2013.04.009>
- Bassett EA, Wallace VA (2012) Cell fate determination in the vertebrate retina. *Trends Neurosci* 35(9):565–573. <https://doi.org/10.1016/j.tins.2012.05.004>
- Gonzalez-Cordero A, Kruczek K, Naeem A, Fernando M, Kloc M, Ribeiro J, Goh D, Duran Y, Blackford SJI, Abelleira-Hervas L, Sampson RD, Shum IO, Branch MJ, Gardner PJ, Sowden JC, Bainbridge JWB, Smith AJ, West EL, Pearson RA, Ali RR (2017) Recapitulation of human retinal development from human pluripotent stem cells generates transplantable populations of cone photoreceptors. *Stem Cell Rep* 9(3):820–837. <https://doi.org/10.1016/j.stemcr.2017.07.022>
- Parfitt DA, Lane A, Ramsden CM, Carr AJ, Munro PM, Jovanovic K, Schwarz N, Kanuga N, Muthiah MN, Hull S, Gallo JM, da Cruz L, Moore AT, Hardcastle AJ, Coffey PJ, Cheetham ME (2016) Identification and correction of mechanisms underlying inherited blindness in human iPSC-derived optic cups. *Cell Stem Cell* 18(6):769–781. <https://doi.org/10.1016/j.stem.2016.03.021>
- Ling JP, Wilks C, Charles R, Leavey PJ, Ghosh D, Jiang L, Santiago CP, Pang B, Venkataraman A, Clark BS, Nellore A, Langmead B, Blackshaw S (2020) ASCOT identifies key regulators of neuronal subtype-specific splicing. *Nat Commun* 11(1):137. <https://doi.org/10.1038/s41467-019-14020-5>
- Kim S, Lowe A, Dharmat R, Lee S, Owen LA, Wang J, Shakoor A, Li Y, Morgan DJ, Hejazi AA, Cvekl A, DeAngelis MM, Zhou ZJ, Chen R, Liu W (2019) Generation, transcriptome profiling, and functional validation of cone-rich human retinal organoids. *Proc Natl Acad Sci U S A* 116(22):10824–10833. <https://doi.org/10.1073/pnas.1901572116>
- Buskin A, Zhu L, Chichagova V, Basu B, Mozaffari-Jovin S, Dolan D, Droop A, Collin J, Bronstein R, Mehrotra S, Farkas M, Hilgen G, White K, Pan KT, Treumann A, Hallam D, Bialas K, Chung G, Mellough C, Ding Y, Krasnogor N, Przyborski S, Zwolinski S, Al-Aama J, Alharthi S, Xu Y, Wheway G, Szymanska K, McKibbin M, Inglehearn CF, Elliott DJ, Lindsay S, Ali RR, Steel DH, Armstrong L, Sernagor E, Urlaub H, Pierce E, Luhrmann R, Grellscheid SN, Johnson CA, Lako M (2018) Disrupted alternative splicing for genes implicated in splicing and ciliogenesis causes PRPF31 retinitis pigmentosa. *Nat Commun* 9(1):4234. <https://doi.org/10.1038/s41467-018-06448-y>
- Dulla K, Aguila M, Lane A, Jovanovic K, Parfitt DA, Schulkens I, Chan HL, Schmidt I, Beumer W, Vorthoren L, Collin RWJ, Garanto A, Duijkers L, Brugulat-Panes A, Semo M, Vugler AA, Biasutto P, Adamson P,

- Cheetham ME (2018) Splice-modulating oligonucleotide QR-110 restores CEP290 mRNA and function in human c.2991+1655A>G LCA10 models. *Mol Ther Nucleic Acids* 12:730–740. <https://doi.org/10.1016/j.omtn.2018.07.010>
14. Capowski EE, Samimi K, Mayerl SJ, Phillips MJ, Pinilla I, Howden SE, Saha J, Jansen AD, Edwards KL, Jager LD, Barlow K, Valiauga R, Erlichman Z, Hagstrom A, Sinha D, Sluch VM, Chamling X, Zack DJ, Skala MC, Gamm DM (2019) Reproducibility and staging of 3D human retinal organoids across multiple pluripotent stem cell lines. *Development* 146(1). <https://doi.org/10.1242/dev.171686>

Open Access This chapter is licensed under the terms of the Creative Commons Attribution 4.0 International License (<http://creativecommons.org/licenses/by/4.0/>), which permits use, sharing, adaptation, distribution and reproduction in any medium or format, as long as you give appropriate credit to the original author(s) and the source, provide a link to the Creative Commons license and indicate if changes were made.

The images or other third party material in this chapter are included in the chapter's Creative Commons license, unless indicated otherwise in a credit line to the material. If material is not included in the chapter's Creative Commons license and your intended use is not permitted by statutory regulation or exceeds the permitted use, you will need to obtain permission directly from the copyright holder.





Chapter 17

Establishment of In Vitro Brain Models for AON Delivery

Elena Daoutsali and Ronald A. M. Buijsen

Abstract

Progress in stem cell biology has made it possible to generate human-induced pluripotent stem cells (hiPSC) that can be differentiated into complex, three-dimensional structures, where the cells are spatially organized. To study brain development, Lancaster and colleagues developed an hiPSC-derived three-dimensional organoid culture system, termed cerebral organoids, that develop various discrete, although interdependent, brain regions. Here we describe in detail the generation of cerebral organoids using a modified version of the culture protocol.

Key words Cerebral organoid, Disease modeling, Induced pluripotent stem cells

1 Introduction

Many brain disorders are hereditary diseases with a known genetic cause, which allowed scientists to generate animal models to study disease progression, understand disease mechanisms, and perform therapeutic intervention studies [1, 2]. However, (1) mice are different from humans, and it is difficult to translate results from animal experiments into clinical application; (2) the genetic cause of many diseases is not yet known; (3) many disease-causing genes are mainly expressed in the cells that are affected; (4) for many of them, there are no (humanized-)mouse models available; (5) there is governmental and public pressure to advance the development of alternative model systems to replace animal studies. This emphasizes the need for patient-derived disease models that bridge the translational gap between animal models and human clinical trials. Progress in stem cell biology has made it possible to generate human induced pluripotent stem cells (hiPSCs) [3] that can be differentiated into the important cell types of the brain, neurons, and astrocytes [4, 5]. The disadvantage of these 2D models is that they are descriptive at a cellular level, but they fail to adequately provide the details that could be derived from a more complex, three-dimensional structure, where the cells are spatially organized

[6]. In 2013, Lancaster and colleagues developed a hiPSC-derived three-dimensional organoid culture system, termed cerebral organoids, that develop various discrete, although interdependent, brain regions [7]. These organoids recapitulate many features of human cortical development, including a progenitor zone organization with abundant outer radial glial stem cells [8].

Here we describe the generation of cerebral organoids using a modified version of the Lancaster protocol [7, 9]. In short, feeder-free cultured hiPSCs were dissociated and replated in neural induction medium in a non-adherent cell culture plate, and differentiated for 100 days (Fig. 1). Cryosections of these organoids can be used for immunofluorescence studies. Organoids can be used for many different purposes including disease modeling, studying disease mechanisms, or analyzing therapeutic interventions (using for example antisense oligonucleotides) at any given time point.

2 Materials

2.1 *Neuroectodermal Differentiation*

1. mTeSR™1.
2. Matrigel.
3. Dulbecco's Modified Eagle's Medium (DMEM) and Ham's F-12 Nutrient Mixture (DMEM/F12).
4. ACCUTASE™.
5. STEMdiff™ Neural Induction Medium (NIM).
6. Y-27632.
7. v-bottom shape 96-well plate.

2.2 *Neurospheres*

1. Neurosphere medium: DMEM/F12 and Neurobasal medium 1:1, 1:200 N2 supplement, 1:100 B-27 supplement (without vitamin A), 1:100 L-glutamine, 0.05 mM non-essential amino acids (MEM-NEAA), 100 U/ml penicillin, 100 µg/ml streptomycin, 1.6 mg/l insulin, 0.05 mM β-mercaptoethanol.
2. Wide orifice pipette tips.
3. Organoid embedding sheet (or parafilm and a 200 µl tip box).

2.3 *Organoids*

1. Brain organoid medium: DMEM/F12 and Neurobasal medium 1:1, 1:200 N₂ supplement, 1:100 B27 supplement w/o vitamin A, 1:100 L-glutamine, 0.05 mM MEM-NEAA, 100 U/ml penicillin, 100 µg/ml streptomycin, 1.6 mg/l insulin, 0.5 µM dorsomorphin, 5 µM SB431542, 0.05 mM β-mercaptoethanol.
2. Spinner flask or 6-well plates.
3. Bioreactor or shaker.

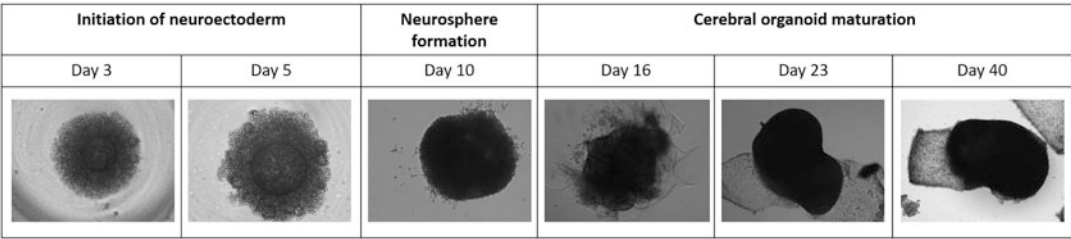


Fig. 1 Cerebral organoids during the various stages of organoid culturing. Organoids are cultured using a modified version of the Lancaster protocol. After 5 days of neuroectodermal differentiation, the neurospheres are embedded in Matrigel and cultured in the neurosphere medium in a 6-well plate for 5 days. For cerebral organoid maturation, the embedded neurospheres are transferred into a spinner flask and can be used for downstream applications if needed

2.4 Fixation and Embedding

- 1. Wide orifice pipette tips.
- 2. Dulbecco’s Phosphate Buffered Saline (DPBS).
- 3. 4% paraformaldehyde (PFA).
- 4. 30% sucrose in distilled water.
- 5. Embedding mold.
- 6. Optimum cutting temperature compound (OCT).

2.5 Cryosectioning and Immunofluorescent Staining

- 1. PLL-coated glass cryoslides.
- 2. Barrier pen.
- 3. PBS-glycine: 200 mM of glycine in DPBS.
- 4. Blocking Solution: 5% goat or horse serum, 0.1% Triton X-100, 200 mM glycine in Dulbecco’s Phosphate-Buffered Saline.
- 5. Immunobuffer solution: 1% goat or horse serum, 0.1% Triton X-100 in Dulbecco’s Phosphate-Buffered Saline.
- 6. Prolong Diamond Antifade Mounting (+DAPI).

3 Methods

3.1 Neuroectodermal Differentiation

- 1. Culture hiPSCs under feeder-free conditions in mTeSR™1 in a culture dish coated with Matrigel. For neuroectodermal differentiation one 100 mm cell culture dish is required (*see Note 1*).
- 2. When the hiPSCs are ready for passaging, wash the hiPSCs with 10 ml pre-warmed (37 °C) DMEM/F12.
- 3. Remove DMEM/F12, add 2 ml pre-warmed ACCUTASE™ and incubate for 5 min at 37 °C and 5% CO₂, allowing cells to detach (*see Note 2*).

4. Pipette the cell suspension up and down 3–5 times using a 1-ml micropipette to make a single-cell suspension and collect the suspension in a 15-ml tube (*see Note 3*).
5. Add 6 ml of pre-warmed DMEM/F12, wash the culture dish and collect the suspension in the same 15-ml tube as in **step 4**.
6. Centrifuge at $300 \times g$ for 5 min at room temperature.
7. Remove supernatant and resuspend the cell pellet in 1 ml of NIM supplemented with 10 μ M Y-27632 and count the cells using a cell counter.
8. Dilute the cell suspension in NIM supplemented with 10 μ M Y-27632 to 4.5×10^5 cells per ml and add 100 μ l per well in a non-adherent, v-bottom shape, 96-well plate (*see Note 4*).
9. Centrifuge the plate at $500 \times g$ for 3 min at room temperature and incubate at 37 °C and 5% CO₂.
10. Change medium by carefully removing 50 μ l NIM from the top of the wells, without disturbing the embryoid bodies, and by adding 50 μ l of fresh NIM. Medium changes should be done daily for the next 5 days (*see Note 5*).

3.2 Neurosphere Embedding

1. Use an 1-ml micropipette with a wide orifice pipet tip to place the neurospheres on a silicone organoid embedding sheet (*see Notes 6 and 7*).
2. Carefully remove the medium from the well, without disturbing the neurosphere, and expel it back to dislodge the neurosphere from the bottom of the well.
3. Use a wide orifice tip to collect the neurosphere and transfer it to the embedding sheet.
4. Carefully remove as much liquid from the embedding sheet as possible.
5. Use an ice-cold tip to add a drop of Matrigel onto each neurosphere.
6. Use an ice-cold tip to place the neurosphere in the center of the Matrigel droplet.
7. Incubate at 37 °C and 5% CO₂ for 15 min.
8. Carefully wash the neurospheres from the embedding sheet into a 100-mm culture dish by flushing them with the neurosphere medium and incubate at 37 °C and 5% CO₂. The total volume of neurosphere medium in the dish is 10 ml (*see Note 8*).
9. Add 2 ml of fresh neurosphere medium on day 2.
10. Use the embedded neurospheres 4 days after the embedding for the next step in the protocol.

3.3 Organoids

1. Carefully transfer the embedded neurospheres into a spinner flask containing 100 ml of pre-warmed organoid medium using a 2-ml serological pipette (*see Note 9*).
2. Place the spinner flask on the magnetic stirring platform in the incubator and use a stirring program at 25 rpm.
3. Culture the organoids on the magnetic stirring platform at 37 °C and 5% CO₂ for up to 100 days (*see Notes 10 and 11*).
4. Change the medium weekly by removing 50 ml of the organoid medium and adding 50 ml of fresh organoid medium (*see Note 12*). To refresh the medium, remove the spinner flask and let the organoids sink to the bottom for 5 min. Then carefully remove the medium, without disturbing the organoids.

3.4 Fixation and Embedding

1. Collect the organoids with an 1-ml micropipette with a wide orifice pipet tip and transfer them in a 60-mm dish or in a 6-well plate (*see Note 6*).
2. Wash the organoids with 5 ml of prewarmed Dulbecco's Phosphate-Buffered Saline.
3. Use a wide orifice tip to transfer each organoid separately into a 1.5-ml Eppendorf tube with 500 µl of 4% PFA. Incubate the organoids for 30 min at room temperature (*see Notes 13 and 14*).
4. Remove the 4% PFA solution and wash the organoids twice with 1 ml DPBS for 5 min (*see Note 15*).
5. Remove DPBS and add 1 ml of 30% sucrose in distilled water per tube to dehydrate the organoids and incubate the organoids at 4 °C overnight (*see Note 16*).
6. Fill a Peel-A-Way embedding molds with 400 µl of optimum cutting temperature compound (until the middle) and use an inoculation loop to place the organoid in the center of the mold. Label the rim of the mold with the sample name (*see Note 17*).
7. Snap-freeze the organoid-containing mold with ethanol on dry-ice and store at –80 °C until further use.

3.5 Cryosectioning and Immunofluorescent Staining

1. Section cryoprotected frozen organoids into 16- to 20-µm-thick slices on PLL-coated glass cryoslides using a cryostat (*see Notes 18 and 19*).
2. Thaw (if they were frozen) and dry the slides for 30 min at room temperature.
3. Draw a hydrophobic barrier around each section using a barrier pen.
4. To quench the PFA-induced autofluorescence wash the slides twice with 200 µL of PBS-glycine for 3 min.

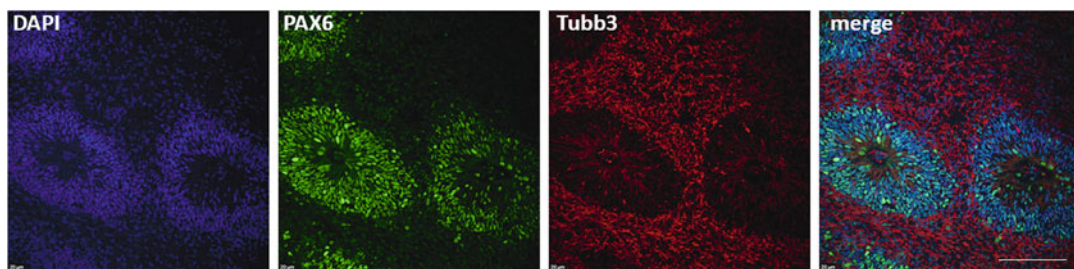


Fig. 2 Immunofluorescent staining of a cortical plate structure. Cortical plate structure in cerebral organoids stained with DAPI (blue), the neural progenitor marker PAX6 (green), and the neural marker TUBB3 (red). The scale bar represents 100 μm

5. Block nonspecific binding by adding 100 μl of Blocking Solution to the section for 1 h at room temperature.
6. Add 100 μl of primary antibody diluted in immunobuffer solution and incubate the slides overnight at 4 $^{\circ}\text{C}$ (*see Note 20*).
7. Wash three times with DPBS for 5 min.
8. Incubate the sections with the secondary antibody in immunobuffer solution for 1.5–2 h at room temperature (*see Note 21*).
9. Wash the slides three times in PBS.
10. Put a drop of Prolong Diamond Antifade Mountant (+DAPI) on the section and put a coverslip on top. Leave overnight at room temperature.
11. Store in fridge at 4 $^{\circ}\text{C}$ until performing microscopy. An example of a cortical plate structure in cerebral organoids stained with the neural progenitor marker PAX6 and the neural marker TUBB3 can be seen in Fig. 2.

4 Notes

1. Change mTeSRTM1 daily and passage hiPSCs after 5–7 days. hiPSCs are ready to passage when the majority of the colonies are large, compact, and have centers that are dense compared to their edges. Only use undifferentiated, high-quality hiPSCs that are fully characterized according to the latest human pluripotent stem cell registry guidelines (<https://hpscreg.eu/>).
2. 1 ml ACCUTASETM per 25 cm^2 surface area.
3. ACCUTASETM is a cell detachment solution of proteolytic and collagenolytic enzymes and does not need to be neutralized.
4. Make sure that the cells are equally distributed in the suspension by mixing the tube regularly.

5. There is more evaporation from the four corner wells. Do not use these wells or add extra medium daily (up to 100 μ l total culture volume).
6. The wide orifice tip can be replaced by a cut tip. The cut on the tip should be done by using sterile scissors. You can effectively sterilize scissors in an autoclave, but tools can also be sterilized in alcohol or a flame.
7. The silicone organoid embedding sheet can be replaced by placing parafilm over an empty 200- μ l tip box and using a finger to make small holes.
8. A maximum of 20 neurospheres per 100-mm cell culture dish.
9. A maximum of 20 organoids per culture flask.
10. When spinner flasks are not available, non-adhesive culture plates on a rotating platform can be used. Use a shaking program of 75 rpm.
11. If an orbital shaker and a 6-well plate are used, do not transfer more than 10 organoids per well. Moreover, monitor the organoids regularly to reduce the chance of them sticking together. If organoids stick together, you can easily separate these by using a sterile pipet tip as a knife.
12. Medium changes need to be done more often when there is a color change of the medium. Check the organoids regularly and replace the medium as done in **step 3** in Subheading 3.3 when needed. For a 6-well plate, a volume of 3-ml medium per well can be used and medium should be changed twice a week and/or when there is a color change of the medium.
13. For a big batch of organoids, fixation can be done in a 6-well plate.
14. For larger organoids (>2 mm), a 4% PFA incubation at 4 °C overnight is recommended.
15. You can store the organoids in 1 ml DPBS at 4 °C for up to 7 days.
16. After the addition of 30% sucrose solution, the organoids should float at the surface, and by the next day, the organoids should sink down to the bottom of the tube. You can keep the organoid in 30% sucrose for up to a month. The recommended time for organoids larger than 4 mm is 5–7 days.
17. To better visualize the organoid while cryosectioning, add Trypan-blue diluted 1:50 in DPBS before embedding the organoids in OCT (and after 30% sucrose) for 15 min at room temperature. The outer area of the organoid will be colored blue.
18. Up to 100 sections can be obtained from one organoid.
19. The slides can be stored at –80 °C.

20. Put a wet tissue inside the box to prevent the slides from drying out.
21. Keep in the dark from here on.

References

1. Chesselet MF, Carmichael ST (2012) Animal models of neurological disorders. *Neurotherapeutics* 9(2):241–244. <https://doi.org/10.1007/s13311-012-0118-9>
2. Berman RF, Buijsen RA, Usdin K, Pintado E, Kooy F, Pretto D, Pessah IN, Nelson DL, Zalewski Z, Charlet-Bergeurand N, Willemsen R, Hukema RK (2014) Mouse models of the fragile X premutation and fragile X-associated tremor/ataxia syndrome. *J Neurodev Disord* 6(1):25. <https://doi.org/10.1186/1866-1955-6-25>
3. Takahashi K, Tanabe K, Ohnuki M, Narita M, Ichisaka T, Tomoda K, Yamanaka S (2007) Induction of pluripotent stem cells from adult human fibroblasts by defined factors. *Cell* 131(5):861–872. <https://doi.org/10.1016/j.cell.2007.11.019>
4. Hu BY, Weick JP, Yu J, Ma LX, Zhang XQ, Thomson JA, Zhang SC (2010) Neural differentiation of human induced pluripotent stem cells follows developmental principles but with variable potency. *Proc Natl Acad Sci U S A* 107(9):4335–4340. <https://doi.org/10.1073/pnas.0910012107>
5. Shi Y, Kirwan P, Livesey FJ (2012) Directed differentiation of human pluripotent stem cells to cerebral cortex neurons and neural networks. *Nat Protoc* 7(10):1836–1846. <https://doi.org/10.1038/nprot.2012.116>
6. Centeno EGZ, Cimarosti H, Bithell A (2018) 2D versus 3D human induced pluripotent stem cell-derived cultures for neurodegenerative disease modelling. *Mol Neurodegener* 13(1):27. <https://doi.org/10.1186/s13024-018-0258-4>
7. Lancaster MA, Knoblich JA (2014) Generation of cerebral organoids from human pluripotent stem cells. *Nat Protoc* 9(10):2329–2340. <https://doi.org/10.1038/nprot.2014.158>
8. Lancaster MA, Renner M, Martin CA, Wenzel D, Bicknell LS, Hurles ME, Homfray T, Penninger JM, Jackson AP, Knoblich JA (2013) Cerebral organoids model human brain development and microcephaly. *Nature* 501(7467):373–379. <https://doi.org/10.1038/nature12517>
9. Gabriel E, Gopalakrishnan J (2017) Generation of iPSC-derived human brain organoids to model early neurodevelopmental disorders. *J Vis Exp* 122:55372. <https://doi.org/10.3791/55372>

Open Access This chapter is licensed under the terms of the Creative Commons Attribution 4.0 International License (<http://creativecommons.org/licenses/by/4.0/>), which permits use, sharing, adaptation, distribution and reproduction in any medium or format, as long as you give appropriate credit to the original author(s) and the source, provide a link to the Creative Commons license and indicate if changes were made.

The images or other third party material in this chapter are included in the chapter's Creative Commons license, unless indicated otherwise in a credit line to the material. If material is not included in the chapter's Creative Commons license and your intended use is not permitted by statutory regulation or exceeds the permitted use, you will need to obtain permission directly from the copyright holder.



Part IV

In Vivo Model Systems



Chapter 18

Considerations for Generating Humanized Mouse Models to Test Efficacy of Antisense Oligonucleotides

Irene Vázquez-Domínguez and Alejandro Garanto

Abstract

Over the last decades, animal models have become increasingly important in therapeutic drug development and assessment. The use of these models, mainly mice and rats, allow evaluating drugs in the real-organism environment and context. However, several molecular therapeutic approaches are sequence-dependent, and therefore, the humanization of such models is required to assess the efficacy. The generation of genetically modified humanized mouse models is often an expensive and laborious process that may not always recapitulate the human molecular and/or physiological phenotype. In this chapter, we summarize basic aspects to consider before designing and generating humanized models, especially when they are aimed to test antisense-based therapies.

Keywords Humanized models, Model systems, Mouse model generation, Splicing defects, Antisense oligonucleotides, In vivo drug testing

1 Introduction

Even though in 2020 the Food and Drug Administration (FDA) approved 53 new drugs (their second biggest approval number ever) [1], the mean annual number of drug approvals was 41 between 2010 and 2018 (approximately 15% of all evaluated drugs until 2019) [2]. It could be argued that this limited success is mainly caused by the insufficient recapitulation of the physiological and pathological of human disease in the preclinical phase. Studying human diseases is often difficult due to the restrictions and ethical concerns regarding the manipulation of human samples or tissues and the use of animal models allows the evaluation of drugs within an entire organism. However, these models are different species, with a different DNA sequence and different behavior, that may not recapitulate the complete human phenotype. Among all animal models, mice and rats are the most frequently used models in early preclinical stages. This is due to their relatively small size, ease of handling and maintenance, short reproductive

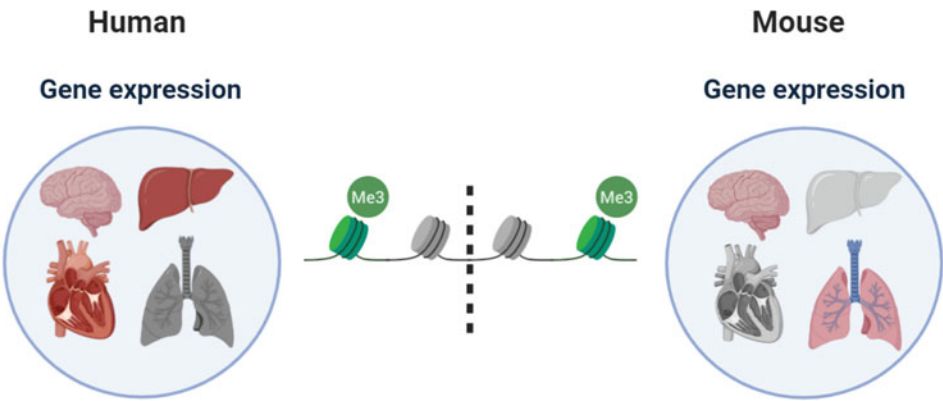
cycle, and the similarities with regard to the genomic and physiological properties compared to humans, as well as the easy genetic manipulation that can be conducted, especially in mice [3].

Antisense oligonucleotide (AON)-based therapies are sequence-specific approaches aimed to either interfere with the splicing mechanism or regulate gene expression, protein translation, or RNA/protein binding [4]. All these processes are highly regulated in cells through different mechanisms such as epigenetics and interactions between mRNA and proteins, which can differ between species [5]. Unfortunately, if the sequence of interest is not completely conserved, the molecule designed to target the human sequence cannot be assessed in the animal model. In this case, the humanization of the models offers the possibility to (partially) replace mouse genes by human counterparts, insert a human copy of the gene in the mouse genome, as well as harbor human tissues [6, 7]. This allows to have the human sequence in an *in vivo* model. However, before generating such a model, it is crucial to first evaluate if the effect of the mutation of interest is also recapitulated in mouse [8]. In this chapter, we discuss the most important considerations to need to be taken into account before generating a genetically modified humanized mouse model to assess the therapeutic effect of AON molecules.

2 Human and Mouse: Species Are Similar But Not Equal

During the last decades, mouse models have served as valuable organisms for investigating human biology and disease as mouse and human are very similar to each other at the cellular as well as the biochemical level. Furthermore, most of the human cellular pathways are conserved in mouse, at the genetic and molecular level [5]. Despite these similarities, mice and humans can also differ in several aspects at multiple levels. For instance, it is described that around 1% of the human genes do not have an ortholog in mouse [9], which means that not all genes are present in both genomes. Furthermore, some data indicate that there is a higher variability of gene expression between the same tissue of two different species, compared to two different tissues within the same species [5]. These findings support the hypothesis that regulatory pathways, like epigenetics, can be responsible for the interspecies differences [5]. Within epigenetics, histone modifications, such as methylation and acetylation of the promoter region, play a crucial role in expression, leading to most of the differences between both species [10] (Fig. 1a). In addition, differences at the individual gene level give rise to different protein isoforms. Finally, the conservation rate of amino acids generates some differences in protein function or substrate recognition [9] (Fig. 1b). These differences can also cause different response to drug administration [11]. All

A) Epigenetics



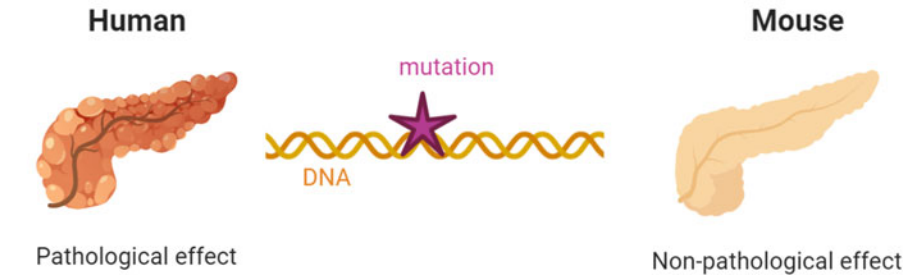
B) Amino acid conservation rate

Human **K**K**A**S**K**P**K**K**A**A**S**K**A**P**T****T**K**K**P**K**A**T**P**V**K**K**A**K**K**K**L**A**A**T**P**K**K**A**K**K**P**K****T**V**K**A**K**P**V**K**A**S**K**P**K**K

Mouse **K**K**A**A**K**P**K**K**A**A**S**K**A**P**S**K**K**P**K**A**T**P**V**K**K**A**K**K**K**P**A**A**T**P**K**K**T**K**K**P**K**A**V**K**V**K**P**V**K**A**S**K**P**K**K**

*** . ***** . ***** ***** ***** . ***** . ** . *****

C) Mutation effect



D) Splicing

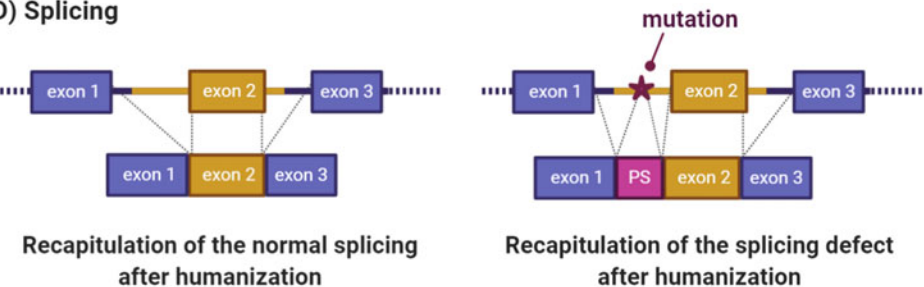


Fig. 1 Summary of some aspects that can differ between human and mouse. (a) Epigenetics. Organs in which the gene of interest is expressed are represented in color while those organs in which the gene is not expressed because of epigenetics regulation (such as methylation, me3) are in gray. As the pattern of gene expression between both organisms (inside the blue circle) is different, the functional role of the gene in both may also be different. (b) Amino acid conservation rate. As an example, part of the human and mouse Histone 1 amino acid sequences is represented. Discrepancies between amino acids are indicated with different symbols (: or .) while conserved regions are marked with an asterisk (*). (c) Mutation effect. Not always the same mutation has the same effect on both species. In humans, the mutation can underlay a pathological defect (left) that is not recapitulated in mice (right). (d) Splicing. The recapitulation of the normal splicing after

these discrepancies can make that a defective gene or pathological mutation in humans may have a completely different outcome when the orthologous gene is mutated or truncated in mice [12–14] (Fig. 1c).

AONs are often used to modulate splicing and correct aberrant splicing. It has been reported that the consensus splice site sequences in mouse and human are highly conserved and comparable even though some small changes in these patterns have been described [15]. That could mean that a human splicing defect may not be completely reproduced in mouse. Some differences between both species at the splicing level have been already described (Fig. 1d). One example is the variant c.315-48T>C in the *FECH* gene, a modifier mutation for erythropoietic protoporphyria [14]. This mutation generates an aberrant splice acceptor site that results in an intron inclusion of 63 nucleotides upstream of exon 4. However, the generated mouse model not only presents this mis-splicing effect but also a strong skipping of the partially humanized exon 3 [14]. This example illustrates how a hybrid gene (or humanized mouse gene) can have undesirable effects on splicing. Another example is the low recognition of the pseudoexon insertion caused by a deep-intronic mutation in the *CEP290* gene (c.2991+1655A>G) in the humanized mouse model carrying this specific variant [13]. Further studies showed that the recognition of the pseudoexon seemed to be specific of primates, and it was less efficient in other species such as pig, dog, mouse, or *Drosophila*. In addition, as shown in *FECH*, additional splicing events not detected in humans were found in the humanized *Cep290* model [16]. Based on all these studies, we recommend performing several in vitro validation steps before generating a humanized mouse model (Fig. 2).

3 Checkpoints Before Generating a Humanized Mouse Model

3.1 Literature Research

An important aspect is to look first in literature or in mouse databases (such as the Mouse Genome Informatics (MGI, <http://www.informatics.jax.org/>) and the International Mouse Phenotyping Consortium (IMPC, <https://www.mousephenotype.org/>)) whether any genetically modified animal model for the gene of interest has already been obtained. With this information, one can avoid the generation of a model already available. In addition, if a humanized model is aimed to study disease, the availability of a

Fig. 1 (continued) humanization is indicated on the left. Mouse regions are indicated in purple and human regions in yellow. On the right, the presence of the splicing-related mutation of interest, located in an intron sequence, causes the insertion of a pseudoexon (PS) in the mRNA transcript. In this situation the splicing defect is recapitulated after the humanization

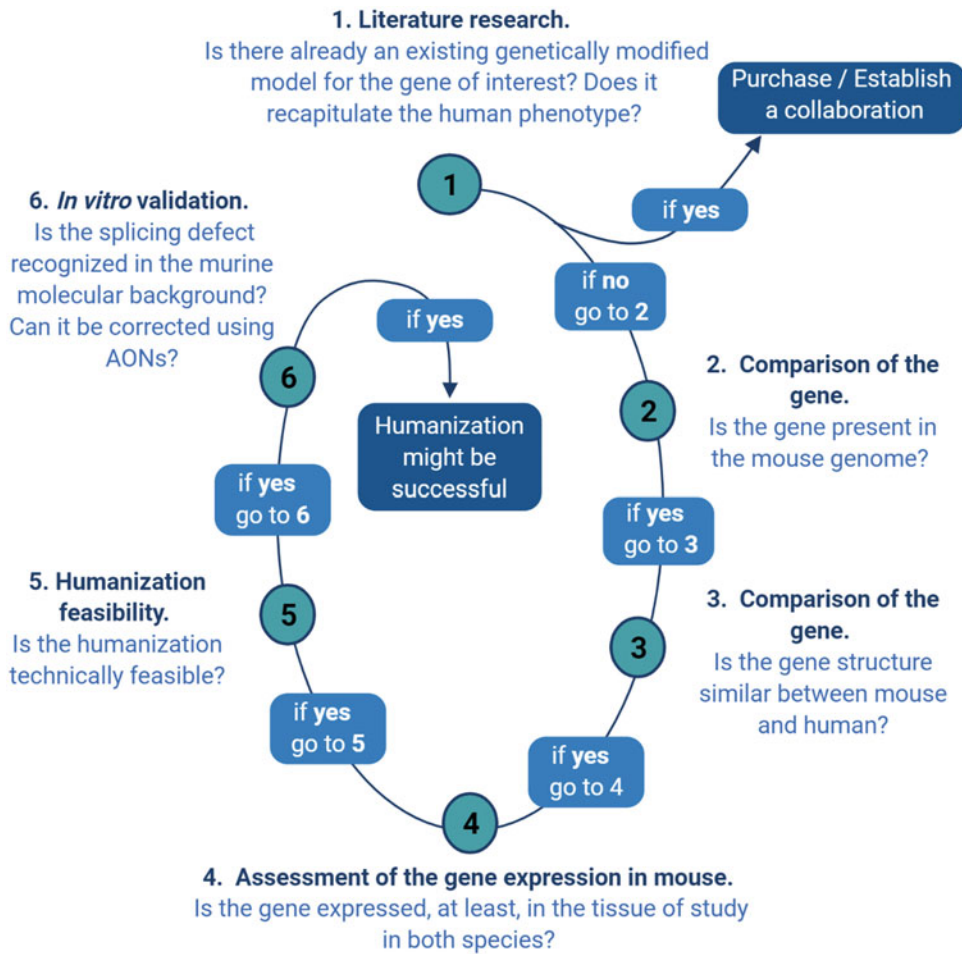


Fig. 2 Schematic representation of the different checkpoints for generating a humanized mouse model

knockout/mutant model will contribute to predict the possible phenotype of the potential new humanized model. For instance, mutations in *ABCA4* generate a non-functional protein involved in the visual cycle that leads to retinal degeneration and subsequent loss of vision, causing Stargardt disease in humans [17–19]. However, the *Abca4*^{-/-} mouse model shows a mild late onset phenotype, despite the fact that no ABCA4 protein is encoded [20]. That means that the defect caused by the absence of this protein is not completely comparable to the human phenotype. Thus, depending on the purpose of study, a humanized mouse model may not be suitable to evaluate antisense therapies for a particular gene.

3.2 Comparison of the Gene Sequence

If the model is not available, the first question that needs to be answered is whether the gene of interest is present in the mouse genome. The probability is high, since only 1% of human genes do not have a mouse orthologue [9]. In addition, it is important to

check the structure of the gene, to ensure it is similar and no relevant exons for the study or protein function are missing. To do so, databases such as Genome Browser (<https://genome.ucsc.edu>) or Ensembl (<https://www.ensembl.org>) can be useful. If the gene name does not coincide, a blast (<https://blast.ncbi.nlm.nih.gov>) at DNA or protein level can be done to search for similar genes or proteins in other species.

3.3 Assessment of Gene Expression in Mouse

Although mouse and human are similar at cellular and molecular levels, some discrepancies between both species have been already reported, including variation in expression levels in different tissues. Therefore, assessing that the gene of interest is expressed in the proper murine tissue (or at least the tissue of study) is crucial. For instance, it is already known that one of the most important pathways in cancer and apoptosis, the phosphoinositide 3-kinase (PI3K) signaling cascade [21], shows high differences in the expression of its two key genes, *mTOR* and *AKT2*, between both species [22]. Thus, mouse is not the best model to conduct oncological studies that aim to investigate this pathway in vivo. In addition, it has been published that muscle, liver, and neuronal cells show a strong similarity of gene expression profiles between both species while other tissues such as testis, lung, and pancreas showed more differences due to the evolution [22]. Therefore, it is important to check expression levels in the tissue(s) of interest in mouse, to ensure that the generation of the humanized model will be useful for future experiments.

3.4 Humanization Feasibility

In general, there are two main ways to introduce the human gene into the mouse genome:

- Introduce the human gene of interest (or part of it) in the mouse genome.
- Replace the corresponding mouse gene (or part of it) by the human one.

In the first option, the complexity lays on where to exactly insert the gene and how to regulate its expression. The second option requires a more in-depth study on the recombination possibilities, the conservation rate between human and mouse, and the resulting humanized gene and protein. For that, first it is important to identify the mouse exons that correspond to the human ones. It is also important to check whether they encode for the same part of the protein and how conserved it is. This can be done with the previously mentioned freely available databases. Finally, the overall procedure needs to be technically feasible, by either homologous recombination in embryonic stem cells or genome editing techniques using a donor template. These steps need to be discussed with

experts on these techniques either at other academic institutes or companies specialized in generating animal models.

3.5 In Vitro Validation

As indicated previously, AONs can be used for splicing modulation. Thus, it is important to study whether the splicing machinery in mouse will allow proper:

- Splicing of the humanized transcript or human gene.
- Recapitulation of the human splicing defect caused by a specific mutation in the mouse molecular background.

One way to perform this validation is by using artificial systems (e.g., mini-/midigenes) harboring the human region of interest either with the “wild-type” sequence or the mutated one [16]. In that way, it can be assessed whether they behave in a mouse-specific environment as expected based on observations in humans. For that, conventional mouse-derived cell lines can be a good start [23]. The data obtained from these studies are crucial to assess if the mouse might be a good animal for the generation of a humanized model.

3.5.1 In Vitro Splicing Assays Considerations

The easiest way for a first screening is to develop human mini-/midigenes with and without the mutation [24] and deliver them to conventional mouse cell lines easy to transfect, such as iMCD3, B16-F10 or N2A. However, depending on the tissue of interest, this information might not be completely accurate. For instance, in human cells, we and others have found differences in pseudoexon recognition, depending on how similar the molecular background was compared to the one of the cell/tissue of interest [24–26], probably due to tissue-specific splicing regulatory elements [27]. Therefore, it is important to choose an appropriate cell line. For instance, if the gene is implicated in neurological disorders affecting the brain, the mouse cell line N2A (derived from mouse brain) might be a better option than using B16-F10, derived from mouse skin or iMCD3, derived from kidney [28]. It is always good to test in several different cell lines: if the splicing pattern observed in humans is well recapitulated in multiple cell lines, most probably the humanized model will also show the same splicing patterns. In case the splicing pattern is not recapitulated at all, we recommend to stop with the generation of the humanized mouse model and try to find alternative models.

Next step, if the splicing defect is recapitulated, is to determine whether the AONs of interest previously designed and tested in vitro human models can also rescue the splicing in the murine molecular background. With that, it is possible to evaluate if those molecules will also be successful in the mouse molecular background. The generation and validation of mini-/midigenes and AON rescue can be done in 3–4 weeks as previously reported

[24, 29] and can contribute significantly to reduce the number of animals by performing initial screenings in vitro [24].

If all the aforementioned points are met successfully (Fig. 2), the chances of success are higher. However, it can still happen that even though the molecular defect is recapitulated, the model does not show a similar phenotype. Unfortunately, this is difficult to predict in vitro. In addition, in order to discern whether the humanization of the model may influence the potential phenotype, especially in those cases where a mutation has been introduced, it is strongly advisable to generate two humanized models, one with only the human “wild-type” region and another one with the mutated sequence.

4 Current Examples of Humanized Mouse Models

Different approaches have been used to generate humanized mouse models, ranging from introducing the entire gene or part of it or replacing specific parts the gene by the human counterpart. Some of these models have also been used to test AON-based therapies for different types of disease.

4.1 Insertion of the Entire Human Gene

One of the approaches frequently used is the introduction of the entire human gene into the mouse genome. This method also takes into account the endogenous expression of the corresponding mouse gene and whether it can affect the development of the desired phenotype. One example of this is the humanized Tg32 FcRn mouse, which harbors the complete human *FCGRT* gene (around 11 kb) plus 5' and 3' untranslated regions (around 10 kb). This transgene is introduced into C57BL/6J oocytes with a null mutation in the *FcRn* mouse gene, which is involved in IgG and serum albumin turnover. As a result, only the human *FcRn* is expressed under the control of its natural human promoter. Besides introducing the “wild-type” sequence in the mouse genome, Anderson and colleagues also generated a defective allele [30]. In this, a neomycin-resistance cassette was inserted, replacing the human “wild-type” located between the promoter end and the beginning on exon 2. This study revealed that the *FcRn*^{+/-} model recapitulated the “wild-type” condition indicating that only one allele is sufficient to regulate the IgG levels and transport [31–33]. However, the defective mouse model (*FcRn*^{-/-}) successfully recapitulated the defective neonatal transport phenotype [30]. This model has already been used in drug preclinical studies [34]. Most of these studies focused on the evaluation and the pharmacokinetics and pharmacodynamics of human IgG [35], but it may also be useful for other therapeutic approaches, such as AONs [36].

Retinitis pigmentosa (RP) is the most frequent inherited retinal disease, for which no therapy is currently available. In this disorder, most of the studies have been focused on the mutation p.P23H of rhodopsin (*RHO*), a recurrent mutation causing autosomal dominant RP [37, 38]. To study this mutation, several animal models have been developed, including the generation of humanized models in either mouse [39] or rats [37, 40]. In all of them, the transgene segregated in an autosomal dominant allele manner and the lines were maintained within the murine wild-type rhodopsin background (*Rho*^{+/+}). However, they differed in the expression levels of the murine and human rhodopsin mRNA. These studies revealed that a higher number of copies of the mutant allele induces a more severe RP phenotype, but also that overexpression of the wild-type allele has a detrimental effect, causing similar RP abnormalities [39, 41–43]. Some of these models have been used to successfully test AON-based therapies aiming to degrade the mutated transcript [44]. These and other results led to a recently started clinical trial (NCT04123626, <http://www.clinicaltrials.gov>).

AON-based therapies have had a major development in neuromuscular disorders [45]. Several mouse models recapitulating muscular dystrophy phenotypic traits have been generated. For instance, the *mdx* model, which harbors a nonsense mutation in exon 23 of the mouse *Dmd* gene causing loss of the functional protein expression, presents a moderate-severe phenotype with an early onset of skeletal muscle degeneration and impairment in muscle functions [46]. However, this model can only be targeted with mouse-specific AONs to the mutation in exon 23 [47–49]. To solve this limitation, the *hDMD/mdx* mouse model was generated by crossing the *mdx* model with a model carrying the entire human *DMD* gene (*hDMD*), allowing the expression of the “wild-type” human dystrophin in the *mdx* model [50]. However, the expression of *hDMD* hampered the development of the dystrophic phenotype caused by the mutation present in the mouse *Dmd* gene. In 2018, the group of Prof. Aartsma-Rus overcame these limitations by generating a new humanized mouse model (*del52hDMD/mdx* mice). This model carries both human and murine *DMD* genes with pathogenic mutations previously described. As a consequence of the nonsense mutation in exon 23 in the mouse *Dmd* gene and the deletion of exon 52 in the *hDMD* gene, none of the genes produce functional dystrophin protein [51]. The absence of dystrophin expression caused a more severe muscular dystrophy phenotype than the one observed in other models. As a result, this model was suitable to test human-specific AONs, and thereby improve AON-based therapies for Duchene muscular dystrophy patients by enabling studies at the mRNA, protein and functional level.

4.2 Replacing Part of the Mouse Gene by the Human Gene

Another way to generate a humanized mouse model is by replacing a specific region in the mouse genome by the human counterpart. One example is the humanized mouse model generated to study the mutation c.2991+1655A>G in the *CEP290* gene. This mutation is the most recurrent mutation underlying Leber congenital amaurosis, accounting up to 15% of all cases in some populations [25, 52]. Two mouse models were generated in which the mouse sequence from exon 25 to exon 26 was replaced by the corresponding human exon 26, intron 26 (with or without harboring the mutation of interest), and exon 27 [13]. In the model *Cep290*^{lca/lca}, human intron 26 harbors the mutation of interest while the model *Cep290*^{hum/hum} does not. In both the models, *Cep290* expression levels and regular splicing of the gene were maintained when compared to “wild-type” mice. However, the splicing defect was barely present in the *Cep290*^{lca/lca} model, the retina being the only tissue where the exon was recognized at detectable levels, but by far not enough to lead to the human phenotype [25]. Subsequent studies, revealed that the pseudoexon recognition strongly correlates with evolutionary distance, being highly recognized in primates, and hardly recognized in lower species such as rodents and fly [16].

5 Conclusions

In summary, the suggestions given in this chapter highlight the importance of performing an accurate study to increase the chances of success when generating a humanized mouse model, e.g., to assess AON-based molecules. Despite similarities, human and mouse are different species and therefore differences are expected at all levels. When aiming to generate a humanized model, it is crucial to determine first if the gene of interest is present in the genome, has a similar structure, and if it is expressed in the same tissue(s) as in humans. Subsequently, when working with splicing defects, it is important to validate that these will be recognized in the murine molecular background, which can be easily done using “artificial systems” in vitro. If everything is conserved, the technical part is also important, is it feasible to humanize the model? If so, the chances of success are high. However, in some cases, it is not feasible, or a mouse model is not an option. In those cases, other models can be explored such as zebrafish or cellular models based on organ-on-a-chip technology. Following these suggestions may increase the success of the generation of humanized models and reduce the number of animals used in research. However, although all these in silico and in vitro tests can help to predict the recapitulation of a molecular defect in a humanized model, it is important to keep in mind that such models may not recapitulate the entire human phenotype.

Acknowledgments

We thank Dr. Rob W.J. Collin for the critical reading of this chapter. The group is financially supported by the Foundation Fighting blindness (PPA-0517-0717-RAD to A.G.), the Curing Retinal Blindness Foundation (to A.G.) as well as the Landelijke Stichting voor Blinden en Slechtzienden, Stichting Oogfonds Nederland (who contributed through UitZicht 2019-17), together with the Rotterdamse Stichting Blindenbelangen, Stichting Blindenhulp, and Stichting Dowilvo (to A.G). The funding organizations had no role in the design or conduct of this research. They provided unrestricted grants. All the figures were made with BioRender.

References

- Mullard A (2021) 2020 FDA drug approvals. *Nat Rev Drug Discov*. 2021 Feb;20(2):85–90. <https://doi.org/10.1038/d41573-021-00002-0>
- Darrow JJ, Avorn J, Kesselheim AS (2020) FDA approval and regulation of pharmaceuticals, 1983-2018. *JAMA* 323(2):164–176. <https://doi.org/10.1001/jama.2019.20288>
- Walsh NC, Kenney LL, Jangalwe S et al (2017) Humanized mouse models of clinical disease. *Annu Rev Pathol* 12:187–215. <https://doi.org/10.1146/annurev-pathol-052016-100332>
- Sardone V, Zhou H, Muntoni F et al (2017) Antisense oligonucleotide-based therapy for neuromuscular disease. *Molecules* 22(4):563. <https://doi.org/10.3390/molecules22040563>
- Lin S, Lin Y, Nery JR et al (2014) Comparison of the transcriptional landscapes between human and mouse tissues. *Proc Natl Acad Sci U S A* 111(48):17224–17229. <https://doi.org/10.1073/pnas.1413624111>
- O'Connell AK, Douam F (2020) Humanized mice for live-attenuated vaccine research: from unmet potential to new promises. *Vaccines (Basel)* 8(1):36. <https://doi.org/10.3390/vaccines8010036>
- Ito R, Takahashi T, Ito M (2018) Humanized mouse models: application to human diseases. *J Cell Physiol* 233(5):3723–3728. <https://doi.org/10.1002/jcp.26045>
- Hammond SM, Aartsma-Rus A, Alves S et al (2021) Delivery of oligonucleotide-based therapeutics: challenges and opportunities. *EMBO Mol Med* 13(4):e13243. <https://doi.org/10.15252/emmm.202013243>
- Mouse Genome Sequencing C, Waterston RH, Lindblad-Toh K et al (2002) Initial sequencing and comparative analysis of the mouse genome. *Nature* 420(6915):520–562. <https://doi.org/10.1038/nature01262>
- Dong X, Greven MC, Kundaje A et al (2012) Modeling gene expression using chromatin features in various cellular contexts. *Genome Biol* 13(9):R53. <https://doi.org/10.1186/gb-2012-13-9-r53>
- Blevitt JM, Hack MD, Herman K et al (2016) A single amino acid difference between mouse and human 5-lipoxygenase activating protein (FLAP) explains the speciation and differential pharmacology of novel FLAP inhibitors. *J Biol Chem* 291(24):12724–12731. <https://doi.org/10.1074/jbc.M116.725325>
- Garanto A, Vicente-Tejedor J, Riera M et al (2012) Targeted knockdown of Cerkl, a retinal dystrophy gene, causes mild affection of the retinal ganglion cell layer. *Biochim Biophys Acta* 8:1258–1269. <https://doi.org/10.1016/j.bbadis.2012.04.004>
- Garanto A, van Beersum SE, Peters TA et al (2013) Unexpected CEP290 mRNA splicing in a humanized knock-in mouse model for Leber congenital amaurosis. *PLoS One* 8(11):e79369. <https://doi.org/10.1371/journal.pone.0079369>
- Barman-Aksozen J, Wiek PC, Bansode VB et al (2017) Modeling the ferrochelatase c.315-48C modifier mutation for erythropoietic protoporphyria (EPP) in mice. *Dis Model Mech* 10(3):225–233. <https://doi.org/10.1242/dmm.027755>
- Abril JF, Castelo R, Guigo R (2005) Comparison of splice sites in mammals and chicken.

- Genome Res 15(1):111–119. <https://doi.org/10.1101/gr.3108805>
16. Garanto A, Duijkers L, Collin RW (2015) Species-dependent splice recognition of a cryptic exon resulting from a recurrent intronic CEP290 mutation that causes congenital blindness. *Int J Mol Sci* 16(3):5285–5298. <https://doi.org/10.3390/ijms16035285>
17. Molday LL, Rabin AR, Molday RS (2000) ABCR expression in foveal cone photoreceptors and its role in Stargardt macular dystrophy. *Nat Genet* 25(3):257–258. <https://doi.org/10.1038/77004>
18. Sun H, Smallwood PM, Nathans J (2000) Biochemical defects in ABCR protein variants associated with human retinopathies. *Nat Genet* 26(2):242–246. <https://doi.org/10.1038/79994>
19. Charbel Issa P, Barnard AR, Herrmann P et al (2015) Rescue of the Stargardt phenotype in Abca4 knockout mice through inhibition of vitamin a dimerization. *Proc Natl Acad Sci U S A* 112(27):8415–8420. <https://doi.org/10.1073/pnas.1506960112>
20. Weng J, Mata NL, Azarian SM et al (1999) Insights into the function of Rim protein in photoreceptors and etiology of Stargardt's disease from the phenotype in abcr knockout mice. *Cell* 98(1):13–23. [https://doi.org/10.1016/S0092-8674\(00\)80602-9](https://doi.org/10.1016/S0092-8674(00)80602-9)
21. Yuan TL, Cantley LC (2008) PI3K pathway alterations in cancer: variations on a theme. *Oncogene* 27(41):5497–5510. <https://doi.org/10.1038/onc.2008.245>
22. Monaco G, van Dam S, Casal Novo Ribeiro JL et al (2015) A comparison of human and mouse gene co-expression networks reveals conservation and divergence at the tissue, pathway and disease levels. *BMC Evol Biol* 15:259. <https://doi.org/10.1186/s12862-015-0534-7>
23. Tsai KW, Tarn WY, Lin WC (2007) Wobble splicing reveals the role of the branch point sequence-to-NAGNAG region in 3' tandem splice site selection. *Mol Cell Biol* 27(16):5835–5848. <https://doi.org/10.1128/MCB.00363-07>
24. Garanto A, Collin RWJ (2018) Design and in vitro use of antisense oligonucleotides to correct pre-mRNA splicing defects in inherited retinal dystrophies. *Methods Mol Biol* 1715:61–78. https://doi.org/10.1007/978-1-4939-7522-8_5
25. Garanto A, Chung DC, Duijkers L et al (2016) In vitro and in vivo rescue of aberrant splicing in CEP290-associated LCA by antisense oligonucleotide delivery. *Hum Mol Genet* 25(12):2552–2563. <https://doi.org/10.1093/hmg/ddw118>
26. Parfitt DA, Cheetham ME (2016) Targeting the proteostasis network in rhodopsin retinitis pigmentosa. *Adv Exp Med Biol* 854:479–484. https://doi.org/10.1007/978-3-319-17121-0_64
27. Lopes-Ramos CM, Paulson JN, Chen CY et al (2017) Regulatory network changes between cell lines and their tissues of origin. *BMC Genomics* 18(1):723. <https://doi.org/10.1186/s12864-017-4111-x>
28. Jiang Z, Cote J, Kwon JM et al (2000) Aberrant splicing of tau pre-mRNA caused by intronic mutations associated with the inherited dementia frontotemporal dementia with parkinsonism linked to chromosome 17. *Mol Cell Biol* 20(11):4036–4048. <https://doi.org/10.1128/mcb.20.11.4036-4048.2000>
29. Sangermano R, Khan M, Cornelis SS et al (2018) ABCA4 midigenes reveal the full splice spectrum of all reported noncanonical splice site variants in Stargardt disease. *Genome Res* 28(1):100–110. <https://doi.org/10.1101/gr.226621.117>
30. Roopenian DC, Christianson GJ, Sproule TJ et al (2003) The MHC class I-like IgG receptor controls perinatal IgG transport, IgG homeostasis, and fate of IgG-Fc-coupled drugs. *J Immunol* 170(7):3528–3533. <https://doi.org/10.4049/jimmunol.170.7.3528>
31. Petkova SB, Akilesh S, Sproule TJ et al (2006) Enhanced half-life of genetically engineered human IgG1 antibodies in a humanized FcRn mouse model: potential application in humorally mediated autoimmune disease. *Int Immunol* 18(12):1759–1769. <https://doi.org/10.1093/intimm/dx1110>
32. Roopenian DC, Akilesh S (2007) FcRn: the neonatal Fc receptor comes of age. *Nat Rev Immunol* 7(9):715–725. <https://doi.org/10.1038/nri2155>
33. Zalevsky J, Chamberlain AK, Horton HM et al (2010) Enhanced antibody half-life improves in vivo activity. *Nat Biotechnol* 28(2):157–159. <https://doi.org/10.1038/nbt.1601>
34. Stein C, Kling L, Proetzel G et al (2012) Clinical chemistry of human FcRn transgenic mice. *Mamm Genome* 23(3–4):259–269. <https://doi.org/10.1007/s00335-011-9379-6>
35. Ward ES, Ober RJ (2009) Chapter 4: multitasking by exploitation of intracellular transport functions the many faces of FcRn. *Adv Immunol* 103:77–115. [https://doi.org/10.1016/S0065-2776\(09\)03004-1](https://doi.org/10.1016/S0065-2776(09)03004-1)
36. Chappell AE, Gaus HJ, Berdeja A et al (2020) Mechanisms of palmitic acid-conjugated antisense oligonucleotide distribution in mice. *Nucleic Acids Res* 48:4382. <https://doi.org/10.1093/nar/gkaa164>

37. LaVail MM, Nishikawa S, Steinberg RH et al (2018) Phenotypic characterization of P23H and S334ter rhodopsin transgenic rat models of inherited retinal degeneration. *Exp Eye Res* 167:56–90. <https://doi.org/10.1016/j.exer.2017.10.023>
38. Gorbatyuk MS, Knox T, LaVail MM et al (2010) Restoration of visual function in P23H rhodopsin transgenic rats by gene delivery of BiP/Grp78. *Proc Natl Acad Sci U S A* 107(13):5961–5966. <https://doi.org/10.1073/pnas.0911991107>
39. Olsson JE, Gordon JW, Pawlyk BS et al (1992) Transgenic mice with a rhodopsin mutation (Pro23His): a mouse model of autosomal dominant retinitis pigmentosa. *Neuron* 9(5):815–830. [https://doi.org/10.1016/0896-6273\(92\)90236-7](https://doi.org/10.1016/0896-6273(92)90236-7)
40. Lewin AS, Drenser KA, Hauswirth WW et al (1998) Ribozyme rescue of photoreceptor cells in a transgenic rat model of autosomal dominant retinitis pigmentosa. *Nat Med* 4(8):967–971. <https://doi.org/10.1038/nm0898-967>
41. Mao H, James T Jr, Schwein A et al (2011) AAV delivery of wild-type rhodopsin preserves retinal function in a mouse model of autosomal dominant retinitis pigmentosa. *Hum Gene Ther* 22(5):567–575. <https://doi.org/10.1089/hum.2010.140>
42. Frederick JM, Krasnoperova NV, Hoffmann K et al (2001) Mutant rhodopsin transgene expression on a null background. *Invest Ophthalmol Vis Sci* 42(3):826–833
43. Orhan E, Dalkara D, Neuville M et al (2015) Genotypic and phenotypic characterization of P23H line 1 rat model. *PLoS One* 10(5):e0127319. <https://doi.org/10.1371/journal.pone.0127319>
44. Murray SF, Jazayeri A, Matthes MT et al (2015) Allele-specific inhibition of rhodopsin with an antisense oligonucleotide slows photoreceptor cell degeneration. *Invest Ophthalmol Vis Sci* 56(11):6362–6375. <https://doi.org/10.1167/iovs.15-16400>
45. Wurster CD, Ludolph AC (2018) Antisense oligonucleotides in neurological disorders. *Ther Adv Neurol Disord* 11:1756286418776932. <https://doi.org/10.1177/1756286418776932>
46. Wu B, Wang M, Shah S et al (2018) In vivo evaluation of dystrophin exon skipping in mdx mice. *Methods Mol Biol* 1828:231–247. https://doi.org/10.1007/978-1-4939-8651-4_14
47. Goyenvallé A, Vulin A, Fougère F et al (2004) Rescue of dystrophic muscle through U7 snRNA-mediated exon skipping. *Science* 306(5702):1796–1799. <https://doi.org/10.1126/science.1104297>
48. Fletcher S, Honeyman K, Fall AM et al (2007) Morpholino oligomer-mediated exon skipping averts the onset of dystrophic pathology in the mdx mouse. *Mol Ther* 15(9):1587–1592. <https://doi.org/10.1038/sj.mt.6300245>
49. Wu B, Lu P, Cloer C et al (2012) Long-term rescue of dystrophin expression and improvement in muscle pathology and function in dystrophic mdx mice by peptide-conjugated morpholino. *Am J Pathol* 181(2):392–400. <https://doi.org/10.1016/j.ajpath.2012.04.006>
50. t Hoen PA, de Meijer EJ, Boer JM et al (2008) Generation and characterization of transgenic mice with the full-length human DMD gene. *J Biol Chem* 283(9):5899–5907. <https://doi.org/10.1074/jbc.M709410200>
51. Veltrop M, van Vliet L, Hulsker M et al (2018) A dystrophic Duchenne mouse model for testing human antisense oligonucleotides. *PLoS One* 13(2):e0193289. <https://doi.org/10.1371/journal.pone.0193289>
52. Coppieters F, Lefever S, Leroy BP et al (2010) CEP290, a gene with many faces: mutation overview and presentation of CEP290base. *Hum Mutat* 31(10):1097–1108. <https://doi.org/10.1002/humu.21337>

Open Access This chapter is licensed under the terms of the Creative Commons Attribution 4.0 International License (<http://creativecommons.org/licenses/by/4.0/>), which permits use, sharing, adaptation, distribution and reproduction in any medium or format, as long as you give appropriate credit to the original author(s) and the source, provide a link to the Creative Commons license and indicate if changes were made.

The images or other third party material in this chapter are included in the chapter's Creative Commons license, unless indicated otherwise in a credit line to the material. If material is not included in the chapter's Creative Commons license and your intended use is not permitted by statutory regulation or exceeds the permitted use, you will need to obtain permission directly from the copyright holder.





Generation of Humanized Zebrafish Models for the In Vivo Assessment of Antisense Oligonucleotide-Based Splice Modulation Therapies

Renske Schellens, Erik de Vrieze, Ralph Slijkerman, Hannie Kremer, and Erwin van Wijk

Abstract

Antisense oligonucleotide (AON)-based splice modulation is the most widely used therapeutic approach to redirect precursor messenger RNA (pre-mRNA) splicing. To study the functional effect of human mutations affecting pre-mRNA splicing for which AON-based splice redirection would be a potential therapeutic option, humanized knock-in animal models are pivotal. A major limitation of using humanized animal models for this purpose is the reported poor recognition of human splice sites by the splicing machineries of other species. To overcome this problem, we provide a detailed guideline for the generation of functional humanized knock-in zebrafish models to assess the effect of mutation-induced aberrant splicing and subsequent AON-based splice modulation therapy.

Keywords Pre-mRNA splicing, Species-specific minigene splice assay, Antisense oligonucleotides, Inherited retinal dystrophies, Usher syndrome, Zebrafish

1 Introduction

Precursor messenger RNA (pre-mRNA) splicing is a tightly regulated and complicated process. The spliceosome, a multicomponent protein complex, removes introns from the pre-mRNA by recognizing and joining each splice donor site, located at the 5' end of the intron, to its corresponding splice acceptor site, located at the 3' end of the intron. The remaining exons are subsequently fused together to form mature mRNA. However, genetic variants in both introns and exons can affect the process of splicing and result in a range of pathogenic phenotypes.

For inherited retinal dystrophies (IRDs), it has been estimated that ~20% of all identified mutations affect pre-mRNA splicing [1]. Numerous of those mutations have already been described in literature [2–4], of which the recurrent deep-intronic

c.7595-2144A > G mutation in *USH2A* intron 40 is an example [5]. This mutation creates a strong splice donor site resulting in the incorporation of a pseudoexon (PE40) into all *USH2A* transcripts and as a consequence, the premature termination of usherin translation. Loss of usherin function in man results in either combined hearing and vision loss (Usher syndrome) or non-syndromic vision loss (retinitis pigmentosa).

Currently, the most widely used approach to interfere with pre-mRNA splicing is antisense oligonucleotide (AON)-based splice modulation. AONs are small single-stranded RNA molecules designed complementary to their target pre-mRNA. Upon binding to splicing regulatory elements within the pre-mRNA transcript, AONs are capable of correcting aberrant pre-mRNA splicing, inducing the skipping of (pseudo)exons or promoting the inclusion of native exons [6].

Humanized animal models, in which a specific part of the species' genomic DNA is replaced by the orthologous human sequence, are pivotal to study the functional effect of aberrant splicing and AON-based splice correction therapy. Multiple vertebrate model organisms, each having their pros and cons, are currently being used for IRD-associated translational research purposes. Among those, the zebrafish represents a fast and inexpensive model which has proven its strength in studying IRDs. Zebrafish are easy to genetically manipulate, have a retinal structure comparable to humans, and for most IRDs (including Usher syndrome) robust phenotypes can already be detected at 5 days post fertilization (dpf) [7].

A major difficulty of using humanized knock-in animal models for the purpose of studying aberrant splicing and evaluating AON-based splice correction is the reported poor recognition of human splice sites by the splicing machineries of other species [8, 9]. As such, thorough *in silico* bio-informatic analyses and *in vitro* cell-based splice assays are essential for the development of a humanized animal model that properly recognizes the splice sites of the introduced human sequence. In this chapter, we will discuss the step-by-step procedure to generate functional humanized zebrafish models, including optimization in cross-species splice-site recognition, to assess the effect of mutation-induced aberrant splicing and subsequent AON-based splice redirection therapies.

2 Materials

2.1 *In Silico* Splice Site Analysis

1. A computer with internet access and a web browser.

2.2 Cloning of a Minigene Splice Vector

1. Forward and reverse primers including attB tails to generate a Gateway[®] cloning-compatible PCR amplicon containing the (pseudo)exon of interest flanked by >500 bp up- and downstream intronic sequence (*see* **Notes 1** and **2**).
2. Gel and PCR Clean-up kit.
3. Gateway[®]BP clonase enzyme mix (Thermo Fisher scientific, Carlsbad (CA), USA).
4. Gateway[®]LR clonase enzyme mix (Thermo Fisher scientific, Carlsbad (CA), USA).
5. Gateway[®] pDONR201 vector (Thermo Fisher scientific, Carlsbad (CA), USA).
6. A pCI-neo-based zebrafish-specific minigene splice assay destination vector [9].
7. DH5 α competent cells.
8. LB agar plates: Dissolve 20 g NaCl, 20 g tryptone, and 10 g yeast extract into 750 ml water. Add 30 g agar and fill up to 1 l. Autoclave the medium and let it cool down to approximately 55 °C. Add the appropriate antibiotics (100 μ g/ml kanamycin or 100 μ g/ml ampicillin) and pour the medium into 10 cm plates. Let the medium solidify and subsequently dry for approximately 10 min. Store the plates at 4 °C until use.
9. LB medium: Dissolve 20 g NaCl, 20 g tryptone, and 10 g yeast extract into 750 ml water. Subsequently, fill up to 1 l total volume and autoclave the solution. LB medium can be stored at room temperature. Prior to use, add 100 μ g/ml kanamycin or 100 μ g/ml ampicillin.
10. Plasmid DNA extraction kit.

2.3 Mutagenesis PCR

1. High-fidelity DNA polymerase.
2. Forward and reverse primers for site-directed mutagenesis, containing the previously identified nucleotide substitution in the splice sites of interest (*see* **Note 3**).
3. *DpnI* restriction enzyme.

2.4 Cell Culture

1. Zendo-1 cells (*see* **Note 4**).
2. L15 medium with L-glutamine (Sigma Aldrich, Saint Louis (MO), USA) (*see* **Note 5**).
3. Fetal calf serum.
4. Penicillin-streptomycin.
5. Isoleucine.
6. Phosphate-buffered saline (PBS) 10 \times : Dissolve 8.1 g NaCl (138 mM), 0.2 g KCl (2.7 mM), 1.15 g Na₂HPO₄·2H₂O (6.5 mM), and 0.2 g KH₂PO₄ (1.5 mM) in 1 l water. Adjust

pH to 7.4 with HCl and autoclave the solution. Dilute ten times with water before use. PBS can be stored at room temperature.

7. Trypsin 1:250. Dissolve 2.5 g trypsin in 100 ml 10× PBS and 900 ml water. Sterilize by filtration.
8. Opti-MEM (Thermo Fisher Scientific, Carlsbad (CA), USA).
9. Liposome-based transfection reagent.

2.5 RNA Isolation

1. RNA isolation kit.

2.6 cDNA Synthesis

1. Reverse transcriptase.
2. Random Hexamers (50 μM) (Thermo Fisher scientific, Carlsbad (CA), USA).
3. RNaseOUT™ Recombinant Ribonuclease Inhibitor (Thermo Fisher scientific, Carlsbad (CA), USA).

2.7 Polymerase Chain Reaction

1. High-fidelity DNA polymerase.
2. dNTP mixture (10 mM each).
3. Target-specific forward and reverse primer (*see Note 6*).

2.8 Agarose Gel Electrophoresis

1. Agarose-gel: Add 150 ml 0.5× TBE buffer to 1.5 g of agarose, and boil the solution until the agarose is completely dissolved. Cool down to approximately 60 °C before adding ethidium bromide to a final concentration of 0.3 μg/ml. Pour the gel into a gel-tray and let it solidify at room temperature (*see Note 7*).

2.9 Donor Template Vector Design and Cloning

1. Forward and reverse primers spanning the human sequence containing the (pseudo)exon of interest flanked by >500 bp up- and downstream intronic sequences.
2. Forward and reverse primers for the amplification of zebrafish-specific homology arms (~900 bp) used for the homologous recombination reaction in zebrafish. Use the GeneArt® Primer and Construct Design Tool (<https://www.thermofisher.com/order/oligoDesigner/type2s>) to design primers compatible with GeneArt® Type II Assembly Kit. The forward primer of the left homology arm and the reverse primer of the right homology arm should contain the sgRNA target site (*see Note 8*).
3. Gel and PCR Clean-up kit.
4. GeneArt® Seamless Cloning and Assembly Kit (Thermo Fisher Scientific, Waltham, MA, USA).

2.10 Animals

1. Tüpfel long fin (TL) zebrafish.

2.11 CRISPR/Cas9 Injections

1. Glass microcapillaries.
2. Micropipette puller.
3. Microinjection plate: Add 80 ml demineralized water to 0.8 g of agarose MP and boil the solution until the agarose is completely dissolved. Cool down to approximately 60 °C before pouring the gel into a dish. Cast the gel with a plastic mold that produces six 1.5-mm-wide trenches [10]. Let the gel solidify at room temperature.
4. Alt-R® S.p. Cas9 Nuclease V3 (Integrated DNA Technologies, Coralville (IA), USA).
5. Potassium chloride.
6. Phenol red.
7. Pneumatic PicoPump pv820 (World Precision Instruments, Sarasota (FL), USA) with foot pedal or similar.
8. Stereo microscope with 10–40× magnification.
9. Micromaster Microscope Stage Micrometer 1 mm (Thermo Fisher Scientific, Waltham, MA, USA).
10. Mineral oil.
11. E3 embryo medium (5 mM NaCl, 0.17 mM KCl, 0.33 mM CaCl₂, 0.33 mM MgSO₄) supplemented with 0.1% methylene blue: Dissolve 34.8 g NaCl, 1.6 g KCl, 5.8 g CaCl₂, and 9.78 g MgCl₂ in 2 l of demineralized water to prepare a 60× stock. Autoclave the 60× stock. To prepare 1× E3 medium, dilute 16.5 ml of the 60× stock to 1 l. Add 100 µl of 1% methylene blue.
12. Zebrafish aquarium and spawning cages.

2.12 Genotyping Materials

1. Lysis buffer (40 mM NaOH and 0.2 mM EDTA in ultrapure water).
2. 2-Phenoxyethanol.
3. 1 M Tris–HCl (pH 7.5).
4. Scissors and forceps.
5. PCR components.

2.13 Quantitative RT-PCR

1. Forward and reverse primers for the specific amplification of fragments with or without the human (pseudo)exon of interest, spanning about 100 bp of expected cDNA sequence (*see Note 9*).
2. gBlocks® Gene Fragments of the PCR targets (Integrated DNA Technologies, IA, USA).
3. Taq polymerase mix.

3 Methods

3.1 Splice Site Optimization

1. The in silico “Berkeley Drosophila Genome Project” splice-site prediction tool (www.fruitfly.org/seq_tools/splice.html) can be used to analyze the strength of splice acceptor and donor sites, using standard settings (*see* **Note 10**). Paste the nucleotide sequence of interest in FASTA format, starting the title line with “>.” Use the submit button to see the resulting splice site prediction scores (*see* **Note 11**).
2. Compare the human splice acceptor and splice donor sequences of interest with the human and zebrafish splice-site consensus sequences [11] (Fig. 1a, b). Identify positions in the human splice acceptor and donor sequences of interest that are markedly different from the zebrafish consensus splice acceptor and donor sequences.
3. Adapt the human splice sites for increased recognition by the zebrafish splicing machinery by substituting nucleotides at the above identified positions in silico (*see* **Note 12**).
4. Analyze the in silico effect of the splice site adaptation(s) using the “Berkeley Drosophila Genome Project” splice-site prediction tool (Fig. 1b).

3.2 Generation of an Engineered Zebrafish-Specific Minigene Splice Vector

1. Perform a PCR using primers that contain Gateway[®]-attB tails to generate a Gateway[®] cloning-compatible PCR amplicon containing the (pseudo)exon of interest flanked by >500 bp up- and downstream intronic sequences (*see* **Notes 1, 2, and 13**). Analyze the PCR products on an agarose gel. Extract and purify the PCR products by using a Gel and PCR Clean-up kit.
2. Perform a Gateway[®] BP-recombination reaction to generate an entry clone containing the purified PCR product. Mix 2 µl of the BP clonase buffer, together with 150 ng pDONR201 vector, 1 µl of the recovered PCR product (~15–150 ng), 4 µl low TE buffer and 2 µl Gateway[®] BP clonase enzyme mix. Incubate the reaction at 25 °C for 2 h (*see* **Note 14**).
3. Terminate the Gateway[®] BP-cloning reaction by adding 1 µl of the Proteinase K solution (2 µg). Vortex briefly. Incubate sample at 37 °C for 10 min.
4. Transform 2.5 µl of the BP reaction into DH5α competent cells according to the manufacturer’s instructions, and plate 200 µl on LB agar plates that contain 100 µg/ml kanamycin as a selection marker for the pDONR201 vector. Incubate overnight at 37 °C (*see* **Note 15**).
5. Inoculate single colonies and culture them overnight in liquid LB medium supplemented with 100 µg/ml kanamycin (*see* **Note 16**).

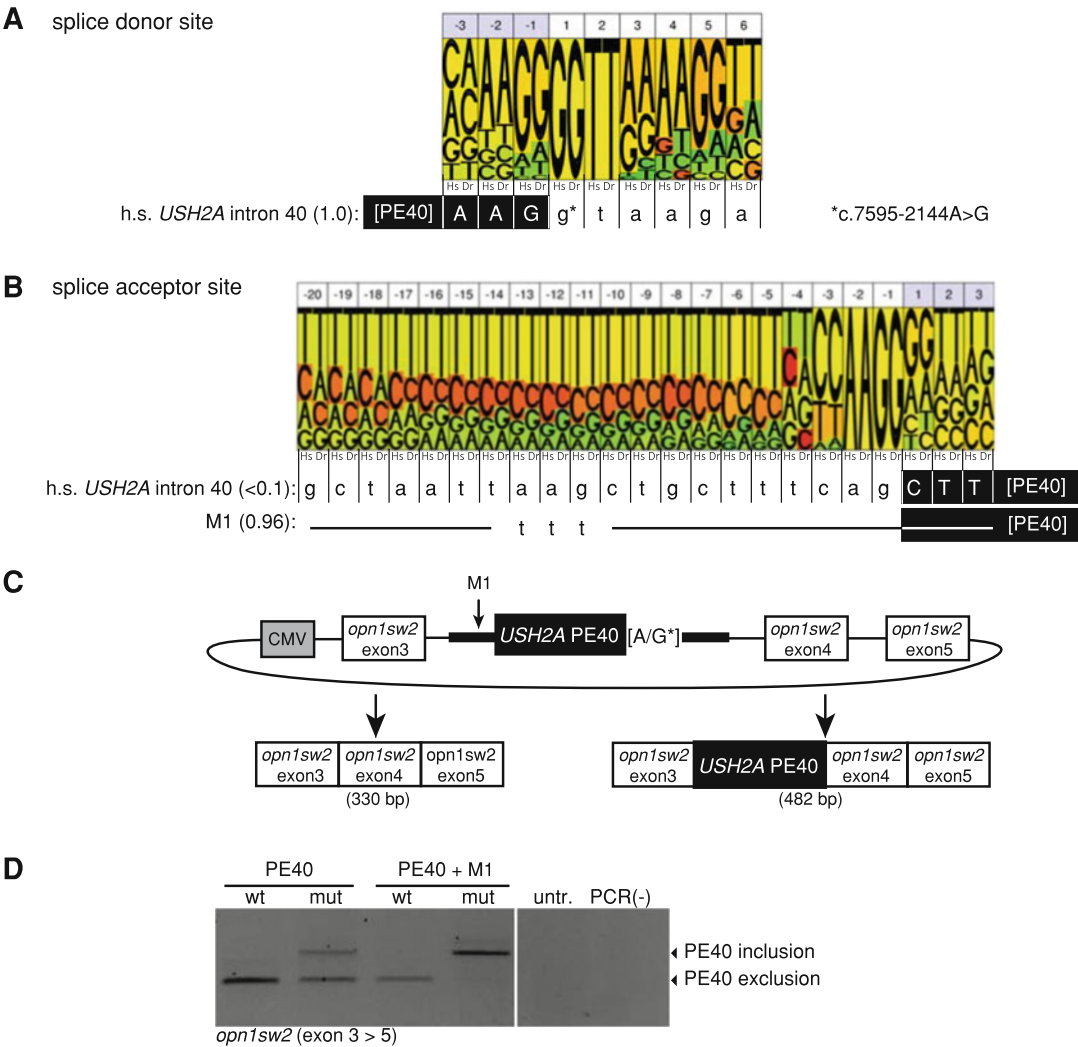


Fig. 1 Optimization of human *USH2A* PE40 splice acceptor site for improved recognition by the zebrafish splicing machinery. **(a)** The nucleotide distribution of the splice donor site found in man (Hs) and zebrafish (Dr). The PE40 splice donor sequence is presented under the splice donor sites with the c.7595-2144A > G mutation, indicated by an asterisk. **(b)** Similar as in **(a)**, the PE40 splice acceptor sequence is presented under the consensus splice acceptor sites as used in human (Hs) and zebrafish (Dr). Based on comparisons, the M1 site was selected for optimization, predicted to result in a stronger PE40 splice acceptor site. The predicted strength of the splice acceptor site is indicated in brackets. **(c)** A zebrafish-specific minigene splice assay containing the human *USH2A* PE40 with flanking sequences was generated. The plasmids, either containing the c.7595-2144A > G mutation (mut) or not (wt), further contained M1 (indicated by vertical arrow). **(d)** The effect of the introduction of M1 on recognition of human *USH2A* PE40 after expression in zebrafish cells (Zendo-1) determined by RT-PCR. untr.: untransfected cells, PCR(–): negative template PCR control. (Reproduced from Slijkerman et al. [9], with permission from Mary Ann Liebert, Inc.)

6. Extract plasmid DNA from the bacterial cultures using a Plasmid DNA extraction kit.

7. Validate the extracted plasmids by Sanger sequencing.
8. Perform mutagenesis PCR to introduce the previously identified nucleotide substitution in the splice sites of interest. Typically, one PCR (50 μ l) contains dNTPs (final concentration of 0.2 mM for each nucleotide), forward and reverse primers containing the nucleotide substitution in the splice site of interest (final concentration of 0.2 mM for each primer), 1 μ l (25–50 ng) entry clone, 0.5 μ l (1 unit) high-fidelity DNA polymerase, and 10 μ l 5 \times reaction buffer. Cycling conditions are: 95 °C for 5 min, followed by 15 cycles with 95 °C for 30 s, “Tm” °C for 1 min and 68 °C for 6 min. The “Tm” temperature depends on the primers used and should be optimized on beforehand. The reaction is finalized by a 5-min incubation step at 68 °C after which the reaction is cooled down to 16 °C until further processing.
9. Analyze the PCR products on an agarose gel.
10. Digest the PCR product with *DpnI* (see **Note 17**).
11. Repeat **steps 4–7** in order to obtain the entry clone with optimized splice site (see **Note 18**).
12. Perform a Gateway[®] LR-recombination reaction to generate a pCI-neo-based zebrafish-specific minigene splice vector. Mix 2 μ l LR clonase buffer with 150 ng of the entry clone, 150 ng pCI-neo-*opn1sw2* exon3–5 destination vector, 2 μ l Gateway[®] LR clonase enzyme mix and low TE buffer to a final volume of 10 μ l. Incubate the reaction at 25 °C for 2 h (see **Note 14**).
13. Repeat **steps 3–7**, using ampicillin instead of kanamycin, in order to obtain the desired zebrafish-specific pCI-neo-based minigene splice vector (Fig. 1c).

3.3 Validation of the Optimized Splice Site Using an Engineered Zebrafish-Specific Minigene Splice Assay

1. Culture Zendo-1 cells at 28 °C. Passage them twice a week in a 1:4 dilution using trypsin (see **Notes 4, 5, and 19**).
2. Seed 1.0×10^6 cells/well into a six-well plate 1 day before transfection (see **Note 20**).
3. Transfect zebrafish-specific pCI-neo-based minigene splice vector into the Zendo-1 cells. Prepare a Lipofectamine[®] 2000 (5 μ l)/Opti-MEM (250 μ l) mixture and a DNA vector (1 μ g)/Opti-MEM (250 μ l) mixture. Incubate both mixtures at room temperature for 5 min before adding them together. Incubate the combined mixture at room temperature for 10 min before adding them drop-wise to the cells (see **Note 21**).
4. Remove the culture medium 4–6 h after transfection and add fresh L15 medium to the cells.
5. Approximately 48 h after transfection, wash the cell with PBS and collect them by using a cell scraper. Centrifuge the cells at

$234 \times g$ for 5 min. Isolate total RNA using a RNA isolation kit, according to manufacturer's instructions.

6. Use 100 ng to 1 μ g of total RNA for cDNA synthesis using Reverse Transcriptase. Prepare a tube for primer annealing and combine 100 ng total RNA, 1 μ l random hexamers (50 μ M), 1 μ l dNTP mix (10 mM) and fill up till 13 μ l with nuclease-free water. Incubate the mixture at 65 °C for 5 min before placing it on ice for at least 1 min. Prepare in a second tube a mixture consisting of 4 μ l 5 \times SSIV buffer, 1 μ l 100 mM DTT, 1 μ l RNaseOUT™ Recombinant Ribonuclease Inhibitor and 1 μ l Reverse Transcriptase (200 U/ μ l). Add the mixture to the annealed primers and incubate the complete reaction mixture at 23 °C for 10 min, 55 °C for 50 min and 80 °C for 10 min.
7. Depending on the RNA input, the cDNA product generated after the reverse transcriptase reaction can be diluted up to 20 \times to serve as a template in a PCR. Typically, one PCR (25 μ l) contains dNTPs (final concentration of 0.2 mM for each nucleotide), forward and reverse primers (final concentration of 0.2 mM for each primer), 0.5–1 μ l (25–50 ng) cDNA, 0.25 μ l (0.5 units) DNA polymerase, and 5 μ l 5 \times reaction buffer. Cycling conditions are: 98 °C for 1 min, followed by 30 cycles with 98 °C for 20 s, “T_m” °C for 20 s and 72 °C for 1 min. The “T_m” temperature depends on the primers used and should be optimized on beforehand. The reaction is finalized by a 5-min incubation step at 72 °C after which the reaction is cooled down to 16 °C until further processing.
8. Analyze the PCR products on an agarose gel. RT-qPCR is recommended when quantification of transcripts is desired to determine the effect of the optimized splice sites. Figure 1d shows the improved recognition of the human PE40 exon in zebrafish after the introduction of the M1 variant in the splice acceptor site.

3.4 Guide RNA Design for CRISPR/ Cas9 Injection

1. Determine the landing site of a given human (pseudo)exon within (the appropriate intronic region of) the corresponding zebrafish gene by using a sequence assembly tool (<https://genome.ucsc.edu/cgi-bin/hgBlat?command=start>). The zebrafish sequence with the highest homology will be exchanged for the human target sequence.
2. The online webtool CHOPCHOP (<https://chopchop.cbu.uib.no/>) can be used to identify candidate Cas9 target sites within the identified zebrafish genomic region of interest and to design corresponding guide RNAs, using standard settings. Select “Paste target” and paste the sequence of interest in FASTA format. Use the “Find Target Sites!” button to predict the Cas9 target sites in your sequence of interest (see Note 22).

3. Select and order the custom guide RNA with no predicted off target binding to other genomic regions (*see* **Note 23**).

3.5 Generation of Donor Template for CRISPR/Cas9-Induced Homology Directed DNA Repair

1. Amplify the human (pseudo)exon of interest with optimized splice sites and surrounding sequences (*see* **Note 24**). Extract and purify the amplified PCR product from an agarose gel using a Gel and PCR Clean-up kit.
2. Design and amplify the left and right homology arm using zebrafish genomic DNA as a template. Homology arms of ~900 bp flanking the target region have shown to be very effective [9, 12]. Extract and purify the PCR products from an agarose gel using a Gel and PCR Clean-up kit.
3. Make use of the GeneArt[®] Seamless Cloning and Assembly Kit to combine the in **steps 1** and **2** amplified PCR products with the supplied linearized pUC19L vector in order to generate a donor template construct containing the human sequence with optimized splice sites flanked by two zebrafish homology arms and sgRNA target sites.
4. Transform 2.5 µl of the GeneArt[®] assembly reaction into DH5α competent cells and plate 200 µl on LB agar plates that contain 100 µg/ml ampicillin as a selection marker for the pUC19 vector. Incubate overnight at 37 °C (*see* **Note 15**).
5. Inoculate single colonies and culture them overnight in liquid LB medium supplemented with 100 µg/ml ampicillin (*see* **Note 16**).
6. Extract plasmid DNA from the bacterial cultures using a DNA extraction kit followed by a phenol/chloroform/isoamyl (25:24:1) extraction and ethanol precipitation.
7. Sanger sequencing verification of the donor template construct.

3.6 Generation of the Humanized Zebrafish Line

1. Use a micropipette puller to prepare glass injection needles from microcapillaries (*see* **Note 25**).
2. Prepare a microinjection plate by casting a 1% agarose gel using a plastic mold that produces six 1.5-mm-wide trenches (*see* **Note 26**).
3. Prepare the injection mixture by combining Cas9 protein (800 ng/µl), sgRNA (100 ng/µl), potassium chloride (0.3 M), phenol red (0.1%), and donor template DNA (25 pg) (*see* **Note 27**). Incubate injection mixture at 37 °C for 5 min prior to injections (*see* **Note 28**).
4. Perform injections by using a Pneumatic Picopump pv280 microinjector, a pipette holder, a foot pedal, and a stereoscope or similar (*see* **Note 29**) (*see* **Note 30**). Load the injection needle with injection mixture and calibrate the needle by

adjusting the pressure and time settings of the microinjector until the injection volume is 1 nl (*see* **Note 31**).

5. Align single-cell-staged fertilized eggs in the trenches of the microinjection plate.
6. Inject embryos by piercing the cell membrane with the injection needle. Press the foot pedal to inject 1 nl of the injection mixture into the cell.
7. Transfer embryos to a new dish containing fresh E3 medium after injection and raise them at 28 °C. Refresh E3 medium on a daily basis and remove dead embryos (*see* **Note 32**).
8. At 5 dpf, transfer the embryos from the dish to a tank in the zebrafish aquarium and raise them for 3 months. At 3 months post-fertilization the injected fish (F0 generation) are sexually mature and can be crossed [13]. The offspring of these F0 fish can be sacrificed for germline transmission analysis of the anticipated recombination event. When positive, F1 of the germline-positive founder fish can be raised for 3 months, and genotyped to identify heterozygous knock-in animals.

3.7 Genotyping After Fin Clipping

1. Prepare for each adult fish one PCR tube containing 75 µl of lysis buffer and one single box containing 1 l of fresh water.
2. Prepare an anesthetic by mixing 250 µl 2-phenoxyethanol with 500 ml water in a beaker.
3. Anesthetize adult zebrafish by putting them in the 2-phenoxyethanol solution for 1–2 min.
4. Manually pick up the anesthetized fish and use scissors to cut a small piece of the caudal fin. Quickly put the fish back into a single box with fresh water. Put the fin in a properly labeled PCR tube using clean forceps. Make sure that both the single box and the PCR tube are labeled with the same number (*see* **Notes 33** and **34**).
5. Incubate the PCR tubes at 95 °C for 20 min (*see* **Note 35**).
6. Add 7.5 µl (10%) 1 M Tris–HCl (pH 7.5) to the lysate (*see* **Note 36**).
7. Dilute the lysate ten times with sterile water and use it directly as a template in a PCR. Typically, one PCR (25 µl) contains dNTPs (final concentration of 0.2 mM for each nucleotide), forward and reverse primers (final concentration of 0.2 mM for each primer), 1 µl lysate, 0.25 µl (0.5 units) DNA polymerase, and 5 µl 5× reaction buffer. Cycling conditions are: 98 °C for 2 min, followed by 30 cycles with 98 °C for 20 s, “Tm” °C for 20 s, and 72 °C for 1 min. The “Tm” temperature depends on the primers used and should be optimized on beforehand. The reaction is finalized by a 5-min incubation step at 72 °C after

which the reaction is cooled down to 16 °C until further processing.

8. Analyze the PCR products on an agarose gel. Confirm the presence or absence of the (pseudo)exon by Sanger sequencing.

3.8 Visualization of Human (Pseudo)Exon Inclusion in Zebrafish

1. Snap freeze 5 dpf larvae in liquid nitrogen and isolate total RNA using an RNA isolation kit.
2. Synthesize cDNA using Reverse Transcriptase. Prepare a tube for primer annealing and combine 100 ng total RNA, 1 µl random hexamers (50 µM), 1 µl dNTP mix (10 mM) and fill up till 13 µl with nuclease-free water. Incubate the mixture at 65 °C for 5 min before placing it on ice for at least 1 min. Prepare in a second tube a mixture consisting of 4 µl 5× SSIV buffer, 1 µl 100 mM DTT, 1 µl RNaseOUT™ Recombinant Ribonuclease Inhibitor, and 1 µl Reverse Transcriptase (200 U/µl). Add the mixture to the annealed primers and incubate the complete reaction mixture at 23 °C for 10 min, 55 °C for 50 min, and 80 °C for 10 min.
3. Dilute your synthesized cDNA 2–10 × (depending on gene expression levels) and use it as a template for PCR amplification. Typically, one PCR (20 µl) contains dNTPs (final concentration of 0.2 mM for each nucleotide), forward and reverse primers (final concentration of 0.2 mM for each primer), 1 µl 2–10× diluted cDNA, 0.25 µl (0.5 units) DNA polymerase, and 4 µl 5× reaction buffer (*see Note 6*). Cycling conditions are: 98 °C for 2 min, followed by 35 cycles with 98 °C for 15 s, “T_m” °C for 20 s, and 72 °C for 45 s. The “T_m” temperature depends on the primers used and should be optimized on beforehand. The reaction is finalized by a 5-min incubation step at 72 °C after which the reaction is cooled down to 16 °C until further processing.
4. Visualize human (pseudo)exon inclusion by analyzing the amplified PCR products on an agarose gel. Figure 2a shows an example of increased in vivo recognition of the (pseudo)-exon after optimization of the splice site.

3.9 Quantification of Human (Pseudo)Exon Inclusion Using Quantitative RT-PCR (RT-qPCR)

1. Order two gBlocks® Gene Fragments, one for each of the RT-qPCR amplicons (*see Note 37*). These synthetic oligonucleotides can be used to generate a standard curve of known copy numbers for each amplicon. Dissolve the gBlocks® Gene Fragments and prepare a stock solution containing 10⁷ copies per µl (*see Note 38*). Generate a 1:1 serial dilution series of the gBlock® stock solution in cDNA of an unrelated species (*see Note 39*).

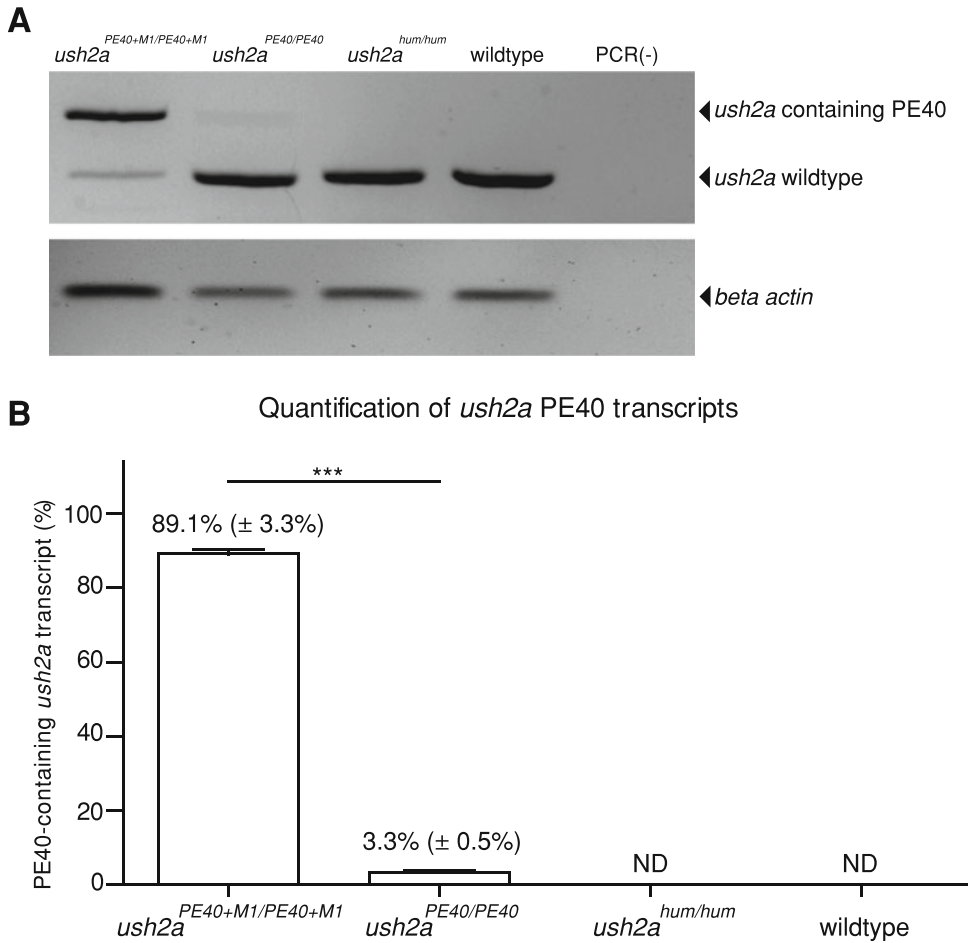


Fig. 2 Human *USH2A* PE40 incorporation in zebrafish *ush2a* transcripts. **(a)** The level of human *USH2A* PE40 incorporation into the zebrafish *ush2a* transcript is analyzed by RT-PCR using cDNA derived from *ush2a*^{PE40 + M1/PE40 + M1}, *ush2a*^{PE40/PE40}, *ush2a*^{hum/hum}, and wild-type larvae (5dpf). *Beta actin* amplification is shown as loading control (lower panel). **(b)** Quantitative RT-PCR analyses to determine the absolute number of PE40-containing *ush2a* transcripts in *ush2a*^{PE40 + M1/PE40 + M1}, *ush2a*^{PE40/PE40}, *ush2a*^{hum/hum}, and wild-type larvae (5dpf). Data are expressed as percentage of PE40-inclusion (mean ± SD). Two-tailed unpaired Student's *t*-test revealed significant differences between groups (*p* = 0.0001). *ND* not detectable

2. Perform a RT-qPCR with a primer pair designed to specifically amplify the exon-inclusion amplicon and a RT-qPCR with a primer pair designed to specifically amplify the exon-exclusion amplicon on the serial gBlocks® dilution and on the zebrafish cDNA samples (see **Note 9**). Amplify all amplicons in duplicate.
3. Analyze the RT-qPCR data by plotting a standard curve of the log values of the copy numbers of the gBlock dilutions against the mean cycle quantification value (Ct or Cq) measured for each gBlock dilution (see **Note 40**). Based on the standard curve, calculate for each cDNA sample, the transcript number

of the exon-inclusion amplicon and of the exon-exclusion amplicon. The amount of product expected from splice site optimization can be calculated as percentage of total *ush2a* transcripts (Fig. 2b). The latter can be calculated as the sum of wild-type product and product expected from splice site optimization (see **Note 41**).

4 Notes

1. Design a forward and reverse primer to generate the amplicon with the sequence of interest. Add a Gateway[®]-compatible attB1 tail to the forward primer (5'-GGGGACAAGTTTGTACAAAAAAGCAGGCT-XXX-3') and attB2 tail to the reverse primer (5'-GGGGACCACTTTGTACAAGAAAGCTGGGT-YYY-3'). XXX indicates the forward primer sequence and YYY indicates the reverse primer sequence from 5' to 3'.
2. The advised maximum fragment size for Gateway cloning reactions is 8 kb.
3. Typically, mutagenesis primers have a length of 25–45 nucleotides with the anticipated mutation in the center. The melting temperature (T_m) must be ≥ 78 °C and a G or C base at the 3' end of each primer is favored, due to the higher stability of GC base pairs (three hydrogen bonds) as compared to AT base pairs (two hydrogen bonds).
4. Use a zebrafish-specific cell line that does not endogenously express the gene of interest (in this case *opn1sw2*). Endogenous expression of the gene of interest can interfere with the analysis of the effect of the mutation on splicing. A detailed protocol for the generation of your own zebrafish-specific cell line is described by Choorapoikayil et al. [14].
5. Culture Zendo-1 cells at 28 °C in L15 medium supplemented with 15% v/v FCS, 1% v/v penicillin/streptomycin and 250 mg/l isoleucine (final concentration in the medium). All cell culture reagents should be pre-warmed to the same temperature as at which the cells are cultured.
6. The total PCR amplicon length should be chosen in such a way that splice redirection results in a markedly different-sized PCR product that can be readily distinguished after agarose gel electrophoresis. The inclusion of multiple flanking exons in the minigene splice assay is of importance since sequence alterations can not only influence the in- and exclusion of the targeted (pseudo)exon but also induce the in- and exclusion of flanking exons [15].

7. Casted agarose gels can be stored at 4 °C for up to 1 month when properly sealed in order to prevent them from drying out.
8. Adding the sgRNA target site to your donor template was found to increase the desired knock-in event up to 20-fold compared to using a donor template vector without those sites [12]. Note that the introduced sgRNA target site should include a canonical PAM site.
9. To specifically amplify transcripts without the target exon, one of the primers must span the exon–exon boundary of the surrounding exons. For the detection of the exon-inclusion transcript, one of the primers must reside within the target exon. Alternatively, custom TaqMan[®] assays (Thermo Fisher scientific, Carlsbad (CA), USA) can be designed for each transcript.
10. The strength of a splice site is conditioned to many different factors, like splice site sequence, the strength of competing splice sites, the relative positions of splice sites, and the presence of tissue-specific *trans*-acting factors [16]. The in silico calculated strength is therefore stochastic.
11. Splice site prediction scores can range from 0 (extremely weak) to 1.0 (extremely strong). Optimize a given splice donor or acceptor site to reach a prediction score as close as possible to 1.0. Keep in mind not to alter the sequence of potential anti-sense oligonucleotide binding sites.
12. Avoid (pseudo)exonic nucleotide substitutions, since those substitutions can result in changes in the encoded amino acids and can potentially affect AON binding sites.
13. Use a high-fidelity DNA polymerase (e.g., Q5[®] High-Fidelity DNA Polymerase). High-fidelity DNA polymerases couple low misincorporation rates with proofreading activity, resulting in near-perfect replication of the target DNA and thereby efficient cloning of the plasmids.
14. We have experienced that extending the incubation time at 25 °C from 2 h to overnight greatly improves the recombination efficiency for difficult cloning reactions (e.g., larger fragments to be cloned).
15. In case no transformants are obtained using DH5 α competent cells, one can consider the use of competent cells with a higher transformation efficiency (e.g., TOP10 competent cells).
16. As a rule of thumb, we generally analyze three clones per reaction.
17. *DpnI* cleaves only methylated recognition sites. It will therefore only cleave the bacterial template DNA and not the amplified DNA.

18. Skip **steps 8–11** to obtain the splice vector without optimized splice sites. Depending on the predicted strengths of the splice sites, it can be useful to first investigate pre-mRNA splicing in a construct without splice site optimization.
19. We culture Zendo-1 cells at 28 °C since they are derived from zebrafish which thrive at an ambient temperature of 28 °C.
20. Seeding density depends on the type of zebrafish-derived cells that are used. Seed cells to be 70–90% confluent at the time of transfection.
21. The two-step dilution method results in higher quality data and generates more reproducible results compared to adding the lipid directly to the diluted DNA. The 10-min pre-incubation stimulates the formation of micelles containing plasmid DNA prior to transfection, resulting in the highest transfection efficiency.
22. The requirement of an NGG PAM site at the target sequence can limit applications of frequently used Cas9 from *Streptococcus pyogenes*. Depending on the target region, other RNA-guided endonucleases can be used, each targeting a unique PAM sequence [17].
23. Single guide RNAs can also be produced manually according to the protocol published by Gagnon et al. [18].
24. Also generate a donor template construct without optimization of the splice sites. This construct can be used as a control to analyze the effect of the splice site optimization.
25. Micropipette puller programs for preparation of injection needles differ between machines and installed heating filaments and should be experimentally optimized according to the device manual.
26. Microinjection plates can be used multiple times upon storage at 4 °C for up to 1 month.
27. Phenol red is added to the injection mixture as a tracer to show which embryo received a dose.
28. Pre-incubation at 37 °C induces Cas9/sgRNA complex formation.
29. The Pneumatic Picopump pv280 microinjector delivers precise volume through pressure pulses of air, which can be adjusted by the user. A foot pedal is connected to the injector and activates the pressure pulse for injection mix delivery. The pipette holder secures the pipette for use during the procedure and connects it to the airline of the injector.
30. A micromanipulator can be used for micro-injections. It allows the researcher to make small and accurate adjustments to the pipette location. However, our experience suggests manual

microinjection since it results in a higher injection speed and accuracy.

31. To calculate the volume of a sphere, use the following formula: *Volume of a sphere (cm³) = $4/3\pi r^3$ (r in cm)*. A 1 nl sphere is 1×10^{-6} cm³. Define the radius of the sphere by using a calibration micrometer.
32. To get an indication of the recombination efficiency, a selection of embryos (~15 embryos) can be sacrificed at 1 day post fertilization for genotyping purposes. Lyse and genotype the embryos individually as described in Subheading 3.8.
33. Fish can be kept in single boxes for a maximum of 5 days without feeding and flow of fresh water, although guidelines and legislation concerning housing can differ between institutions. Consult your local institutional guidelines for the most accurate information.
34. Check if all tails are immersed in the lysis buffer.
35. Flick the PCR tubes to mix and disintegrate the tissue.
36. Tris-HCl neutralizes the lysis buffer and stabilizes DNA, thereby supporting long-term storage.
37. gBlocks[®] Gene Fragments are affordable and easy to obtain. Using gBlock fragments as DNA standards in a RT-qPCR assay decreases time, reagents, and costs of creating a standard curve [19].
38. Use the mass of the gBlocks fragments (provided by manufacturer) to calculate the amount of DNA copies in the gBlock standard by using the following formula: *weight per copy = (# bp in gBlocks) × 617.5 g/mol/bp × (1 mol/6.02 × 10²³ molecules)* [19].
39. Diluting the gBlock in cDNA of an unrelated species provides a cDNA context in which off-target binding of the primers is included in the RT-qPCR efficiency, without the presence of on-target transcripts.
40. Adjust the gBlock dilution range if amplification of the used gBlock dilution series did result in amplification values outside of the qPCR detection range.
41. A third primer pair and gBlock can be used to quantify the total number of transcripts by amplifying other exons of the transcript.

Acknowledgments

The authors would like to thank Dr. Jeroen den Hertog for sharing his zebrafish cell line Zendo-1. The authors acknowledge the

facilities and personnel of the Zebrafish Facility at the Faculty of Science of the Radboud University Nijmegen. The authors received funding from the Foundation Fighting Blindness USA (FFB PPA-0517-0717-RAD to EvW) and Stichting Ushersyndroom (to EvW and EdV) for the research that led to the protocol.

References

1. Liu MM, Zack DJ (2013) Alternative splicing and retinal degeneration. *Clin Genet* 84: 142–149. <https://doi.org/10.1111/cge.12181>
2. Cremers FP, van de Pol DJ, van Driel M et al (1998) Autosomal recessive retinitis pigmentosa and cone-rod dystrophy caused by splice site mutations in the Stargardt's disease gene ABCR. *Hum Mol Genet* 7:355–362. <https://doi.org/10.1093/hmg/7.3.355>
3. Hollander den AI, Koenekoop RK, Yzer S et al (2006) Mutations in the CEP290 (NPHP6) gene are a frequent cause of Leber congenital amaurosis. *Am J Hum Genet* 79:556–561. <https://doi.org/10.1086/507318>
4. Thompson DA, Gyürüs P, Fleischer LL et al (2000) Genetics and phenotypes of RPE65 mutations in inherited retinal degeneration. *Invest Ophthalmol Vis Sci* 41:4293–4299
5. Vaché C, Besnard T, le Berre P et al (2012) Usher syndrome type 2 caused by activation of an USH2A pseudoexon: implications for diagnosis and therapy. *Hum Mutat* 33:104–108. <https://doi.org/10.1002/humu.21634>
6. Hammond SM, Wood MJA (2011) Genetic therapies for RNA mis-splicing diseases. *Trends Genet* 27:196–205. <https://doi.org/10.1016/j.tig.2011.02.004>
7. Slijkerman RWN, Song F, Astuti GDN et al (2015) The pros and cons of vertebrate animal models for functional and therapeutic research on inherited retinal dystrophies. *Prog Retin Eye Res* 48:137–159. <https://doi.org/10.1016/j.preteyeres.2015.04.004>
8. Garanto A, van Beersum SEC, Peters TA et al (2013) Unexpected CEP290 mRNA splicing in a humanized knock-in mouse model for Leber congenital amaurosis. *PLoS One* 8: e79369. <https://doi.org/10.1371/journal.pone.0079369>
9. Slijkerman R, Goloborodko A, Broekman S et al (2018) Poor splice-site recognition in a humanized zebrafish knockin model for the recurrent deep-Intronic c.7595-2144A>G mutation in USH2A. *Zebrafish* 15:597. <https://doi.org/10.1089/zeb.2018.1613>
10. Westerfield M (2000) The zebrafish book : a guide for the laboratory use of zebrafish. http://zfin.org/zf_info/zfbook/zfbk.html
11. Abril JF, Castelo R, Guigó R (2005) Comparison of splice sites in mammals and chicken. *Genome Res* 15:111–119. <https://doi.org/10.1101/gr.3108805>
12. Irion U, Krauss J, Nüsslein-Volhard C (2014) Precise and efficient genome editing in zebrafish using the CRISPR/Cas9 system. *Development* 141:4827–4830. <https://doi.org/10.1242/dev.115584>
13. Singleman C, Holtzman NG (2014) Growth and maturation in the zebrafish, *Danio rerio*: a staging tool for teaching and research. *Zebrafish* 11:396–406. <https://doi.org/10.1089/zeb.2014.0976>
14. Choorapoikayil S, Overvoorde J, Hertog den J (2013) Deriving cell lines from zebrafish embryos and tumors. *Zebrafish* 10:316–325. <https://doi.org/10.1089/zeb.2013.0866>
15. Lenassi E, Saihan Z, Bitner-Glindzicz M, Webster AR (2014) The effect of the common c.2299delG mutation in USH2A on RNA splicing. *Exp Eye Res* 122:9–12. <https://doi.org/10.1016/j.exer.2014.02.018>
16. Fu XY, Manley JL (1987) Factors influencing alternative splice site utilization in vivo. *Mol Cell Biol* 7:738–748. <https://doi.org/10.1128/mcb.7.2.738>
17. Yao R, Liu D, Jia X et al (2018) CRISPR-Cas9/Cas12a biotechnology and application in bacteria. *Synth Syst Biotechnol* 3:135–149. <https://doi.org/10.1016/j.synbio.2018.09.004>
18. Gagnon JA, Valen E, Thyme SB et al (2014) Efficient mutagenesis by Cas9 protein-mediated oligonucleotide insertion and large-scale assessment of single-guide RNAs. *PLoS One* 9:e98186. <https://doi.org/10.1371/journal.pone.0098186>
19. Conte J, Potoczniak MJ, Tobe SS (2018) Using synthetic oligonucleotides as standards in probe-based qPCR. *BioTechniques* 64: 177–179. <https://doi.org/10.2144/btn-2018-2000>

Open Access This chapter is licensed under the terms of the Creative Commons Attribution 4.0 International License (<http://creativecommons.org/licenses/by/4.0/>), which permits use, sharing, adaptation, distribution and reproduction in any medium or format, as long as you give appropriate credit to the original author(s) and the source, provide a link to the Creative Commons license and indicate if changes were made.

The images or other third party material in this chapter are included in the chapter's Creative Commons license, unless indicated otherwise in a credit line to the material. If material is not included in the chapter's Creative Commons license and your intended use is not permitted by statutory regulation or exceeds the permitted use, you will need to obtain permission directly from the copyright holder.





Use of Small Animal Models for Duchenne and Parameters to Assess Efficiency upon Antisense Treatment

Ngoc Lu-Nguyen, Alberto Malerba, and Linda Popplewell

Abstract

Duchenne muscular dystrophy (DMD) is a rare genetic disease affecting 1 in 5000 newborn boys. It is caused by mutations in the *DMD* gene with a consequent lack of dystrophin protein that leads to deterioration of myofibers and their replacement with fibro-adipogenic tissue. Using antisense oligonucleotides (AONs) to modify out-of-frame mutations in the *DMD* gene, named exon skipping, is currently considered among the most promising treatments for DMD patients. The development of this strategy is rapidly moving forward, and AONs designed to skip exons 51 and 53 have received accelerated approval in the USA. In preclinical setting, the *mdx* mouse model, carrying a point mutation in exon 23 of the murine *Dmd* gene that prevents production of dystrophin protein, has emerged as a valuable tool, and it is widely used to study in vivo therapeutic approaches for DMD. Here we describe the methodology for intravenous delivery of AONs targeting dystrophin through tail vein of *mdx* mice. Furthermore, the most relevant functional analyses to be performed in living mice, and the most informative histopathological and molecular assays to evaluate the effect of this treatment are detailed.

Key words Antisense oligonucleotides, Duchenne muscular dystrophy, Dystrophin, Exon skipping, *mdx*

1 Introduction

Duchenne muscular dystrophy (DMD) is due to mutations on the *DMD* gene and the consequent loss of the dystrophin protein in skeletal and cardiac muscles [1]. The loss of dystrophin makes the muscle fibers extremely fragile and susceptible to cycles of tissue degeneration and regeneration causing depletion of muscle stem cells and massive deposition of fat/connective tissue finally leading to muscle weakness, respiratory insufficiency, and cardiac failure [2]. Mutations of the *DMD* gene often lead to the disruption of the reading frame. Exon skipping, based on the selective removal of exons flanking the out-of-frame mutations using antisense oligonucleotides (AONs), has been used to re-frame the mRNA transcript to allow the expression of a partially functional Becker

muscular dystrophy (BMD)-like protein [3, 4]. To study this approach in vivo, AONs targeting exon 23 of the mouse *Dmd* gene have been tested by local and systemic delivery in *mdx* mice, the most used animal model of DMD, from neonatal to very late (>15-month old) stages of development [5–8].

In this chapter, we focus on systemic intravenous administration of AONs that allows their body-wide distribution. We provide a detailed description of intravenous infusion of AONs through the mouse tail vein. Phosphorodiamidate morpholino oligomers (PMOs) with or without the conjugation with a cell-penetrating peptide have been used for this approach [4–8]. We also list methods for assessing the animal locomotor activities, forelimb strength, treadmill and wheel exercise, and in situ muscle physiology. *Post-mortem* protocols for RT-PCRs measuring the level of exon skipping for *DMD* exon 23, Western blot for quantifying the level of dystrophin protein, and immunofluorescence for evaluating muscle histology and the effect of the treatment on muscle size, muscle fibrosis, and myofiber cross-sectional area are additionally described.

2 Materials

2.1 PMO and PMO Conjugate

1. PMO-DMD inducing skipping of murine *Dmd* exon 23 (5'-GGCCAAACCTCGGCTTACCTGAAAT-3') is synthesized and conjugated to an arginine-rich cell-penetrating peptide (so-called B-peptide: RXRRBRRXRBRXB) at the 3'-end of the PMO by Sarepta Therapeutics Inc. (see **Note 1**).
2. BPMOs, as lyophilized powder, are kept at -20°C .
3. Resuspended BPMOs (at 10 mg/ml), in sterile ddH₂O, are kept at 4°C .

2.2 Animals

1. All animal procedures are performed in accordance with the UK Animals (Scientific Procedures) Act, 1986.
2. *Mdx* (C57BL/10ScSn-Dmdmdx) and C57BL/10 mice are bred in an authorized animal facility and are maintained in a standard 12-h light/dark cycle with free access to food and water. Both *mdx* and C57BL/10 mice are also available from The Jackson laboratory (<https://www.jax.org>).

2.3 Intravenous Tail Vein Injection

1. BPMOs (as described in Subheading 2.1).
2. 0.9% saline.
3. BD Microfine Insulin 0.3-ml syringes with 30G needles attached.
4. 70% ethanol.
5. ddH₂O.

6. Heat chamber (set at 40 °C).
7. Mouse restrainer.
8. Clean cages with bedding, food, and water.

2.4 Postmortem Tissue Processing

1. CO₂ chamber.
2. Liquid nitrogen (N₂).
3. Isopentane, isopentane container.
4. 70% ethanol.
5. Dissection tools (i.e., scalpels, scissors, tweezers, forceps).
6. Raymond lamb cork disc for cryostat use (20 mm x 3 mm), cork holder.
7. Optimal cutting temperature (OCT) embedding medium.
8. 1.5-ml tubes.
9. Scales to weigh mice and samples harvested.

2.5 RNA Extraction and RT-PCR

1. RNeasy Fibrous Tissue kit (QIAgen).
2. Tungsten Carbide beads, 3 mm (QIAgen).
3. TissueLyser II (QIAgen).
4. ND-1000 NanoDrop spectrophotometer.
5. GoScript Reverse Transcription System.
6. GoTaq Polymerase.
7. Reverse transcription master mix: 2.5 mM MgCl₂, 0.5 mM dNTPs, 1x GoScript Reverse Transcription buffer, 8 units of GoScript Reverse Transcriptase, ddH₂O up to 10 µl/reaction.
8. PCR master mix: 200 nM forward/reverse primer, 1.5 mM MgCl₂, 0.2 mM dNTPs, 1x GoTaq buffer, 1.25 units of GoTaq Polymerase, ddH₂O up to 21 µl/reaction.
9. Agarose.
10. 1x TAE buffer: 40 mM Trizma base, 20 mM glacial acetic acid, 1 mM Na₂EDTA, pH 7.6.
11. GeneTools Image Analysis software 4.02 (Syngene) or ImageJ (NIH, free download at <https://imagej.nih.gov/ij/download.html>).
12. PCR primers, see below:

Primer name	Sequence (5'–3')
mDmd SDY 20x21 (F)	GTAAGGATGAAGTCAACAGATTG
mDmd ASDY 25 (R)	TCCCACTGAGTGTTAAGCTC
mDmd ASDY 24 (R)	GCCATCCATTTCTGTAAG

2.6 Protein Extraction and Western Blot

1. Lysis buffer: 0.15 M NaCl, 0.05 M HEPES, 1% NP-40, 0.5% sodium deoxycholate, 0.1% sodium dodecyl sulfate, 0.01 M EDTA, protease inhibitor (Roche, 1 tablet/50 ml). Aliquot and store at -20°C .
2. Tungsten Carbide beads, 3 mm.
3. TissueLyser II.
4. DC Protein Assay.
5. NuPAGE 3–8% Tris–Acetate gels, Tris–Acetate running and transfer buffers.
6. HiMark Pre-stained Protein Ladder.
7. HyBond nitrocellulose membrane, 0.45 μm pore size.
8. 1x Phosphate-buffered saline (PBS) solution: 137 mM NaCl, 2.7 mM KCl, 4.3 mM Na_2HPO_4 , 1.47 mM KH_2PO_4 , pH 7.4.
9. Blocking buffer: 5% skimmed milk, 1x PBS, 0.2% Tween-20.
10. Washing buffer: 1x PBS, 0.1% Tween-20.
11. Primary antibodies: Mouse monoclonal anti-dystrophin 6C5 (Novocastra Laboratories), rabbit anti- α tubulin (Abcam).
12. Secondary antibodies (LI-COR Biosciences): goat anti-mouse IRDye800, goat anti-rabbit IRDye680.
13. Odyssey Infrared Imaging System (LI-COR Biosciences).

2.7 Immunohisto- chemistry Staining and Histological Analyses

1. OTF 5000 cryostat (Bright).
2. Superfrost[®] Plus microscopy slides, coverslips.
3. Dako (hydrophobic) pen.
4. 100% acetone, 100% ethanol, 100% xylene.
5. 1x PBS solution: 137 mM NaCl, 2.7 mM KCl, 4.3 mM Na_2HPO_4 , 1.47 mM KH_2PO_4 , pH 7.4. Store at room temperature.
6. 4% paraformaldehyde (PFA): dissolve 40 g PFA in 700 ml of 1x PBS at 60°C . Top up with 260 ml dH_2O to cool down solution. Add few drops of 5 M NaOH and adjust to pH 7.4. Aliquot and store at -20°C .
7. 0.3% Picro sirius red: 0.3 g sirius red in 100 ml of saturated picric acid solution, filter through filter paper.
8. 0.5% acetic acid: 100% acetic acid diluted in tap water.
9. Mouse-On-Mouse (MOM) Basic kit (Vector Laboratories).
10. Blocking buffer: MOM blocking reagent (supplied with the MOM kit, 1 drop in 1.25 ml 1x PBS), 1% bovine serum albumin, 1% goat serum, 0.1% Triton X-100.
11. Washing buffer: 1x PBS, 0.05% Tween-20.

12. Primary antibodies: mouse monoclonal anti-dystrophin 6C5 (Novocastra Laboratories), rabbit polyclonal anti-laminin (Abcam), rabbit polyclonal anti-collagen VI (Abcam).
13. Secondary antibodies (Life Technologies): goat anti-mouse Alexa488 and goat anti-rabbit Alexa568.
14. 4',6-Diamidino-2-phenylindole (DAPI).
15. 0.1% *p*-Phenylenediamine (PPD) anti-bleaching solution: dissolved in water, stored at -20°C , and protected from light.
16. Mowiol solution: stir 4.8 ml glycerol, 2.4 g Mowiol in 6 ml water for 2 h, at room temperature. Add 12 ml of 0.2 M Tris buffer pH 8.5, 0.02% sodium azide. Incubate solution in $50\text{--}60^{\circ}\text{C}$ water bath for 10 min, stirring frequently. Centrifuge at $5000 \times g$ for 15 min. Collect supernatant, aliquot and store at -20°C (*see Note 2*).
17. Mounting solution: mix 1 part of 0.1% PPD solution with 9 parts of Mowiol solution, maintain at room temperature, protect from light and use within a day.
18. DPX mountant (Sigma Aldrich).
19. Microscope (e.g., Axio Observer D1, ZEISS).
20. Image acquisition and analysis software (e.g., ZEN software, Fiji—free downloaded at <https://imagej.net/Fiji/Downloads>).

3 Methods

3.1 Intravenous Tail-Vein Injection (*See Note 3*)

1. Dilute BPMO in sterile 0.9% saline at a desired concentration, immediately prior to injection, and keep on ice during the procedure.
2. Weigh mouse and calculate the dose of BPMO needed in a total volume of $200\text{ }\mu\text{l}$ /mouse.
3. Place mouse in a heat chamber for about 10 min.
4. Load BPMO solution into syringe, remove all air bubbles.
5. Transfer the mouse into a restrainer leaving the tail outside.
6. Hold the tail all the time to avoid the mouse withdrawing its tail.
7. Close the restrainer tightly so that the mouse can breathe but barely move back and forth (*see Note 4*).
8. Turn restrainer on its side, this will also turn the mouse on the side.
9. Wipe the tail with 70% ethanol.
10. Identify the lateral veins (the tail has one vein on each side).

11. Hold the tail on your left hand (for right-handed researchers). Hold the needle (with bevel up) on your right hand and inject BPMO. If injection fails, try few more times on that side prior to changing to the other side.
12. Slowly remove the needle and apply gentle compression (with a thumb) until bleeding ceases.
13. Place mouse into a clean cage.

3.2 Functional Tests

TREAT-NMD has provided exhaustive experimental protocols for DMD animal models (<http://www.treat-nmd.eu/resources/research-resources/dmd-sops/>). Below are four functional tests we use to assess muscle function, usually 1 or 2 weeks before the experiment ends:

1. Behavioral and locomotor measurements using open field animal activity monitoring system (SOP ID No.: DMD_M.2.1.002).
2. Use of treadmill and wheel exercise to assess dystrophic state (SOP ID No.: DMD_M.2.1.003).
3. Use of grip strength meter to assess the limb strength of *mdx* mice (SOP ID No.: DMD_M.2.2.001).
4. Measuring isometric force of isolated mouse skeletal muscles in situ (TREAT-NMD, SOP ID No.: DMD_M.2.2.005).

3.3 Postmortem Tissue Processing

1. Weigh mouse before sacrificing by CO₂ exposure and confirm the death by neck dislocation.
2. From each mouse, we usually collect heart, diaphragm, extensor digitorum longus, gastrocnemius, soleus, and tibialis anterior.
3. Tissues from one side of the body are frozen immediately in liquid N₂ for RNA and protein extraction while tissues from the other side are embedded in OCT and subsequently frozen in liquid N₂-cooled isopentane for cryo-sectioning (*see Note 5*).
4. All samples are kept at −80 °C until use.
5. If required, collect total blood by cardiac puncture into 1-ml syringe (*see Note 6*). Transfer the blood into an ice-cold 1.5-ml tube, keep on ice for at least 4 h or overnight prior to serum extraction: (1) centrifuge at $8000 \times g$ for 10 min at 4 °C; (2) transfer supernatant to fresh tubes; (3) repeat centrifugation; (4) collect the supernatant and store at −80 °C.

**3.4 RNA Extraction
and RT-PCR
Quantifying Exon
Skipping Efficiency**

1. Place samples on ice immediately after taking them out of -80°C freezer.
2. Add lysis buffer RLT provided with RNeasy Fibrous Tissue kit and wait until samples thawed down.
3. Disrupt and homogenize samples with 3 mm Tungsten Carbide beads at 25 Hz for 2 x 2 min (*see Note 7*) on a TissueLyser II.
4. Follow manufacturer's instructions to complete RNA extraction process (*see Note 8*).
5. Quantify RNA concentration using a ND-1000 NanoDrop spectrophotometer.
6. Make first strand cDNA: 500–1000 ng RNA, 0.5 μg oligo dT, 0.5 μg random primers, ddH₂O up to 10 μl /reaction. Run program: 70°C for 5 min, 4°C for at least 5 min.
7. Reverse Transcription: add 10 μl of the master mix into 10 μl of first strand cDNA. Run program: 25°C for 5 min, 42°C for 1 h, 70°C for 15 min (*see Note 9*).
8. Mix 4 μl cDNA (made in **step 7**, equivalent to 100–200 ng cDNA) with 21 μl PCR master mix and run PCR programs as below.
9. First-round PCR program: 94°C for 2 min, 30 cycles (94°C for 1 min, 57°C for 1 min, 72°C for 1 min), 72°C for 5 min, 4°C for infinity.
10. Nested PCR program: 94°C for 2 min, 30 cycles (94°C for 1 min, 54°C for 1 min, 72°C for 45 sec), 72°C for 5 min, 4°C for infinity.
11. PCR products are loaded onto 2% agarose gels, with HyperLadderIV used as a size standard. Expected sizes: 577 bp (unskipped), 346 bp (skipped exon 23), 218 bp (skipped exons 22 + 23).
12. Densitometric analysis of gel electrophoresis results can be done using GeneTools Image Analysis or ImageJ software.
13. Evaluate the efficiency of dystrophin exon skipping as the percentage of the density of skipped products against the total density of unskipped and skipped products.

**3.5 Protein
Extraction and
Western Blot
Quantifying Dystrophin
Expression**

1. Place samples on ice immediately after taking them out of -80°C freezer.
2. Add lysis buffer (*see Note 10*) and wait until samples thawed down.
3. Disrupt and homogenize samples with 3 mm Tungsten Carbide beads at 25 Hz for 2 x 2 min (*see Note 7*) on a TissueLyser II.
4. Centrifuge at $14,000 \times g$, 10 min, 4°C .

5. Transfer the supernatant to fresh pre-chilled 1.5-ml tubes. Repeat centrifugation if required.
6. Quantify the total protein with *DC* Protein Assay following the manufacturer's instructions.
7. Reduced protein samples (100–200 µg) are resolved on NuPAGE 3–8% Tris–Acetate gels with HiMark Pre-stained Protein Ladder used as a size standard.
8. Run gel at 150 V for 1.5 h (or until the dye reaches the bottom of gel) in Tris–Acetate buffer and blot onto HyBond nitrocellulose membranes for 2 h at 30 V.
9. Block in blocking buffer for 1 h, at room temperature, with gentle agitation.
10. Primary antibody incubation for overnight at 4 °C (with gentle agitation) with either mouse monoclonal anti-dystrophin 6C5 (1:100) or rabbit anti- α tubulin (1:2500), diluted in blocking buffer (*see Note 11*).
11. Wash for 3 x 5 min in washing buffer with gentle agitation.
12. Secondary antibody incubation for 1 h at room temperature (with gentle agitation) with goat anti-mouse IRDye800 and goat anti-rabbit IRDye680 (1:10,000, diluted in blocking buffer), protect from light afterwards.
13. Wash for 3 x 5 min in washing buffer with gentle agitation.
14. Analyze on an Odyssey Infrared Imaging System (ImageJ software can be used alternatively). Expected size: 427 kDa for dystrophin and 50 kDa for α tubulin.
15. The values of dystrophin intensity are normalized to the values of corresponding α -tubulin intensity and subsequently quantified based on a standard curve of dystrophin (*see Note 12*).

3.6 Immunostaining for Dystrophin, Laminin, or Collagen VI

For histological analyses, muscles are sectioned and co-immunostained for dystrophin/laminin to assess the percentage of dystrophin positive fibers and the muscle cross sectional area or immunostained for collagen VI to assess the amount of muscle fibrosis.

1. Section frozen tissue on an OTF 5000 cryostat at 10-µm thickness through the muscle length. Cutting temperature is between –24 and –20 °C.
2. Collect transverse sections onto Superfrost® Plus microscopy slides, keep at –80 °C for long-term storage (*see Note 13*) or proceed to immunostaining (as below).
3. Air-dry samples for 15 min.
4. Fix in ice-cold acetone for 10 min.

5. Air-dry for 10 min. During this time, limit with a Dako (hydrophobic) pen the area to be stained.
6. Rehydrate samples in 1x PBS for 2 x 2 min.
7. Use a Mouse-on-Mouse (MOM) Basic kit (*see Note 14* for collagen VI staining) and block samples in blocking buffer for 1 h, at room temperature (*see Note 15*).
8. Wash 3 x 5 min in washing buffer with gentle agitation.
9. Incubate with MOM diluent buffer (supplied with the kit, 80 µl reagent in 1 ml of 1x PBS) for 5 min, at room temperature. Tap off excess.
10. Incubate with mouse monoclonal anti-dystrophin 6C5 (1:50) and rabbit polyclonal anti-laminin (1:400) (or with rabbit polyclonal anti-collagen VI, 1:300), diluted in MOM diluent, for overnight, at 4 °C.
11. Wash 3 x 5 min in washing buffer with gentle agitation.
12. Incubate with goat anti-mouse Alexa488 (1:500) and goat anti-rabbit Alexa568 (1:500), diluted in 1% goat serum, 1x PBS, 0.05% Tween-20, for 1 h, at room temperature. Protect from light afterwards.
13. Wash 3 x 5 min in washing buffer with gentle agitation.
14. Incubate with 1 µg/ml DAPI diluted in 1x PBS for 15 min, at room temperature.
15. Rinse with 1x PBS.
16. Add mounting solution (50–100 µl/slide) and cover with coverslips.
17. Air-dry slides and store at 4 °C.

3.7 Picro Sirius Red Staining for Detecting Collagen I and III

Deposition of muscle fibrosis can also be assessed following staining with picro sirius red that stains collagen in red and cytoplasm in yellow:

1. Air-dry tissue sections for 15 min.
2. Fix in 4% PFA for 10 min.
3. Wash 2 x 5 min in tap water and hydrate in dH₂O for 5 min.
4. Immerse in 100% ethanol for 5 min.
5. Air-dry completely for at least 20 min (*see Note 16*).
6. Stain with 0.3% picro sirius red for 1 h.
7. Rinse quickly in dH₂O.
8. Fix staining in 0.5% acetic acid for 2 x 5 min.
9. Dehydrate in 100% ethanol for 3 x 5 min.
10. Clear in 100% xylene for 2 x 10 min.

11. Mount in DPX mountant and cover with coverslips.
12. Air-dry slides and store at room temperature.

3.8 Histological Analyses

1. Immunostainings are visualized under an inverted fluorescence Axio Observer D1 microscope and taken by an AxioCam MR3 camera combined with ZEN imaging software (*see Note 17*).
2. Ideally a mosaic image of the whole muscle section is acquired by overlapping and stitching individual images of that section together.
3. For quantifying dystrophin expression: use ZEN software to score the mean intensity of dystrophin and subsequently normalize to the mean intensity of laminin of the same section.
4. For quantifying dystrophin-positive fiber numbers: use ImageJ, manually count the number of positive fibers, and evaluate as the percentage of the number of total fibers within the same image field that are positive with laminin staining (*see Note 18*).
5. For quantifying the frequency distribution of fiber size: see TREAT-NMD, SOP ID No.: DMD_M.1.2.001.
6. For quantifying the level of central nucleation: use ImageJ, manually count the number of fibers having centralized nuclei (as shown by DAPI staining) and evaluate as the percentage of the number of total fibers within the same image field that are positive with laminin staining.
7. For quantifying muscle fibrosis: use ZEN software to score the mean intensity of collagen VI and evaluate as the percentage of wild-type values obtained in the same way. For measuring the collagen area positive with collagen VI or sirius red staining: use ImageJ and select the area covered by the section. Then using the threshold function, highlight only the portion of the section positive for collagen staining and evaluate as the percentage of the total area of the muscle cross-section (*see Note 19*).

4 Notes

1. BPMOs have been used to describe these experiments; however, other chemistries can be used if preferred (e.g., unconjugated PMO, vivo-PMO by Genetools, 2OMePS, etc.).
2. Mowiol may not be dissolved completely, but the pellet must be colorless. After centrifugation, collect and aliquot the supernatant and store at -20°C until use. Do not disturb the pellet.
3. Four to 6 weeks after in vivo delivery, the efficacy of the AONs reaches a plateau. Intravenous injections can be repeated

weekly for several weeks to boost the antisense efficacy and make a more robust exon skipping.

4. In case the mouse is particularly weak or very old, a general anesthesia may be preferable to avoid the mouse feeling too distressed by the procedure. In this case, in addition to the standard materials you will need: anesthesia chamber, isoflurane, isoabsorber, 100% oxygen, heat pads. Place mouse into an anesthesia chamber and induce with 5% isoflurane in 100% O₂ until the animal goes into deep anesthesia (heart beats slowly and regularly). Transfer the mouse onto a heat pad, with anesthesia maintained at approximately 2.5% isoflurane in 100% O₂. The animal is ready for injection following loss of pedal withdrawal reflex and eye-blink reflex. Monitor the state of anesthesia throughout the procedure. Turn the mouse on the side, identify the tail vein, and proceed with the injection.
5. Cover samples on cork discs with silver foil before immersing in liquid N₂ for additional tissue protection.
6. The volume of total blood depends on how quickly you reach this stage after the animal dies (also depends on animal strain); we usually get 200–600 µl/mouse.
7. Homogenization can be extended to maximum 10 min if required.
8. All centrifuge steps are performed at 8000 × *g*.
9. Store cDNA at –20 °C, if can't proceed to PCR.
10. Recommended volume for diaphragm, heart, tibialis anterior (25–30 mg): 200–300 µl; for gastrocnemius (70–90 mg): 300–400 µl; for extensor digitorum longus or soleus: 50–100 µl.
11. To avoid cross-reactivity, cut the membrane between the fourth and fifth bands (counted from top to bottom) equivalent to 117 and 71 kDa bands. Incubate top segment with mouse anti-dystrophin and bottom segment with rabbit anti-α tubulin.
12. For dystrophin standard curve, different protein amounts extracted from C57 mice are mixed with those from *mdx* mice (muscle type-matched) such that in each 100–200 µg protein mixture there is 100, 75, 50, 25, 0% of C57 dystrophin.
13. Transverse sections can be maintained at room temperature during sectioning for few hours but must be stored at –80 °C afterwards.
14. The MOM kit is not strictly needed in case of Collagen VI staining. In this case, a blocking with 5% skimmed milk in 1x PBS, 0.05% Tween-20 is sufficient. Similarly, 2.5% milk in 1x

PBS, 0.05% Tween-20 can be used to dilute primary and secondary antibodies.

15. We usually use 200–350 μ l reagent/slide, depending on the number of sections on each slide.
16. If samples are not completely dry, the cytoplasm of myofibers will also be colored in orange.
17. Select the mid-belly muscle section (for hind-limb muscles), usually the biggest section on the slide, or nearly the biggest one, which shows the best sectioning and staining. This is important as suboptimal sectioning forms artefacts that interferes with the analysis.
18. Determine the area of a single image field or of the whole muscle section using rectangle or polygon tool of ZEN software, respectively. Express data as the number of dystrophin-positive fibers per mm^2 . This method takes less time and effort but is still informative.
19. Analysis should be performed in a blinded manner and by a single operator to avoid bias.

Acknowledgments

The authors thank the Muscular Dystrophy UK (London, UK) for funding the study (grant reference number: RA/893) and Sarepta Therapeutics Inc. (Cambridge, Massachusetts, USA) for their sponsorship. The authors declare that they have no conflict of interest.

References

1. Koenig M, Hoffman EP, Bertelson CJ et al (1987) Complete cloning of the Duchenne muscular dystrophy (DMD) cDNA and preliminary genomic organization of the DMD gene in normal and affected individuals. *Cell* 50(3): 509–517
2. Bonilla E, Samitt CE, Miranda AF et al (1988) Duchenne muscular dystrophy: deficiency of dystrophin at the muscle cell surface. *Cell* 54(4):447–452
3. Dunckley MG, Eperon IC, Dickson G (1996) Modulation of pre-mRNA splicing in the Duchenne muscular dystrophy gene. *Biochem Soc Trans* 24(2):276S
4. Malerba A, Sharp PS, Graham IR et al (2011) Chronic systemic therapy with low-dose morpholino oligomers ameliorates the pathology and normalizes locomotor behavior in mdx mice. *Mol Ther* 19(2):345–354
5. Malerba A, Kang JK, McClorey G et al (2012) Dual myostatin and dystrophin exon skipping by morpholino nucleic acid oligomers conjugated to a cell-penetrating peptide is a promising therapeutic strategy for the treatment of Duchenne muscular dystrophy. *Mol Ther Nucleic Acids* 1: e62. <https://doi.org/10.1038/mtna.2012.54>
6. Lu-Nguyen NB, Jarmin SA, Saleh AF et al (2015) Combination antisense treatment for destructive exon skipping of myostatin and open reading frame rescue of dystrophin in neonatal mdx mice. *Mol Ther* 23(8):1341–1348
7. Lu-Nguyen N, Malerba A, Popplewell L et al (2017) Systemic antisense therapeutics for dystrophin and myostatin exon splice modulation improve muscle pathology of adult mdx mice. *Mol Ther Nucleic Acids* 6:15–28. <https://doi.org/10.1016/j.omtn.2016.11.009>

8. Lu-Nguyen N, Ferry A, Schnell FJ et al (2019) aged mdx mice. *Hum Mol Genet* 28(18): 3091–3100
Functional muscle recovery following dystrophin and myostatin exon splice modulation in

Open Access This chapter is licensed under the terms of the Creative Commons Attribution 4.0 International License (<http://creativecommons.org/licenses/by/4.0/>), which permits use, sharing, adaptation, distribution and reproduction in any medium or format, as long as you give appropriate credit to the original author(s) and the source, provide a link to the Creative Commons license and indicate if changes were made.

The images or other third party material in this chapter are included in the chapter's Creative Commons license, unless indicated otherwise in a credit line to the material. If material is not included in the chapter's Creative Commons license and your intended use is not permitted by statutory regulation or exceeds the permitted use, you will need to obtain permission directly from the copyright holder.





In Vivo Models for the Evaluation of Antisense Oligonucleotides in Skin

Jeroen Bremer and Peter C. van den Akker

Abstract

Here, we describe an in vivo model in which antisense oligonucleotides were preclinically evaluated in reconstituted patient and healthy control skin. The aim was to investigate the effect of antisense oligonucleotides upon local or systemic administration. This allows for clinically relevant evaluation of antisense oligonucleotides in an in vivo setting. In this model, primary human keratinocytes and fibroblasts were placed into silicone grafting chambers, implanted onto the back of athymic nude mice. After sufficient cells were expanded, within a few weeks, human skin grafts were generated with a high success rate. These mice bearing grafts were subsequently treated with antisense oligonucleotides targeting exon 105 of the *COL7A1* gene which encodes type VII collagen. Patients completely lacking expression of type VII collagen develop severe blistering of skin and mucosa, i.e., recessive dystrophic epidermolysis bullosa. In this chapter, we describe the in vivo model used for the preclinical evaluation of antisense oligonucleotides as therapeutic approach for recessive dystrophic epidermolysis bullosa.

Keywords Epidermolysis bullosa, Therapy, Exon skipping, Antisense RNA, Skin equivalent mouse model, Splice modulating

1 Introduction

Antisense oligonucleotide (ASO)-mediated exon skipping has been shown to have great potential as therapeutic approach for the devastating heritable skin blistering disease dystrophic epidermolysis bullosa (DEB) [1, 2]. Severe recessive DEB (RDEB-gen sev) is caused by biallelic null variants in the *COL7A1* gene, which encodes type VII collagen (C7). C7 is an extracellular matrix molecule that secures attachment of the epidermis to the dermis by the formation of anchoring fibrils. Imaginably, the complete absence of C7 results in severe blistering of skin and mucosa and early demise [3]. The aim of ASO-mediated exon skipping is to remove the exon from the transcriptome in which the disease-causing variant resides. As a result, a slightly shorter protein is expressed which is functional [4]. In this chapter, we describe the evaluation of ASO targeting

skin in an in vivo setting. The model is based on the cell sorting principle, in which cells are of the same cell type cluster; in this case, primary human fibroblasts and keratinocytes [5]. Athymic nude mice were used for several reasons, foremost, these mice are highly suitable for xenografting as the mice do not possess a thymus and therefore do not display graft rejection. Second, morphological changes, like pigmentation or blistering, can be easily observed as the mice have little to no fur. These mice are bred and kept in individually ventilated cages (IVC), as they are vulnerable to pathogens.

Initially, a submerged culture was established in silicone grafting chambers that were implanted onto the back of these mice. This submerged culture allows for proliferation, clustering, and attachment of fibroblasts and keratinocytes onto the muscle fascia. After 10 days, the silicone grafting chamber is removed, which creates an air–liquid interface. It is well known that an air–liquid interface is essential for differentiation of the keratinocytes and form a stratum corneum. These principles are similar to the principles of 3D skin-equivalent culture in vitro.

The major advantage of this model is the ability to evaluate ASOs that are systemically administered. Additionally, this model allows treatment for longer periods than in vitro. The major disadvantage of this model is the need for, in comparison with in vitro 3D-culture, high numbers of patient cells. Primary cells were used; however, cell lines or iPSC-derived cells could be used as well. When using primary cells, the lower the passage, the better-defined strata of skin as the proliferative potential and differential is the highest. In this chapter, we describe the grafting model that was used to evaluate ASO-mediated exon skipping upon systemic treatment using primary cultured fibroblasts and keratinocytes.

2 Materials

1. Primary cultured human skin fibroblasts ($5\text{--}6 \times 10^6$ per animal).
2. Primary cultured human skin keratinocytes ($5\text{--}6 \times 10^6$ per animal).
3. Phosphate-buffered saline (PBS).
4. HEPES-buffered saline solution (HBSS).
5. Hyclone fetal bovine serum (Chelex 100 treated) (*see Note 1*).
6. Grafting medium (1:1 DMEM:Ham-F12 + 5% FBS).
7. Silicone grafting chamber (made by medical instrument maker).
8. Surgical instruments: scissors (Metzenbaum), tweezers, forceps.

9. Suture wire (5-0).
10. Biotechnical surgery equipment.
11. Buprenorphine (0.01 mg/ml).
12. Chlorhexidine 2% for topical application.
13. 70% alcohol.
14. Weighing scale for mice.

3 Methods

3.1 *Anesthesia and Handling*

Due to the wide variability in laboratory animal practices and surgical instruments used in laboratories, we generally describe the anesthesia procedure. Anesthesia of the animal was induced using 5% isoflurane gas in a closed induction chamber designed for mice with continuous flow of 5% isoflurane gas carried by oxygen. After induction, the animal was transferred onto a heated pad where anesthesia was maintained using 2% isoflurane gas by placing the head of the mouse into a breathing conduit through which the gas continuously flows. All handling and surgery were performed inside a laminar biohazard flow cabinet.

3.2 *Surgical Procedure*

1. Harvest $5\text{--}6 \times 10^6$ fibroblasts and $5\text{--}6 \times 10^6$ keratinocytes. Spin down at $200 \times g$ and remove supernatant. Resuspend and pool pellets in 4 ml grafting medium. Spin down at $200 \times g$ and remove supernatant. Keep pellet on ice and proceed to the animal laboratory.
2. Take the IVC cage containing the animal and spray it down with 70% alcohol, then place the cage in the flow cabinet.
3. Open the cage and transfer the mouse into the induction chamber containing 5% isoflurane gas and write the time in your log as the start of the operation.
4. Once induced, weigh the mouse and transfer the mouse onto the heated pad and place the head of the mouse into the breathing conduit. Make sure the mouse is under by pinching a paw. Only when completely under anesthesia, continue.
5. With a sterile gauze use chlorhexidine to sanitize the neck and tail base of the mouse.
6. Inject 10 $\mu\text{l/g}$ buprenorphine at the tail base subcutaneously.
7. Using a permanent marker, draw an 8–10 mm diameter circle between the shoulder blades loose skin.
8. Using a tweezer, lift the skin in the middle of the circle and excise a full skin thickness circle revealing the muscle fascia (Fig. 1a).

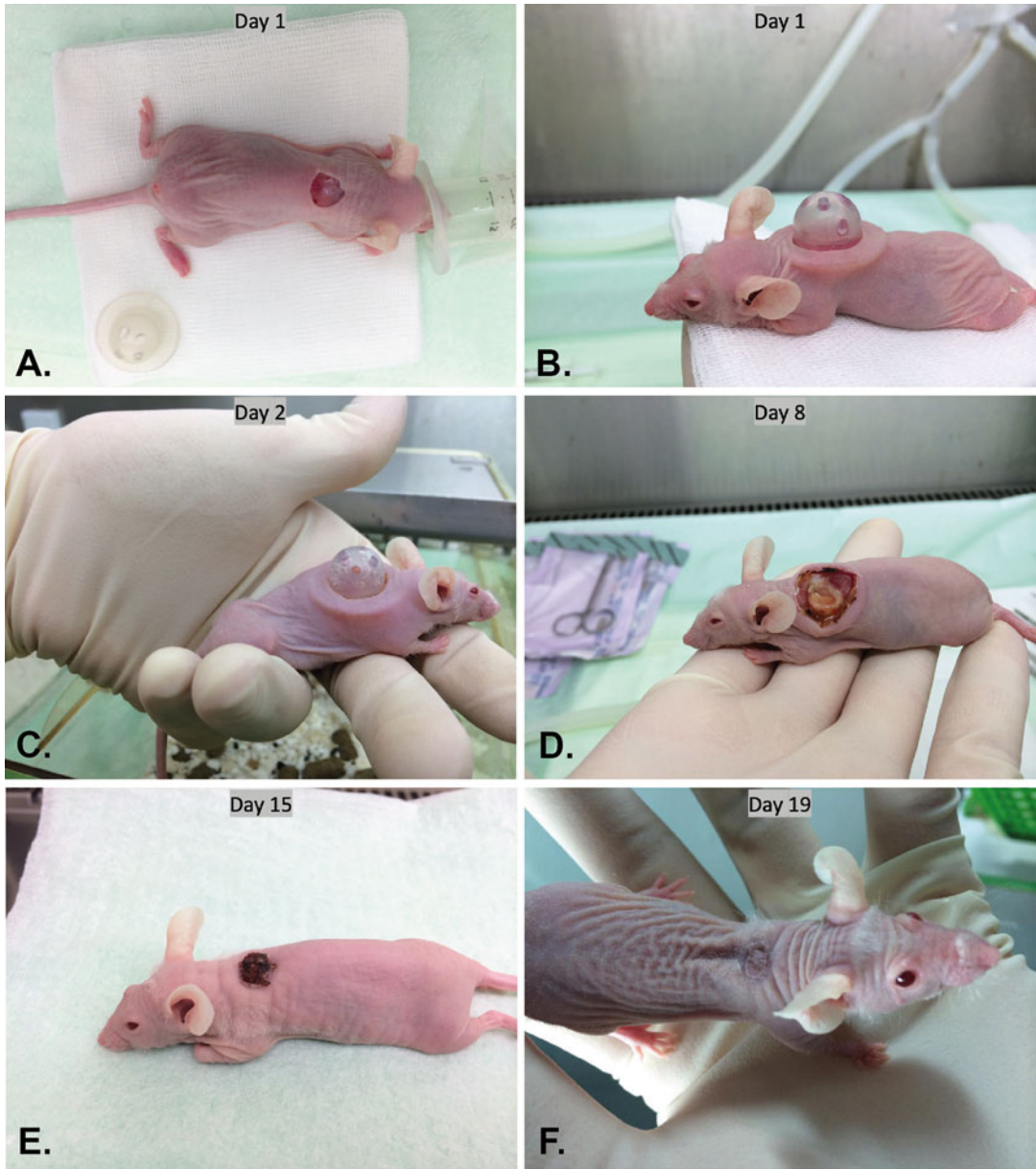


Fig. 1 Grafting procedure. In this figure, the steps of the grafting procedure are explained. (a) First, a full-thickness skin excision is made. (b) Then the silicone grafting chamber is implanted, followed by injection of the cells in grafting medium in the chamber. (c) Subsequently, the chamber will be filled with wound fluid and after (d) 7 days, the grafting chamber is removed. (e) A scab will be formed on the wound which will (f) fall off around 10 days after removal of the chamber and a patch of human skin is revealed

9. Once removed, use the surgical scissors to separate the skin from the fascia surrounding the excision.
10. Insert the silicone grafting chamber in the excised area.

11. Once the grafting chamber is implanted, the chamber should be securely held in place by the surrounding skin. If necessary, suture the skin surrounding the chamber together, thereby securing the chamber in place.
12. Resuspend the pellet in grafting medium and pipet gently dropwise into the grafting chamber. Write the time in your log (Fig. 1b).
13. Reduce the isoflurane to 1.75% (*see Note 2*) and cover the lower part of the mouse with a few gauzes to make sure the mouse remains warm.
14. 40 min after the cells are pipetted onto the muscle fascia in the grafting chamber, gently place the mouse back into the IVC cage, close the lid, and monitor the mouse as it recovers from anesthesia.
15. Every 8 h, the mouse is treated with 10 μ L/g buprenorphine for 48 h. After 48 h, the mice should be monitored daily for behavior (*see Note 3*) (Fig. 1c).

3.3 Removal of the Grafting Chambers

Ten days post operation, the grafting chambers are removed.

1. Induce anesthesia as described above. Carefully using precision tweezers release the graft from the inside of the grafting chamber (*see Note 4*) and the grafting chamber from the skin surrounding the chamber. Remove sutures if necessary.
2. Once free, carefully remove the grafting chamber using tweezers, revealing the white-yellow graft in the middle (Fig. 1d).
3. The mouse is kept under anesthesia for 10 min after removal by 2% isoflurane gas in oxygen.
4. Gently place the mouse back into the IVC cage and monitor the mouse as it comes back to esthesia.
5. Within 24 h, a scab will form (Fig. 1e). Generally, the scab will fall off after a week (*see Note 5*) revealing the human skin graft (Fig. 1f).

4 Notes

1. Hyclone fetal bovine serum is chelated using 4 g Chelex 100 (Bio-Rad)/100 mL FBS. Left to rotate overnight at 4 °C, paper filtrated to remove residual resin, then sterile filtered and kept in aliquots at -20 °C. It is essential to use low calcium serum, as calcium will induce premature differentiation of keratinocytes.
2. It is essential to monitor mice under isoflurane anesthesia. Try to find the minimum required to sustain anesthesia, as the mice are sensitive to isoflurane.

3. Injections are given under short general anesthesia to minimize the risk of damaging the chambers/grafts. The mice are housed individually, as mice will eat the silicone grafting chamber. Additionally, remove cage enrichment where the chamber can get stuck behind, e.g., small houses or tubes. Sterilized tissues can be used as replacement for cage enrichment. The mice will build burrows with them, and they cannot damage the grafting chamber or graft.
4. Make sure the graft and skin are completely cleared from the chamber. Otherwise, lifting the chamber could remove (part of) the graft.
5. Do not physically remove the scab. The time required for the scab to fall off varies. Usually between 7 and 10 days.

References

1. Bremer J, Bornert O, Nystrom A, Gostynski A, Jonkman MF, Aartsma-Rus A, van den Akker PC, Pasmooij AM (2016) Antisense oligonucleotide-mediated exon skipping as a systemic therapeutic approach for recessive dystrophic epidermolysis bullosa. *Mol Ther Nucleic Acids* 5(10):e379. <https://doi.org/10.1038/mtna.2016.87>
2. Bremer J, van der Heijden EH, Eichhorn DS, Meijer R, Lemmink HH, Scheffer H, Sinke RJ, Jonkman MF, Pasmooij AMG, Van den Akker PC (2019) Natural exon skipping sets the stage for exon skipping as therapy for dystrophic epidermolysis bullosa. *Mol Ther Nucleic Acids* 18: 465–475. <https://doi.org/10.1016/j.omtn.2019.09.009>
3. Has C, Bauer JW, Bodemer C, Bolling MC, Bruckner-Tuderman L, Diem A, Fine JD, Heagerty A, Hovnanian A, Marinkovich MP, Martinez AE, McGrath JA, Moss C, Murrell DF, Palisson F, Schwieger-Briel A, Sprecher E, Tamai K, Uitto J, Woodley DT, Zambruno G, Mellerio JE (2020) Consensus reclassification of inherited epidermolysis bullosa and other disorders with skin fragility. *Br J Dermatol* 183(4): 614–627. <https://doi.org/10.1111/bjd.18921>
4. Bornert O, Kuhl T, Bremer J, van den Akker PC, Pasmooij AM, Nystrom A (2016) Analysis of the functional consequences of targeted exon deletion in COL7A1 reveals prospects for dystrophic epidermolysis bullosa therapy. *Mol Ther* 24(7): 1302–1311. <https://doi.org/10.1038/mt.2016.92>
5. Wang CK, Nelson CF, Brinkman AM, Miller AC, Hoeffler WK (2000) Spontaneous cell sorting of fibroblasts and keratinocytes creates an organotypic human skin equivalent. *J Invest Dermatol* 114(4):674–680. <https://doi.org/10.1046/j.1523-1747.2000.00938.x>

Open Access This chapter is licensed under the terms of the Creative Commons Attribution 4.0 International License (<http://creativecommons.org/licenses/by/4.0/>), which permits use, sharing, adaptation, distribution and reproduction in any medium or format, as long as you give appropriate credit to the original author(s) and the source, provide a link to the Creative Commons license and indicate if changes were made.

The images or other third party material in this chapter are included in the chapter's Creative Commons license, unless indicated otherwise in a credit line to the material. If material is not included in the chapter's Creative Commons license and your intended use is not permitted by statutory regulation or exceeds the permitted use, you will need to obtain permission directly from the copyright holder.





Delivery of Antisense Oligonucleotides to the Mouse Retina

Alejandro Garanto 

Abstract

The eye is the organ in charge of vision and, given its properties, has become an excellent organ to test genetic therapies, including antisense oligonucleotide (AON) technology. In fact, the first AON receiving FDA and EMA approval was meant to treat an eye condition. Currently, dozens of clinical trials are being conducted for a variety of subtypes of inherited retinal disease. Although most of them are based on gene augmentation therapies, a phase 3 and two phase 1/2 clinical trials using AONs are ongoing. Since the retina is a layered structure of nondividing cells, obtaining human retinal tissue and expanding it in the lab is not possible, unless induced pluripotent stem cell technology is used. Mouse models have helped to elucidate the function of many genes, and the retinal structure is quite similar to that of humans. Thus, drug delivery to the mouse eye can provide valuable information for further optimization of therapies. In this chapter, the protocol for intravitreal injections of AONs is described in detail.

Keywords Retina, Intravitreal injection, Mouse, Inherited retinal diseases, Antisense oligonucleotide, Drug delivery, Intraocular injection

1 Introduction

The eye is the window to the world around us. Vision occurs thanks to a thin neuronal layer located at the back of the eye called the retina. When light enters the eye, the photosensitive cells (photoreceptors) capture the photons and convert them into chemical and electrical signals that travel to the brain, where the final image will be generated [1].

Inherited retinal diseases (IRDs) are monogenic disorders affecting approximately 1 in 3000 individuals worldwide [2]. So far, mutations in more than 250 genes have been associated with IRDs (RetNet: <https://sph.uth.edu/retnet/>). IRDs are highly heterogeneous, but in general, the first symptoms appear during the first decade of life, and the disease progresses with age, often leading to total blindness.

Although no cure is available for IRDs, the eye is at the forefront of the development of molecular therapies. Its accessibility, containment, immune-privileged status, together with the window

of opportunity that IRDs present, make the eye a model organ for therapeutics. An example is Luxturna, an adeno-associated virus (AAV)-based therapy, which has become the first gene therapy treatment with market approval for an eye disease [3]. This achievement has sped up the development of many other potential treatments currently under investigation at both preclinical and clinical levels for a variety of retinal diseases. Another example of molecules that have shown promising results in humans is antisense oligonucleotides (AONs). These 18–21 nucleotide oligonucleotides are able to bind to the pre-mRNA and, among other functions, can modulate splicing or degrade RNA transcripts [4]. After the promising results obtained in a phase 1/2 clinical trial [5], a phase 2/3 clinical trial (NCT03913143) using AONs to correct a splicing defect in *CEP290*-associated IRD has recently started. Furthermore, two other phase 1/2 clinical trials have also commenced for specific mutations in the IRD-causing genes *USH2A* (NCT03780257) and *RHO* (NCT04123626).

When considering testing AON efficacy in the mouse eye, it is important to remember that AONs are sequence-specific molecules. In the past, we developed a humanized mouse model for the intronic variant c.2991+1655A>G in *CEP290* [6]. This model contained a ~6 kb fragment of the human *CEP290* including the intronic mutation, and the splicing defect associated with this mutation was only slightly recapitulated [6]. Despite, using a previously efficacious AON characterized in patient-derived cells [7], a single dose of 60 µg of AON was delivered to the retina intravitreally, and pseudoexon skipping was observed up to 30 days after injection [8].

Delivery to the eye can be performed in multiple ways. The most common ones are intravitreal and subretinal injections. For AONs, intravitreal injections are a good choice since the entire retina can be targeted (Fig. 1). There are several ways to perform intravitreal injections, and in this chapter, the protocol we successfully use in our lab is described step by step. For this procedure, no sophisticated equipment is required.

2 Materials

2.1 For Injections

1. Permission from the animal ethical committee and a safe place to work (*see Note 1*).
2. Stereomicroscope.
3. Balance to weigh the animals.
4. Microdissection scissors (e.g., Vannas 8 cm str).
5. Dumont #5 forceps.
6. Dumont #5 curve 45-degree forceps.

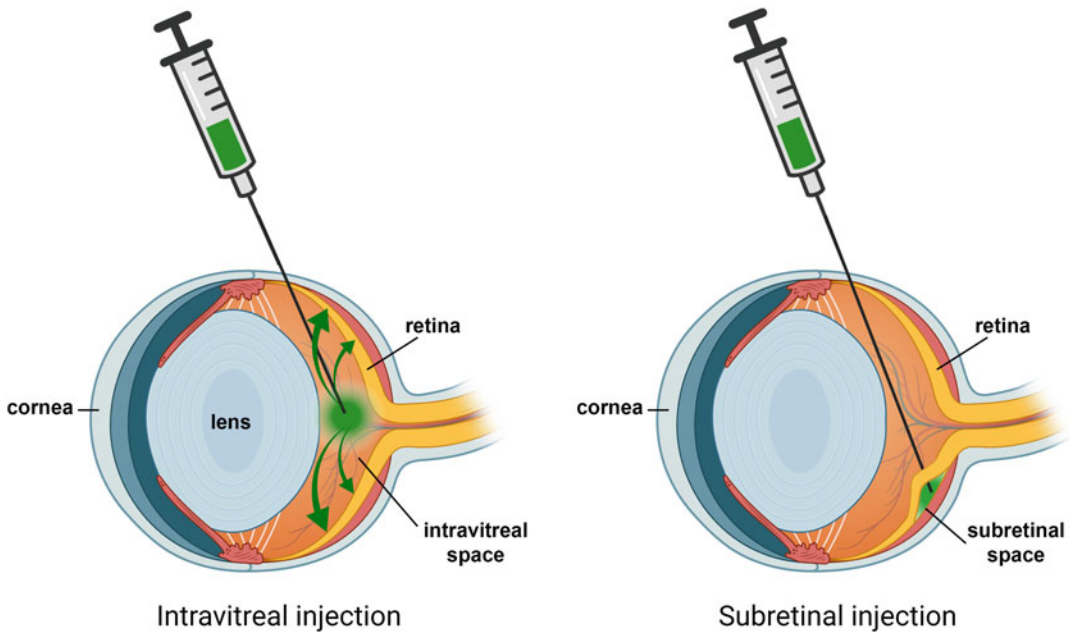


Fig. 1 Schematic representation of an intravitreal (left) and subretinal (right) injections. The figure was made with Biorender

7. 30G needles.
8. 25G needles.
9. 1-ml plastic syringes.
10. 10 μ l Hamilton syringe without needle (e.g., 1701 RN or 701 RN).
11. Hamilton needles: 33G, 51 mm, blunt end or 34G, 12.7 mm, blunt end (*see Note 2*).
12. Sterile gauzes.
13. Isoflurane or other types of anesthetics.
14. In case of using isoflurane, a box to anaesthetize the animals, and corresponding tubes (including a stopcock to allow distribution of the isoflurane to the box, but also to the animal undergoing the procedure).
15. Analgesic such as carprofen (stock 50 mg/ml).
16. Tropicamide ophthalmic solution (*see Note 3*).
17. Antibiotics, formulated as eye ointments (e.g., PRED-G, TobraDex, etc.).
18. Heat pad to warm up the animals during the recovery time.
19. 1-ml tips.
20. Ethanol 70%.
21. Sterile deionized water (in a falcon tube).

22. 1.5-ml Eppendorf tubes.
23. Bench diapers.
24. The solution to resuspend the molecule of interest (in this case, sterile PBS 1× or saline commercial).
25. The molecule of interest (in this case AONs) resuspended at the proper concentration in the appropriate solution (between 5 and 20 µg/µl).
26. A colleague willing to help and that is allowed to work with animals (*see* **Note 4**).
27. Mice to inject (*see* **Note 5**).

2.2 For Harvesting Eyes

1. Dumont #5 forceps.
2. 2-ml Eppendorf tubes.
3. Scissors.
4. Small blades.
5. OCT compound.
6. Molds for cryoblocks.
7. Liquid nitrogen.
8. Polystyrene box.
9. Isopentane.
10. Aluminum boxes (to store the cryoblocks individually (14.5 mm) or in groups (29 mm)).

3 Methods

3.1 Before Starting

Prepare the selected spot with enough space to place a stereomicroscope, sit in a comfortable way, have safe connection to isoflurane (*see* **Note 6**), and have enough room to have all the necessary tools around. For administering AONs, a safety cabinet is not per se needed; however depending on the animal facility, the animal handling must be conducted inside the cabinet, meaning that the procedure is too (*see* **Note 7**). Last but not least, remember to sterilize the forceps and scissors before the procedure.

3.2 Preparation for the Procedure

Once at the location, prepare the place for the procedure:

1. Cover the surface with the bench diapers.
2. Place the microscope on top of it.
3. Connect the box to the isoflurane using a tube with a stopcock and an extra exit tube.
4. Place a 1-ml tip at the end of the extra tube (cut the 1 cm of the tip first) if performed in the cabinet, or use a safe tube connected to the aspirating system.

5. Put the balance in a stable place.
6. Wash the Hamilton syringes with deionized water (MQ), then ethanol 70%, and then water again.
7. Prepare all the tools around the microscope: forceps, scissors, a 1-ml syringe with a 30G needle (for the procedure), the AONs, and antibiotics.
8. Prepare the carprofen at the correct concentration (usually 1:100 in saline, to inject 10 μ l for each gram of weight). Alternatively, carprofen can be added to the drinking water 24 h prior to the procedure in a 1:1000 dilution (stock 50 mg/ml). In this case, injection is not needed.
9. Prepare a 1-ml syringe with a 33G needle (to inject the carprofen).
10. Prepare the heat pad.
11. Prepare the animals for the procedure.

3.3 The Procedure

1. Take the first animal.
2. Weight the animal and write down the weight in grams.
3. Place the mouse in the box with the isoflurane at 4–5% for induction.
4. Once the animal is asleep, transfer it under the stereomicroscope and place the extra tube in the mouth/nose of the mouse, using the 1-ml tip if working on the cabinet or the safe tube. Reduce the isoflurane to 2–2.5%.
5. Tape the tip to the base of the microscope to avoid it moving and the mouse waking up during the procedure.
6. Deliver the carprofen via subcutaneous injection (10 μ l of a solution 0.5 mg/ml (dilution 1:100) for each gram of weight). Alternatively, carprofen can be added to the drinking water 24 h prior to the procedure (dilution 1:1000), in this case injection is not needed.
7. Place the animal in a position such as the eye is clearly visible through the center of the stereomicroscope (*see Note 8*). In our lab, left eye is injected first by a right-handed person (*see Notes 8 and 9*).
8. Prepare the volume to be injected in one of the Hamilton syringes. For adult mice, this is usually 2 μ l. In this example, the left eye is injected first, thus the solution will be PBS 1 \times .
9. With the forceps, take the conjunctiva below the upper eyelid. Pull it a bit to the outside, and with the surgery, scissors make a small cut to clearly see the eyeball toward the inner part. Make sure you do not cut the conjunctiva in the border, otherwise it will not be possible to pull it in the next steps (*see Note 10*).

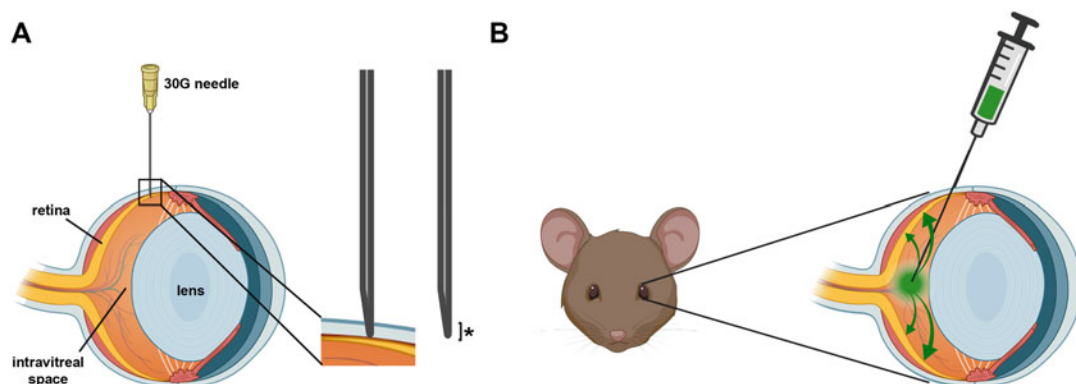


Fig. 2 Schematic representation of the steps to perform an intravitreal injection in mice. **(a)** The 30G needle is used to make a small hole in the eye to be able to introduce the Hamilton needle with a blunt end in the intravitreal space. It is important to only perform the incision with the very tip part of the needle (marked with an asterisk). **(b)** Schematic representation of the intravitreal injection of the left eye. The figure was made with Biorender

The cut should be done in the area behind the ora serrata, to make sure we inject in the retina.

10. Leave the scissors and take the syringe with the 30G needle.
11. While still holding the conjunctiva with the forceps, use the syringe with the 30G needle to make a tiny hole in the clean area (without any type of membrane) of the eyeball (Fig. 2a), by only using the tip of the needle (*see Note 11*).
12. Leave the syringe and grab the Hamilton loaded with 2 μ l of PBS 1 \times .
13. Place the needle of the Hamilton in the hole previously made, for intravitreal injection, carefully and slowly placing the needle into the eye in the intravitreal space (Fig. 2b). Release slowly the content of the syringe with the help of a colleague (*see Notes 12–14*).
14. Leave the needle a couple of seconds to avoid reflux.
15. Slowly remove the needle from the eye (*see Note 15*).
16. Release also the conjunctiva.
17. Turn the animal and perform the same procedure (**steps 7–15**) on the right eye, but now injecting the AON instead of PBS 1 \times (*see Note 16*).
18. Once both eyes have been injected, remove the mouse from the isoflurane.
19. Place some antibiotic on top of each eye.
20. Transfer the mouse to the cage located on top of the heat pad.
21. Label the cage properly to avoid confusions (*see Note 17*).

22. After a couple of minutes, the animal should wake up and start moving around.
23. Clean with ethanol the forceps, scissors.
24. Continue with the next animal following the same steps as described above (*see* **Note 18**).
25. If multiple AONs are injected, clean the Hamilton syringe as described in **step 6** of Subheading 3.2 and proceed with the same steps described in Subheading 3.3.

3.4 After the Procedure

1. Stop the isoflurane.
2. Check that all animals are awake.
3. Place them back in the corresponding rack and recheck again that labels are correctly placed.
4. Clean the needles first with MQ water (to remove any kind of possible tissue left), then with 70% ethanol, and then with MQ water again and allow to dry (*see* **Note 19**).
5. Discard all the 30G and 33G needles used in the proper container.
6. Clean the scissors and forceps with 70% ethanol and water.
7. Discard the bench diaper, the tip, and syringes used to inject carprofen.
8. Clean the working space.

3.5 Follow-Up

During the next 2 days, it is important to check the eyes of the animals on a daily basis in order to detect possible infections. In our hands, we have never observed any infection or complication derived from the injections (*see* **Note 20**).

3.6 Harvesting the Tissue and Read-Outs

Depending on the molecule injected and the purpose of the experiment, the harvesting time will vary. For instance, it is known that when injecting viruses such as adeno-associated viruses (AAVs), the highest expression is obtained after 3–4 weeks [9]. In contrast, the effect of an AON can be already detected a couple of days after injection [8]. Therefore, the timing on tissue collection will be based on the specific project and the expected efficacy of the therapeutic molecule.

The way to sacrifice the mice can also modify the read out. In our group, we sacrifice the animals by cervical dislocation to collect the samples as quickly as possible and avoid possible changes triggered by CO₂ inhalation (the other type of euthanasia approved in our facility).

AON efficacy assessment can be done at RNA or protein level. For example, checking by RT-PCR if the splicing is redirected, or by Western blot whether protein levels were increased or decreased, depending on the purpose of the study. For that, the retina needs to

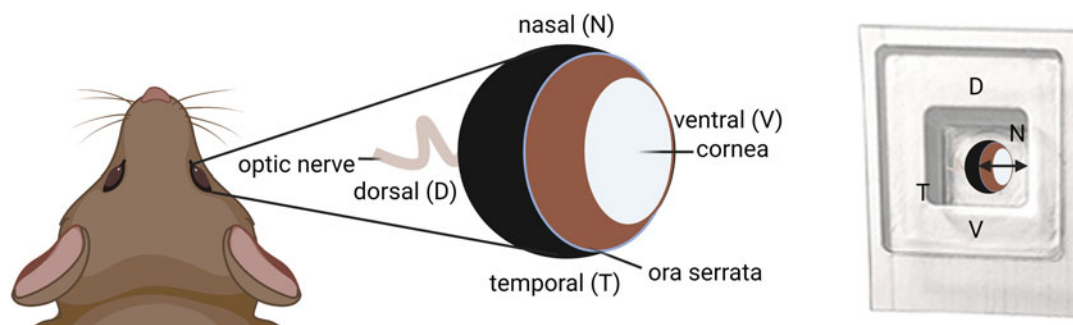


Fig. 3 Schematic representation on how to place the right eye in the cryomold. The figure shows the different areas of the eye in the position of the mouse. When placing the eye in the mold, we put the dorsal (D) and the ventral (V) areas as indicated. Nasal (N) area will be at the bottom of the mold and the temporal (T) at the top. Arrows indicate the side of the mold used as reference to place the ora serrata of the eye in parallel. This is the common procedure we use in our lab, but the position of the eye can be done in different ways. Also the eye can be marked with a dye or by carefully burning the cornea at a specific position to recognize the orientation. The figure was made with Biorender

be harvested, and this can be done easily following the instructions previously described elsewhere [10]. Once the tissue is collected, it can be processed according to standard protocols for RNA isolation and protein lysates [6].

Morphological studies can also be performed. These tests are important for example, to study if the newly created protein localizes at the proper place or if the AON itself is creating any toxic effect. For that, the entire eye will be collected and subsequently sectioned to analyze these aspects by conventional eosin/hematoxylin or toluidine-blue staining or immunohistochemical studies. In order to prepare the samples, the eye needs to be sectioned. Here, there are two options. (A) The eye is fixed and dissected, removing the cornea and lens, cryopreserved in sucrose, and embedded in OCT, as previously described elsewhere [10], or (B) embedded directly in OCT. In general terms, fixed eyes will give better morphology than non-fixed. However, in our experience, often primary antibodies work only in unfixed tissue (especially those that are home-made). Therefore, choosing the best protocol to follow will depend on the reagents that will be employed for the different readouts. Since option A has already been described in detail previously [10], option B is explained below:

1. Add OCT to the cryomold (*see Note 21*).
2. Enucleate the eye using the forceps.
3. Pull the eye from the animal.
4. Place the eye in the OCT with the cornea looking to the right side (right eye) or left side (left eye) (Fig. 3, *see Note 22*).
5. Make sure the eye is entirely submerged in the OCT.

6. Align the ora serrata parallel to the border of the cryomold.
7. Add isopentane in an aluminum box.
8. Place the aluminum box with isopentane in a polystyrene box.
9. Place the mold on top of the aluminum box, making sure the lower part is in contact with the isopentane.
10. Add some liquid nitrogen in the polystyrene box.
11. Allow the sample to freeze slowly.
12. Once completely frozen, unmold and store for sectioning in an aluminum box properly labeled at -80°C until sectioning (*see Note 23*).

4 Notes

1. Before starting the procedure, please make sure that permission by the corresponding ethical committee of the research institute has been granted. Subsequently, find a location where the injections can be performed in the most comfortable way, and adhering to the rules for animal experimentation and the animal facility.
2. Depending on the skills of the person, the stereomicroscope (space left to perform the injection), the angle, etc., you can use long or short needles. Long needles allow more flexibility in terms of space (the Hamilton does not interfere with the stereomicroscope); however, small movements are more noticeable. Also, a second person needs to help by pressing the syringe to deliver the volume. In our experience, for adult mice long needles are better.
3. Tropicamide ophthalmic solution can be used to relax the musculature of the eye and therefore dilate the pupils by applying one drop on the eye, and after 1 or 2 min, dry it with a gauze. It is not per se needed, but it might help.
4. During the injection procedure, a third hand is needed to press the syringe and release the content. This colleague can also help with the preparations, for instance, while one person injects, the other can already weigh and prepare the next animal, in order to optimize time as much as possible.
5. It is recommended to start with pigmented animals. This will allow to perform the procedure easily since all the membranes and the eyeball will be completely distinguishable. Having acquired more practice, albino animals can also be injected. If this is not possible, practicing with albino mice can be done using some type of dye that will allow to observe where the liquid is being injected.

6. Isoflurane is the method we use in the lab. Animals fall asleep and recover fast. However, other types of analgesia are also possible if they are accepted by the ethics committee and animal facility.
7. In general, animal facilities are relatively far away from the regular labs; therefore, if the animal facility does not have a stock of materials, such as needles, syringes, tubes, tips, etc., take more materials than needed just in case.
8. Depending on the person, the right or left eye might be easier to inject. Based on our experience, left-handed persons find it easier to inject the left eye, while the opposite is observed for right-handed persons.
9. One of the benefits of working in the eye field is that each animal is its own control. To avoid confusion and perform the procedure in a systematic way, we deliver the control solution to the left eye, and the AON molecule to the right eye. However, it may happen that both eyes might be injected with the same molecule. This will be determined based on the hypothesis and study design.
10. It is really important to have a small area without any membrane, otherwise future steps will be complicated. Multiple cuts might be needed.
11. It is very important to make the hole with the very beginning of the tip of the needle; otherwise, the hole might be too big, or the needle might penetrate into the eye, damaging the retina (Fig. 2a).
12. Sometimes a possibility is to find the lens carefully and go back 1–2 mm, in that way you know you are in intravitreal space.
13. While releasing, hold the syringe in a way that it will not move. Practice first with your colleague and make sure you both adapt to each other. Be clear with the person assisting you by using a specific quote such as “inject,” “now,” etc. It is very important that the person pressing is also aware of doing it gently and slowly to avoid moving, or even pushing the syringe deeper.
14. When injecting, you should see that the solution gets into the eye.
15. When removing the needle there can be some reflux. This happens often, and it is more obvious when injecting 3 μ l. With 2 μ l it can be observed depending on the size of the eye and with 1 μ l it is rare. However, with 1 μ l it can happen that the molecules do not reach the entire retina. Removing the needle slowly after a couple of seconds (instead of immediately) after injection also reduces the amount of reflux.
16. To avoid having to clean the Hamilton syringe and needle between left and right eye, the use of two syringes, one for

the PBS 1×, and the other for the AON, is recommended. This will ensure no traces of AON in the control eye and will contribute to reduce the overall intervention time.

17. When injecting the mice, make sure that the accompanying labels are moved, and the treatment is clearly stated in the label. Usually, it is also needed to identify individual animals. This can be done with earmarks or any other system used at the facility.
18. The 30G and 33G needles often get less sharp after a couple of injections. So replace them every time you feel they are not as sharp as they used to.
19. When cleaned directly with ethanol, the salts tend to precipitate, and the needle can get clogged. Therefore, the extra step with MQ water after ethanol is to remove the possible salts that could precipitate and therefore cause malfunction of the Hamilton syringe or needle.
20. We have not observed any discomfort or side effect caused by the procedure. However, some spontaneous casualties may occur due to aging, spontaneous tumors, or fights between animals. This highly depends on the age of the animals at the moment of injection, and the period of time they need to be in the experiment until analysis.
21. Make sure that no bubbles are present. If so, remove them since they can affect the sectioning procedure.
22. This is the way we do it to differentiate left and right eyes but also knowing the orientation of the eye. Alternatively, the eye can be marked to identify the orientation after sectioning.
23. A couple of hours before sectioning, we usually move the cryoblocks to -20°C .

Acknowledgments

The author wants to acknowledge Prof. Rob W.J. Collin and Dr. Irene Vázquez Domínguez for critical review of this chapter. The group is financially supported by the Foundation Fighting Blindness (PPA-0517-0717-RAD), the Curing Retinal Blindness Foundation, as well as the Landelijke Stichting voor Blinden en Slechthzienden and Stichting Oogfonds via Uitzicht 2019-17, together with Stichting Blindenhulp, Rotterdamse Stichting Blindenbelangen, and Dowilwo. The funding organizations had no role in the design or conduct of this research and provided unrestricted grants. All figures were made with BioRender.

References

1. Kolb H (2003) How the retina works. *Am Sci* 91(1):28–35. [citeulike-article-id:1560678](https://doi.org/10.1560678)
2. Vazquez-Dominguez I, Garanto A, Collin RWJ (2019) Molecular therapies for inherited retinal diseases-current standing, opportunities and challenges. *Genes (Basel)* 10(9):654. <https://doi.org/10.3390/genes10090654>
3. Keeler AM, Flotte TR (2019) Recombinant adeno-associated virus gene therapy in light of Luxturna (and Zolgensma and Glybera): where are we, and how did we get here? *Annu Rev Virol* 6(1):601–621. <https://doi.org/10.1146/annurev-virology-092818-015530>
4. Hammond SM, Wood MJ (2011) Genetic therapies for RNA mis-splicing diseases. *Trends Genet* 27(5):196–205. <https://doi.org/10.1016/j.tig.2011.02.004>
5. Cideciyan AV, Jacobson SG, Ho A, Drack A, Pfeifer W, Charng J, Taiel M, Schwartz M, Biasutto P, de Wit W, Cheetham ME, Adamson P, Rodman D, Nerinckx F, De Zaeytijd J, van Cauwenbergh C, Leroy BP, Russel S (2018) Intravitreal antisense oligonucleotide therapy (QR-110) for the Treatment of Leber Congenital Amaurosis due to Photoreceptor Cilium Defect in Subjects with the CEP290 p.Cys998X Mutation. Paper presented at the RD2018 XVIIIth international symposium on retinal degeneration, Killarney, Ireland
6. Garanto A, van Beersum SE, Peters TA, Roepman R, Cremers FP, Collin RW (2013) Unexpected CEP290 mRNA splicing in a humanized knock-in mouse model for Leber congenital amaurosis. *PLoS One* 8(11):e79369. <https://doi.org/10.1371/journal.pone.0079369>
7. Collin RW, den Hollander AI, van der Velde-Visser SD, Benniselli J, Bennett J, Cremers FP (2012) Antisense oligonucleotide (AON)-based therapy for Leber congenital amaurosis caused by a frequent mutation in CEP290. *Mol Ther Nucleic Acids* 1:e14. <https://doi.org/10.1038/mtna.2012.3>
8. Garanto A, Chung DC, Duijkers L, Corral-Serrano JC, Messchaert M, Xiao R, Bennett J, Vandenberghe LH, Collin RW (2016) In vitro and in vivo rescue of aberrant splicing in CEP290-associated LCA by antisense oligonucleotide delivery. *Hum Mol Genet* 25(12):2552–2563. <https://doi.org/10.1093/hmg/ddw118>
9. Surace EM, Auricchio A (2008) Versatility of AAV vectors for retinal gene transfer. *Vis Res* 48(3):353–359. <https://doi.org/10.1016/j.visres.2007.07.027>
10. Toulis V, Garanto A, Marfany G (2016) Combining zebrafish and mouse models to test the function of deubiquitinating enzyme (Dubs) genes in development: role of USP45 in the retina. *Methods Mol Biol* 1449:85–101. https://doi.org/10.1007/978-1-4939-3756-1_3

Open Access This chapter is licensed under the terms of the Creative Commons Attribution 4.0 International License (<http://creativecommons.org/licenses/by/4.0/>), which permits use, sharing, adaptation, distribution and reproduction in any medium or format, as long as you give appropriate credit to the original author(s) and the source, provide a link to the Creative Commons license and indicate if changes were made.

The images or other third party material in this chapter are included in the chapter's Creative Commons license, unless indicated otherwise in a credit line to the material. If material is not included in the chapter's Creative Commons license and your intended use is not permitted by statutory regulation or exceeds the permitted use, you will need to obtain permission directly from the copyright holder.





Delivery of Antisense Oligonucleotides to the Mouse Brain by Intracerebroventricular Injections

Tom Metz, Elsa C. Kuijper, and Willeke M. C. van Roon-Mom

Abstract

The use of antisense oligonucleotides (AONs) is a promising therapeutic strategy for central nervous system disorders. However, the delivery of AONs to the central nervous system is challenging because their size does not allow them to diffuse over the blood–brain barrier (BBB) when injected systemically. The BBB can be bypassed by administering directly into the brain. Here we describe a method to perform single and repeated intracerebroventricular injections into the lateral ventricle of the mouse brain.

Key words Intracerebroventricular injections, Stereotactic surgery, Cannula, Antisense oligonucleotides

1 Introduction

There has been a recent revival of interest in the use of antisense oligonucleotides (AONs) to treat neurodegenerative disorders with one approved central nervous system AON therapy and several in clinical trials [1]. This is largely due to the remarkably widespread distribution and cellular uptake of AONs once delivered into the brain. However, for drugs to reach the nervous system, they first have to cross the blood–brain barrier (BBB). Since the molecular weight of AONs is approximately 6000–10,000 Da, they are too large to cross the BBB by simple diffusion when delivered systemically. During the study of therapeutic efficacy of AONs in mouse models, AONs are often infused intracerebroventricularly (ICV). The BBB is bypassed by injecting the AON directly into the lateral ventricle, after which the AONs pass the ependymal cell layer that lines the ventricular system and enters the brain parenchyma.

One group of disorders for which these AON therapies are being studied in mouse models are the polyglutamine disorders. In these disorders, the disease is caused by CAG triplet repeat expansions in the coding region of a gene that is subsequently translated into an expanded stretch of glutamine amino acids in

the protein. The disease-causing proteins for each of these polyglutamine (polyQ) disorders are different, but in each case, the expanded stretch of glutamines results in a toxic gain of function of the protein leading to neurodegeneration. To date, a total of nine polyQ disorders have been described: dentatorubral-pallidoluysian atrophy (DRPLA), Huntington's disease (HD), spinal bulbar muscular atrophy (SBMA), and spinocerebellar ataxias (SCA1, 2, 3, 6, 7, and 17) [2, 3]. There is an inverse correlation of disease onset and polyQ length in the protein; the longer the CAG repeat, the earlier the age of onset of the disease [2]. Protein aggregates are found in the nucleus and cytoplasm of cells, indicating that protein misfolding is a common feature of these disorders. Using RNA breakdown [4] or RNA splice modulating AONs [5, 6], it is possible to reduce the toxicity of the mutant proteins, which can hopefully halt the disease progression in patients.

Because of the limited volume that can be injected into the mouse brain, multiple injections can be required to reach the desired dose. Repeated injections of AONs lead to a widespread distribution throughout the entire mouse brain, and the protein modifying effect can be detected in the cortex, cerebellum, and brainstem [6]. In this chapter, we describe a method for ICV delivery of AONs through a single injection or repeated injections using a cannula (Fig. 1).

2 Materials

2.1 Mice (See Note 1).

2.2 Disposables

1. Infusion cannula (PlasticsOne C315IS-5/SPC).
2. Tubing (PlasticsOne C313CT).
3. Cannula guide (PlasticsOne C315GS-5-SP).
4. Dummy cannula (PlasticsOne C315DCS-5-SPC).
5. MRI-compatible cannula guide (PlasticsOne C315GS-5-Pk/SPC) (see Note 2).
6. MRI-compatible dummy cannula (PlasticsOne C315DCNS-5/SPC) (see Note 2).
7. Dental cement (DiaFil Flow 1928–5005-01 DiaDent).
8. Primer (OptiBond® All-In-One 33381-E; Kerr Dental, Bioggio, Switzerland).
9. Analgesia (Carprofen 50 mg/mL).
10. Ocular lubricant (Added Pharma 220201).
11. Petroleum jelly.
12. Small piece of paper.

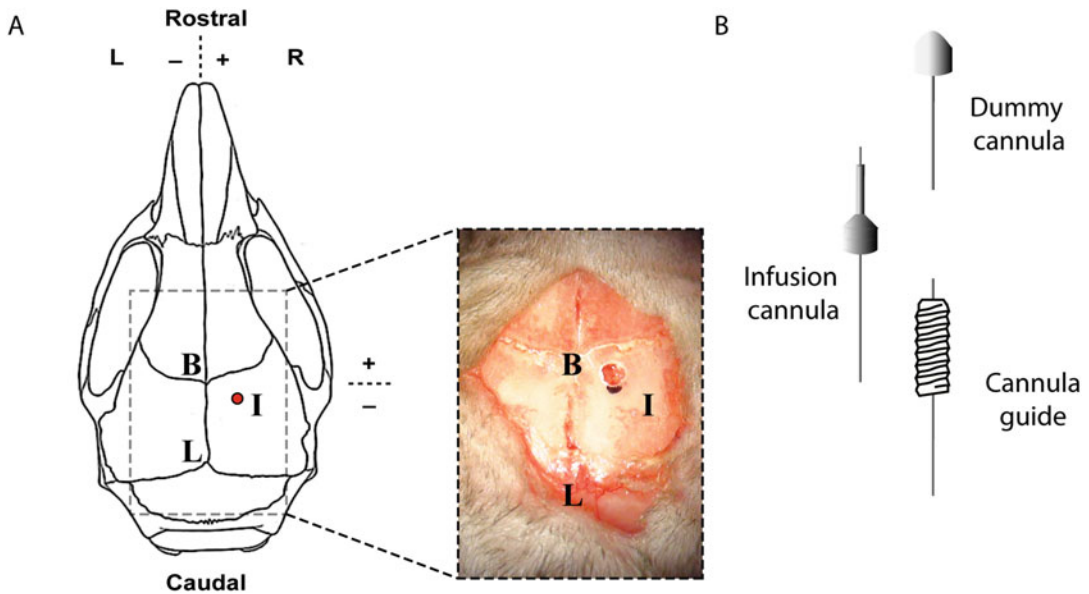


Fig. 1 Location and tools for intracerebroventricular injection. (a) Schematic and photographic outline of the injection site (I), bregma (B), and lambda (L) as points of reference. (b) Cannula types required for intracerebroventricular injection. The infusion cannula is connected to the syringe tubing and guided through the cannula guide to inject into the lateral ventricle. The cannula guide is attached to the skull and can be closed using a dummy cannula

13. Anesthesia (oxygen/isoflurane system with box and mouthpiece).
14. 70% ethanol.
15. Isopropanol.
16. MilliQ water.
17. 25 G disposable needle (for subcutaneous injection of analgesia).
18. 23 G disposable needle (for flushing cannula tubing).
19. 1 mL disposable syringe.
20. Tape (to remove dust from skull after drilling).
21. Cotton cloths.

2.3 Fixed Equipment

1. Stereotactic setup.
 - (a) Noninvasive ear bars.
 - (b) Stereotactic arm that fits the cannula guide.
2. Drill (Meisinger 310104001001005).
3. Macroscopic + light.
4. UV light source.

5. Hamilton syringe (gastight Hamilton #1701, including blunt needle 32 G).
6. Heating pad.
7. Heating lamp.
8. Animal shaver.
9. Waterproof marker.
10. Forceps (2×).
11. Scissors (skin).

2.4 Solutions

1. Reconstituted AON in DPBS (Gibco 14190144).

3 Methods

The limit of a bolus injection in the adult mouse brain is about 10 μL . In order to reach a sufficient dose of AON in the mouse brain, multiple injections over a longer period of time can be used (*see Note 3*). To make consecutive injections more easy and more animal-friendly, a cannula guide is placed on the mouse skull (*see Note 4*). The following injections can be given without surgery (*see Note 5*). The animal only has to be anesthetized and injected, which will not take longer than 10 min.

3.1 Preparation

1. Prepare the stereotactic setup.
 - (a) Stereotactic apparatus with arm with holder for cannula.
 - (b) Isoflurane setup.
 - (c) Heating pad.
2. Prepare the AON at the desired concentration.
3. Clean the infusion cannula, tubing, cannula guide, and dummy cannula with 70% ethanol.
4. Attach about 30 cm of tubing to an infusion cannula (*see Note 6*).
5. Flush the tubing and infusion cannula using a 23 G needle and a 1-mL syringe filled with MilliQ water.
6. Withdraw the syringe slightly, creating an air bubble in the tubing (*see Note 7*).
7. Attach the tubing to the 10- μL Hamilton syringe.
8. Withdraw 10 μL of the AON into the tubing using the Hamilton syringe and make sure the AON is at room temperature when injecting.
9. Prepare carprofen in NaCl at 0.5 mg/mL from 50 mg/mL stock.

3.2 Surgical Procedure

1. Weigh the mouse.
2. Induce anesthesia by placing the mouse in a box with 4% isoflurane (0.8 L/min) to induce anesthesia.
3. Prepare carprofen analgesia (5 mg/kg) in a 1-mL syringe with 25 G needle at room temperature.
4. When the mouse is fully sedated, shave the head of the mouse from the ears until the eyes.
5. Lower the isoflurane to 2% (0.4 L/min), switch the isoflurane from the box to the stereotactic apparatus, place the mouse in the stereotactic setup and make sure the mouthpiece is over the entire snout.
6. Make sure the mouse is placed on the heating pad, place the temperature probe in the anus of the mouse using lubricant gel and set the heating pad to 37 °C.
7. Cover the eyes of the mouse with ocular lubricant in order to prevent corneal dehydration.
8. Place a small piece of paper over the eyes to protect against UV light.
9. Apply carprofen subcutaneously using a 25 G needle.
10. Mount the mouse with noninvasive ear bars.
11. Turn on macroscope light.
12. Use 70% ethanol to clean the shaved area.
13. Make an incision in the skin from the ears until the eyes using a pair of scissors and a pair of forceps.
14. Use forceps and, under the macroscope, remove meninges and apply isopropanol to the skull where the cement will be located to make sure that the skull surface is dry.
15. The head of the mice should be placed parallel to the stereotactic apparatus, so that bregma and lambda are at the same Z coordinate in accordance with the flat-skull principle used in stereotactic rodent surgery.
16. Set the isoflurane to 1.5% (*see Note 8*).
17. Secure the cannula guide in the arm of the stereotactic device.
18. Assess bregma and mark it with a marker.
19. Bring the cannula guide onto the marked point on bregma and note the coordinates of bregma.
20. Apply primer to the whole area of the skull and also apply primer on the edge of the skin (*see Note 9*). Harden the primer with UV light 2×10 s. Ensure the primer has hardened properly and is dry.

21. Set the coordinates of the injection site in the stereotactic device: 0.2 mm posterior and 1.0 mm lateral to bregma (*see Note 1*).
22. Apply a mark in the area where the cannula guide is expected. Bring the cannula guide down to the surface of the skull, which will leave a mark in the ink of the marker.
23. Drill a hole in the skull on the place where the cannula guide made a mark in the ink using a dental drill and remove any dust by applying and removing tape. Remove any blood or liquid with a cotton cloth.
24. Lower the cannula guide to a depth of 2.2 mm from the skull surface.
25. Mount the infusion cannula into the cannula guide (click-on).
26. Inject by hand at 1 $\mu\text{L/s}$ and let the syringe in place to prevent outflow.
27. Apply dental cement in layers, starting between the cannula guide and the skull working up to the skin (*see Note 10*). Use 2×10 s of UV light on each layer to harden the cement.
28. Detach the cannula guide from the stereotactic arm and carefully move the stereotactic arm upwards while leaving the cannula guide in place.
29. Add a last layer of dental cement and harden with UV light.
30. Screw the dummy cannula onto the cannula guide (*see Note 11*).
31. Unmount the mouse from the stereotactic device and place it under a heating lamp for 15 min to recover (*see Note 12*).

3.3 Consecutive Injection

1. Weigh the mouse.
2. Induce anesthesia by placing the mouse in a box with 4% isoflurane (0.8 L/min) to induce anesthesia until it is fully sedated.
3. Lower the isoflurane to 2% (0.4 L/min), switch the isoflurane from the box to the stereotactic apparatus and place the mouse in the stereotactic setup (or other isoflurane mask).
4. Make sure the mouse is placed on the heating pad, place the temperature probe in the anus of the mouse using lubricant gel, and set the heating pad to 37 °C.
5. Cover the eyes of the mouse with ocular lubricant in order to prevent corneal dehydration.
6. Gently remove the dummy cannula from the cannula guide (*see Note 11*).
7. Mount the infusion cannula into the cannula guide (click-on).

8. Inject by hand at 1 $\mu\text{L/s}$ and let the syringe in place to prevent outflow.
9. Screw the dummy cannula onto the cannula guide.
10. Unmount the mouse from the stereotactic device and place it under a heating lamp for 15 min to recover (*see* **Note 13**).

4 Notes

1. For our experiments, we have used different mouse models with a C57BL/6 background in the age range of 2–6 months. The coordinates of the injection site may vary among mouse strains and ages at injection.
2. When MRI is part of the experiment, use MRI-compatible cannula guide and dummy cannula (Fig. 2a).
3. The technique described here has been applied to do three AON injections over a period of 4 weeks. There should be at least 1 week between injections to let the mice recover. Sometimes the cannula guide comes off the skull of the mouse; however, in our hands, the cannula guide stays attached to the skull for a period of 6 months. After 6 months, we observed indentation of the skull in around 20% of the animals (Fig. 2b). Animals do not seem to suffer from this, but it could potentially influence the experiment depending on outcome measurements. For example, mice can have such a deformation that their MRI scans cannot be used.
4. When a single injection is sufficient to reach the desired dose, a fixed cannula guide is not needed. The cannula guide is not attached to the skull after injection and the skin is sutured.
5. Because of the protrusion of the cannula from the skull, the environment of the mouse might need adjustments. The cannula can get stuck in cage enrichment and experimental setups might need adjusting (MRI-coil, behavioral assays).
6. Infusion cannula and tubing can be used multiple times, if cleaned with MilliQ water and 70% ethanol.
7. The air bubble in the tubing creates a barrier between the water and the AON. By filling up the dead volume with water, less AON is wasted.
8. Keep an eye on the temperature and breathing of the mouse. When the breathing pattern becomes too low, isoflurane should be decreased. If the mouse starts waking up (you can check by pinching its paw), increase the isoflurane.
9. Make sure that the primer is not past its expiration date, the cement will detach if the primer is out of date. The primer should be kept at 4 °C, but it should be room temperature

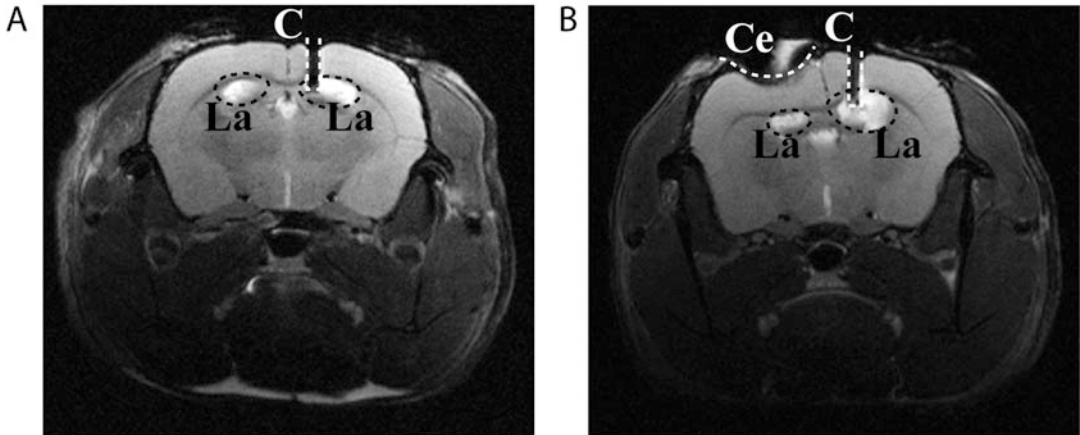


Fig. 2 MRI of mouse brains holding an ICV cannula. (a) Axial image of mouse brain depicting the lateral ventricles (La) showing the protrusion of the cannula (C, white dashed line) into the right lateral ventricle. (b) Axial image of mouse brain showing skull malformation by intrusion of cement (Ce, white dashed line) oppressing the brain

before applying. Make sure the skull is very dry before applying primer, if necessary use a cloth.

10. It is important to add cement one layer at the time and let it set before adding a next layer. Build the cement a few millimeters up the cannula guide, but you still need to be able to screw the dummy onto the cannula guide.
11. It happens that the dummy cannula is unscrewed from the cannula guide. This can be prevented by tightening the dummy onto the cannula guide using forceps.
12. We found that mice can be placed back into group housing after cannula placement.
13. Be careful with postmortem removal of the cannula guide, the inner part of the cannula guide can cause damage to the underlying brain tissue if not removed properly.

Acknowledgments

The research of the group is supported by: Campagne Team Huntington. “Antisense oligonucleotide disease modifying treatment for Huntington’s disease”; AFM Telethon. “Final proof of concept for the advancement of antisense oligonucleotide treatment for SCA3 towards the clinic” (Project number 20577); and ZonMW Memorabel. “RNA modulating therapy for Alzheimer’s disease” (Project number 733050818).

References

1. Aartsma-Rus A (2017) FDA approval of Nusinersen for spinal muscular atrophy makes 2016 the year of splice modulating oligonucleotides. *Nucl Acid Ther* 27(2):67–69. <https://doi.org/10.1089/nat.2017.0665>
2. Cummings CJ, Zoghbi HY (2000) Fourteen and counting: unraveling trinucleotide repeat diseases. *Hum Mol Genet* 9(6):909–916. <https://doi.org/10.1093/hmg/9.6.909>
3. Nakamura K, Jeong SY, Uchihara T, Anno M, Nagashima K, Nagashima T, Ikeda S, Tsuji S, Kanazawa I (2001) SCA17, a novel autosomal dominant cerebellar ataxia caused by an expanded polyglutamine in TATA-binding protein. *Hum Mol Genet* 10(14):1441–1448. <https://doi.org/10.1093/hmg/10.14.1441>
4. Tabrizi SJ, Leavitt BR, Landwehrmeyer GB, Wild EJ, Saft C, Barker RA, Blair NF, Craufurd D, Priller J, Rickards H, Rosser A, Kordasiewicz HB, Czech C, Swayze EE, Norris DA, Baumann T, Gerlach I, Schobel SA, Paz E, Smith AV, Bennett CF, Lane RM (2019) Targeting huntingtin expression in patients with Huntington's disease. *N Engl J Med* 380(24):2307–2316. <https://doi.org/10.1056/NEJMoa1900907>
5. Evers MM, Tran HD, Zalachoras I, Meijer OC, den Dunnen JT, van Ommen GJ, Aartsma-Rus A, van Roon-Mom WM (2014) Preventing formation of toxic N-terminal huntingtin fragments through antisense oligonucleotide-mediated protein modification. *Nucl Acid Ther* 24(1):4–12. <https://doi.org/10.1089/nat.2013.0452>
6. Toonen LJA, Rigo F, van Attikum H, van Roon-Mom WMC (2017) Antisense oligonucleotide-mediated removal of the polyglutamine repeat in spinocerebellar ataxia type 3 mice. *Mol Ther Nucl Acids* 8:232–242. <https://doi.org/10.1016/j.omtn.2017.06.019>

Open Access This chapter is licensed under the terms of the Creative Commons Attribution 4.0 International License (<http://creativecommons.org/licenses/by/4.0/>), which permits use, sharing, adaptation, distribution and reproduction in any medium or format, as long as you give appropriate credit to the original author(s) and the source, provide a link to the Creative Commons license and indicate if changes were made.

The images or other third party material in this chapter are included in the chapter's Creative Commons license, unless indicated otherwise in a credit line to the material. If material is not included in the chapter's Creative Commons license and your intended use is not permitted by statutory regulation or exceeds the permitted use, you will need to obtain permission directly from the copyright holder.



Part V

Safety and Toxicology



Chapter 24

Intrathecal Delivery of Therapeutic Oligonucleotides for Potent Modulation of Gene Expression in the Central Nervous System

Zachary Kennedy, James W. Gilbert, and Bruno M. D. C. Godinho

Abstract

Therapeutic oligonucleotides hold tremendous potential for treating central nervous system (CNS) disorders. The route of administration of oligonucleotides significantly impacts both distribution and silencing efficiency. Here, we describe a technically simple, clinically relevant method to administer oligonucleotide compounds into the CNS via direct intrathecal injections. This method achieves distribution throughout the CNS rapidly and permits high-throughput testing of oligonucleotide efficacy and potency in mammals.

Keywords siRNA, Antisense oligonucleotides, CSF infusion, IT dosing, Intrathecal injections, Modified oligonucleotides, Gene silencing, Therapeutic oligonucleotides, CNS administration

1 Introduction

Therapeutic oligonucleotides hold tremendous potential for treating disorders of the central nervous system (CNS), but numerous factors can hinder the delivery of these compounds. Among the major determinants affecting delivery of drugs to the CNS is the route of administration.

Drug delivery to the CNS can be performed through two general approaches: (a) systemic, where oligonucleotides are initially delivered outside of the CNS, or (b) direct, where oligonucleotides are delivered directly within the CNS. Systemic delivery strategies (e.g., intravenous or subcutaneous) are technically simple and easy to perform, but require significantly higher doses and result in very low efficacy in the CNS, mostly due to the inability of oligonucleotides to pass the blood–brain barrier [1–3]. Direct delivery methods, on the other hand, are comparatively more technical, but require much lower doses and enable significantly better

Zachary Kennedy and Bruno M. D. C. Godinho have contributed equally to this work.

distribution, efficacy, and potency throughout the CNS than systemic methods [4, 5]. The most commonly used direct delivery methods, especially in rodent models, are intracerebroventricular (ICV) injections or lumbar intrathecal (IT) injections.

From a technical perspective, IT injections are easier to perform than ICV injections—they require less setup/procedural time and do not require stereotactic equipment [6, 7]. IT administration is also favored from a clinical perspective because it is less invasive than ICV injections; IT injections do not require brain surgery and can be performed as an outpatient procedure. IT injections can be performed with or without a catheter. Currently, IT injections are the only clinically approved route of administration for therapeutic oligonucleotide treatment of CNS disorders [8].

Given its ability to deliver to the CNS, the comparatively quick operation time, and the clinical relevance of the route of administration, IT injections are an attractive delivery method for which to screen oligonucleotide compounds for CNS applications. In this chapter, we describe how to perform direct IT injections in mice without using a catheter. Special attention is given to the preparation of the oligonucleotide compounds, prepping the mouse for the injections, and ensuring successful delivery.

2 Materials

2.1 Preparation of Test Oligonucleotides

1. SpeedVac™ concentrator.
2. NanoDrop™.
3. Bench top centrifuge.
4. 3 kDa cutoff Amicon spin column (0.5 mL or larger).
5. 5 mM sterile calcium chloride (CaCl₂) solution.
6. Sterile phosphate-buffered saline (PBS).

2.2 Direct Intrathecal Injections

1. Gas tight Hamilton syringe, 25 µL 1702RN with a 30 G needle, 0.5 in. long, and point style 4 (12° angle bevel).
2. Electric shaver.
3. Dry bead sterilizer.
4. Weigh scale.
5. Cotton-tipped applicators (Q-tips).
6. Eye lubricant.
7. Anesthetics (Isoflurane or Ketamine/Xylazine).
8. Analgesic (Ketoprofen or Meloxicam SR).
9. Antiseptic Povidone-Iodine Solution (5–10%).
10. Ethanol solution (70%).

11. Oligonucleotide preparation (antisense oligonucleotides, ASOs; small interfering RNAs, siRNAs) at desired concentration.
12. Sterile gloves.

3 Methods

Oligonucleotides must be prepared aseptically in a laminar flow cabinet to avoid contamination and maintain sterility. All procedures performed in live animals must be approved by the Institutional Animal Care and Use Committee (IACUC) prior to executing the experiment.

3.1 Preparation of Test Oligonucleotides

It is recommended that test oligonucleotides be treated with a calcium solution to minimize acute in vivo toxicities (*see Note 1*). ASOs can be treated immediately after synthesis, whereas siRNAs should be treated after duplexing of the guide and passenger strands (*see Note 2*).

1. Add the entire oligonucleotide solution into a 3 kDa cutoff Amicon spin column. For a 0.5-mL Amicon column, add ~300 μ L of 5 mM CaCl_2 solution, sterilized using an autoclave.
2. Elute by centrifugation at $14,000 \times g$ for 10 min (min) at room temperature (RT) and discard the flow-through. Repeat **steps 1 and 2**.
3. Remove excess CaCl_2 , add ~400 μ L of nuclease-free water, centrifuge at $14,000 \times g$ for 10 min at RT, and discard flow-through. Repeat this step.
4. Wash compounds by adding ~400 μ L of $1 \times$ sterile PBS, centrifuge at $14,000 \times g$ for 10 min at RT, and discard flow-through.
5. Transfer compounds to sterile tubes by adding $1 \times$ PBS to the Amicon column and mixing the solution up and down (*see Note 3*). To recover as much compound as possible, invert the Amicon filters into the collection tubes and centrifuge at $2000 \times g$ for 5 min at RT.
6. Determine the concentration of the test oligonucleotide preparation using a NanoDropTM. Adjust to the desired concentration using sterile $1 \times$ PBS.

While the aforementioned CaCl_2 wash steps minimize toxicity, recovery of oligonucleotides from the columns is often incomplete, resulting in reduced yields. If the initial amount of oligonucleotides is low, an alternative strategy would be to evaporate oligonucleotides in SpeedVac (using the no temperature option for drying rate) and resuspend at the desired concentration with the chosen buffer.

3.2 Direct Intrathecal Injection

1. Gather all materials and set up a clean area for the procedure. If possible, the procedure should be done in a laminar flow cabinet (Fig. 1a).
2. Record the weight of each animal. This is important to perform prior to injections, in order to monitor the well-being of the animal after the procedure concludes.
3. Anesthetize the mouse according to the approved IACUC protocol (e.g., isoflurane, ketamine/xylazine, avertin). If isoflurane is used, induction is carried out with 4–5%, and maintenance with 1.5% by continuous administration through a nose cone.
4. Ensure the mouse is sufficiently sedated by gently pinching hind paws. If properly sedated, the mouse should not respond to the pinch.
5. Cover both the eyes with eye lubricant using a sterile cotton-tipped applicator.
6. Using an electric shaver, shave hair around the lower spine, starting from the base of the tail and spanning an area approximately 3×3 cm.
7. Clean the shaved area with an antiseptic 5–10% povidone-iodine solution, then wipe with 70% ethanol. Repeat this step three times.
8. Place a 15-mL conical tube under the abdomen of the mouse to expose a bigger area of the interspinous ligament, which is punctured by the needle to access the intradural space (see Fig. 1b). Positioning the mouse on a 15-mL conical tube also makes it easier to find and grasp the iliac crest.
9. Identify the iliac crest by finding the two pits formed at the interface of the muscle and the hip bone (see Fig. 1b, black dotted lines).
10. The injection site (L5–L6) will be directly above the iliac crest (marked with an asterisk in Fig. 1b). Determine the position of the L6 vertebra by identifying the most protruding spinal process (see Fig. 1b). Injection at this position reduces the possibility of spinal damage, since this site is where the spinal cord ends and the cauda equina begins.
11. Prepare and load the Hamilton Syringe with a test compound (5–10 μ L) (see Note 4). The same syringe can be used for multiple animals; however, use only one syringe per compound to avoid cross contamination. Syringes should be cleaned and the tip sterilized in the bead sterilizer between animals (see Note 5).

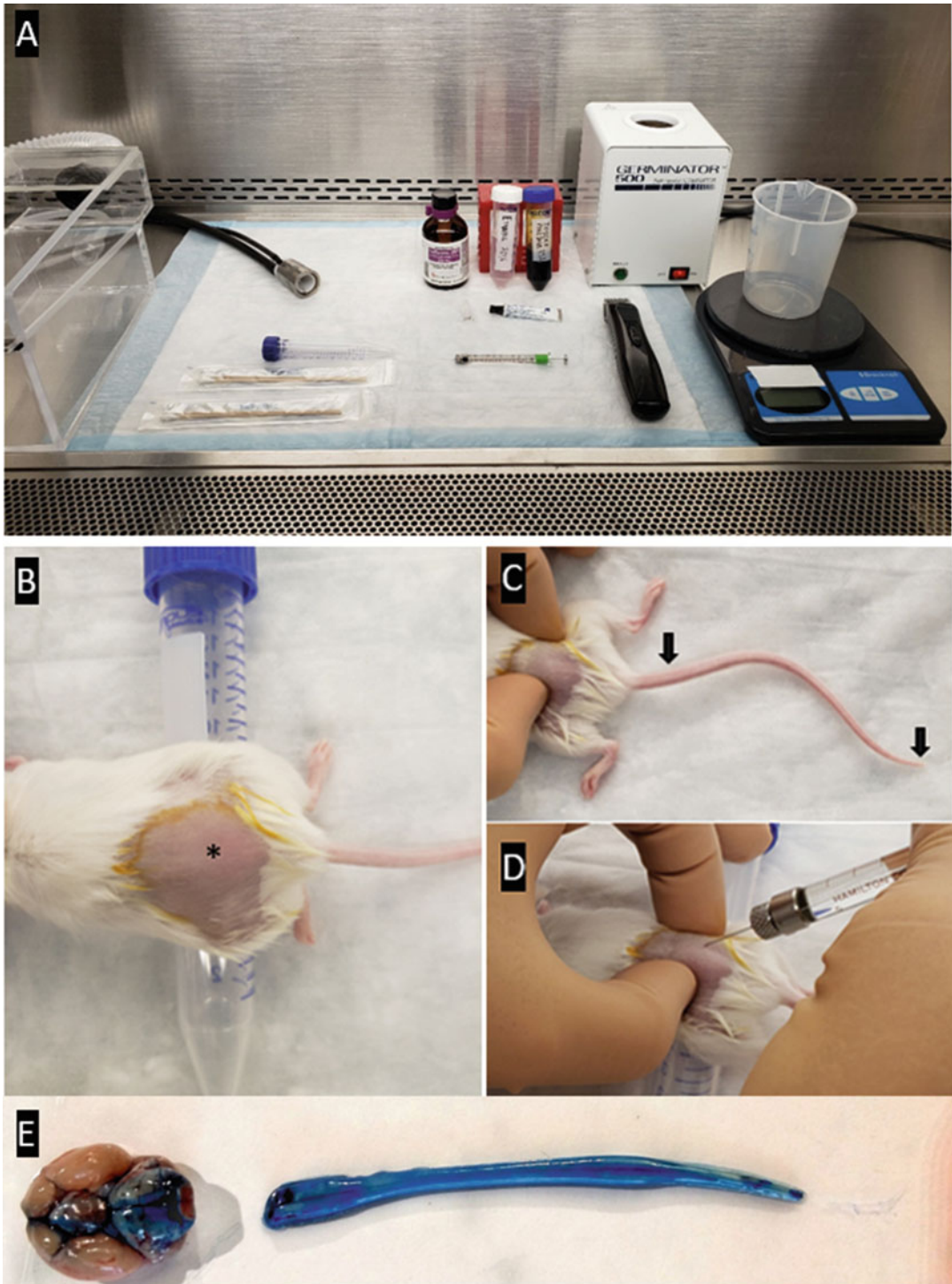


Fig. 1 Intrathecal injection procedures. **(a)** Setup and materials needed for intrathecal injections. **(b)** Placement of anesthetized mice. After shaving the mice, the mouse is placed on a 15-mL conical tube placed under the lower stomach, allowing for easy visualization of the hip and spinal cord protrusions. Asterisk indicates injection site. Dotted lines indicate the superficial depression formed by spinal cord and iliac crests. **(c)** Placement of hands during procedure. Mouse is grasped by pinching the hips and lifting slightly, allowing for

12. Grasp the animal by pinching just above the hips, taking care to ensure that the tail is visible (see Fig. 1c).
13. Insert the needle between the groove of L5 and L6 vertebrae at a $\sim 30^\circ$ angle, and to a depth of approximately 0.5 cm. Once the needle has successfully entered the intradural space, the tail of the mouse will move or “flick” (see Note 6, and Fig. 1c, d).
14. After observation of the tail flick, slowly and continuously inject oligonucleotides. After the entire volume of test oligonucleotide has been injected, keep the needle in the intradural space for 5–10 s to prevent or reduce backflow.
15. Carefully remove the needle and inspect the site for backflow.
16. Administer analgesia as per IACUC protocol.
17. Return the animal to its cage and monitor for pain and discomfort for at least 30 min. Until animals regain sternal recumbency, supplemental heat should be provided. This can be achieved by keeping the cage on top of a heating pad. Monitor animals daily for 3 days after the procedure, and weekly thereafter. IT injections may be repeated as necessary (see Notes 7 and 8).

When establishing this methodology in the lab, it is recommended to first practice using Evans blue dye. A successful injection will result in immediate distribution of the dye throughout the spinal cord and periphery of the brain (see Fig. 1e). It is also important to consider that distribution of therapeutic oligonucleotides is highly dependent on its conjugated ligand modality. Thus, in studies investigating biodistribution, oligonucleotides are often labeled with fluorescent tags, such as Cy3. Figure 2 shows the distribution of a Cy3-labeled Di-siRNA scaffold (20 nmol in 10 μ L) 48 h after a single IT injection.

3.3 Suggestions for Tissue Collection and Processing

For microscopy, the whole spine may be fixed in decalcifier/formalin after perfusion of the animal with cold $1\times$ PBS. For RNA and protein analyses, the spinal cord can be either dissected or flushed out of the spine. After identifying the different segments of the spinal cord, these can be divided longitudinally to generate two samples per region for: (1) RNA assessment and (2) protein evaluation. RNA analyses can be carried out by RT-qPCR, bDNA, or other methods. Protein analyses can be performed by Western blot, ELISA, or other methods.

Fig. 1 (continued) maximum exposure of the cartilage between the L4 and L5 spinal segments. Successful needle insertion is often accompanied with a subtle tail-flick, which can be observed at the base of the tail or the very tip (see arrows), (d) Placement of needle during procedure. Dotted lines indicate the superficial depression formed by the spinal cord and iliac crest, where the hip meets the spinal cord. (e) Ventral view of brain and spinal cord immediately after IT injection of Evans blue dye

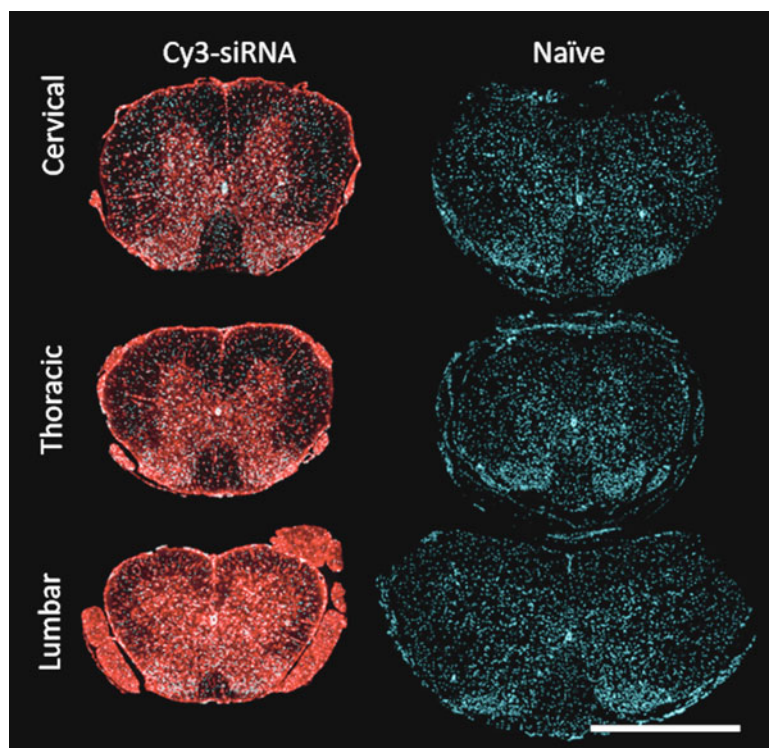


Fig. 2 Distribution pattern of Cy3-labeled oligonucleotide within the spinal cord. Horizontal cross sections of spinal cord segments following intrathecal injection of Cy3 labeled Di-siRNA oligonucleotides (20 nmol). Mice were euthanized 48 h post injection and tissues processed for microscopy. Tiled fluorescent images were acquired using 10× objective and displayed as overlay images: Cyan (DAPI, Nuclei), red (Cy3-labeled oligo). Scale bar 1 mm

4 Notes

1. Upon injection into the CSF, the negatively charged phosphate backbone of therapeutic oligonucleotides can rapidly sequester divalent ions (Ca^{2+} , Mg^{2+}), causing acute adverse events (e.g., seizures). To minimize toxicity in vivo, a calcium treatment can be performed to saturate every phosphate position.
2. ASOs and siRNAs can be either synthesized in-house or acquired through a vendor or a contract research organization. If test oligonucleotides are delivered in dried form, they should be resuspended in nuclease-free water or other appropriate buffers. In the case of siRNA, guide and passenger strands can be annealed in equimolar amounts after the determination of initial concentration.

3. To ensure compounds are not overdiluted, it is important to start with small volumes (e.g., 50–100 μL) and wash the filter several times.
4. Based on previous literature, we found that 10 μL injections in adult mice are well-tolerated and do not cause neuronal loss, astrogliosis, or microgliosis [9]. We do not recommend injecting in less than 5 μL due to higher chance of pipetting error while preparing the compounds.
5. Syringes should be cleaned right after use to avoid clogging. Rinse the syringe with: Milli-Q purified (or deionized) water (5 \times), diluted Hamilton cleaning solution (P/N 18311) (5 \times), then Milli-Q purified (or deionized) water (5 \times) again. Sterilize the tip by dipping it on a dry bead sterilizer for 15–20 s and allow it to cool. Rinse the syringe with 1 \times PBS before drawing the compound for the next injection. Disinfectants, such as Microcide SQ[®] (P/N 3995–01), can be used to eliminate a variety of common bacteria, fungi, and viruses. Before storage, and after using a cleansing agent or disinfectant, rinse with Milli-Q purified (or deionized) water and with acetone. Air dry and store in case.
6. The flick of the tail can be very subtle; while advancing the needle into the skin, it is important to focus your attention on the tail. If the tail flick event is missed, and the needle is pulled back and re-inserted, the likelihood of observing a tail flick on a second attempt is significantly lower. Tail flicks are somewhat inversely correlated with the deepness of the anesthesia—very deep anesthesia will make it harder to see the tail flick event occur.
7. Immediately after the procedure, mice should be warmed with thermal support (i.e., a heating pad or a heat lamp) and observed until they are ambulatory. After mice are ambulatory, return mice to their cages and make sure food and water are easily accessible to mice. This can be achieved by adding food pellets to the floor of the cage and supplanting the cage with gel water. After the procedure, mice should be monitored at least once every 24 h for 3 days. Monitor for signs of stress that could indicate pain, including weight loss, lethargy, reduction in rearing behavior, excessive barbering, urine stain, and changes in behavior. If at any point, the mice show signs of pain, they should be given analgesics or euthanized in accordance with the IACUC-approved protocol.
8. Depending on the dosing strategy and the individual IACUC protocol, IT injections can be performed on a single mouse up to three times per 24 h.

Acknowledgments

The authors would like to thank Dr. Anastasia Khvorova of the RNA Therapeutics Institute (University of Massachusetts Medical School) for continuous mentorship and research support. The authors would also like to thank Jake Metterville of Wave Life Sciences, Greg Cottle, and Van Gould of the Department of Animal Medicine (University of Massachusetts Medical School) for expert advice on technical details and animal welfare compliance. The authors acknowledge Dr. Emily Haberlin for editorial feedback on the manuscript.

References

1. Relizani K, Goyenvallé A (2018) Use of Tricyclo-DNA antisense oligonucleotides for exon skipping. *Methods Mol Biol* 1828: 381–394. https://doi.org/10.1007/978-1-4939-8651-4_24
2. Godinho B, Henninger N, Bouley J, Alterman JF, Haraszti RA, Gilbert JW, Sapp E, Coles AH, Biscans A, Nikan M, Echeverria D, DiFiglia M, Aronin N, Khvorova A (2018) Transvascular delivery of hydrophobically modified siRNAs: gene silencing in the rat brain upon disruption of the blood-brain barrier. *Mol Ther* 26(11): 2580–2591. <https://doi.org/10.1016/j.ymthe.2018.08.005>
3. Boursereau R, Donadieu A, Dabertrand F, Dubayle D, Morel JL (2015) Blood brain barrier precludes the cerebral arteries to intravenously-injected antisense oligonucleotide. *Eur J Pharmacol* 747:141–149. <https://doi.org/10.1016/j.ejphar.2014.11.027>
4. Miller TM, Pestronk A, David W, Rothstein J, Simpson E, Appel SH, Andres PL, Mahoney K, Allred P, Alexander K, Ostrow LW, Schoenfeld D, Macklin EA, Norris DA, Manousakis G, Crisp M, Smith R, Bennett CF, Bishop KM, Cudkowicz ME (2013) An antisense oligonucleotide against SOD1 delivered intrathecally for patients with SOD1 familial amyotrophic lateral sclerosis: a phase 1, randomised, first-in-man study. *Lancet Neurol* 12(5):435–442. [https://doi.org/10.1016/S1474-4422\(13\)70061-9](https://doi.org/10.1016/S1474-4422(13)70061-9)
5. Njoo C, Heintz C, Kuner R (2014) In vivo siRNA transfection and gene knockdown in spinal cord via rapid noninvasive lumbar intrathecal injections in mice. *J Vis Exp* (85):51229. <https://doi.org/10.3791/51229>
6. Chen Y, Mazur C, Luo Y, Sun L, Zhang M, McCampbell A, Tomassy GS (2019) Intrathecal delivery of antisense oligonucleotides in the rat central nervous system. *J Vis Exp* (152). <https://doi.org/10.3791/60274>
7. Hylden JL, Wilcox GL (1980) Intrathecal morphine in mice: a new technique. *Eur J Pharmacol* 67(2–3):313–316. [https://doi.org/10.1016/0014-2999\(80\)90515-4](https://doi.org/10.1016/0014-2999(80)90515-4)
8. Corey DR (2017) Nusinersen, an antisense oligonucleotide drug for spinal muscular atrophy. *Nat Neurosci* 20(4):497–499. <https://doi.org/10.1038/nn.4508>
9. Guo Y, Wang D, Qiao T, Yang C, Su Q, Gao G, Xu Z (2016) A single injection of recombinant adeno-associated virus into the lumbar cistern delivers transgene expression throughout the whole spinal cord. *Mol Neurobiol* 53(5): 3235–3248. <https://doi.org/10.1007/s12035-015-9223-1>

Open Access This chapter is licensed under the terms of the Creative Commons Attribution 4.0 International License (<http://creativecommons.org/licenses/by/4.0/>), which permits use, sharing, adaptation, distribution and reproduction in any medium or format, as long as you give appropriate credit to the original author(s) and the source, provide a link to the Creative Commons license and indicate if changes were made.

The images or other third party material in this chapter are included in the chapter's Creative Commons license, unless indicated otherwise in a credit line to the material. If material is not included in the chapter's Creative Commons license and your intended use is not permitted by statutory regulation or exceeds the permitted use, you will need to obtain permission directly from the copyright holder.





Preclinical Safety Assessment of Therapeutic Oligonucleotides

Patrik Andersson 

Abstract

During the last decade, therapeutic oligonucleotide drugs (OND) have witnessed a tremendous development in chemistry and mechanistic understanding that have translated into successful clinical applications. Depending on the specific OND mechanism, chemistry, and design, the DMPK and toxicity properties can vary significantly between different OND classes and delivery approaches, the latter including lipid formulations or conjugation approaches to enhance productive OND uptake. At the same time, with the only difference between compounds being the nucleobase sequence, ONDs with same mechanism of action, chemistry, and design show relatively consistent behavior, allowing certain extrapolations between compounds within an OND class. This chapter provides a summary of the most common toxicities, the improved mechanistic understanding and the safety assessment activities performed for therapeutic oligonucleotides during the drug discovery and development process. Several of the considerations described for therapeutic applications should also be of value for the scientists mainly using oligonucleotides as research tools to explore various biological processes.

Keywords Oligonucleotide drugs, ASO, siRNA, Antisense, Non-clinical safety assessment, Preclinical safety assessment, Toxicity

1 Introduction: Oligo Classes, Chemistries, and Designs

Oligonucleotide drugs (OND) of different classes range from 10–12 up to 100 nucleotides in length, often with chemical modifications of the backbone and ribose sugar. The chemistry and design used are dictated by the desired mechanism of action, resulting in different classes of therapeutic oligos with specific properties. The most common classes in clinical studies target RNA and rely on Watson-Crick hybridization for selectivity and affinity, where antisense oligonucleotides (ASOs) and short interfering RNAs (siRNAs) are the most common, with several examples of approved products [1, 2].

ASOs are single-stranded ONDs of 12–20 nucleotides in length, often with a phosphorothioate (PS) backbone and 2′ribose

modifications like OMe, MOE, LNA, and cEt that improve drug properties like metabolic stability, tissue uptake, and increased affinity to the target transcript [3–5]. The ASO class can be further subdivided into ASO gapmers that trigger RNase H-mediated cleavage and degradation of target transcripts and steric blocking ASOs that modulate splicing events or inhibit activity of, e.g., microRNA (miR) [6–8]. For ASOs with a steric blocking activity, use of other chemistries resulting in neutral backbones like Phosphorodiamidate Morpholinos (PMO), Peptide nucleic acids (PNA) and tricyclo-DNA (tcDNA) is possible and quite common [9–13].

siRNAs and microRNA-mimics have a double-stranded design with each strand approximately 20–24 nucleotides in length and rely on loading of the antisense strand into RISC for activity [14, 15]. The design of siRNA results in cleavage and subsequent degradation of the target transcript, whereas miR mimics regulate gene expression by binding to miR sites in mRNA, inducing degradation and regulating protein translation [8].

In addition to hybridization dependent ASOs, miR mimics, and siRNA, there are several classes of hybridization independent ONDs including aptamers [16, 17] and immunostimulatory CpG oligos [18–21]. Rather than binding to RNA, the three-dimensional structure of folded RNA of a given sequence is combined with chemical modifications to achieve specific binding to proteins. Other therapeutic approaches such as mRNA therapy and the guide RNA in various gene editing approaches (e.g., CRISPR/CAS9) utilize nucleotides and but are commonly not classified as ONDs.

This chapter will focus on safety assessment of the hybridization dependent PS backbone ASOs and siRNA.

2 Delivery

The activity of ASOs, siRNA, and miR mimics rely on reaching the interior of the target cells. Uptake per se is not enough; the oligo needs to access the right subcellular compartments for activity, e.g., the cytosol for RISC loading or the nucleus for splice modulation or RNase H activity. Cellular uptake leading to pharmacodynamic effects are often referred to as “productive uptake” [22–24]. For ASOs, the best productive uptake after systemic delivery is often observed in the liver, in particular hepatocytes [24, 25]. Early siRNA candidates were delivered in protective formulations that also showed best uptake into hepatocytes [26]. Local delivery has successfully been used to bypass the blood–brain barrier, resulting in good therapeutic effects after local delivery to CNS [27–29], and the eye [30–33]. However, for use of therapeutic oligos beyond hepatocytes [3, 5, 34–37] and local delivery, achieving sufficient productive uptake has become one of the biggest challenges and

numerous ways to overcome this has been proposed [36, 38, 39]. One approach is delivery in different types of formulations like the lipid nanoparticle (LNP) used to deliver Onpattro [26], the first siRNA receiving regulatory approval by FDA in 2018 [40]. However, although efficient delivery at low doses can be achieved, the LNP triggers proinflammatory flu-like responses that are managed by pre-medication before administration [41]. Since discovery of this LNP, a number of alternative formulations have been presented with different tissue distribution and improved efficacy:safety relationship.

An alternative way to improve the productive uptake is conjugation of the oligo to a targeting ligand, utilizing binding to cell surface receptors that internalize the oligo conjugate. An excellent example of this strategy is conjugation of the GalNAc carbohydrate, resulting in significantly improvements in productive uptake of both siRNA and ASOs [42, 43]. This GalNAc-mediated improvement in productive uptake is mediated by the binding of the conjugate to the asialoglycoprotein receptor (ASGR), which mainly is expressed on hepatocytes. Although non-conjugated ASOs show hepatocyte activity, adding GalNAc conjugates increased the clinical potency 20–30-fold for several re-formatted ASOs with hepatocyte targets [44]. Combining GalNAc conjugation with nuclease-resisting chemical stabilization has led to a tremendous increase in the utility of siRNA in the clinic, with several recent approvals with no need for the pre-medication required for LNP formulated Onpattro [2].

3 Safety Assessment of Therapeutic Oligos

The focus of this chapter is the preclinical safety assessment of therapeutic oligos intended to enter clinical trials to get regulatory approval for use in patients. With increasing experience and mechanistic understanding, screening cascades, study designs and data interpretations for ONDs are constantly improving, leading to more potent clinical candidates with better safety profiles. As described below, safety assessment of clinical OND candidates is a highly regulated process that at first sight could be of less interest for scientists primarily using oligonucleotides as tools to dissect and understand basic biological process. However, several of the considerations for bringing safe candidates to clinical trials could also be of value when developing optimal tool oligos and study designs for basic research. This includes cross species activity, restricted uptake distribution, long tissue half-life and effect duration, hybridization dependent off-target effects and the need to screen away from sequence dependent toxicities.

**3.1 Discovery Phase:
Selecting the Oligo
Candidate with the
Best Balance Between
Potency and Safety**

The potential safety concerns with therapeutic oligos can be divided into:

1. Sequence and hybridization dependent (Sect. 3.1.1).
2. Sequence and hybridization independent (Sect. 3.1.2).
3. Sequence dependent, but hybridization independent (Sect. 3.1.3).

**3.1.1 Sequence and
Hybridization Dependent
Effects: Assessing On- and
Off-Target Safety**

On-target toxicities, also known as exaggerated pharmacology, are dependent on sequence and RNA hybridization for ASOs, siRNA, and miR mimics. It can manifest in too strong intended effect or an adverse consequence of the pharmacological response in an unintended organ. A first assessment of potential on-target safety risks should be a theoretical exercise compiling available information on the biological role, tissue expression pattern, competitor information, etc. to assess the likelihood and potential adverse impact of the identified risks in the intended patient population. Considerations for assessing on-target toxicities for ONDs has been discussed by Kornbrust et al. [45].

Another safety concern dependent on Watson-Crick base pairing is hybridization dependent **off-target risks**. In contrast to the risk for on-target toxicity described above where the oligo has the intended, but exaggerated activity, this off-target risk relates to oligo activity on other transcripts than the intended target. Key features determining likelihood for hybridization dependent off-target effects have been discussed in depth elsewhere [46–50] and several recommendations [51] are summarized below:

1. Identify candidates for off-target hybridization by in silico screening of the entire transcriptome of the pre-mRNA.
2. In vitro confirmation: experimentally assess potency of sequences meeting the in silico criteria in vitro, establishing margins to activity on the primary target transcript.
3. For off-targets with insufficient in vitro margins, assess potential consequences using the principles for on-target safety assessment.

There are some specific considerations when assessing potential hybridization-dependent safety concerns. First, due to species differences in sequence, it is often difficult to achieve pharmacological activity with the same OND in other species and it is common practice to use surrogate molecules with sufficient potency in the model species of choice.

Second, the chemical modifications used in therapeutic oligos lead to slow tissue elimination and extended effect duration [52]. This is convenient from a delivery perspective, but the wash-out period needed for the adverse effects to cease would be equally long should on- or off-target toxicities be observed.

Third, the restricted productive uptake of ASOs and siRNA to many cell types needs to be considered, as there is a large difference in the uptake between different cells and tissues. The oligo distribution can change with other administration routes and delivery systems like conjugates or formulations, so understanding the productive uptake distribution for such new conditions is critical for proper risk assessment of potential on- and off- target toxicities.

3.1.2 Sequence and Hybridization Independent Effects: Coagulation Time and Complement Activation

A couple of toxicities that are dependent on plasma C_{\max} but independent of both hybridization and sequence can be observed at relative high doses of PS backbone ASOs. This includes prolongation of coagulation time and activation of the alternative complement system. Acutely, activation of the alternative complement system can lead to significant drops in blood pressure. Repeated complement activation can result in “consumption” of complement factor C3 with impaired complement-mediated clearance of antibody aggregates resulting in vascular inflammation [53]. Data from in vitro, in vivo, and clinical studies clearly show that cynomolgus monkeys are significantly more sensitive than humans for this lowered threshold of complement activation [54, 55].

Both these effects are driven by the plasma C_{\max} levels [56–60] and transient in nature. With increased potency of modern ASOs and adapted dosing in current clinical studies, plasma concentrations rarely exceed these activation thresholds [55, 61, 62].

3.1.3 Sequence Dependent, But Hybridization Independent: Inflammation, Liver, and Kidney Toxicities

In contrast to these plasma C_{\max} -driven effects, other hybridization independent toxicities are highly dependent on the OND sequence. This includes proinflammatory manifestations and effects in high exposure organs such as liver and kidney that can sometimes be observed during the discovery phase. For siRNA, liver toxicity has been explained to be caused by off-target effects in the seed-region of the siRNA [48]. For PS backbone ASOs, liver toxicity is more frequently observed with higher affinity chemistry like LNA and cEt. It is clear from a number of published and unpublished observations that this liver toxicity observed during the screening process of PS backbone ASO gapmers is *not* caused by knockdown of the intended target transcript or liver concentration per se, see e.g. [63]. ASO sequence motifs associated with liver tox [64, 65] and different molecular mechanisms have been proposed, including cell death as a cellular consequence to exaggerated RNase H activity resulting from non-selective hybridization [66, 67]. An alternative mechanism proposed involves PS backbone-dependent binding to key intracellular proteins in a sequence and chemistry-dependent manner. Being more hydrophobic, the higher affinity modifications showing higher incidence of liver toxicity also show higher affinity to a number of intracellular proteins compared to the same sequence with, e.g., MOE chemistry [68–71]. Importantly,

predictive in vitro models for liver and kidney toxicity have been developed [67, 72, 73], and design modifications reducing ASO toxicity without compromising potency have been proposed [69, 74] demonstrating that highly potent ASO sequences that do not show liver toxicity can be identified and progressed to clinical trials.

Immune-stimulatory effects have long been a prominent feature of ONDs, where responses may vary widely between species and depend on oligonucleotide design and sequence, as well as chemical modifications [75–85]. The immunomodulatory potential can deliberately be used to design nucleotide-based immunotherapies and vaccine adjuvants, often harboring so-called CpG motifs [18–21], but for most other ONDs these effects are unwanted. Despite avoiding established CpG motifs in the design phase, some therapeutic oligos induce clear proinflammatory effects that can show in several different ways in the clinic, including injection site or infusion related reactions, flu-like symptoms and thrombocytopenia [86–90]. These effects are dose-dependent and can occur at different time points after first administration of the drug. Rodents are particularly sensitive to the immunostimulatory effects of ONDs [91, 92]. Similar to the liver toxicity described above, oligo sequence is a key parameter defining the proinflammatory property of therapeutic oligos and subtle and systematic sequence modifications to a proinflammatory ASO resulted in clear differences in proinflammatory potential [93]. Chemical modifications can modify the immune stimulatory potential of ONDs of a given sequence: PS modification of the backbone has long been known to increase the immune stimulatory properties of ONDs [80, 85, 94], whereas the neutral backbone in PMOs does not evoke an immune response [95]. 5'-methylation of cytosine is frequently used to suppress the immune stimulatory effect of CpG DNA sequences [76, 79]. 2'OMe modification of ssRNA or siRNA sequences inhibit immune stimulation, whereby even single modifications can significantly reduce the cytokine upregulation [78, 84]. Other 2'-ribose modifications (2'F, 2'H, 2'MOE, LNA) have also been described to reduce proinflammatory effects [76, 83]. Therapeutic oligos administered in lipid formulations have been shown to induce inflammatory responses, and humans seem to be more sensitive to these effects than both rodents and NHPs [96–98].

Thrombocytopenia (TCP), i.e., low concentration of circulating platelets, has been observed in NHP toxicity studies with ASOs. In most cases, the platelet counts show around 30% reduction from baseline and then stabilize at a non-adverse level. However, in some drug programs, a few individual monkeys have experienced severe TCP [99]. Severe TCP was observed in the phase 3 studies for volanesorsen and inotersen as well as for drisapersen [86, 100, 101]. These TCP events occurred in the highest dose group, and

platelet counts increased after drug cessation. A combination of high dose of proinflammatory ASOs and possibly patient susceptibility factors seem to be the most likely cause: a high frequency of severe TCP in cynomolgus monkeys of Mauritian origin whereas no cases of severe TCP were observed when the same ASO was given to non-Mauritian cynomolgus monkeys in a follow-up study [102].

3.2 Development Phase: In-Depth Characterization and Documentation of the Oligo Candidate

3.2.1 Preclinical Safety Assessment During the Development Phase

Strategies for preclinical safety assessment of therapeutic oligos have been discussed elsewhere [22, 89]. Results from a survey across 23 companies developing therapeutic oligos performed in 2018 showed that most companies follow the two species small molecule approach as outlined by the ICH M3(R2) guideline [103]. Although a guideline recently was adopted by Japanese regulators, most health authorities lack formal regulatory guidelines for therapeutic oligos, so the expectations and experience may vary between regions and even within health authorities [103]. However, white papers published by cross-pharma groups like OSWG (Oligo Safety Working Group) on best practice recommendations are frequently used as informal guidelines [45, 51, 96, 104–110].

For the common situation with a human active candidate having limited cross-species activity for meaningful assessment of potential on-target toxicity, a surrogate molecule can be included in parallel to the clinical candidate. Such surrogate molecules should be of the same design and chemistry as the clinical candidate and have a good general safety profile to allow meaningful assessment and documentation of potential on-target toxicities. Such surrogate molecules are mostly designed to be active in the rodent species of choice.

Despite lack of positive results in regulatory genotoxicity studies as discussed in the OSWG white paper by Berman et al. [105], several health authorities still request in vitro and in vivo assessment of genotoxicity [103].

For small molecules, in vitro and in vivo safety pharmacology studies are important to rule out adverse functional effects on key organs such as the CNS, cardiovascular and respiratory systems. Safety pharmacology assessment has been discussed in another OSWG white paper [106]. To the knowledge of the author, there is no information on systemically administered ASOs or siRNA showing activity in vitro or in vivo safety pharmacology studies, including activity on the hERG channel or any other ion channels important for cardiovascular or neuronal function. However, direct delivery into heart and CNS is a different story and could result in functional effects.

Similar to small molecules, the general toxicity studies for ASOs and siRNA are performed in a rodent and a non-rodent species. The duration of these Good Laboratory Practice (GLP) studies range from 1 to 3 months in the beginning of a program to chronic

studies of 6 and 9 months in duration for rodents and non-rodents, respectively. For double-stranded siRNA and microRNA mimics, the rat is by far the most commonly used rodent species whereas the mouse is rodent species of choice for most single stranded PS backbone ASO candidates [103]. Although rat is the most common rodent for toxicity studies of small molecules, rat specific lesions like Chronic Progressive Nephropathy (CPN) [91, 92] are aggravated by the high kidney concentrations resulting from systemic delivery of PS backbone ASO. CPN is of no human relevance [111] but can become problematic in toxicity studies of long duration.

Due to the highest likelihood of sequence-dependent crossover on activity and a robust historical background record, the non-human primate (NHP), is by far the most common non-rodent species used for both ASO and siRNA candidates, but other non-rodents have been evaluated [103], including the pig [112]. Other in vivo studies required before regulatory approval include developmental and reproductive toxicology studies (DART) and carcinogenicity studies. Considerations for the DART studies are described in an OSWG white paper [108] and is normally run in mouse, rat or rabbit. Carcinogenicity studies are commonly run as a lifelong (2 years) studies in rat and mice or a 2-year study in rat combined with a 6-month study in a transgenic mouse model. The relevance of these carcinogenicity studies for ASOs and siRNA has been questioned, but most health authorities are likely waiting for more data before discussing whether these studies can get a waiver or not.

3.2.2 *Regulatory Perspective*

Several of the oligonucleotide products approved to date (e.g., eteplirsen, mipomersen, inotersen, volanesorsen) are aimed at treating rare, often genetic diseases for which no alternative treatment is available. In such cases, the presence of some safety signals has been judged to be acceptable. However, with some recent projects aiming at targeting significantly larger populations with more common disease, like the cholesterol-lowering siRNA inclisiran targeting PCSK9 and for which other treatments exist, the risk:benefit assessment will likely be different. At the same time as ONDs are considered for much larger and broader patient populations than before, exciting opportunities on the other end of the patient population spectrum are emerging. Milasen is a splice modulating ASO developed to treat a fatal neurodegenerative condition unique to a single patient [113]. With increasingly refined and optimized screening cascades, OND treatments for $N = 1$ and other ultrarare conditions will most likely become more common practice.

In summary, safety of ONDs depend on sequence, chemistry, design, and delivery approach. Several properties like limited species cross-reactivity, long tissue half-life and restricted productive

uptake distribution needs to be considered when designing interpreting results for hybridization dependent on – and off-target safety assessment studies. Together with liver and kidney toxicity, proinflammatory effects are the most commonly observed safety findings in preclinical studies. With improved mechanistic understanding and screening approaches, more potent OND candidates with better safety profile can be identified for treatment of an increasing range of diseases and patient populations.

References

1. Crooke ST, Witztum JL, Bennett CF, Baker BF (2018) RNA-targeted therapeutics. *Cell Metab* 27(4):714–739. <https://doi.org/10.1016/j.cmet.2018.03.004>
2. Zhang MM, Bahal R, Rasmussen TP, Manautou JE, Zhong XB (2021) The growth of siRNA-based therapeutics: updated clinical studies. *Biochem Pharmacol* 189:114432. <https://doi.org/10.1016/j.bcp.2021.114432>
3. Khvorova A, Watts JK (2017) The chemical evolution of oligonucleotide therapies of clinical utility. *Nat Biotechnol* 35(3):238–248. <https://doi.org/10.1038/nbt.3765>
4. Seth PP, Swayze EE (2014) Unnatural nucleoside analogs for antisense therapy. In: Hanessian S (ed) *Natural products in medicinal chemistry*, 1st edn. Wiley-VCH Verlag, Weinheim, pp 403–439
5. Wan WB, Seth PP (2016) The medicinal chemistry of therapeutic oligonucleotides. *J Med Chem* 59(21):9645–9667. <https://doi.org/10.1021/acs.jmedchem.6b00551>
6. Bennett CF (2019) Therapeutic antisense oligonucleotides are coming of age. *Annu Rev Med* 70:307–321. <https://doi.org/10.1146/annurev-med-041217-010829>
7. Krutzfeldt J, Rajewsky N, Braich R, Rajeev KG, Tuschl T, Manoharan M, Stoffel M (2005) Silencing of microRNAs in vivo with ‘antagomirs’. *Nature* 438(7068):685–689. <https://doi.org/10.1038/nature04303>
8. Rupaimoole R, Slack FJ (2017) MicroRNA therapeutics: towards a new era for the management of cancer and other diseases. *Nat Rev Drug Discov* 16(3):203–222. <https://doi.org/10.1038/nrd.2016.246>
9. Carver MP, Charleston JS, Shanks C, Zhang J, Mense M, Sharma AK, Kaur H, Sazani P (2016) Toxicological characterization of exon skipping Phosphorodiamidate Morpholino oligomers (PMOs) in non-human primates. *J Neuromusc Dis* 3(3): 381–393. <https://doi.org/10.3233/JND-160157>
10. Goyenvallé A, Leumann C, Garcia L (2016) Therapeutic potential of tricyclo-DNA antisense oligonucleotides. *J Neuromusc Dis* 3(2):157–167. <https://doi.org/10.3233/JND-160146>
11. Hammond SM, Hazell G, Shabanpoor F, Saleh AF, Bowerman M, Sleigh JN, Meijboom KE, Zhou H, Muntoni F, Talbot K, Gait MJ, Wood MJ (2016) Systemic peptide-mediated oligonucleotide therapy improves long-term survival in spinal muscular atrophy. *Proc Natl Acad Sci U S A* 113(39): 10962–10967. <https://doi.org/10.1073/pnas.1605731113>
12. Montazersaheb S, Hejazi MS, Nozad Charoudeh H (2018) Potential of peptide nucleic acids in future therapeutic applications. *Adv Pharmaceut Bull* 8(4):551–563. <https://doi.org/10.15171/apb.2018.064>
13. Saleh AF, Arzumanov AA, Gait MJ (2012) Overview of alternative oligonucleotide chemistries for exon skipping. *Methods Mol Biol* 867:365–378. https://doi.org/10.1007/978-1-61779-767-5_23
14. Titze-de-Almeida R, David C, Titze-de-Almeida SS (2017) The race of 10 synthetic RNAi-based drugs to the pharmaceutical market. *Pharm Res* 34(7):1339–1363. <https://doi.org/10.1007/s11095-017-2134-2>
15. Bobbin ML, Rossi JJ (2016) RNA interference (RNAi)-based therapeutics: delivering on the promise? *Annu Rev Pharmacol Toxicol* 56:103–122. <https://doi.org/10.1146/annurev-pharmtox-010715-103633>
16. Nimjee SM, White RR, Becker RC, Sullenger BA (2017) Aptamers as therapeutics. *Annu Rev Pharmacol Toxicol* 57:61–79. <https://doi.org/10.1146/annurev-pharmtox-010716-104558>
17. Zhou J, Rossi J (2017) Aptamers as targeted therapeutics: current potential and challenges.

- Nat Rev Drug Discov 16(3):181–202. <https://doi.org/10.1038/nrd.2016.199>
18. Jackson S, Candia AF, Delaney S, Floettmann S, Wong C, Campbell JD, Kell S, Lum J, Hessel EM, Traquina P, McHale M, Robinson I, Bell J, Fuhr R, Keeling D, Coffman RL (2018) First-in-human study with the inhaled TLR9 oligonucleotide agonist AZD1419 results in interferon responses in the lung, and is safe and well-tolerated. *Clin Pharmacol Ther* 104(2): 335–345. <https://doi.org/10.1002/cpt.938>
 19. Krieg AM (2006) Therapeutic potential of toll-like receptor 9 activation. *Nat Rev Drug Discov* 5(6):471–484. <https://doi.org/10.1038/nrd2059>
 20. Holtick U, Scheulen ME, von Bergwelt-Baildon MS, Weihrauch MR (2011) Toll-like receptor 9 agonists as cancer therapeutics. *Expert Opin Investig Drugs* 20(3):361–372. <https://doi.org/10.1517/13543784.2011.553187>
 21. Vollmer J, Krieg AM (2009) Immunotherapeutic applications of CpG oligodeoxynucleotide TLR9 agonists. *Adv Drug Deliv Rev* 61(3):195–204. <https://doi.org/10.1016/j.addr.2008.12.008>
 22. Andersson P, Den Besten C (2019) Preclinical and clinical drug-metabolism, pharmacokinetics and safety of therapeutic oligonucleotides. In: Agrawal S, Gait MJ (eds) *Advances in nucleic acid therapeutics*. Drug discovery series, 1st edn. Royal Society of Chemistry, London, pp 474–531
 23. Crooke ST, Wang S, Vickers TA, Shen W, Liang XH (2017) Cellular uptake and trafficking of antisense oligonucleotides. *Nat Biotechnol* 35(3):230–237. <https://doi.org/10.1038/nbt.3779>
 24. Koller E, Vincent TM, Chappell A, De S, Manoharan M, Bennett CF (2011) Mechanisms of single-stranded phosphorothioate modified antisense oligonucleotide accumulation in hepatocytes. *Nucleic Acids Res* 39(11):4795–4807. <https://doi.org/10.1093/nar/gkr089>
 25. Hung G, Xiao X, Peralta R, Bhattacharjee G, Murray S, Norris D, Guo S, Monia BP (2013) Characterization of target mRNA reduction through in situ RNA hybridization in multiple organ systems following systemic antisense treatment in animals. *Nucl Acid Ther* 23(6): 369–378. <https://doi.org/10.1089/nat.2013.0443>
 26. Kulkarni JA, Cullis PR, van der Meel R (2018) Lipid nanoparticles enabling gene therapies: from concepts to clinical utility. *Nucl Acid Ther* 28(3):146–157. <https://doi.org/10.1089/nat.2018.0721>
 27. Khorkova O, Wahlestedt C (2017) Oligonucleotide therapies for disorders of the nervous system. *Nat Biotechnol* 35(3):249–263. <https://doi.org/10.1038/nbt.3784>
 28. Querbes W, Ge P, Zhang W, Fan Y, Costigan J, Charisse K, Maier M, Nechev L, Manoharan M, Kotlianski V, Sah DW (2009) Direct CNS delivery of siRNA mediates robust silencing in oligodendrocytes. *Oligonucleotides* 19(1):23–29. <https://doi.org/10.1089/oli.2008.0165>
 29. Rigo F, Chun SJ, Norris DA, Hung G, Lee S, Matson J, Fey RA, Gaus H, Hua Y, Grundy JS, Krainer AR, Henry SP, Bennett CF (2014) Pharmacology of a central nervous system delivered 2'-O-methoxyethyl-modified survival of motor neuron splicing oligonucleotide in mice and nonhuman primates. *J Pharmacol Exp Ther* 350(1):46–55. <https://doi.org/10.1124/jpet.113.212407>
 30. Henry SP, Miner RC, Drew WL, Fitchett J, York-Defalco C, Rapp LM, Levin AA (2001) Antiviral activity and ocular kinetics of antisense oligonucleotides designed to inhibit CMV replication. *Invest Ophthalmol Vis Sci* 42(11):2646–2651
 31. Danis RP, Henry SP, Ciulla TA (2001) Potential therapeutic application of antisense oligonucleotides in the treatment of ocular diseases. *Expert Opin Pharmacother* 2(2): 277–291. <https://doi.org/10.1517/14656566.2.2.277>
 32. Leeds JM, Henry SP, Bistner S, Scherrill S, Williams K, Levin AA (1998) Pharmacokinetics of an antisense oligonucleotide injected intravitreally in monkeys. *Drug Metab Dispos* 26(7):670–675
 33. Solano EC, Kornbrust DJ, Beaudry A, Foy JW, Schneider DJ, Thompson JD (2014) Toxicological and pharmacokinetic properties of QPI-1007, a chemically modified synthetic siRNA targeting caspase 2 mRNA, following intravitreal injection. *Nucl Acid Ther* 24(4): 258–266. <https://doi.org/10.1089/nat.2014.0489>
 34. Dowdy SF (2017) Overcoming cellular barriers for RNA therapeutics. *Nat Biotechnol* 35(3):222–229. <https://doi.org/10.1038/nbt.3802>
 35. Juliano R, Alam MR, Dixit V, Kang H (2008) Mechanisms and strategies for effective delivery of antisense and siRNA oligonucleotides. *Nucleic Acids Res* 36(12):4158–4171. <https://doi.org/10.1093/nar/gkn342>

36. Juliano RL (2016) The delivery of therapeutic oligonucleotides. *Nucleic Acids Res* 44(14): 6518–6548. <https://doi.org/10.1093/nar/gkw236>
37. Juliano RL, Alahari S, Yoo H, Kole R, Cho M (1999) Antisense pharmacodynamics: critical issues in the transport and delivery of antisense oligonucleotides. *Pharm Res* 16(4): 494–502
38. Godfrey C, Desviat LR, Smedsrod B, Pietri-Rouxel F, Denti MA, Disterer P, Lorain S, Nogales-Gadea G, Sardone V, Anwar R, El Andaloussi S, Lehto T, Khoo B, Brolin C, van Roon-Mom WM, Goyenvallé A, Aartsma-Rus A, Arechavala-Gomez V (2017) Delivery is key: lessons learnt from developing splice-switching antisense therapies. *EMBO Mol Med* 9(5):545–557. <https://doi.org/10.15252/emmm.201607199>
39. Hammond SM, Aartsma-Rus A, Alves S, Borghos SE, Buijsen RAM, Collin RWJ, Covello G, Denti MA, Desviat LR, Echevarría L, Foged C, Gaina G, Garanto A, Goyenvallé AT, Guzowska M, Holodnuka I, Jones DR, Krause S, Lehto T, Montolio M, Van Roon-Mom W, Arechavala-Gomez V (2021) Delivery of oligonucleotide-based therapeutics: challenges and opportunities. *EMBO Mol Med* 13(4):e13243. <https://doi.org/10.15252/emmm.202013243>
40. Ledford H (2018) Gene-silencing technology gets first drug approval after 20-year wait. *Nature* 560(7718):291–292. <https://doi.org/10.1038/d41586-018-05867-7>
41. Coelho T, Adams D, Silva A, Lozeron P, Hawkins PN, Mant T, Perez J, Chiesa J, Warrington S, Tranter E, Munisamy M, Falzone R, Harrop J, Cehelsky J, Bettencourt BR, Geissler M, Butler JS, Sehgal A, Meyers RE, Chen Q, Borland T, Hutabarat RM, Clausen VA, Alvarez R, Fitzgerald K, Gamba-Vitalo C, Nochur SV, Vaishnav AK, Sah DW, Gollob JA, Suhr OB (2013) Safety and efficacy of RNAi therapy for transthyretin amyloidosis. *N Engl J Med* 369(9):819–829. <https://doi.org/10.1056/NEJMoa1208760>
42. Nair JK, Willoughby JL, Chan A, Charisse K, Alam MR, Wang Q, Hoekstra M, Kandasamy P, Kel'in AV, Milstein S, Taneja N, O'Shea J, Shaikh S, Zhang L, van der Sluis RJ, Jung ME, Akinc A, Hutabarat R, Kuchimanchi S, Fitzgerald K, Zimmermann T, van Berkel TJ, Maier MA, Rajeev KG, Manoharan M (2014) Multivalent N-acetylgalactosamine-conjugated siRNA localizes in hepatocytes and elicits robust RNAi-mediated gene silencing. *J Am Chem Soc* 136(49):16958–16961. <https://doi.org/10.1021/ja505986a>
43. Prakash TP, Graham MJ, Yu J, Carty R, Low A, Chappell A, Schmidt K, Zhao C, Aghajan M, Murray HF, Riney S, Booten SL, Murray SF, Gaus H, Crosby J, Lima WF, Guo S, Monia BP, Swayze EE, Seth PP (2014) Targeted delivery of antisense oligonucleotides to hepatocytes using triantennary N-acetyl galactosamine improves potency 10-fold in mice. *Nucleic Acids Res* 42(13): 8796–8807. <https://doi.org/10.1093/nar/gku531>
44. Crooke ST, Baker BF, Xia S, Yu RZ, Viney NJ, Wang Y, Tsimikas S, Geary RS (2019) Integrated assessment of the clinical performance of GalNAc3-conjugated 2'-O-Methoxyethyl chimeric antisense oligonucleotides: I. Human volunteer experience. *Nucl Acid Ther* 29(1):16–32. <https://doi.org/10.1089/nat.2018.0753>
45. Kornbrust D, Cavagnaro J, Levin A, Foy J, Pavco P, Gamba-Vitalo C, Guimond A (2013) Oligo safety working group exaggerated pharmacology subcommittee consensus document. *Nucl Acid Ther* 23(1):21–28. <https://doi.org/10.1089/nat.2012.0399>
46. Hagedorn PH, Hansen BR, Koch T, Lindow M (2017) Managing the sequence-specificity of antisense oligonucleotides in drug discovery. *Nucleic Acids Res* 45(5):2262–2282. <https://doi.org/10.1093/nar/gkx056>
47. Jackson AL, Linsley PS (2010) Recognizing and avoiding siRNA off-target effects for target identification and therapeutic application. *Nat Rev Drug Discov* 9(1):57–67. <https://doi.org/10.1038/nrd3010>
48. Janas MM, Schlegel MK, Harbison CE, Yilmaz VO, Jiang Y, Parmar R, Zlatev I, Castoreno A, Xu H, Shulga-Morskaya S, Rajeev KG, Manoharan M, Keirstead ND, Maier MA, Jadhav V (2018) Selection of GalNAc-conjugated siRNAs with limited off-target-driven rat hepatotoxicity. *Nat Commun* 9(1):723. <https://doi.org/10.1038/s41467-018-02989-4>
49. Kamola PJ, Kitson JD, Turner G, Maratou K, Eriksson S, Panjwani A, Warnock LC, Douillard Guilloux GA, Moores K, Koppe EL, Wixted WE, Wilson PA, Gooderham NJ, Gant TW, Clark KL, Hughes SA, Edbrooke MR, Parry JD (2015) In silico and in vitro evaluation of exonic and intronic off-target effects form a critical element of therapeutic ASO gapmer optimization. *Nucleic Acids Res* 43(18):8638–8650. <https://doi.org/10.1093/nar/gkv857>

50. Watt AT, Swayze G, Swayze EE, Freier SM (2020) Likelihood of nonspecific activity of Gapmer antisense oligonucleotides is associated with relative hybridization free energy. *Nucl Acid Ther* 30(4):215–228. <https://doi.org/10.1089/nat.2020.0847>
51. Lindow M, Vornlocher HP, Riley D, Kornbrust DJ, Burchard J, Whiteley LO, Kamens J, Thompson JD, Nochur S, Younis H, Bartz S, Parry J, Ferrari N, Henry SP, Levin AA (2012) Assessing unintended hybridization-induced biological effects of oligonucleotides. *Nat Biotechnol* 30(10):920–923. <https://doi.org/10.1038/nbt.2376>
52. Ray KK, Landmesser U, Leiter LA, Kallend D, Dufour R, Karakas M, Hall T, Troquay RP, Turner T, Visseren FL, Wijngaard P, Wright RS, Kastelein JJ (2017) Inclisiran in patients at high cardiovascular risk with elevated LDL cholesterol. *N Engl J Med* 376(15):1430–1440. <https://doi.org/10.1056/NEJMoal615758>
53. Engelhardt JA, Fant P, Guionaud S, Henry SP, Leach MW, Loudon C, Scicchitano MS, Weaver JL, Zabka TS, Frazier KS, Society of Toxicologic Pathology Vascular Injury Working G (2015) Scientific and regulatory policy committee points-to-consider paper*: drug-induced vascular injury associated with non-small molecule therapeutics in preclinical development: part 2. Antisense oligonucleotides. *Toxicol Pathol* 43(7):935–944. <https://doi.org/10.1177/0192623315570341>
54. Henry SP, Jagels MA, Hugli TE, Manalili S, Geary RS, Giclas PC, Levin AA (2014) Mechanism of alternative complement pathway dysregulation by a phosphorothioate oligonucleotide in monkey and human serum. *Nucl Acid Ther* 24(5):326–335. <https://doi.org/10.1089/nat.2014.0491>
55. Shen L, Frazer-Abel A, Reynolds PR, Giclas PC, Chappell A, Pangburn MK, Younis H, Henry SP (2014) Mechanistic understanding for the greater sensitivity of monkeys to antisense oligonucleotide-mediated complement activation compared with humans. *J Pharmacol Exp Ther* 351(3):709–717. <https://doi.org/10.1124/jpet.114.219378>
56. Bosgra S, Sipkens J, de Kimpe S, den Besten C, Datson N, van Deutekom J (2019) The pharmacokinetics of 2'-O-methyl Phosphorothioate antisense oligonucleotides: experiences from developing exon skipping therapies for Duchenne muscular dystrophy. *Nucl Acid Ther* 29(6):305–322. <https://doi.org/10.1089/nat.2019.0805>
57. Geary RS, Norris D, Yu R, Bennett CF (2015) Pharmacokinetics, biodistribution and cell uptake of antisense oligonucleotides. *Adv Drug Deliv Rev* 87:46–51. <https://doi.org/10.1016/j.addr.2015.01.008>
58. Levin AA, Yu RZ, Geary RS (2008) Basic principles of the pharmacokinetics of antisense oligonucleotide drugs. In: Crooke ST (ed) *Antisense drug technology—principles, strategies, and applications*, 2nd edn. CRC Press, Taylor and Francis Group, Boca Raton, FL, pp 183–215
59. Yu RZ, Kim TW, Hong A, Watanabe TA, Gaus HJ, Geary RS (2007) Cross-species pharmacokinetic comparison from mouse to man of a second-generation antisense oligonucleotide, ISIS 301012, targeting human apolipoprotein B-100. *Drug Metab Dispos* 35(3):460–468. <https://doi.org/10.1124/dmd.106.012401>
60. Yu RZ, Lemonidis KM, Graham MJ, Matson JE, Crooke RM, Tribble DL, Wedel MK, Levin AA, Geary RS (2009) Cross-species comparison of in vivo PK/PD relationships for second-generation antisense oligonucleotides targeting apolipoprotein B-100. *Biochem Pharmacol* 77(5):910–919. <https://doi.org/10.1016/j.bcp.2008.11.005>
61. Crooke ST, Baker BF, Kwok TJ, Cheng W, Schulz DJ, Xia S, Salgado N, Bui HH, Hart CE, Burel SA, Younis HS, Geary RS, Henry SP, Bhanot S (2016) Integrated safety assessment of 2'-O-Methoxyethyl chimeric antisense oligonucleotides in NonHuman primates and healthy human volunteers. *Mol Ther* 24(10):1771–1782. <https://doi.org/10.1038/mt.2016.136>
62. Shen L, Engelhardt JA, Hung G, Yee J, Kikkawa R, Matson J, Tayefeh B, Machemer T, Giclas PC, Henry SP (2016) Effects of repeated complement activation associated with chronic treatment of Cynomolgus monkeys with 2'-O-Methoxyethyl modified antisense oligonucleotide. *Nucl Acid Ther* 26(4):236–249. <https://doi.org/10.1089/nat.2015.0584>
63. Hagedorn PH, Persson R, Funder ED, Alback N, Diemer SL, Hansen DJ, Moller MR, Papargyri N, Christiansen H, Hansen BR, Hansen HF, Jensen MA, Koch T (2018) Locked nucleic acid: modality, diversity, and drug discovery. *Drug Discov Today* 23(1):101–114. <https://doi.org/10.1016/j.drudis.2017.09.018>
64. Burdick AD, Sciabola S, Mantena SR, Hollingshead BD, Stanton R, Warneke JA, Zeng M, Martsen E, Medvedev A, Makarov SS, Reed LA, Davis JW 2nd, Whiteley LO

- (2014) Sequence motifs associated with hepatotoxicity of locked nucleic acid—modified antisense oligonucleotides. *Nucleic Acids Res* 42(8):4882–4891. <https://doi.org/10.1093/nar/gku142>
65. Hagedorn PH, Yakimov V, Ottosen S, Kammiller S, Nielsen NF, Hog AM, Hedtjarn M, Meldgaard M, Moller MR, Orum H, Koch T, Lindow M (2013) Hepatotoxic potential of therapeutic oligonucleotides can be predicted from their sequence and modification pattern. *Nucl Acid Ther* 23(5):302–310. <https://doi.org/10.1089/nat.2013.0436>
66. Burel SA, Hart CE, Cauntay P, Hsiao J, Machemer T, Katz M, Watt A, Bui HH, Younis H, Sabripour M, Freier SM, Hung G, Dan A, Prakash TP, Seth PP, Swayze EE, Bennett CF, Crooke ST, Henry SP (2016) Hepatotoxicity of high affinity gapmer antisense oligonucleotides is mediated by RNase H1 dependent promiscuous reduction of very long pre-mRNA transcripts. *Nucleic Acids Res* 44(5):2093–2109. <https://doi.org/10.1093/nar/gkv1210>
67. Dieckmann A, Hagedorn PH, Burki Y, Brugmann C, Berrera M, Ebeling M, Singer T, Schuler F (2018) A sensitive in vitro approach to assess the hybridization-dependent toxic potential of high affinity Gapmer oligonucleotides. *Mol Ther Nucl Acids* 10:45–54. <https://doi.org/10.1016/j.omtn.2017.11.004>
68. Liang XH, Sun H, Shen W, Crooke ST (2015) Identification and characterization of intracellular proteins that bind oligonucleotides with phosphorothioate linkages. *Nucleic Acids Res* 43(5):2927–2945. <https://doi.org/10.1093/nar/gkv143>
69. Shen W, De Hoyos CL, Migawa MT, Vickers TA, Sun H, Low A, Bell TA 3rd, Rahdar M, Mukhopadhyay S, Hart CE, Bell M, Riney S, Murray SF, Greenlee S, Crooke RM, Liang XH, Seth PP, Crooke ST (2019) Chemical modification of PS-ASO therapeutics reduces cellular protein-binding and improves the therapeutic index. *Nat Biotechnol* 37(6):640–650. <https://doi.org/10.1038/s41587-019-0106-2>
70. Shen W, De Hoyos CL, Sun H, Vickers TA, Liang XH, Crooke ST (2018) Acute hepatotoxicity of 2' fluoro-modified 5-10-5 gapmer phosphorothioate oligonucleotides in mice correlates with intracellular protein binding and the loss of DBHS proteins. *Nucleic Acids Res* 46(5):2204–2217. <https://doi.org/10.1093/nar/gky060>
71. Shen W, Liang XH, Sun H, Crooke ST (2015) 2'-Fluoro-modified phosphorothioate oligonucleotide can cause rapid degradation of P54nrb and PSF. *Nucleic Acids Res* 43(9):4569–4578. <https://doi.org/10.1093/nar/gkv298>
72. Moisan A, Gubler M, Zhang JD, Tessier Y, Dumong Erichsen K, Sewing S, Gerard R, Avignon B, Huber S, Benmansour F, Chen X, Villasenor R, Braendli-Baiocco A, Festag M, Maunz A, Singer T, Schuler F, Roth AB (2017) Inhibition of EGF uptake by nephrotoxic antisense drugs in vitro and implications for preclinical safety profiling. *Mol Ther Nucl Acids* 6:89–105. <https://doi.org/10.1016/j.omtn.2016.11.006>
73. Sewing S, Boess F, Moisan A, Bertinetti-Lapatki C, Minz T, Hedtjaern M, Tessier Y, Schuler F, Singer T, Roth AB (2016) Establishment of a predictive in vitro assay for assessment of the hepatotoxic potential of oligonucleotide drugs. *PLoS One* 11(7):e0159431. <https://doi.org/10.1371/journal.pone.0159431>
74. Vasquez G, Freestone GC, Wan WB, Low A, De Hoyos CL, Yu J, Prakash TP, Ostergaard ME, Liang XH, Crooke ST, Swayze EE, Migawa MT, Seth PP (2021) Site-specific incorporation of 5'-methyl DNA enhances the therapeutic profile of gapmer ASOs. *Nucleic Acids Res* 49(4):1828–1839. <https://doi.org/10.1093/nar/gkab047>
75. Hamm S, Latz E, Hangel D, Muller T, Yu P, Golenbock D, Sparwasser T, Wagner H, Bauer S (2010) Alternating 2'-O-ribose methylation is a universal approach for generating non-stimulatory siRNA by acting as TLR7 antagonist. *Immunobiology* 215(7):559–569. <https://doi.org/10.1016/j.imbio.2009.09.003>
76. Henry S, Stecker K, Brooks D, Monteith D, Conklin B, Bennett CF (2000) Chemically modified oligonucleotides exhibit decreased immune stimulation in mice. *J Pharmacol Exp Ther* 292(2):468–479
77. Hornung V, Ellegast J, Kim S, Brzozka K, Jung A, Kato H, Poeck H, Akira S, Conzelmann KK, Schlee M, Endres S, Hartmann G (2006) 5'-triphosphate RNA is the ligand for RIG-I. *Science* 314(5801):994–997. <https://doi.org/10.1126/science.1132505>
78. Judge AD, Sood V, Shaw JR, Fang D, McClintock K, MacLachlan I (2005) Sequence-dependent stimulation of the mammalian innate immune response by synthetic siRNA. *Nat Biotechnol* 23(4):457–462. <https://doi.org/10.1038/nbt1081>

79. Krieg AM (2002) CpG motifs in bacterial DNA and their immune effects. *Annu Rev Immunol* 20:709–760. <https://doi.org/10.1146/annurev.immunol.20.100301.064842>
80. Liang H, Nishioka Y, Reich CF, Pisetsky DS, Lipsky PE (1996) Activation of human B cells by phosphorothioate oligodeoxynucleotides. *J Clin Invest* 98(5):1119–1129. <https://doi.org/10.1172/JCI118894>
81. Robbins M, Judge A, Liang L, McClintock K, Yaworski E, MacLachlan I (2007) 2'-O-methyl-modified RNAs act as TLR7 antagonists. *Mol Ther* 15(9):1663–1669. <https://doi.org/10.1038/sj.mt.6300240>
82. Sewing S, Roth AB, Winter M, Dieckmann A, Bertineti-Lapatki C, Tessier Y, McGinnis C, Huber S, Koller E, Ploix C, Reed JC, Singer T, Rothfuss A (2017) Assessing single-stranded oligonucleotide drug-induced effects in vitro reveals key risk factors for thrombocytopenia. *PLoS One* 12(11):e0187574. <https://doi.org/10.1371/journal.pone.0187574>
83. Sioud M (2006) Single-stranded small interfering RNA are more immunostimulatory than their double-stranded counterparts: a central role for 2'-hydroxyl uridines in immune responses. *Eur J Immunol* 36(5):1222–1230. <https://doi.org/10.1002/eji.200535708>
84. Tluk S, Jurk M, Forsbach A, Weeratna R, Samulowitz U, Krieg AM, Bauer S, Vollmer J (2009) Sequences derived from self-RNA containing certain natural modifications act as suppressors of RNA-mediated inflammatory immune responses. *Int Immunol* 21(5):607–619. <https://doi.org/10.1093/intimm/dxp030>
85. Zhao Q, Temsamani J, Iadarola PL, Jiang Z, Agrawal S (1996) Effect of different chemically modified oligodeoxynucleotides on immune stimulation. *Biochem Pharmacol* 51(2):173–182
86. Chi X, Gatti P, Papoian T (2017) Safety of antisense oligonucleotide and siRNA-based therapeutics. *Drug Discov Today* 22(5):823–833. <https://doi.org/10.1016/j.drudis.2017.01.013>
87. Goemans NM, Tulinius M, van den Hauwe M, Kroksmark AK, Buyse G, Wilson RJ, van Deutekom JC, de Kimpe SJ, Loubakos A, Campion G (2016) Long-term efficacy, safety, and pharmacokinetics of Drisapersen in Duchenne muscular dystrophy: results from an open-label extension study. *PLoS One* 11(9):e0161955. <https://doi.org/10.1371/journal.pone.0161955>
88. Kwok TJ (2008) An overview of the clinical safety experience of first-and second-generation antisense oligonucleotides. In: Crooke ST (ed) *Antisense drug technology: principles, strategies and applications*, 2nd edn. CRC Press, Carlsbad, CA, pp 365–399
89. Mustonen EK, Palomaki T, Pasanen M (2017) Oligonucleotide-based pharmaceuticals: non-clinical and clinical safety signals and non-clinical testing strategies. *Regul Toxicol Pharmacol* 90:328–341. <https://doi.org/10.1016/j.yrtph.2017.09.028>
90. van Meer L, Moerland M, Gallagher J, van Doorn MB, Prens EP, Cohen AF, Rissmann R, Burggraaf J (2016) Injection site reactions after subcutaneous oligonucleotide therapy. *Br J Clin Pharmacol* 82(2):340–351. <https://doi.org/10.1111/bcp.12961>
91. Frazier KS (2015) Antisense oligonucleotide therapies: the promise and the challenges from a toxicologic pathologist's perspective. *Toxicol Pathol* 43(1):78–89. <https://doi.org/10.1177/0192623314551840>
92. Henry SP, Kim T-W, Kramer-Stickland K, Zanardi TA, Fey RA, Levin AA (2008) Toxicologic properties of 2'-methoxyethyl chimeric antisense inhibitors in animals and man. In: Crooke ST (ed) *Antisense drug technology: principles, strategies and applications*, 2nd edn. CRC Press, Taylor and Francis Group, Boca Raton, FL, pp 327–363
93. Paz S, Hsiao J, Cauntay P, Soriano A, Bai L, Machemer T, Xiao X, Guo S, Hung G, Younis H, Bennett CF, Henry S, Yun TJ, Burel S (2017) The distinct and cooperative roles of toll-like receptor 9 and receptor for advanced glycation end products in modulating in vivo inflammatory responses to select CpG and non-CpG oligonucleotides. *Nucl Acid Ther* 27(5):272–284. <https://doi.org/10.1089/nat.2017.0668>
94. Jeske S, Pries R, Wollenberg B (2013) CpG-induced IFN- α production of plasmacytoid dendritic cells: time and dosage dependence and the effect of structural modifications to the CpG backbone. *Nucl Acid Ther* 23(2):118–124. <https://doi.org/10.1089/nat.2012.0384>
95. Iversen PL (2008) Morpholinos. In: Crooke ST (ed) *Antisense drug technology: principles, strategies and applications*, 2nd edn. CRC Press, Carlsbad, CA, pp 565–582
96. Marlowe JL, Akopian V, Karmali P, Kornbrust D, Lockridge J, Semple S (2017) Recommendations of the oligonucleotide safety working Group's formulated oligonucleotide subcommittee for the Safety

- Assessment of formulated oligonucleotide-based therapeutics. *Nucl Acid Ther* 27(4): 183–196. <https://doi.org/10.1089/nat.2017.0671>
97. Suhr OB, Coelho T, Buades J, Pouget J, Conceicao I, Berk J, Schmidt H, Waddington-Cruz M, Campistol JM, Bettencourt BR, Vaishnav A, Gollob J, Adams D (2015) Efficacy and safety of patisiran for familial amyloidotic polyneuropathy: a phase II multi-dose study. *Orphanet J Rare Dis* 10: 109. <https://doi.org/10.1186/s13023-015-0326-6>
98. Tabernero J, Shapiro GI, LoRusso PM, Cervantes A, Schwartz GK, Weiss GJ, Paz-Ares L, Cho DC, Infante JR, Alsina M, Gounder MM, Falzone R, Harrop J, White AC, Toudjarska I, Bumcrot D, Meyers RE, Hinkle G, Svrzikapa N, Hutabarat RM, Clausen VA, Cehelsky J, Nochur SV, Gamba-Vitalo C, Vaishnav AK, Sah DW, Gollob JA, Burris HA 3rd (2013) First-in-humans trial of an RNA interference therapeutic targeting VEGF and KSP in cancer patients with liver involvement. *Cancer Discov* 3(4):406–417. <https://doi.org/10.1158/2159-8290.CD-12-0429>
99. Henry SP, Narayanan P, Shen L, Bhanot S, Younis HS, Burel SA (2017) Assessment of the effects of 2'-Methoxyethyl antisense oligonucleotides on platelet count in Cynomolgus nonhuman primates. *Nucl Acid Ther* 27(4):197–208. <https://doi.org/10.1089/nat.2017.0666>
100. Crooke ST, Baker BF, Witztum JL, Kwoh TJ, Pham NC, Salgado N, McEvoy BW, Cheng W, Hughes SG, Bhanot S, Geary RS (2017) The effects of 2'-O-Methoxyethyl containing antisense oligonucleotides on platelets in human clinical trials. *Nucl Acid Ther* 27(3):121–129. <https://doi.org/10.1089/nat.2016.0650>
101. EMA (2018) Kynamro assessment report. http://www.ema.europa.eu/docs/en_GB/document_library/EPAR_-_Public_assessment_report/human/002429/WC500144511.pdf
102. Andersson P, den Besten C (2019) Chapter 20. Preclinical and clinical drug-metabolism, pharmacokinetics and safety of therapeutic oligonucleotides. In: *Advances in nucleic acid therapeutics*. The Royal Society of Chemistry, London, pp 474–531. <https://doi.org/10.1039/9781788015714-00474>
103. Tessier Y, Achanzar W, Mihalcik L, Amuzie C, Andersson P, Parry JD, Moggs J, Whiteley LO (2021) Outcomes of the European Federation of Pharmaceutical Industries and Associations Oligonucleotide Working Group Survey on nonclinical practices and regulatory expectations for therapeutic oligonucleotide safety assessment. *Nucl Acid Ther* 31(1):7–20. <https://doi.org/10.1089/nat.2020.0892>
104. Alton EW, Boushey HA, Garn H, Green FH, Hodges M, Martin RJ, Murdoch RD, Renz H, Shrewsbury SB, Seguin R, Johnson G, Parry JD, Tepper J, Renzi P, Cavagnaro J, Ferrari N (2012) Clinical expert panel on monitoring potential lung toxicity of inhaled oligonucleotides: consensus points and recommendations. *Nucl Acid Ther* 22(4):246–254. <https://doi.org/10.1089/nat.2012.0345>
105. Berman CL, Barros SA, Galloway SM, Kasper P, Oleson FB, Priestley CC, Sweder KS, Schlosser MJ, Sobol Z (2016) OSWG recommendations for genotoxicity testing of novel oligonucleotide-based therapeutics. *Nucl Acid Ther* 26(2):73–85. <https://doi.org/10.1089/nat.2015.0534>
106. Berman CL, Cannon K, Cui Y, Kornbrust DJ, Lagrutta A, Sun SZ, Tepper J, Waldron G, Younis HS (2014) Recommendations for safety pharmacology evaluations of oligonucleotide-based therapeutics. *Nucl Acid Ther* 24(4):291–301. <https://doi.org/10.1089/nat.2013.0477>
107. Capaldi D, Teasdale A, Henry S, Akhtar N, den Besten C, Gao-Sheridan S, Kretschmer M, Sharpe N, Andrews B, Burm B, Foy J (2017) Impurities in oligonucleotide drug substances and drug products. *Nucl Acid Ther* 27(6):309–322. <https://doi.org/10.1089/nat.2017.0691>
108. Cavagnaro J, Berman C, Kornbrust D, White T, Campion S, Henry S (2014) Considerations for assessment of reproductive and developmental toxicity of oligonucleotide-based therapeutics. *Nucl Acid Ther* 24(5): 313–325. <https://doi.org/10.1089/nat.2014.0490>
109. Henry SP, Seguin R, Cavagnaro J, Berman C, Tepper J, Kornbrust D (2016) Considerations for the characterization and interpretation of results related to alternative complement activation in monkeys associated with oligonucleotide-based therapeutics. *Nucl Acid Ther* 26(4):210–215. <https://doi.org/10.1089/nat.2015.0593>
110. Schubert D, Levin AA, Kornbrust D, Berman CL, Cavagnaro J, Henry S, Seguin R, Ferrari N, Shrewsbury SB (2012) The oligonucleotide safety working group (OSWG). *Nucl Acid Ther* 22(4):211–212. <https://doi.org/10.1089/nat.2012.0383>

111. Hard GC, Johnson KJ, Cohen SM (2009) A comparison of rat chronic progressive nephropathy with human renal disease-implications for human risk assessment. *Crit Rev Toxicol* 39(4):332–346. <https://doi.org/10.1080/10408440802368642>
112. Braendli-Baiocco A, Festag M, Dumong Erichsen K, Persson R, Mihatsch MJ, Fisker N, Funk J, Mohr S, Constien R, Ploix C, Brady K, Berrera M, Altmann B, Lenz B, Albassam M, Schmitt G, Weiser T, Schuler F, Singer T, Tessier Y (2017) From the cover: the Minipig is a suitable non-rodent model in the safety assessment of single stranded oligonucleotides. *Toxicol Sci* 157(1):112–128. <https://doi.org/10.1093/toxsci/kfx025>
113. Kim J, Hu C, Moufawad El Achkar C, Black LE, Douville J, Larson A, Pendergast MK, Goldkind SF, Lee EA, Kuniholm A, Soucy A, Vaze J, Belur NR, Fredriksen K, Stojkowska I, Tsytsykova A, Armant M, Di Donato RL, Choi J, Cornelissen L, Pereira LM, Augustine EF, Genetti CA, Dies K, Barton B, Williams L, Goodlett BD, Riley BL, Pasternak A, Berry ER, Pflock KA, Chu S, Reed C, Tyndall K, Agrawal PB, Beggs AH, Grant PE, Urion DK, Snyder RO, Waisbren SE, Poduri A, Park PJ, Patterson A, Biffi A, Mazzulli JR, Bodamer O, Berde CB, Yu TW (2019) Patient-customized oligonucleotide therapy for a rare genetic disease. *N Engl J Med* 381(17):1644–1652. <https://doi.org/10.1056/NEJMoal813279>

Open Access This chapter is licensed under the terms of the Creative Commons Attribution 4.0 International License (<http://creativecommons.org/licenses/by/4.0/>), which permits use, sharing, adaptation, distribution and reproduction in any medium or format, as long as you give appropriate credit to the original author(s) and the source, provide a link to the Creative Commons license and indicate if changes were made.

The images or other third party material in this chapter are included in the chapter's Creative Commons license, unless indicated otherwise in a credit line to the material. If material is not included in the chapter's Creative Commons license and your intended use is not permitted by statutory regulation or exceeds the permitted use, you will need to obtain permission directly from the copyright holder.





Preclinical Evaluation of the Renal Toxicity of Oligonucleotide Therapeutics in Mice

Lucía Echevarría and Aurelie Goyenvalle

Abstract

Antisense oligonucleotides (ASO) therapeutics hold great promise for the treatment of numerous diseases, and several ASO drugs have now reached market approval, confirming the potential of this approach. However, some candidates have also failed, due to limited biodistribution/uptake and poor safety profile. In pursuit of better delivery and higher cellular uptake, ASO are being optimized, and new chemistries are developed or conjugated with various ligands. While these developments may lead to candidates with higher potency, it is important to keep the safety aspects in sight and screen for potential toxicity in early phases of preclinical development to avoid subsequent failure in clinical development. Our understanding of ASO-mediated toxicity keeps improving with increased preclinical and clinical data available. In this chapter, we will focus on the assessment of renal toxicity in mice and describe methods to measure the levels of general urinary biomarkers as well as acute kidney injury biomarkers following ASO treatment.

Key words Antisense oligonucleotides (ASO), Safety, Toxicology, Kidney toxicity, Acute kidney injury biomarker, Preclinical evaluation, Mouse model

1 Introduction

The field of synthetic antisense oligonucleotide (ASO) has advanced remarkably in the last decade, and ASOs represent a very promising therapeutic platform that keeps evolving rapidly, in particular in pursuit of delivery improvement. Many preclinical studies in the antisense area focus on improving ASO delivery and assessing their efficacy in target tissues, often neglecting the evaluation of toxicity, at least in early phases of development. However, safety assessment is particularly important when developing new generations of ASOs or novel delivery systems to avoid the potential failure of a new drug in further toxicological studies, as it happened with a peptide conjugated PMO (PPMO) targeting the human dystrophin exon 50 which was found to cause mild tubular degeneration in the kidneys of cynomolgus monkeys [1].

Toxicological properties of ASO have been comprehensively and extensively summarized previously [2, 3], and our understanding of them has allowed the development of predictive tests to select the best preclinical candidates.

Following systemic administration, the highest concentrations of ASO, independently of their chemistry, are found in liver and kidney, which are therefore considered as high-exposure organs. Importantly, tissue concentration does not further increase upon re-administration once steady-state is reached [2]. Accumulated ASOs can often be visualized at the histopathology level as basophilic granules on tissue sections stained with hematoxylin and eosin, but these effects are regarded as nonadverse because of their reversible nature upon treatment cessation. In rodents treated with high dose of PS-ASO, it is also frequent to observe tissue macrophages with a foamy appearance, referred to as histiocytes, which store cytokines in response to an activated state [3].

Considering the high concentrations of ASO accumulating in the kidneys, including the charge-neutral backbone such as PMO [4, 5], they are regarded as a common organ for toxicity. The highest uptake is generally observed in the proximal tubular epithelial cells of the convoluted tubule, whereas uptake in tubular cells in kidney medulla is much lower [6, 7]. Renal effects therefore tend to be more tubular than glomerular, apart from the reported glomerulopathies in mouse and monkey studies with the 2'OMe PS Dri-sapersen developed for the treatment of DMD [8]. However, it appears that this toxicity was linked to the chronic complement activation and inflammatory effects of the ASO and therefore over-predicted in animal studies since humans are less susceptible to these effects. Much more common are the lesions observed in the proximal tubules, which typically appear in animals treated with much higher doses of ASOs than the clinically relevant doses. Renal toxicity is mostly regarded as an accumulation-related toxicity and mostly sequence unspecific, except for more acute tubular lesions reported with high-affinity ASO such as locked nucleic acid (LNA) [9]. These effects might be related to excessive accumulation of RNase H-dependent off-target transcripts and/or specific protein binding [2] and a predictive EGF-based assay has recently been developed to exclude this type of kidney-toxic candidates [10].

Besides this EGF-based assay, several specific and early biomarkers of toxicity can be evaluated in mice (treated with high doses of ASO) to predict toxicity in preclinical development and exclude nephrotoxic candidates [8]. Evaluation of renal toxicology typically includes macroscopic examination of the kidneys upon necropsy of the animals followed by microscopic examination and careful histopathology analysis. General biomarkers of renal toxicity can be measured in the serum or plasma of treated mice such as urea, albumin, creatinine, and total protein. In this chapter, we focus on urinary biomarkers of kidney toxicity and describe the methods

to measure the levels of total protein, albumin, creatinine as well as specific kidney injury biomarkers as a way of evaluating the potential renal toxicity of antisense oligonucleotides in mice. For this assessment, urines are collected from ASO-treated mice either shortly after ASO injection to evaluate the potential acute kidney toxicity or after several weeks of repeated treatment to evaluate the potential long term renal toxicity induced by the accumulation of ASO in kidneys.

2 Materials

For all analysis described in this chapter, urine is collected using metabolic cages for rodents (e.g., metabolic cages for mice ref. 52–6731, Harvard apparatus, Holliston, MA).

2.1 Evaluation of Creatinine Levels in Urine

1. Creatinine assay kit (*see Note 1*).
2. Microplate reader capable of measuring absorbance at 490 nm.
3. Deionized or distilled water.
4. Test tubes for dilution of standards and samples.

2.2 Evaluation of Total Protein Level in Urine

1. Deionized or distilled water.
2. Acetone (pre-chilled overnight at -20°C).
3. Microplate reader capable of measuring absorbance at 562 nm.
4. Pierce BCA assay (*see Note 2*).
5. Test tubes for dilution of standards and samples.
6. Clear polystyrene microplates (96 well).

2.3 Evaluation of Albumin Level in Urine

1. Albumin ELISA kit (*see Note 3*).
2. Microplate reader capable of measuring absorbance at 450 nm.
3. Deionized or distilled water.
4. Test tubes for dilution of standards and samples.

2.4 Evaluation of Acute Kidney Injury Biomarkers (AKI) Level in Urine

1. Multiplex kidney injury panels (panel 1: MKI1MAG-94K and panel 2: MKI2MAG-94K, Merck-Millipore).
2. Luminex xMAP[®] technology compatible reader such as Luminex 200[™], HTS, FLEXMAP 3D[®] or MAGPIX[®] with xPONENT[®] software or Bio-Plex manager 6.1 software.
3. Automatic plate washer for magnetic beads (such as BioTek[®] 405 LS and 405 TS, EMD Millipore catalog #40–094, #40–095, #40–096, #40–097, or equivalent) or handheld magnetic separation block (EMD Millipore catalog #40–285 or equivalent).

4. Luminex sheath fluid (EMD Millipore catalog # SHEATH FLUID) or Luminex drive fluid (EMD Millipore catalog #MPXDF-4PK).
5. Adjustable pipettes with tips capable of delivering 25–1000 μL .
6. Multichannel pipettes capable of delivering 5–50 μL or 25–200 μL .
7. Reagent reservoirs.
8. Polypropylene microfuge tubes.
9. Rubber bands.
10. Aluminum foil.
11. Absorbent pads.
12. Laboratory vortex mixer.
13. Titer plate shaker (Lab-Line Instruments Model #4625 or equivalent).

3 Methods

3.1 Evaluation of Creatinine Levels in Urine

1. Collect urine using metabolic cages over 24 h, directly in refrigerated tubes (4 °C).
2. Record the total volume of collected urine.
3. Upon collection, centrifuge urines at $10,000 \times g$ for 10 min and aliquot supernatant.
4. Freeze aliquots at -80°C for further analysis (Fig. 1) (*see Note 4*).

Urine creatinine is measured using a creatinine assay kit (in our case R&D Systems), based on the Jaffe reaction where creatinine is treated with an alkaline solution to yield a bright orange-red complex. Intensity of the color at 490 nm corresponds to the concentration of creatinine in samples.

1. Dilute the urine samples 20-fold as follows: 10 μL of urine sample + 190 μL of deionized or distilled water.
2. Prepare the alkaline picrate solution: for one plate, add 2.5 mL of NaOH to 12.5 mL of picric acid reagent (provided in the kit). Mix well. 100 μL of alkaline picrate solution is required per well.
3. Prepare the standard curve from the stock solution provided at 100 mg/dL. Label 7 microcentrifuge tubes from 20 mg/dL to 0.31 mg/dL. For the first point at 20 mg/dL, add 200 μL of stock into 800 μL of deionized or distilled water. The 20 mg/dL standard serves as the high standard. For the six subsequent tubes, serial dilute (1:2) by pipetting 500 μL of standard into 500 μL of deionized or distilled water made of 7 points from

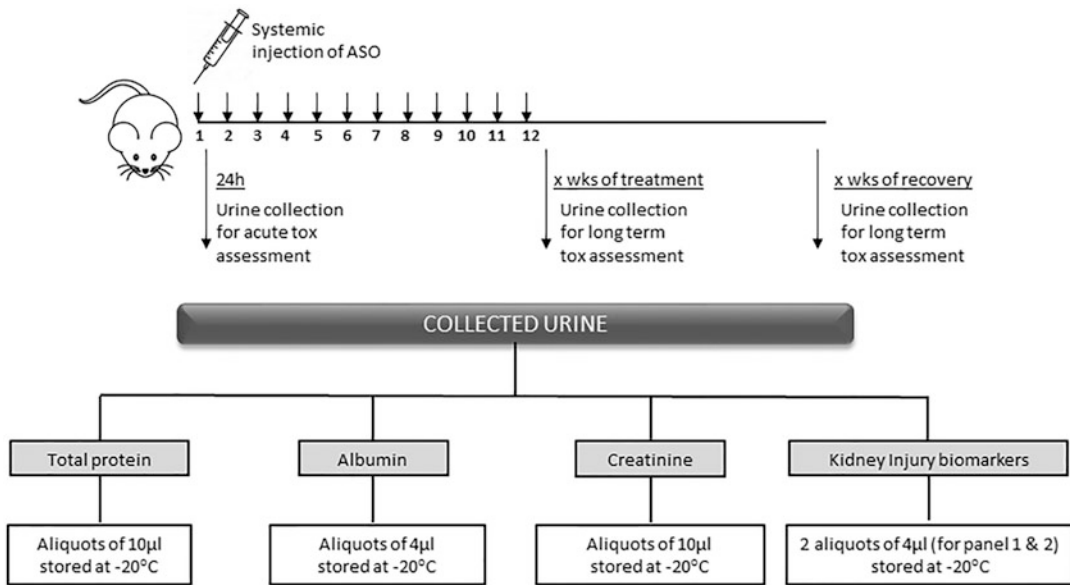


Fig. 1 Schematic representation of urine collection possibilities following ASO treatment in mice and possible urine analysis

20 mg/dL to 0.31 mg/dL. Mix each tube thoroughly before the next transfer. Use deionized or distilled water as the zero standard (0 mg/dL).

4. Once all reagents, samples and creatinine standards are ready, remove excess microplate strips from the plate frame, return them to the foil pouch, and reseal.
5. Add 50 µL of standard, control, or sample to each well.
6. Add 100 µL alkaline picrate solution to each well.
7. Incubate for 30 ± 5 min at room temperature.
8. Determine the optical density of each well using a microplate reader set to 490 nm.
9. Calculate the creatinine concentration in your samples using the optical density measurements and the standard curve.
10. Since samples have been diluted, the concentration read from the standard curve must be multiplied by the dilution factor (i.e., 20) to obtain the sample concentration.

3.2 Evaluation of Total Protein Level in Urine

1. Precipitate the protein in the urine samples by adding 40 µL dH₂O and 200 µL of prechilled acetone to 10 µL of urine.
2. Incubate samples at -20°C for 30 min, and then centrifuge 15 min at $14,000 \times g$ at 4°C .
3. Resuspend pellets in 40 µL of dH₂O.
4. Measure protein concentration using a BCA assay:

- (a) Prepare the standards from the 2 mg/mL albumin provided in the BCA assay, preferably using the same diluent as the one used for the samples. Nine standard tubes are prepared at concentrations 2000 (stock), 1500, 1000, 750, 500, 250, 125, 25, and 0 µg/mL of BSA.
- (b) Prepare the working reagent (WR). First, determine the total volume of WR required:

$$(n \text{ standards} + n \text{ unknowns}) \times (n \text{ replicates}) \times (\text{volume of WR per sample}) = \text{Total V required.}$$
 Prepare the WR by mixing 50 parts of BCA Reagent A with 1 part of BCA Reagent B (50:1; A:B).
- (c) Then add 10 µL of each standard or unknown sample replicate into a microplate well (working range = 20–2000 µg/mL). Add 200 µL of WR to each well and mix plate thoroughly on a plate shaker for 30 s. Cover the plate and incubate at 37 °C for 30 min.
- (d) Cool the plate at room temperature.
- (e) Measure the absorbance at 562 nm on a plate reader.
- (f) Calculate the total protein concentration in your samples using the optical density measurements and the standard curve.

3.3 Evaluation of Albumin Levels in Urine

Albumin levels from urine samples are measured using an albumin ELISA kit. All reagents must be at room temperature before use. We describe the method below using the albumin ELISA kit from Bethy Laboratories:

1. Prepare 1× dilution buffer C by diluting 25 mL of 20× dilution buffer C into 475 mL of ultrapure water. Mix well.
2. Prepare standards: reconstitute the 900 ng albumin standard vial (included in the kit) with 1 mL of 1× dilution buffer C (all buffers mentioned are included in the kit) to achieve a final concentration of 900 ng/mL. Mix well. Label seven tubes, one for each standard curve point: 300, 100, 33.3, 11.1, 3.7, 1.23, and 0 ng/mL. Serially dilute 1:3 by adding 150 µL of the 900 ng/mL standard into the first tube containing 300 µL of 1× dilution buffer C. Mix well. Continue the dilution by adding 150 µL of the previous standard into 300 µL of 1× dilution buffer C in the next tube until the sixth tube. Last tube is the blank.
3. Prepare the urine samples. The recommended dilution is 1/1000. First perform a 1:25 dilution by adding 4 µL of urine to 96 µL of dilution buffer C, and then perform a 1:40 dilution by adding 6 µL of the 1:25 dilution into 234 µL of dilution buffer C.

4. Prepare the 1× wash buffer by diluting the 20× wash buffer in ultrapure water. For 1 L, dilute 50 mL of 20× wash buffer into 950 mL of ultrapure water.
5. Perform the assay: add 100 µL of standard or sample to designated wells (run each standard or sample in duplicate).
6. Cover the plate and incubate at RT for 1 h.
7. Gently remove the well content and wash the plate four times with 250 µL/well of 1× washing buffer.
8. Add 100 µL of anti-albumin detection antibody to each well and carefully attach a new adhesive plate cover. Incubate at RT for 1 h.
9. Gently remove the well content and wash the plate four times with 250 µL/well of 1× washing buffer.
10. Add 100 µL of HRP Solution A to each well and carefully attach a new adhesive plate cover. Incubate at RT for 30 min.
11. Gently remove well contents and wash the plate four times with 250 µL/well of 1× washing buffer. Blot off any residual liquid at the bottom of the wells.
12. Add 100 µL of TMB solution (included in the kit) to each well.
13. Do not cover the plate with a plate sealer.
14. Incubate the plate in the dark at RT for 30 min.
15. Stop the reaction by adding 100 µL of stop solution (included in the kit) to each well.
16. Measure absorbance on a plate reader at 450 nm.
17. Calculate the albumin concentration in your samples using the optical density measurements and the standard curve.

3.4 Evaluation of Acute Kidney Injury Biomarkers (AKI) Level in Urine

Acute kidney injury (AKI) biomarkers levels are analyzed by multiplex assays (MILLIPLEX® MAP) using the Luminex® technology.

The multiplex kidney injury panels (panel 1: MKI1MAG-94K and panel 2: MKI2MAG-94K, Merck-Millipore) are used according to the manufacturer's instructions to measure levels of β -2-microglobulin (B2M), renin, kidney injury molecule 1 (KIM-1), interferon-gamma induced protein 10 (IP-10), vascular endothelial growth factor (VEGF) (panel 1) and Cystatin C, epidermal growth factor (EGF), Lipocalin-2-NGAL, clusterin and osteopontin (OPN) (panel 2).

3.4.1 Evaluation of β 2-Microglobulin, Renin, Kim-1, IP-10, and VEGF Levels in Mouse Urines

β 2-Microglobulin, Renin, Kim-1, IP-10, VEGF are measured using the panel 1 (ref MKI1MAG-94K from Merck-Millipore).

1. Allow all reagents to warm to room temperature (20–25 °C) before use in the assay (except antibodies and beads).

2. Prepare the dilution of urine samples. For panel 1: dilute sample 1:25 in the assay buffer provided in the kit by adding 4 μL of urine to 96 μL of assay buffer.
3. Prepare the antibody-immobilized beads. For individual vials of beads, vortex for 1 min. Add 150 μL from each antibody-bead vial to the mixing bottle and bring final volume to 3.0 mL with assay buffer. Vortex the mixed beads well (*see Note 5*). There are 5 biomarkers in panel 1: add 150 μL from each of the five bead vials to the Mixing Bottle. Then add 2.25 mL assay buffer.
4. Prepare the quality controls (*see Note 6*):
 - (a) Reconstitute quality control 1 and quality control 2 with 250 μL deionized water.
 - (b) Invert the vial several times to mix and vortex.
 - (c) Allow the vial to sit for 5–10 min.
5. Prepare the standards:
 - (a) Reconstitute the mouse kidney injury panel 1 standard with 250 μL deionized water.
 - (b) Invert the vial several times to mix. Vortex the vial for 10 s.
 - (c) Allow the vial to sit for 5–10 min.
 - (d) This will be used as standard 7 (*see Note 6*).
 - (e) Label 6 Eppendorf microfuge tubes standard 1 through standard 6.
 - (f) Add 150 μL of assay buffer to each of the six tubes.
 - (g) Prepare serial dilutions (1:4) by adding 50 μL of the reconstituted standard to the standard 6 tube, mix well and transfer 50 μL of standard 6 to the standard 5 tube, mix well and transfer 50 μL of standard 5 to the standard 4 tube, mix well and transfer 50 μL of standard 4 to the standard 3 tube, mix well and transfer 50 μL of standard 3 to the standard 2 tube, mix well and transfer 50 μL of standard 2 to the standard 1 tube and mix well.
 - (h) The 0 pg/mL standard (background) will be assay buffer.
6. Perform the immunoassay procedure making sure that all reagents are warmed at room temperature (20–25 °C).
 - (a) Add 200 μL of assay buffer into each well of the plate. Seal and mix on a plate shaker for 10 min at room temperature (20–25 °C).
 - (b) Decant assay buffer and remove the residual amount from all wells by inverting the plate and tapping it smartly onto absorbent towels several times.

- (c) Add 25 μ L of each standard or control into the appropriate wells. Assay buffer should be used for 0 pg/mL standard (background).
 - (d) Add 25 μ L of sample (diluted) into the appropriate wells.
 - (e) Add 25 μ L of assay buffer to all wells.
 - (f) Add beads: vortex mixing bottle and add 25 μ L of the mix to each well (*see Note 7*).
 - (g) Seal the plate with a plate sealer.
 - (h) Wrap the plate with foil and incubate with agitation on a plate shaker (~700 rpm) overnight (16–18 h) at 2–8 °C.
 - (i) Place the plate on magnetic holder (handheld magnet, EMD Millipore Catalog #40–285) and rest plate on magnet for 60 s to allow complete settling of magnetic beads.
 - (j) Remove well contents by gently decanting the plate in an appropriate waste receptacle and gently tapping on absorbent pads to remove residual liquid.
 - (k) Wash plate with 200 μ L of wash buffer by removing plate from magnet, adding wash buffer, shaking for 30 s, reattaching to magnet, letting beads settle for 60 s, and removing well contents as previously described after each wash. Repeat wash steps three times.
 - (l) Add 25 μ L of detection antibodies into each well. Allow the detection antibodies to warm to room temperature prior to addition.
 - (m) Seal, cover with foil and incubate with agitation on a plate shaker (~900 rpm) for 1 h at room temperature (20–25 °C). Do not aspirate after incubation.
 - (n) Add 25 μ L streptavidin-phycoerythrin to each well containing the 25 μ L of detection antibodies.
 - (o) Seal, cover with foil and incubate with agitation on a plate shaker for 30 min at room temperature (20–25 °C).
 - (p) Gently remove well contents (after placing the plate on magnetic holder) and wash plate three times following instructions listed above (**Step k**).
 - (q) Add 150 μ L of Sheath Fluid (or Drive Fluid if using MAGPIX[®]) to all wells. Resuspend the beads on a plate shaker for 5 min.
 - (r) Run plate on Luminex 200[™], HTS, FLEXMAP 3D[®] or MAGPIX[®] with xPONENT[®] or Bio-Plex manager 6.1 software.
7. Analysis: Save and analyze the median fluorescent intensity (MFI) data using a 5-parameter logistic or spline curve-fitting

method for calculating analyte concentrations in samples. For diluted samples, final sample concentrations should be multiplied by the dilution factor (25 as per protocol instructions). If using another dilution factor, multiply by the appropriate dilution factor.

3.4.2 Evaluation of Cystatin C, Epidermal Growth Factor (EGF), Lipocalin-2-NGAL, Clusterin, and Osteopontin (OPN) Level in Urine

Cystatin C, epidermal growth factor (EGF), Lipocalin-2-NGAL, Clusterin, and Osteopontin (OPN) levels are measured using the panel 2 (ref MKI2MAG-94K from Merck-Millipore):

1. Allow all reagents to warm to room temperature (20–25 °C) before use in the assay (except antibodies and beads).
2. Prepare the dilution of urine samples. For panel 1: dilute sample 1:1000 in the assay buffer provided in the kit by adding first 4 µL of urine to 96 µL of assay buffer, and then 2 µL of this dilution into 78 µL of assay buffer.
3. Prepare the antibody-immobilized beads:
 - (a) For individual vials of beads, vortex for 1 min.
 - (b) Add 150 µL from each antibody-bead vial to the mixing bottle and bring final volume to 3.0 mL with assay buffer.
 - (c) Vortex the mixed beads well (*see Note 5*).
 - (d) There are five biomarkers in panel 1: using five antibody-immobilized beads, add 150 µL from each of the five bead vials to the Mixing Bottle. Then add 2.25 mL assay buffer.
4. Prepare the quality controls:
 - (a) Reconstitute quality control 1 and quality control 2 with 250 µL deionized water. Invert the vial several times to mix and vortex.
 - (b) Allow the vial to sit for 5–10 min (*see Note 6*).
5. Prepare the standards:
 - (a) First, reconstitute the mouse kidney injury panel 2 standard with 250 µL deionized water. Invert the vial several times to mix. Vortex the vial for 10 s. Allow the vial to sit for 5–10 min. This will be used as Standard 6 (*see Note 6*).
 - (b) Label 5 Eppendorf microfuge tubes standard 1 through standard 5.
 - (c) Add 150 µL of assay buffer to each of the five tubes.

- (d) Prepare serial dilutions (1:4) by adding 50 μL of the reconstituted standard to the standard 5 tube, mix well and transfer 50 μL of standard 5 to the standard 4 tube, mix well and transfer 50 μL of standard 5 to the standard 3 tube, mix well and transfer 50 μL of standard 3 to the Standard 2 tube, mix well and transfer 50 μL of standard 2 to the standard 1 tube and mix well.
 - (e) The 0 pg/mL standard (background) will be assay buffer.
6. Perform the immunoassay procedure making sure that all reagents are warmed at room temperature (20–25 °C).
- (a) Add 200 μL of assay buffer into each well of the plate. Seal and mix on a plate shaker for 10 min at room temperature (20–25 °C).
 - (b) Decant assay buffer and remove the residual amount from all wells by inverting the plate and tapping it smartly onto absorbent towels several times.
 - (c) Add 25 μL of each standard or control into the appropriate wells. Assay buffer should be used for 0 pg/mL standard (background).
 - (d) Add 25 μL of sample (diluted) into the appropriate wells.
 - (e) Add 25 μL of assay buffer to all wells.
 - (f) Add beads: Vortex mixing bottle and add 25 μL of the mix to each well. During addition of beads, shake bead bottle intermittently to avoid settling.
 - (g) Seal the plate with a plate sealer.
 - (h) Wrap the plate with foil and incubate with agitation on a plate shaker (~700 rpm) overnight (16–18 h) at 2–8 °C.
 - (i) Place the plate on magnetic holder (handheld magnet, EMD Millipore Catalog #40–285) and rest the plate on magnet for 60 s to allow complete settling of magnetic beads.
 - (j) Remove well contents by gently decanting the plate in an appropriate waste receptacle and gently tapping on absorbent pads to remove residual liquid.
 - (k) Wash plate with 200 μL of wash buffer by removing plate from magnet, adding wash buffer, shaking for 30 s, reattaching to magnet, letting beads settle for 60 s, and removing well contents as previously described after each wash. Repeat wash steps three times.
 - (l) Allow the detection antibodies to warm to room temperature.
 - (m) Add 25 μL of detection antibodies into each well.

- (n) Seal, cover with foil, and incubate with agitation on a plate shaker (~900 rpm) for 1 h at room temperature (20–25 °C). Do not aspirate after incubation.
 - (o) Add 25 µL streptavidin-phycoerythrin to each well containing the 25 µL of detection antibodies.
 - (p) Seal, cover with foil and incubate with agitation on a plate shaker for 30 min at room temperature (20–25 °C).
 - (q) Gently remove well contents (after placing the plate on magnetic holder) and wash plate three times following instructions listed above (**Step k**).
 - (r) Add 150 µL of sheath fluid (or drive fluid if using MAG-PIX[®]) to all wells. Resuspend the beads on a plate shaker for 5 min.
 - (s) Run plate on Luminex 200™, HTS, FLEXMAP 3D[®], or MAGPIX[®] with xPONENT[®] or Bio-Plex manager 6.1 software.
7. Analysis: Save and analyze the median fluorescent intensity (MFI) data using a five-parameter logistic or spline curve-fitting method for calculating analyte concentrations in samples. For diluted samples, final sample concentrations should be multiplied by the dilution factor (1000 as per protocol instructions). If using another dilution factor, multiply by the appropriate dilution factor (*see* **Note 8**).

4 Notes

1. We describe methods using the creatinine assay kit from R&D Systems, including all reagents mentioned.
2. We describe methods using the Pierce BCA assay from Thermo Scientific, including all the reagents mentioned.
3. We describe methods using the albumin ELISA kit from Bethy Laboratories, including all the reagents mentioned.
4. Avoid multiple (>2) freeze/thaw cycles of urine samples. Urine samples should be aliquoted upon collection and just after centrifugation according to further analysis requirements (*see* Fig. 1). When using frozen samples, it is recommended to thaw the samples completely, mix well by vortexing, and centrifuge prior to use in the assay to remove particles.
5. The unused portion of prepared antibody-immobilized beads may be stored at 2–8 °C for up to 1 month.
6. The unused portion of prepared quality controls and standards may be stored at ≤ −20 °C for up to 1 month.

7. During addition of beads, shake bead bottle intermittently to avoid settling.
8. All the quantification methods described here measure the concentration of analyte (Albumin, KIM-1, etc.) in the collected urines (e.g., as ng/ μ L). Data can also be normalized to the levels of creatinine. Alternatively, data can be expressed as total quantity/24 h when the volume of urine collected in the metabolic cage (per 24 h) is taken into account.

Acknowledgments

LEZ is an employee of SQY Therapeutics and AG is funded by the Institut National de la santé et la recherche médicale (INSERM); the Association Monegasque contre les myopathies (AMM); and the Duchenne Parent project France (DPPF).

References

1. Moulton HM, Moulton JD (2010) Morpholinos and their peptide conjugates: therapeutic promise and challenge for Duchenne muscular dystrophy. *Biochim Biophys Acta* 1798: 2296–2303. <https://doi.org/10.1016/j.bbmem.2010.02.012>
2. Andersson P, den Besten C (2019) Chapter 20. Preclinical and clinical drug-metabolism, pharmacokinetics and safety of therapeutic oligonucleotides. In: *Advances in nucleic acid therapeutics*. The Royal Society of Chemistry, London, pp 474–531
3. Frazier KS (2015) Antisense oligonucleotide therapies: the promise and the challenges from a toxicologic pathologist's perspective. *Toxicol Pathol* 43:78–89. <https://doi.org/10.1177/0192623314551840>
4. Carver MP, Charleston JS, Shanks C et al (2016) Toxicological characterization of exon skipping Phosphorodiamidate Morpholino oligomers (PMOs) in non-human primates. *J Neuromusc Dis* 3:381–393. <https://doi.org/10.3233/JND-160157>
5. Szani P, Ness KPV, Weller DL et al (2011) Repeat-dose toxicology evaluation in cynomolgus monkeys of AVI-4658, a phosphorodiamidate morpholino oligomer (PMO) drug for the treatment of duchenne muscular dystrophy. *Int J Toxicol* 30:313–321. <https://doi.org/10.1177/1091581811403505>
6. Hung G, Xiao X, Peralta R et al (2013) Characterization of target mRNA reduction through in situ RNA hybridization in multiple organ systems following systemic antisense treatment in animals. *Nucl Acid Ther* 23: 369–378. <https://doi.org/10.1089/nat.2013.0443>
7. Butler M, Stecker K, Bennett CF (1997) Cellular distribution of phosphorothioate oligodeoxynucleotides in normal rodent tissues. *Lab Invest* 77:379–388
8. Frazier KS, Sobry C, Derr V et al (2014) Species-specific inflammatory responses as a primary component for the development of glomerular lesions in mice and monkeys following chronic administration of a second-generation antisense oligonucleotide. *Toxicol Pathol* 42:923–935. <https://doi.org/10.1177/0192623313505781>
9. Engelhardt JA, Fant P, Guionaud S et al (2015) Scientific and regulatory policy committee points-to-consider paper*: drug-induced vascular injury associated with nonsmall molecule therapeutics in preclinical development: part 2. Antisense oligonucleotides. *Toxicol Pathol* 43:935–944. <https://doi.org/10.1177/0192623315570341>
10. Moisan A, Gubler M, Zhang JD et al (2017) Inhibition of EGF uptake by nephrotoxic antisense drugs in vitro and implications for pre-clinical safety profiling. *Mol Ther Nucl Acids* 6: 89–105. <https://doi.org/10.1016/j.omtn.2016.11.006>

Open Access This chapter is licensed under the terms of the Creative Commons Attribution 4.0 International License (<http://creativecommons.org/licenses/by/4.0/>), which permits use, sharing, adaptation, distribution and reproduction in any medium or format, as long as you give appropriate credit to the original author(s) and the source, provide a link to the Creative Commons license and indicate if changes were made.

The images or other third party material in this chapter are included in the chapter's Creative Commons license, unless indicated otherwise in a credit line to the material. If material is not included in the chapter's Creative Commons license and your intended use is not permitted by statutory regulation or exceeds the permitted use, you will need to obtain permission directly from the copyright holder.





Protocol for Isolation and Culture of Mouse Hepatocytes (HCs), Kupffer Cells (KCs), and Liver Sinusoidal Endothelial Cells (LSECs) in Analyses of Hepatic Drug Distribution

Kjetil Elvevold, Ingelin Kyrrestad, and Bård Smedsrød

Abstract

Development of the new generation of drugs (e.g., oligo- and polynucleotides administered intravascularly either as free compounds or as nano-formulations) frequently encounters major challenges such as lack of control of targeting and/or delivery. Uncontrolled or unwanted clearance by the liver is a well-known and particularly important hurdle in this respect. Hence, reliable techniques are needed to identify the type(s) of liver cells, receptors, and metabolic mechanisms that are responsible for unwanted clearance of these compounds.

We describe here a method for the isolation and culture of the major cell types from mouse liver: hepatocytes (HCs), Kupffer cells (KCs), and liver sinusoidal endothelial cells (LSECs). The presently described protocol employs perfusion of the liver with a collagenase-based enzyme preparation to effectively transform the intact liver to a single cell suspension. From this initial cell suspension HCs are isolated by specified centrifugation schemes, yielding highly pure HC preparations, and KCs and LSECs are isolated by employing magnetic-activated cell sorting (MACS). The MACS protocol makes use of magnetic microbeads conjugated with specific antibodies that bind unique surface antigens on either KCs or LSECs. In this way the two cell types are specifically and separately pulled out of the initial liver cell suspension by applying a magnetic field, resulting in high purity, yield, and viability of the two cell types, allowing functional studies of the cells.

If the drug compound in question is to be studied with respect to liver cell distribution of intravascularly administered drug compounds the isolated cells can be analyzed directly after isolation. Detailed studies of receptor-ligand interactions and/or dynamics of intracellular metabolism of the compound can be conducted in primary surface cultures of HCs, LSECs, and KCs established by seeding the isolated cells on specified growth substrates.

Key words Mouse liver cells, Cell isolation, Kupffer cells, Liver sinusoidal endothelial cells, Hepatocytes, Cell culture, Magnetic-activated cell sorting, MACS

1 Introduction

Modern drug treatment modalities frequently include i.v. administration of large molecule compounds or nano-formulations. In either case oligonucleotides may represent the active principle.

Lack of targeting control is a general challenge when these therapeutics are injected i.v. The main cause of targeting failure is unwanted uptake in liver [1]. Apart from the one noteworthy example of i.v. administered oligonucleotide therapeutics patisiran that successfully targets the major type of liver cells, the hepatocytes (HCs) [2], the general rule is that large molecules/nano-formulations are rapidly cleared from the circulation by specialized scavenger cells lining the wall of the several hundred million capillary-like liver vessels called liver sinusoids. The scavenger cells of the liver sinusoids represent two cell types: the liver sinusoidal endothelial cells (LSECs) and the Kupffer cells (KCs). The KCs are the resident mononuclear phagocytes of the liver and represent by far the largest population of macrophages in the body. These cells are geared to carry out phagocytosis of large blood-borne material (>200 nm). In contrast the LSECs, representing the great majority of endothelial cells of the liver, are unable to perform phagocytosis under normal conditions, but are among the most active endocytic cells of the body, using clathrin-mediated endocytosis and a set of unique endocytosis receptors [3].

Although the LSECs and KCs make up only 3.3% and 2.5% of the total liver volume, the numberwise distribution of same cells is 21% and 8.5% [4]. The following anatomical and physiological relationships strongly support the notion that LSECs are optimally geared to carry out extremely efficient blood clearance: (a) The liver receives as much as 25% of the blood volume that is pumped through the heart at any time unit; (b) The KCs and LSECs represent the surface that the blood encounters on its journey through the liver; (c) The total surface of the LSECs in the human liver facing the sinusoidal lumen is that of a tennis court [3]; (d) The ad- and ab-luminal surfaces of LSECs carry unique endocytosis receptors that recognize and internalize an array of blood-borne waste substances, including several nanoparticles as well as oligo- and polynucleotides [5–8]; (e) The endocytosis receptors in LSECs mediating blood clearance recycle back to the cell surface only seconds after they have delivered their cargo to the primary endosomes, making these receptors extremely efficient. Moreover, considering the effective intracellular transport toward lysosomes and their unusually high contents of lysosomal enzymes, there should be no surprise that the LSECs and KCs represent very active scavenger cells contributing importantly to the high blood clearance capacity of the liver.

Based on the remarkable scavenging activity of the LSECs and KCs, projects including development of large molecule compounds and nano-formulated therapeutics should include studies to determine (a) if the drug candidates accumulate preferentially in LSECs and/or KCs, (b) and if so, what receptors are involved in the recognition. Exact studies designed to determine to what extent any i.v. administered compound accumulates in the different types of liver cells require reliable methods to isolate pure preparations of LSECs, KCs, and HCs from a single liver.

We pioneered the method of preparing LSECs, KCs, and HCs from a single rat liver, using collagenase perfusion to disperse the liver cells, followed by density separation on Percoll, and selective substrate adherence [9]. This method, which has been used with or without modifications by several laboratories, was later adapted by us for isolation and culture of mouse LSECs, KCs, and HCs [10].

While the procedure for isolation of HCs is rather straightforward and will be only briefly mentioned later in the present methods description, techniques for isolation of LSECs and KCs are more elaborate and will therefore be dealt with in greater detail in the present chapter. The great majority of the techniques used nowadays to generate initial single cell suspensions of liver include perfusion with a collagenase solution through the portal vein. The further steps comprise either centrifugal elutriation [11], Percoll density separation followed by selective adherence [10], or magnetic-activated cell sorting (MACS). Fluorescence-activated cell sorting (FACS) is frequently used to isolate KCs and LSECs. However, this method subjects the cells to considerable shear stress, which is probably why cell cultivation and functional studies of LSECs and KCs purified by FACS have been so scantily described in the literature. It has been reported that FACS of murine liver cells to produce LSECs resulted in a higher purity compared to MACS but was associated with a lower yield and recovery rate [12]. See [13] for a systematic review on methods for isolation and purification of murine LSECs. What is clear is that the cell yield, viability, and purity are affected by several steps in the cell isolation procedure, including the enzyme and technique used to disperse the liver cells, buffers, centrifugation steps, and antibody used for sorting. In rat, highly pure LSECs are reported with MACS isolation [14, 15] using the LSEC-specific antibody SE-1 [16], which targets the FcγRIIb2 in these cells [17].

We here describe the MACS procedure that we have developed for isolation of mouse KCs and LSECs, using F4/80 and CD146 as cell markers, which allows simultaneous isolation of highly pure HCs, LSECs, and KCs. The method is reliable because specific antibodies are commercially available for recognition of either KCs or LSECs in a suspension of mixed liver cells. Moreover, the procedure is fast and reproducible, and gives good cell yields. In addition, the MACS isolation procedure requires equipment that is considerably less expensive and easier to operate than elutriation centrifuges or flow cytometry cell sorters. During the isolation procedure, the cells and buffers are kept cold to minimize intracellular metabolic processes. After the final isolation step the cells can be seeded in culture dishes and maintained for functional studies or pelleted and used for further analysis. This allows for both *in vivo* liver cell distribution of intravascularly administered compounds, as well as *in vitro* analysis of how compounds interact with isolated cultures of KCs, LSECs, and HCs.

2 Materials

2.1 Perfusion System (Fig. 1)

1. Water bath.
2. Heat exchanger with bubble trap.
3. Pump.
4. Silicone tubing (use tubes with small diameter to avoid formation of air bubbles) (*see* **Notes 1**).
5. Intravenous cannula 22G.
6. Magnifier.

2.2 Materials for Perfusion

1. Small styrofoam “bed” for the mouse + tissue paper rolled to form a pillow.
2. Good scissors, forceps, surgical dressing tweezers.
3. Fridge/ice box for buffers.
4. Perfusion buffer (*see* **steps 1** and **2** in Subheading **2.3** for preparation).
5. Liberase™ Research Grade, rehydrated and aliquoted in 1 mg batches according to the manufacturer’s protocol, and kept frozen until perfusion starts.



Fig. 1 Equipment for the perfusion system

6. Liberase buffer (= perfusion buffer with 4.76 mM CaCl_2 , *see steps 2 and 3* in Subheading 2.3) for dissolution of the defrosted Liberase™.
7. Cold AIM V medium (30 ml/mouse liver) for collection of cells after perfusion with Liberase™.
8. Petri dish (10 cm diameter) for releasing cells from liver following perfusion with Liberase™.
9. The present protocol has been set up for C57BL/6 mice (*see Note 2*).

2.3 Buffers, Density Medium, Liberase™, Cell Culture Media, Coating of Cell Culture Dishes with Fibronectin, Magnetic-Activated Cell Sorting (MACS) Isolation System (Hardware and Buffers)

1. Perfusion buffer: Dilute 40 ml of perfusion buffer concentrate (see below) in milliQ sterile water to a total volume of 1 l.
2. Perfusion buffer concentrate: Dissolve 103.75 g NaCl, 6.25 g KCl, and 28.70 g Hepes in 350 ml milliQ H_2O while stirring. When all has been dissolved add 75 ml of 1 M NaOH. Add H_2O to a total volume of 500 ml. Filter (pore size 0.45 μm) the solution and distribute in tubes (50 ml); freeze in portions of 40 ml. *See [4]* for more details on buffer compositions.
3. Liberase buffer: Add 0.5 ml of 476 mM CaCl_2 to 49.5 ml of perfusion buffer to obtain a final concentration of 4.76 mM CaCl_2 . Add 1.0 mg of freshly defrosted stock of Liberase™ to give a working concentration of 0.02 mg/ml immediately before perfusion starts. *See Note 3* regarding Liberase™ concentration.
4. Percoll (100%): Mix 13.5 ml stock Percoll™ with 1.5 ml 10× PBS to make 15 ml 100% Percoll™.
5. Medium for cultivation of HCs: Add 1 kit of Gibco™ Primary Hepatocyte Maintenance Supplements to 1 bottle (500 ml) of Gibco™ William's E Medium, no phenol red to prepare medium for culture of HCs.
6. Medium for cultivation of LSECs and KCs: Gibco™ AIM V™ Medium, liquid.
7. Coating of cell culture dishes with fibronectin for cultivation of LSECs and HCs: Use fibronectin prepared from bovine plasma (1 mg/ml) to coat culture dishes at a concentration of 1–5 $\mu\text{g}/\text{cm}^2$. Coat culture surface with a minimal volume, just enough to cover the surface. Leave for 10 min at room temperature. Once the entire area is covered, remove excess solution, which can be reused to coat another well/plate. Leave for 10 min at room temperature. Wash 3× with PBS and let stand in PBS in the incubator until seeding of cells. PBS must be removed before cells are added.
8. MACS isolation system: CD146 MicroBeads (Miltenyi); anti-F4/80 MicroBeads (Miltenyi); LS Columns (Miltenyi); QuadroMACS™ Separator (Miltenyi).

9. Prepare MACS buffer: Mix autoMACS Rinsing Solution (Miltenyi) and MACS BSA Stock Solution (Miltenyi) according to instructions by the manufacturer.

3 Methods

If the aim is to study the distribution of an injected compound in the different types of liver cells, the compound must be injected before starting at Subheading 3.1. The time from injection of compound until the animal is euthanized, and the liver perfusion and cell isolation procedure start depends on the anticipated rate of metabolism of the injected compound. The faster the metabolism, the faster is the disappearance of the compound from the liver cells, and accordingly, the shorter should the time be from compound injection to cell isolation.

If the aim is to study interaction of compound with isolated liver cells, without prior intravenous administration, start directly at Subheading 3.1.

3.1 Preparing the Perfusion System

1. Heat perfusion buffer to approx. 70 °C, and let it cool down. This operation drives air of the perfusion buffer, lowering the risk of bubble formation during the perfusion.
2. Wash the system with 10 ml perfusion buffer (*see Note 1*).
3. Allow the water bath to attain the correct working temperature (*see Note 4*).
4. Make sure there are no bubbles in the system (*see Note 1*).
5. Flow rate before starting the liver perfusion: approx. 9 ml/min.
6. Make sure there is at least 50 ml perfusion buffer in the tube before starting the liver perfusion.
7. Shortly before starting the liver perfusion, rapidly defrost Liberase™, add it to the Liberase buffer and mix.

3.2 Running the Liver Perfusion to Generate Single Cell Suspension of Liver Cells

1. The entire procedure is carried out postmortem and must be started immediately after the animal has been euthanized according to the protocol of the ethical review permission that covers the research. The mouse images shown in Figs. 2, 3, 4, 5, 6, and 7 are from an in vitro experiment (euthanasia before sampling), and the experimental protocol and animal handling were approved by the competent institutional authority at UiT The Arctic University of Norway, which is licensed by the National Animal Research Authority at the Norwegian Food Safety Authority (Mattilsynet; Approval ID: UiT 02/20), and experiments were performed in compliance with the European Convention for the protection of Vertebrate Animals used for Experimental and Other Scientific Purposes.



Fig. 2 Position of the mouse organs



Fig. 3 Position of the portal vein and inferior vena cava

2. Place the animal on the bed with the tissue paper pillow under the abdomen, to position the liver at a slightly higher level than the rest of the organs.
3. Carefully open the abdomen by midline incision, making sure not to injure the liver. The abdominal cavity has to be well exposed for better visualization and access (Fig. 2).

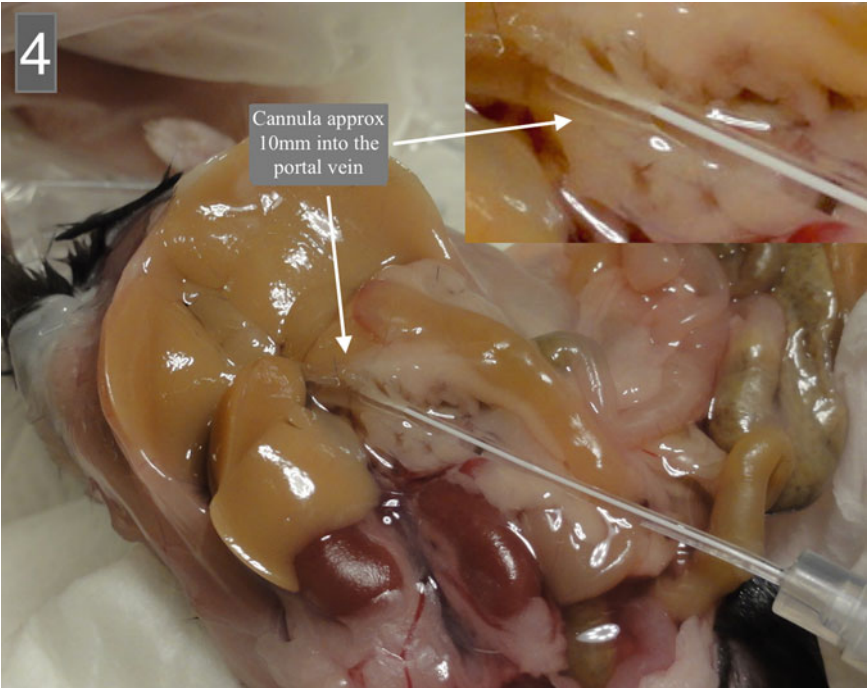


Fig. 4 Position of the cannula in the portal vein

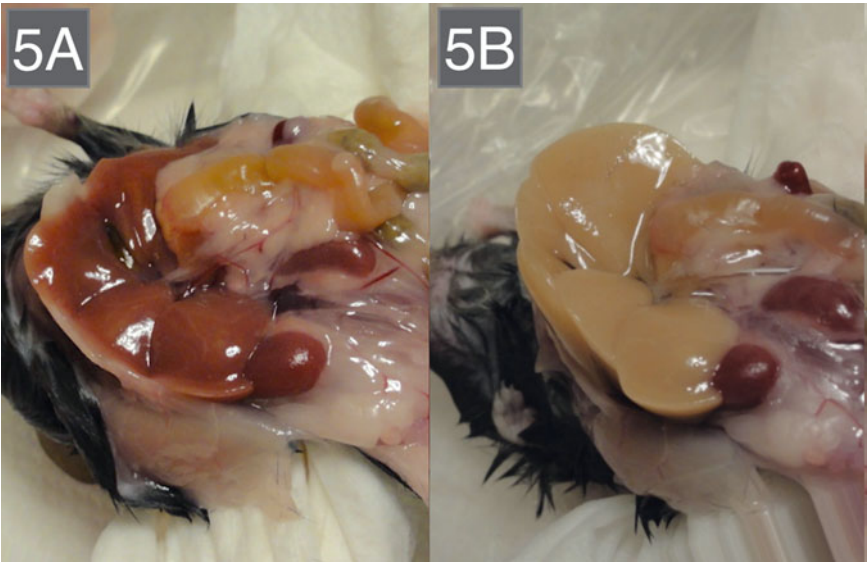


Fig. 5 Color shift of the organs



Fig. 6 Removal of the liver

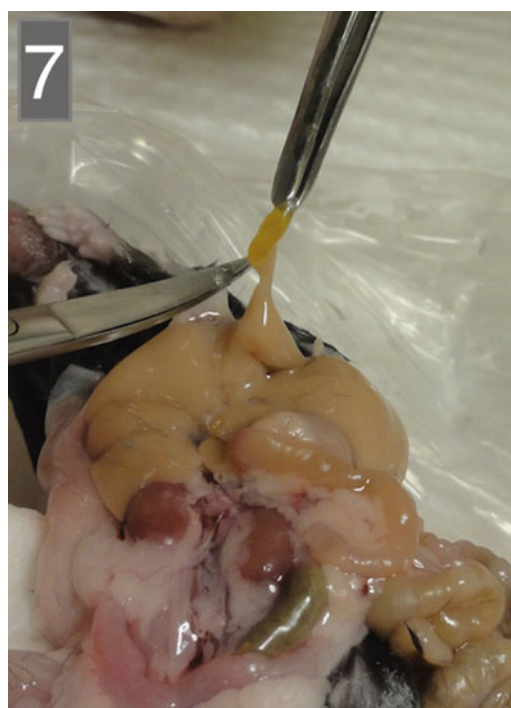


Fig. 7 Removal of the gall bladder

4. Move the intestines to the side to expose the portal vein (Fig. 3).
5. Before reducing the flow rate to 4 ml/min flick the tubing all the way from the heat exchanger to the tubing tip to get rid of all visible air bubbles (*see Note 1*).
6. Reduce the flow rate to 4 ml/min (make sure that there is a surplus of perfusion buffer in the 50 ml tube in case more time is needed for the operation). Note that it is important to maintain this low flow rate during the insertion of the tubing cannula. Never stop the flow rate completely during any step of the operation.
7. Focus the magnifier on the portal vein and make a small incision (approx. 1/3 of the vein diameter). Do not cut the portal vein completely, as this will make it very difficult to insert the cannula. The incision should be made close to where the splenic vein enters the portal vein. In this way one ensures that the distance from the incision to the point where the portal vein enters the liver is sufficient to give the cannula a stable position, and at the same time the tip of the cannula will rest in a position that allows the perfusion of all liver lobes (Fig. 4).
8. Insert the cannula, by carefully moving it through the incision of the portal vein, in a movement nearly parallel to the vessel. In this way the cannula will slide smoothly in, and the risk of rupturing the vessel wall is minimized. A certain sign that the cannula has entered the vein is a rapid color shift of the liver from dark red (Fig. 5a) to yellow (Fig. 5b).
9. Cut the inferior vena cava as indicated with the arrow in Fig. 3 to allow the perfusion buffer to flow freely through the liver.
10. Increase the flow rate to 7–10 ml/min depending on the animal weight.
11. Keep on perfusing the liver with perfusion buffer to make sure no more blood is left (normally 10–20 ml).
12. Change to the Liberase buffer. Avoid entrance of air bubbles into the portal vein during this operation (*see Note 1*).
13. When the liver cells are well dissociated by the perfusion with Liberase™ (as judged by swelling, increased size and a softer appearance of the liver, pale color, and a tendency of Glisson's capsule to separate from the parenchyma), remove the cannula from the portal vein (*see Note 5*).
14. Carefully remove the liver from the body, by cutting the ligaments using a small, sharp pair of scissors. Use the magnifier as a guide to fine-tune the cutting of ligaments around the stomach. Avoid rupturing the esophagus or intestines (Fig. 6) (*see Note 5*).
15. Carefully remove the gall bladder (Fig. 7) (*see Note 5*).

16. Place the liver in the petri dish (with 10 ml cold AIM V) and remove Glisson's capsule (*see* **Notes 5** and **6**).
17. Shake the liver gently to release the cells that have been dissociated during the Liberase™ perfusion. When no more cells seem to be released, pour the cell suspension into a 50 ml tube and ice-cold AIM V medium to approx. 40 ml (*see* **Note 5**).
18. Keep the cell suspension at 4 °C.
19. Repeat perfusion operation with a new mouse or end by washing the system with 50 ml of sterile water, fill with 70% ethanol, and leave it until next liver perfusion.
20. Release the tubings from the pump.

3.3 Cell Isolation

1. Very gently mix the cell suspension.
2. Spin down the HCs by differential centrifugation ($35 \times g$ for 2 min at 4 °C; max acceleration/deceleration). The resulting pellet is enriched in HCs, and the supernatant is enriched in KCs and LSECs.
3. Pipette the KC/LSEC-enriched supernatant to a new centrifuge tube and repeat the differential centrifugation ($35 \times g$ for 2 min at 4 °C; max acceleration/deceleration) (*see* **Note 7**).
4. To increase the yield of KC/LSECs resuspend the HC-enriched pellet in 40 ml perfusion buffer and repeat the differential centrifugation at $35 \times g$ for 2 min at 4 °C; max acceleration/deceleration (*see* **Note 7**).
5. For isolation of HCs, resuspend the HC-enriched pellet from **step 4** in 20 ml William's E medium and continue at **step 3** in Subheading 3.3.3 (procedure for isolation and culture of HCs).
6. For isolation of KC/LSECs, collect the resulting supernatants from **steps 3** and **4** in Subheading 3.3, and centrifuge ($300 \times g$ for 10 min at 4 °C; max acceleration/deceleration). Small, light-colored pellets indicate that the content of HCs is low, and the procedure can continue at **step 10** in Subheading 3.3. Big, darker colored pellets indicate high content of HCs, and a density separation on Percoll is recommended to deplete HCs from KCs and LSECs: to do this, resuspend the pellet in 11 ml MACS buffer and mix with 9 ml 100% Percoll to make a 20 ml mix of 45% Percoll solution and cells. Carefully add 8 ml MACS buffer on top (*see* **step 9** in Subheading 2.3).
7. Centrifuge the 45% Percoll gradient: $1350 \times g$ for 25 min at 4 °C. Set acceleration/deceleration to 5 (on scale from 1 to 9).
8. By means of a 10 ml pipette collect the HC-depleted KCs and LSECs (non-HCs) from the top of the 45% Percoll cushion and resuspend in 5 ml MACS buffer. Count the cells.

9. Centrifuge ($300 \times g$ for 10 min at 4°C ; max acceleration/deceleration).
10. Resuspend pellet in MACS buffer to make a cell number/volume ratio of 5×10^6 non-HCs per 100 μl . (If you go directly from **step 6** to **step 10** in Subheading 3.3, first resuspend the non-HC pellet in 5 ml MACS buffer, count the cells, and centrifuge at $300 \times g$ for 10 min at 4°C ; max acceleration/deceleration.)

3.3.1 MACS Isolation of KCs and LSECs

1. Mix 2/3 of the total volume of non-HCs with 20 μl of anti-F4/80 MicroBeads (for isolation of KCs). Mix the remaining 1/3 with 20 μl of anti-CD146 MicroBeads (for isolation of LSECs). Incubate both non-HC suspensions for 15 min at 4°C in 5 ml centrifuge tubes.
2. Fill each of the two 5 ml tubes with MACS buffer and centrifuge ($300 \times g$ for 10 min at 4°C ; max acceleration/deceleration). Aspirate both supernatants completely.
3. Resuspend each of the two pellets in 0.5 ml MACS buffer and apply to two LS columns for magnetic isolation according to the instructions given by the manufacturer.
4. Wash the column with 3×3 ml MACS buffer. Discard the flow-through.
5. Remove the column from the magnetic field and fill it with 5 ml MACS buffer. Immediately flush out the magnetically labeled cells by firmly pushing the plunger into the column. Collect the eluted volumes in two 15 ml centrifuge tubes—one tube for the cells incubated with anti-F4/80 MicroBeads, and the other for the cells incubated with anti-CD146 MicroBeads. Spin the tubes ($300 \times g$ for 10 min at 4°C ; max acceleration/deceleration), resuspend the resulting pellets in 1 ml AIM V medium, and count the cells. See **Note 8** for details regarding yield, purity, and viability of isolated KCs and LSECs.
6. At this point the KCs and LSECs may be analyzed for contents of drug administered prior to the liver perfusion procedure.
7. If cells are to be used for *in vitro* analysis of drug uptake and intracellular processing, they may be cultured according to the following procedure.

3.3.2 Culturing LSECs (Continue Here After **Step 5** in Subheading 3.3.1)

1. Seed 0.25×10^6 LSECs/200 μl AIM V medium/ cm^2 growth area in fibronectin-coated cell culture wells. Place in a humidified CO_2 incubator at 5% O_2 .
2. After 35 min carefully wash with PBS or medium.
3. The LSEC cultures are now ready for experiments. Characteristic morphology of cultured LSECs is shown in Fig. 8a, b. See **Note 9** for details regarding purity of cultured LSECs.

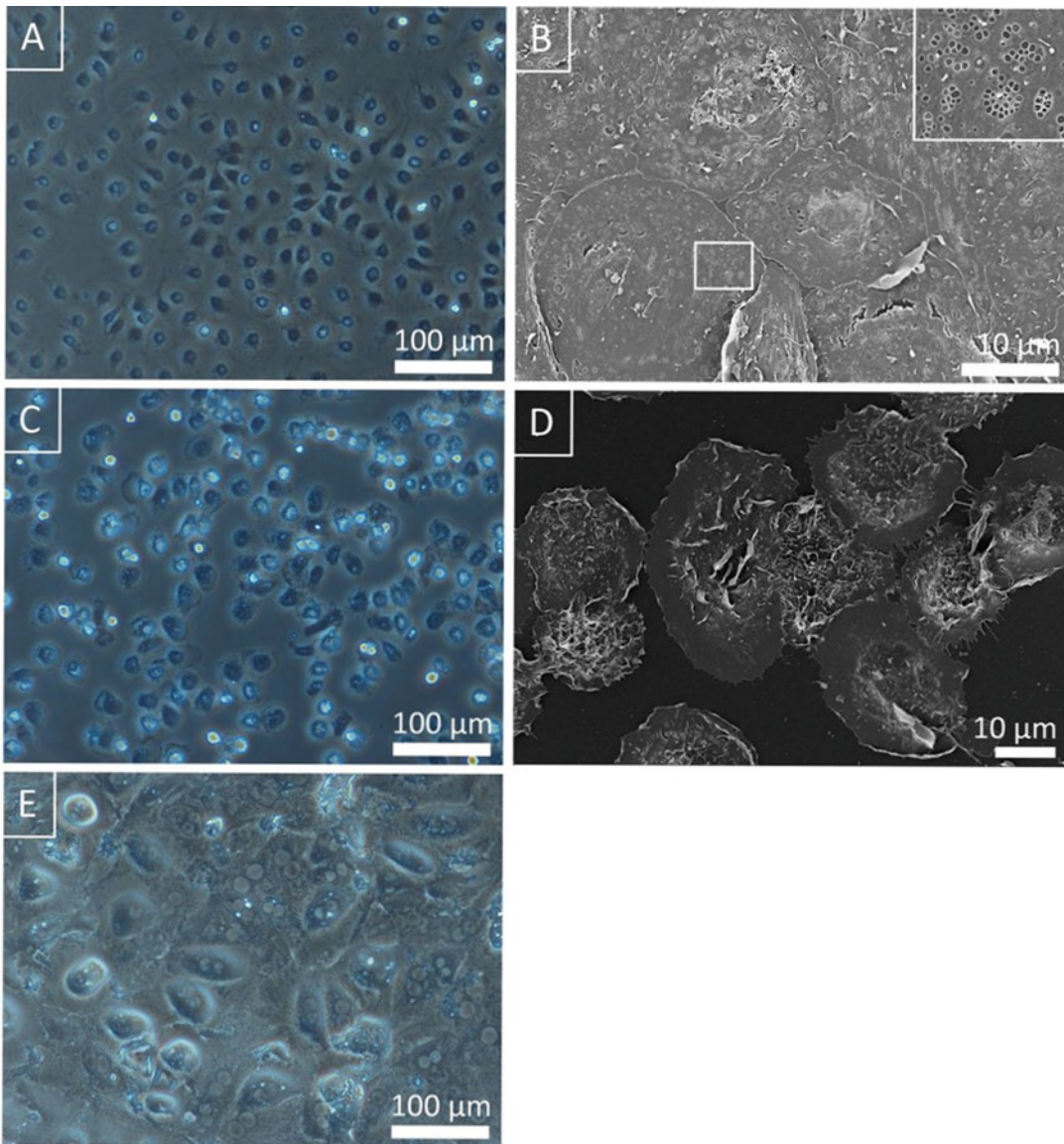


Fig. 8 Characteristics of the LSEC cultures. Phase contrast (**a**, **c**, **e**) and scanning electron micrographs (**b**, **d**) of mouse liver cells following isolation and culture. Liver cells were isolated as outlined in Subheading 3.3 and established in monolayer cultures. (**a**, **b**) LSECs 2 h following seeding. The inset in **b** shows typical LSEC fenestrations (open trans-cytoplasmic pores), which are a hallmark of these cells. (**c**, **d**) KCs 1 h following seeding. (**e**) HCs 48 h following seeding. LSECs and HCs were seeded on fibronectin-coated tissue culture plastic, and KCs were seeded on non-coated culture plastic. KCs and LSECs were cultured in AIM V medium, in 5% O₂ and 5% CO₂ atmosphere, whereas HCs were cultured in William's E medium with supplements, 5% fetal bovine serum, 0.1 μM dexamethasone, and 20% O₂ and 5% CO₂. Following the indicated cultivation times the cultures for scanning electron microscopy were gently washed with medium prewarmed to 37 °C, fixed in McDowell's fixative for electron microscopy [18], and processed according to the protocol in [14], and examined in a Zeiss Sigma field emission scanning electron microscope, run at 2 kV. Phase contrast micrographs were taken with a 20× objective lens in a Nikon Eclipse TE300 inverted microscope, equipped with a Zeiss AxioCam MRC digital camera

3.3.3 Culturing KCs

(Continue Here After **Step 5** in Subheading 3.3.1)

1. Seed 0.20×10^6 KCs/200 μ l AIM V medium/cm² growth area in non-coated cell culture wells. Place in a humidified CO₂ incubator at 5% O₂.
2. After 35 min carefully wash with PBS or medium.
3. The KCs are now ready for experiments. Characteristic morphology of cultured KCs is shown in Fig. 8c, d. See **Note 10** for details regarding purity of cultured KCs.

3.3.4 Isolation and Culturing of HCs (Continue Here After **Step 4** in Subheading 3.3)

1. Filter the resuspended HC-enriched pellet through a 70 μ m cell strainer to get rid of debris and cell aggregates that remain undissociated after the Liberase™ and centrifuge the filtrate ($54 \times g$ for 2 min at 4 °C; max acceleration/deceleration).
2. Mix resulting pellet with 45% Percoll and centrifuge ($1350 \times g$ for 25 min at 4 °C; set acceleration/deceleration to 5 on scale from 1 to 9).
3. After centrifugation remove the Percoll above the cell layer, fill up the tube with William's E medium, and mix with the remaining bottom layer of Percoll which contains the purified HCs. Spin down the HCs ($54 \times g$ for 2 min at 4 °C; max acceleration/deceleration).
4. Resuspend in William's E medium and count the HCs. At this point the HCs may be analyzed for contents of drug if administered prior to the liver perfusion procedure. Determine viability, e.g., by the trypan blue exclusion test. See **Note 11** for details regarding viability of HCs.
5. If the HCs are to be used for *in vitro* analysis of drug uptake and intracellular processing, they may be cultured according to the procedure described in steps 5–7 in Subheading 3.3.4.
6. Seed 0.15×10^6 HCs/200 μ l William's E medium with supplements (see step 5 in Subheading 2.3) and 5% fetal bovine serum/cm² growth area in fibronectin-coated cell culture wells. Place in a humidified CO₂ incubator at 20% O₂ (see **Note 12**).
7. After 4 h very carefully wash with William's E medium using a 1 ml pipette. Continue cultivating the HCs in William's E medium with supplements (see step 5 in Subheading 2.3), with or without serum. See **Note 13** regarding maintenance and serum requirement for HC cultures.
8. The HC cultures are now ready for experiments. Characteristic morphology of cultured HCs is shown in Fig. 8e. See **Note 14** regarding purity of HC cultures.

4 Notes

1. Great care must be taken to avoid the formation of air bubbles in the perfusion system, as trapping of air bubbles in the vascular system of the liver during perfusion will obstruct perfusion and greatly reduce the yield of cells.
2. The present protocol has been set up for C57BL/6 mice. Cell yields and time needed for cells to attach and spread optimally on growth substrates may vary between different mouse strains.
3. Although a concentration of 1 mg Liberase™/50 ml Liberase buffer (0.02 mg/ml buffer) is recommended to disperse liver cells from normal mouse liver, it is advisable to use a somewhat stronger concentration when cells are to be isolated from the liver of old mice or from mice with fibrotic liver. For these purposes the Liberase™ concentration may be increased to 0.03 mg/ml, although it is recommended that tests be performed to establish the adequate concentration.
4. The working temperature of the water bath must be adjusted to give the buffer a temperature of 38 °C at the tip of the cannula. (Tubing diameter, distance from heat exchanger, and flow rate affect the temperature drop along the tubing.)
5. For optimal viability, yield, and purity of isolated liver cells it is essential that the cells of the initial liver cell suspension following perfusion of the liver with Liberase™ are well dispersed as single cells, and with a minimum of aggregated cells and debris. A word of caution: if the liver is not satisfactorily transformed into a single cell suspension after the enzyme perfusion it is of little help to use mechanical force to tear the tissue apart, as this will result in massive formation of debris and dead cells. DNA leaking from dead cells will contribute to clumping of cells, and the result will be greatly reduced cell yield and viability.
6. It is not necessary to remove absolutely all of the Glisson's capsule; Glisson's capsule has to be ruptured and pulled off by means of tweezers to the extent that the dissociated liver cells can be gently shaken out into the buffer.
7. The purpose of the second differential centrifugation of the KC/LSEC-enriched supernatant is to remove more HCs which is important before the MACS isolation step, whereas the purpose of the second differential centrifugation of the resuspended HC pellet is to extract even more LSECs and KCs, which may still be present in the first HC pellet. The total yield of LSECs and KCs can be increased 20% by running a second differential centrifugation. Repeating this

centrifugation step further will not give significantly increased yields of LSECs and KCs.

8. Yield, purity, and viability of isolated KCs and LSECs. With the method outlined here, using female C57BL/6 mice of 15–20 g body weight, and isolating all three cell types from the same liver we obtain >95% pure preparations of KCs (yield: $2\text{--}4 \times 10^6$ cells per 3 mice) and LSECs (yield: $3\text{--}6 \times 10^6$ cells per 3 mice). Of note, the presently described method has been set up to isolate KCs and LSECs from 2/3 and 1/3 of the initial liver cell suspension. If more KCs are needed, the cell yield can be increased up to $3\text{--}6 \times 10^6$ KCs per 3 mice by using the entire initial liver cell suspension. Similarly, the yield of LSECs can be increased up to $5\text{--}10 \times 10^6$ per mouse by using the entire initial liver cell suspension to make LSECs. Viability as judged by trypan blue exclusion is $\geq 95\%$ for both KCs and LSECs.
9. Typical purity of cultured LSECs: 95–98% (fenestrated cells assessed by scanning EM), with KCs as the dominating contaminating cell.
10. Typical purity of cultured KCs: Between 98% and 100%.
11. Viability of HCs should be >80%. If viability is <80% it is recommended that the cells be discarded. Viability routinely varies between 80% and 95%.
12. HCs may be seeded in William's E medium with supplements (*see step 5* in Subheading 2.3) with or without 5% fetal bovine serum and allowed to attach and spread on the growth substrate for 4 h. Following washing the HC cultures may be continued by culturing in William's E medium with supplements (without serum *see* Subheading 2.3, **step 5**). HCs must be cultured in 20% O₂; they will not survive in 5% O₂.
13. Our experience is that HC cultures can be maintained up to at least 48 h without serum added to the medium.
14. Typical purity of cultured HCs: >99%.

Acknowledgments

The authors wish to acknowledge Prof. Karen Kristine Sørensen at UiT The Arctic University of Norway for assisting in proof reading of the manuscript, and also for providing light and electron microscopic images shown in Fig. 8.

References

1. Godfrey C, Lourdes D, Smedsrød B, France P-R, Denti M, Disterer P, Lorain S, Nogales-Gadea G, Sardone V, Rayan A, EL-Andaloussi S, Lehto T, Khoo B, Hjortkjær C, van Roon-Mom W, Goyenvallé A, Aartsma-Rus A, Arechavala-Gomez V (2017) Delivery is key: lessons learnt from developing splice switching antisense therapies. *EMBO Mol Med* 9:545–557. <https://doi.org/10.15252/emmm.201607199>
2. Setten RL, Rossi JJ, Han SP (2019) The current state and future directions of RNAi-based therapeutics. *Nat Rev Drug Discov* 18(6): 421–446. <https://doi.org/10.1038/s41573-019-0023-6>
3. Sørensen KK, Smedsrød B (2020) The liver sinusoidal endothelial cell: basic biology and pathobiology. In: Arias IM, Alter HJ, Boyer JL, Cohen DE, Shafritz DA, Thorgeirsson SS, Wolkoff AW (eds) *The liver: biology and pathobiology*, 6th edn. Wiley, New York, pp 422–434
4. Pertoft H, Smedsrød B (1987) Separation and characterization of liver cells. In: Pretlow TGII, Pretlow TP (eds) *Cell separation: methods and selected applications*, vol 42. Academic Press, New York, pp 1–24. <https://doi.org/10.1016/B978-0-12-564504-1.50004-0>
5. Sørensen KK, Simón-Santamaría J, McCuskey RS, Smedsrød B (2015) Liver sinusoidal endothelial cells. *Compr Physiol* 5:1751–1774. <https://doi.org/10.1002/cphy.c140078>
6. Liu F, Shollenberger LM, Conwell CC, Yuan X, Huang L (2007) Mechanism of naked DNA clearance after intravenous injection. *J Gene Med* 9:613–619
7. Hisazumi J, Kobayashi N, Nishikawa M, Takakura Y (2004) Significant role of liver sinusoidal endothelial cells in hepatic uptake and degradation of naked plasmid DNA after intravenous injection. *Pharm Res* 21:1223–1228
8. Miller CM, Tanowitz M, Donner AJ, Prakash TP, Swayze EE, Harris EN, Seth PP (2018) Receptor-mediated uptake of phosphorothioate antisense oligonucleotides in different cell types of the liver. *Nucleic Acids Ther* 28: 119–127. <https://doi.org/10.1089/nat.2017.0709>
9. Smedsrød B, Pertoft H (1985) Preparation of pure hepatocytes and reticuloendothelial cells in high yield from a single rat liver by means of Percoll centrifugation and selective adherence. *J Leukoc Biol* 38:213–230
10. Hansen B, Arteta B, Smedsrød B (2002) The physiological scavenger receptor function of hepatic sinusoidal endothelial and Kupffer cells is independent of scavenger receptor class A type I and II. *Mol Cell Biochem* 240:1–8
11. Knolle PA, Gerken G, Loser E, Dienes HP, Gantner F, Tiegs G, Meyer Zum Buschenfelde KH, Lohse AW (1996) Role of sinusoidal endothelial cells of the liver in concanavalin A-induced hepatic injury in mice. *Hepatology* 24:824–829
12. Bartneck M, Topuz F, Tag CG, Sauer-Lehnen S, Warzecha KT, Trautwein C, Weiskirchen R, Tacke F (2015) Molecular response of liver sinusoidal endothelial cells on hydrogels. *Mater Sci Eng C Mater Biol Appl* 51:64–72. <https://doi.org/10.1016/j.msec.2015.02.045>
13. Meyer J, Gonelle-Gispert C, Morel P, Bühler L (2016) Methods for isolation and purification of murine liver sinusoidal endothelial cells: a systematic review. *PLoS One* 11:e0151945. <https://doi.org/10.1371/journal.pone.0151945>
14. Bhandari S, Li R, Simón-Santamaría J, McCourt P, Johansen SD, Smedsrød B, Martínez-Zubiaurre I, Sørensen KK (2020) Transcriptome and proteome profiling reveal complementary scavenger and immune features of rat liver sinusoidal endothelial cells and liver macrophages. *BMC Mol Cell Biol* 21:85. <https://doi.org/10.1186/s12860-020-00331-9>
15. Tokairin T, Nishikawa Y, Doi Y, Watanabe H, Yoshioka T, Su M et al (2002) A highly specific isolation of rat sinusoidal endothelial cells by the immunomagnetic bead method using SE-1 monoclonal antibody. *J Hepatol* 36(6): 725–733
16. Ohmura T, Enomoto K, Satoh H, Sawada N, Mori M (1993) Establishment of a novel monoclonal antibody, SE-1, which specifically reacts with rat hepatic sinusoidal endothelial

- cells. *J Histochem Cytochem* 41(8): 1253–1257
17. March S, Hui EE, Underhill GH, Khetani S, Bhatia SN (2009) Microenvironmental regulation of the sinusoidal endothelial cell phenotype in vitro. *Hepatology* 50(3):920–928
 18. McDowell EM, Trump BF (1976) Histologic fixatives suitable for diagnostic light and electron microscopy. *Arch Pathol Lab Med* 100: 405–414. <https://pubmed.ncbi.nlm.nih.gov/60092/>

Open Access This chapter is licensed under the terms of the Creative Commons Attribution 4.0 International License (<http://creativecommons.org/licenses/by/4.0/>), which permits use, sharing, adaptation, distribution and reproduction in any medium or format, as long as you give appropriate credit to the original author(s) and the source, provide a link to the Creative Commons license and indicate if changes were made.

The images or other third party material in this chapter are included in the chapter's Creative Commons license, unless indicated otherwise in a credit line to the material. If material is not included in the chapter's Creative Commons license and your intended use is not permitted by statutory regulation or exceeds the permitted use, you will need to obtain permission directly from the copyright holder.



Part VI

Intellectual Property



Chapter 28

Patent Considerations When Embarking on New Antisense Drug Programs

Laurence D. S. Gainey

Abstract

The aim of this chapter is to provide some key information on patents and the patent system to assist someone embarking on the design, development, and commercialization of new antisense drugs.

Here I outline certain key topics such as what is a patent? why patent? how do I protect my molecule with a patent? confidentiality, searching for the same or similar molecules in the prior art, data requirements, the patenting timeline and freedom to operate.

Keywords Patent, Intellectual property, Patentability, Prior art, Searching, Patent filing, Exclusivity, Freedom to operate, Confidentiality

1 Introduction

When embarking on a research and development program for any therapeutic, including an antisense drug, it is crucial that appropriate consideration be given to patents and the patent system. A patent protecting a therapeutic is often the main tool to keep bioequivalent versions off the market for a limited period, thus allowing the innovator time to recoup and secure a return on their investment. It is also important to consider third-party patents in case these impede the ability to commercialize the therapeutic.

The aim of this chapter is to provide a basic understanding of the patent system for someone embarking on a research program to discover and develop a therapeutic antisense drug. However, as patent decisions for any particular project will be case specific, appropriate legal advice should be sought from a qualified patent attorney.

The chapter is split into sections that discuss:

- What is a patent?
- Why patent inventions?
- Types of inventions to consider.

- Patenting requirements.
- Importance of confidentiality.
- Patent timeline.
- Data requirements.
- Searching.
- Freedom to operate considerations.

The patenting of a putative therapeutic molecule is usually crucial to the commercial success of the therapeutic. It is therefore recommended that you engage the services of a patent professional with expertise in handling antisense oligonucleotide patent portfolios at the earliest opportunity and keep them apprised of developments in the research program throughout.

2 What Is a Patent?

A patent is a property right given by a country's government to an inventor, or their successor, that protects a new and useful invention. It is a reward for publishing the invention and provides the recipient with an exclusive right, for a limited period of time, to prevent others from exploiting, such as making, using, importing, offering for sale or selling, the invention in the country. Once this period of exclusivity has expired the public are free to exploit the invention and this arrangement with the state—a limited period of exclusivity in exchange for publishing and teaching the world what the invention is, is often referred to as the “patent bargain” and is what helps to stimulate and drive innovation.

Some important features of a patent are:

1. It is a country-specific right. Anyone wishing to secure patent protection in multiple countries will need to secure a granted patent in each of these countries.
2. The period of time (often referred to as “the term”) of the right is governed by the patent legislation in the country, but in the vast majority of countries, this is 20 years from the filing date of the patent application. Certain countries also have provisions to extend the term of the patent or award a separate extension right, typically for a maximum of 5 years, for pharmaceutical or agrochemical products that were required to undergo regulatory approval.
3. The exclusive right is an exclusionary right. It does not necessarily allow the owner to work (use) the invention. It merely allows them to prevent others from working the invention. For example, if the patent is to a new therapeutic compound the patent does not give you the right to make and sell the compound as this will require separate approval from the health

authority. Also, exploitation of the invention may fall within the scope of someone else's patent and so authorization, such as via a license, from this entity may be needed to work the invention.

4. The patent right must be applied for via the filing of a patent application that describes the invention in enough detail so that the invention can be understood and reproduced by a skilled reader.
5. A patent is only enforceable (via the relevant national court system) once it has been examined and granted by the patent office of the relevant country.
6. The invention is defined by a series of sentences termed "claims" that describe the invention and help to define the scope of protection (i.e., whether something falls within the patent or not). An analogy for the claims in a patent is the boundary fence that defines a field.
7. The claimed invention must meet certain requirements to become a "granted patent"—see Sect. 5.

3 Why Patent Inventions?

The cost of research and development (R&D) for therapeutic molecules is significant. In 2016, the Tufts Center for Drug Development estimated R&D costs per approved drug to be in excess of \$2.5bn [1]. In order to drive investment in therapeutic R&D there must be means to recoup and provide a return on this investment. The patent system has evolved to stimulate innovation and is one of the key mechanisms to provide an environment for securing a return on the investment.

3.1 Exclusive Market Position

Patents provide a legal right to stop others from working a patented invention for a period of time. Provided the patent owner or their licensee has all other necessary freedom to operate, it can mean that they can establish exclusivity to sell their product in the market.

During this period of exclusivity, when there is no direct competition for the same product, it is often easier to commercialize the product and so recoup the costs invested in the R&D and obtain a return on that investment.

3.2 Opportunity to License or Sell the Invention

A patent is a property right which can be sold or licensed to another party. In exchange for granting a licensee the rights to work under the patent, the applicant/licensor can secure financial or other compensation. This means that patent owners who are unable to fully exploit the invention independently can, for example, leverage the patent for revenue, cross-licensing purposes and/or open up valuable collaborations. Thus, a patent protecting a therapeutic

antisense oligonucleotide product or its use can also be very valuable to individual inventors, small companies, and academic institutions.

3.3 Collateral for Raising Funding

Because of the opportunity to secure an exclusive market position as in Sect. 3.1, a strong patent portfolio is attractive to investors and so can assist with company flotations or raising further capital.

3.4 Incentive to Invest in Research and Development

Without the existence of a patent protecting a therapeutic antisense oligonucleotide molecule or its use in treating a particular disease or patient group, there may be significant disincentives to invest in the research and development costs and lost commercial opportunities.

4 Types of Inventions to Consider

A patent protecting the oligonucleotide drug molecule being developed, often defined by its sequence, is likely to be particularly desirable as this will protect the molecule regardless how it is used.

However, in addition to a new oligonucleotide defined by its sequence and/or particular chemical modifications (e.g., to the backbone, sugars, bases) throughout or at specific positions, it is important to recognize that valuable patenting opportunities might also be found for new types of chemical modifications, fusions or conjugates, manufacturing processes, formulations, drug delivery technologies, particular diseases to be treated (therapeutic uses), particular patient populations to target, dosage forms of the drug, and/or dosage treatment regimens, to name just some categories of invention. It is therefore important to think beyond the specific molecule/compound to see if there are other patentable opportunities that can be captured to enhance the patent portfolio protecting your entire research program.

5 Patenting Requirements

Each country (jurisdiction) has its own legal requirements (legislation) of what constitutes a patentable invention, but typically the claims that define the invention must meet certain criteria, including (1) novelty (new); (2) inventive step (not obvious) over what is already known; and (3) industrial utility (be useful). In addition, the application must include an adequate description of how to carry out the invention.

Individual country legislation may also preclude the patenting of certain types of subject matter in that country. For example, certain countries do not permit patents directed to *methods of treatment, surgery or diagnosis practised on the human body*.

However, antisense oligonucleotide molecules, particularly those with chemical modifications, constitute patentable subject matter all the key countries (including US, Europe, Japan, China).

5.1 Novelty

The claimed invention must not have been disclosed in the public domain prior to the filing date of the invention.

According to Article 54(1) of the European Patent Convention [2]:

An invention shall be considered to be new if it does not form part of the state of the art.

Thus, a claimed invention is novel/new if it does not form part of “the state of the art,” the state of the art being everything that was available to the public by way of written (including via electronic means) or oral publication, use or any other way, in any country of the world and in any language before the effective filing date of the invention. The effective filing date of the invention is the date of filing of the first patent application (e.g., priority application or International application—see 7(b)) that appropriately discloses the claimed invention. Novelty is an objective measure. Each and every feature of the claimed invention must have been disclosed together in the prior art to preclude patenting based on novelty.

An ideal antisense molecule may be the culmination of optimum choice of a number of features including, target sequence, length, complementarity, and chemistry. Thus, even with recognized therapeutic targets, there is often scope for establishing novelty over the prior art molecules. What will likely determine the ability to secure a patent on the molecule will be inventive step or non-obviousness.

5.2 Inventive Step (or Non-Obviousness)

It is somewhat subjective, and the assessment of inventive step differs from one country to another but, in essence, it is an assessment of whether the difference between the claimed invention and the state of the art, as assessed by the person skilled in the art, is obvious.

According to Article 56, first sentence, of the European Patent Convention [2]:

An invention shall be considered as involving an inventive step if, having regard to the state of the art, it is not obvious to a person skilled in the art.

Because this assessment is to be made by the notional “person skilled in the art,” it is intrinsically more difficult to gauge whether a claimed invention is inventive and is the main discussion point between a patent examiner and the patent attorney seeking to secure grant of the patent.

However, indicators of inventive step accepted by most patent offices include surprising and/or unpredictable results. To demonstrate this, it will likely be necessary to have comparative data which

demonstrates that the new antisense molecule, as claimed, possesses some superior property, perhaps much greater affinity or half-life, compared to that of the closest prior art molecule.

5.3 Industrial Utility

The claimed invention must be capable of being made or used in any type of industry.

According to Article 57 of the European Patent Convention [2]:

An invention shall be considered as susceptible of industrial application if it can be made or used in any kind of industry, including agriculture.

In general, this is an easy criterion to meet, and it is difficult to see how an antisense oligonucleotide invention would not meet this requirement.

5.4 Sufficiency/ Written Description

Finally, the application must include sufficient information to allow the person skilled in the art to work the invention across the whole area claimed without undue burden or requiring inventive skill.

According to Article 83 of the European Patent Convention [2]:

The European patent application shall disclose the invention in a manner sufficiently clear and complete for it to be carried out by a person skilled in the art.

Similar or equivalent provisions to those above, illustrated using the European Patent Convention [2], are to be found in the patent legislation of most countries.

6 Confidentiality

As noted above, to be patentable an invention must be novel.

The invention must therefore have not been disclosed to anyone outside of a confidentiality agreement or put into the public domain by any means. Numerous patent applications have failed to meet the novelty or inventive step criteria due to an inventor's own disclosure/publication.

Aside from publication in a scientific journal, other publications to be aware of include, website postings, or poster or oral presentation at a scientific conference. If the researcher is from an academic institution, other potential publications include: an internal academic presentation attended by individuals from outside the institution or under no obligation of confidentiality, a PhD thesis, a discussion with an academic from a different institution, indeed any oral disclosure to someone not required in law to keep the information confidential.

While some countries, such as USA, provide for a “*grace period*” that allow prior publications from the inventor, made

within a limited period before the filing date of their patent application, to be discounted from the prior art when assessing patentability, thus allowing a patent application to be filed after an earlier publication, it is a mistake to rely on this facility because “grace period” provisions only exist in a few countries. As noted above, therapeutic drug development costs are very high. In order to recoup such investment, it is typically desirable or necessary to be able to sell the drug globally, and thus important that patent protection for the drug be secured in the major markets. Many of the major pharmaceutical market countries do not have a *grace period* provision. An ill-timed publication could therefore undermine the opportunity to secure a patent in certain of the major markets which will have serious commercial implications. For example, it may dissuade a potential licensee or could be a reason for ceasing development of the molecule.

It is therefore crucial that the invention is kept confidential, at least until the patent application has been filed (*see Note 1*).

7 Patent Timeline

There are various routes available for seeking a patent in a particular country.

However, in situations where the applicant desires patent protection in multiple countries the following route is commonly adopted:

- (a) First filing of a patent application in a reference country, typically the home country of the applicant. This first application is often referred to as the priority application. Optionally, one or more subsequent priority application filings may follow within the next 12-month period.
- (b) At or prior to the 12-month anniversary of the first priority application a single application claiming priority from the earlier priority application(s) is filed under the Patent Co-operation Treaty (often referred to as a PCT or international application). By designating all available states in the PCT application, it is possible to convert this single international application into separate national patents in most countries of the world.
- (c) A search and preliminary non-binding opinion on the patentability of the claims is carried out by the patent office processing the PCT application and sent to the applicant, typically around 16 months from the filing of the earliest priority application.
- (d) 18 months from filing of the earliest priority application the PCT application is published.

- (e) Typically, at 30 months from the earliest priority date (*see Note 2*) the applicant must convert the international (PCT) application into separate national or regional applications (*see Note 3*). At this stage, the PCT application ceases to exist.
- (f) The national or regional applications are then examined by each respective national or regional patent office. Such examination will typically take 2–8 years culminating either in grant of the national or regional patent or refusal. On grant of a regional patent the applicant must then decide which countries within the region to convert the patent into. These then become national patents.
- (g) During the term of the regional or national patent applications or granted patents, it is typically necessary to pay ongoing fees (typically referred to as annuity or renewal fees) for keeping the application/patent in force. The term of any granted national patent is typically 20 years from the filing date (using the PCT system described above, the PCT application filing date in (b)).
- (h) In some countries, certain pharmaceutical or agrochemical patents may be entitled to a patent term extension for up to 5 years from the normal expiry date of the national patent. In Europe, rather than a patent term extension, a separate intellectual property right termed a Supplementary Protection Certificate (SPC) with a term of up to 5 years may be available. The patent extension or SPC referred to herein is to compensate, in part, for the period of time that the pharmaceutical or agrochemical compound was subjected to regulatory assessment by the authority responsible for regulating such products.

A typical timeline that uses the PCT system outlined above is shown in Fig. 1.

More details on the PCT system can be found on the PCT website [3].

8 Data Requirements

Patent attorneys are often asked how much and what type of data must be included in the patent application. There is no hard and fast rule on this. Generally, it is case specific and will depend on various factors such as the complexity in the art.

The majority of patent systems typically do not mandate that the patent application contain any number of specific examples, nor that these examples be actual worked examples with real data. However, in order to be patentable, the invention must be sufficiently described and enabled (or supported) to permit a person of

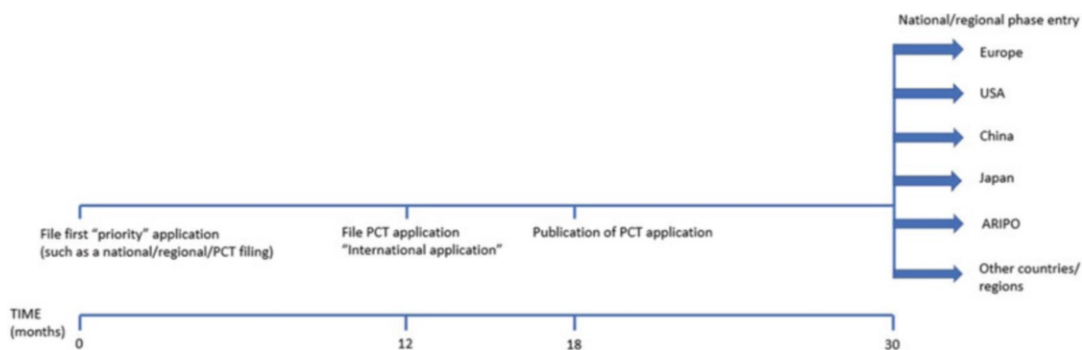


Fig. 1 Basic timeline for Patent Cooperation Treaty (PCT) patent application filling

skill in the art to practice the invention. With predictable technologies, such as mechanical devices, disclosure of a single means for making or using the invention may suffice. The person skilled in the art can easily make the invention and understand whether and how it works. In more unpredictable fields, such as therapeutic agents acting within biological systems, it is likely that the amount and type of data needed to demonstrate that the invention works and that the person skilled in the art can practice the invention will be greater. Thus, in practice, with therapeutic-type inventions, the presence of worked examples with relevant data plays a significant part in satisfying the patent examiner (and/or court) that the invention as claimed is supported/enabled and works.

Antisense oligonucleotide inventions, as with other therapeutic molecules, particularly those in established fields would benefit from two categories of data.

The first are data that would convince the person skilled in the art that the molecule has the necessary biological effect to make it credible that it would work as claimed (supporting data). Thus, if a disease pathology is manifest by expression of a particular protein, data demonstrating that the antisense oligonucleotide can, for example, impede production of the protein would be advantageous.

It is not necessary that the application include actual clinical trial data demonstrating efficacy in the relevant subjects (e.g., human patients). Suitable *in vivo* or *ex vivo* animal data or even cell data from an *in vitro* system, demonstrating that the antisense molecule impedes protein production, for example, may be sufficient and should be included in the patent application.

The second are data that demonstrate that the claimed invention performs better than what is already known (comparative data). Comparative data is particularly helpful, indeed often necessary, if the claimed invention is close to and thus potentially *prima facie* obvious over what is already known (in the public domain). Data comparing the claimed invention with the closest prior art

molecule can help support the position that the claimed invention meets the inventive step (non-obviousness) criterion.

While it may be possible to supply this comparative data during the patent examination/prosecution stage it is advantageous to have this in the application as filed. However, in order to be able to do this, the researcher must have identified which molecule is likely to be determined to be the “closest prior art molecule” and then to have synthesized and tested this molecule against those of the claimed invention.

9 Searching

As will be appreciated from the above, the claimed invention is assessed against what is already known (in the public domain).

When embarking on a research program for a new antisense oligonucleotide, it is recommended that the researcher conduct or commission searches of the published literature, including published patent applications, to identify, for example, the various molecules against the target sequence that are in the public domain. This information can assist on two fronts. First, it offers the opportunity to conduct research in novel space and design novel molecules; secondly, it should identify the molecule(s) that are likely to be considered the closest prior art molecules against which the new molecule will be assessed for patentability.

Prior art and patent searching is a skill that requires access to and an understanding of how to search particular databases of published documents. The ways of conducting searches of the prior art is beyond the scope of this chapter. The researcher may have the tools (e.g., databases of publications) and skills to conduct their own prior art searching. Otherwise, it is recommended that this be commissioned from an appropriate search firm.

10 Freedom to Operate (FTO)

The final topic to flag is that of freedom to operate. As noted above, a patent on your product (e.g., antisense oligonucleotide drug) is an exclusionary right. It does not give the right to commercialize the product, and one obstacle to exploitation may be the existence of one or more third-party patents that dominate the ability to make, use or sell the product. Examples of dominating third-party patents might be those that cover a broad class of molecules that your development candidate falls within or claims to the precise therapeutic use (e.g., disease to be treated) that a molecule such as the one you are developing is to be used for.

It is therefore also important to consider third-party patents in case these impede the ability to commercialize the product. An

FTO assessment for third party patents starts with searching for the existence of relevant pending applications or granted patents. It is highly recommended that such searching be conducted by professional searchers and the search output should then be assessed by a suitably qualified patent attorney. Once potentially relevant third-party patent property, both pending applications and granted patents have been identified, strategies to mitigate the risk of patent infringement can be devised. This could include securing legal opinions on infringement and validity, initiating challenges to the validity of such patents and/or securing appropriate patent licenses to any dominating patents.

The most meaningful FTO assessment can only be carried out when the actual product and its method of manufacture have been identified. However, if FTO assessments are carried out at an early stage it may help to gauge risk and potentially allow the design of molecules that avoid problematic third-party patents. For example, if equivalent chemical modifications are feasible, only one of which is protected by third-party patents, it may be possible to utilize the patent-free modification to avoid the FTO risk.

11 Summary

When embarking on a research program to develop a therapeutic antisense oligonucleotide, it is important to consider and incorporate a patent strategy that includes seeking protection for patents on the product and being aware of third-party patents that might be an impediment to commercialization.

It is advantageous to conduct prior art searches early on to ensure that your molecule is novel over those already known and to identify the closest prior art molecules against which your product will be assessed for patentability, in particular inventive step. It is imperative that the details of the invention are kept confidential until after the patent application has been filed, at least.

It is important to generate data that demonstrates that the molecule has the biological properties likely to be of use in the purported treatment and to include this data in the patent application. In vitro cell data may be sufficient.

It may also be advantageous to generate comparative data to demonstrate that the claimed molecule has some unexpected beneficial property or improvement over the closest prior art compound. If this data is included in the patent application, it could help to satisfy the patent examiner that the claimed molecule meets the inventive step criterion and thus greatly facilitate the patent prosecution. If it is not available at the time of filing it may be useful, if not actually necessary, to generate this data for use in the patent prosecution stage.

It is important to recognize that valuable patenting opportunities may exist for subject matter other than the antisense compound itself and its particular use and you should consider whether seeking patent protection for these would strengthening the overall patent portfolio.

Finally, you should engage the services of a patent professional with expertise in handling antisense oligonucleotide patenting at the earliest opportunity. They can provide counsel on the appropriateness of the data generated and the strategy for filing and prosecuting the patent application(s), including which territories to pursue for patent protection. They can draft and file the patent application(s) and manage the patent portfolio. They can also assist with any necessary prior art or third-party patent searching and advise on the best time to undertake the necessary freedom to operate assessments.

12 Glossary

Applicant—the individual or legal entity that has filed for and has claimed initial ownership of a patent application.

Freedom to operate (FTO)—is the ability to develop, make, sell, offer for sale (i.e., market) the product without legal liabilities to third parties, including third party patent owners.

Licensor—the person or entity that grants formal permission to make or do something. In the context of a patent the right to perform certain acts protected by the patent.

Licensee—the individual who obtains the license from the licensor to make or do something.

Patent claims—a series of independent or linked (dependent) sentences that define the scope of what is being claimed as the invention. The patent claims form one section of the patent application.

Patent Cooperation Treaty (PCT)—is an international patent law treaty which provides a unified procedure for filing patent applications in each of its contracting states. It is administered under the auspices of the World Intellectual Property Organization (WIPO). A patent application filed under the PCT is typically referred to as an international application, or PCT application. The PCT application is merely a vehicle to facilitate grant of individual national patents. It is not, and cannot, become a patent itself. There is no such thing as an international patent.

Patent office—is a governmental or intergovernmental organization which processes and awards patents.

Patent portfolio—refers to the collection of patent applications and granted patents owned by an applicant.

Patent prosecution—is the process taken to establish whether the patent application meets the criteria for grant of a patent. It may also be referred to as patent examination.

Patent term (or “term”)—is the length or period of time that a patent can remain in force. Once this term has finished the patent expires and the invention enters the public domain, so anyone is entitled to freely exploit the invention.

Patent term extension—is an extension of time to the usual patent term.

Person skilled in the art—is a fictitious individual used in many patent laws of the world as the individual that is used as reference to determine whether the claimed invention is patentable (e.g., inventive) and the application sufficiently disclosed, among other things. Often the person skilled in the art is a technician skilled in the technical area of the invention who is aware of the prior art and has common general knowledge but no scintilla of ingenuity or inventiveness. Sometimes the person skilled in the art can be a team of individuals. It is a legal fiction.

Prior art—refers to all information that has been made available to the public prior to the effective filing date of the claimed invention. The effective filing date being the date of filing of the application that first discloses the claimed invention. This could be, for example, the date of one of the priority applications or the substantive application.

Priority application or priority patent application—a patent application filed in a national or regional state (including PCT application) that can be used to claim priority to from a subsequently filed national, regional or international application.

Public domain—refers to information or inventions which are freely available to the public, in particular, where no exclusive intellectual property rights exist or are possible. It can refer to patented inventions whose term has expired or information which has been published and so no longer protectable by a patent.

State of the art—refers to information which is known, or is capable of being known, by the public. It is often a synonym for prior art (information known before the patent filing date).

Substantive application—is the national or international application which will be subjected to patent examination and whose text can no longer be changed. Such filing may claim priority from an earlier “priority” application.

Supplementary Protection Certificate (SPC)—is a distinct intellectual property right available in countries of the European Economic Area that extends the term of certain rights under a patent for pharmaceutical or agrochemical products that have had to undergo regulatory assessment. It enters into force immediately the patent on which it is based expires. The SPC is designed to compensate the applicant for delays incurred in securing regulatory approval for a product, and it effectively extends the monopoly right for the product for a limited period of time.

13 Notes

1. There may be advantages to delaying publication until the substantive application filing date or even the patent application publication date, and these should be discussed with your patent professional.
2. The time limit to enter the national phase for most states/countries signed up to the PCT is 30 months from the priority date; however, the patent legislation of a country or region may set a time limit which expires later than 30 months from the priority date.
3. There are four regional contracting states to the PCT: African Regional Intellectual Property Organization (ARIPO), Eurasian Patent Office (EAPO), European Patent Office (EPO), and African Intellectual Property Organization (OAPI).

References

1. DiMasi JA, Grabowski HG, Hansen RW (2016) Innovation in the pharmaceutical industry: new estimates of R&D costs. *J Health Econ* 47: 20–33. <https://doi.org/10.1016/j.jhealeco.2016.01.012>
2. European patent convention (2016) ISBN 978-3-89605-152-3
3. International Patent System website (2021). <https://www.wipo.int/pct/en/>

Open Access This chapter is licensed under the terms of the Creative Commons Attribution 4.0 International License (<http://creativecommons.org/licenses/by/4.0/>), which permits use, sharing, adaptation, distribution and reproduction in any medium or format, as long as you give appropriate credit to the original author(s) and the source, provide a link to the Creative Commons license and indicate if changes were made.

The images or other third party material in this chapter are included in the chapter's Creative Commons license, unless indicated otherwise in a credit line to the material. If material is not included in the chapter's Creative Commons license and your intended use is not permitted by statutory regulation or exceeds the permitted use, you will need to obtain permission directly from the copyright holder.



INDEX

A

- ABCA4* 36, 39, 145–151, 157–159, 162, 271
 Acute kidney injury (AKI) 373, 374, 377–381
 Agarose 56, 60, 66, 70, 79,
 93, 97, 101, 117–126, 148, 150, 155, 159, 162,
 171, 175, 177, 182, 194, 199, 200, 203, 204,
 218, 220, 224, 226, 237, 284–286, 288–290,
 292, 293, 295, 303, 307
 Agarose retardation gel 117–126
 Analyses 67, 68, 70, 80, 81,
 83–85, 90, 91, 93, 95–98, 101, 125, 140, 145,
 152, 154–157, 159–161, 164, 172, 174–179,
 181–183, 193–195, 198–201, 203, 204, 208,
 213, 214, 218–220, 222, 224, 225, 228–230,
 239, 252, 282, 291, 293, 303–305, 307, 308,
 310, 312, 331, 350, 372–375, 379, 381, 382,
 387, 396, 398
 Anthrax toxin 130, 131
 Antisense oligonucleotides (AON/ASO) 3–5,
 8, 9, 11, 12, 14–16, 20, 33–39, 41, 43, 53–61,
 130, 146, 149, 158–161, 163, 168, 185–192,
 207–214, 218, 220, 221, 223, 224, 226,
 228–230, 235, 237, 239, 240, 246, 250, 251,
 257–263, 267–276, 282, 295, 301, 315–331,
 333–340, 347, 355, 356, 359–362, 371–373,
 375, 406, 408–410, 413–416
 Antisense technology 36, 43

B

- Bifunctional oligonucleotides 54, 55, 57, 58
 Biodistribution 8, 42, 350
 Biomarkers 8, 372–374, 377–381
 Brain 8, 13, 42, 257–264,
 273, 321, 333–340, 345, 346, 350, 356

C

- Cannula 334–340, 388, 394, 399
 Cationic polymers 117–126
 cDNA synthesis 56, 60, 93, 97,
 149, 160, 172, 194, 198, 237, 241, 284, 289
 Cell isolation 387, 390–398
 Cellular models 54, 65, 66, 79, 84, 169, 183, 276
 Cellular systems 65, 145–164
 Cerebral organoids 258, 259, 262

- Chemistries 3–23, 38, 39, 41,
 130, 136, 192, 355–356, 359, 360, 362, 372, 409
 Clinical 5, 8, 9, 12–14, 16,
 18–21, 33, 38–42, 159, 208, 257, 322, 346, 355,
 357, 359, 360
 Clinical trials 4, 8, 9, 12, 21, 33, 38–40,
 42, 219, 257, 275, 322, 333, 357, 360, 413
 Cloning 6, 65–70, 78, 84, 146,
 147, 150–155, 162, 181, 283, 284, 290, 293, 295
COL7A1 35, 185, 315
 Confidentiality 406, 410, 411
 Conjugating peptide 20, 39, 302, 371
 Conjugations 18, 20, 21, 42,
 105, 113, 130, 133, 135, 136, 138, 140, 302, 357
 COST Action 43
 CRISPR-Cas9 21, 22, 167–183
 CRISPR technology 168

D

- Delivery 8, 9, 15, 16, 18,
 20, 21, 38, 39, 41–43, 63–85, 103, 104, 118, 119,
 130, 131, 177, 181, 191–204, 237, 239, 240,
 242, 257–264, 296, 302, 310, 322, 334,
 345–353, 356–360, 362, 371
 Delivery of Antisense RNA (DARTER) v, 43
 Designs 5, 12, 15, 16, 23,
 33, 38, 39, 42, 43, 54, 55, 57, 58, 61, 65–70, 78,
 81, 83, 84, 89–101, 147, 148, 150–155, 157,
 158, 162, 164, 168, 169, 172, 173, 175, 178,
 179, 182, 192, 195, 218, 237, 277, 284, 289,
 290, 293, 330, 331, 355–357, 360, 362, 414, 415
 Differentiation 193, 197, 199,
 201, 210, 211, 220, 223, 224, 226, 229, 230,
 236–241, 245, 247, 249–252, 258–260, 316, 318
 Disease modeling 236, 258
 Dissection 303
 DNA 3, 4, 6, 7, 9, 14, 18, 21,
 22, 33, 37, 56, 60, 66, 68, 70, 78, 81, 82, 85,
 92–97, 105, 107, 111, 119, 120, 123, 125, 129,
 147–153, 155, 158, 162, 168, 171, 173–177,
 179–183, 191, 194, 204, 211, 213, 218, 220,
 224, 267, 272, 282–285, 287–292, 295–297,
 360, 399
 DNA analogue 13
 Dot blot 207–214

Drug delivery 104, 119, 345, 408
 Drugs 4, 5, 8, 9,
 12–19, 22, 33, 37–39, 41–43, 54, 103–115, 191,
 208, 218, 221, 236, 267, 268, 274, 333, 345,
 355, 356, 360, 361, 371, 385–400, 405–418
 Duchene muscular dystrophy (DMD) 8, 9, 12,
 13, 21, 34, 35, 38, 39, 54, 191–193, 199, 201,
 203, 217–231, 275, 301, 302, 306, 310, 372
 Dystrophin 8, 34, 38, 54,
 191, 193, 217–231, 275, 301, 302, 307–311, 371

E

Efficacies 18, 20, 38–40,
 42, 80–85, 100, 158, 192, 218, 219, 239, 240,
 267–276, 310, 311, 322, 326, 333, 345, 346,
 357, 371, 413
 Electrophoresis gel 60, 93, 97,
 120, 124–126, 148, 150, 151, 153, 158, 160,
 199, 200, 221, 230, 284, 294, 307
 Electroporation 77, 79, 80, 100, 191–204
 Endothelial cells 386
 Epidermolysis bullosa 35, 315
 Eteplirsen 5, 8, 38, 39, 54, 191, 192, 218, 362
 Exclusivity 41, 406, 407
 Exons 12, 13, 34–40,
 53–61, 91, 93, 94, 97, 98, 101, 146, 149, 150,
 153, 157, 162, 163, 168, 186, 191–193, 195,
 199, 201, 218, 221, 222, 224, 226, 230, 270,
 272, 274–276, 281–286, 289, 290, 292–295,
 297, 301, 302, 307, 315, 371
 Exon skipping 8, 12, 21, 35,
 38, 54, 61, 90, 164, 169, 185, 186, 188, 189,
 191–193, 195, 199, 201, 203, 204, 217–231,
 301, 302, 307, 311, 315, 316
 Eye 33, 39, 40, 174, 245,
 246, 253, 321–323, 325, 326, 328, 330, 331,
 339, 346, 348, 356

F

Fibroblasts 55, 56, 58, 60, 76,
 77, 84, 91, 93, 94, 96–98, 100, 101, 150,
 186–189, 236, 316, 317
 Freedom to operate (FTO) 406, 407, 414–416

G

Gapmers 4, 5, 12, 14–17,
 20, 23, 34, 36, 37, 40, 103, 104, 356, 359
 Gene delivery 119
 Gene editing 167–183, 356
 Genetics 40, 41, 53, 70, 90,
 104, 145, 146, 168, 169, 178, 207, 235, 257,
 268, 281, 362
 Gold nanoparticles 103–115

H

Haploinsufficiency 36, 64, 65
 Hepatocytes 18, 21, 356, 357, 386, 389
 HepG2 72, 77, 167–183
Homo sapiens 92
 Human 7, 9, 39, 42, 55, 57, 65–68,
 80, 84, 90, 91, 93, 94, 96–100, 146, 162, 167,
 169, 178, 203, 235–242, 246, 252, 257, 258,
 262, 267–276, 282, 284–287, 289, 290, 292,
 293, 316, 318, 322, 360, 362, 371, 386, 408, 413
 Human cells 7, 8, 42, 64, 273
 Humanized models 42, 270–276
 Hybridization 7, 355–359, 363

I

Immunohistochemistry 304, 305
 Induced pluripotent stem cells (iPSCs) 236,
 245–248, 250, 252, 253, 257
 Inherited metabolic diseases 168
 Inherited retinal diseases 145, 245, 275, 321
 Intellectual property 412, 416–418
 Internalization 79, 103, 104, 118
 Intracerebroventricular injections 335
 Intrathecal injections 192, 346–351
 Intravitreal injections 322, 326
 Intronic mutations 322
 Introns 35, 36, 41,
 54, 55, 57–59, 147, 151, 153, 186, 194, 270,
 276, 281, 282
In vitro 54, 65, 83, 84, 90, 91,
 93, 94, 96–99, 146, 147, 156–158, 179, 185,
 186, 192, 193, 217–231, 235–242, 245,
 257–263, 270, 273–274, 276, 282, 316,
 358–360, 387, 390, 396, 398, 413, 415
In vivo 7–9, 14, 15, 18, 20,
 54, 65, 83, 84, 98, 130, 208, 236, 246, 268, 272,
 281–297, 302, 310, 316, 347, 351, 359, 360,
 362, 387, 413

K

Keratinocytes 186–189, 316–318
 Kidney 8, 21, 42, 273,
 359–363, 371–373, 377, 378

L

Lipid nanoparticles 18, 21, 357
 Liver 8, 12, 17, 18, 20,
 21, 42, 43, 130, 169, 272, 356, 359–361, 363,
 372, 386, 387, 389–391, 393–400
 Locked nuclei acids (LNA) 12, 14, 16,
 17, 22, 23, 37, 58, 208, 356, 359, 360, 372
 Long non-coding RNA (lncRNAs) 64, 70

M

- Magnetic-activated cell sorting (MACS).....387,
389–391, 396, 399
- Maxigenes.....147, 148, 151, 153–156, 163
- MDx* mouse model12, 21, 275
- Mechanism of action.....5–7, 9, 19,
23, 33, 35, 37, 118, 355
- 2'-*O*-methoxyethyl (2'-MOE)5, 12,
13, 16, 20, 37, 192, 208, 220, 253
- 2'-*O*-methyl (2'-OMe)12, 13, 16,
17, 22, 37, 58, 186, 253
- Mice8, 9, 15, 19, 38, 54,
57, 64, 65, 67, 77, 84, 162, 208, 257, 267–276,
302–306, 308, 309, 311, 316–331, 333–340,
346, 348–352, 362, 371–383, 387–391, 395,
397, 399, 400
- Midigenes146–163, 273
- Minigene.....100, 283, 286–289, 293
- Model systems65, 68, 70, 71,
81, 83, 85, 158, 257
- Morpholino4, 8, 11, 38,
129–140, 208, 237, 253, 302
- Morphology.....201, 328, 396, 398
- mRNA.....3, 7, 8, 21, 22, 33,
34, 36–38, 41, 43, 64, 65, 70, 71, 80, 82, 83, 85,
90, 118, 169, 178, 186, 191, 246, 268, 270, 275,
281, 301, 356
- Mucopolysaccharidosis90
- Muscles20, 21, 33, 38, 39,
192, 201, 208, 217, 220, 235, 236, 241, 242,
272, 275, 301, 302, 306, 308–312, 316, 317,
319, 348
- Mutations34–42, 90, 91,
93–95, 98, 99, 101, 104, 129, 146–148, 151,
152, 154, 155, 162, 163, 168, 173, 176,
178–180, 182, 183, 185, 186, 191–193, 217,
218, 221, 268–271, 273–276, 281, 282, 287,
293, 301, 321, 322
- Myoblasts.....191–204, 207–214
- Myoblots.....219, 220, 222, 224, 226, 228–230
- Myotonic dystrophy21, 207–214
- Myotonic dystrophy type 1 (DM1)207–209,
211, 213
- Myotubes.....192, 193, 195,
197, 199, 201, 220, 235–242

N

- Nanoparticles.....103, 104, 108, 113, 114, 386
- Nucleofection.....194–197, 199, 201–203

O

- Off-target.....8, 9, 17, 70, 83,
98, 183, 297, 357–359, 363, 372

- Oligonucleotides3–14, 20, 21, 33, 38–40,
54, 55, 61, 103–105, 107, 108, 110–114, 159,
179–181, 191, 201, 208, 211, 292, 322,
345–353, 355–363, 371–383, 385, 386, 408
- On-target183, 297, 358–360
- Organoids146, 158, 245,
246, 248–253, 258–261, 263

P

- Patentability.....411, 414, 415
- Patent filing417
- Patents405–418
- Patient-derived cells35, 42, 90, 220, 322
- Phenylketonuria (PKU)169
- Phosphorodiamidate morpholino oligomers
(PMOs)4, 5, 8, 21,
38, 39, 129–131, 133, 135, 137, 138, 140, 192,
193, 196, 197, 199, 202, 208, 237, 239, 241,
242, 302, 310, 356, 371, 372
- Phosphorothioates (PS).....3–5, 7–9,
11–13, 22, 23, 36, 38–41, 180, 186, 192, 208,
220, 253, 270, 355, 356, 359, 360, 362, 372
- Photoreceptor cells245
- Pompe disease236
- Preclinical.....4, 9, 14, 19, 20, 39,
40, 185, 218, 220, 230, 267, 274, 322, 357, 360,
362, 363, 371, 372
- Preclinical evaluations17
- Pre-mRNA.....12, 34, 36, 53, 54, 129, 146, 150,
157, 162, 164, 186, 235, 281, 282, 296, 322, 358
- Prior art409–411, 413–417
- Protection195, 311, 390, 406,
407, 411, 412, 415, 416, 418
- Protective antigen129–140
- Protein quantification80, 210, 213, 219, 220
- Pseudoxons.....34, 36, 39, 40,
150, 164, 168, 270, 273, 276, 282, 322

Q

- Quantitative polymerase chain reaction
(qPCR).....56, 80–82,
85, 218, 219, 241, 252, 297

R

- Rare diseases42, 43, 169, 185
- Read-out157, 159, 163, 251, 326
- Retina.....35, 38, 42, 147, 156,
164, 245–247, 250, 253, 276, 321–331
- Reverse transcription polymerase chain reaction
(RT-PCR)91, 93, 97, 98,
101, 104, 149, 150, 157–160, 163, 177, 183,
193–195, 198–200, 203, 219, 230, 237, 252,
285, 287, 292–294, 303, 307, 326

RNA..... 3, 4, 6–9, 11, 12, 14–18,
20–22, 33–43, 53–56, 60, 61, 64, 65, 67, 69, 70,
74, 81, 83, 84, 89, 90, 97, 117–126, 129, 146,
158, 168, 169, 171, 173, 177, 179–181, 186,
188, 191, 194, 195, 197, 198, 203, 207,
218–220, 224, 229, 230, 239–241, 247, 251,
253, 268, 281, 282, 289, 290, 292, 303, 306,
307, 322, 326, 334, 340, 350, 353, 355, 356, 358
RNA-based therapies 235–242
RNA isolation..... 56, 93, 149, 156,
157, 160, 171, 172, 176, 177, 194, 198, 203,
237, 240, 241, 284, 289, 292, 328
RNase H 5, 8, 9, 11, 12,
14–17, 177, 356, 359

S

Safety..... 5, 6, 9, 12, 16, 17, 19,
40–42, 67, 236, 250, 323, 355–363, 371, 390
Searching 406, 414–416
Sensors 104
sgRNA 284, 290, 295, 296
Short interfering RNA (siRNAs) 3–7, 17–19,
21, 40, 43, 103, 104, 118–126, 201, 347, 351,
355–360, 362
Skeletal muscles..... 192, 193, 220,
235, 236, 275, 306
Skin 35, 56, 65, 104,
185–190, 203, 273, 315–320, 336–339, 352
Skin grafts 318
Spherical nucleic acids..... 104
Splicing 5, 8, 13,
34–36, 41, 53–55, 57, 58, 60, 61, 89–101, 129,
145–164, 167–169, 177, 178, 180, 182, 183,
186, 191, 207, 235, 236, 246, 252, 268–270,
273, 274, 276, 281, 282, 286, 287, 293, 296,
322, 326, 356
Splicing modulation..... 14, 34–36,
39, 245–253, 273
Splicing variants..... 146, 167–183
Splicing vectors..... 151
Stereotactic surgery..... 337
Synthetic long non-coding RNAs
(SINEUPs) 63–85
Systemic administration 9, 20, 372

T

Therapeutics 3–23, 33–43, 53,
54, 64, 65, 84, 91, 93, 94, 96–98, 101, 104, 118,
119, 129, 130, 146, 159, 185, 218, 245, 252,
257, 258, 268, 274, 302, 312, 315, 322, 326,
333, 345–353, 355–363, 371–383, 386,
405–409, 411, 413–415
Therapeutic tools 36, 64
Therapies 22, 33, 38, 41, 54,
64, 98, 104, 118, 146, 167–183, 192, 218, 268,
271, 274, 275, 281–297, 321, 322, 333, 340, 356
3D culture 316
Toxicology 362, 372
Transcript degradation..... 34, 36, 37, 39
Transcripts 34–37, 41, 60, 64,
67–70, 80–85, 157, 159, 161, 163, 164, 186,
191, 193, 199, 218, 270, 273, 275, 282, 289,
293–295, 297, 301, 322, 356, 358, 359, 372
Transfection 56, 58, 61, 66, 79,
91, 93, 95–97, 100, 101, 103, 104, 118, 146,
147, 149, 150, 156–160, 163, 169, 171–174,
177, 178, 180, 181, 186–190, 192, 201, 210,
211, 213, 220, 223–226, 239, 241, 284, 287, 296

U

U1 small nuclear ribonucleoprotein
(U1 snRNP) 89
USH2A 35, 39, 40, 282,
287, 293, 294, 322
Usher syndrome 35, 40, 282

V

Variants 35, 36, 90, 145, 146,
148, 150, 151, 157, 167–169, 208, 235, 241,
246, 251, 270, 281, 289, 315, 322

W

Watson-Crick 355, 358
Western blot 57, 67, 80, 81, 98,
183, 208, 214, 302, 304, 307, 308, 326, 350

Z

Zebrafish 74, 84, 276, 281–298